6th International Symposium on Focused Ultrasound 2018

Reston, Virginia | October 21-25, 2018

Abstract Book

Hyatt Regency Reston
Reston, Virginia, USA

Focused Ultrasound Foundation

Sponsor Acknowledgements

Diamond Sponsor

INSIGHTEC

Platinum Sponsor

PROFOUND MEDICAL

Gold Sponsor

KOCH™
DISRUPTIVE TECHNOLOGIES

Silver Sponsors

BRACCO
LIFE FROM INSIDE

ISTU
International Society for Thearapeutic Ultrasound

KAI RESEARCH
AN ALTARUM COMPANY

MEGGiTT

Welcome Messages

From the Honorary President

This week, I join my colleagues as we convene for the Focused Ultrasound Foundation's biennial event. I am honored to be a part of this invaluable opportunity to gather and learn of the latest advances and techniques in the field of therapeutic ultrasound.

In my clinical practice, I have personally seen this technology change lives. Focused ultrasound has enabled a four-year-old child with a desmoid tumor in her forearm to participate in gymnastics again. It has made it possible for a 78-year-old man with painful metastatic melanoma to stop his narcotics for the first time in years and ride his horse to his cabin in the mountains. And it has allowed an 84-year-old woman who was isolated by her hand and vocal tremor to feel confident about speaking with her friends and family on the phone and eating with them at a restaurant. I truly believe that focused ultrasound is an incredibly effective, noninvasive solution for many patients, and yet, we have just begun to scratch the surface of its applications.

The Symposium is an opportunity to broaden focused ultrasound's impact into new indications and innovative uses of the technology. We are able to draw inspiration from work being done around the world and create collegial contacts with whom we can collaborate on future projects.

I encourage you to spend this week exploring new ideas and establishing new partnerships, allied to expand the field of therapeutic ultrasound beyond its current achievements.

Pejman Ghanouni, MD, PhD
Assistant Professor of Radiology, and, by courtesy, of Neurosurgery and of Urology
Stanford University Medical Center
Honorary Symposium President

From the Foundation Chairman

Dear Colleagues:

Welcome to the 6th International Symposium on Focused Ultrasound. There has never been a more important time to convene as we acknowledge the field's immense growth in the past two years. There are now more than 100 clinical indications for which focused ultrasound is in various stages of research, development, and commercialization. This is an astonishing increase since the Foundation was created in 2006, and this progress is the result of your hard work, dedication, and innovation.

Over the next four days, we will share data, foster collaboration, and identify applications that offer maximum value to patients. We will hear from leading experts in this innovative field as they share findings through a record 240 oral and poster presentations.

I cannot stress enough the importance of exploring new partnerships this week as you are surrounded by leaders in all stages of focused ultrasound research and commercialization. The event provides unique value to all attendees: clinicians can communicate their medical needs, manufacturers have the opportunity to showcase their products, and scientists will share newly identified mechanisms of action that can translate into treatments.

We appreciate your participation in the Symposium and your steadfast commitment to advancing focused ultrasound technology. I am confident that at the close of this event, you will feel inspired to pursue the important research and collaborations that will make tangible progress toward improving patients' lives.

In closing, I would like to acknowledge the generosity of our donors and the support of our sponsors. They have made this meeting possible. Thank you.

Be well,

Neal F. Kassell, MD
Chairman, Focused Ultrasound Foundation

Table of Contents

Symposium Organizer
About the Foundation 4

Scientific Program Committee 5

Map 7

General Information 8

Program at a Glance
Keynotes and Special Lecture 9
Sunday, 21 October 2018 9
Monday, 22 October 2018 10
Tuesday, 23 October 2018 11
Wednesday, 24 October 2018 12
Thursday, 25 October 2018 13

Session Moderators 14

Abstracts
Oral Abstracts 15
Poster Abstracts 207

Awards
Ferenc Jolesz Memorial Award 321
Visionary Award 322

Young Investigator Awards
Young Investigator Awards Program 323
Young Investigator Award Recipients 324

Charles Steger Memorial Internship Program
2017 and 2018 Summer Interns 330
2017 Global Interns 331
2018 Global Interns 332

Sponsors and Exhibitors
Sponsor and Exhibitor Information 333

Partners
Partner Information 339

Symposium Organizer

FOCUSED ULTRASOUND FOUNDATION

About the Focused Ultrasound Foundation

The Focused Ultrasound Foundation is a medical technology research, education, and advocacy organization dedicated to improving the lives of millions of people with serious medical disorders by accelerating the development and adoption of focused ultrasound.

Positioned at the nexus of a large, diverse group of stakeholders comprising the focused ultrasound community, the Foundation functions as an independent, unbiased third party, aligning organizations into a cohesive ecosystem with a single goal: to make this technology available to patients in the shortest time possible. It strives to catalyze progress while instilling a patient-centric sense of urgency.

The Foundation works to clear the path to global adoption by organizing and funding research, fostering collaboration at our various workshops and symposia, building awareness, and cultivating the next generation through internships and fellowships.

The Foundation is on the leading edge of the venture philanthropy and social entrepreneurship movements and is a model of how private philanthropy can work in concert with academia, industry, and government to bridge the gap between research and commercialization.

To learn more about focused ultrasound and the Focused Ultrasound Foundation, visit the Foundation's website: www.fusfoundation.org

Scientific Program Committee

Roberto Blanco Sequeiros, MD, PhD
Turku University Hospital
Turku, Finland

Kim Butts Pauly, PhD
Stanford University
Stanford, California, United States

Alexandre Carpentier, MD, PhD
Hôpitaux Universitaires Pitié-Salpêtrière
Paris, France

Charles Caskey, PhD
Vanderbilt University
Nashville, Tennessee, United States

Rajiv Chopra, PhD
University of Texas Southwestern
Dallas, Texas, United States

Paul Fishman, MD, PhD
University of Maryland
Baltimore, Maryland, United States

Jessica Foley, PhD, Co-Chair
Focused Ultrasound Foundation
Charlottesville, Virginia, United States

Wladyslaw Gedroyc, MBBS
St. Mary's Hospital
London, United Kingdom

Chandan Guha, MBBS, PhD
Montefiore Medical Center
Bronx, New York, United States

Joo Ha Hwang, MD, PhD
Stanford University
Stanford, California, United States

Tatiana Khokhlova, PhD
University of Washington
Seattle, Washington, United States

Elisa Konofagou, PhD
Columbia University
New York, New York, United States

Cyril Lafon, PhD
LabTAU, Inserm
Lyon, France

Nir Lipsman, MD, PhD
Sunnybrook Health Sciences Centre
Toronto, Ontario, Canada

Hao-Li Liu, PhD
Chang-Gung University
Taoyuan, Taiwan

Nathan McDannold, PhD
Brigham and Women's Hospital
Boston, Massachusetts, United States

Tim Meakem, MD, Co-Chair
Focused Ultrasound Foundation
Charlottesville, Virginia, United States

Franco Orsi, MD, PhD
Instituto Europeo di Oncologia
Milan, Italy

Karun Sharma, MD
Children's National Health System
Washington, DC, United States

Gail ter Haar, PhD
Institute of Cancer Research
London, United Kingdom

Joan Vidal-Jove, MD, PhD
Hospital Universitari Mútua Terrassa
Barcelona, Spain

Bradford Wood, MD
National Institutes of Health Clinical Center
Bethesda, Maryland, United States

Zhen Xu, PhD
University of Michigan
Ann Arbor, Michigan, United States

Lian Zhang, MD
Chongqing Medical University
Chongqing, China

Notes

Map | Grand Ballroom and Regency Ballroom

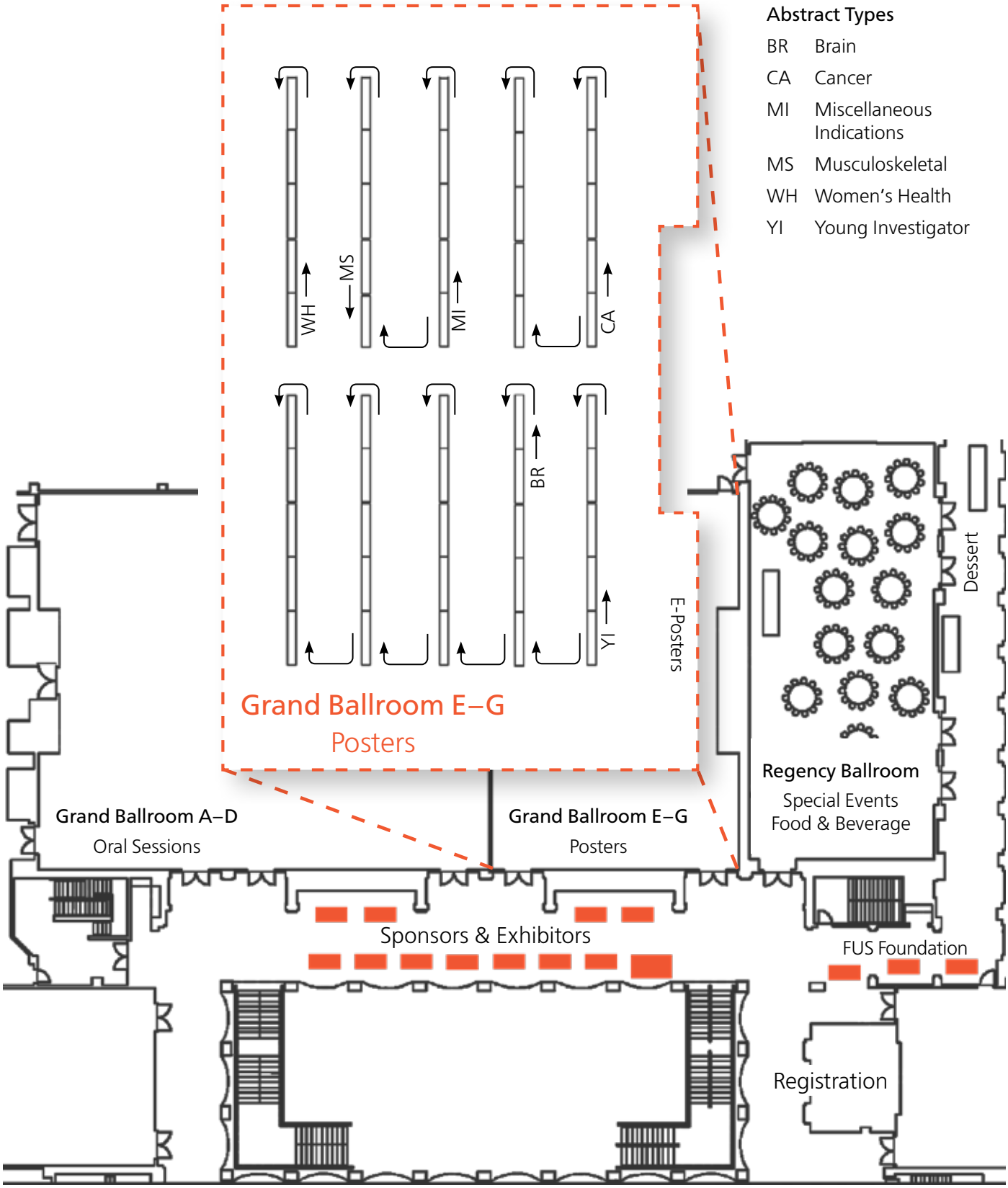

General Information

Registration & Information Hours

Sunday	16:00 – 20:00
Monday	7:00 – 18:30
Tuesday	7:00 – 18:00
Wednesday	7:00 – 18:00
Thursday	7:00 – 14:00

Internet Access in Meeting Rooms

Wireless internet access is complimentary in the hotel lobby and in guest rooms that were reserved at the special conference rate.

Network: @Hyatt_Meetings
Access Code: FUS2018

Symposium Mobile App

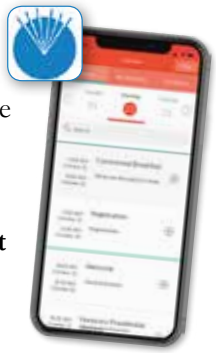

The FUS Symposium app is available from the App Store or Google Play. **Scan** the QR code below to **Download**. **Accept** the cookie popup. Tap **Log In**, enter your **First Name** and **Last Name**, and tap **Next**. You will receive a validation code. Enter the four-digit code, and tap **Verify**. You will be redirected to the Welcome screen. Go to the **Schedule** tab and tap on a ⊕ to add a session to your personalized symposium schedule.

Download on the App Store

GET IT ON Google play

E-Poster Library

A library of e-posters is available in Grand Ballroom E–G and will also be available online after the symposium.

The mobile app and e-poster library are both sponsored by:

INSIGHTEC

Speaker Ready Room Hours

Sunday	16:00 – 18:30
Monday	7:30 – 17:30
Tuesday	7:30 – 17:30
Wednesday	7:30 – 17:30
Thursday	7:00 – 12:00

Local Transportation

Information about taxis and other local transportation options is available from the hotel Concierge Desk located in the lobby.

Meals

Included in Symposium Registration

Registration includes continental breakfast, lunch, break refreshments and special events (see below). The Tuesday afternoon break is sponsored by **HistoSonics**. The Wednesday morning break is sponsored by **Profound Medical Corp.**

Dinner Options

Symposium registration does not include dinner. Options include two restaurants at the Hyatt Regency Reston as well as nearby restaurants. More information is available from the hotel Concierge Desk located in the lobby.

Special Events

Sunday, 21 October 2018

Welcome Reception sponsored by:

KOCH DISRUPTIVE TECHNOLOGIES

18:00–20:00 | Regency Ballroom
Includes drinks and hors d'oeuvres

Tuesday, 23 October 2018

Poster Session and Young Investigator Spotlight sponsored by:

INSIGHTEC

18:00–20:00 | Grand Ballroom E-G
Includes drinks and hors d'oeuvres

Symposium Feedback Survey

To assist the Focused Ultrasound Foundation in evaluating the success of the symposium, attendees will be asked to complete a brief, anonymous online survey each day of the meeting and at the end of the event.

Daily Surveys

Monday:	www.surveymonkey.com/r/FUSFMON
Tuesday:	www.surveymonkey.com/r/FUSFTUES
Wednesday:	www.surveymonkey.com/r/FUSFWED
Thursday:	www.surveymonkey.com/r/FUSFTHUR

Overall Survey: www.surveymonkey.com/r/KH9ZWKP

Program at a Glance

Sunday

21 October

16:00

17:00

18:00

19:00

20:00

Welcome Reception sponsored by

KOCH DISRUPTIVE TECHNOLOGIES

Ferenc Jolesz Memorial Award sponsored by INSIGHTEC (p. 15)

Visionary Award (p. 16)

Regency Ballroom 18:00–20:00

Registration

Ballroom Foyer 16:00–20:00

Keynotes and Special Lecture

Gary Shapiro

Tuesday, 23 October 2018 | 11:46–12:16

Gary Shapiro, President and CEO of the Consumer Technology Association (CTA)™, which annually produces CES®, the largest technology and innovation show in the world, will deliver a keynote address on the importance of innovation at the intersection of technology, business, and healthcare.

Scott Whitaker

Wednesday, 24 October 2018 | 8:00–8:30

Scott Whitaker is President and CEO of the Advanced Medical Technology Association (AdvaMed). A top healthcare advocate and policy expert, Whitaker will discuss the benefits of technology in medicine – including focused ultrasound – for improving the lives of patients and for society in general, as well as current challenges and obstacles facing the industry during an onstage interview.

Mary Lou Jepsen, PhD

Thursday, 25 October 2018 | 8:00–8:20

Mary Lou Jepsen, Founder and CEO of Openwater, will deliver a special lecture entitled, "Can a Consumer Electronics Wearable Leapfrog MR and Ultrasound Imaging and Revolutionize Focused Ultrasound Therapy?"

Program at a Glance (continued)

Monday
22 October

7:00 — Continental Breakfast
Regency Ballroom 7:00–8:00

8:00 — Opening Remarks | Honorary President's Address
Presentation by Ferenc Jolesz Memorial Award Winner
Grand Ballroom A–D 8:00–8:42

9:00 — Movement Disorders
Grand Ballroom A–D 8:42–9:54

10:00 — Break
Regency Ballroom 9:54–10:24

11:00 — Movement Disorders (continued)
Grand Ballroom A–D 10:24–11:36

General Discussion Grand Ballroom A–D 11:36–11:56

12:00 — Lunch
Regency Ballroom 11:56–13:56

13:00

14:00 — Pyschiatric Disorders
Grand Ballroom A–D 13:56–14:20

15:00 — Neurodegenerative Disorders
Grand Ballroom A–D 14:20–15:16

Break
Regency Ballroom 15:16–15:46

16:00 — Blood-Brain Barrier Opening
Grand Ballroom A–D 15:46–16:34

17:00 — Epilepsy, Stroke, Neuropathic Pain
Grand Ballroom A–D 16:34–17:38

18:00 — Neuromodulation
Grand Ballroom A–D 17:38–18:26

Registration and Exhibits Ballroom Foyer 7:00–18:30
Posters Grand Ballroom E–G 7:00–18:30

Program at a Glance (continued)

Tuesday
23 October

7:00 — Continental Breakfast
Regency Ballroom 7:00–8:00

8:00 — Brain — Technical
Grand Ballroom A–D 8:00–9:20

9:00 — Break
Regency Ballroom 9:20–9:50

10:00 — Brain Tumors
Grand Ballroom A–D 9:50–11:02

11:00 — Panel Discussion: Sonodynamic Therapy Grand Ballroom A–D 11:02–11:22

Brain Tumors (continued) Grand Ballroom A–D 11:22–11:46

12:00 — Keynote: Gary Shapiro Grand Ballroom A–D 11:46–12:16

13:00 — Lunch
Regency Ballroom 12:16–13:36

14:00 — Cancer Immunotherapy
Grand Ballroom A–D 13:36–14:48

15:00 — Panel Discussion: Cancer Immunotherapy
Grand Ballroom A–D 14:48–15:08

Break Regency Ballroom 15:08–15:38
sponsored by **HistoSonics**

16:00 — Liver/Pancreas/Kidney
Grand Ballroom A–D 15:38–16:42

17:00 — Bone Grand Ballroom A–D 16:42–17:06

Panel Discussion: Osteoid Osteoma Grand Ballroom A–D 17:06–17:16

Bone (continued)
Grand Ballroom A–D 17:16–17:56

18:00 — Poster Session and Young Investigator Spotlight
sponsored by
INSIGHTEC
Grand Ballroom E–G 18:00–20:00

19:00

20:00

Registration and Exhibits Ballroom Foyer 7:00–18:00
Posters Grand Ballroom E–G 7:00–18:00

Program at a Glance (continued)

Wednesday 24 October

7:00 — Continental Breakfast
Regency Ballroom 7:00–8:00

8:00 — Keynote Conversation: Scott Whitaker
Grand Ballroom A–D 8:00–8:30

Prostate
Grand Ballroom A–D 8:30–9:10

9:00

Miscellaneous Tumors
Grand Ballroom A–D 9:10–10:30

10:00

Break Regency Ballroom 10:30–11:00
sponsored by **Profound Medical Corp.**

11:00 — Breast
Grand Ballroom A–D 11:00–11:24

Gynecological
Grand Ballroom A–D 11:24–12:28

12:00

Lunch
Regency Ballroom 12:28–13:58

13:00

Musculoskeletal
Grand Ballroom A–D 13:58–15:10

14:00

Cardiovascular
Grand Ballroom A–D 15:10–15:42

15:00

Break
Regency Ballroom 15:42–16:12

16:00

Miscellaneous Indications
Grand Ballroom A–D 16:12–17:24

17:00

Advocacy Partnerships Grand Ballroom A–D 17:24–17:40

18:00

Registration and Exhibits Ballroom Foyer 7:00–18:00
Posters Grand Ballroom E–G 7:00–18:00

Program at a Glance (continued)

Thursday 25 October

7:00 — Continental Breakfast
Regency Ballroom 7:00–8:00

8:00 — Special Lecture: Mary Lou Jepsen Grand Ballroom A–D 8:00–8:20

Technology
Grand Ballroom A–D 8:20–8:50

9:00 — Treatment Success
Grand Ballroom A–D 8:50–9:20

Regulatory Collaboration
Grand Ballroom A–D 9:20–9:50

10:00 — Block Chain and AI Grand Ballroom A–D 9:50–10:10

Break
Regency Ballroom 10:10–10:40

11:00 — Panel Discussion: Clinical Trials and Registries
Grand Ballroom A–D 10:40–11:25

Open Science Grand Ballroom A–D 11:25–11:30

Panel Discussion: Training and Credentialing
Grand Ballroom A–D 11:30–12:00

12:00 — Pick Up Box Lunch Ballroom Foyer 12:00–12:10

Development and Regulatory Approval
Grand Ballroom A–D 12:10–12:40

Obtaining Venture Capital; FUS Partners Grand Ballroom A–D 12:40–13:00

13:00 — Panel Discussion: Crystal Ball — FUS in Ten Years
Grand Ballroom A–D 13:00–13:30

Closing Remarks Grand Ballroom A–D 13:30–13:40

14:00

Registration Ballroom Foyer 7:00–14:00

Session Moderators

Jean-François Aubry, PhD
Institut Langevin
Paris, France

Alberto Bazzocchi, MD, PhD
Istituto Ortopedico Rizzoli
Bologna, Italy

Henry Brem, MD
Johns Hopkins University
Baltimore, Maryland, United States

Matthew Bucknor, MD
University of California, San Francisco
San Francisco, California, United States

Kim Butts Pauly, PhD
Stanford University
Stanford, California, United States

Alexandre Carpentier, MD, PhD
Hôpitaux Universitaires Pitié-Salpêtrière
Paris, France

Jin Woo Chang, MD, PhD
Yonsei University Health System, Severance Hospital
Seoul, Korea

G. Rees Cosgrove, MD
Brigham and Women's Hospital
Boston, Massachusetts, United States

Patrick Dillon, MD
University of Virginia
Charlottesville, Virginia, United States

Katherine Ferrara, PhD
Stanford University
Stanford, California, United States

Paul Fishman, MD, PhD
University of Maryland
Baltimore, Maryland, United States

Joseph Frank, MD
National Institutes of Health
Bethesda, Maryland, United States

Dheeraj Gandhi, MBBS
University of Maryland
Baltimore, Maryland, United States

Wladyslaw Gedroyc, MBBS
St. Mary's Hospital
London, United Kingdom

Jürgen Götz, PhD
University of Queensland
Brisbane, Queensland, Australia

Arik Hananel, MD, MBA
FUSMobile, Inc.
Alpharetta, Georgia, United States

Joo Ha Hwang, MD, PhD
Stanford University
Stanford, California, United States

Michael Kaplitt, MD, PhD
Weill Cornell Medicine
New York, New York, United States

Tatiana Khokhlova, PhD
University of Washington
Seattle, Washington, United States

Vera Khokhlova, PhD
University of Washington
Seattle, Washington, United States

AeRang Kim, MD, PhD
Children's National Health System
Washington, DC, United States

Vibhor Krishna, MBBS
Ohio State University
Columbus, Ohio, United States

Cyril Lafon, PhD
LabTAU, Inserm
Lyon, France

Suzanne LeBlang, MD
University MRI & Diagnostic Imaging Centers
Boca Raton, Florida, United States

Nir Lipsman, MD, PhD
Sunnybrook Health Sciences Centre
Toronto, Ontario, Canada

Nathan McDannold, PhD
Brigham and Women's Hospital
Boston, Massachusetts, United States

Chrit Moonen, PhD
Universitair Midsch Centrum Utrecht
Utrecht, Netherlands

Alessandro Napoli, MD, PhD
Università degli Studi di Roma 'La Sapienza'
Rome, Italy

Jill O'Donnell-Tormey, PhD
Cancer Research Institute
New York, New York, United States

Dennis L. Parker, PhD
University of Utah
Salt Lake City, Utah, United States

Richard J. Price, PhD
University of Virginia
Charlottesville, Virginia, United States

Narendra Sanghvi
SonaCare Medical, LLC
Charlotte, North Carolina, United States

Jonathan R. Sukovich, PhD
University of Michigan
Ann Arbor, Michigan, United States

Claire Tempany, MD
Brigham and Women's Hospital
Boston, Massachusetts, United States

Gail ter Haar, PhD
Institute of Cancer Research
London, United Kingdom

Joan Vidal-Jove, MD, PhD
Hospital Universitari Mútua Terrassa
Barcelona, Spain

Seung-Schik Yoo, PhD, MBA
Brigham and Women's Hospital
Boston, Massachusetts, United States

Oral Abstracts

BR	Brain	16
CA	Cancer	84
CV	Cardiovascular	137
GI	Gastrointestinal	141
MI	Miscellaneous Indications	142
MS	Musculoskeletal	164
WH	Women's Health	175
YI	Young Investigator (Oral/Poster)	189

In accordance with author requests, the following abstracts are not included in this publication:

BR-7	CA-8	CA-14	MS-4	YI-7
BR-8	CA-9	CA-36	MS-9	
BR-44	CA-13	MI-12	WH-10	

The following abstracts were withdrawn by the authors:

BR-17	CA-37	WH-8
BR-26	MI-14	

BR-1

Monday

22 October 2018

Topic: Movement Disorders

Presentation Type: Oral

Six year outcome of focused ultrasound thalamotomy for essential tremor

Diane Huss, Aaron Bond, Tony Wang, Jeff Elias

University of Virginia, Charlottesville, Virginia, United States

Background: Focused ultrasound thalamotomy has been recently accepted as a treatment option for medication-refractory essential tremor. Class 1 evidence led to FDA approval in July 2016 following results of a multicenter double-blind randomized trial. In the United States, Medicare approved it as a covered treatment option for unilateral treatment of Essential Tremor in 2018. One and two year outcomes have been published, and now we share outcomes for 13 of the first 15 patients in the original Essential Tremor pilot study. The Pilot study was conducted from February through December of 2011 with a safety as a primary objective.

Methods: The pilot study of 15 ET patients, treated with unilateral FUS Vim thalamotomy, was conducted in 2011. Clinical outcomes were assessed for tremor, disabilities, quality of life, MRI, and adverse event reporting. These patients were recently assessed in the fall of 20178 at six years post treatment with CRST, QUEST, global impression of clinical change and +/- treatment response. A correlation analysis of their long term clinical outcomes was conducted.

Results: Thirteen patients (87%) were assessed at 6 years post thalamotomy. One patient was lost to follow-up and another has passed away. There were no latent adverse effects or procedural morbidity.

Mean hand tremor scores (baseline: 20.4+5.2), which were improved by 74% (5.2+4.8) at one year, remained improved by 36% (12.5+11.4) at 6 years but with some loss of effect. Six of the thirteen patients available for follow-up had over 50% reduction of hand tremor at 6 years.

Mean disability scores remained improved from baseline by 50% at long term. Additional outcomes including total CRST, simulated eating task, and quality of life from the QUEST are improved at long term. Of note is that 9 of the 13 retested subjects retained ability to eat, drink and write functionally six years after treatment.

Conclusions: FUS thalamotomy can provide long term benefit for ET, but recurrence certainly occurs. These long term results from an early stage pilot study provides additional insight into the procedure as the treatment evolves as a medically acceptable and insurance reimbursable procedure.

BR-2

Monday

22 October 2018

Topic: Movement Disorders

Presentation Type: Oral

MR-guided focused ultrasound thalamotomy for treatment of essential tremor: A two-year outcome study

Ying Meng[1], Benjamin Solomon[1], Alexander Boutet[2], Maheleth Llinas[1], Nadia Scantlebury[1], Yuexi Huang[3], Kullervo Hynynen[4], Alfonso Fasano[2], Andres Lozano[2], Nir Lipsman[3], Michael Schwartz[1]

[1]Sunnybrook Health Sciences Centre, Toronto, Ontario, Canada
[2]Toronto Western Hospital, Toronto, Ontario, Canada
[3]Sunnybrook Research Institute, Toronto, Ontario, Canada
[4]University of Toronto, Toronto, Ontario, Canada

Objectives: MR-guided focused ultrasound is an emerging, minimally-invasive thermoablation technique for medically refractory essential tremor. Beyond the initial year, data regarding efficacy and potential predictors of efficacy are still preliminary. To assess the outcome at two-years and the association between lesion volume and outcome at one-year after treatment.

Methods: We reviewed data from 37 patients who underwent unilateral MR-guided focused ultrasound thalamotomy, with primary outcome being dominant tremor subscore of the Clinical Rating Scale for Tremor. We used multivariable linear regression to model initial lesion volume with one-year outcome, adjusting for other clinically relevant variables.

Results: While we detected a trend in loss of clinical benefit within the first year, the dominant tremor score at two-years continued to be significantly improved (43.4%, 95% CI 27.8 – 59.0%) from baseline (Figure 1). Secondarily, initial lesion volume is significantly associated with one-year outcome ($p = 0.02$, Figure 2).

Conclusions: Our findings support MR-guided focused ultrasound as a comparable treatment option for medically refractory essential tremor even in the long-term, and highlight areas for improvement.

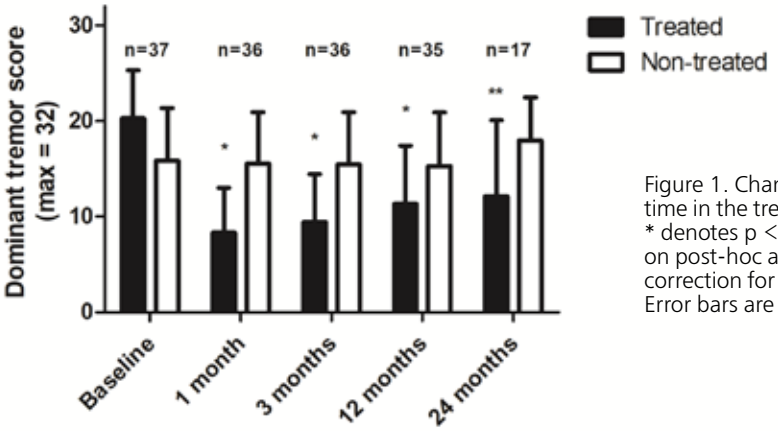

Figure 1. Change in tremor score over time in the treated and nontreated side. * denotes $p < 0.001$ and ** $p < 0.05$ on post-hoc analysis with Bonferroni correction for multiple comparisons. Error bars are standard deviations.

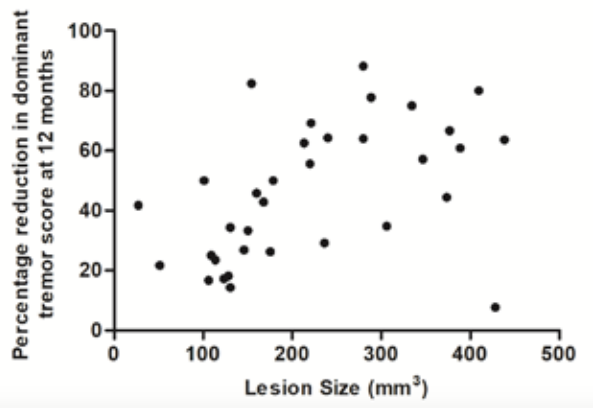

Figure 2. Lesion volume *versus* percentage reduction in dominant tremor score at twelve months after treatment

BR-3

Monday

22 October 2018

Topic: Movement Disorders

Presentation Type: Oral

Is trans-cranial MR-guided focused ultrasound a repeatable treatment option? Report of a successfully re-treated patient

Cesare Gagliardo[1], Francesca Valentino[1], Rosario Maugeri[1], Giusepe Cosentino[1], Maurizio Marrale[1], Alessandro Napoli[2], Domenico Gerardo Iacopino[1], Carlo Catalano[2], Massimo Midiri[3]

[1]University of Palermo, Palermo, Italy
[2]Sapienza University of Rome, Rome, Italy
[3]Universita Degli Studi Di Palermo, Palermo, Italy

Background: In recent years, transcranial Magnetic Resonance-guided Focused UltraSounds (tcMRgFUS) treatments for functional neurological disorders are giving a new thrust to the field of therapeutic brain lesioning. This technique has been proven safe and effective in selected patients. Here we present the case of a patient affected by tremor combined with parkinsonism who underwent a second tcMRgFUS thalamotomy because of relapsing tremor after a few months from the first tcMRgFUS treatment.

Methods: A 72-year-old, right-handed man, who came to our observation because of a disabling tremor affecting mainly his upper right limb and refusing any invasive surgical procedure. His past medical history was notable for arterial hypertension, diabetes mellitus and hereditary hemochromatosis (homozygous H63D mutation). Patient underwent a tcMRgFUS thalamotomy (target: left VIM) which resulted in a meaningful reduction of 46.9% of the global tremor at the FTM, with a persistent reduction of 57.1% of the treated hand tremor and a 33.9% improvement in patient's quality of life at a 3 months follow-up. Four months after the treatment, a progressive recurrence of the disabling tremor on the right upper limb was noticed by the patient. The decision to re-treat the patient was taken.

Results: The re-treatment session was planned six month after the former and, again, the treatment resulted in an immediate and complete relief from right upper limb tremor. At a clinical and electrophysiological assessment performed six months after the second treatment, a clinical benefit on postural and kinetic tremor of the right upper limb persisted; patients showed only a slight and inconstant resting tremor. A significant reduction of 41.7% of the global tremor was reported by the FTM scale, with a persistent reduction of 71.4% of the treated hand tremor. Moreover, an improvement of 29.2% in patient's quality of life was reported by the QUEST questionnaire.

Conclusions: Since tcMRgFUS doesn't use ionizing radiations and it is incision-less, repeated and staged treatment procedures have always been hypothesized. Our report suggests that tcMRgFUS re-treatment might be actually a feasible, safe and effective option in selected patients in whom an optimal clinical outcome is not achieved after the first treatment session. During the re-treatment session no technical issues were faced focusing the HI-FU beam in proximity to the previously targeted area and it was still possible to exploit the typical closed-loop feedback and control system which characterizes tcMRgFUS procedures. However, future well-designed studies in large samples are needed to assess the possible risks of retreatment and the optimal timing of reintervention.

Acknowledgements: The installation of the tcMRgFUS equipment named in this abstract was funded by the Italian Ministry of Education, University and Research (MIUR) within the project "Programma Operativo Nazionale 2007-3013" (PONa3_00011; Project Leader: Prof. Carlo Catalano). The research leading to these results has received funding from the Italian Ministry of Health's "Ricerca Finalizzata 2016" (GR-2016-02364526; Principal Investigator: Dr. Cesare Gagliardo).

BR-4

Monday

22 October 2018

Topic: Movement Disorders

Presentation Type: Oral

Association between improvement in tremor severity and functional connectivity changes after MRgFUS thalamotomy in essential tremor patients

Li Jiang, Jiachen Zhuo, Dheeraj Gandhi, Charlene Aldrich, Howard Eisenberg, Paul Fishman, Elias Melhem, Rao Gullapalli

University of Maryland School of Medicine, Baltimore, Maryland, United States

Background: Thalamotomy of the ventral intermediate nucleus (VIM) using MR guided Focused Ultrasound (MRgFUS) with real-time guidance from MR thermometry is effective in alleviating medication-resistant tremor in patients with essential tremor. However, there is substantial lack of knowledge regarding functional brain changes before and after the treatment and even less is known about its correlation with the tremor severity changes after treatment. In this study, we aimed at investigating the resting-state functional connectivity (rs-FC) changes between pre-treatment and one year post-treatment; and the association between the rs-FC changes and the corresponding tremor severity changes.

Methods: Medication refractory ET patients were recruited at the University of Maryland Medical Center and underwent unilateral MRgFUS thalamotomy. All patients obtained resting-state fMRI (rs-fMRI) scans on a 3T TrioTim Siemens Scanner at pre-treatment (baseline), within 24 hours post-treatment (post-24h), and 1-year post-treatment (post-1y). We examined 15 of the 19 ET patients recruited into the study at our site who had MRgFUS thalamotomy of the left VIM. No resting state scans were available on two of the remaining 4 patients and the other two had. thalamotomy performed on the right VIM. Clinical rating for tremor (CRST) scores were available for all patients.

The rs-fMRI data were preprocessed using SPM12 standard procedures (http://www.fil.ion.ucl.as.uk/spm) including slice timing, realignment, normalized to the MNI template space, spatially smoothed with 6mm FWHM Gaussian Kernel, and temporally band-pass filtered from 0.008-0.1 Hz. Nuisance variables including the six motion parameters as well as the principle components of the averaged BOLD time signals from WM and CSF were regressed out to remove motion and non-neuronal contributions. Seed-to-whole brain functional connectivity analysis was performed using the CONN toolbox (http://www.nitrc.org/projects/conn). The T1-MPRAGE images were segmented into gray matter (GM), white matter (WM), and cerebral spinal fluid (CSF) and normalized to MNI template space. The coordinates of the left VIM (for right-handed patients) where the lesioning was performed were estimated from the normalized T1 images acquired at 24-hour post-treatment since most of the thermal lesions resolved at 1-year post-treatment. A 6-mm spherical ROI on the left VIM on the pre-treatment and one year data was used to perform a bivariate analysis to estimate the Pearson correlation map between the averaged BOLD time series from the seed and the whole brain. The association map between the FC changes of left VIM (post-pre) and contralateral upper extremity(UE)-tremor improvement (pre-post) was estimated with age as a covariate using a threshold of voxel-wise uncorrected p-value of 0.009 and cluster-wise FDR-corrected p value of 0.05 for multiple comparison. Using the significant clusters thus obtained, we performed a seed-to-cluster ROI analysis using the left VIM as a seed. The FC between the left VIM and clusters were Fisher-z transformed and their association with the contralateral upper extremity-tremor improvement was also assessed.

Results: A repeated measure ANOVA with Greenhouse-Geisser correction was applied to determine if the UE-tremor changed significantly following the treatment. As shown in Fig. 1, the percentage change of contralateral UE-tremor significantly reduced from baseline to 42.5% ($p < 0.0001$) by 1-month post-treatment, and this reduction persisted throughout the 12-month study period (40.8% of baseline). However, although non-significant, the non-dominant hand UE-tremor increased slightly and remained at an elevated level over one year of observation.

Fig.2 shows the correlation maps between the changes of FC of left VIM (post-pre) and the difference of contralateral UE-tremor (pre-post). Increased functional connectivity was associated with greater reduction in tremor symptoms in the motor, spatial learning and visual processing areas. Whereas a reduction in functional connectivity ($r = -0.88$, $p < 0.001$) was associated with greater reduction in tremor symptoms in the superior parietal lobule,

supramarginal gyrus, occipital cortex, visuo-spatial, visuomotor, pre/post central gyrus, supplemental motor area (SMA).

Conclusions: To our knowledge this is the first study that examined the FC changes in the brain and its association with longitudinal change of tremor severity for treated and non-treated side of the upper extremity separately. We observed that the unilateral VIM lesioning improved tremor symptoms only on the side that was treated immediately following treatment and lasted for at least 1 year. Our results also demonstrate significant connectivity changes between the VIM of the treated side to other cortical and sub-cortical regions involving motor, and visuospatial regions. Additionally, the changes in functional connectivity correlated with the changes in tremor symptoms related to Part A and B scores on the CRST.

BR-5

Monday

22 October 2018

Topic: Movement Disorders

Presentation Type: Oral

tMRgFUS thalamotomy modifies cerebello-thalamo-cortical structural connectivity in essential tremor

Jose Angel Pineda-Pardo, Raul Martínez-Fernández, Rafael Rodríguez-Rojas, Marta Del-Alamo, Frida Hernández, Lydia Vela, José Obeso

CINAC, Hospital Universitario HM Puerta del Sur, Móstoles, Universidad CEU-San Pablo, Madrid, Spain and Mostoles, Spain

Background: MR guided focused ultrasound (MRgFUS) thalamotomy has been proven to be effective in the treatment of medication-refractory essential tremor[1]. Recent evidence suggests that the clinical benefit in tremor when targeting at the ventral intermediate (VIM) nucleus of the thalamus should be related to the interruption of the propagation of tremor activity along the cerebello-thalamic pathway to the cortex[2]. However, how thalamotomy impacts on the anatomical tracts in the vicinity of the VIM is still unclear. In here, we acquired DWI to resolve the effects of thalamotomy in the microstructural integrity of the cerebello-thalamic tract and its neighbours, and to quantify how these changes are related to the resulting clinical outcome.

Methods: Twenty-four patients with disabling and medication-refractory essential tremor underwent MRgFUS thalamotomy targeting the VIM of the thalamus. MRI was obtained on a 3T GE scanner for all patients at baseline, 1-day post-treatment, and 3-months post-treatment. DWI was acquired along 60 directions (b=1000s/mm^2) with 2mm isotropic resolution. Tremor was assessed in all sessions using the Fahn-Tolosa-Marín Scale for Tremor.

DWI was pre-processed for motion and field-inhomogeneities, and DTI was estimated to generate fractional anisotropy (FA), mean-, axial- and radial diffusivity maps (MD, AD, RD). Three anatomical pathways were reconstructed across subjects using constrained spherical deconvolution and probabilistic tractography: cortico-spinal tract, medial lemniscus, and the cerebello-thalamic tract (CBTT). Standardized representations of these tracts were created in MNI, and intersecting planes were defined along their trajectories for statistical analyses. Scalar measures were extracted across subjects in all intersecting planes, and compared between baseline and 3-months post-treatment images using paired t-test comparison.

Results: DTI analysis along the CBTT revealed a significant decrease in FA local to the lesion site, as well as an FA decrease together with an RD/MD increase in the white matter adjacent to ipsilateral motor cortex (P<0.01). No significant differences were found in the medial lemniscus, but decrease in cortical FA was found for the cortico-spinal projection (P<0.01) (Figure 1). Furthermore changes in DTI along the CBTT were correlated with the clinical improvement in tremor (P<0.05). No significant changes were found in the contralateral hemisphere to the lesion.

Conclusions: Using DWI we mapped the impact of MRgFUS thalamotomy over the thalamo-motor connections. We found that several DTI metrics were sensitive to local and distant alterations after thalamotomy, as reported for FA in[3]. By informing our DTI comparison with the pathway's trajectories we gained analytical specificity about how distant white matter was affected after the lesion. Our results suggest that clinical improvement in ET after thalamotomy is supported by a reduction in the integrity along the CBTT, both locally at the thalamic level and distantly below the motor cortex, while the ML and the CST are spared. Therefore using probabilistic tractography it seems possible to gain specificity in the definition of a successful, safer and personalized target for tMRgFUS thalamotomy.

Figure 1. A. Voxel-based changes in DTI measures. B. Changes in DTI along the cerebello-thalamic tract.

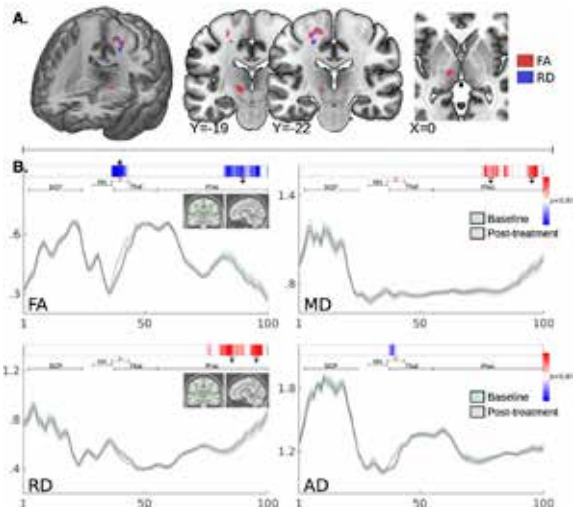

References

1. Elias WJ et al. A Randomized Trial of Focused Ultrasound Thalamotomy for Essential Tremor. *N Engl J Med.* 2016;375(8): 730–39.
2. Klein JC et al. The tremor network targeted by successful VIM deep brain stimulation in humans. *Neurology.* 2012;78(11):787–95.
3. Wintermark, M et al. Thalamic Connectivity in Patients with Essential Tremor Treated with MR Imaging-Guided Focused Ultrasound: *In vivo* Fiber Tracking by Using Diffusion-Tensor MR Imaging. *Radiology.* 2014;272(1):202–9

BR-6

Monday

22 October 2018

Topic: Movement Disorders

Presentation Type: Oral

Unilateral magnetic resonance guided focused ultrasound pallidotomy for Parkinson's disease

Jin Woo Chang

Yonsei University College of Medicine, Seoul, Republic of Korea

Background: Recently, magnetic resonance-guided focused ultrasound (MRgFUS) is emerging as an innovative new treatment method to treat many neurological disorders. This research was designed to identify the feasibility, effectiveness, and potential side effects of unilateral MRgFUS pallidotomy for the treatment of Parkinsonian dyskinesia.

Methods: Ten patients with severe, medication-refractory Parkinson's disease (PD) with motor fluctuation underwent unilateral MRgFUS pallidotomy using the Exablate 4000 device (INSIGHTEC, Israel) since December 2013. All patients had fully informed written consent. The patients` clinical assessments were obtained at baseline, 1 week, 1, 3, 6, and 12 months following MRgFUS pallidotomy. Technical failure as well as safety issues were also carefully determined by monitoring every event throughout the study period.

Results: Seven out of ten patients can finish more than 6 months follow up study. Three patients were dropped from the study with various reasons. All patients who underwent MRgFUS showed immediate and sustained improvements in dyskinesia, particularly in the treated hand. And this reduction was accompanied by functional improvement of activity of daily living. However, we also encountered several failure cases of thermal lesion with MRgFUS. There were also several side effects along with MRgFUS even though no patient suffered noticeable or significant complications.

Conclusions: This is the world's first pilot study of unilateral MRgFUS pallidotomy for advanced PD. In this study, we thus demonstrated the both benefits of unilateral MRgFUS pallidotomy in PD as well as a certain limitation of this technique because of the incomplete thermal lesioning in globus pallidus interna.

Acknowledgements: Grant from Michael J Fox Foundation

BR-7

Monday

22 October 2018

Topic: Movement Disorders

Presentation Type: Oral

Bilateral MR-guided focused ultrasound (MRgFUS) ablation of the pallido-thalamic tract for the treatment of advanced Parkinson's disease: Safety, feasibility and effectiveness study

Toshio Yamaguchi[1], Fusako Yokochi[2], Keiichi Abe[3], Hiroki Hori[1], Shiro Horisawa[3], Takaomi Taira[3]

[1]Shin-yurigaoka General Hospital, Kawasaki, Japan
[2]Tokyo Metropolitan Neurological Hospital, Fuchuu, Japan
[3]Tokyo Women's Medical University, Tokyo, Japan

In accordance with author request, this abstract is not available for publication.

BR-8

Monday

22 October 2018

Topic: Movement Disorders

Presentation Type: Oral

MR-guided focused ultrasound (MRgFUS) ventro-oral thalamotomy for focal hand dystonia (musician's dystonia): Safety and feasibility study

Toshio Yamaguchi[1], Keiichi Abe[2], Hiroki Hori[1], Shiro Horisawa[2], Takaomi Taira[2]

[1]Shin-yurigaoka General Hospital, Kawasaki, Japan
[2]Tokyo Women's Medical University, Tokyo, Japan

In accordance with author request, this abstract is not available for publication.

BR-9

Monday

22 October 2018

Topic: Movement Disorders

Presentation Type: Oral

Focused ultrasound thalamotomy for multiple sclerosis-associated tremor: A case report

Jorge Máñez-Miró[1], Raul Martinez-Fernández[2], Beatriz Fernandez[1], Marta Del Alamo[1], Jose A. Pineda-Pardo[2], Rafael Rodriguez-Rojas[2], Frida Hernandez-Fernandez[3], Fernando Alonso-Frech[3], Esther De Luis-Pastor[4], Lydia Vela[5], José Obeso[5]

[1]HM Puerta del Sur-CINAC, Mostoles, Spain
[2]Centro Integral de Neurociencias AC, University Hospital HM Puerta del Sur, Madrid, Spain
[3]CINAC-HM Puerta del Sur Hospital, Madrid, Spain
[4]HM Puerta del Sur-Radiology, Móstoles, Spain
[5]CINAC, Hospital Universitario HM Puerta del Sur, Móstoles, Universidad CEU-San Pablo, Madrid, Spain and Mostoles, Spain

Background: Tremor is the most common movement disorder related to MS, with a prevalence ranging from 25% to 58%[1] depending on the series. MS-associated tremor can be refractory to medical treatment and thus become highly disabling. Both thalamic deep brain stimulation and radiofrequency thalamotomy have shown to provide sustained benefit in selected patients[2]. However, risk-benefit ratio of applying invasive techniques is often a major cautionary drawback. MRgFUS has been developed as an incisionless technique which allows performing focal brain lesions in a controlled manner.[3] MRgFUS thalamotomy has been recently approved by FDA as a treatment for essential tremor[4] and some preliminary evidence suggests that it could also improve tremor of other origins.[5] Here, we report for the first time a successful unilateral MRgFUS thalamotomy in a patient with MS-associated tremor.

Methods: A 28-year-old female diagnosed with MS was referred for MRgFUS VIM thalamotomy to treat right upper limb tremor refractory to medical treatment and highly disabling. Assessment was performed both at baseline and 3 and 6 months after treatment through the Clinical Rating Scale for Tremor (CRST), as well as with EMG-accelerometer recordings (Figure 1A). Abolition of tremor was achieved intraprocedure after initial therapeutic sonications.

Results: The next day, postural and action tremor had decreased strikingly with only minimal bouts of tremor in certain manoeuvres. She could use her right upper limb for daily living performance almost normally. Mild facial asymmetry, moderate dysarthria and unsteadiness were present. MRI 12 hrs. post-procedure (Figure 2A) showed an acute left thalamic lesion with perilesional oedema spreading into the internal capsule. Patient was discharged 24 hrs. after treatment on corticosteroid (prednisone, 60/mg daily) therapy. Follow-up assessment at 3 and 6-months showed persistent tremor effect and marked improved of neurological side-effects. At 3 and 6-months post-treatment, the CRST score of the treated hand was reduced by 79.3% (from 29 at baseline to 6) and 75.6% (29 *vs.* 7) respectively. EMG-accelerometer recordings supported the observed clinical improvement (Figure 1B). Follow-up MRIs exhibited the left thalamic lesion greatly reduced in size (Figure 2B-2D).

Conclusions: This is, to our knowledge, the first report of a MS associated-tremor successfully treated with MRgFUS thalamotomy. This poses a potentially new therapeutic option for carefully selected MS patients suffering of tremor refractory to medical treatment.

References

1. Pittock S, McClelland R, Mayr W, et al. Prevalence of tremor in multiple sclerosis and associated disability in the Olmsted County population. *Mov Disord.* 2004;19:1482-1485.
2. Schuurman PR, Bosch DA, Merkus MP, Speelman JD. Long-term follow-up of thalamic stimulation *versus* thalamotomy for tremor suppression. *Mov Disord.* 2008;23(8):1146-53.
3. Lipsman N, Schwartz ML, Huang Y, et al. MR-guided focused ultrasound thalamotomy for essential tremor: a proof-of concept study. *Lancet Neurol.* 2013;12:462-8.
4. Elias WJ, Lipsman N, Ondo WG, et al. A randomized trial of focused ultrasound thalamotomy for essential tremor. *N Engl J Med.* 2016;375: 30–39.
5. Fasano A, Llinas M, Munhoz RP, Hlasny E, Kucharczyk W, Lozano AM. MRI-guided focused ultrasound thalamotomy in non-ET tremor syndromes. *Neurology.* 2017;89:771–75.

BR-10

Monday

22 October 2018

Topic: Movement Disorders

Presentation Type: Oral

MRI guided focused ultrsound for movement disorders-success and pitfalls in 71 consecutive cases

Menashe Zaaroor[1], Alon Sinai[2], Maria Nassar[2], Ayelt Eran[2], Ilana Schlesinger[2]

[1]Technion-Faculty of Medicine, Tiberias, Israel
[2]Rambam Health Care Campus, Haifa, Israel

Background: VIM Thalamotomy is effective in alleviating medication resistant tremor. MRI guided focused ultrasound (MRgFUS) is an innovative technology that enables thalamotomy via thermal ablation through an intact skull.

Methods: To evaluate MRgFUS VIM thalamotomy in the treatment of tremor. Seventy-one patients (72 procedures), 36 Essential tremor (ET), 28 Parkinson's disease (PD), 4 ET-PD (ET patients which developed PD years later) and 1 Multiple System Atrophy (MSA) patient with severe refractory tremor underwent the treatment. Effect was evaluated using Tremor Rating Scale (CRST) in ET patients and Unified PD Rating Scale (UPDRS) motor part in PD, ET-PD and MSA patients. Quality of life was assessed by Quality of life in ET Questionnaire (QUEST) and PD Questionnaire (PDQ-39).

Results: Tremor stopped in the treated arm in all but one patient immediately following treatment. Tremor in chin, leg and head, when present, was stopped, in most patients. At one month, ET patients' CRST score decreased from 44.4±12.1 to 14.7±8.6 ($p<0.001$) and QUEST scores decreased from 44.8±18.6 to 10.9±14.9 ($p<0.001$). In PD, ET-PD and MSA patients UPDRS (motor part) decreased from 23.6±6.5 to 12.7±8.8 ($p<0.001$) and PDQ39 decreased from 39.1±18.7 to 28.3±18.2 ($p=0.001$). During follow up tremor reappeared in twelve patients but usually, to a lesser degree than before treatment. Significant adverse events included unsteady feeling when walking, gait ataxia, unilateral taste disturbances and hand ataxia that lasted up to 3 months.

Conclusions: MRgFUS VIM thalamotomy to relieve medication resistant tremor was safe and effective. Still large randomized studies are needed to assess prolonged efficacy and safety.

BR-11

Monday

22 October 2018

Topic: Movement Disorders

Presentation Type: Oral

Lesion size prediction during focused ultrasound treatment of Parkinson's disease

Sijia Guo[1], Jiachen Zhuo[2], Rao Gullapalli[2], Dheeraj Gandhi[1], Mor Dayan[3]

[1]University of Maryland School of Medicine, Baltimore, Maryland, United States
[2]University of Maryland, Baltimore, Maryland, United States
[3]INSIGHTEC, Dallas, Texas, United States

Background: The FDA approval of MR-guided focused ultrasound (MRgFUS) using the ExAblate 4000 system (INSIGHTEC, Haifa, Israel) to ablate the ventral intermediate nucleus to treat essential tremors has opened the door for other treatments that attempt at ablating targets that are away from the center of focus for the system including Parkinson's disease where Globus Pallidus interna (GPi) is targeted. Of specific interest when intervening with such off-center targets is to be able to arrive at a thermal threshold that reliably predicts the lesion size. Using the data from patients that participated in the PD002 feasibility study for medically-refractory dyskinesia symptoms of advanced idiopathic Parkinson's Disease where unilateral lesioning was performed, we assessed the temperature that best predicted the 24-hour lesion as seen on T2-weighted MRI.

Methods: Data from 13 subjects that participated in the treatment of Parkinson's disease was retrospectively analyzed. Whole brain T2-weighted MR images were obtained one day (all 13 patients) and 30 days (9 patients) after the treatment to visualize the thermal lesion size. Unlike essential tremor[1] where the VIM is centrally located with respect to the ExAblate transducer, the GPi is slightly off-center and hence the shape of the lesion is elongated and more ellipsoid in shape. MR thermometry images were used and the maps were thresholded at various temperatures (52°C, 50°C, 48°C, 46°C, 44°C) indicating that the area with the GPi (focal spot) that survived a given threshold received a minimum temperature determined by that threshold. To make a comparison between thermal thresholding areas and thermal lesions at 24 hours, two vectors (x and y) were used for area determination of the lesion and also to assess the shape and the direction on the 24h T2-weighted image (Fig. 1), with θ being the angle between x-axis and horizontal line in the images. Similar vectors (x2, y2) were also created based on the thermal maps on the day of the procedure at the same location. As the targeted location of FUS will usually be moved (typically 2~3 times) during the treatment as shown in Fig. 1 for improving the treatment response, we considered that the movement on RL, AP and SI directions would have an effect on the thermal threshold acheived. The function used to compare termal threshoulding areas and lesion areas is also shown in Fig. 1 based on the average of 5 sonications with the highest temperature rises. The temperature at which there was maximum concordance with the area determined by the temperature map and those determined by the 24 hour lesion volume was determined from all the 13 cases.

Results: An example of thermal thresholding areas at different temperature and the corresponding thermal lesion is shown in Fig. 2 along with the temperature rise at the spot, in which the red line indicates the peak temperature and the green line is the average temperature of the surrounding pixels. These thermal areas at different temperatures were compared with the thermal lesion of 1-day T2-weighted MR images (Fig. 3). Based on an average of the differences on 13 patients, 48°C was the minimum threshold that provides the best estimation for final lesions determined from 24h T2-weighted lesions. The 48°C threshold model had the lowest bias of all thresholds studied.

Conclusions: In this retrospective review of 13 PD patients, sonication at a minimum temperature of 48°C sonication appeared to best predict the 24 hour T2-weighted lesion. In contrast, previous reports for ET reported a minimum temperature of 51°C to create a lesion. The low temperature threshold for PD lesions may be due to reduced acoustic transmission efficiency when targeting GPi, which is more off-center, compared to essential tremor cases.

Reference

1. A. Bond and W. Elias. Predicting lesion size during focused ultrasound thalamotomy: a review of 63 lesions over 3 clinical trials. *Neurosurgical Focus*. 2018;44(2).

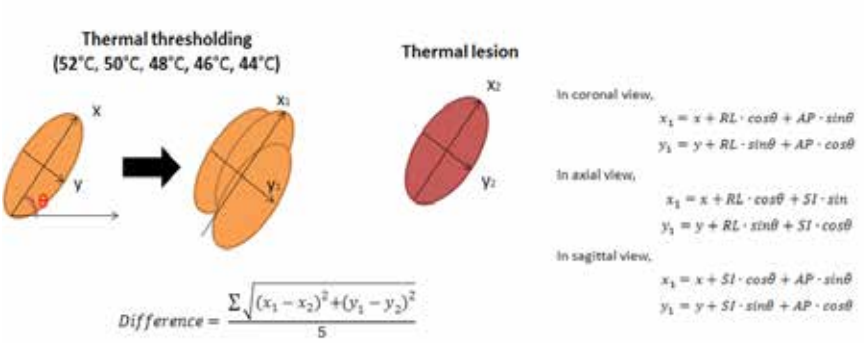

Figure 1. Thermal thresholding areas from MR thermometer and thermal lesion of post-treatment T2-weighted images. The differences between thermal thresholding areas and thermal lesion were calculated based on the five highest-temperature sonications.

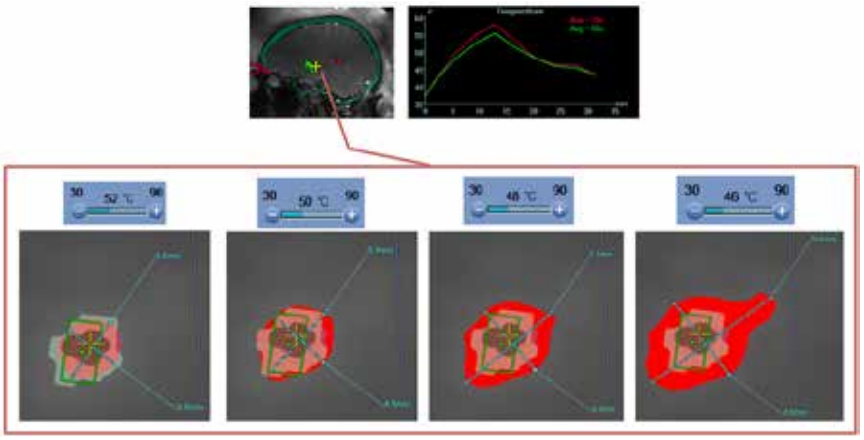

Figure 2. Thermal areas with different thresholds acquired from MR thermometry during PD treatment.

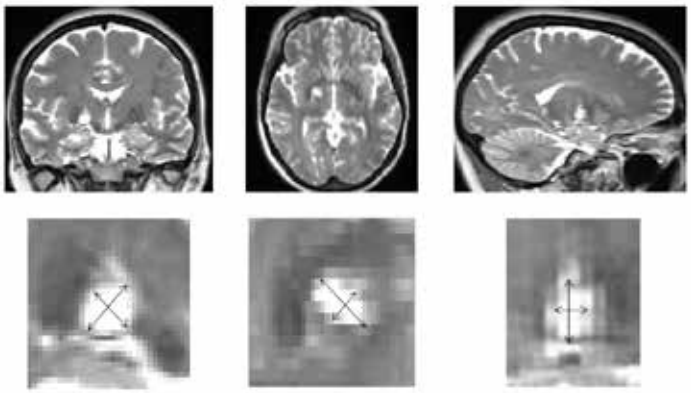

Figure 3. Visible thermal lesion from 1-day post-treatment T2-weighted MR images.

BR-12

Monday

22 October 2018

Topic: Movement Disorders

Presentation Type: Oral

Cortico-spinal tract visualization with double inversion recovery sequences in magnetic resonance guided focused ultrasound (MRgFUS) ventral intermediate nucleus thermal ablation: A preliminary study

Giuseppe Kenneth Ricciardi[1], Elisa Ciceri[1], Roberto Israel Foroni[2], Stefano Tamburin[2], Michele Longhi[1], Tommaso Bovi[1], Antonio Nicolato[1], Carlo Cavedon[1], Michele Tinazzi[2], Stefania Montemezzi[1]

[1]University Hospital of Verona, Verona, Italy
[2]University of Verona, Verona, Italy

Background: The ventral intermediate nucleus (VIM) is the preferential target for transcranial MRgFUS treatment of essential tremor (ET). Post-treatment limb weakness has been reported among possible reversible side effects of this treatment between 4 and 6% of cases. This may be due to unexpected mass effect on cortico-spinal tract (CST) axons. The CST has been reported to be located in the posterior limb of the internal capsule (PLIC); it is not readily visible on conventional structural magnetic resonance imaging (MRI). The precise position of the CST can be demonstrated by means of diffusion tensor imaging (DTI) tractography, but this technique is often limited in precision because of image distortion due to intrinsic artifacts of DTI sequences. We propose a volumetric (3D) Double Inversion Recovery (DIR) sequence, as a mean to directly visualize the CST on structural imaging, in order to rapidly assess its relationships with nearby structures in patients treated with VIM thermal ablation by MRgFUS.

Methods: 8 patients with ET underwent MRgFUS VIM thermal ablation. Pre-treatment imaging included 3D-DIR (TR 6002, TE 110, TI 2518 TI 300), together with other conventional structural sequences and DTI. 3D-DIR sequence was also acquired in all patients within 6 to 10 hours and one month after treatment. We evaluated the ability of DIR sequence to depict the lateral border of the thalamus, to isolate the CST within the PLIC and from adjacent thalamus and to distinguish CST from post-ablation VIM hyperintensity.

Results: 3D-DIR acquired before treatment depicted in all patients most of the internal capsule (IC) as an hypointense band, while the surrounding basal ganglia appeared from slightly to highly hyperintense. Concerning the thalamus, it appeared always hyperintense to the IC, although degree of hyperintensity varied among patients and was higher in the medial nuclei compared to the lateral ones.

After FUS treatment the location of the CST was clearly visible and may be isolated both from the adjacent thalamus and from post-ablation thalamic hyperintensity in 6/8 patients. In 2/8 patients, the day after treatment, edema surrounding the ablated tissue masked the CST. These two patients developed contralateral limb weakness on the 4th and 6th post-op day, respectively.

Conclusions: In our series, when compared to other structural imaging techniques, 3D-DIR improved visualization of the CST in ET patients treated by MRgFUS VIM thermal ablation. The location of CST was clearly visible and isolated both from the adjacent thalamus and post-ablation thalamic hyperintensity in 6/8 patients. In 2/8 patients, who developed limb weakness within a week of FUS treatment, hyperintensity surrounding the ablation area masked the CST within the IC. This may be due to peculiar characteristics of CST axons compared to other motorneurons located in the IC. 3D-DIR sequence may help predicting development of limb weakness after MRgFUS VIM thermal ablation. Further experience is needed to properly correlate clinical and imaging findings in these patients.

BR-13

Monday

22 October 2018

Topic: Movement Disorders

Presentation Type: Oral

Intraoperative, diffusion-weighted, MR imaging immediately after transcranial FUS thalamotomy

Steven Allen[1], Xue Feng[1], W. Jeffrey Elias[1], Craig Meyer[3], Kim Butts Pauly[4]

[1]University of Virginia, Charlottesville, Virginia, United States
[2]University of Utah, Salt Lake City, Utah, United States
[3]Stanford University, Stanford, California, United States

Background: Essential tremor (ET) is a debilitating movement disorder affecting up to 10% of the population. Transcranial focused ultrasound (FUS) thalamotomy can reduce ET symptoms in many patient populations. This procedure uses clinical and magnetic resonance imaging (MRI) feedback to guide the lesioning process. However, feedback is limited by both technical difficulties that suppress image quality and delayed lesion maturation. For example, T2-contrast-generating edema takes tens of minutes to develop and cannot differentiate between coagulation and vasogenic edema.[1,2]

Previous work in a pig model suggests that diffusion-weighted MRI (dw) contrast forms minutes after sonication and differentiates between coagulation and edema[3]. Previous studies in humans indicate dw contrast formation,[3,4] but are limited by the use of a dedicated head coil—which requires removing the transducer and, consequently, delaying image acquisition to at least 30 minutes after treatment[2,3].

Methods: Here, we introduce a novel T2-w and dw-MRI sequence designed for immediate image acquisition with the transducer remaining in place. We report its use immediately after clinical FUS thalamotomy procedures. Magnetic and transmit field inhomogeneities remain primary impediments to quality MR imaging during FUS thalamotomy. Eddy current fields and an artificially large field-of-view induced by the coupling water bath remain secondary impediments. To mitigate these difficulties, we have developed a multi-shot, twice-refocused, adiabatic, dw-MRI pulse sequence that employs a retraced, spiral acquisition scheme. The adiabatic RF pulses partially mitigate the transmit field inhomogeneity effects; the multi-shot, retraced spiral acquisition mitigates the effects of patient motion, magnetic field inhomogeneities, and the large field of view; and the twice-refocused design mitigates eddy current field artifacts. T2-w images can be acquired by deactivating the diffusion-encoding gradients. This pulse sequence is shown in Figure 1.

ET patients underwent a standard FUS thalamotomy procedure[3]. After sonication, the water bath was drained but the transducer remained installed on the patient. The proposed sequence acquired dw and T2-w MR images using the scanner's body coil. Data were acquired for 2 minutes for the dw and T2-w versions of the sequence, respectively. After acquisition, magnetic field inhomogeneities were corrected using a semi-automatic method.[4]

Results: Example T2-w and dw images are shown in Figure 2 with the thalamotomy lesion demarcated by an arrow. Contrast-to-noise ratios of the lesion are also provided. The lesion is hyper-intense in both the T2-w and dw images, consistent with previous observations using a head coil[2].

Figure 1. A multi-shot, twice-refocused, adiabatic, dw-MRI pulse sequence that employs a retraced, spiral acquisition scheme. This sequence produces intraoperative dw and T2-w MR images during FUS thalamotomy.

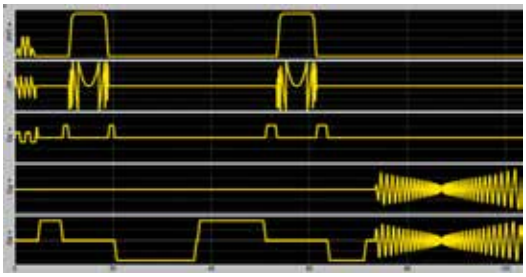

Conclusions: We found immediate dw-MRI to be feasible for FUS thalamotomy procedures using the proposed sequence. The resulting images are both sensitive to thalamic lesioning and robust against technical challenges such as field inhomogeneity, patient motion, and eddy current fields. Future work includes imaging with the water bath in place.

Acknowledgements: This work is funded by a contract with the Focused Ultrasound Foundation

References

1. Vykhodtseva et al. *Ultrasound Med. Biol.* 2000;26(5).
2. Plata et al. *ISTU*. 2016;16:O42
3. Wintermark et al, *AJNR*.. 2014;35(5).
4. Elias et al, *N. Engl. J. Med.* 2016;375(8).
5. Allen et al. *Proc. Intl. Soc. Mag. Reson. Med.* 2018;26:2680

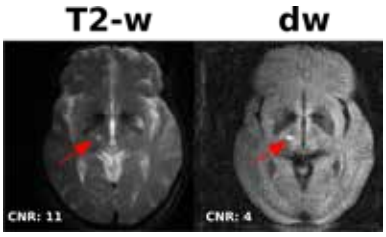

Figure 2. T2-w and dw images acquired in an ET patient using the proposed sequence. The arrows indicate the thermal lesion. Contrast-to-noise ratios are also provided. The lesion is hyper-intense in both the T2-w and dw images.

BR-14

Monday

22 October 2018

Topic: Movement Disorders

Presentation Type: Oral

Impact of skull density ratio on efficacy and safety of magnetic resonance guided focused ultrasound treatment of essential tremor

Pejman Ghanouni[1], Mor Dayan[2], Kim Butts Pauly[1]

[1]Stanford University, Stanford, California, United States
[2]INSIGHTEC, Dallas, Texas, United States

Background: Selection of patients with essential tremor (ET) for treatment with magnetic resonance guided focused ultrasound (MRgFUS) is based in part on patient skull density ratio (SDR). SDR reflects the heterogeneity of the bone and is calculated from the minimum to maximum attenuation on computed tomography (CT) of the skull. The SDR threshold for enrollment in clinical trials of MRgFUS in the US was SDR > 0.45 ± 0.05. We compared the efficacy and safety of MRgFUS treatment of 189 patients with essential tremor divided into groups based on SDR thresholds of 0.45 and 0.40.

Methods: Efficacy was based on improvement in Clinical Rating Scale for Tremor (CRST) scores at 1 year after MRgFUS. Safety was based on the rate of the most severe procedure or thalamotomy related adverse event reported for a patient, with severity of adverse events as previously defined.[1]

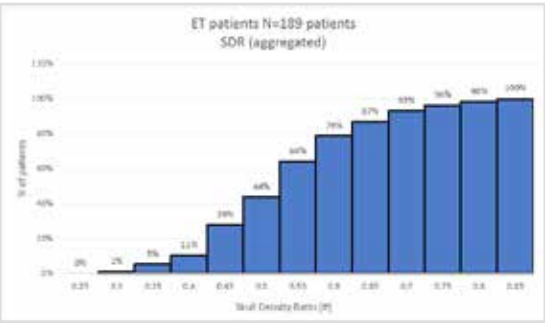

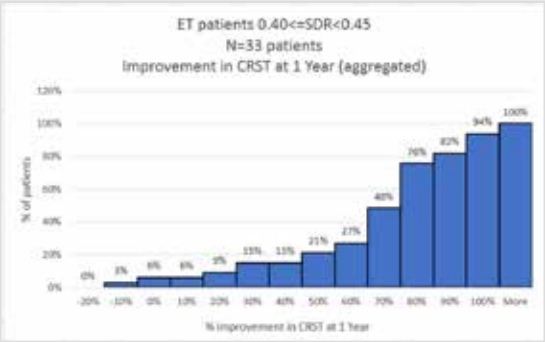

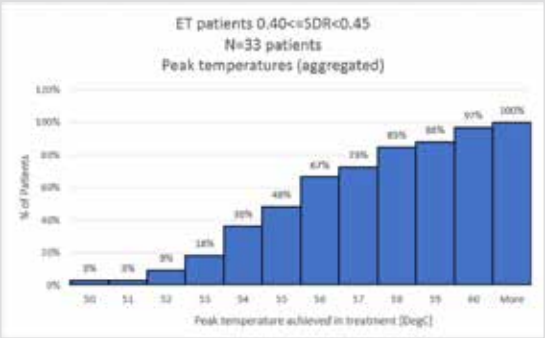

Results: Fifty-three (28%) of the patients had an SDR < 0.45 and 20 had an SDR < 0.40 (Figure 1). Of 33 patients with 0.40 ≤ SDR < 0.45, 26 (79%) had at least 50% improvement in CRST at 1 year (Figure 2) and 21 (64%) achieved peak average temperature at the focal spot of at least 54°C (Figure 3). Of 20 patients with SDR < 0.40, 50% had at least 50% improvement in CRST at 1 year. The rates of adverse events for patients based on SDR were: SDR< 0.4 (mild: 40%, moderate: 0%, severe: 0%), 0.40 ≤ SDR < 0.45 (mild: 39.4%, moderate: 12.1%, severe: 0%), and SDR ≥ 0.45 (mild: 60.3%, moderate: 14.7%, severe: 2.2%) (Table 1).

Conclusions: SDR is an indicator of the acoustic transparency of the skull to the ultrasound beam. In general, the lower the SDR, the higher the energies needed to reach ablative temperature, but the prediction is not perfect. Indeed, our analysis shows that treatment is frequently beneficial for some patients with skull density ratio (SDR) of less than 0.45; overall, 36 of 53 (68%) of these patients showed at least a 50% improvement in CRST at 1 year. Treatment of patients with SDR < 0.45 was performed without an increase in the rate of adverse events.

Reference

1. Fishman PS, Elias WJ, Ghanouni P, Gwinn R, Lipsman N, Schwartz M, et al. Neurological adverse event profile of magnetic resonance imaging-guided focused ultrasound thalamotomy for essential tremor. *Mov Disord.* 2018;33(5):843–847.

Figure 1. Skull density ratio distribution of 189 patients with essential tremor, showing cumulative percentage of patients as SDR increases. 28% of treated patients had SDR < 0.45, and 11% had SDR < 0.40.

Figure 2. Percentage of patients with 0.40 ⩽ SDR < 0.45 compared to percent improvement in tremor score at 1 year. As an example, only 21% of patients in this cohort had <50% improvement in CRST scores at 1 year.

Figure 3. Percentage of patients with 0.40 ⩽ SDR < 0.45 compared with peak average temperature achieved at the focal spot. Only 36% of treatments resulted in peak average temperatures < 54C.

By most Severe AE per patient (both procedure and thalamotomy related):

	% Patients with Mild AE	% Patients with Moderate AE	% Patients with Severe AE	Number of patients
SDR < 0.40	40.0%	0.0%	0.0%	20
0.40 <= SDR <0.45	39.4%	12.1%	0.0%	33
SDR >= 0.45	60.3%	14.7%	2.2%	136

Table 1. Rates of adverse events after MRgFUS for ET among patients grouped based on SDR ranges.

BR-15

Monday

22 October 2018

Topic: Movement Disorders

Presentation Type: Oral

MR Guided focused ultrasound ablation of globus pallidus interna using 3D FGATIR imaging fused with diffusion tensor MRI of the cortico-spinal tracts: Description of technique and initial experience

Dheeraj Gandhi[1], Jiachen Zhuo[2], Timothy Miller[2], Howard Eisenberg[2], Paul Fishman[3], Elias Melhem[2], Rao Gullapalli[2]

[1]University of Maryland School of Medicine, Baltimore, Maryland, United States
[2]University of Maryland, Baltimore, Maryland, United States
[3]VA Maryland Health Care System, Baltimore, Maryland, United States

Background: Successful focused ultrasound ablation of globus pallidus interna (GPi) requires accurately placed thermal lesions into the GPi motor territory. Standard imaging techniques such as T1W, T2W and FLAIR sequences neither reliably delineate the boundaries of globes pallidus nor the lamina between globes pallidus externa (GPe) and GPi. Use of these sequences therefore necessitates use of indirect, consensus based coordinates for the ablation procedure. We describe a novel technique that uses FGATIR (Fast gray matter acquisition T1 Weighted inversion recovery) sequence fused with the diffusion tensor imaging of the cortico-spinal tract. This technique allows direct, image based targeting of the motor GPi during FUS treatment.

Methods: A total of thirteen patients met inclusion criteria and were recruited from our institution in a prospective, multi center MRgFUS ablation feasibility study (PD002) for medically-refractory dyskinesia symptoms of advanced PD. All patients underwent comprehensive clinical assessment as well as MRI of the brain inclusive of 3D FGATIR and DTI. Deterministic Fiber Tracking was carried out on a Siemens Leonardo workstation (Siemens Medical Solutions) using Neuro3D task card (Siemens Medical Solutions). We began fiber tracking with a VOI (volume of interest) defining the cerebral peduncle and hand knob of the pre-central gyrus ipsilateral to the target GPi on high-resolution 3D FGATIR MRI. 3D FGATIR sequence was co-registered and fused with tractography images of the pyramidal tract and imported into INSIGHTEC MRgFUS workstation. These images were independently reviewed by two experienced neuroradiologists and differences resolved with consensus. Fused images were utilized for direct targeting of GPi with FUS while choosing the target location in GPi that was minimum of 2 mm away from the pyramidal tract and optic radiation. Intra-operative as well as post-treatment imaging at day 1 and day 30 were reviewed.

Results: All patients underwent successful treatment of GPi and demonstrated significant improvement of their clinical symptoms. FGATIR imaging reliably demonstrated the boundaries of the Globus pallidus as well as the lamina between GPe and GPi in all patients. Locations of the optic tracts and the coticospinal tracts could be confidently inferred from the fused images and helped in guiding the ablation of GPi while avoiding lesion encroachment on to the optic and motor tracts. Post-operative MR imaging demonstrated ellipsoid high T2 signal lesions that are oriented obliquely (superomedial to inferolateral) in the coronal axis, surrounded by area of vasogenic edema that resolves on follow-up studies.

Conclusions: The use of FGATIR imaging allows direct targeting of GPi motor territory as it reliably demonstrates the boundaries of Globus pallidus and presents excellent spatial and contrast resolution. Superimposition of cortico-spinal tract on FGATIR images allows for excellent surgical planning so that the lesions do not encroach on the motor tract.

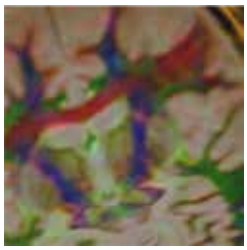

Figure 1. Oblique cross sectional image of FGATIR superimposed on fiber tractography reveals the relationship of GPi with pyramidal tract and optic tract.

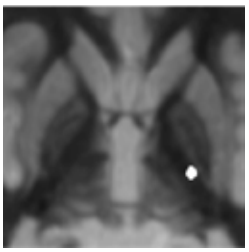

Figure 2. Axial high resolution FGATIR image of globes plallidus. Please note the pyramidal tract superimposed on this image. These images are directly imported into FUS workstation, assisting with surgical planning.

BR-16

Monday

22 October 2018

Topic: Psychiatric Disorders

Presentation Type: Oral

Bilateral thermal capsulotomy with focused ultrasound for treatment-refractory obsessive-compulsive disorder: 2-year follow-up

Jin Woo Chang

Yonsei University College of Medicine, Seoul, Republic of Korea

Background: We investigated the efficacy and safety of bilateral thermal lesioning of the anterior limb of internal capsule (ALIC) using magnetic resonance-guided focused ultrasound (MRgFUS) in patients with treatment-refractory obsessive-compulsive disorder (OCD).

Methods: Eleven patients with treatment-refractory OCD were included. Clinical outcomes were evaluated using the Yale-Brown Obsessive-Compulsive Scale (Y-BOCS), Clinical Global Impression (CGI) including improvement (CGI-I) and severity (CGI-S), Hamilton Rating Scale for Depression (HAM-D), and Hamilton Rating Scale for Anxiety (HAM-A) at 1 week and 1, 3, 6, 12, and 24 months following MRgFUS. Neuropsychological functioning, Global Assessment of Functioning (GAF), and adverse events were also assessed.

Results: After MRgFUS, Y-BOCS scores significantly decreased across the 24-month follow-up period (mean Y-BOCS score, 34.4±2.3 *vs.* 21.3±6.2, $p<0.001$). HAM-D and HAM-A scores also significantly decreased (mean HAM-D score, 19.0±5.3 *vs.* 7.6±5.3, $p<0.001$; mean HAM-A score, 22.4±5.9 *vs.* 7.9±3.9, $p<0.001$). GAF score significantly improved (mean GAF score, 35.8±4.9 *vs.* 56.0±10.3, $p<0.001$). Memory Quotient significantly improved after MRgFUS. Wechsler Adult Intelligence Scale, Controlled Oral Word Association Test, Color-Word Stroop Test, and Digit Span Test scores were unchanged. Adverse events were mild and transient.

Conclusions: The results suggest that bilateral thermal lesioning of the ALIC using MRgFUS may improve obsessive-compulsive, depressive, and anxiety symptoms in treatment-refractory OCD patients without serious adverse events. However, since this is an open-label, single arm study, randomized controlled trials are needed to validate the results.

BR-18

Monday

22 October 2018

Topic: Psychiatric Disorders

Presentation Type: Oral

MR-guided focused ultrasound bilateral capsulotomy for refractory OCD and major depression

Karim Mithani, Anusha Baskaran, Nir Lipsman

Sunnybrook Research Institute, Toronto, Ontario, Canada

Obsessive-compulsive disorder (OCD) and Major Depressive Disorder (MDD) are amongst the most common, challenging, and debilitating psychiatric disorders. A large proportion of OCD and MDD patients remain symptomatic despite optimal medical and psychotherapeutic care, and may benefit from surgical treatment. Current neurosurgical approaches, however, require cranial access, with attendant risk of brain injury and infection. Two prospective, single-arm, non-randomized, Phase I, pilot trials of MR-guided Focused Ultrasound (MRgFUS) for non-invasively treating refractory OCD and MDD have been initiated with the goal of recruiting 10 patients with each diagnosis. MRgFUS will be used to create an ~5mm lesion in the anterior limbs of the internal capsule bilaterally. Treatments are administered by a neurosurgeon, and supported by anesthesiologists, engineers, and psychiatrists. Patients are being followed-up at 1 month, 3 months, 6 months, and 12 months post-operatively. These visits involve evaluation of general health, psychiatric symptoms, neuropsychological effects, and device-/procedure-related adverse events. Various PET and MR imaging are also being performed, including diffusion tensor imaging and functional magnetic resonance imaging. Adverse events are being recorded and categorized by severity, and efficacy is being evaluated using various psychiatric scales such as the Yale-Brown Obsessive Compulsive Scale (YBOCS) and the Hamilton Depression Scale (HAM-D). Preliminary safety and clinical results, as well as neuroimaging correlates of psychosurgical treatment, including an approach to personalized tractography-based targeting in MRgFUS capsulotomy (e.g. Figure 1, Figure 2), will be presented. As this is a pilot, phase I study, there is no statistical endpoint and primary outcomes are assessments of safety and efficacy. These are ongoing clinical trials (ClinicalTrials.gov: OCD #NCT03156335, MDD: # NCT03421574), and results will be updated as the study progresses.

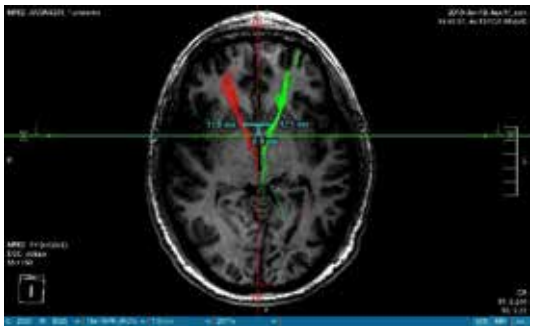

Figure 1. Anterior limbs of the internal capsule, identified with diffusion tensor imaging tractography (axial view)

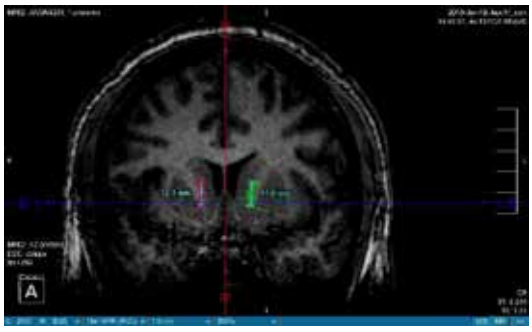

Figure 2. Anterior limbs of the internal capsule, identified with diffusion tensor imaging tractography (coronal view)

BR-19

Monday

22 October 2018

Topic: Neurodegenerative Disorders

Presentation Type: Oral

Blood-brain barrier opening in Alzheimer's disease: Safety data from a phase I trial

Nir Lipsman[1], Ying Meng[2]

[1]Sunnybrook Research Institute, Toronto, Ontario, Canada
[2]Sunnybrook Health Sciences Centre, Toronto, Ontario, Canada

Blood-brain barrier opening in Alzheimer's disease using MR-guided focused ultrasound

Background: MR-guided focused ultrasound (MRgFUS) in combination with intravenously injected microbubbles (MB) has been shown to transiently open the blood-brain barrier (BBB), and reduce beta-amyloid and tau pathology in animal models of Alzheimer's disease (AD). Here, we investigated the safety and feasibility of MRgFUS to open the BBB within the right prefrontal cortex, on two occasions, in six patients with mild-to-moderate AD.

Methods: We enrolled patients diagnosed with Alzheimer's disease with Mini-Mental Status Exam score between 18 and 28 and [18F]-florbetaben PET positivity in the right frontal lobe, area of target. Patients underwent two BBB opening procedures using the ExAblate 220 KHz system (INSIGHTEC, Haifa, Israel), one month apart, and followed for a total of three months. Primary outcome measures were safety, in the number of adverse events, and feasibility by the leakage of gadolinium contrast on MRI due to increased BBB permeability. Secondary outcome measures were change in [18F]-florbetaben tracer uptake in the region of interest, and change in neuropsychological tests (e.g. ADAS-cog). Exploratory measures included changes in resting state connectivity following BBB opening.

Results: In all patients, the blood-brain barrier within the target volume was safely and repeatedly opened, with closure observed on follow-up MRI within 24 hours. Opening the blood-brain barrier did not result in serious clinical or radiographic adverse events. The average maximum sonication power was 4.6W with an average of 3.6 sonications administered for stage 1 and 4.5W for 7.5 sonications for stage 2. Changes in group ADAS-cog scores at three months and baseline, as well as tracer uptake after stage 1 and 2 were not statistically different ($p > 0.05$).

Conclusions: The results of this safety and feasibility study support the continued investigation of focused ultrasound as a potential novel treatment and delivery strategy for patients with Alzheimer's disease.

BR-20

Monday

22 October 2018

Topic: Neurodegenerative Disorders

Presentation Type: Oral

Clearance of the Aβ and tau pathology of Alzheimer's disease using scanning ultrasound (SUS)

Gerhard Leinenga[1], Rucha Pandit[2], Rebecca Nisbet[2], Juergen Goetz[1]

[1]The University of Queensland, Brisbane, Queensland, Australia
[2]University of Queensland, Queensland Brain Institute, Brisbane, Queensland, Australia

Background: Alzheimer's disease is characterized by amyloid-β deposition leading to extracellular plaques and tau deposition leading to intraneuronal tangles (Polanco et al., Nature Reviews Neurology 2018). Treatment strategies for neurodegenerative diseases such as Alzheimer's disease are hampered by the fact that the blood-brain barrier (BBB) establishes an efficient barrier for therapeutic agents (Leinenga et al., Nature Reviews Neurology 2016). We have previously shown that scanning ultrasound (SUS) allows microglia-mediated clearance of extracellularly deposited amyloid-β in APP mutant APP23 mice and restores memory functions in three cognitive tests to wild-type levels, in the absence of overt damage to the brain (Leinenga and Götz, Science Translational Medicine 2015). We also determined that ultrasound augments the therapeutic effects of an antibody fragment directed against a specific form of Tau (2N Tau), using Tau mutant pR5 mice (Nisbet et al, Brain 2017). Because different from amyloid, tau deposits intracellularly, ultrasound-mediated clearance of tau is unlikely mediated by microglia. Extending the clearance studies of tau and amyloid, we firstly aimed to determine the efficacy of SUS in aged APP23 mice that are characterized by a pronounced cerebral amyloid angiopathy, and secondly to understand how Tau clearance is facilitated by SUS.

Methods: We firstly treated 2 years-old APP23 mice four times weekly with SUS and analyzed them histologically. Bleeds were assessed by staining with hematoxylin & eosin and Perl's Prussian Blue. Plaque load was assessed with methoxy-XO4. Microglial analysis was done by staining for Iba1. To determine whether microglia are attracted to amyloid plaques following SUS treatment, we performed co-staining followed by a Deming best fit regression analysis - We secondly treated Tau mutant K3 mice that are characterized by a pronounced motor phenotype characteristic of a subset of frontotemporal dementia (Ittner et al., PNAS 2008). The mice were treated 15 times weekly with SUS starting at 5 weeks of age (onset of motor phenotype), followed by a comprehensive analysis using histology, immunoblotting and memory and motor tests (Rotarod and grip strength).

Results: We firstly found that SUS in aged mice that had been exposed to four SUS sessions spread out over 8 weeks and analyzed 4 weeks later did not show evidence of increased CAA or microbleeds. Furthermore, amyloid was reduced by 58% as assessed by methoxy-XO4 fluorescence, and the proportion of large plaques was reduced. In addition, plaque-associated microglia were more numerous in SUS-treated mice. We found that there was a significant correlation between plaque area and the number of microglia in close proximity to plaques for both sham [$F(1, 80) = 113.9$, $p < 0.0001$] and SUS [$F(1, 95) = 92.94$, $p < 0.0001$] groups.

In the K3 mice we found a SUS-mediated reduction in tau phosphorylation by immunohistochemistry and western blotting. Motor and memory functions were improved. We will further present data of the underlying tau clearance mechanism.

Conclusions: Together this adds to the notion that SUS may be a treatment modality for human neurodegenerative diseases.

BR-21

Monday

22 October 2018

Topic: Neurodegenerative Disorders

Presentation Type: Oral

Ultrasound-mediated blood-brain barrier disruption improves anti-pyroglutamate antibody efficacy in aged Alzheimer's disease-like mice

Qiaoqiao Shi[1], Tao Sun[1], Yongzhi Zhang[2], Chanikarn Power[2], Jens-Ulrich Rahfeld[3], Torsten Hoffmann[3], Inge Lues[3], Stephan Schilling[3], Nathan McDannold[2], Cynthia A Lemere[1]

[1]Brigham and Women's Hospital; Harvard Medical School, Boston, Massachusetts, United States
[2]Brigham and Women's Hospital, Boston, Massachusetts, United States
[3]Probiodrug AG, Halle (Saale), Germany

Background: Pyroglutamate-3 amyloid-β (pGlu3 Aβ) is a pathological, highly neurotoxic form of amyloid-β which can be found in deposits and water-soluble aggregates of human AD brain. We present a nonpharmacological approach, focus ultrasound (FUS) with intravenous injection of microbubbles, for facilitating intravenous delivery of an anti-pGlu3 Aβ monoclonal antibody (mAb) through the blood-brain barrier (BBB), clearing Aβ and improving hippocampal function of aged APP/PS1 Alzheimer's Disease (AD)-like mice.

Methods: Sixteen month-old, male WT C57BL/6J and APPswe/PS1dE9 AD mice were divided into 6 groups: WT+PBS, WT+FUS, APP/PS1+PBS, APP/PS1+FUS, APP/PS1+Ab, APP/PS1+Ab+FUS). Intravenous infusion of 500 μg murine anti-pyroGlu3 Aβ IgG2a mAb (07/2a; kindly provided as a gift from Probiodrug AG, Halle, Germany) was administered immediately prior to FUS treatment. FUS was applied under anesthesia using an 837 kHz transducer (diameter 10 cm, focal length 8 cm) in conjunction with intravenous 100 μl/kg Optison microbubbles. Burst sonications (10ms at 2 Hz) were applied for 100 s at two locations in each hemisphere in the hippocampus. Animals received three weekly treatments. Behavior tests were conducted 1 week later followed by euthanasia. Brains were examined for amyloid burden, inflammation, and microhemmorhage.

Results: Combination treatment (Ab+FUS) showed a significant improvement, and Ab alone a strong trend, in learning in the Water T-Maze test after this short term treatment compared to PBS controls. FUS alone improved learning in WT mice and memory in AD mice in the contextual fear conditioning test compared to PBS controls. The combination treatment significantly lowered the Aβ42 and pGlu3-Aβ plaque load and increased synaptic markers in the hippocampus of AD mice compared to PBS control AD mice. Iba-1-positive, plaque-associated microglia/macrophages were observed in AD mice with Ab alone and Ab+FUS, while Ab+FUS also induced Ly6G+ monocyte/granulocyte/neutrophil infiltration and association with Aβ plaques. No changes in microhemorrhage were seen following FUS, Ab or the combination treatment.

Conclusions: Our findings suggest that FUS may be a useful tool for facilitating the efficacy of anti-Aβ mAb immunotherapy presumably by increasing delivery to the brain, resulting in better Aβ clearance, synaptic protection and hippocampal function. Interestingly, the combination treatment resulted in the presence of peripheral immune cells within plaques. Thus, this noninvasive method may have therapeutic potential when used in combination with mAbs for AD treatment.

BR-22

Monday

22 October 2018

Topic: Movement Disorders

Presentation Type: Oral

Focused-ultrasound mediated anti-alpha-synuclein antibody delivery for the treatment of Parkinson's disease

Hairong Zhang[1], Carlos Sierra[1], Nancy Kwon[1], Marilena Karakatsani[1], Mark Burgess[1], Vernice R. Jackson-Lewis[1], Serge Przedborski[1], Elisa Konofagou[2]

[1]Columbia University, New York, New York, United States
[2]Columbia University Medical Center, New York, New York, United States

Background: Parkinson's disease (PD) is associated with the selective death of dopaminergic (DA) neurons in the substantia nigra pars compacta (SNpc). While the specific cause of the neuronal loss remains elusive, the abnormal accumulation of alpha synuclein (α-syn), a major constituent of Lewy bodies, is considered to play a central role in the pathology of PD. Previous passive immunization studies remain ineffective due to the presence of the blood-brain barrier (BBB), which hinders most therapeutic agents to diffuse to the brain parenchyma. Focused ultrasound in conjunction with microbubbles (MB) is a technique to achieve noninvasive, transient, and localized BBB opening to enhance drug delivery to the brain. Therefore, the objective of this study is to explore the potential of FUS-mediated delivery of anti α-syn antibodies for the treatment of Parkinson's disease.

Methods: The study group consisted of ten A53T mice expressing the human α-syn which were divided into three groups: control, FUS-only, and FUS combined with anti-α-syn monoclonal antibodies (mAb). Mice were sonicated with FUS at the left hippocampus, left caudate putamen, and left substantia nigra at an acoustic pressure of 450 kPa, and the microbubbles were injected intravenously (with or without antibodies) through the tail vein immediately prior to sonication. To investigate neuroprotective effects of FUS/mAb, mice received three weekly treatments at 6-7 months of age before significant alpha synuclein aggregation and were euthanized one month after the last treatment for perfusion and immunohistochemical analysis.

Results: FUS mediated successful delivery of mAb by a 3-fold in a transgenic mouse model of Parkinson's disease (Figure 1), demonstrating its potential role in elevating to therapeutic dose.

Quantification using a minimum error thresholding technique demonstrated reduced α-syn load in mice treated with both FUS and antibody compared to the control mice ($p<0.01$ by one-way ANOVA and multiple comparison test), without a significant change in neuronal cell counts ($p>0.5$ by one-way ANOVA, Figure 2).

Microglia were found not to be activated neither as a result of the pathology at the age of the mice studied nor as a result of the FUS. The FUS treatment was found to be safe as assessed by both MRI and TUNEL staining.

Conclusions: Repeated FUS in conjunction with MB can successfully deliver anti-α-syn mAb and achieve neuroprotective effects such as reducing α-syn in transgenic mouse models of PD. The results demonstrated the potential role of FUS-mediated drug delivery for the treatment of neurodegenerative diseases such as the Parkinson's disease. Ongoing work aims at using more clinically-relevant MB dosages as well as a larger study group for the assessment of therapeutic role of FUS/mAb treatment.

Figure 1. Fluorescence intensity quantification for antibody delivery. There is a ~3 fold increase in fluorescence in FUS-treated side with 100 μg mAb.

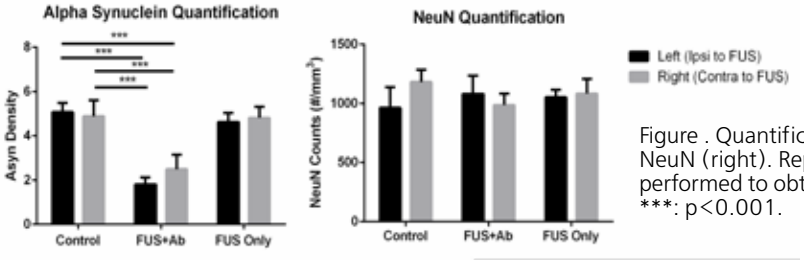

Figure . Quantification of αsyn (left) and NeuN (right). Repeated ANOVA was performed to obtain statistical significance. ***: $p<0.001$.

BR-23

Monday

22 October 2018

Topic: Neurodegenerative Disorders

Presentation Type: Oral

Intranasal GDNF pDNA nanoparticles combined with focused ultrasound increases transgene expression and alters cellular transfection

Amirah Aly[1], Zejun Li[2], Margee Kyada[2], Tao Sun[3], Yongzhi Zhang[4], Ozge Sesenoglu-Laird[5], Linas Padegimas[6], Mark Cooper[5], Nathan McDannold[4], Qingxi Ma[2], Barbara Waszczak[7]

[1]University of British Columbia, Vancouver, British Columbia, Canada
[2]Northeastern University, Boston, Massachusetts, United States
[3]Brigham and Women's Hospital; Harvard Medical School, Boston, Massachusetts, United States
[4]Brigham and Women's Hospital, Boston, Massachusetts, United States
[5]Copernicus Therapeutics, Cleveland, Ohio, United States
[6]Abeona Therapeutics, Inc., Cleveland, Ohio, United States
[7]Northeastern University, Boston, Massachusetts, United States

Background: Glial cell line-derived neurotrophic factor (GDNF) is a promising disease-modifying approach for treatment of Parkinson's disease due to its ability to protect and promote the survival of dopaminergic neurons in the brain. However, its therapeutic potential has been limited by its inability to cross the blood-brain barrier (BBB). We previously demonstrated that intranasal administration of PEGylated lysine 30-mer (CK30PEG10K) plasmid DNA nanoparticles (NPs) encoding hGDNF overcomes the BBB and generates a continuous source of GDNF expression in the rat brain for at least 6 months. We also showed, using ELISA and double-label immunohistochemistry (DL-IHC), that transgene expression is widespread in the rat brain, and the transfected cells are consistently located abluminal to the vascular endothelium and resemble pericytes morphologically. Despite its advantages, intranasal administration is a low efficiency route and results in brain-wide distribution with no means of targeting specific regions. Here we investigated whether focused ultrasound (FUS) combined with circulating microbubbles could enhance intranasal delivery of pGDNF NPs to specific brain areas, promote tissue penetration, and alter cellular transfection patterns.

Methods: We used a reporter plasmid (pUGG), which produces an eGFP-GDNF fusion protein. All rats received 90 μg of pUGG NPs intranasally. FUS bursts (32 msec bursts at 4 Hz for 100 sec) at 274 kHz were applied to the right forebrain and midbrain before and after intranasal delivery, respectively, during the infusion of Optison microbubbles. Rats were sacrificed 1 week later and eGFP expression was assessed throughout the brain by eGFP-ELISA, and by IHC to examine regional and cellular transfection patterns. To identify the cell type(s) transfected, DL-IHC was carried out for eGFP and a second cellular maker, i.e., NeuN for neurons, GFAP for astrocytes, RECA-1 for endothelial cells, and Iba1 for microglia.

Results: FUS with circulating microbubbles significantly increased eGFP expression in the sonicated hemisphere compared to non-sonicated side, confirming that FUS enhanced intranasal pGDNF NP delivery and transfection in the brain. IHC showed that the transfected cells in areas distant from sonication sites in both hemispheres were again typically perivascular, with eGFP-positive cells closely aligned along microvessels. However, at sonication sites, FUS caused transfection of cells that were not consistently perivascular in location, and were neither neurons nor astrocytes. At these apparent sonication sites, the eGFP-positive cells were deeper in the parenchyma in discrete clumps or clusters, and the majority expressed the microglial marker Iba1. Subtle changes Iba1 labeling were also observed away from sonication sites on the sonicated side. Specifically, the right forebrain and midbrain had a somewhat higher percentage of eGFP-positive cells that also co-expressed Iba1 than the non-sonicated left forebrain and midbrain, suggesting enhanced microglial recruitment and transfection on the sonicated *versus* non-sonicated side.

Conclusions: These results demonstrate that FUS with circulating microbubbles enhances transfection and transgene expression after intranasal administration of DNA NPs, and that the transfected cells at sonication sites are predominantly microglia.

Acknowlegements: Supported by the Focused Ultrasound Foundation

BR-24

Monday

22 October 2018

Topic: Neurodegenerative Disorders

Presentation Type: Oral

Amyloid beta plaque reduction with antibodies crossing the blood-brain barrier using focused ultrasound in a mice model

Christakis Damianou[1], Marinos Giannakou[2], Georgios Menikou[1], Nickolas Evripidou[1], Andreas Mylonas[1], Ioanna Kousiappa[3], Stella Angeli[3], Savvas Papacostas[3]

[1]Cyprus University of Technology, Limassol, Cyprus
[2]Cyrpus University of Cyprus, Limassol, Cyprus
[3]Cyprus Institute of Neurology and Genetics, Nicosia, Cyprus

Background: The main objective of the study was to remove Amyloid beta plaques using focused ultrasound (FUS) induced blood-brain barrier (BBB) opening using microbubbles with endogenous antibodies in a mice model.

Methods: The 5XFAD transgenic mice model was used. An MRI compatible positioning device was designed to navigate an MRI compatible transducer for sonicating a mouse placed in supine position. A spherically FUS transducer of 5 cm diameter; focusing at 10 cm and operating at 0.5 MHz was used.

Results: The effect of treatment using BBB opening using FUS showed some reduction of Amyloid plaques. The positioning device and transducer were evaluated extensively for their MRI compatibility and effectiveness.

Conclusions: This feasibility study demonstrated that by opening the BBB, it will be possible to allow endogeneous antibodies to enter the brain, thus eliminating Amyloid β plaques. A novel and simple positioning device was evaluated and was proven very effective in sonicating mice brain inside the MRI environment.

BR-25

Monday

22 October 2018

Topic: Neurodegenerative Disorders

Presentation Type: Oral

Transcranial and pulsed focused ultrasound that activates brain can accelerate remyelination in a mouse model of multiple sclerosis

Pierre Mourad

University of Washington, Seattle, Washington, United States

Multiple sclerosis (MS) impacts approximately 400,000 in the United States and is the leading cause of disability among young to middle aged people in the developed world. Characteristic of this disease, myelin within generally focal volumes of brain tissue wastes – either inexorably or through a cycle of demyelination and re-myelination – away under an autoimmune assault. This results in central and peripheral symptoms tied to the portion of brain within the MS lesion site. Gibson and colleagues (Gibson et al., 2014) noted that optical activation of transgenically tagged central neurons increased the thickness of the myelin sheath around those neurons. Since ultrasound, delivered transcranially, can also activate brain focally, we hypothesized that ultrasound stimulation of MS lesions in a mouse model that followed the temporal pattern of Gibson et al might either decelerate the demyelination phase of MS or accelerate the re-myelination phase. We first identified a range of pulsed and focused ultrasound (pFU) protocols capable of activating brain, including mice with developing MS lesions, as measured by subdermal EEG. We then tested three pFU protocols with minimal ultrasound intensity that produced consistent brain activation during each of the demyelinating and re-myelinating phases of this mouse model. We identified one ultrasound protocol that robustly accelerated re-myelination, as demonstrated with histological analysis. MRI can readily identify MS lesions: indeed, it is the clinical gold standard. MRI-guided focused ultrasound systems exist that can, in principle, deliver the ultrasound protocol we successfully tested here. Given the relatively low intensity values of our ultrasound protocol – close to FDA limits – we anticipate that future success with this approach to MS therapy on more realistic MS mouse models may one day translate to clinical trials that help address this devastating disease.

BR-27

Monday

22 October 2018

Topic: Blood-Brain Barrier Opening

Presentation Type: Oral

Enhanced microbubble contrast agent oscillation following 250 kHz insonation for blood-brain barrier opening in mice

Tali Ilovitsh[1], Asaf Ilovitsh[1], Josquin Foiret[1], Charles F. Caskey[2], Jiro Kusunose[2], Brett Z. Fite[1], Hua Zhang[1], Lisa M. Mahakian[3], Sarah Tam[3], Kim Butts Pauly[4], Shengping Qin[3], Kathy Ferrara[1]

[1]Stanford University, Palo Alto, California, United States
[2]Vanderbilt University, Nashville, Tennessee, United States
[3]University of California, Davis, Davis, California, United States
[4]Stanford University, Stanford, California, United States

Background: Microbubble contrast agents are widely used in ultrasound imaging and therapy, typically with transmission center frequencies in the MHz. Currently, an ultrasound center frequency near 250 kHz is proposed for therapeutic clinical human studies in which ultrasound combined with microbubble contrast agents is applied to open the blood-brain barrier. This work is focused on characterizing the microbubble oscillation at this frequency to determine a safe range of parameters for enhanced brain delivery, and implementing the results in blood-brain barrier opening through transcranial ultrasound in mice.

Methods: Theoretical predictions of microbubble oscillations were performed using the modified Rayleigh–Plesset equation and the Marmottant model. An ultra high-speed optical imaging setup, operating at 100 Mfps was used to record the oscillations of single microbubbles following a short ultrasound pulse with a center frequency of 250 kHz. The vibrational response for steady state excitation of microbubbles driven at 250 kHz was recorded using a passive cavitation detection system. Results are compared to those obtained using a higher center frequency of 1 MHz typically used in clinical ultrasound imaging and therapy. Lastly, the estimated safe range of parameters were implemented in *in vivo* transcranial ultrasound for blood-brain barrier opening in mice, where blood-brain barrier opening was observed through contrast enhancement using magnetic resonance imaging.

Results: As compared with the 1 MHz center frequency, microbubble expansion is enhanced for 250 kHz transmission, a frequency that is well below the resonance frequency of these contrast agents (Fig. 1). Following 250 kHz insonation, microbubble expansion increases nonlinearly with increasing ultrasonic pressure above the Blake threshold, and is accurately predicted by either the modified Rayleigh–Plesset equation for a clean bubble or the Marmottant model of a lipid-shelled bubble. The expansion ratio reaches 35-fold with 250 kHz at a peak negative pressure of 500 kPa, as compared to a predicted expansion ratio of 3.5 fold for 1 MHz transmission at a similar peak negative pressure (Fig. 2). Further, the range of peak negative pressure yielding stable cavitation is narrow for the 250 kHz transmission frequency (75-190 kPa for a microbubble with a radius of 0.75 μm) as compared to the higher frequency (245-500 kPa for the same microbubble radius). Blood-brain barrier opening observed through *in vivo* transcranial ultrasound in mice followed the same trend as the *in vitro* experiments. At a pressure of 75 kPa, no blood-brain barrier opening was observed. For pressures of 100 and 150 kPa, safe blood-brain barrier opening was observed; however, at pressures above 190 kPa (e.g. 190 and 250 kPa), inertial cavitation resulted in hemorrhage (Fig. 3).

Conclusions: Due to the high nonlinear expansion of microbubbles at a center frequency of 250 kHz, the development of safe and successful protocols for therapeutic delivery to the brain utilizing a similar center frequency requires consideration of the narrow pressure window between stable and inertial cavitation.

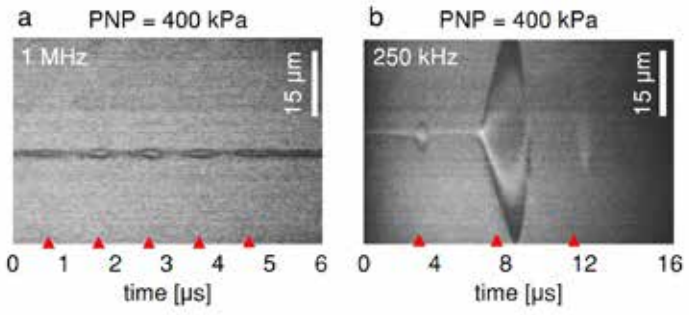

Figure 1. Ultra high-speed camera streak images of oscillating microbubbles for a peak negative pressure of 400 kPa at a center frequency of (a) 1 MHz. (b) 250 kHz.

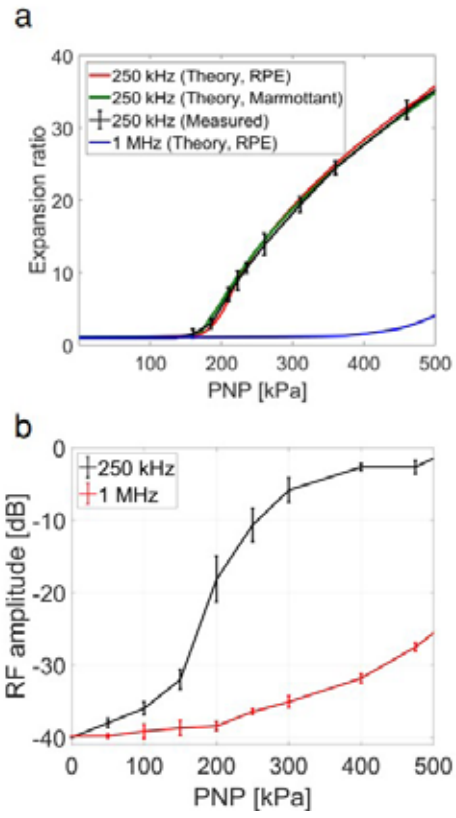

Figure 2. (a) Ultra high-speed camera experimental observations for microbubble's expansion ratio, as a function of peak negative pressure. (b) Passive cavitation detection of the second harmonic RF amplitude as a function of the peak negative pressure

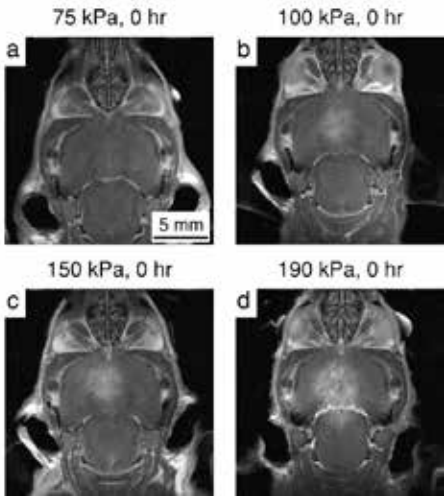

Figure 3. Coronal T1-weighted MR images, for mice treated with microbubbles and ultrasound using a peak negative pressure of: (a) 75 kPa. (b) 100 kPa (c) 150 kPa. (d)190 kPa.

BR-28

Monday

22 October 2018

Topic: Blood-Brain Barrier Opening

Presentation Type: Oral

Feasibility studies in mice and sheep to validate ultrasound-mediated blood-brain barrier opening for potential therapeutic interventions

Juergen Goetz[1], Mathew Pelekanos[2], Gerhard Leinenga[1], Mostafa Odabaee[2], Maryam Odabaee[2], Daniel Blackmore[2], Fabrice Turpin[2]

[1]The University of Queensland, Brisbane, Queensland, Australia
[2]University of Queensland, Queensland Brain Institute, Brisbane, Queensland, Australia

Background: Neurological disorders constitute a substantial social and economic burden. Treatment strategies for these diseases are hampered by the fact that the blood-brain barrier (BBB) establishes an efficient barrier for therapeutic agents (Leinenga et al., Nature Reviews Neurology 2016). We and others have shown that ultrasound (used by us in a scanning mode termed SUS for scanning ultrasound) together with retro orbitally injected microbubbles can be effectively used to transiently open the BBB and thereby remove toxic protein aggregates and ameliorate memory functions in mouse models of Alzheimer's disease (Leinenga et al., Science Translational Medicine 2015). As an underlying principle we identified the activation of microglia by unidentified blood-borne factors entering the brain. In order to develop SUS into a treatment modality for human patients it is important to establish the technology in larger animals (such as sheep) and to establish long-term safety.

Methods: In a stepwise manner, we used a total of 12 sheep to establish a sonication protocol using a spherically focused transducer. This was assisted by *ex vivo* simulations based on CT scans to establish suitable sonication parameters. BBB opening was assessed by Evans blue staining and a range of histological tests. - To assess long-term safety, we treated 12 month-old wild-type mice weekly over six weeks with SUS, followed by a multimodal analysis for up to 18 months of age.

Results: We demonstrate noninvasive microbubble-mediated BBB opening through the intact sheep skull. Our non-recovery protocol allowed for BBB opening at the base of the brain, but also in areas relevant for AD, including the cortex and hippocampus. Linear time-shift invariant analysis and finite element analysis simulations were used to optimize the position of the transducer and to predict the acoustic pressure and location of the focus. - In mice, we found that spatial memory and neuronal morphology was not adversely affected nor was long-term potentiation (LTP) as a cellular correlate of memory.

Conclusions: Our study firstly establishes sheep as a novel animal model for ultrasound-mediated BBB opening and highlights opportunities and challenges in using this model. Moreover, as sheep develop an AD-like pathology with aging, they represent a large animal model that could potentially complement the use of non-human primates (Pelekanos et al., Theranostics 2018). - Secondly, the multimodal analysis in mice indicates that therapeutic ultrasound is safe in the long-term, underscoring its validity as a potential treatment modality for diseases of the brain (Blackmore et al., submitted).

BR-29

Monday

22 October 2018

Topic: Blood-Brain Barrier Opening

Presentation Type: Oral

In vivo imaging of microbubble circulation in the human brain using intraoperative contrast-enhanced ultrasound (iCEUS) during neurosurgical procedures: Pictorial essay and implications for treatment

Francesco Prada[1], Frederic Padilla[2]

[1]Focused Ultrasound Foundation, Charlottesville, Virginia, United States
[2]LabTAU, Inserm, Lyon, France

Background: The correlation between MBs circulation and their interaction with focused ultrasound (FUS) in different brain areas has never been specifically investigated, nor the impact of FUS has been correlated with the microbubble distribution in the brain, according to time-intensity curves. Microbubble concentrations in fact changes in time with different vascular phases (arterial-parenchymal and venous) and showed different concentrations according to vessel density (gray/white matter - basal ganglia), probably also depending on their behaviour. The purpose of this pictorial essay is to briefly describe our intra-operative imaging technique, show the normal distribution of ultrasound contrast agent in different brain areas, demonstrate the appearence of a spectrum of different cerebral lesions and discuss the implications for focused ultrasound treatments.

Methods: We retrospectively evaluated data regarding a series of > 500 patients who underwent iCEUS imaging in an off-label setting while being operated on for different cerebral tumor and vascular lesions since 2010. We analyzed iCEUS imaging obtained after craniotomy, before dural opening, after intravenous injection of ultrasound contrast agent. A semiquantitative, offline interobserver analysis was performed to visualize each brain lesion and to characterize its perfusion features (timing - degree - patterns of enhancement). In specific cases a quantitative anlysis with dedicated software has been performed.

Results: In all case the lesion and the surrounding parenchyma were visible with iCEUS, permitting perfusion assessment.

- MBs highlighted different brain tissues without relying on its echogenicity but on its vascularization.
- The degree of contrast enhancement is a consequence of the MBs concentration in time and density of the capillaries (Fig. 1).
- Different lesions show different kinetic and morphologic patterns (Fig.2, 3).
- Different brain areas and structures show different MBs kinetics and morphologic patterns: large and small vessels > basal ganglia > sulci and gray matter > white matter (Fig. 4).
- MBs distribution changes according to way of administration (bolus *versus* infusion).

Conclusions: Brain perfusion characteristics, assessed with iCEUS, shed lights on previously unknown features regarding microbubble distribution in normal and pathological conditions and might have important consequences predicting therapeutic US behaviour. It is foreseeable that to achieve certain biological effects FUS parameters should be adjusted according to different organ areas/disease or else attention should be paid in order not to damage surrounding vital structures.

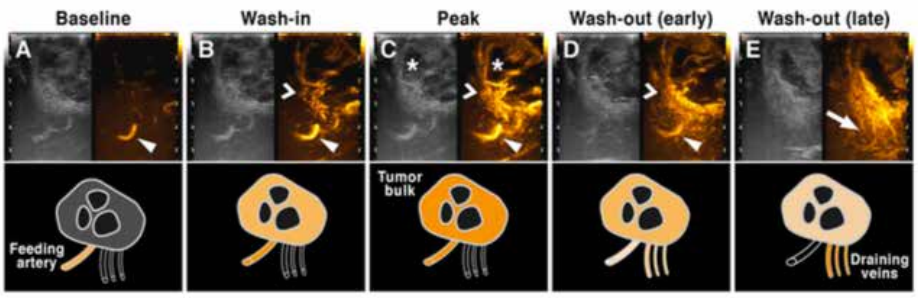

Figure 1. Time frame of how a glioblastoma (right parietal) is visualized by ultrasound (both B-mode and contrast-enhanced ultrasound; top row), along with a schematic representation of it (bottom row). Note how the microbubble contrast medium allows the neurosurgeon to visualize the feeding artery (full arrowhead; A), the arterial phase, and the tumor parenchyma (B and C; the empty arrowhead points at the secondary arteries, and the star shows the cystic/necrotic areas), followed by the venous phase and the draining veins (arrow) of the lesion (D and E).

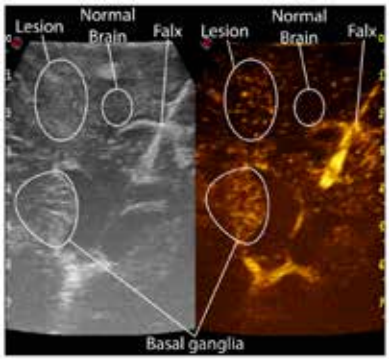

Figure 2. Normal brain parenchyma enhancement. Axial/frontal CEUS scan in a case of a right frontal low grade glioma. Normal parenchyma shows only slight contrast enhancement, while basal ganglia typically show higher degree of contrast enhancementand lower grade gliomas has tipically mild contrast enhancement.

Figure 3. Time frame of how different grades of glioma are visualized with CEUS. In the first column of each row low mechanical index US and baseline CEUS (CA arrival – *t*0) are displayed; then different CEUS phases (time is displayed in the top right corner of each image) are displayed only. The image clearly shows the differences in terms of timing, degree of enhancement, and CEUS patterns for different types of glioma, in a continuous and dynamic modality.

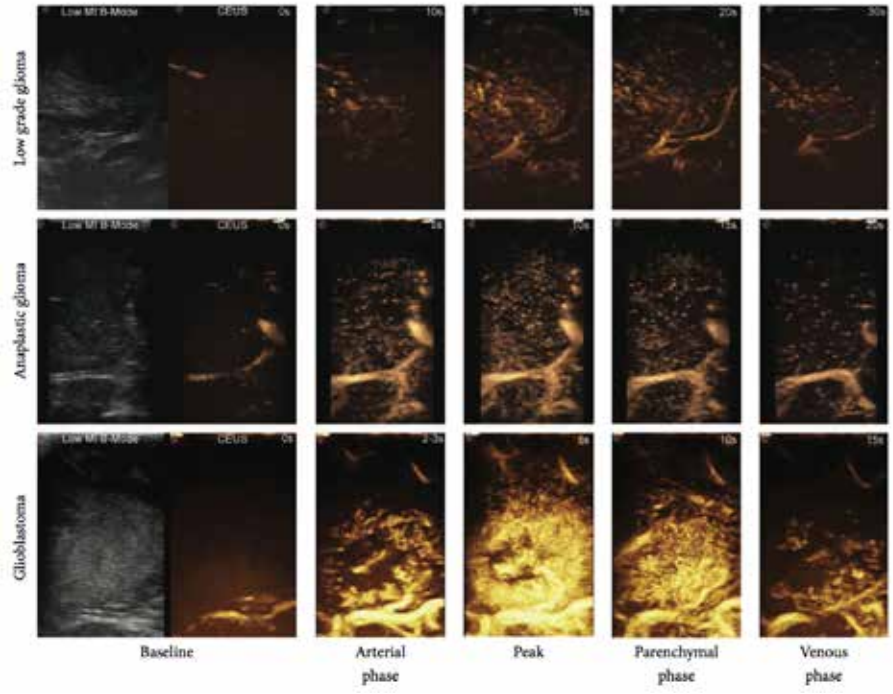

Figure 4. Quantitative analysis in a case of mesial temporal high grade glioma performed with proprietarty software (VueBox, Bracco, Milan, Italy). Two region of interest (ROI) have been placed on the tumor bulk and on the normal temporal parenchyma: the two derived time intensity curves show how MB dynamics differs in the two regions (green: neoplastic tissue - yellow: temporal parenchyma).

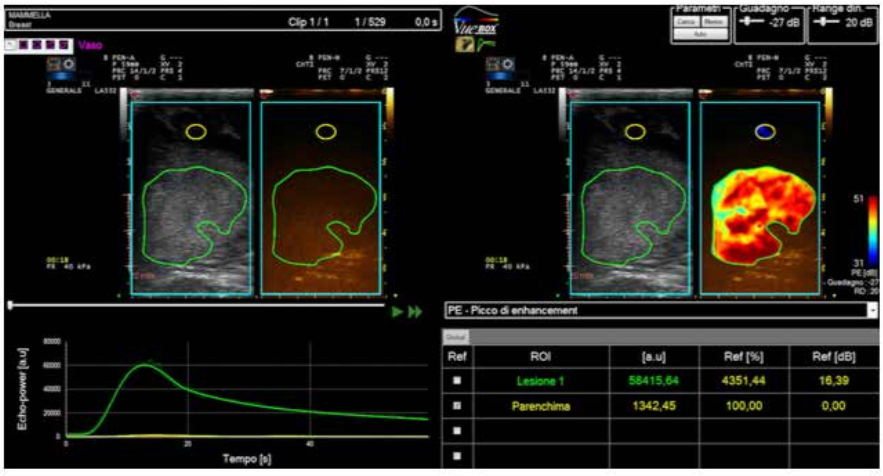

BR-30

Monday

22 October 2018

Topic: Blood-Brain Barrier Opening

Presentation Type: Oral

Influence of nanobubble concentration on blood-brain barrier opening using focused ultrasound under real-time acoustic feedback control

Bingbing Cheng, Chenchen Bing, Debra Szczepanski, Rajiv Chopra

UT Southwestern Medical Center, Dallas, Texas, United States

Background: Real-time acoustic feedback control based on harmonic emissions of stimulated microbubbles may be a way to achieve reliable blood-brain barrier (BBB) opening in the brain. Previously, we demonstrated BBB opening was possible using sub-micron bubbles and produced comparable results to commercialized microbubbles (Optison™, Definity®, etc). However, the harmonic emissions and acoustic control was more consistent using sub-micron bubbles. This study further evaluates BBB opening using a custom-made nanobubble (200-300 nm) under different conditions, including: nanobubble concentration, feedback control threshold, and/or treatment duration.

Methods: Nanobubbles were synthesized by dissolving lipids DBPC, DPPA, DPPE, and mPEG-DSPE in chloroform at a mass ratio of 6:1:2:1. Following solvent evaporation, the lipids were hydrated in a solution containing 50 µl of glycerol and 1 mL of phosphate buffered saline (PBS) containing Pluronic L10 (0.6 mg/mL) at 80°C for 30 minutes. Once hydrated, the air inside of the vial was replaced with octafluoropropane gas. The vial was then agitated using a Vialmix shaker (Bristol-Meyers Squibb Medical Imaging, N. Billerica, MA) for 45 s. A custom-built focused ultrasound transducer with f0 = 0.5MHz was attached to a stereotactic system to achieve spatially targeted transcranial exposures (Figure 1). A piezocomposite hydrophone (central frequency: 0.75MHz) was built to capture the acoustic signals emitted from stimulated nanobubbles. A feedback control algorithm was implemented in LabVIEW to quantify the area under curve (AUC) within ultra-harmonic bands (0.75±0.05MHz) during the ultrasound exposure and to adjust the focal pressure accordingly based on the difference between current AUC and a desired threshold. Initial *in vitro* tests were performed in which nanobubbles with different concentrations were infused into a single tube (0.15 ml/min, tubing I.D. = 1mm). *In vivo* studies were performed in a rat model to evaluate the acoustic emissions and BBB opening at different nanobubble concentrations. Evans blue dye was used as an indicator of BBB opening.

Results: Nanobubbles with an average diameter of 280 nm and a concentration of 1011 particles/mL were successfully synthesized (Figure 2). Both *in vitro* and *in vivo* AUC response from nanobubbles during focused ultrasound exposures increased with the pressure increase as expected. The data suggested nanobubbles have an *in vitro* persistence of ~10, 5, and 1 mins and *in vivo* circulation time of ~10, 5, and 6 mins at concentrations of 1:1, 1:10, and

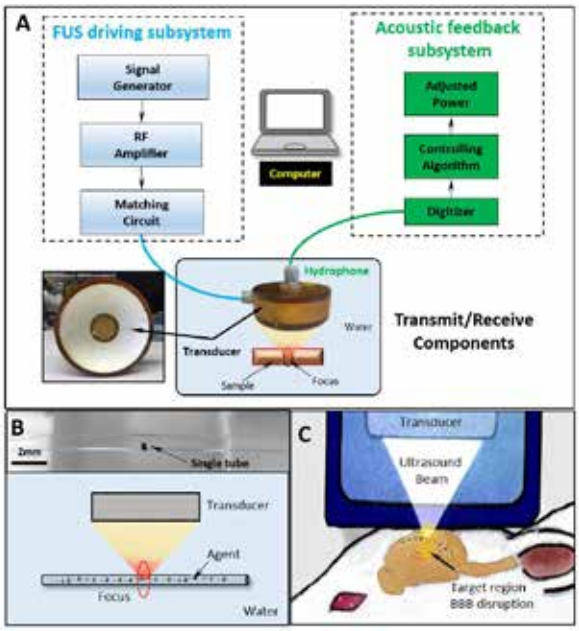

Figure 1. (left) Experimental setup. A: Components of the focused ultrasound system. B: *In vitro* tube phantom setup. C: *In vivo* FUS-induced BBB opening setup.

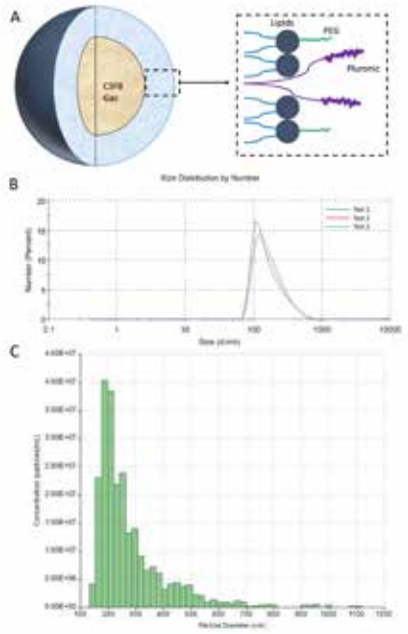

Figure 2. (right) Nanobubble structure and characterization. A: A schematic diagram of the synthesized nanobubbles. B and C: Representative size distribution and concentration measured by DLS and qNano platform.

1:100, respectively (Figure 3). Lastly, successful maintenance of the AUC at a target level was achieved *in vivo* with different bubble concentrations, and BBB opening was confirmed by the leakage of Evans Blue at the target locations (Figure 4).

Conclusions: A nano-sized bubble was synthesized and utilized for the BBB opening with focused ultrasound. Nanobubbles have long persistence and *in vivo* circulation time. Evans Blue dye leakage confirmed the reliable and successful BBB disruption with bubble concentrations at 1:1, 1:10, and 1:100 under real-time acoustic feedback control.

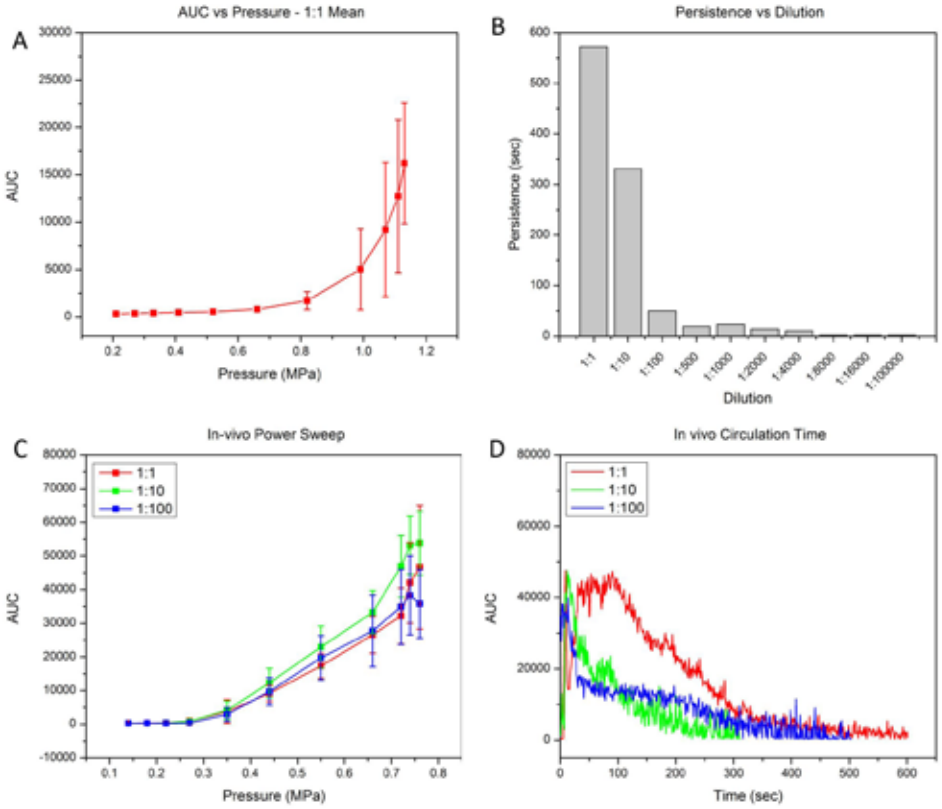

Figure 3. *In vitro* and *in vivo* characterization of acoustic emissions from stimulated nanobubbles

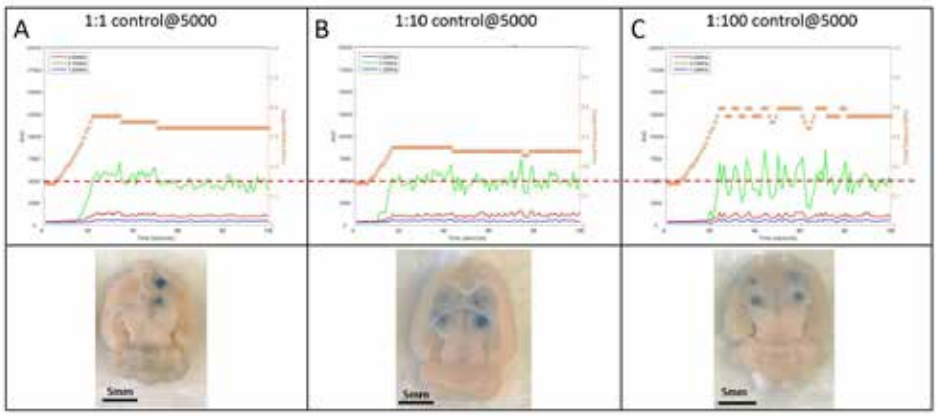

Figure 4. BBB opening under feedback control with nanobubbles in a rat model with three different concentrations A: 1:1, B: 1:10, and C: 1:100

BR-31

Monday

22 October 2018

Topic: Blood-Brain Barrier Opening

Presentation Type: Oral

NaviFUS: A neuronavigation-guided focused ultrasound device for clinical transcranial brain application

Hao-Li Liu[1], Arthur Lung[2], Cheng-Chia Lee[3], Kuo-Chen Wei[4]

[1]Chang Gung University, Taoyuan City, Taiwan
[2]NaviFus Corp, Taipei, Taiwan
[3]Taipei Veterans General Hospital, Taipei, Taiwan
[4]Chang Gung Memorial Hospital, Taoyuan City, Taiwan

Focused ultrasound is a promising intervention tools to transcranially deliver targeted energy into the brain noninvasively with the potential for clinical CNS indication application such as thermal tissue ablation, thermal thalamotomy, blood-brain barrier (BBB) opening, as well as neuromodulation. Current available approach relies on the use of MRI-compatible device, with MR-thermometry to guide the focused energy to hit the correct targeted position, with its accuracy reaching sub-millimeters. Although MRI provides pre-operational focal position identification, intra-operational treatment monitoring can only be applied for thermal ablation application. For BBB opening application, the CNS permeability can be confirmed through post-operational contrast-agent administration for outcome confirmation. In addition, for neuromodulation application, the evaluation of neuronal activity requires more interaction between physicians and patients, yet MR-guided platform is a closed system design which requires environment to be isolated, including personals and other evaluation equipment contact to patients. As an alternative, neuronavigation tool has long been employed and widely accepted for neurosurgical procedure. With its original intention for solid-tool guidance, it is feasible to be adapted to guide virtual focused ultrasound energy. In this presentation, we aim to introduce a neuronavigation-guided focused ultrasound system designed for clinical application. A multiple-channel focused ultrasound phased array system is available, with its focal steering beam can be guided via commercial neuronavigation system. In this presentation, we aim to share the concept of neuronavigation-guided focused ultrasound, including its preclinical validation, system design, performance, its recently clinical application status, as well as its future developments.

Figure 1. NaviFUS: A Neuronavigation-Guided Focused Ultrasound Device for Clinical Transcranial Brain Application

BR-32

Monday

22 October 2018

Topic: Blood-Brain Barrier Opening

Presentation Type: Oral

Transcranial imaging of acoustic cavitation with high temporal and spatial resolution in non-human primates

Mark Burgess[1], Maria Eleni Karakatsani[1], Iason Zacharias Apostolakis[1], Elisa Konofagou[2]

[1]Columbia University, New York, New York, United States
[2]Columbia University Medical Center, New York, New York, United States

Background: Detection of focused ultrasound (FUS)-stimulated microbubble activity (i.e. acoustic cavitation) is the fundamental strategy to guide and monitor promising FUS therapies that harness acoustic cavitation-mediated bioeffects, such as blood-brain barrier (BBB) opening. The magnitude, location, and persistence of acoustic cavitation over time are critical measurements for successful monitoring. Passive cavitation imaging with ultrasound arrays has emerged as the standard technique to quantify these parameters; however, current beamforming methods were developed for monitoring high-intensity focused ultrasound ablation and suffer from poor axial image resolution. The objective of this study was to implement passive cavitation imaging with broadband FUS pulses and beamforming techniques similar to B-mode ultrasound imaging to improve the axial image resolution. Additionally, clutter filtering techniques developed for ultrafast Doppler imaging were explored to improve image sensitivity.

Methods: Transcranial passive cavitation imaging was performed in non-human primates (NHP) with a 1.5D imaging array (M5Sc-D, bandwidth: 1.7 – 4.2 MHz, GE Medical Systems) located in the central opening of a 0.5 MHz FUS transducer (H204, Sonic Concepts) (Figure 1A). A bolus injection of Definity (Lantheus Medical Imaging) was intravenously injected at five times the clinical dose (50 μL/kg) during imaging. The hippocampal region of the NHP was targeted using a neuronavigation system (Brainsight, Rogue Research) (Figure 1B). Broadband FUS pulses were used along with synchronous transmit and receive sequences to perform delay and sum beamforming with absolute time delays. Image sets were acquired at ultrafast frame rates (>1000 frames per second) for calculation of mean intensity images, i.e. power cavitation images. Spatiotemporal clutter filtering based on singular value decomposition (SVD) was used to increase power cavitation image contrast over a range of FUS peak negative pressures (0.1 – 0.9 MPa).

Results: Delay and sum beamforming with absolute time delays significantly improved the axial resolution of passive cavitation imaging. The full width half max (FWHM) of an acoustic cavitation source at the focus was quantified *in vitro* to be approximately 2.4 mm by 0.44 mm in the lateral and axial dimensions, respectively. Clutter filtering improved the sensitivity of power cavitation images by removing slow moving tissue and skull reflections. The contrast-to-noise ratio for a region of interest in the focal area was increased by up to 40 dB (Figure 1C). Power cavitation images were registered with pre-acquired MRI images to identify the spatial distribution of acoustic cavitation in the underlying vasculature (Figure 1D). Acoustic cavitation was not only localized to the focal region, but also prefocally and along the muscle/skull/brain interface.

Conclusions: By combining the improved resolution of transcranial passive cavitation imaging with the processing techniques developed for ultrafast ultrasound imaging, acoustic cavitation can be detected with high temporal and spatial resolution in non-human primates. Future work will explore the use of this image-guided method for safe and controlled BBB opening.

Acknowlegements: This work was supported in part by National Institutes of Health (NIH) grants R01AG038961 and R01EB009041

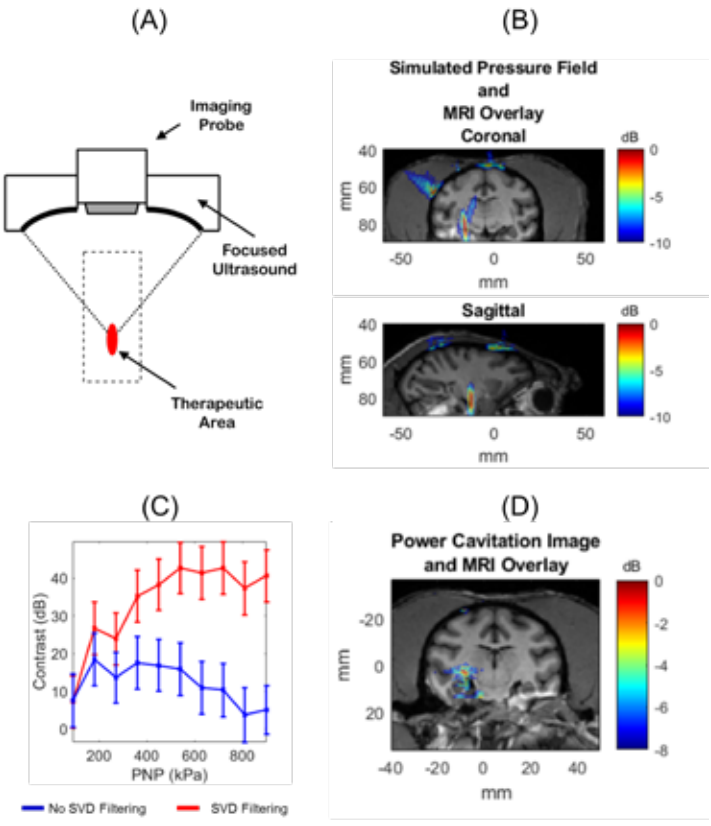

Figure 1. (A) Experimental setup. (B) Simulated pressure field and MRI overlay showing hippocampal targeting. (C) Impact of clutter filtering on image contrast. (D) Power cavitation image and pre-acquired MRI overlay.

BR-33

Monday

22 October 2018

Topic: Epilepsy
Presentation Type: Oral

A pilot open-label clinical trial evaluating focused ultrasound thalamotomy for the prevention of secondary generalization in focal onset epilepsy

Vibhor Krishna[1], Francesco Sammartino[1], Carson Reider[1], Angela Emerson[1], Matthew Eames[2], Jacquelyne Cios[1], William Bell[1], Cady Block[1], Jesse Mindel[1]

[1]The Ohio State University, Columbus, Ohio, United States
[2]Focused Ultrasound Foundation, Charlottesville, Virginia, United States

Background: Focused ultrasound ablation (FUSA) is an emerging treatment for neurological and psychiatric disorders. We describe the design of a pilot, open–label, prospective intervention clinical trial using FUSA of the anterior nucleus of the thalamus (AN) in patients with treatment-refractory epilepsy.

Methods: Ten (10) adults with treatment-refractory, focal-onset epilepsy will be enrolled. The AN will be identified using direct visualization and a formulaic method based on atlas coordinates. The patients will receive AN ablation using Exablate 4000 (INSIGHTEC, Inc.) mid-frequency (650k Hz) device. The outcomes will be assessed through clinical- and imaging-based follow-up after the intervention and compared with baseline measurements.

Results: This trial will assess the safety and feasibility of FUSA in patients with partial- or focal-onset epilepsy. Safety will be assessed by the absence of side effects, defined as new-onset neurological deficits or performance deterioration on neuropsychological testing. Feasibility is defined as the ability to create lesion within the AN. Secondary outcomes will include changes in seizure frequency and patient reported quality of life measures. Imaging analyses will be performed to study changes in functional connectivity, as well as in structural and microstructural brain anatomy.

Conclusions: This is the first known clinical trial to assess the safety and feasibility of FUSA of AN in patients with treatment-refractory partial-onset epilepsy.

BR-34

Monday

22 October 2018

Topic: Epilepsy
Presentation Type: Oral

Non-invasive neuronal lesions sparing non-targeted cellular structures

Yi Wang[1], Matthew Anzivino[1], Yanrong Zhang[2], Max Wintermark[2], James Woznak[1], Alexander Klibanov[1], Erik Dumont[3], Edward Bertram[1], Kevin Lee[1]

[1]University of Virginia, Charlottesville, Virginia, United States
[2]Stanford University, Stanford, California, United States
[3]Image Guided Therapy, Pessac, France

Resection or ablation of brain tissue can be quite effective for treating medically-intractable neurological disorders, such as drug resistant epilepsy. However, existing surgical procedures possess considerable limitations and potential complications. Resective surgery can be highly invasive, resulting in bleeding, infection, blood clots, strokes, seizures, swelling of the brain, and off-target damage. Moreover, functional deficits in memory, language comprehension, and visual processing can occur with the removal of large amounts of brain tissue. More recent advances using minimally-invasive and non-invasive procedures are promising, but also have potential risks. For instance, thermal ablation produced by Laser Interstitial Thermal Therapy or high-intensity focused ultrasound result in comprehensive tissue damage affecting vascular, ventricular, and axonal elements in the target area. Radiosurgery can be effective, but also appears to produce pan-necrosis in the target area, and requires a latency period of months to be effective. It therefore remains of critical importance to identify alternative interventions that lessen the complications of surgery, do not require the removal of large areas of the brain, minimize injury to functional circuitries and patent vasculature, but still provide effective outcomes.

Our studies take advantage of the ability of low-intensity, magnetic resonance-guided focused ultrasound, combined with intravenous microbubbles, to transiently disrupt the blood-brain barrier (BBB) in a targeted manner. The period of reversible BBB-opening is exploited to focally deliver to the brain parenchyma a neurotoxin that is otherwise BBB-impermeable, and is tolerated after systemic (i.e. intravenous or intraperitoneal) administration. This strategy, termed Precise, Intracerebral, Non-invasive Guided-surgery (PING), produces neuronal damage in the targeted area. Several brain regions have been targeted in the rodent brain (neocortex, hippocampus, thalamus, striatum, etc.), and each area exhibited degenerating neurons post-PING. However, it is notable that axons of passage, ventricular structures, and vasculature in the target area are apparently spared by PING.

PING thus possesses several significant strengths for the targeted disconnection of neural circuitry. It is non-invasive and can be precisely directed to an area of interest. It destroys neurons, while sparing non-targeted features or the parenchyma such as vascular and ventricular structures. This avoids secondary ischemia to neighboring tissues that share vascular supply with the target area. It also circumvents leakage that can occur after compromise to the ventricular-parenchymal barrier. PING spares axons of passage, the compromise of which can result in functional deficits. It allows conformal targeting, which is a key advantage when irregularly shaped structures, such as seizure-genic dysplasias, are involved. It allows the targeting of tissue that would be difficult or impossible to treat with invasive procedures. Finally, inasmuch as PING utilizes low-intensity focused ultrasound, it should have a broader treatment envelope than high-intensity focused ultrasound, allowing the targeting of a wider range of brain regions. PING could thus prove useful to disconnect dysfunctional brain circuitry in a precise, conformal, and non-invasive fashion, and may do so in a manner that limits collateral damage to cellular structures that are not the object of the intervention.

BR-35

Monday

22 October 2018

Topic: Neuropathic Pain
Presentation Type: Oral

A pilot study of focused ultrasound medial thalamotomy for the treatment of trigeminal neuropathic pain

Shayan Moosa, Robert Goldstein, Jeff Elias

University of Virginia, Charlottesville, Virginia, United States

Focused ultrasound has proven effective for deep brain lesioning through the intact skull, and MRI can be utilized for stereotactic targeting and continuous temperature monitoring. Recently, focused ultrasound was used to successfully perform ventrolateral thalamotomy to alleviate essential tremor – an event paving the way for the first FDA approval in brain.

Historically, medial thalamotomy, the termination of the primary pain pathway from the spinal cord, has suggested efficacy for the treatment of various pains. Neurosurgical interventions for pain have been plagued, however, by open label studies confounded by heterogenous pain conditions and imperfect outcome measures.

This pilot study will investigate the feasibility of focused ultrasound to safely perform a medial thalamotomy and the potential to relieve neuropathic pain. The neuropathic pain from chronic acquired peripheral neuropathy represents a homogenous condition that is disabling and notoriously refractory to medical treatment. This study is rigorously designed as a randomized, sham-controlled trial where the ten patients and their assessors are blinded to the treatment assignment. Validated pain scales and neuropathy-specific scales will be utilized by a multidisciplinary team of experts in the fields of focused ultrasound, pain, and peripheral neuropathy. Objective measures of treatment effect will be determined by functional brain imaging.

BR-36

Monday

22 October 2018

Topic: Neuropathic Pain
Presentation Type: Oral

Intense focused ultrasound (iFU) stimulation of intact *versus* transected peripheral nerves

Pierre Mourad

University of Washington, Seattle, Washington, United States

People with amputation often experience residual limb pain, and phantom limb sensation and pain. However, it is often difficult to distinguish if pain originates from transected nerves, from surrounding tissue, and/or has central contributions via central sensitization. As a step towards understanding amputee patient's pain, we sought to determine if transected nerves after amputation are or more or less sensitive to intense focused ultrasound (iFU) stimulation relative to intact nerves. To do so we applied iFU to two cohorts of participants: standard amputees with transected nerves and health volunteers. As controls, we stimulated ipsilateral muscle, contralateral, intact nerves in the amputation cohort, and intact nerves in healthy volunteers. Our iFU sources, guided with diagnostic ultrasound, emitted individual bursts of 2 MHz ultrasound lasting 0.1 seconds. We started at low intensity values, increasing the intensity until either the test subjects experienced a sensation associated with successful stimulation of the nerve or reached the upper bound on the intensity emitted by our device (820 W/cm^2 spatial peak temporal average intensity - Ispta), defined as the iFU threshold intensity value or iFU_t. We found that all nerves were more sensitive than surrounding, muscular tissue. Intact nerves across all cohorts had comparable iFU_t values, on average. 5/13 (38%) of amputees had substantially lower (by an order of magnitude) ipsilateral iFU_t than contralateral iFU_t, while the rest had comparable values of iFU_t between ipsilateral and contralateral nerves. This study demonstrates the feasibility of using high intensity focused ultrasound to distinguish between neuropathic tissue and surrounding non-neuropathic tissue.

BR-37

Monday

22 October 2018

Topic: Neuromodulation
Presentation Type: Oral

Cortical transcranial ultrasound stimulation: Assessment of off-line activity change using functional MRI

Jérôme Sallet[1], Lennart Verhagen[2], Cécile Gallea[3], Davide Folloni[2], Charlotte Constans[4], Stéphane Lehericy[3], Daria Jensen[2], Harry Ahnine[3], Léa Roumazeilles[2], Mathieu Santin[3], Bashir Ahmed[2], Miriam Klein-Flügge[2], Kristine Krug[2], Rogier Mars[2], Matthew Rushworth[2], Pierre Pouget[3], Jean-François Aubry[5]

[1]University of Oxford, Oxford, United Kingdom
[2]Wellcome Centre for Integrative Neuroimaging (WIN), Centre for Functional MRI of the Brain (FMRIB), Oxford, United Kingdom
[3]Institute du Cerveau et de la Moelle épinière (ICM), Centre for NeuroImaging Research (CENIR), Paris, France
[4]Institut Langevin, ESPCI Paris, PSL Research University, CNRS 7587, UMRS 979 Inserm, Sorbonne Univer, Paris, France
[5]Institut Langevin, Paris, France

Background: Transcranial ultrasound stimulation (TUS) has been shown to modify brain activity in non-human primates (Wattiez, Brain Stimulation, 2017). Coupled to functional magnetic resonance imaging (fMRI), it could be used as a non-invasive way to manipulate and record brain activity. In this paper, we used off line transcranial ultrasound stimulation in non-human primates followed by fMRI in an ultrasound-free environment.

Methods: We used TUS to modify brain activity in the supplementary motor area (SMA), the frontal polar cortex (FPC) and the Anterior Cingulate Cortex (ACC) in N=3 non-human primates. A single element ultrasound transducer (H115-MR, diameter 64 mm, Sonic Concept, Bothell, WA, USA) was operated at 250 kHz with 30 ms bursts of ultrasound with a pulse repetition rate of 10Hz. The total duration of the stimulation was 40 seconds, with a peak-to-peak voltage of 130V, corresponding to a peak negative pressure of 1.2MPa measured in water with an in house heterodyne interferometer. Sonication was performed off line and whole-brain BOLD fMRI data were collected in a 3 T MRI scanner with a full-size horizontal bore from each animal at least 20 minutes after sonication: 36 axial slices; in-plane resolution, 2 x 2 mm; slice thickness, 2 mm; no slice gap; TR, 2000 ms; TE, 19 ms; a total of 2400 volumes were acquired in 3 runs over 80 minutes.

Results: Transcranial focused ultrasound stimulation of SMA and FPC induced spatially specific changes to SMA and FPC connectivity profiles respectively (Fig. 1, non-parametric permutation tests, SMA: $p = 0.017$, FPC: $p = 0.027$). For all sites tested, TUS led to more restricted interactions of the stimulated area with the rest of the brain, reflected in a sharpening of its connectivity profile. These site-specific changes in cortical signal were superimposed on more widespread changes driven by signal in a cerebral spinal fluid compartment (CSF). These widespread signal changes were well captured by the mean time course and first five principal components of the WM and CSF signals, adhering to conventional resting-state approaches to account for global signal contributions. Following these modulations of superficial cortical activity, we confirmed these effects in a deeper cortical region, the ACC. Again, we observed similarly altered brain connectivity, as compared to control (Fig. 2). However we did not observe strong CSF related widespread changes. The maximum temperature elevation inside the brain below the dura (mean thickness 0.5mm) was estimated to 1.0°C. Temperature elevation at the stimulation site was estimated to be below 0.5°C.

Conclusions: TUS induces a sustained impact on the network of connectivity of non human primates, in an ultrasound-free environment thanks of offline stimulation prior to fMRI. The impacts differ significantly when ultrasound stimulation is applied to two different areas in the frontal cortex.

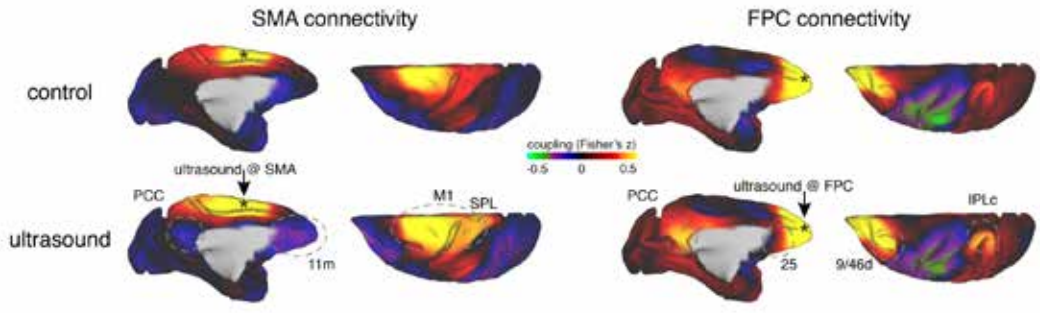

Figure 1. Coupling of activity between stimulated area (SMA: left and FPC: right) and the rest of the brain with (bottom row) and without (top row, control) ultrasound sonication

Figure 2. Coupling of activity between ACC and the rest of the brain with (bottom row) and without (top row, control) ultrasound sonication

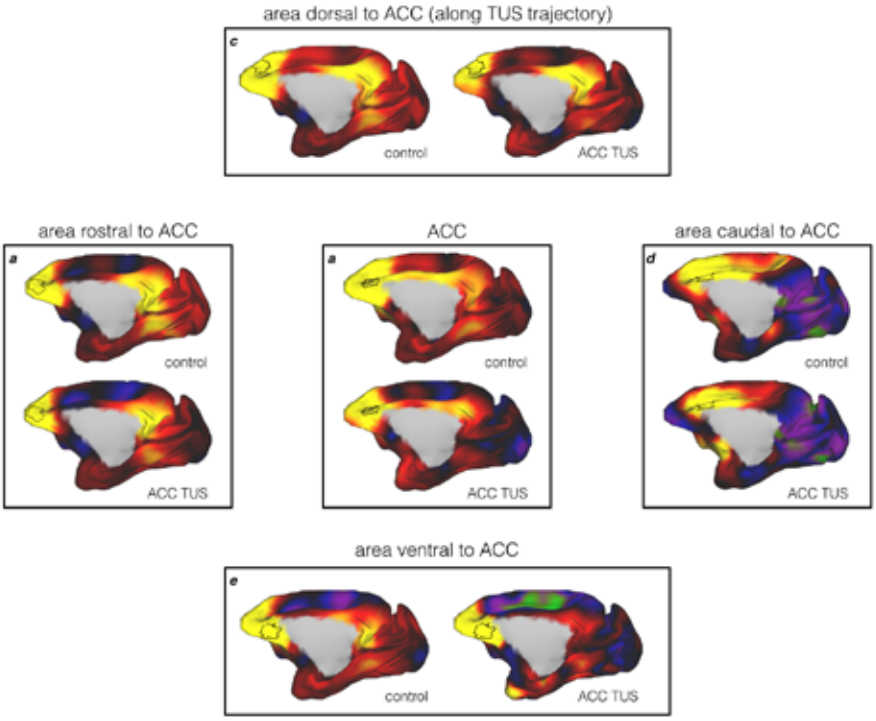

BR-38

Monday

22 October 2018

Topic: Neuromodulation
Presentation Type: Oral

Elimination of auditory pathway activation does not affect motor neuromodulation responses in rodents

Morteza Mohammadjavadi, Gerald R. Popelka, Patrick Peiyong Ye, Kim Butts Pauly

Stanford University, Stanford, California, United States

Background: Transcranial ultrasound (US) stimulation of the motor system can activate the auditory pathway (Foster et al.,1977, Sato et al., 2017). Previously (ISTU 2018) we showed that the auditory brainstem response (ABR) resulting from a pulsed US stimulus capable of eliciting a motor response is much smaller than the ABR resulting from an auditory stimulus too low (40 dB SPL acoustic click) to elicit a startle reflex. In this study, we investigate the effect of US stimulus envelope on the ABR in normal hearing mice and the US-stimulated EMG motor responses in deaf knockout mice.

Methods: Wild-type C57BL/6 hearing mice (n=8) and genetically deaf homozygous samba mutant (LOXHD1) knockout mice (Grillet et al., 2009) (n=4) were used with intraperitoneal anesthesia (ketamine/xylazine). A single-element planar transducer (500 kHz, 25.4 mm diameter) was coupled via 2 mm aperture waveguide on the midline over the caudal brain.

The US stimuli were pulsed wave (PW) with 1.5 kHz pulse repetition frequency (PRF), PW(1.5kHz), and 8 kHz PFR, PW(8kHz), continuous wave (CW) with rectangular envelope, CW(RE), or smoothed envelope CW(SE), a no-stimulus sham condition, (Sham) and a broad band acoustic 100 μs click at 40 dB SPL, (Click). Sonication duration (80 ms) and ISPTA (2.9 W/cm^2) were held constant.

The ABR was measured from needle electrodes placed on the animal's head, processed off-line (MATLAB with bandpass filtering, 200 to 2500 Hz averaged over 1000 trials) with ABR signal power calculated over a 6 ms period after stimulus onset. The motor responses were recorded from EMG signals from forelimb muscles and calculated as success percentage rate (number of EMG responses divided by 100 sonications, including 10 sham stimulations in random order).

Results: Hearing mice showed clear ABR responses for PW(1.8kHZ), PW(8kHz) and CW(RE) US stimuli and no ABR responses for CW(SE) US stimuli or the sham control conditions (Fig.1), differences that were statistically significant ($P < 0.01$, 2-tailed unpaired t-test). The mean ABR for PW(1.5kHZ), PW(8kHz) and CW(RE) US stimuli were smaller than the ABR for the 40-dB SPL acoustic click that is well below levels that cause an acoustic startle reflex.

A rectangular envelope US stimulus elicits ABRs at both the sharp on and sharp off portion of the envelope (Fig.2) that are eliminated by smoothing the waveform envelope (Fig.1 & 2). The rectangular envelope US stimulus with ABR, CW(RE), and the smoothed US stimulus envelope, CW(SE), with no ABR, induce equivalent motor responses (Fig 2).

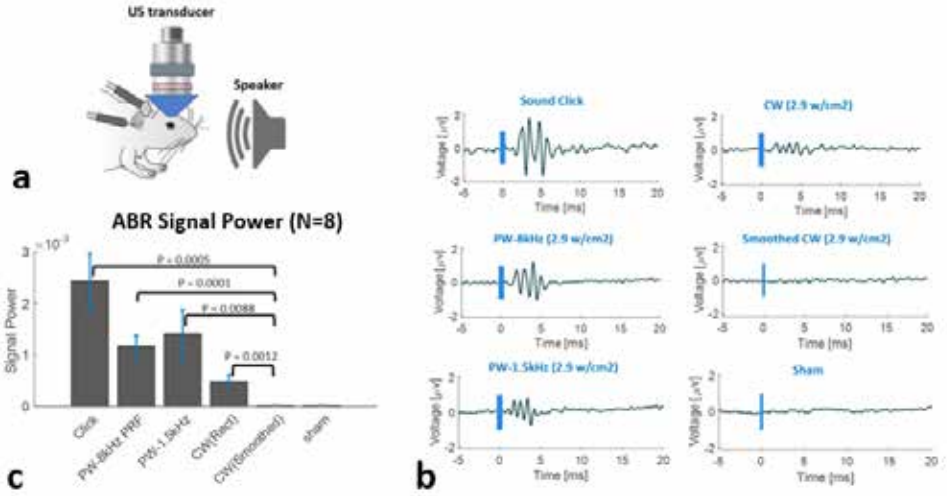

Figure 1.

a) Experiment setup b) *ABR signal power for different ultrasound stimuli or a broadband acoustic click c) Representative ABR responses*

The EMG responses were equivalent for all US waveforms in the knockout (LOXHD1) deaf mice (Fig.3) that have no measurable ABR over the entire frequency range of hearing (Grillet et al., 2009).

Conclusions: The broad-band, generally high frequency components of an US rectangular envelope stimulus can activate the cochlea and generate signals in the afferent auditory pathway. Smoothing the US waveform eliminates the auditory responses without affecting the motor responses.

Acknowlegements: The authors would like to thank Anthony Ricci for his advice and guidance on

this study and Nicolas Grillet for providing us with genetically knockouts (LOXHD1) and Anping Xia for her help in recording auditory brainstem responses.

This work was supported by the funding sources: NIH R01 EB019005, R01 MH111825, INSIGHTEC.

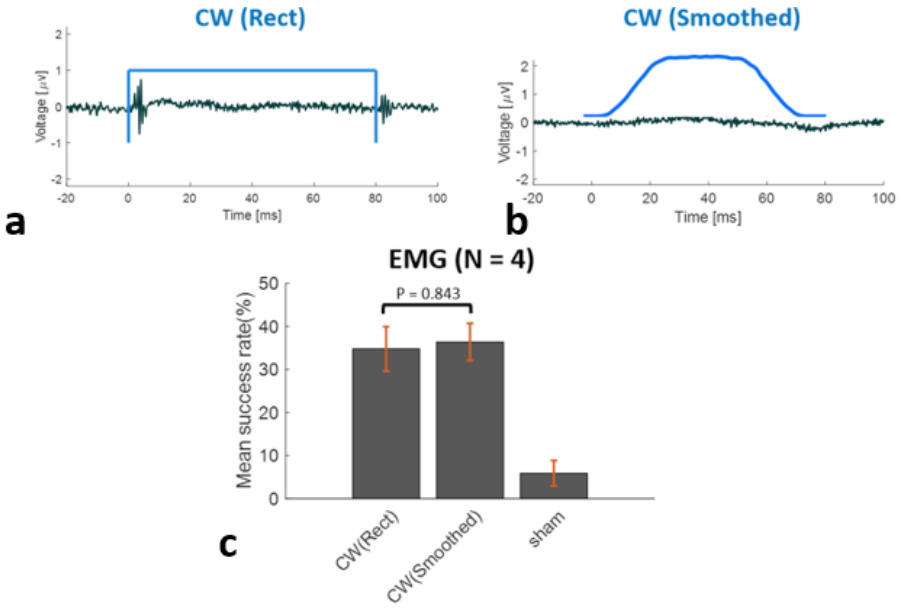

Figure 2.

a) ABR responses observed at the rapid on and off portion of the rectangular envelope continuous waveform US b) ABR responses eliminated by smoothing the US waveform envelope c) EMG responses for smoothed and rectangular US pulses are equivalent

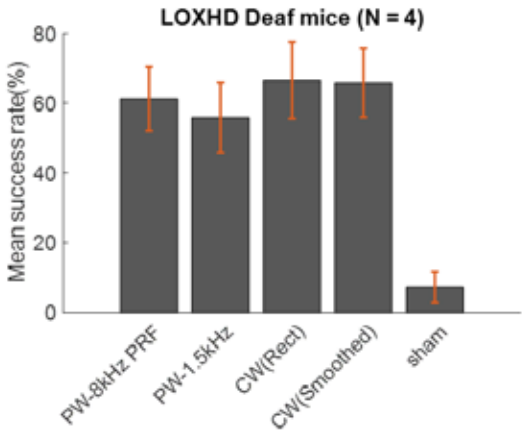

Figure 3.

EMG success rate for different US stimuli for deaf knockout Samba LOXHD1 mutants

BR-39

Monday

22 October 2018

Topic: Neuropathic Pain
Presentation Type: Oral

Temperature and cavitation monitoring for FUS peripheral neuromodulation

Hermes Kamimura[1], Min Kim[1], Antonios Pouliopoulos[1], Stephen Lee[1], Elisa Konofagou[2]

[1]Columbia University, New York, New York, United States
[2]Columbia University Medical Center, New York, New York United States

Background: Noninvasive focused ultrasound (FUS) is capable of modulating the central and the peripheral nervous system (PNS).[1, 2] FUS modulation of the PNS is a promising approach to treat neuropathic diseases as an alternative to drug therapy, electrical stimulation and surgical intervention. Although, a range of acoustic parameters (< 5.7 MPa) was found safe in mice,[2] the clinical translation of this technique requires a reliable control of parameters. Monitoring thermal and cavitation effects in real time allow conducting safe sonication in humans. In this study, thermal evaluation and cavitation mapping were performed in chicken breast samples and in murine tibialis anterior muscle *in vivo* as a preliminary evaluation of our human setup.

Methods: Sonications were performed at 3.1 MHz (Sonic Concepts) in male C57BL/6 mice *in vivo* and *ex vivo* chicken breast samples with average pressure attenuation of 3.5 dB/cm@1 MHz (similar to human muscle) were sonicated with pulse durations (PD) varying within 32-1000 µs and peak negative pressure (PNP) levels from 3 to 11 MPa. Thermal assessments were performed using a T-type thermocouple. A P12-5 (Philips) array passively recorded cavitation signals, which were processed with a passive cavitation imaging (PCI) algorithm[3] to map acoustic emissions.

Results: PCI revealed a threshold of 4.2 MPa for broadband and ultra-harmonic emissions in the muscle in mice (Figures 1, 2). Modest temperature increase (<2°C, 5 min, Figure 3) was detected 5 mm from the focus at 11 MPa, 1 ms PD and 1 Hz PRF. Tissue fragmentation was observed in chicken sample (Figure 4) for PNP ≥ 7 MPa, 161 µs PD, 0.3 Hz PRF and sonication duration of 2 min. Safe sonication was thus found to be limited to PNP < 7 MPa despite the fact that the thermal dose remained under 0.001 CEM at lower PRF (≤1 Hz).

Conclusions: These results indicate a PNP range (4.2 - 7 MPa) where cavitation is present without measurable thermal effects or any gross damage. In ongoing studies, EMG measurements will be conducted in human subjects at the identified safe PNP levels where cavitation can be minimized (≤4.2 MPa) and explore whether these safe cavitation levels (at 4.2≤PNP<7MPa) and thermal effects (at PRF>1Hz) can enhance neuromodulatory responses in humans.

Acknowlegements: Supported by Soundstim, DARPA (HR0011-15-2-0054) and NIH (R01EB009041).

References

1. Kamimura et al. *Med Phys.* 2016;43:5730-5
2. Downs et al. *Phys Med Biol.* 2018;63:035011
3. Haworth et al. *IEEE T Ultr Ferroelec Fr eq Contr.* 2017;64:177-191

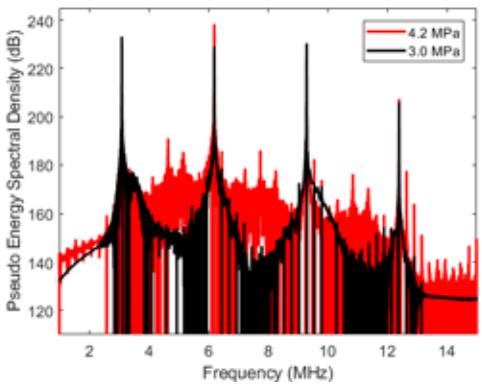

Figure 1. (left) Cavitation spectrum from mouse tibialis anterior muscle *in vivo* under sonications at 3.0 and 4.2 MPa.

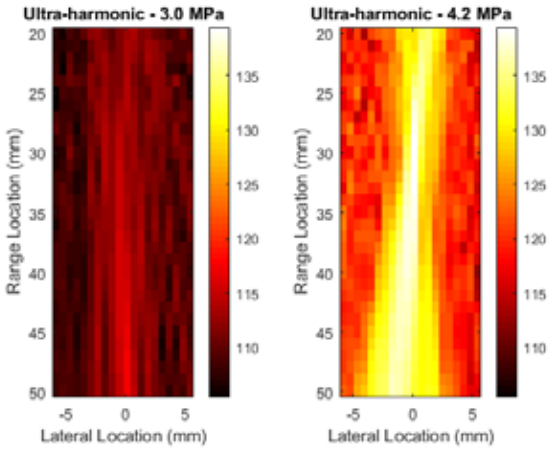

Figure 2. (right) Passive cavitation imaging of mouse tibialis anterior muscle *in vivo*.

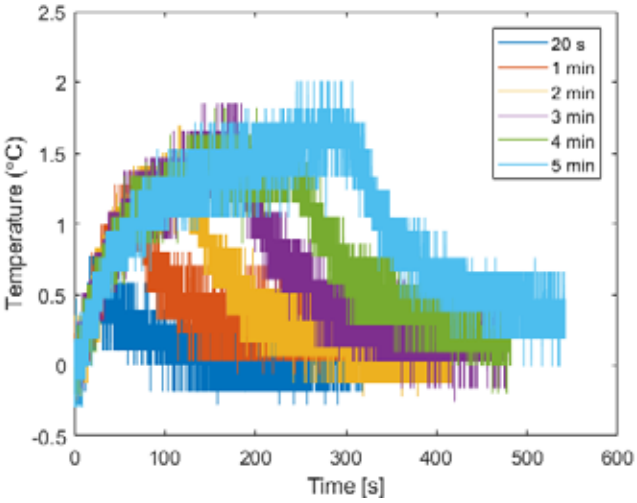

Figure 3. Temperature recordings during sonication of mouse tibialis anterior muscle *in vivo*

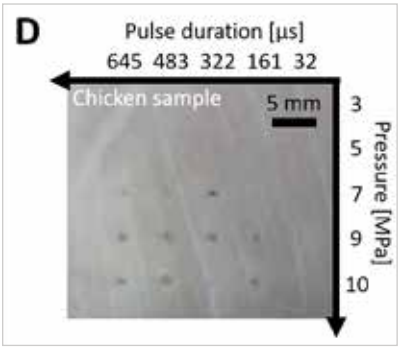

Figure 4. Tissue fragmentation observed in chicken breast samples under sonication.

BR-40

Monday

22 October 2018

Topic: Neuromodulation
Presentation Type: Oral

Transcranial FUS-mediated motor cortical stimulation in freely-moving awake rats using wearable headgear system

Phillip Croce, Ryan W. Margolin, Amanda Cammalleri, Kyungho Yoon, Seung Schik Yoo, Wonhye Lee

Brigham and Women's Hospital, Harvard Medical School, Boston, Massachusetts, United States

Background: Transcranial focused ultrasound (FUS) with a low-intensity has gained momentum as a novel modality for regional brain neuromodulation with superior spatial selectivity and depth penetration. Typically, animal experiments utilize anesthetic states to provide a controlled environment for FUS administration. However, the type/depth of anesthesia is known to affect the overall responsiveness to the sonication. Due to the confounding effects of anesthesia, further study is needed in awake small animals (e.g. rats) to better understand the efficacy of FUS brain stimulation.

Methods: We developed a 3D-printed wearable headgear system with a miniature single-element FUS transducer (16 mm diameter, 12 mm height, ~6 g weight, with a PZT piezoelectric ceramic) capable of being mounted to the skull of a Sprague-Dawley rat (male, n=7, 299–466 g). When operated at 600 kHz, the transducer generated an acoustic focus ~10 mm away from the exit plane. The size of the focus, measured at full-width at 90%-maximum, was 3.5 mm in length and 1.0 mm in diameter. In order to reproducibly place the wearable headgear on the rat's head, a pedestal was implanted on the skull, allowing for the transcranial delivery of FUS to the motor cortical areas in freely-moving awake rats. While targeting the motor cortices of the tail/limbs/whiskers, sonication-related behavioral responses were examined using video recordings across three different conditions—awake status, ketamine/xylazine anesthesia, and isoflurane anesthesia, and the response rates/latencies were compared. The 300 ms-long pulsed sonication (with 1 ms tone-burst-duration and 500 Hz pulse-repetition-frequency; 50% duty-cycle) was given every 5–10 s, with an intensity range of 3.4–21.6 W/cm^2 Isppa. After repeated FUS sessions, histological analysis was conducted on the sonicated brain tissues. All animal procedures were conducted under the approval of the local IACUC.

Results: FUS stimulation elicited movements from various anatomical locations such as the tail/limbs/whiskers. Head/neck twitches and chewing behaviors were also detected. In the awake status, the response rate was higher while the latency to stimulation was shorter than those under light ketamine/xylazine or isoflurane anesthesia. The variability in response rates decreased during the awake condition compared to the anesthetic conditions. Further analysis on the distribution of movement latencies implicated the possible coexistence of acoustic startle responses with FUS-mediated movements. Post-FUS animal behaviors did not demonstrate any abnormalities, and histological analysis showed no signs of tissue damage.

Conclusions: Transcranial FUS was successfully applied over the rat's motor cortical areas using a wearable transducer headgear and elicited sonication-related movements under both awake and anesthetized conditions. Diverse physical responses were observed from the awake conditions compared to those reported in previous studies. The capability of conducting experiments in freely-moving awake animals would pave the way to examine the effects of FUS neuromodulation without the confounding factors from anesthesia, and provide a translational study platform to large animals and humans.

Acknowlegements: This study was supported by the Focused Ultrasound Foundation (FUS461 to WL) and the National Institutes of Health (RO1MH111763 to SSY).

BR-41

Monday

22 October 2018

Topic: Neuromodulation
Presentation Type: Oral

Mechanisms and applications of focused ultrasound tissue modulation for augmented nanoparticle penetration and efficacy in the CNS

Brian Mead[1], Colleen Curley[1], William Garrison[1], Wilson Miller[1], Namho Kim[2], Karina Negron[2], Jung Soo Suk[2], Justin Hanes[2], Richard Price[1]

[1]University of Virginia, Charlottesville, Virginia, United States
[2]Johns Hopkins University, Baltimore, Maryland, United States

Background: Microbubble (MB) activation with focused ultrasound (FUS) facilitates the noninvasive, MR image-guided, and spatially targeted delivery of heavily-PEGylated brain-penetrating nanoparticles (BPN) across the blood-brain barrier (BBB) to the central nervous system (CNS). There is evidence that FUS also augments the penetration of nanoscale therapeutics through brain tissue; however, this secondary effect has not been leveraged therapeutically and its mechanisms have not been well-elaborated. Here, we tested whether pre-treating brain tissue with pulsed FUS may be used to (i) enhance BPN dispersion in the CNS via activation of mechanosensitive TrpA1 and/or TrpV1 channels and (ii) augment BPN-mediated transfection following trans-BBB delivery of BPN.

Methods: Pulsed FUS pre-treatment, with or without i.v. MBs, was applied to the left striatum of rats (Sprague-Dawley) or mice (C57Bl6, TrpV1-/- or TrpA1-/-), followed by convection-enhanced delivery (CED) of ZsGreen plasmid bearing-BPN. Transfection volume was assessed at day two by imaging of the ZsGreen reporter. To test whether FUS pre-treatment enhances transgene expression after BPN delivery across the BBB, FUS pre-treatment was first applied (2 or 4 MPa; 45 ms pulses, 2.25% duty cycle, 10 min) to either the left or right striatum in rats. MBs and luciferase-BPN were then i.v. injected, followed by BBB opening in both striata with FUS and MBs (0.6 MPa, 10 ms pulses, 0.5% duty cycle, 2 min, 1x105 MB/g). Acoustic emissions data were collected throughout. Reporter transgene expression was assessed by bioluminescence imaging. MR thermometry was performed during FUS pre-treatments, and additional T1 contrast MRI was done to test whether FUS pre-treatment affected subsequent BBB opening.

Results: FUS pre-treatment increased the volume of transfected brain tissue (1.8- and 2.5-fold in C57Bl6 mice and Sprague-Dawley rats, respectively) after CED of gene-vector BPN. This effect was abolished in TrpA1-/- mice, but not in TrpV1-/- mice, thereby identifying TrpA1 as a key biological mediator of FUS-enhanced penetration (Figure 1). FUS pre-treatment prior to trans-BBB nanoparticle delivery elicited up to a 5-fold increase in subsequent transgene expression (Figure 2), but had no detectable impact on subsequent BBB opening or acoustic emissions (Figure 3), thereby confirming that augmented transfection occurs through parenchymal modulation. FUS pre-treatment elicited a minimal temperature rise and median CEM43°C of 0.73, which is below the threshold for CNS damage (Figure 4). GFAP and Iba1 immunolabeling indicated no overt signs of astrogliosis and microgliosis, respectively (Figure 4).

Conclusions: Here, we identified TrpA1 channels as novel FUS mechanosensors and regulators of FUS-enhanced tissue permeability. Further, in a clinically-operable treatment paradigm guided entirely by MR imaging, we demonstrated that pre-conditioning brain tissue with pulsed FUS before opening the BBB elicits multi-fold enhancements in subsequent transgene expression, without significant tissue heating or overt signs of gliosis. The FUS pre-treatment strategies advanced here may be appended to already-established protocols to augment the efficacy of drug or gene therapy strategies in the CNS.

Acknowledgements: Supported by NIH R01CA164789, R01CA197111, and R01EB020147.

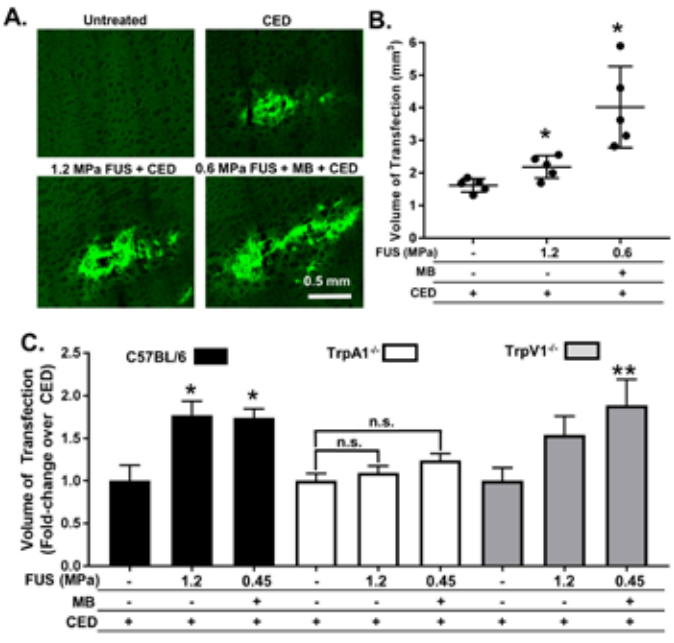

Figure 1. A,B: ZsGreen expression after CED. *p<0.01 *vs.* CED. C: ZsGreen transfection volume as a fold change over CED in mice. *p<0.05 *vs.* CED in C57BL/6 and TrpA1. **p<0.025 *vs.* CED in TrpV1.

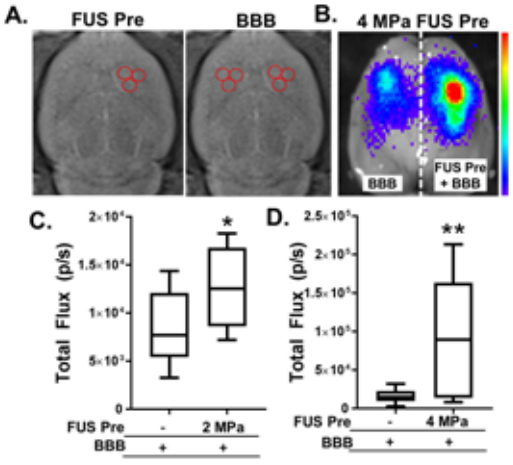

Figure 2. A: Treatment planning. Red spots = sonications. B: *Ex vivo* bioluminescence image 2 days after treatment. C,D: Luciferase expression is significantly enhanced with FUS pre-conditioning at 2 and 4 MPa. *p<0.01.

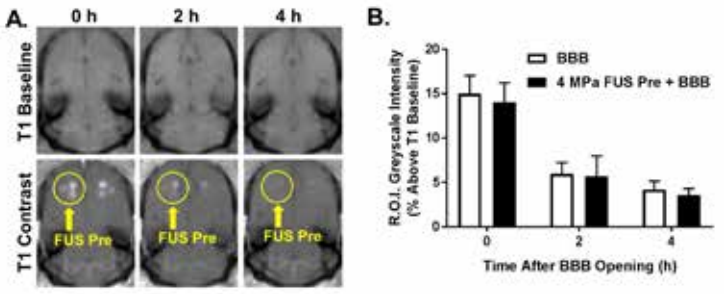

Figure 3. A: T1 contrast MRI images showing BBB opening, with and without 4 MPa FUS pre-conditioning. B: Mean greyscale intensity as a percentage over pre-conditioning baseline from T1 contrast MRIs. No significant differences were observed.

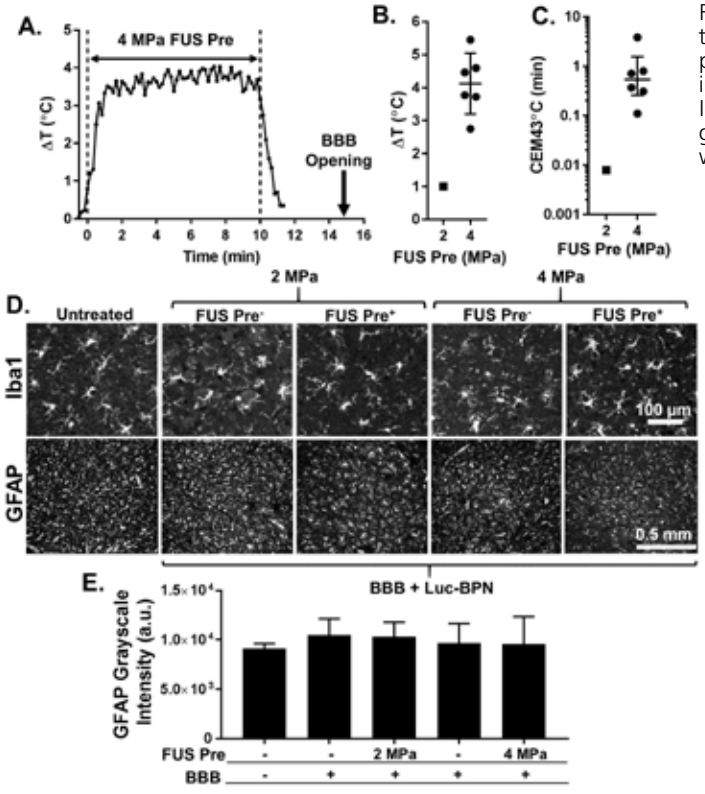

Figure 4. A: Representative MR thermometry data for 4 MPa FUS pre-conditioning. B: Temperature increases. C: CEM43°C values. D: Iba1 and GFAP staining. E: GFAP grayscale. No significant differences were observed.

BR-42

Monday

22 October 2018

Topic: Neuromodulation
Presentation Type: Oral

Modulation of visual evoked response by non invasive GABA delivery in non-human primates

Pierre Pouget[1], Charlotte Constans[2,3,4,5], Harry Ahnine[1], Mathieu Santin[1], Stéphane Leherícy[1], Mickael Tanter[2,3,4], Jean-François Aubry[2,3,4]

[1]Institut du Cerveau et de la Moelle épinière, ICM, Inserm U 1127, CNRS UMR 7225, Sorbonne Université, Paris, France
[2]Inserm U979, Institut Langevin, Paris, France
[3]ESPCI Paris, PSL Research University, Institut Langevin, Paris, France
[4]CNRS UMR 7587, Institut Langevin, Paris, France
[5]Université Paris Diderot, Sorbonne Paris Cité, Paris, France

Background: Blood-brain barrier (BBB) opening induced by focused ultrasound coupled with microbubbles has been previously achieved in rodents and primates, holding promises for targeted drug delivery. Here we investigate the feasibility of local, non-invasive delivery of an inhibitory neurotransmitter (GABA) to modulate the visual cortex activity of non-human primates.

Methods: The BBB was opened in the visual cortex of two macaques using a single element focused ultrasound transducer (Sonic Concepts, Bothell, WA, USA) at 245 kHz and microbubbles (SonoVue Bracco, Milan, Itay)). The *in situ* pressure delivered to the monkey brain transcranially was estimated to 0.50 MPa. The harmonic responses of the microbubbles were recorded with a PCD and used as real-time control of efficiency and safety.

The animals were installed in front of a black screen, eyes opened. A run of visual stimuli consisted in 200 full field white flashes separated by 2s. Two electrodes were implanted intracutaneously above the V1 regions to record the electrophysiological activity. Figure 1 displays the timeline of the procedure. Control runs (baseline, after ultrasound alone and after ultrasound + microbubbles) were performed before GABA was injected intravenously (0.1 to 6 mg/kg) and the 'GABA' runs were conducted. Electrophysiological data were filtered and averaged. We calculated, for each session, the decrease of the VEPs amplitudes as the difference between the maximum and the minimum P1 peaks over the five first GABA runs.

Results: Figure 2 displays the VEP results of one session (monkey A, GABA dose=5 mg/kg). We considered the decay of the VEPs P1 amplitudes when the GABA dose increases. Figure 3 shows that the impact on P1 amplitude gets stronger with the GABA dose increase. We observed in 5 cases out of 7 a significant neuromodulation effect. We therefore calculated the average contribution from ultrasound alone, BBB opening and GABA through the spectral power decrease, over all sessions with a GABA dose of at least 4mg/kg, for three different time periods: 0-100ms, 100-200ms and 200-300ms after the stimulus onset (figure 3). Results showed that FUS + microbubbles influence got stronger as time increases after the visual stimulus onset, compared to GABA-induced effects. GABA accounts for 90% of the effects during the first 100 ms, 42% during the 100-200ms period and 50% during the 200-300ms period.

Conclusions: The modulatory impact of the local delivery of GABA in the brain is at maximum (90%) within the first 100ms after the visual stimulus onset.

Figure 1. Timeline of the experiments. Each bar represents a VEP run (measurement of the visual responses to 200 full field flashes)

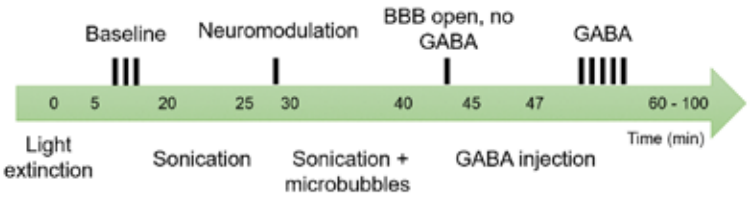

Figure 2. Mean VEP recordings for each run from baseline to the last GABA run for sham session (left) and session 6 mg/kg GABA dose (right) for monkey B. The legend describes the runs in the chronological order. Each curve is the average of 200 VEP recordings of one run. The visual stimuli occur at time 0. The names of the sham sessions runs were kept similar to the non-sham sessions ('baseline', 'neuromodulation', 'no GABA', 'GABA') to place their occurrence on the timeline, even though there was no neuromodulation nor GABA injection.

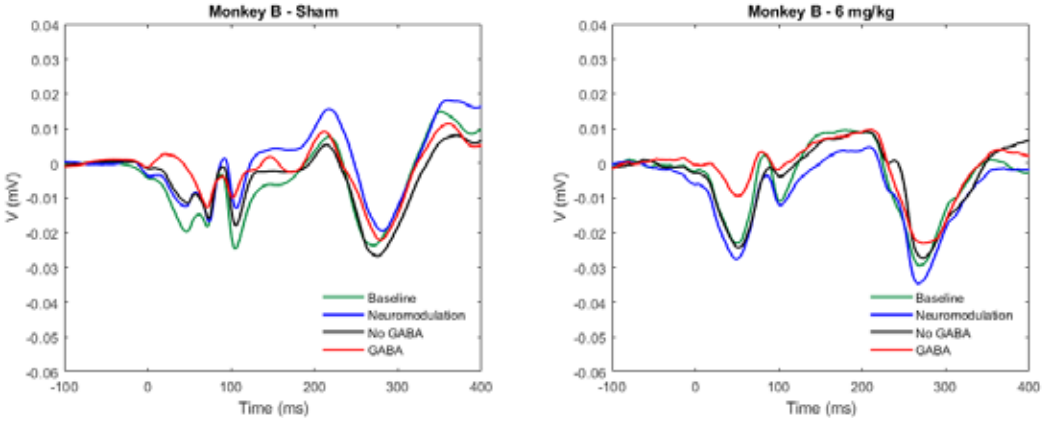

Figure 3. VEPs decrease of amplitude (maximum P1 amplitude – minimum P1 amplitude over all GABA runs) after GABA injection, as a function of GABA dose for monkey A (left) and monkey B (right).

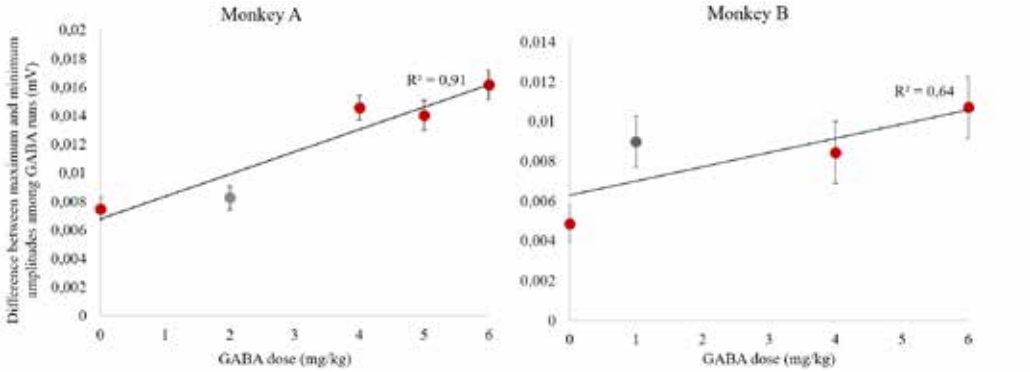

BR-43

Tuesday

23 October 2018

Topic: Brain – Technical
Presentation Type: Oral

Accelerated real-time 3D MR thermometry using a retraced spiral-in/out trajectory

Xue Feng, Steven Allen, Samuel Fielden, Craig Meyer

University of Virginia, Charlottesville, Virginia, United States

Background: Real-time MR thermometry, usually based on the proton-resonance frequency shift, is a key aspect of MR-guided ultrasound procedures. The desire to monitor the entire insonicated volume has led the development of rapid, 3D methods; however, acquiring fully sampled 3D volumetric data is time consuming so that fast methods must be developed. Spiral k-space trajectories have higher acquisition efficiency than Cartesian scanning so that they are an attractive way to improve the temporal and spatial resolution in MR thermometry. Furthermore, temporal redundancy can be exploited with real-time reconstruction models such as the Kalman Filter to accelerate the scan. The purpose of this study was to develop the accelerated real-time 3D MR thermometry using a retraced spiral-in/out (RIO) trajectory with Kalman filter reconstruction.

Methods: A 3D RIO thermometry sequence based on stack-of-spirals was implemented on the RTHawk platform (HeartVista, Inc.) to enable real-time sequence control and monitoring of a FUS insonication. A fully sampled spiral k-space trajectory was designed with 24 interleaves and 12 slice-encoding steps. The supported field-of-view was 280 mm^2 with 1.5 mm^2 in-plane resolution and 36 mm with 3 mm through-plane resolution. The other sequence parameters were: FA=5-10°, TR/TE = 22.0/12.8 ms. During acquisition, the interleaves were looped inside the phase encoding steps and the time to cover the entire k-space was 6.3 seconds. To double the temporal resolution, reconstruction can be performed when half of the k-space is updated with the rest of k-space filled from the previous frame, which is called view sharing but suffers from temporal blurring. Kalman filter method only relies on the updated k-space data and use an optimization model to get the unaliased images, given as

$$x_k = x_{k-1} + w_{k-1}$$

$$z_k = U_k F x_k + v_k$$

in which x_k is the target image; w_k is the system noise modeling the image changes due to heating; z_k is the measurement with undersampling pattern U_k; F is the Fourier transform matrix and v_k is the measurement noise. The distribution of w_k is designed to focus on the area around the focal spot so that it can get more accurate estimation of the temperature changes. To compare the two reconstruction methods, a 2x retrospective undersampling was performed on the acquired data set from a phantom study with insonications.

Figure 1. Temperature maps at peak temperature frame are shown for all 12 slices (left to right, then top to bottom). Multiple slices show the temperature changes.

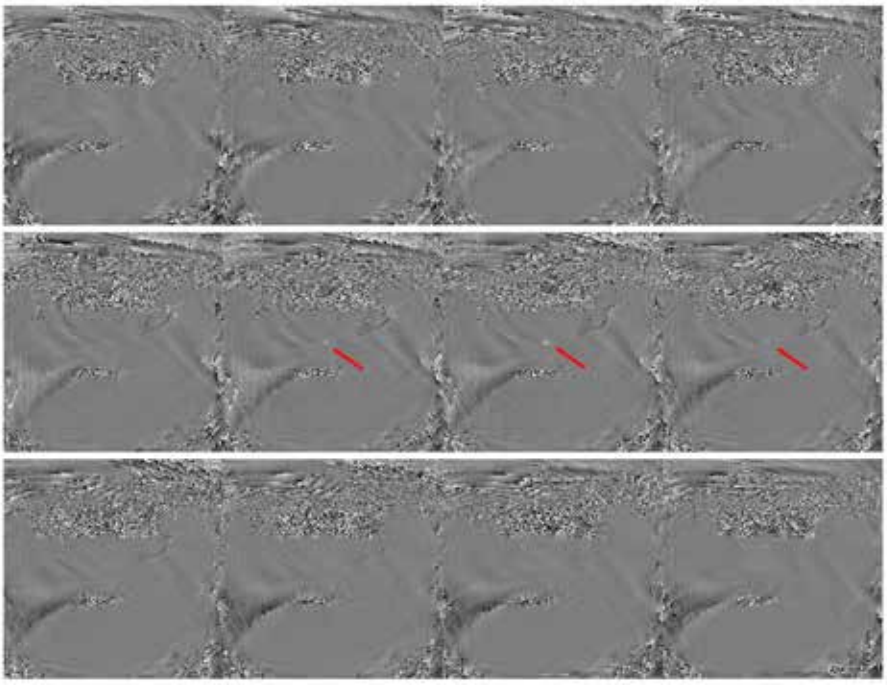

Results: Temperature maps at peak temperature frame are shown in Fig. 1 for all 12 slices. Two neighboring slices of the focal spot (slice 7) also have significant temperature changes, showing the necessity of a 3D monitoring. Fig. 2 shows the comparison of the two reconstruction methods. The view sharing method underestimated the peak temperature due to temporal blurring and the Kalman filter method provided a much more accurate temperature measurement.

Conclusions: The efficiency of spiral readouts supports rapid generation of 3D temperature maps and the Kalman filter method can further accelerate the sequence so that it can become a more superior MR thermometry tool.

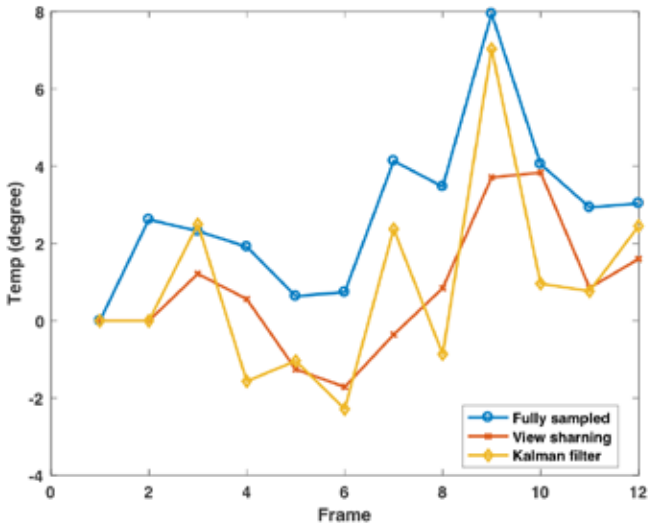

Figure 2. Temperature changes at the hottest spot using the view sharing and Kalman filter based reconstruction as well as the fully sampled data. Kalman filter yielded a more accurate peak temperature.

BR-44

Tuesday

23 October 2018

Topic: Brain – Technical
Presentation Type: Oral

Closed-loop control of cavitation activity using passive acoustic mapping

Scott Schoen[1], Arpit Patel[1], Costas Arvanitis[1,2]

[1]Georgia Institute of Technology, Atlanta, Georgia, United States
[2]Emory University, Atlanta, Georgia, United States

In accordance with author request, this abstract is not available for publication.

BR-45

Tuesday

23 October 2018

Topic: Brain – Technical
Presentation Type: Oral

Effect of CT exam protocols on skull-density-ratio calculations performed for MRgFUS brain treatment planning

Zaiyang Long, Krzysztof Gorny, Michael Bruesewitz, Marissa Suchyta, Christopher Favazza, Aiming Lu, Timothy Kaufmann, Lifeng Yu

Mayo Clinic, Rochester, Minnesota, United States

Background: MR-guided focused ultrasound treatment of the brain requires a head CT scan to assess skull density ratio (SDR). Treatment on the INSIGHTEC Exablate Neuro system (INSIGHTEC Ltc., Israel) requires CT images using a defined scan protocol and reconstructed with a specific reconstruction kernel, which is not available on all scanner platforms. It is unclear how other kernels or alternate exam protocols would affect the SDR calculations.

Methods: A fixed head specimen was scanned on a Siemens SOMATOM Flash scanner (Siemens Healthcare, Germany) using our clinical protocol (120 kV, pitch 0.6, 350 mAs without tube current modulation, 53.5 mGy CTDIvol) under IRB approval. According to INSIGHTEC, reconstructed slice thickness was 1 mm with 1 mm increment with a sharp H60 kernel. In addition, scans were also performed on a Siemens SOMATOM Force scanner using the same technique. Images were reconstructed with an "H60-equivalent" Hr59 kernel, which is not recommended by INSIGHTEC. Other variations in exam protocols were also tested, including different mAs, slice thickness, smoother kernels such as H30 and Hr38, and various head positions relative to the scanner (up to 50 degree lateral rotation or tilting superiorly or inferiorly using the standard head holder). In addition, raw data of a patient's head exams on the two scanners were obtained and used to reconstruct anonymized H60 and Hr69 images. Images were exported to the treatment system where SDR scores were computed.

Results: SDR scores obtained using the H60 kernel on the Flash were identical to those obtained using Hr59 on the Force, 0.405 ± 0.005. On both platforms, using smoother kernels led to 32-35% higher SDR scores (difference ranged from +0.13 to +0.14), relative to H60 or Hr59. While thinner slice and increment did not cause changes, thicker slice of 2mm resulted in 15-17% increases in SDR scores (difference +0.06 -- +0.07). Changing the relative position of the head resulted in 5% differences in SDR scores (difference -0.02 -- +0.01). Increasing mAs by 100 or reducing by 200 resulted in consistent SDR scores (i.e. 0.40, difference 0.005) on the Force, and SDR scores of 0.38-0.39 (difference 0.015-0.025) on the Flash. Patient images demonstrated SDR of 0.47 on the Flash and 0.48 on the Force.

Conclusions: Hr59 kernel on the Force scanner resulted in same or very close SDR scores as the recommended H60 kernel on the Flash scanner based on specimen and clinical images. This suggests that patient scans don't have to be limited to the Flash, which would lead to enhanced clinical efficiency. Smoother kernels and thicker slice thickness caused SDR score differences higher than published standard deviation of SDR score measurements (0.05), and therefore, should be avoided. On the other hand, changing head positioning or radiation dose within certain range caused difference less than 0.05, and therefore, judged to be acceptable. These results suggest patient head positioning does not have to be stringently restricted and there is potential to reduce radiation dose.

BR-46

Tuesday

23 October 2018

Topic: Brain – Technical
Presentation Type: Oral

Evaluation and tradeoffs of 2D and 3D Cartesian MR temperature imaging (MRTI) for brain applications

Henrik Odéen[1], Sunil Patil[2], John Roberts[1], Bradley Bolster[3], Himanshu Bhat[4], Dennis Parker[1]

[1]University of Utah, Salt Lake City, Utah, United States
[2]Siemens Medical Solutions, Baltimore, Maryland, United States
[3]Siemens Medical Solutions, Salt Lake City, Utah, United States
[4]Siemens Medical Solutions, Burlington, Massachusetts, United States

Background: MR temperature measurements for FUS brain applications ideally have high enough spatial and temporal resolution (on the order of 1x1x3mm and 3-5s) to accurately monitor the fast temperature changes occurring in FUS. The monitored field of view ideally covers the full brain so that any un-intentional heatings in the ultrasound near- and far-fields can be detected. However, currently only a single 2D slice through the focal spot is imaged. In this work we evaluate a flexible approach for single-/multi-slice 2D or volumetric 3D imaging based on a GRE echo planar imaging (EPI) pulse sequence. FUS heatings were performed in a gelatin phantom. MRTI precision was evaluated in *in vivo* scans with no heating.

Methods: The pulse sequence can perform 2D (single- and multi-slice) and 3D imaging with echo train length (ETL) from 1 (i.e., GRE) to the number of phase-encoding lines (i.e., single shot, SS) and odd numbers in-between (i.e., segmented/multi-shot), with and without different types of parallel imaging (GRAPPA and CAIPI in 1D and 2D). A 2D RF pulse-based B0-navigator was implemented to monitor and correct for bulk phase drift, and the frequency encoding can be performed with flyback gradients (i.e., mono-polar) to minimize off-resonance effects due to temperature change and fat/water frequency offsets in EPI. 16-bit (216 data points) phase imaging dynamic range is implemented to minimize the likelihood of phase wraps. 6 different protocols were tested; a) 2D GRE, b) 2D segmented-EPI, c) 2D single-shot EPI, d) 3D GRE, e) 3D segmented-EPI without flyback, and f) 3D segmented-EPI with flyback (with and without GRAPPA, R=2) – Table 1. Phantom heatings (256-element phased array transducer, 1-MHz, 13-cm radius of curvature, Imasonic/IGT, France) in a gelatin phantom using an in-house-built 5-channel coil array and *in vivo* imaging using a 20-channel head coil were performed on a 3T scanner (PrismaFIT, Siemens, Germany). All reconstructed temperature change maps were corrected for field drift using the B0-navigator.

Results: Figure 1 shows temperature maps overlaid on magnitude images for the 6 protocols, and Figure 2 shows temperature precision measured as standard deviation through time. GRE imaging (ETL=1) shows the least amount of image distortion while SS EPI has the worst distortions. SS EPI has the best thermometry precision due to the long TE, with 3D GRE having the worst precision. Segmented EPI approaches demonstrate a good tradeoff between small distortions and high precision. GRAPPA can be used to speed up the acquisitions, however with an ~√2 SNR-penalty (2 f)). The B0-navigator accurately monitors and correct for field-drifts.

Protocol	Slices	TR/TE (ms)	ETL	FE-BW (Hz/px)	FUS (W, s)	t_{acq} (s)
a) 2D GRE	1 x 3 mm	23/10	1	260	23, 30	2.9
b) 2D seg. EPI	1 x 3 mm	39/19	7	260	23, 30	0.7
c) 2D SS EPI	1 x 3 mm	160/73	125	260	23, 30	0.2
d) 3D GRE	10 x 2.5 mm	10/5.5	1	930	15, 61	10.2
e) 3D seg. EPI	12 x 2.5 mm	25/18	5	1302	23, 30	5.9
f) 3D seg. EPI Flyback	12 x 2.5 mm	23/13	5	1302	23, 30	5.4 2.7 (R=2)

Table 1. All protocols used a FOV of 240x240mm in-plane, and resolution 0.94x1.88mm. FUS is listed as Power in W and duration in seconds. For all 3D protocols 6/8 partial Fourier in the slice-encoding direction was utilized. tacq = acquisition time.

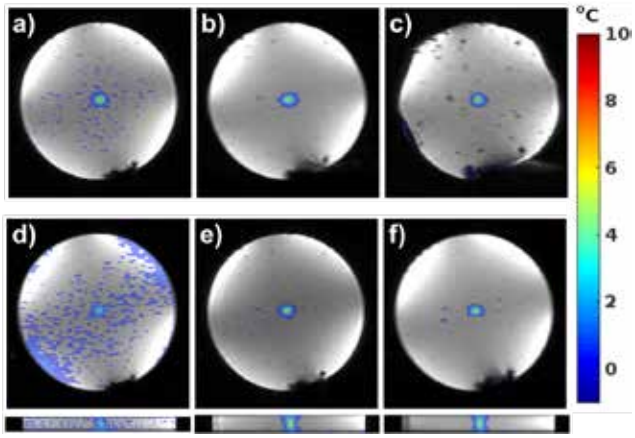

Figure 1. Temperature maps from HIFU heating in phantom overlaid on magnitude images for a) 2D GRE b) 2D segmented-EPI c) 2D single-shot EPI d) 3D GRE e-f) 3D segmented-EPI without/with flyback, respectively. For d)-f) 2 orthogonal views are shown.

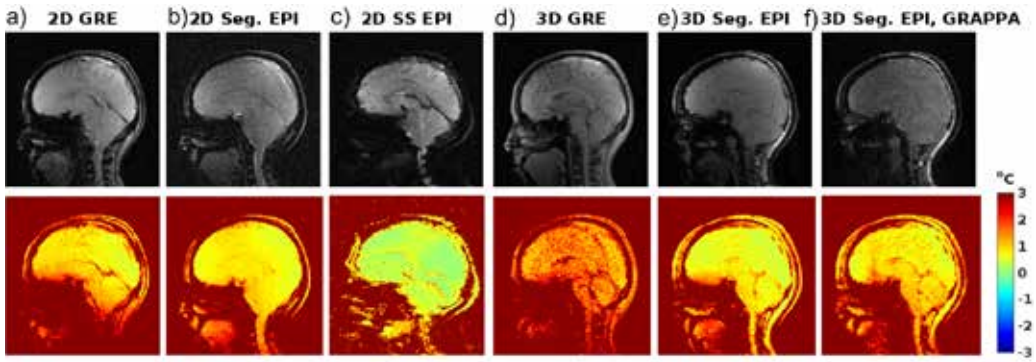

Figure 2. *In vivo* volunteer scans showing magnitude(top row) and temperature standard deviation through time (bottom row). 2DSS EPI has best precision but worst distortions. 2D/3D segmented EPI (b,e,f) show good tradeoff between precision and distortions.

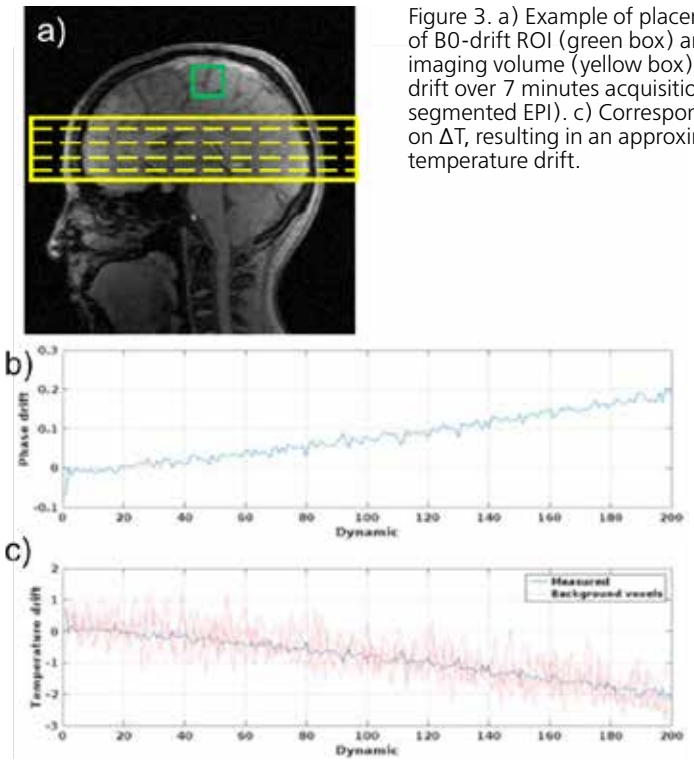

Figure 3. a) Example of placement of B0-drift ROI (green box) and 3D imaging volume (yellow box). b) Phase drift over 7 minutes acquisition (3D segmented EPI). c) Corresponding effect on ΔT, resulting in an approximately 2C temperature drift.

BR-47

Tuesday

23 October 2018

Topic: Brain – Technical
Presentation Type: Oral

Real-time transcranial histotripsy treatment monitoring and localization using acoustic cavitation emission feedback

Jonathan Sukovich, Timothy Hall, Jonathan Macoskey, Zhen Xu

University of Michigan, Ann Arbor, Michigan, United States

Background: Transcranial MR-guided focused ultrasound (MRgFUs) has been explored as a non-invasive treatment option for various brain applications. To detect cavitation during these therapies, passive cavitation detection has been investigated, which requires an ultrasound transducer separate from the therapy transducer. Histotripsy is a cavitation-based ultrasound therapy which is being investigated for transcranial applications, and has been demonstrated to rapidly and accurately generate lesions through the skull. Cavitation events generated during histotripsy generate large acoustic cavitation emission (ACE) signals which can be detected through the skull using the elements of the histotripsy array as receivers. This study investigates the feasibility of using these ACE signals to monitor and localize cavitation activity in real-time during transcranial histotripsy treatments. The goal is to show that this is a viable technique for monitoring and localizing histotripsy-induced cavitation during treatments using the same transducer for both treatment and detection.

Methods: Histotripsy pulses were delivered through three excised human skullcaps using a 256-element, 500kHz, hemispherical histotripsy transducer with transmit-receive capable elements. Pulses were electronically steered through a 1cm diameter spherical volume centered at the geometric focus of the array through the skullcaps at PRF's of 1Hz, 30Hz, and 100Hz to generate cavitation. During experiments, ACE signals were collected in real-time using the elements of the array as receivers. Treatment monitoring and localization was accomplished by back-projecting the acquired ACE signals into the field to form signal intensity maps of the transducer's focal volume. To assess the effectiveness of the ACE-based cavitation monitoring and localization, concurrent optical images of the cavitation events were acquired using a multi-camera imaging system for comparison.

Results: Using the ACE signals, we were able to monitor and localize cavitation activity in real-time through the skulls. There was good agreement between the locations of the bubbles found by back-projecting the ACE signals into the field and those measured using the cameras through all skullcaps, and deviations between the two measurements were generally bounded to within the measured diameters of the generated bubbles (<1.5mm). The locations of the cavitation events predicted using ACE signals were preferentially biased in the prefocal direction of the array compared to camera measurements. The accuracy of the ACE predictions was observed to be affected by the PRF and deviated most from the camera measurements at 100Hz. This is likely due to the re-excitement of undissolved bubble nuclei in the field from previous pulses, which generate additional emission signals that act as noise in the ACE reconstructions.

Conclusions: In this study we have demonstrated the feasibility of using ACE signals to monitor transcranial histotripsy therapies in real-time. The locations of the bubble clouds predicted using the ACE signals, with respect to those measured via optical imaging, were found to be accurate to within the measured diameters of the generated bubbles. The performance of the ACE monitoring and mapping was found to be negatively impacted by higher PRFs, likely due to emissions from the re-excitement of undissolved bubble nuclei in the field from previous pulses. Strategies are being investigated to address this issue.

Acknowledgements: This work was funded through the Focused Ultrasound Foundation.

BR-48

Tuesday

23 October 2018

Topic: Brain – Technical
Presentation Type: Oral

Targeting focused ultrasound neuromodulation in non-human primates with optical tracking-guided MR-ARFI

Sumeeth Jonathan, M Anthony Phipps, Vandiver Chaplin, Aparna Singh, Pai-Feng Yang, Allen Newton, John Gore, Li-Min Chen, Charles Caskey, William Grissom

Vanderbilt University, Nashville, Tennessee, United States

Background: Magnetic resonance-acoustic radiation force imaging (MR-ARFI) pulse sequences enable localization and targeting during focused ultrasound (FUS) therapy. MR-ARFI uses motion-encoding gradients (MEGs) to visualize the tissue displacement caused by the acoustic beam's radiation force. However, a priori knowledge of the acoustic beam's propagation direction is critical for MR-ARFI so that the MEGs can be placed in the proper orientation. We used an optical tracking system to inform the geometry of MR-ARFI acquisitions for targeting focused ultrasound neuromodulation experiments in non-human primates.

Methods: Transcranial MR-ARFI-derived displacement images were acquired on an *in vivo* experimental platform of ultrasonic neuromodulation in non-human primate (M fascicularis) somatosensory networks (Fig 1). Displacement images were acquired using a diffusion-weighted spin echo 2D MR-ARFI pulse sequence implemented on a high-field 7.0 Tesla scanner (Philips Achieva). Sonications were performed at 802 kHz with a low duty cycle (2.9 MPa free-field peak negative pressure/3.1 mechanical index) using an MRI-compatible FUS transducer (Sonic Concepts). An optical tracking system (Polaris Vicra) was used with 3DSlicer (http://slicer.org/) to determine the location of the transducer in real-time, and this information was used to prescribe MR-ARFI scans parallel to the ultrasound propagation axis to maximally encode displacement (Fig 2). Our current protocol for *in vivo* ultrasonic neuromodulation uses prone/head first positioning, targeting the somatosensory network (right S1 areas 3a/3b) of sedated adult macaque monkeys. Transcranial displacement images were acquired *in situ* after determining the location of the acoustic beam with optical tracking. Touch circuit-specific neuromodulation effects were further characterized using functional MRI (fMRI), with manual tactile stimulation used as a reference.

Results: In two separate macaques, we observed focal displacements of about 1 μm transcranially (Fig 2). Our results are among the first demonstrations of MR-ARFI feasibility in a large animal for targeting transcranial focused ultrasound therapy *in vivo*. In separate *ex vivo* studies, we show that knowledge of the acoustic beam's propagation direction is critical for MR-ARFI, and can be determined using optical tracking (data not shown). In some cases, the observed displacement was completely missed if MR-ARFI was prescribed in the wrong orientation.

Conclusions: The proposed optical tracking workflow was used to guide MR-ARFI to produce acoustic beam maps for targeting ultrasonic neuromodulation *in vivo*. Our ongoing studies will demonstrate the effectiveness of focused ultrasound in modulating the function of relevant neural circuits in non-human primates.

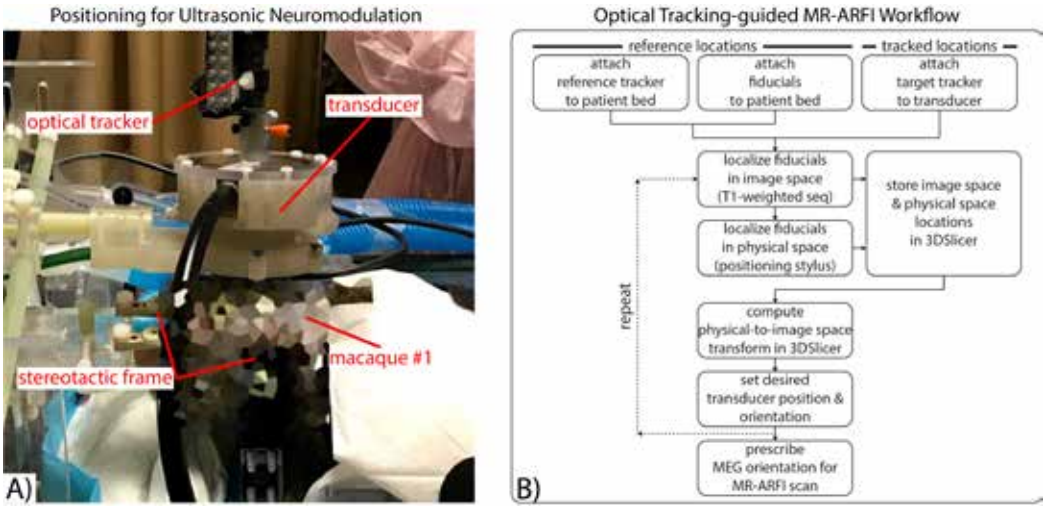

Figure 1. (A) Non-human primate positioning for ultrasonic neuromodulation, targeting right S1 areas 3a/3b. (B) Transcranial MR-ARFI-derived displacement images were acquired *in situ* after determining the location of the acoustic beam with optical tracking.

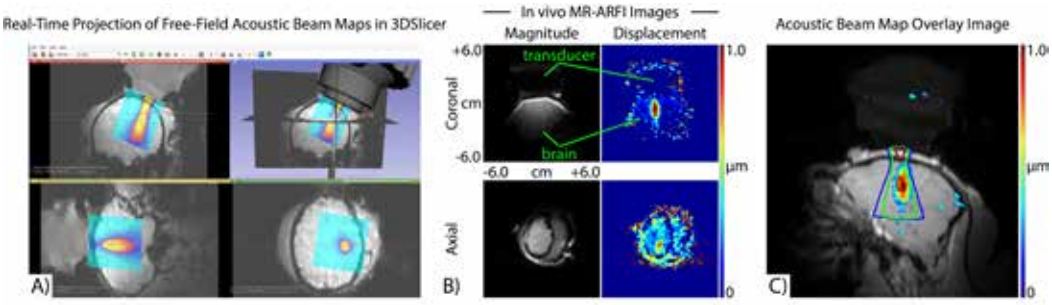

Figure 2. Our optical tracking workflow uses a Polaris Vicra with 3DSlicer to determine the location of the transducer in real-time. Transcranial MR-ARFI-derived beam maps acquired with optical tracking guidance show good agreement with free-field beam maps.

BR-49

Tuesday

23 October 2018

Topic: Brain – Technical
Presentation Type: Oral

The effect of study-dependent acoustic property relationships on transcranial focused ultrasound simulation results

Steve Leung, Taylor Webb, Rachelle Bitton, Pejman Ghanouni, Kim Butts Pauly

Stanford University, Stanford, California, United States

Background: In transcranial focused ultrasound (FUS) applications, the heterogeneity of skull alters the position, intensity, and shape of the beam's focus. 3D numeric simulations can be used to predict these focal spot characteristics and correct for them.

In general, numeric simulations use patient-specific skull models derived from computed tomography (CT) images of individual patients. For every voxel in a skull model, acoustic properties can be assigned according to its CT Hounsfield unit (HU) value. However, in the literature, there is substantial variability in the acoustic properties that are used for transcranial FUS simulations (Figure 1). Moreover, the acoustic property relationships can have [Webb2018, Leung2018] and not have [Connor2002, Aubry2003, Pinton2011, Pichardo2011, Kyriakou2015, Vyas2016, Robertson2017] specific dependence on CT acquisition parameters. The purpose of this work was to take a step back and investigate how a specific set of simulations can be affected by different published values for acoustic properties.

Methods: Patient-specific skull models were derived from computed tomography (CT) images, which were acquired on a General Electric scanner with 120 kVp, medium filter, and BONEPLUS reconstruction kernel. Every voxel was assigned acoustic properties according to its CT Hounsfield unit (HU) value using the curves given in Figure 1. We used the hybrid angular spectrum (HAS) method [Vyas2012] for simulations.

MR thermometry data were acquired during FUS treatment of patients with essential tremor, in which the ventral intermediate nucleus of the thalamus was the primary target. We compared the MR thermometry and simulation focal spots to evaluate simulation accuracy. Acoustic properties were modified to investigate their effect on simulation accuracy.

Results: The mean position errors are shown in Figure 2 for the frequency and phase encode directions. The mean position errors were not statistically significant across sets, indicating that the variations seen in Figure 1 (left) had little effect on the position.

The study-dependent acoustic properties resulted in a large range of simulated temperatures. While each attenuation curve from Figure 1 (right) gives a good fit to a line between MR thermometry temperature and simulation temperature ($r2 > 0.720$), the slopes of these curves are quite different from unity, indicating that the variations seen in Figure 1 (right) have a large impact on simulation.

Conclusions: Across studies, there is substantial variability in the acoustic properties used for transcranial focused ultrasound simulation. Only recently has there been work to measure how this variability is dependent on CT parameters [Webb2018].

Mean position error was not significantly different across the eight sets of acoustic properties, therefore the variability seen in the acoustic velocity relationships was not very influential. However, attenuation can greatly affect the simulated temperature.

It is important to note that this study does not help determine the optimal set of acoustic properties to use for simulation in general. The mappings from CT HU to acoustic properties are highly dependent on CT acquisition parameters, and there also exists variability between subjects [Webb2018].

Acknowledgements: NIH grant R01 MH111825, INSIGHTEC, FUSF

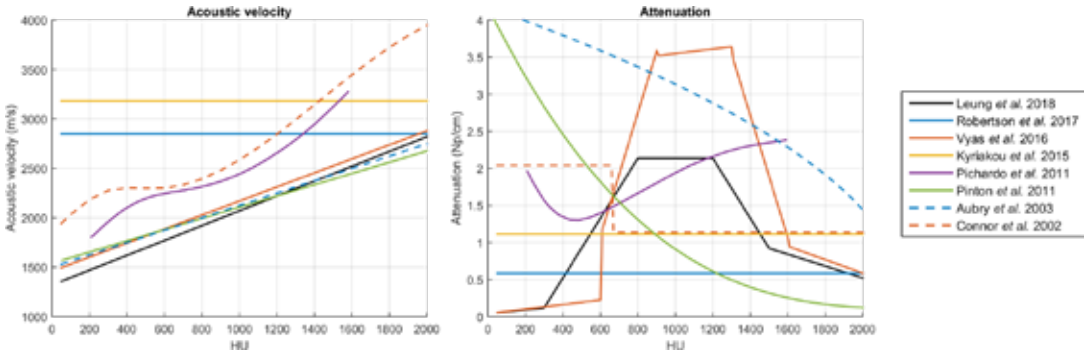

Figure 1. Study-dependent acoustic properties. There is little consensus in the literature as to the underlying relationships with HU.

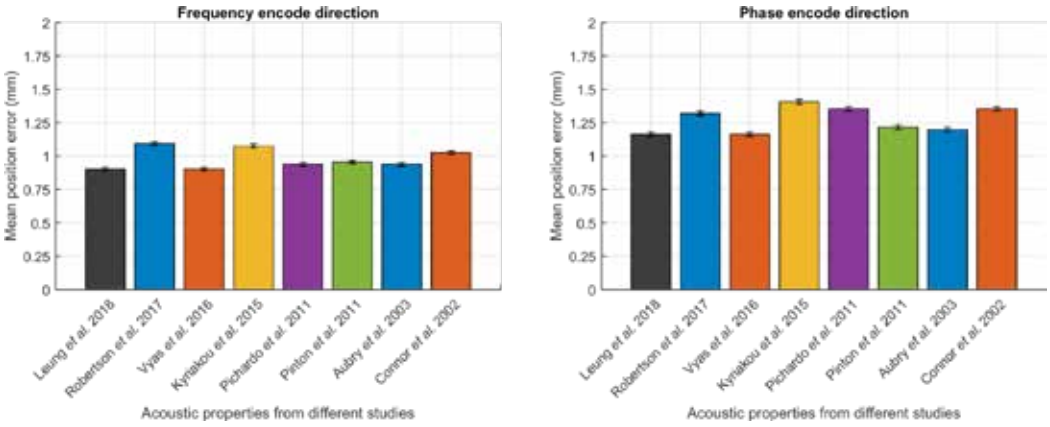

Figure 2. Mean position error due to study-dependent acoustic properties. The mean position error across 63 sonications is shown. Standard error bars are included.

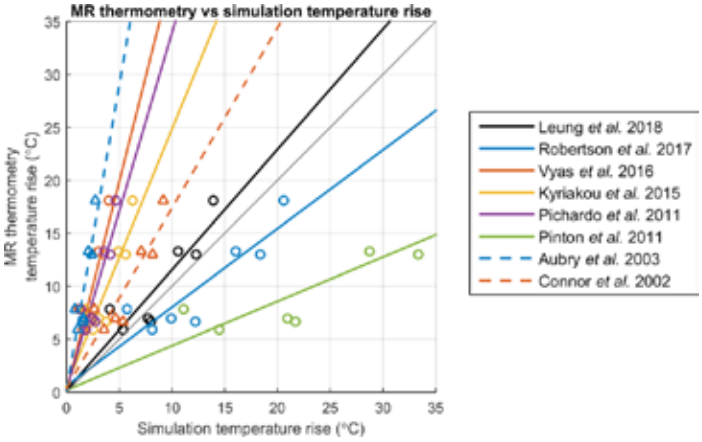

Figure 3. Comparison of MR thermometry and simulation temperature rise. The study-dependent acoustic properties result in a range of simulated temperature rises. Unity line is in gray.

BR-50

Tuesday

23 October 2018

Topic: Brain – Technical
Presentation Type: Oral

Towards an expanded transcranial treatment envelope: Update on the volumetric thermometry challenge

William Grissom[1], Henrik Odeen[2], Sumeeth Jonathan[1], Xue Feng[3], Dennis Parker[2], Craig Meyer[2], Kim Butts Pauly[4], John Snell[5]

[1]Vanderbilt University, Nashville, Tennessee, United States
[2]University of Utah, Salt Lake City, Utah, United States
[3]University of Virginia, Charlottesville, Virginia, United States
[4]Stanford University, Stanford, California, United States
[5]Focused Ultrasound Foundation, Charlottesville, Virginia, United States

Background: Whole-brain real-time MRI Temperature imaging is needed to expand the MRgFUS treatment envelope beyond the midbrain to include targets closer to the skull where reflections and locally high through-skull power densities increase the risk of unintended heating. Several groups have proposed new imaging pulse sequences and reconstructions to meet this need, but they have each been implemented on different scanner platforms (GE, Siemens, and Philips) and with different focused ultrasound systems, and a careful comparison between approaches has not been completed. To address this, we proposed the Volumetric Thermometry Challenge at the 2016 FUS Symposium, which comprises a head-to-head comparison of 3D segmented echo-planar (EPI) [Todd, MRM 2012], retraced in-out (RIO) stack-of-spirals [Fielden, MRM 2018], and EPI stack-of-stars [Jonathan, MRM 2018] acquisitions on the same scanner and with the same transcranial focused ultrasound device, to evaluate the strengths and weaknesses of each approach and make practical recommendations to the FUS community. Here we provide an update on the Challenge.

Methods: k-Space trajectories from each acquisition are shown in Figure 1. The major achievement to date is that all three sequences have been implemented in RTHawk 2.4.1 (HeartVista, Los Altos, CA, USA) on a GE Discovery MR750T 3T scanner (GE Healthcare, Waukesha, WI, USA) equipped with an INSIGHTEC ExAblate 650 focused ultrasound system (INSIGHTEC Ltd, Tirat Carmel, IL). The 3D segmented EPI acquisition is reconstructed using model-predictive filtering [Todd, MRM 2010], the RIO stack-of-spirals acquisition is reconstructed using gridding and Kalman filtering [Fielden, ISMRM 2014], and the stack-of-stars EPI acquisition is reconstructed using the k-space hybrid method [Gaur, MRM 2015].

Results: Figure 2 shows a table of the acquisition parameters for each method at the time of their original publication; these are also the default parameters of their RTHawk implementations. Figure 3 plots one TR for each pulse sequence as it appears in SpinBench, the RTHawk sequence editor. All three sequences collect a large 28 cm FOV to prevent the water bath from aliasing into the brain, and all have similar spatial resolution of 1.5-2 mm in-plane/3 mm through-plane. Figure 4 shows representative images or temperature maps from each acquisition, to illustrate their quality and coverage.

Conclusions: In addition to the parameters in Figure 2, for comparison the scans will be run in frame rate-matched (3-4 seconds/volume) mode to compare volume coverage, and in volume coverage-matched (FOV 28 x 28 x 12 cm^3, resolution 1.5 x 1.5 x 3 mm^3) mode to compare their frame rates. Scans in each mode will be collected *in vivo* without heating but with the water bath filled, to measure temperature precision. Scans will also be collected during phantom heating through a skull, to characterize hot spot distortion compared to a single-slice multi-echo 2DFT sequence.

Acknowledgements: Focused Ultrasound Foundation, NIH R01 DA 019912, T32 GM 007347, UVA-Coulter Translational Research Partnership, NIH R21 EB022309, NIH R01 EB013433, NIH R01 CA172787

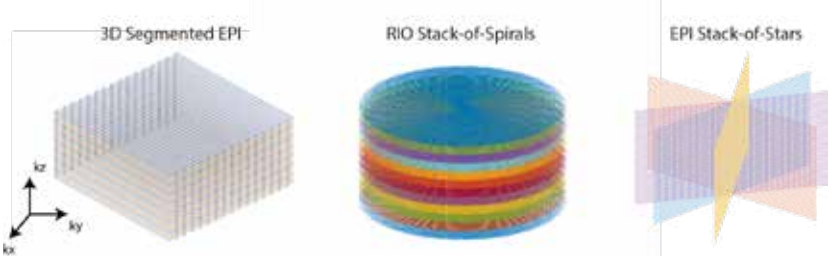

Figure 1. k-space trajectories. All sequences are phase-encoded in z. In each TR, the 3D Segmented EPI and RIO stack-of-spirals scans collect one z phase encode, while the EPI stack-of-stars scan collects all z phase encodes for one x/y projection.

	3D Segmented EPI	RIO Stack-of-spirals	EPI Stack-of-Stars
FOV	22 x 22 x 14.5 cm^3	28 x 28 x 3.6 cm^3	28 x 28 x 12 cm^3
Resolution	1.15 x 1.15 x 2.9 mm^3	1.5 x 1.5 x 3 mm^3	1.5 x 1.5 x 3 mm^3
Volume Scan Time	6.8 s	3.2 s	3.3 s
°C per pixel/direction	60°C/y	75°C/x-y (equivalent)	25°C/z

Figure 2. Sequence parameters. °C per pixel is the temperature rise at 3T required to cause a one pixel shift; the value reported for the RIO stack-of-spirals sequence is its approximate equivalent 2DFT value.

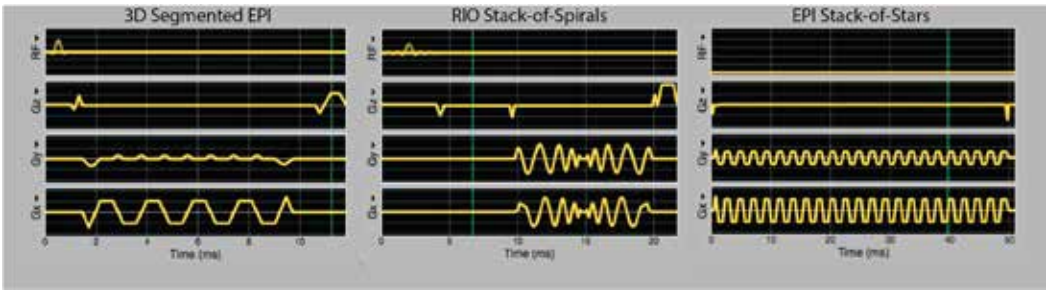

Figure 3. One TR of each sequence as it appears in SpinBench, the RTHawk sequence development environment. The slab excitation pulse of the EPI stack-of-stars sequence is in a separate subsequence, to facilitate rotating the readout gradients.

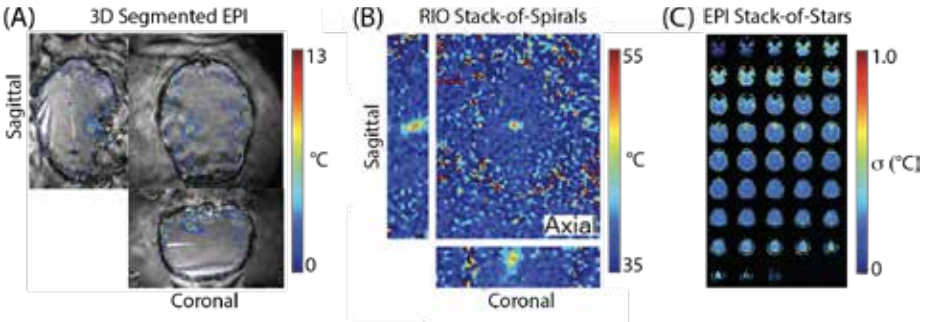

Figure 4. (A) Phantom temperature maps acquired with the 3D Segmented EPI scan. (B) Maps acquired with the RIO stack-of-spirals scan during porcine brain heating. (C) Temperature precision maps from the EPI stack-of-stars scan in a volunteer.

BR-51

Tuesday

23 October 2018

Topic: Brain – Technical
Presentation Type: Oral

Towards low-cost transcranial focused ultrasound: Pushing the limits of single element technology

Guillaume Maimbourg, Alexandre Houdouin, Roxane Lahady, Bruno Souchu, Mickael Tanter, Jean-François Aubry

Institut Langevin, ESPCI Paris, CNRS UMR7587, Inserm U 979, PSL Research University, Paris, France

Background: Transcranial focused ultrasound has shown efficacy in a growing number of brain conditions. The development of the next generation of transcranial devices should aim at reducing their cost without compromising on efficiency or safety. To address these challenges, we have developed disruptive technologies to:

1. compensate the aberrations induced by the human skull by using a single element transducer covered with a patient and target specific 3D-printed acoustic lens[1];
2. binary localize (inside/outside the brain) cavitation activity based on the lowpass filter effect of the skull on the harmonic content of the acoustic bubble response recorded by a single element passive cavitation detector (PCD)[2].

Methods:

1. The study were conducted on N=3 human skulls. A numerical simulation based on CT data provides the phase shifts for each skull. This shift is converted into local thickness (Error! Reference source not found.(b)) of the acoustic lens. The acoustic lens is casted in silicone (c_silicone=1000 "m/s"), thanks to a 3D-printed mold. Then, the quality of the focusing through the skull is assessed by performing a 3D scan of the pressure field (Error! Reference source not found.(a)). Finally, we assessed the steering capability of such a device. The transducer is moved relatively to the skull to target areas up to 10mm away from the initial target into the transverse and longitudinal direction.
2. A PCD recorded the acoustic activity during thermal necrosis (Figure 2(a)). Experiments were conducted *in vitro* with N=6 human skulls and one monkey skull. To achieve the binary localization of microbubbles activity, we computed ultraharmonics ratios.

Results:

1. The acoustic lens qualitatively restores the focusing: the energy is concentrated at the immediate vicinity of the target without side lobe effects. Over three skulls, the average acoustic intensity at the target is ten times higher when using the acoustic lens. Concerning the steering capability, transverse error is always below 1mm for x-steering up to 11.2mm but maximum acoustic intensity significantly decreases (50%) for a 11.2mm steering compared to the case without any steering.
2. Cavitation induced sub and ultra harmonics (Figure 2(a), in grey). Ultraharmonics ratios significantly decreases when the acoustic signal propagates through human or monkey skulls (Figure 2(b)), blue plots compared to black one). A 22dB threshold discriminates cavitation occurring inside or outside the skull.

Conclusions: We showed that a single element covered with a patient specific acoustic lens is able to restore a good focusing though the skull. Furthermore, we established that the safety can be improved by binary localizing cavitation activity with one single PCD. These approaches pave the way to low cost and yet efficient transcranial brain therapy.

This work was supported by the Bettencourt Schueller Foundation and the Agence Nationale de la Recherche under the program Future Investments with the reference ANR-10-EQPX-15.

References

1. Maimbourg, G., et al. 3D-printed adaptive acoustic lens as a disruptive technology for transcranial ultrasound therapy using single-element transducers. *Physics in Medicine and Biology*, 2017.
2. Maimbourg, G., et al. Inside/outside the brain binary cavitation localization based on the lowpass filter effect of the skull on the harmonic content: a proof of concept study. *Physics in medicine and biology*, 2018.

Figure 1

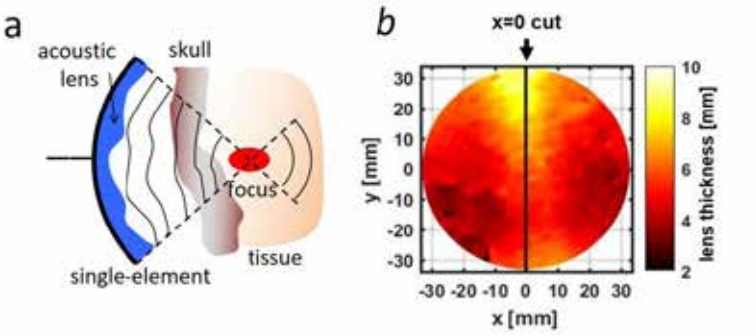

Figure 2

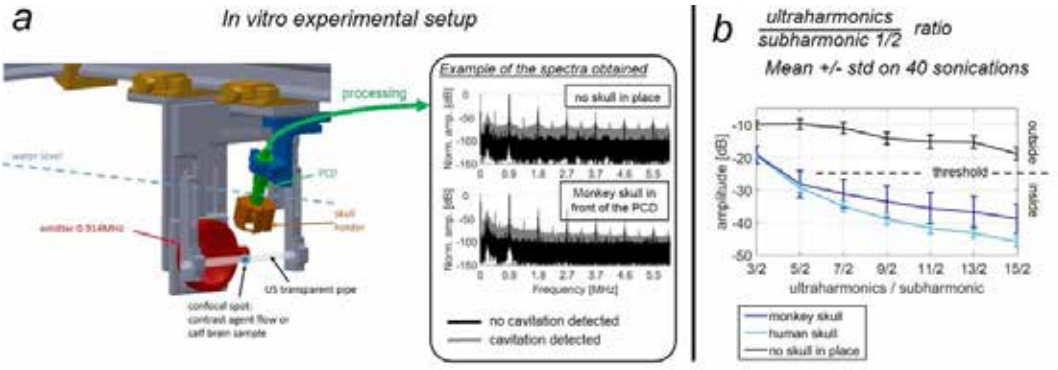

BR-52

Tuesday

23 October 2018

Topic: Stroke
Presentation Type: Oral

FUS combined with intra-arterial mitochondria transplantation for ischemic stroke

Pedro Norat[1], Catherine Gorick[1], Petr Tvrdik[1], Richard Price[1], Melanie Walker[2], Michael Levitt[2], Yashar Kalani[3]

[1]University of Virginia, Charlottesville, Virginia, United States
[2]University of Washington, Seattle, Washington, United States
[3]University of Virginia School of Medicine, Charlottesville, Virginia, United States

Background: Stroke is the third leading cause of death and the leading cause of long-term morbidity in the United States[1]. In 2008, the cost of care for stroke patients amounted to $18.8 billion, and it is estimated that this population had an additional $15.5 billion in loss of productivity. The state of Virginia has an annual age-adjusted stroke rate of 3%, placing it amongst the states most affected by stroke. This means that this year, 199,319 Virginians have had a stroke and are living with the disability caused by this stroke; and, that in the past year nearly 3,300 Virginians have died due to stroke[2]. Focused ultrasound (FUS) has recently been demonstrated to have the efficacy and safety for selective targeting of deep-seated regions of the brain[3]. In this work, we used FUS to selectively open the blood-brain barrier (BBB) at the site of stroke-induced injury and delivered therapeutics, notably mitochondria to assist with minimizing reperfusion injury in the ischemic penumbra after stroke.

Methods: Cerebral ischemia was modeled in mice by performing selective middle cerebral artery occlusion (MCAO) for 1 hour followed by reperfusion. Six hours after reperfusion the mice were treated with microbubbles and FUS to open the blood barrier followed by intra-arterial delivery of 109 prospectively isolated mitochondria from muscle. The animals were then sacrificed at the completion of experiments, the brain dissected and subjected to immunohistochemical analysis.

Results: As expected stroke induces partial opening of the blood-brain barrier at the site of ischemia. The addition of FUS allows for a more robust opening of the blood-brain barrier. Intra-arterial delivery of mitochondria to the ischemic penumbra in enhanced with use of FUS with microbubbles.

Conclusions: Given the impact of ischemic stroke on the population of the United States and the lack of availability of agents that can assist with post-stroke recovery, a therapeutic regimen targeting this patient population is greatly needed. The ability of FUS to selectively open the BBB allows for the systemic delivery of reagents that may be able to decrease the severity of reperfusion injury. Therapies that can aid improve patient outcomes after stroke have the potential to improve patient quality of life and decrease costs to the health-care system and the families of patients afflicted by stroke.

References

1. Tymianski M. Novel approaches to neuroprotection trials in acute ischemic stroke. *Stroke* 2013;44(10):2942-50.
2. VDH Division of Population Health Data, Virginia Health Information, 2017.
3. Elias WJ et al. A Randomized Trial of Focused Ultrasound Thalamotomy for Essential Tremor. *N Engl J Med* 2016;275:730-9.

BR-53

Tuesday

23 October 2018

Topic: Psychiatric Disorders

Presentation Type: Oral

Bilateral thermal capsulotomy with MR-guided focused ultrasound for patients with treatment-resistant depression: A proof of concept study

Jin Woo Chang

Department of Neurosurgery, Yonsei University College of Medicine, Seoul, Republic of Korea

Background: This preliminary study investigated the use of a magnetic resonance-guided focused ultrasound (MRgFUS), novel, minimally invasive, noncranium-opening surgical technique in bilateral thermal capsulotomy for patients with treatment-resistant depression.

Methods: Four patients with treatment resistant depression received open-label bilateral thermal capsulotomy at anterior limb of internal capsule via MRgFUS. Patients underwent comprehensive neuropsychological evaluations and imaging at baseline, 1 week, 1 month, 6 months and 12 months following treatment. Outcomes were measured with the Hamilton Rating Scale for Depression (HAM-D) and Beck Depression Inventory (BDI), and treatment-related adverse events were evaluated.

Results: Three out of four patient showed almost immediate and sustained improvements in depression (a mean reduction of 61.1%). No adverse events (physical or neuropsychological) were reported in relation to the procedure. In addition, there were no significant differences found in the comprehensive neuropsychological test scores between the baseline and 6 or 12 months time points.

Conclusions: This study demonstrates that bilateral thermal capsulotomy with MRgFUS can be used without inducing side effects to treat patients with treatment resistant depression. If larger trials validate the safety, effectiveness and long-term durability of this new approach, this procedure could considerably change the clinical management of treatment resistant depression.

Acknowledgements: This work was supported by the Focused Ultrasound Foundation (Charlottesville, VA).

BR-54

Tuesday

23 October 2018

Topic: Neuropathic Pain
Presentation Type: Oral

Treatment of neuropathic pain in amputated patients using MRgFUS technology

Alicia Nachtigal[1,2], Ronen Cozacov[3], Shlomi Rudich[4], Lilach Shay[4], Gena Korol[4], Anat Grinfeld[5], Motti Tamansky[6], Elon Eisenberg[1,3]

[1]Hillel Yaffe Medical Center, Hadera, Israel
[2]Technion–Israel Institute of Technology, Haifa, Israel
[3]Institute of Pain Medicine, Rambam Health Care Campus, Haifa, Israel
[4]INSIGHTEC Ltd, Tirat Carmel, Israel
[5]Rambam Health Care Campus, Haifa, Israel
[6]Pain Clinic, Loewenstein Hospital, Raanana, Israel

Background: Neuroma is a non-neoplastic lesion that develops following nerve injury, due to trauma or surgical procedures (e.g., amputation), and most commonly found in the extremities of the body. This lesion can cause neuropathic pain, resulting in limited physical functioning and significant decrease in quality of life. Current treatment modalities are various and include pain control using analgesics, re-approximation of nerve endings in injury site and re-embedding of the nerve stump into a different tissue away from scar tissue.

In this work we present our initial clinical experience in employment of Magnetic Resonance Imaging guided Focused Ultrasound (MRgFUS) as a novel, non-invasive approach for treatment of traumatic neuropathic pain.

Methods: From August 2017, 5 patients suffering from painful traumatic neuromas in their lower limbs following amputation, were treated under an IRB approved study. The study is performed using a 3T MRI scanner (Discovery MR750, GE, Milwaukee, WI), equipped with an MRgFUS system with a 208 elements phased array transducer (Exablate 2100V1, INSIGHTEC, Haifa, Israel). All patients were positioned on the MRgFUS table, with the neuroma centered within the acoustic window of the transducer and anesthetized using general anesthesia. Skin hair was removed from treatment area pass-zone, and water bags and gel pads were used to achieve optimal acoustic coupling. A three-plane localizer was performed to verify adequate acoustic coupling and patient positioning, followed by T2-weighted treatment planning sequences, which were then loaded into the Exablate workstation. After a treatment plan was prescribed on the workstation by the operator, a low-energy test sonication was performed to confirm accuracy of system setup and ultrasound beam. Then, therapeutic sonications were delivered, using an ultrasound frequency in the range of 1-1.15 MHz and energies reaching up to 4800J, to ablate the lesion. Post-treatment T1-weighted contrast enhanced sequences were used to evaluate treatment outcome.

Results: No safety events were reported in this study so far. As the study is currently ongoing, efficacy results are still preliminary, and showing ability to target and ablate neuroma using focused ultrasound (FUS). Several factors seem to contribute to ablation of the neuroma, including: (1) usage of high energy sonications, (2) hypo-intensity of the neuroma on T2-weighted images, (3) location of bone tissue in the far field and adjacent to the neuroma and (4) homogeneity of tissue in the near field of the neuroma. Initial results also suggest that partial ablation of neuroma might have beneficial clinical effect (e.g., pain reduction) as well.

Conclusions: Initial clinical experience with MRgFUS for treatment of neuropathic pain in amputated patients, show high safety profile and suggest that this non-invasive procedure is a feasible treatment modality. Additional clinical experience is required to fully evaluate the limitations of this novel treatment approach, as well as to optimize patient selection and treatment methods for improved clinical outcome.

CA-1

Tuesday

23 October 2018

Topic: Brain Tumors
Presentation Type: Oral

A feasibility safety study using transcranial magnetic resonance image-guided focused ultrasound in the management of benign centrally located intracranial tumors which require clinical intervention in pediatric and young adult subjects

Travis Tierney[1], Kambiz Alavian[2], Nolan Altman[3], Michael Duchowny[3], Ann Hyslop Segeren[3], Ian Miller[3], John Ragheb[3], Prasanna Jayakar[3]

[1]Miami Children's Hospital, Coral Gables, Florida, United States
[2]Imperial College London, London, United Kingdom
[3]Nicklaus Children's Hospital, Miami, Florida, United States

Background: Under an Investigational Device Exemption (IDE no. G160189), we are evaluating the safety and feasibility of transcranial magnetic resonance image-guided focused ultrasound thermoablation for the treatment of benign centrally-located brain tumors in 10 children and young adults. This report describes our first three cases.

Methods: IRB approval and informed consent were obtained to treat 2 females with a hypothalamic hamartoma remnant and one male with a subependymal giant cell astrocytoma under general anesthesia. The study is open to subjects 8 to 22 years of age who require surgical intervention for a benign centrally-located brain tumor. Please see ClinicalTrials.gov identifier NCT03028246 for full exclusion and inclusion criteria. In each case, the Exablate 4000 system (INSIGHTEC, Haifa, Israel) was used to target and thermally ablate target tissue. The patients have been follow for 15, 6 and 3 months, respectively, according to the study protocol.

Results: Successful thermoablation of target tissue was achieved in both hamartoma cases with immediate cessation of gelastic seizures. The first patient had transitory relapse around the time of an unplanned antiepileptic drug withdrawal, but is seizure free at 15 months. The second patient remained seizure free through interval 6 month follow up. In both cases, durable cessation of epilepsy was accompanied by subjective improvement in mood and memory. Near-field calcium and acoustic cavitation events precluded complete thermal ablation of the subependymal giant cell astrocytoma in the third patient. No postoperative endocrine, cognitive or motor complications occurred in any case.

Conclusions: Focused ultrasound surgery can be used safely to treat epilepsy associated with hypothalamic hamartomas. It is less certain that calcium-bearing tumors like subependymal giant cell astrocytomas can be treated with focused ultrasound. More work is necessary to further refine optimal patient selection criteria and definitively demonstrate the safety of focused ultrasound in treating other subcortical tumors younger children.

Acknowledgements: The Focused Ultrasound Foundation of Virginia (no. FUS 530 to TST) funded this trial (ClinicalTrials.gov identifier NCT03028246). The device manufacturer, INSIGHTEC, is our FDA regulatory sponsor but we have not requested any commercial financial support for this study. We thank Mor Dyan and Jacob Chen for invaluable advice and technical support of these cases.

CA-2

Tuesday

23 October 2018

Topic: Brain Tumors
Presentation Type: Oral

Focused ultrasound stimulates glioma-derived extracellular vesicle release *in vitro*

Alec Batts, Natasha Sheybani, Richard Price

University of Virginia, Charlottesville, Virginia, United States

Background: Extracellular vesicles (EVs) are characterized as a population of cell-derived vesicles ranging from 50-500 nm in size whose biological function remains to be elucidated. Microvesicles and exosomes constitute two classes of EVs, and can vary extensively in origin and proteomic content. Microvesicles arise from exophytic budding of plasma membrane, while exosomes (ranging in size from 30-100 nm) arise endosomally, via endocytic vesicle fusion to plasma membrane and subsequent exophytic budding. Although specific distinctions between these types of EVs are poorly characterized, both subpopulations contain representative proteins, mRNA, miRNA, lipids and DNA of their parent cell, pointing to a potential role in intercellular signaling. Given the emerging role of EVs in signaling in the tumor microenvironment (TME), FUS-elicited changes in EV release from cancer cells could exert a strong influence on tumor biology. Here, using *in vitro* platforms, we tested the hypothesis that FUS-mediated hyperthermia and/or microbubble-activation elicits increased EV secretion from glioma cells.

Methods: For hyperthermia experiments: GL261-luc2 murine glioma cells were seeded into Celartia PetakaG3-HOT chambers ~24 hours before FUS exposure (1.1 MHz, 252 sonications, 5W input power, 5s duration) (Figure 1A-B). A MATLAB simulation was used to estimate the expected heating profile at the surface of the PetakaG3 (Figure 1C-D). For FUS+MB cavitation experiments: Nunc OptiCell culturing devices seeded with U87-MG human glioma cells were supplemented with 1.5e+07 microbubbles/ml albumin-shelled MB immediately prior to FUS treatment. A 1 MHz unfocused transducer was positioned ~1.5 in above the OptiCell (transducer-chamber orientation orthogonal to that displayed in Figure 1A), for insonation of cells at a peak negative pressure (PNP) of either 300 or 500 kPa via raster scan (0.5% duty cycle, translation speed ~ 2.0 mm/s). Fifteen minutes following FUS exposure, supernatant was isolated and clarified for EV isolation. EVs were purified by differential ultracentrifugation. Particle concentration and size distributions were determined using NanoSight nanoparticle tracking analysis.

Results: Both FUS hyperthermia and FUS+MB cavitation elicited a statistically significant increase in EV release from their respective glioma cell lines compared to untreated controls. Hyperthermia resulted in a ~42% increase in GL261-luc2-derived EVs (Figure 2A) and a maximum CEM43C of 0.14 min. FUS+MB cavitation conferred a ~5-fold increase above control in mean U87-MG-derived EV concentration across both PNPs evaluated (Figure 2B). PNP did not significantly impact EV secretion. EV size distribution (Figure 2C) did not change significantly as a function of FUS exposure. The mode size across all samples was 102.24 ± 5.02 nm.

Figure 1 (A-D)

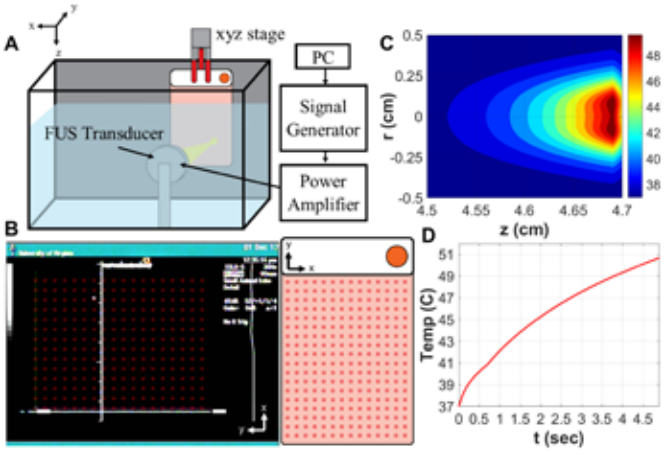

Figure 2 (A-C)

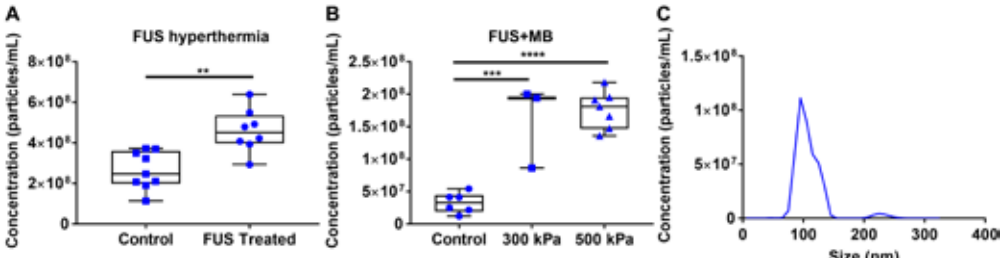

Conclusions: Our results indicate that direct application of both FUS-mediated hyperthermia and microbubble activation elicits a marked increase in glioma-derived EV release into surrounding environment. This effect could have significant implications for altering cell-cell signaling in the TME. Ongoing studies are aimed at validating the prevalence of EV subtypes in our isolates and evaluating whether thermal and mechanical FUS exposure differentially impact the proteomic profile of glioma-derived EVs. Our future efforts will be directed toward testing this hypothesis in other tumor cell lines and performing mechanistic studies aimed at uncovering the biological implications of our findings.

CA-3

Tuesday

23 October 2018

Topic: Brain Tumors
Presentation Type: Oral

Results from 72 transient blood-brain barrier (BBB) disruptions by an implantable low intensity pulsed ultrasound (LIPU) device: A safety and feasibility study in recurrent glioblastoma patients

Alexandre Carpentier[1], Michael Canney[2], Carole Desseaux[2], Alexandre Vignot[2], Bruno Law-Ye[1], Delphine Leclercq[1], Lisa Belin[1], Marc Sanson[1], Khe Hoang-Xuan[1], Jean-Yves Delattre[1], Ahmed Idbaih[1]

[1]APHP, Paris, France
[2]CarThera, Paris, France

Background: The BBB limits the efficacy of drug therapies in the brain by blocking the passage of systemically administered drugs to diseased tissue. Two to four minutes of LIPU in combination with injection of micron-sized microbubbles can transiently disrupt the BBB to increase the passage of drugs such as carboplatin.

Methods: This first-in-man, single arm, monocentric trial was performed at Hôpital Universitaire Pitié-Salpêtrière, Paris, France from 2014-2018. GBM patients at any recurrence were implanted with (1) or (3) 1 MHz, 10-mm diameter cranial devices (SonoCloud®) in burr holes during debulking surgery or during a dedicated procedure under local anesthesia. Ultrasound dose was escalated over 7 patient cohorts in a 3+3 design. The implantable ultrasound device was activated monthly in a <15 minute procedure to transiently disrupt the BBB before intravenous administration of carboplatin (AUC4-6). BBB disruption was visualized using T1w contrast-enhanced magnetic resonance imaging (MRI) and patients were monitored clinically.

Results: Twenty-seven patients were implanted with LIPU devices and 25 per-protocol were sonicated from 2014-2018. A total of 19 patients were treated with (1) US emitter, SonoCloud-1 (SC1), and six patients were treated with (3) US emitters, SonoCloud-3 (SC3). In 85 ultrasound sessions, BBB disruption was visible on post-sonication T1w MRI for 72 sonications was ultrasound pressure dependent. Reported device or procedure-related adverse events were transient and manageable: two cases of transient edema (H1 and D15) and one transient facial palsy. No carboplatin-related neurotoxicity was observed nor infection.

In the SC1 group, patients with no or poor BBB disruption (n=8) had a shorter median PFS and OS than patients with clear BBB disruption (n=11). Two patients in the SC1 group had 10 monthly sonications and 1 patient in the SC3 group had 12 monthly sonications. Patients treated by repeated sonications showed no signs of attenuation of BBB disruption over time or evidence of additional toxicity.

Conclusions: LIPU was well-tolerated and may increase the effectiveness of drug therapies in the brain. The sonication of larger volumes of brain in recurrent GBM will be investigated in a future trial using a larger SonoCloud device and may further enhance the observed effectiveness of this treatment modality. Clinical trial information: NCT02253212.

CA-4

Tuesday

23 October 2018

Topic: Brain Tumors
Presentation Type: Oral

The feasibility of achieving peritumoral blood-brain barrier opening using focused ultrasound with nanobubbles under real-time acoustic feedback control in a F98 glioma-bearing rodent model

Bingbing Cheng, Chenchen Bing, Vamsidhara Vemireddy, Debra Szczepanski, Ming Xu, Robert Bachoo, Rajiv Chopra

UT Southwestern Medical Center, Dallas, Texas, United States

Background: Glioblastoma multiforme (GBM) is the most lethal primary brain tumor, with aggressive and fatal progression of disease inevitable. During the early infiltration of GBM cells into normal brain regions surrounding the primary tumor, this peritumoral environment has an intact blood-brain barrier (BBB) which inhibits the delivery of therapeutic agents. BBB disruption with focused ultrasound (FUS) could be used to achieve peritumoral delivery of therapeutic agents to tackle infiltrative cancer progression. Previously, we have demonstrated BBB opening in normal rat brain using focused ultrasound with nanobubbles under real-time acoustic feedback control. The goal of this study is to evaluate the feasibility of BBB opening in a region encompassing both tumor and peripheral tissues in F98 glioma-bearing rats and to evaluate the brain vascular/tissue response to the FUS exposures.

Methods: F98 tumor cells (10,000 cells) were injected slowly into the striatum of the brain (Fisher rats). Subsequent tumor growth was monitored using contrast enhanced gradient echo MRI (GRE, TE: 2.8ms, TR: 13.2ms, flip: 30°, 80mm FOV, 256×256, 1mm slice). Eight days post-implantation, pulsed focused ultrasound exposures (f0 = 0.5MHz, pulse duration = 10ms, period = 1s, duration = 30s) were delivered using a custom stereotactic system (Figure 1). The exposures were delivered in a 3x3 grid with 2 mm spacing to cover both the tumor and peritumoral region (Figure 2). At each target, stimulated acoustic emissions were monitored and controlled to a target threshold at an ultra-harmonic frequency (0.75 MHz). The infusion rate of nanobubbles during FUS was 0.3 ml/min. Contrast enhanced MRI were used to evaluate the BBB opening. The brain tissue response was evaluated by immunohistochemistry at time points of 6 hours, 24 hours, 3 and 7 days post-treatment.

Results: Figure 3 shows the tumor growth rate. By 9 days, tumor diameter was approximately 2-3 mm. Histology performed on the tumors confirmed the exposed region included peritumoral regions with infiltrative tumor cells. The mean pressure using feedback control across all locations was 0.3 MPa. Contrast enhanced MRI images acquired before and after the treatment identified the GBM tumor and BBB opening (Figure 4).

Conclusions: It is feasible to open the BBB of the peritumoral region using focused ultrasound with nanobubbles under real-time acoustic feedback control in a GBM tumor-bearing rat model.

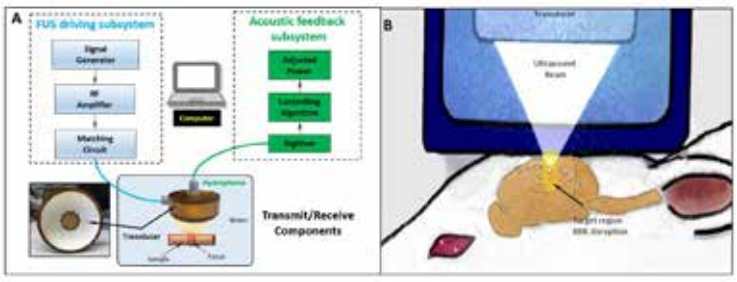

Figure 1. Experimental setup. A: Components of the ultrasound system used in this study, including: a focused ultrasound transducer driving subsystem and a hydrophone-based acoustic feedback subsystem. B: *In vivo* FUS-induced BBB opening setup.

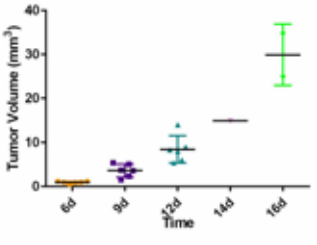

Figure 2. FUS exposure strategy for GBM tumor implants. The ellipsoidal focal volume (dashed line) of the ultrasound beam will be overlapped in a 2D raster fashion to open the BBB in the GBM tumor and margin.

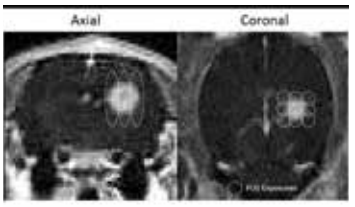

Figure 3. (top right) GBM tumor volume as a function of time. The x axis represents days after implantation.

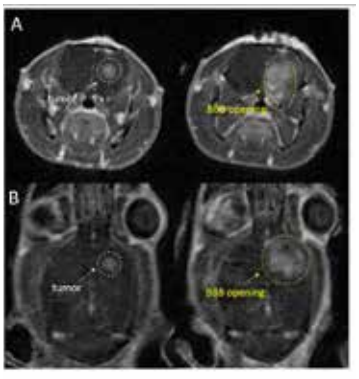

Figure 4. (bottom right) Contrast enhanced MR images of GBM tumor before and after ultrasound exposures in axial (A) and coronal (B) scan.

CA-5

Tuesday

23 October 2018

Topic: Brain Tumors
Presentation Type: Oral

Focused ultrasound treatment of cerebral cavernous malformations

Pedro Norat[1], Min Park[1], Petr Tvrdik[1], Kevin Lee[1], Yashar Kalani[2]

[1]University of Virginia, Charlottesville, Virginia, United States
[2]University of Virginia School of Medicine, Charlottesville, Virginia, United States

Background: Stroke is the leading cause of morbidity in the United States. Hemorrhagic stroke constitutes 15% of all stroke and can be caused by rupture of aneurysms or vascular malformations. Cerebral cavernous malformations (CCMs) have a prevalence of 0.5% in the general population, meaning 1,800,000 Americans harbor a CCM. These lesions represent a significant cause of disability in the young. Current treatment options for patients with CCMs are observation or surgery. Surgery for superficial lesions is well-tolerated but results of surgery for deep-seated lesions are less favorable, with up to 50% of patients suffering deficits, in the most experienced hands. Therefore, an alternative regimen for treatment of deep-seated CCMs is greatly needed. We aimed to use FUS to target and treat deep-seated CCM in a mouse model of the disease.[1,2,3] FUS can be safely used to target deep-seated vascular lesions, and if this technology proves efficacious in treating CCMs, it would provide a minimally invasive modality for treatment of a common and devastating cause of stroke in the young.

Methods: Animal models of CCM disease in mice were generated using established induced endothelial knockout of the CCM1 gene on postnatal day 1. At 30 days of age, the animals in the disease cohort were randomized to treatment with FUS or sham treatment. A baseline MRI and MRIs after treatment or sham were performed. Both non-thermal and thermal FUS were used. After MRI the animals were sacrificed 6 hours after intervention, the brain dissected and subjected to immunohistochemical analysis. A cohort of animals were treated with 5-Aminolevulinic acid (5-ALA) to assess if this drug collects into the caverns of the vascular malformation with the aim of using 5-ALA as a sono-sensitizer.

Results: The CCM1 conditional knockout mouse generated cavernous malformations as expected. The addition of 5-ALA allowed for accumulation within the caverns of the cavernous malformation suggesting that this drug could be used as a sono-sensitizer to focus a more robust dose of FUS to these malformations while sparing unaffected brain.

Conclusions: Given the prevalence of CCMs, the morbidity associated with their hemorrhage, and risks associated with surgery, a non-surgical treatment for CCMs is greatly needed. Identification of an alternative treatment modality, such as FUS, with efficacy at modulating CCM biology will greatly improve care of this patient population while minimizing cost associated with the care of this often-young cohort of patients affected by stroke.

References

1. Mleynek TM et al. Lack of CCM1 induces hypersprouting and impairs response to flow. *Hum Mol Genet.* 2014;23:6223-34.
2. Boulday G et al. Tissue-specific conditional CCM2 knockout mice establish the essential role of endothelial CCM2 in angiogenesis: implications for human cerebral cavernous malformations. *Dis Model Mech.* 2009;2:168-77.
3. Zhou JH et al. Endothelial exocytosis of angiopoietin-2 resulting from CCM3 deficiency contributes to cerebral cavernous malformation. *Nat Med.* 2016;22:1033-1042.

CA-6

Tuesday

23 October 2018

Topic: Brain Tumors
Presentation Type: Oral

Sonodynamic therapy for glioblastoma cells using 220-kHz transcranial MRI-guided focused ultrasound system and 5-aminolevulinic acid

Hiroyuki Kobayashi[1], Michiharu Yoshida[2], Shunsuke Terasaka[1], Hajime Kamada[2], Kiyoihro Houkin[1]

[1]Hokkaido University, Sapporo, Japan
[2]Hokuto Hospital, Obihiro, Japan

Background: Malignant glioma, particularly glioblastoma multiforme has one of the worst prognoses among brain tumors, because existing adjuvant therapies such as radiation or chemotherapy has not exerted sufficient effect. Therefore it is indispensable to develop totally different ideas and methods. Among the new attempts, sonodynamic therapy (SDT) has been a unique presence. We focused on this and investigated the effect of SDT for glioma cell line using lower frequency focused ultrasound (FUS) device with 5-aminolevulinic acid (ALA) as a sonosensitizer.

Methods: In this study, our group investigated the efficacy of SDT using a 220-kHz transcranial MRI-guided FUS (TcMRgFUS) system (INSIGHTEC, Israel) in combination with 5-ALA for the treatment of malignant glioma cells *in vitro*. Cultured F98 rat glioblastoma cells were co-incubated with 5-ALA 4 hours before SDT. Cells were transferred into a black polypropylene test tube and then sonicated with FUS. To determine optimal condition, sonication was performed with 1024 transducer elements under the following conditions: frequency, 220 kHz; total energy, 400–4000 J; output power, 10–20 W; duration of irradiation, 120–240 s; duty cycle, 10–100%. During sonication, target medium temperature was kept < 42 °C. Cell morphology, viability and apoptosis were evaluated by microscopy, WST-1 (cell proliferation) assay, fluorescence staining and western blot analysis at 20 hours after SDT.

Results: WST-1 assay showed reduction of cell viability depended on both duration of sonication and output power. Regarding total energy, at least 2000 J was necessary for cytotoxic effect, and about 80 % of cells were killed by 4000 J SDT. Besides, the relation between cell damage and the duty ratio was not observed. Fluorescence microscopic observation showed that most cells in the SDT group were in the late phase of apoptosis. And a western blot analysis of cytosolic extracts revealed, comparing with control, 5-ALA group and FUS group, that SDT induced caspase-3 cleavage.

Conclusions: Our *in vitro* data suggested the possibility that even a lower total ultrasound energy can achieve cytotoxic effects using the 220-kHz TcMRgFUS in conjunction with 5-ALA as compared to treatment aiming thermal coagulation by FUS alone. And it was demonstrated that induction of apoptosis was a key mechanism of cell damage in SDT. Further, efficacy of SDT was observed within the range of physiological temperature. Although various conditions should be improved, SDT can be expected as a less-invasive, safe and sustainable novel treatment strategy for malignant gliomas.

Acknowledgements: This project was supported by a grant from Takeda Pharmaceutical Company, Japan (no. RS2016A001453). The authors thank INSIGHTEC Ltd. (Tirat Carmel, Israel) for technical support.

CA-7

Tuesday

23 October 2018

Topic: Brain Tumors
Presentation Type: Oral

Sonodynamic therapy in malignant glioma model and future direction of personalized focused ultrasound therapy for brain tumors

Michiharu Yoshida[1], Yasutaka Kato[2]

[1]Hokuto Hospital, Obihiro, Japan
[2]Hokuto Hospital/Keio University, Obihiro, Japan

Background: Sonodynamic therapy (SDT), Blood-brain barrier (BBB) opening, thermal ablation are expected as new therapeutic ultrasound modality for brain tumors. SDT is based on non-thermal synergistic effect of ultrasound and the specific sonosensitizers, such as 5-aminolevulinic acid (ALA). The work reported here aimed to develop personalized focused ultrasound (FUS) therapy for brain tumors by establishment of primary human glioblastoma cells to evaluate the cancer genes & 5-ALA intake after pilot study by using rat glioblastoma model.

Methods:

1. F98 rat glioblastoma models were irradiated with 220-kHz transcranial MRI-guided FUS (TcMRgFUS) system (INSIGHTEC, Israel) (total energy, 500 J; output power, 18 W; duration of irradiation, 30 s; duty cycle, 100%; target temperature ≤ 42 °C; 10 repeats) following 100 mg/kg 5-ALA treatment, and the anti-tumor effects were assessed based on changes in tumor volume and histology.
2. A glioblastoma patient-derived fresh tissue was collected with written informed patient consent, and target gene panels of 160 genes for whole body cancer & 50 genes for brain tumors were run using next-generation sequencing (NGS). The accumulation of 200 μg/ml 5-ALA after 4 h co-incubation was evaluated with the primary glioblastoma cell cultures.

Results:

1. The TcMRgFUS/5-ALA combination suppressed tumor proliferation and invasion, while causing minimal damage to normal brain tissue.
2. Remarkable CDK4 amplification was detected and suggested CDK4/6 inhibitor (Palbociclib) treatment recommendation. In addition, high up-take of 5-ALA was detected in the primary cells.

Conclusions: SDT with 220-kHz TcMRgFUS and 5-ALA can be safely used for the treatment of malignasnt glioma. Technology of SDT & drug assay by using primary cell culture & NGS may enable personalized FUS therapy for brain tumors.

Acknowledgements: The authors thank INSIGHTEC Ltd. (Tirat Carmel, Israel) for technical support and the Department of Neurosurgery, Graduate School of Medicine, Hokkaido University (Sapporo, Japan) for excellent assistance.

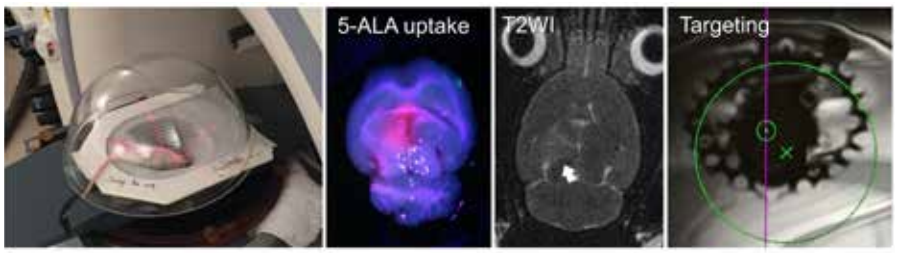

Figure 1. (top) Setup of F98 rat glioblastoma model

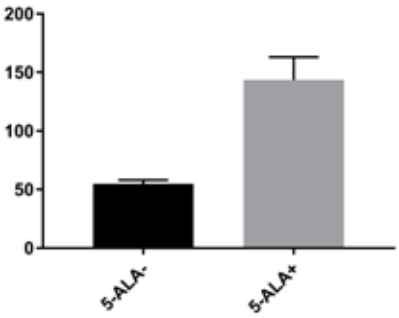

Figure 2. (bottom) 5-ALA uptake in primary glioblastoma cells

CA-8

Tuesday

23 October 2018

Topic: Brain Tumors
Presentation Type: Oral

Sonodynamic therapy with Fluorescein for the treatment of sub-cutaneous C6 glioma in a rat model

Francesco Prada[1], Diogo Cordeiro[2], Dave Moore[1], Kelsie Timbie[1], Zhiyuan Xu[2], Neal Kassell[1]

[1]Focused Ultrasound Foundation, Charlottesville, Virginia, United States
[2]University of Virginia, Charlottesville, Virginia, United States

In accordance with author request, this abstract is not available for publication.

CA-9

Tuesday

23 October 2018

Topic: Brain Tumors
Presentation Type: Oral

Focused ultrasound – induced mild hyperthemia improves immune cell infiltration in a mouse GL261 intracranial glioma model

Anastasia Velalopoulou[1], Yutong Guo[1], Arpit Patel[1], Johannes Leisen[1], Costas Arvanitis[1,2]

[1]Georgia Institute of Technology, Atlanta, Georgia, United States
[2]Emory University, Atlanta, Georgia, United States

In accordance with author request, this abstract is not available for publication.

CA-10

Tuesday

23 October 2018

Topic: Cancer Immunotherapy

Presentation Type: Oral

A pre-clinical investigation of the immunological effects of pulsed focused ultrasound and immune checkpoint inhibitors in pancreatic cancer

Petros Mouratidis[1], Gail ter Haar[2]

[1]The Institute of Cancer Research, London, United Kingdom
[2]The Institute of Cancer Research, Sutton, United Kingdom

Background: The clinical benefit of immunotherapy has not yet been realised in pancreatic cancer, which is characterised by a low antigenicity and dense stroma profile. Focused ultrasound (FUS) can be used in the treatment of solid tumours, either by inducing necrosis (using ablative temperatures), or by creating cavitation which results in mechanical disruption of the stroma. Both of these processes may regulate the immune response and make the tumours more susceptible to immunotherapeutic treatments. In this study, pancreatic tumours have been exposed to FUS and co-treated with immune checkpoint inhibitors (ICI) to explore whether control of the tumour growth can be achieved.

Methods: Syngeneic orthotopic KPC pancreatic tumours (KrasLSL.G12D/+; p53R172H/+; PdxCre tg/+) were grown in immune-competent murine C57BL/6 subjects (> 15 weeks old). Tumours were exposed to pulsed FUS using the small animal Alpinion VIFU 2000 Therapeutic Ultrasound platform. Pulsed FUS exposure parameters were designed to result in cavitation (power = 250 W, duty cycle = 1 %, pulse repetition frequency = 1 Hz, 60 repeats) in the target tissue. A passive, weakly focused, broadband (0.1 to 20 MHz) sensor was used to detect cavitation. A combination of anti-CTLA4 and anti-PD-1 antibodies (200 mg per antibody per subject), or their respective isotypes, were administered intraperitoneally 3 days before treatment, and every 3 days thereafter. Tumour growth was estimated using high frequency ultrasound imaging, and with callipers at the time of culling. The biological effects of the treatments on the tumours and the extracellular matrix were investigated using H&E and trichrome staining of formalin-fixed, paraffin-embedded histological sections, and using immunohistochemistry to detect CD4+ and CD8+ tumour infiltrating lymphocytes. Results were quantified using ImageJ. The immunological effects of the treatments were investigated in the blood, spleen and the pancreaticoduodenal and gastric lymph nodes of the treated and sham-exposed subjects with multi-colour flow cytometry of white blood cells and splenocytes. Staining patterns typical of T_{helper}, $T_{cytotoxic}$, $T_{regulatory}$, $T_{effector}$ and Myeloid-derived suppressor cells were used. Their relative abundances were quantified using Flow Jo.

Results: Pulsed FUS treatment of pancreatic tumours resulted in cell and collagen depleted regions in the tumours, associated with an extensive rearrangement of the extracellular matrix. Broadband signal (suggestive of cavitation) was detected. No skin damage was observed. Combination of a single pulsed focused ultrasound treatment with administration of ICIs resulted in improved control of tumour growth relative to the monotherapies and sham exposures. Survival of subjects treated with the combination treatment was extended relative to the survival of subjects treated with the monotherapies. Additional results for the systemic and localised relative abundance of immune cells will be presented.

Conclusions: FUS can be used in combination with antibody immunotherapy to control the growth of pancreatic tumours. These results suggest that focused ultrasound can turn an immunologically "cold" tumour into an immunologically "hot" tumour and should be trialled with additional immunotherapies.

CA-11

Tuesday

23 October 2018

Topic: Cancer Immunotherapy

Presentation Type: Oral

Boiling histotripsy ablation of renal carcinoma in the Eker rat increases effector memory T-cells

George Schade

University of Washington, Seattle, Washington, United States

Background: Focused ultrasound (FUS) exposures have demonstrated immunomodulatory effects suggestive of an anti-tumor immune response following tumor ablation in numerous models. Our group has been developing boiling histotripsy (BH) as a non-invasive FUS treatment for renal carcinoma (RCC) and have previously shown short-term changes in systemic and local cytokines and infiltration of CD8+ T-cells following BH treatment *in vivo*. We characterized the long-term changes in immune cell populations following BH RCC tumor ablation in a rat model.

Methods: RCC bearing genotyped Eker rats (Tsc2 heterozygotes) were randomly assigned to transcutaneous BH or FUS SHAM procedure targeting ~0.5 cc of RCC or non-tumor bearing normal kidney. BH was delivered with a 1.5 MHz US-guided small animal FUS system (VIFU-2000, Alpinion) operated at duty cycles of 1-2%, 10-20 ms pulses, 525-600 W electric power. Following treatment rats were recovered, underwent serial US imaging surveillance and serial blood draws, and were survived for 7, 14, or 56 days. Following euthanasia, the treated and contralateral kidney, tumor draining lymph nodes (TDLN), and spleen were collected. Flow-cytometry was performed on processed tissues and blood to analyze for changes in circulating and local immune cell populations.

Results: BH RCC treatment was associated with significant alterations in the immune system *vs.* sham treatment at 14 days post-treatment. Specifically, BH was associated with a significant 1.3-fold increase in CD4+ CD62L- CD44+ effector memory T-cells and near-significant 1.8-fold ($p=0.08$) increase in central memory CD4+ CD62L+ CD44- cells in TDLNs. Additionally, BH treatment resulted in significant alterations in cytotoxic CD8+ T-cell populations. Specifically, BH treatment was associated with significantly increased CD8+ CD62L- CD44+ effector memory cells in both TDLNs and spleen (3.0-fold, $p<0.01$ and 2.9-fold, $p=0.03$, respectively) and central memory CD8+ CD62L+ CD44- cells in TDLNs (6.8-fold, $p<0.01$) with a corresponding significant decrease in CD8+ CD62L+ CD44+ naïve cells in TDLNs (0.4-fold, $p=0.01$) (see figure 1). At 56 days, significantly increased effector memory CD8+ CD62L- CD44+ T-cells persisted within TDLN (2.7-fold, $p<0.01$) with a similar 1.9-fold increase observed in the treated tumor and 1.7-fold increase observed in contralateral untreated tumors (see figure 2).

Conclusions: These data represent the first extensive analysis of the immune response to BH tumor treatments and suggest that BH RCC ablation produces significant changes to the immune system suggestive of an anti-tumor response. Future studies will further evaluate the specificity of this response and whether it can improve clinically relevant outcomes.

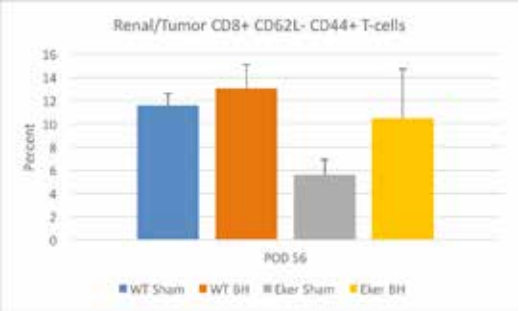

Figure 1. Flow cytometry results for CD8+ CD62L- CD 44+ effector memory cells in tumor derived lymph nodes

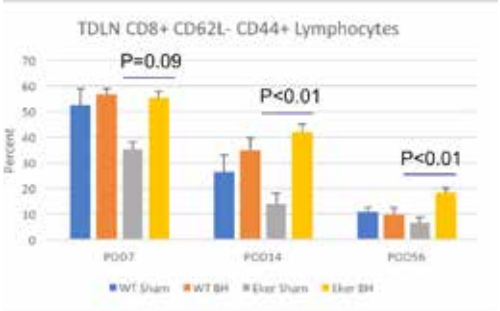

Figure 2. Flow cytometry results for CD8+ CD62L- CD 44+ effector memory cells in treated RCC

CA-12

Tuesday

23 October 2018

Topic: Cancer Immunotherapy

Presentation Type: Oral

Evaluating the immune response following mouse brain tumor ablation with MRI-guided focused ultrasound

Marc Santos[1], Sharshi Bulner[2], Sheng-Kai Wu[1], David Goertz[1], Kullervo Hynynen[1]

[1]University of Toronto, Toronto, Ontario, Canada
[2]Sunnybrook Research Institute, Toronto, Ontario, Canada

Background: Glioblastoma multiforme (GBM) continues to have a dismal prognosis and significant efforts are being made to develop more effective treatment methods. Recent work has suggested the potential of immunotherapies to treat GBM, though as with other tumor types it is likely that only subsets of patients will respond and combinatorial approaches may ultimately be favored. The ability of different types of focused ultrasound (FUS) to evoke an immune response has been previously established, suggesting its potential to augment immunotherapies. However, understanding the mechanisms and duration of the effects are required to provide a rational basis for its use in conjunction with immunotherapies. The objective of this work is to investigate the immune response of gliomas in mice following ablative ultrasound treatments.

Methods: Experiments were performed using a GL261 intracranial tumor model in immune-competent C57 BL/6 albino female mice. To reduce superficial heating craniotomies were performed immediately preceding tumor cell implantation. Tumors then grew for 14 days (Figure 1), whereupon experiments commenced. Ultrasound exposures were carried out in a 7T MRI scanner (Bruker) using a preclinical MRgFUS system (FUS Instruments). MRI thermometry was performed to monitor temperatures during sonication. Ultrasound based thermal treatments in the mouse brain pose considerable challenges in that the small spatial scale favors higher frequencies, while superficial heating favors the use of lower frequencies. An extensive pilot study was first conducted to determine appropriate frequencies, power levels, and durations (n=19). The transducer employed (focal length 20mm; f-number 0.8) was driven at 3.3, 5.5 or 7.7MHz. Subsequently, data was acquired at day 21 (7 days post ablation or sham treatment) for tumor growth, histology and flow cytometry. Histologic analysis focused on CD4+ and CD8+ T-cells, while flow cytometry focused on a wider range of immune cell markers.

Figure 1. (A) Coronal image of a GL261 tumor grown for 14 days in a mouse brain. (B) Axial image of the same tumor. The tumor is indicated in both images by a white arrow.

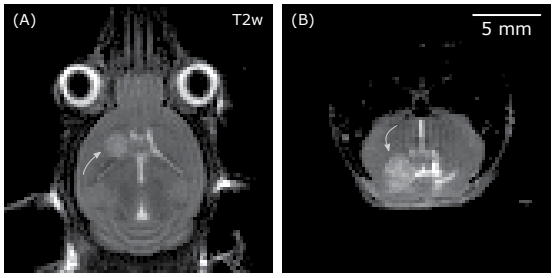

Figure 2. (A) Coronal and (B) axial imaging plane during MRI thermometry with image magnitude signal in gray scale and temperature data overlaid in color above 45°C. (C) Temperature profile in a 3x3 voxel region at the ultrasound focus.

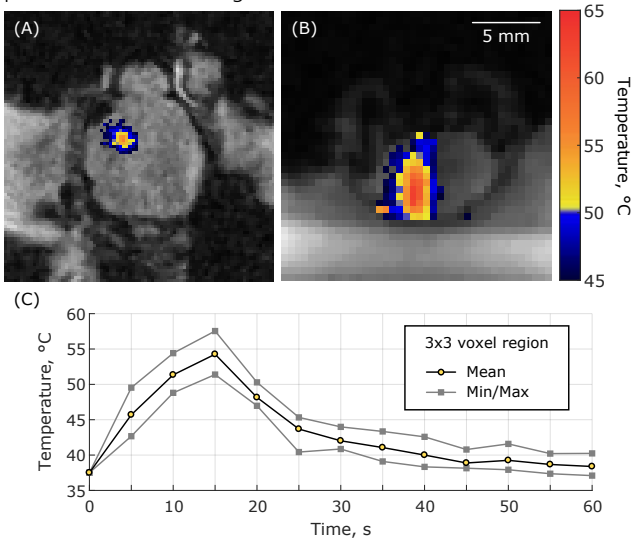

Results: Lesions in the brain were induced at all three frequencies assessed. However, the 3.3MHz exposures were frequently associated with skull based heating due to the focal depth of field. At 7.7MHz, superficial heating was frequently observed that posed challenges to heat at a sufficient tumor depth, and was associated with small lesions. Experiments were therefore carried out at 5.5MHz, which in general produced heating within the desired depth range. The bulk of the work was comprised of 15s sonications and an acoustic power level of 2.45W, where either single or multiple exposures were performed within tumors. Temperature monitoring was used to determine if exposures resulted in a sufficient thermal dose for lesion production. Figure 2 shows an example MRI thermometry dataset obtained during a 15s ablative sonication. Histology and cytometry data is accumulating and the results for these will be presented.

Conclusions: Targeted MRgFUS ablation of an orthotopic GBM tumor model in mice is feasible and experiments are currently being conducted to establish the immune response following treatments. These experiments have the potential to yield results relevant for providing a rational basis for combining ablation with immunotherapies in patients with GBM.

CA-13

Tuesday

23 October 2018

Topic: Cancer Immunotherapy

Presentation Type: Oral

Identification of genes responsive to pulsed focused ultrasound stimulation using melanoma and breast cancer xenograft models

Gadi Cohen, Rebecca Lorsung, Scott R Burks, Joseph A Frank

National Institutes of Health, Bethesda, Maryland, United States

In accordance with author request, this abstract is not available for publication.

CA-14

Tuesday

23 October 2018

Topic: Cancer Immunotherapy

Presentation Type: Oral

Immune cell modulation of pulsed focused ultrasound in murine melanoma and breast cancer models

Parwathy Chandran, Gadi Cohen, Rebecca Lorsung, Omer Aydin, Scott R Burks, Joseph A Frank

National Institutes of Health, Bethesda, Maryland, United States

In accordance with author request, this abstract is not available for publication.

CA-15

Tuesday

23 October 2018

Topic: Cancer Immunotherapy

Presentation Type: Oral

Immunogenic cell death mediated by calreticulin-nanoparticle synergizes melanoma immunotherapy of focused ultrasound

Sri Nandhini Sethuraman, Mohit Pratap Singh, Girish Patil, Shitao Li, Jerry Malayer, Ashish Ranjan

Oklahoma State University, Stillwater, Oklahoma, United States

Background: Malignant melanoma in advanced stages is a highly lethal form of cancer, refractory to chemo- and radio-therapy, with median survival as low as 6-9 months. To improve response rates, focused ultrasound (FUS) immunomodulation is currently a major focus of melanoma research, but the local and systemic antitumor effects remain moderate in treated patient. Recent studies indicate that activation of immunogenic cell death (ICD) in melanoma cells by expression of endogenous calreticulin (CRT) in tumor cells stimulates innate and adaptive immunity. The objective of this study was to investigate the combination of FUS with ICD-enhancing CRT-nanoparticle (CRT-NP) for synergistic enhancement of immune effects in murine melanoma.

Methods: To characterize the impact of ICD on the efficacy of FUS, we compared the following groups in a murine model of B16F10 melanoma (~50mm^3): 1) Control, 2) FUS, 3) CRT-NP, and 4) CRT-NP/FUS. For CRT-NP synthesis, full-length clone DNA of human calreticulin was encapsulated in liposome-NP made from DOTAP and cholesterol. Three CRT-NP intratumoral injections of 20 μg each were given 2 days apart, and FUS heating (43-45°C, ~15min; 1.5 MHz central frequency) was applied sequentially 24h after each injection to evaluate tumor regression. To investigate ICD specific systemic effects, the splenocytes of mice vaccinated with CRT-NP (± FUS) treated B16F10 cells were evaluated *ex vivo* for TRP-2 antigen specific immunity. Additionally, long-term protection mediated by the combination of FUS/CRT-NP was evaluated by rechallenging with the melanoma cells in the flank regions of tumor bearing mice.

Results: CRT-NP and FUS combination suppressed B16 melanoma growth in tumor-bearing mice *in vivo* by >85% *vs.* that seen in untreated controls, and >~50% *vs.* CRT-NP or FUS alone. FUS/CRT-NP combination synergistically enhanced the population of CD8+ cytotoxic T cells positive for IFN-γ and granzyme-B in tumors, and the ratio of M1 to M2 macrophages in the spleen compared to all the groups. A two-fold higher frequency of TRP-2 specific IFN-γ producing CD4+ and CD8+ T cells was noted in the spleen compared to CRT-NP indicating melanoma specific immunization. These findings were also verified in rechallenge experiments where 80% mice (4/5) treated with CRT/FUS combination remained tumor-free compared to the controls (0%; 0/4).

Conclusions: We demonstrate for the first time that combining FUS with ICD activating CRT-NP achieves dependable clearance of melanoma cancer cells and provide long-term protection against recurrence. This combinatorial technology has the potential for clinical translation.

Acknowledgements: CVHS Kerr Chair & RED FUNDING

CA-16

Tuesday

23 October 2018

Topic: Cancer Immunotherapy

Presentation Type: Oral

Single cell RNA sequencing analysis of HIFU treated breast cancer enables rationale immune checkpoint inhibitor combinations

Kensuke Kaneko, Shinya Abe, Takuya Osada, Pankaj Agarwal, Joshua Snyder, Pei Zhong, H. Kim Lyerly

Duke University, Durham, North Carolina, United States

Background: In a novel breast cancer model in immunocompetent mice, we used single cell RNA sequencing (scRNAseq) of leukocytes in the tumor microenvironment after Thermal (T)- or Mechanical (M)-High Intensity Focused Ultrasound (HIFU) to characterize cell populations and expression of immune checkpoints. We had reported that M-HIFU induced stronger antitumor immune response than conventional T-HIFU in murine colon cancer model, so we studied both methods in breast cancers to provide a rationale for combination HIFU with immune checkpoint blockade.

Methods: The murine mammary epithelial cell line (MM3MG) was transduced with human HER2 to generate a tumorigenic model (MM3MG-HER2) in immune competent mice (BALB/c). The VIFU 2000 system (Alpinion Medical Systems, Bothell, WA) was used for planning treatment strategy, HIFU exposure and monitoring during treatment. Established tumors were treated using a 1.5 MHz HIFU transducer under two different protocols (50% duty cycle, 1 Hz pulse repetition frequency, 20W, 10 seconds or 2% duty cycle, 5 Hz pulse repetition frequency, 200W, 20 seconds) to produce either thermal necrosis or mechanical lysis of the tumor cells. We evaluated the efficacy of HIFU treatment in MM3MG-HER2 breast cancer and characterized tumor-infiltrating immune cells after T- or M-HIFU treatment by scRNAseq as well as FACS.

Results: In MM3MG-HER2 tumor-bearing mice, both modes of HIFU treatments suppressed tumor growth, but M-HIFU treatment showed higher efficacy, leading to 40% mice cured (Figure 1). IFN-gamma ELISpot assay showed the induction of systemic antigen-specific immune response by both T- and M-HIFU treatment. FACS analysis revealed that M-HIFU treatment improved infiltration of immune cells in tumors, including T cells and NK cells, but reduced macrophages (Figure 2). In addition, M-HIFU treatment increased activation and lysis markers, including CD69, inducible co-stimulatory molecule (ICOS) and Granzyme B on tumor-infiltrating T cells. On the other hand, M-HIFU treatment increased immune checkpoint molecules on immune cells, such as PD-L1 (Figure 3) and lymphocyte activation gene 3 (LAG-3). To further characterize leukocyte populations in tumors after HIFU treatment, scRNAseq analysis was conducted, which revealed that most T cells in treated tumors showed not only high ICOS expression but also CTLA-4 (CD4+) or PD-1 (CD8+) expression (Figure 4). Accordingly, we conducted the combination treatment of M-HIFU with PD-1/PD-L1 blockade for MM3MG-HER2 tumor-bearing mice, and demonstrated that the combination strategy induced the strongest HER2-specific immune response and had the most potent antitumor efficacy. These results suggested that appropriate immune checkpoint blockade could enhance the treatment efficacy of HIFU.

Conclusions: M-HIFU showed higher antitumor efficacy than T-HIFU in murine breast cancer model with greater expansion of T cells and NK cells in breast cancer. Blockade of PD-1/PD-L1 pathway based on scRNAseq and FACS analyses improved the treatment efficacy of M-HIFU. Thus, scRNAseq analysis of immune infiltrates provides a rationale approach to develop combination strategies of immune checkpoint molecules in combination therapy with HIFU treatment, and to monitor non-responsiveness or resistance.

Acknowledgements: The study was supported by Duke MEDx funding.

Figure 1. Tumor growth and mouse survival after HIFU treatment.

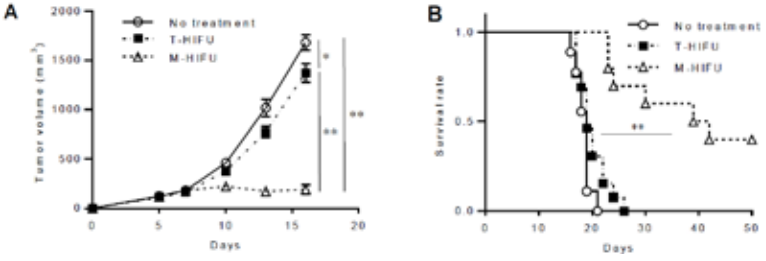

Figure 2. FACS analysis of leukocytes isolated from breast tumors after HIFU treatment.

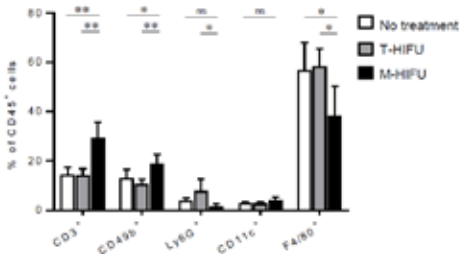

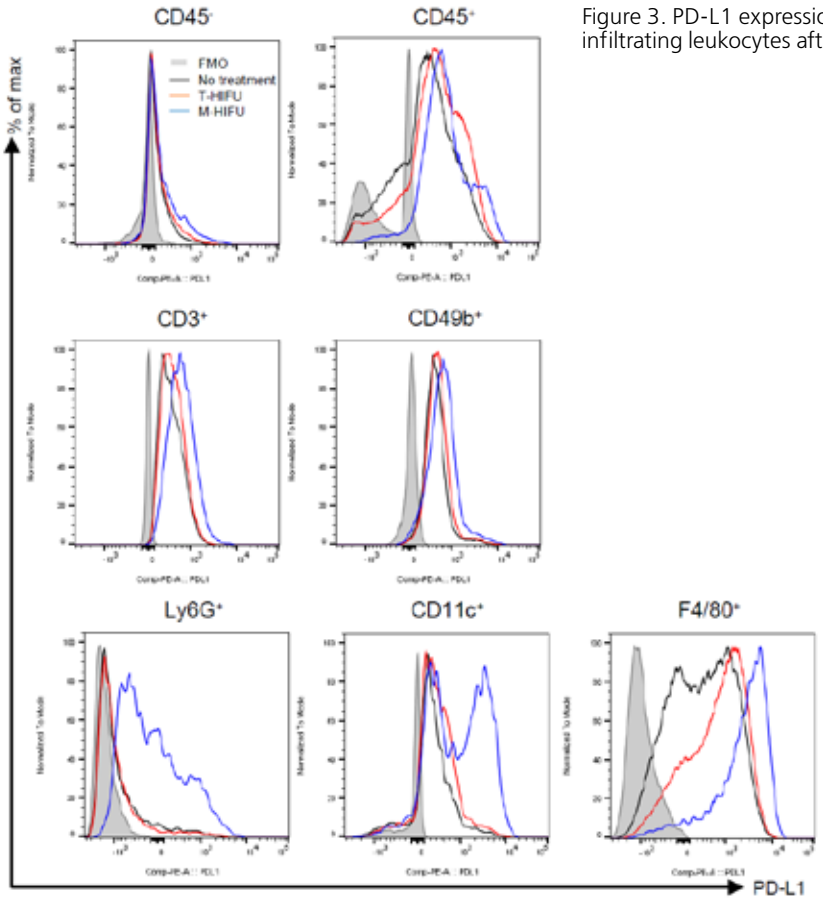

Figure 3. PD-L1 expression on tumor-infiltrating leukocytes after HIFU treatment.

Figure 4. Single cell RNAseq analysis of CD45+ leukocytes isolated from HIFU treated or untreated MM3MG-HER2 tumor.

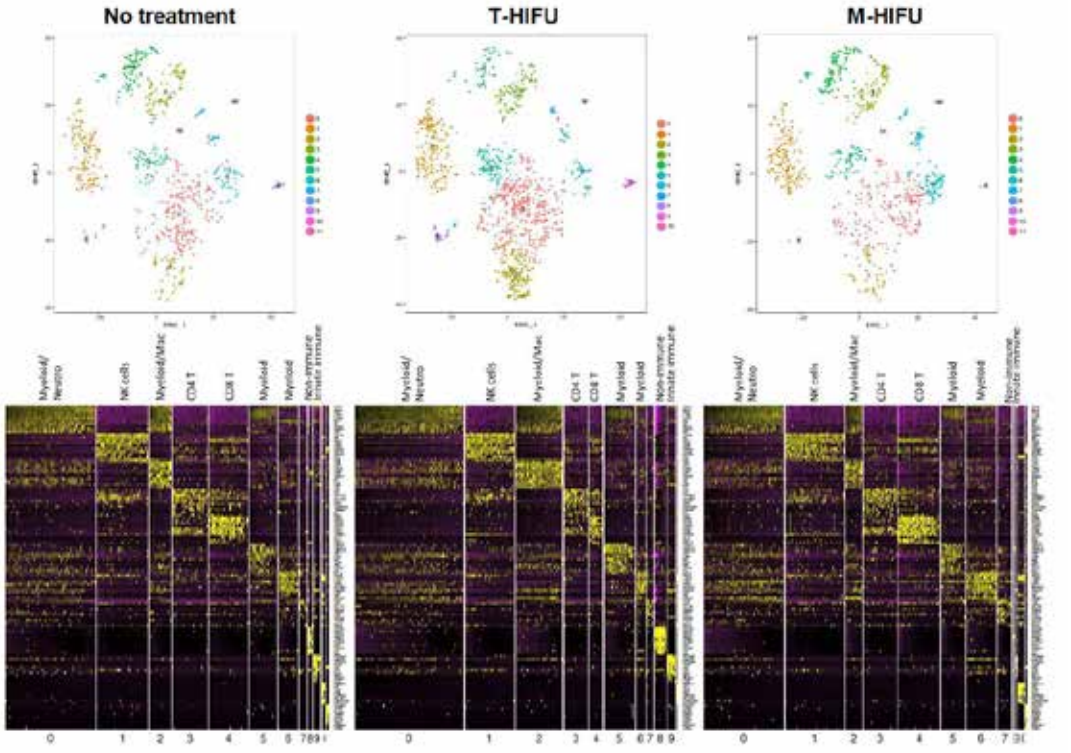

CA-17

Tuesday

23 October 2018

Topic: Liver
Presentation Type: Oral

High intensity focused ultrasound for hepatic gene transfer

Cynthia Anderson[1], Ralph Shohet[2]

[1]University of Hawaii, Honolulu, Hawaii, United States
[2]University of Hawaii, John A. Burns School of Medicine, Honolulu, Hawaii, United States

Background: The development of nonviral ultrasound-based strategies for delivering therapeutic agents to different anatomical regions would be useful for enhancing the safety and efficacy of gene therapy. Many current approaches use viral vectors, which can deliver transgenes with high efficiency but are often associated with undesirable systemic effects including immune responses and transduction of non-target organs. An alternative approach, Ultrasound Targeted Microbubble Destruction (UTMD), can deliver gene-expression vectors bound to the shells of lipid microbubbles. These are administered intravenously, and deposited at the target organ by acoustic cavitation of the microbubbles. While UTMD provides a relatively safe and highly specific alternative to viral-based gene therapies, the technology is limited by low transfection efficiency. Integration of high intensity focused ultrasound (HIFU) into the current UTMD technique may improve gene transfer efficiency by enhancing transient vascular permeability in the liver. The goal of our study is to evaluate the potential of HIFU for enhancing the efficiency of hepatic gene transfer.

Methods: Multiple HIFU parameters, including pulse repetition frequency (PRF), amplitude signal, pulse duration, acoustic exposure time, and targeting depth, were evaluated to optimize the delivery of liver-specific reporter plasmids to the livers of mice using HIFU-targeted microbubble destruction. We used bioluminescence and immunofluorescence to determine hepatic transfection efficiency and the distribution and intensity of reporter expression. We assessed the effects of HIFU exposure at different planes in the medial and left liver lobes for the various ultrasound parameters and targeting depths (5mm-18mm) with histology.

Results: Ultrasound parameters were identified in unfocused UTMD studies that produced site specific transfection of hepatocytes with plasmids encoding reporters or the therapeutic human blood coagulation factor IX (hFIX) without substantial damage in the livers of wild-type and Hemophilia B mice. Using the new HIFU-based strategy, we observed similar levels of reporter expression compared to the unfocused technique 24-48 hours after transfection (P=0.95). Increasing the HIFU PRF (50-60 Hertz range) while maintaining a low duty cycle with short pulse durations of ≤20μs has produced the greatest average radiance for reporter expression (~1.0 x 104-105 photons/sec/cm^2/sr, Figure 1A-B). Robust clusters of reporter gene expression were observed in distinct regions of the liver after HIFU compared to the diffuse pattern of expression observed for unfocused treatments (Figure 1C-D). We are now modulating the HIFU targeting depth between 5-18mm in a single UTMD treatment as a strategy to target multiple anatomical planes in the liver and augment transfection efficiency.

Conclusions: We are evaluating the efficiency and bioeffects of varying HIFU parameters on gene transfer in the livers of wild-type mice. Our optimized HIFU-based UTMD approach will then be used to direct the delivery of hFIX to the livers of FIX-/- mice. The goal of this work is to advance the development of an anatomically targeted, minimally invasive, DNA delivery strategy that is robust enough to treat genetic deficiency disorders such as Hemophilia B.

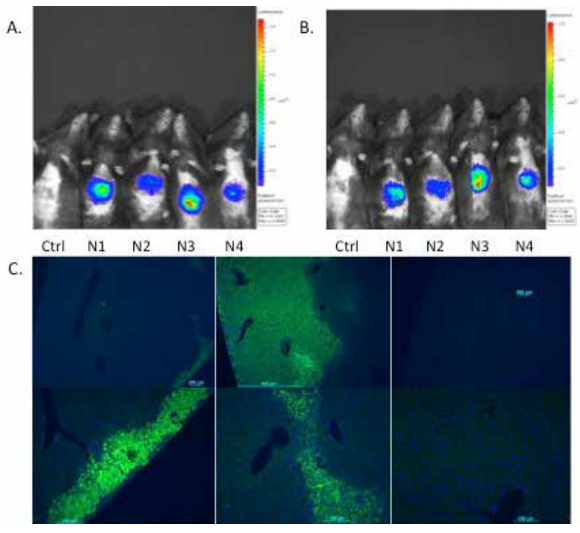

Figure 1. HIFU delivery of reporter plasmids to the liver.

Acknowledgements: Chad Walton, PhD (HIFU technology development). Funding support from NIH T32HL115505 and AHA Postdoctoral Fellowship 33990116 (CDA).

CA-18

Tuesday

23 October 2018

Topic: Pancreas
Presentation Type: Oral

MRI biomarkers for focused ultrasound treatment of pancreatic ductal adenocarcinoma

Yak-Nam Wang[1], Ezekiel Maloney[1], Ravneet Vohra[1], Tanya Khokhlova[1], Stella Whang[1], Helena Son[1], Joshua Park[1], Kayla Gravelle[1], Joo Ha Hwang[2], Donghoon Lee[1]

[1]University of Washington, Seattle, Washington, United States
[2]Stanford University, Stanford, California, United States

Background: Pancreatic ductal adenocarcinoma (PDA) is the fourth leading cause of cancer-related deaths in the United States. Advanced stage diagnosis and the ineffectiveness of standard treatments contribute to the poor overall prognosis. Standard chemotherapeutic treatments are largely ineffective due to the robust desmoplastic stroma and resulting high interstitial fluid pressures characteristic of PDA. In a transgenic mouse model of PDA (KPC mouse), pulsed focused ultrasound (pFUS) has been shown to disrupt dense fibrotic stroma and increase chemotherapeutic penetration. A recent phase 1 clinical trial of pFUS in combination with chemotherapy, doubled median overall survival in patients with inoperable PDA *versus* chemotherapy alone. As new promising treatments are developed, methods to assess treatment efficacy are a critical consideration. The purpose of this study was to implement non-invasive MRI methods to assess pFUS treatment effects for PDA.

Methods: Three murine models of PDA (subcutaneous, orthotopic, and a transgenic) were evaluated with multi-parametric MRI at 14T (Paravision 5.1 software, Bruker Corp, Billerica, MA) to assess tumor response to ultrasound-guided pFUS treatments (VIFU 2000 Alpinion Medical Systems; 475 W peak electric power, 1 millisecond pulse duration, 1 Hz, duty cycle 0.1%) or sham treatments. The focal spot was raster-scanned with a step size of 1 mm, and 60 pulses were delivered at each focal spot. Cavitation activity was recorded during treatment. MR images were collected 48 hrs pre-pFUS and immediately post-pFUS therapy. Maps for T1 and T2 relaxation, apparent diffusion coefficient (ADC), magnetization transfer ratio (MTR), and chemical exchange saturation transfer (CEST) for the amide proton and glycosaminoglycan (gag) spectrum were generated. Tumors were excised and prepared for histological and biochemical evaluation. Sulfated glycosaminoglycans (sGAG) and hyaluronan (HA) concentration was measured using standard techniques.

Results: Cavitation activity was achieved in all three murine PDA models. Treated areas demonstrated predominantly isointense signal on T1 weighted anatomic scans, in some instances with an associated peripheral ring of T1 hypoinense signal. However, overall there was no significant difference in mean tumor T1 relaxation time. Following pFUS treatment, mean ADC increased significantly for all animal models, and was most pronounced in the KPC model. Mean gag CEST and T2 map quantitations decreased significantly post-treatment only for the KPC group. HA and sGAG tissue concentrations were found to be lower in the treated animals. Mean MTR values increased 21.6% for the KPC group. Mean amide CEST values increased 14.5% for the KPC group. Other parameters tested were not significantly changed post-pFUS treatment. There were no significant differences in any parameters for the sham group animals.

Conclusions: Variable changes in T1 relaxation, and significantly increased MTR and amide CEST signals post-pFUS-treatment most likely represent sequelae of hyperacute hemorrhage from microcapillary vessels. Decreases in gag CEST and T2 relaxation may represent disruption of glycosaminoglycans and associated liberation of complexed water molecules from within the tumor stroma. Significant increase in ADC likely reflects increased diffusivity within the treated PDA tumors. T2 relaxation, gag CEST, and ADC may provide reliable quantitation for monitoring therapeutic effect of pFUS for PDA

CA-19

Tuesday

23 October 2018

Topic: Bone
Presentation Type: Oral

A two-center phase III, randomized, controlled study of MRgFUS *versus* EBRT in patients with metastatic non-spinal bone disease: Palliative strategy for cancer-induced bone pain

Alessandro Napoli[1], Roberto Scipione[2], Fabrizio Andrani[2], Carola Palla[2], Cristina Marrocchio[2], Carlo Catalano[1]

[1]Sapienza University of Rome, Rome, Italy
[2]Policlinico Umberto I - Sapienza University of Rome, Rome, Italy

Background: Bone metastases are the most common cause of cancer-related pain and often determine a considerable impairment in quality of life.

The current standard of care for metastatic bone pain is external-beam radiation therapy (EBRT); however, 20%–30% of treated patients reportedly do not experience adequate pain relief, and a substantial number of them shows recurrent pain, with limited possibility for repeating treatment because of radiation toxic effects. Most importantly, EBRT involves long latency periods, requiring up to 4 weeks before pain palliation is achieved.

MR-guided Focused Ultrasound (MRgFUS) is a non-invasive radiation-free ablative procedure that has become a valid alternative for a wide range of pathologies and received FDA approval for pain palliation in patients with bone metastases. Multiple mechanisms may explain MRgFUS effects in terms of pain relief: periosteum denervation, tumor debulking (with reduction in the pain related to the expansion of the mass), and the reduction of chemical mediators' release and the degree of osteoclast-mediated osteolysis. The variation of some technical parameters could also induce complete lesion ablation with local tumor control.

The purpose of this study was to examine and compare the clinical outcomes of MRgFUS and EBRT in patients with painful bone metastasis.

Methods: Patients with breast cancer, prostate cancer, or other solid tumours and one or more bone metastasis were included. Eligible patients were ≥18 years of age, had radiologically proven bone metastases, were scheduled for radiotherapy, could safely undergo both MRgFUS and radiotherapy and had pain scores ≥ 4 (on 0-to-10 numeric rating scale). Participants were randomly assigned (1:1 ratio) to receive MrgFUS or EBRT. Outcomes were compared at 4 weeks. The primary end point was treatment response, defined as a reduction of ≥ 2 points in worst pain by week 4, accompanied by a stable or reduced opioid dose, compared with baseline. Secondary end points assessed average pain, interference of pain with activity, breakthrough pain, mood, quality of life, and adverse events.

Results: 233 patients (M: 125; F: 108) were enrolled and randomly assigned: 116 to MRgFUS and 117 to EBRT. The most common cancers were prostate (n=88; 38%), breast (n=78; 33%), and lung (n=44; 19%). In the MRgFUS arm 91 patients (78.4%) achieved the primary end point, compared with 85 (72.6%) in the EBRT arm (adjusted odds ratio, 1.3; p = 0.21). There were no statistically significant differences in average pain, pain interference with activity, breakthrough pain, mood and quality of life between arms.

Conclusions: Although no strongly significant difference in clinical outcomes was recorded between MRgFUS and EBRT, a general trend of better results was documented towards non-invasive procedure. MRgFUS combines effective pain palliation with the advantages of radiation-free and single-session procedure, but is limited to non-spinal locations. MRgFUS represents a valid treatment option in cancer-induced bone pain and could be routinely introduced in the management of painful bone metastases that are technically accessible and do not respond to conventional treatment.

Figure 1. Pre- and post-procedural CE- MRI scans shows local tumor control in a 67-yo patient with bone metastases from renal cell carcinoma; this patient experienced pain relief as well (from VAS 8 to 0)

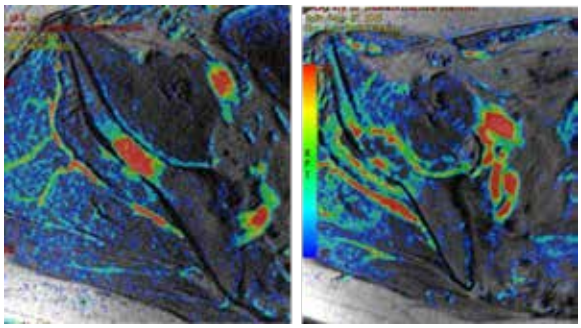

Figure 2. Pre and post-procedural CE-MRI scans of a 57-yo patient with bone metastases on the falanx of the thumb from lung cancer; local tumor control and pain relief were described (from VAS 8 to 0)

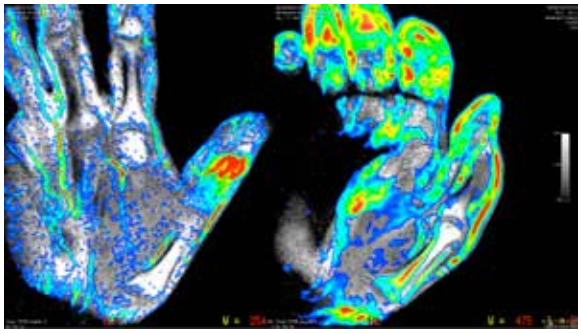

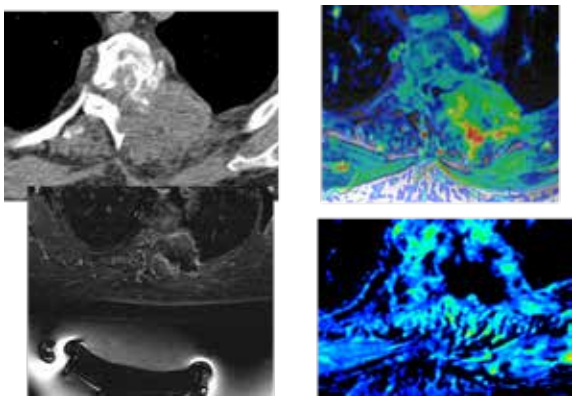

Figure 3. Painful bone metastases on pedicle and transverse process of a vertebra; pre- and post- images are presented showing tumor devascularization. This patient also reported clinical benefit (from VAS 9 to 2)

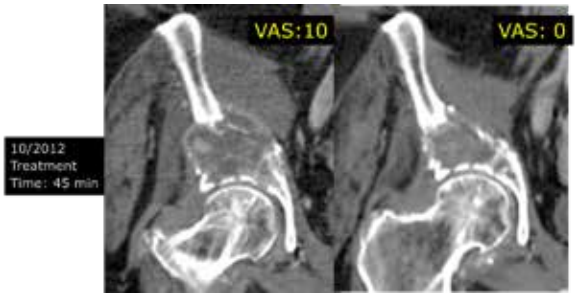

Figure 4. Pre- and post-procedural scan CT scan of a on the right iliac bone shows lesion size reduction and bone sclerosis and remodeling. Palliative effect was achieved (from VAS 8 to 0).

CA-20

Tuesday

23 October 2018

Topic: Bone
Presentation Type: Oral

Magnetic resonance guided focused ultrasound (MRgFUS) in the management of osteoid osteoma: A new first-line technique? Long-term results from a dual-center prospective study

Alessandro Napoli[1], Roberto Scipione[2], Carola Palla[2], Fabrizio Andrani[2], Hans-Peter Erasmus[2], Andrea Leonardi[2], Carlo Catalano[1]

[1]Sapienza University of Rome, Rome, Italy
[2]Policlinico Umberto I - Sapienza University of Rome, Rome, Italy

Background: Osteoid osteoma (OO) is a painful benign bone tumor that mainly affects children and young adults. The most frequent symptom is localized dull pain that increases at night and promptly subsides with non-steroidal anti-inflammatory drugs (NSAIDs). Conventional therapy options for OO include surgery, medications and/or percutaneous treatment; pain-relievers are considered the treatment of choice but a long-lasting NSAIDs intake could cause gastrointestinal, renal or other side effects; surgical resection can be challenging in many cases, and it needs post-surgery therapy and a prolonged rehabilitation time; minimally invasive therapies are constantly growing in clinical routine, and radiofrequency (RF) ablation is currently considered the standard of care, despite an incomplete treatment rate of 2%, recurrent pain of 4.9% and complications of 2.1%.

MR-guided Focused Ultrasound (MRgFUS) is a non-invasive radiation-free technique that has become a valid alternative for a wide range of pathologies and represents a feasible option for selected patients with OO: combining periosteal neurolysis and a focal ablation of the nidus, a complete pain relief with no need for medication can be achieved.

The purpose of this work was to demonstrate that non-invasive radiation-free ablation of OO with MRgFUS is a safe, effective and durable treatment option

Methods: Patients with typical clinical and radiological findings of OO, suitable for MRgFUS and anaesthesia, were enrolled in this dual-centre prospective observational study. Vertebral locations were excluded as considered inaccessible. MrgFUS was performed using INSIGHTEC-ExAblate2100 system. Safety (rate of complications), clinical effectiveness (Visual Analogue Scale[VAS] pain score reduction) and durability (stability of results over time) of MRgFUS were evaluated as primary outcomes; tumour control (nidus ablation) at dynamic contrast enhanced MR imaging (Discovery 750, GE;Gd-BOPTA, Bracco) was considered as secondary outcome. All patients underwent a minimum follow-up period of 5 years.

Results: Out of 50 subjects screened, 45 were enrolled and submitted to MRgFUS. No treatment-related complications were observed. Complete and durable response was achieved in 80% of cases. Median VAS pain score dropped from 8 (IQR 7-9) to 0 at 1-week, and at all subsequent follow-ups (1-, 6-,12-,24-,36-,48- and 60-month). Scores evaluating interference of pain with sleep, physical and daily activities showed similar improvement. Among subjects with partial response (20%), 4 received a second treatment(3 with CT-guided Radiofrequency Ablation, 1 with MRgFUS), and 5 did not need any other treatment. All re-treated patients achieved 0 VAS score. Overall, 87% of patients after MRgFUS treatment reached and maintained a stable 0 VAS score during follow-up. At final follow-up MRI, OO showed no vascularization in 32/42 patients (76%) treated with MRgFUS alone (Figure 1).

Conclusions: Our data suggest that MRgFUS is a safe, effective and durable option in the treatment of non-spinal OO (Figures 2-4). Without relevant side effects, with this proof of efficacy and with the chance of repeatability we are using the MRgFUS as a first-line treatment in patient with Osteoid Osteoma and we propose this technique as the new treatment of choice in these patients.

Figure 1. Clinical results of patients undergoing MRgFUS procedure during our follow-up period.

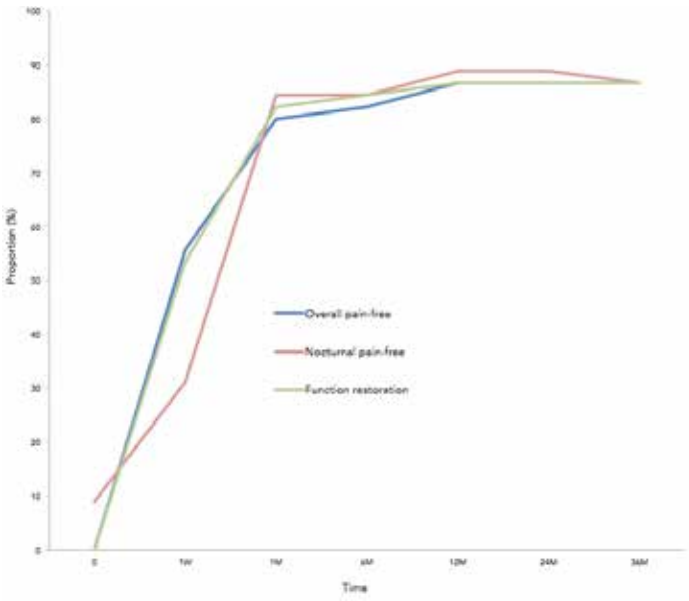

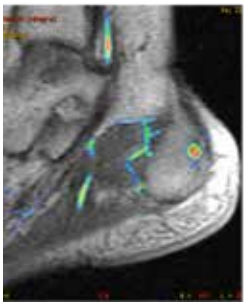

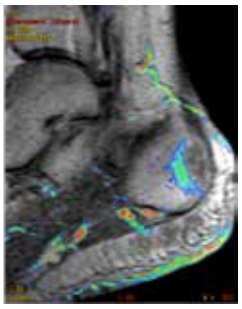

Figure 2. Baseline MRI scan of 21 year old woman suffering from a painful osteoid osteoma in the calcaneus (VAS=8), compared with post-treatment results: complete disappearance of the nidus and resolution of pain (VAS 0).

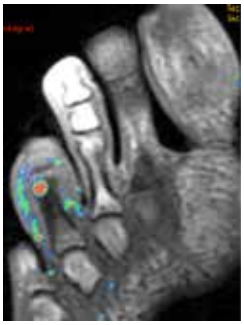

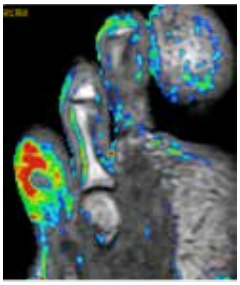

Figure 3. Painful OO on the toe of a young football player (VAS 9); post-treatment results show a complete disappearance of nidus vascularity and complete clinical benefits (VAS 0)

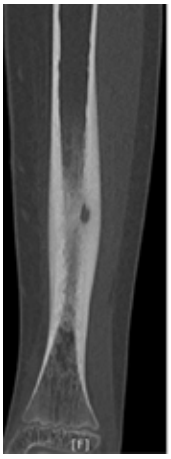

Figure 4. Serial CT examinations (baseline-18 months-3years) showing the progressive restitutio ad integrum of the bone after MRgFUS treatment

CA-21

Tuesday

23 October 2018

Topic: Bone
Presentation Type: Oral

MR guided high intensity focused ultrasound (MRgFUS) for the Treatment of oligometastatic prostate cancer bone metastasis. Can sound waves downstage cancer spread?

Alessandro Napoli[1], Roberto Scipione[2], Fabrizio Andrani[2], Carola Palla[2], Susan Dababou[2], Michele Anzidei[2], Carlo Catalano[1]

[1]Sapienza University of Rome, Rome, Italy
[2]Policlinico Umberto I - Sapienza University of Rome, Rome, Italy

Background: Prostate cancer is the most common malignancy in male population; the presence of bone metastases is detected in up to 70% of affected patients and considerably worsens overall survival and quality of life, causing pain, fractures and other complications. Systemic therapy represents the main first-line treatment in patients with metastatic prostate cancer, with only palliative intent. Nevertheless, due to the improvement in diagnostic modalities, the detection of metastases is currently increasing and occurs at very early stages, when there are limited number of lesions and no symptoms; emerging data suggest that oligometastatic patients have more prolonged survival rates compared to patients with widely diffuse disease. Therefore, metastasis-directed therapies (MDT) aiming to local control may alter the prognosis of the disease, resulting in prolonged survival, or even cure.

Magnetic Resonance-guided Focused Ultrasound (MRgFUS) is a non-invasive procedure that uses high-intensity ultrasound to induce coagulative necrosis in target lesions. MR-guidance allows precise targeting and real-time temperature monitoring, resulting into efficient ablation and ensuring safety of surrounding healthy tissues.

MRgFUS would be an ideal treatment for oligometastatic prostate cancer as it is non-invasive, has a high safety profile, does not need ionizing radiations nor the interruption of concurrent cancer treatments. Moreover, it has the additional benefit of pain palliation of bone lesions, for which is an approved second-line strategy.

Our aim was to determine MRgFUS ability to downstage patients with oligometastatic bone disease with single session of non-invasive metastasis-directed therapy.

Methods: The study was designed with intention-to-treat metastatic bone lesions. Patients were enrolled if they had accessible bone metastasis and could safely undergo MRgFUS (Exablate 2100, INSIGHTEC, Israel). Baseline measurable characteristics included dynamic contrast enhanced MRI study (Gd-BOPTA, Bracco; GE 750 3T magnet) with semiquantitative perfusion analysis, PSA level (ng/ml) and choline PET (SUV). Measurable variables were obtained at treatment time, 3 months, 12 months and 24 months follow-up.

Figure 1. PET study before and after treatment in a 70-year-old patient with bone metastases on the left ilium from prostate cancer. The radiotracer uptake was significantly reduced after MRgFUS.

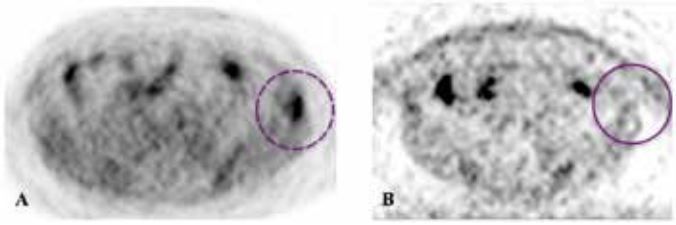

Figure 2. DCE MRI scans before and after the procedure in a 64-year-old patient with bone metastases on the left scapula from prostate cancer. The colorimetric perfusion maps show the absence of perfusion in the lesion after MRgFUS.

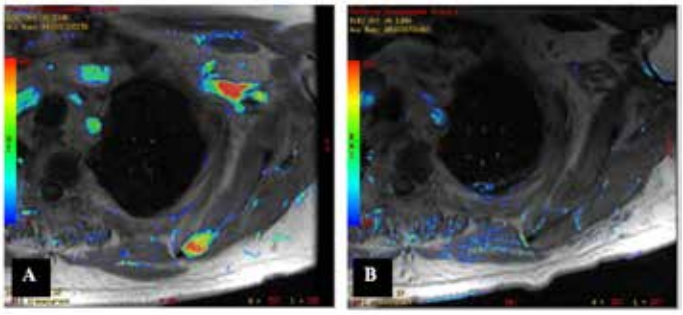

Results: 18 patients fulfilled the inclusion criteria and safely underwent MRgFUS procedure of metastatic bone ablations. Lesions were located in the pelvis (11), scapula (3) and long bones (4). At baseline all lesions showed a significant DCE perfusion (highly vascular) with mean perfusion reduction of 88% at 3 months follow-up (CI: 100-50; $p<0.001$) stable at subsequent follow-up scans. Similarly PSA levels decreased from a mean baseline of 19 (ng/ml) to 7.1, 2.9 and 2.1, at 3-12 and 24 moths respectively. SUV values showed similar trend with reduction from baseline (mean 8.9 to 3.0, 2.3 and 1.7: $p<0.001$). In all patients single MRgFUS session was appropriate without any major or minor adverse events reported.

Conclusions: MRgFUS is a totally non-invasive procedure that can obtain nearly complete bone ablation in patients with oligometastatic prostate disease (Figures 1-4). The technique features a radiation-free approach that can be of incremental value in long-survivor subset on oncological patients, significantly reducing risk of toxic effects. MRgFUS could be routinely introduced as a treatment option for oligometastatic bone disease non-responding to conventional treatment.

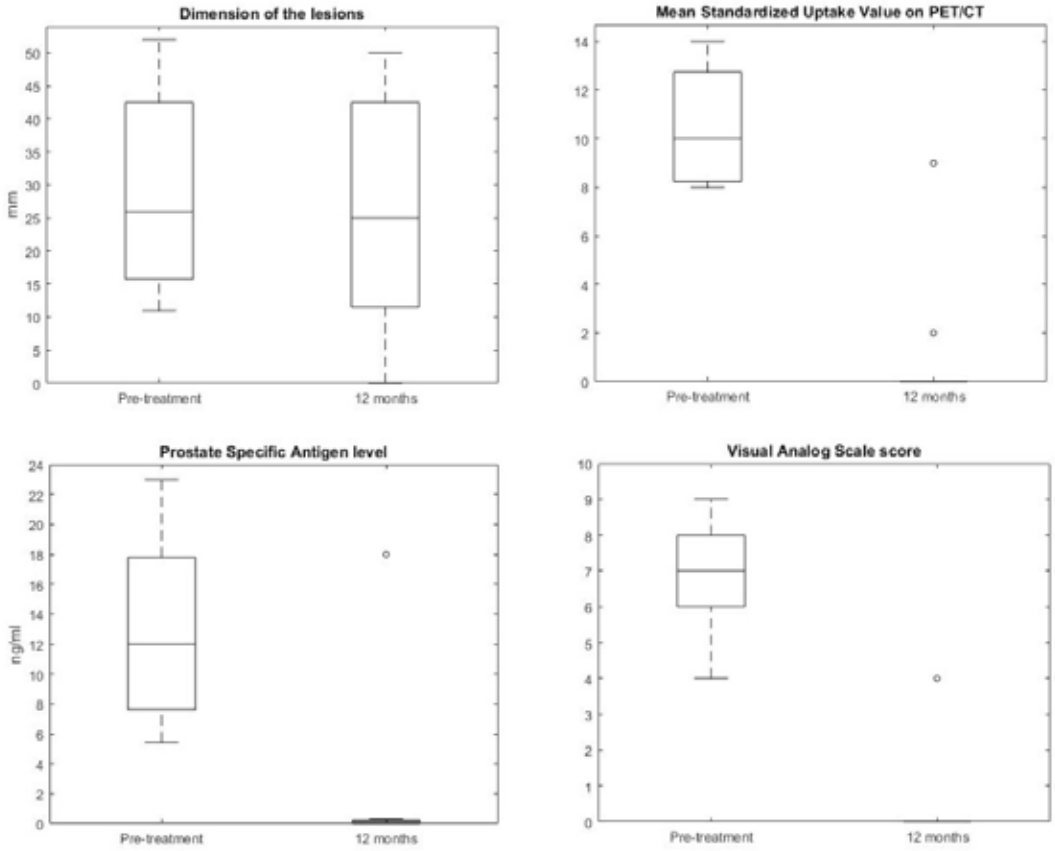

Figure 3. Boxplots showing results at 12 months follow-up; evaluated parameters include lesion dimension, μSUV on 18F Choline-PET/CT, PSA levels, VAS score.

CA-22

Tuesday

23 October 2018

Topic: Bone
Presentation Type: Oral

Bone pain palliation: Early clinical experiences

Sin Yuin Yeo[1], Grischa Bratke[2], Edwin Heijman[3], Michael Püsken[2], David Maintz[2], Holger Gruell[1]

[1]Klinikum der Universitaet zu Koeln, Cologne, Germany
[2]Uniklinik Köln, Cologne, Germany
[3]Philips Research Germany, Cologne, Germany

Background: Bone pain as a result of bone metastases, osteoid osteoma, or soft tissue tumor with bone infiltration is debilitating and reduces patients' quality of life. Depending on the origin of bone pain, standard treatments include radiation therapy (RT), surgery, radiofrequency ablation, chemotherapy or a combination of these treatment options. Despite that, pain recurrence is common and necessitates an alternative treatment option to manage the corresponding pain. Magnetic resonance-guided high intensity focused ultrasound (MR-HIFU) ablation is a promising treatment, which has been shown to reduce bone pain. Here, we present our early clinical experiences using MR-HIFU ablation for bone pain palliation.

Methods: Eight patients experiencing bone pain due to bone metastases (4), soft tissue sarcoma with osteolysis (2), osteoid osteoma (1) and desmoid tumor (1) were treated with a Sonalleve® MR-HIFU system (Profound Medical). The treated bone regions include ilium (5), rib (1), femur (1) and humerus (1). Prior to MR-HIFU treatments, all patients were placed under general anesthesia and the intended treatment regions were centered on the therapy window. T1-weighted images were acquired for treatment planning. The lesions were treated with acoustic powers between 40-170W. Following treatments, contrast-enhanced T1-weighted images were acquired to assess the non-perfused volume (NPV), and patients were monitored overnight for complications. The visual analog scale (VAS) pain scores were documented before and up to 3 months post therapy. Patient respond was defined by a minimum of 2-point reduction in VAS score without analgesic increase or 25% reduction in analgesic intake without increase in pain. Depending on patients' conditions, MRI follow-up was performed at 1.5- and 3-month time points. Currently, complete follow-up is pending, and 3 representative cases are discussed below.

Results: Pain relief was observed in 100% patients (7/7).

Bone metastases: Patient had an osteolytic destruction of left ilium and non-responsive to RT. The lesion was 127.5cm^3 in volume. Immediately after MR-HIFU, NPV ratio was 80%. The VAS score increased from 7 to 8 at 1 week after MR-HIFU. Interestingly, at 4 weeks after the treatment, VAS score reduced to 0, demonstrating complete response. The lesion volume was 136.3cm^3 at 6 weeks follow-up.

Osteoid osteoma: Patient had a nidus in the right femur. As shown in Figure 1, immediately after the ablation, the nidus was completely non-perfused. The pain score reduced from 6 to 0 at 1 day after treatment. Patient remained pain-free at 2-week follow-up.

Desmoid tumor: Patient had a painful (VAS=7) lesion with two recurrences after surgeries within 12 months, and osteolytic bone infiltration. Immediately after HIFU, NPV was 87%, but with no changes in the VAS scores within the first 3 days after MR-HIFU. At 1.5-month follow-up, VAS score reduced to 0, and a 50% volume reduction was observed. Pain relief was stable, and tumor reduced by 72% at 3-month follow-up.

There were no treatment-related complications.

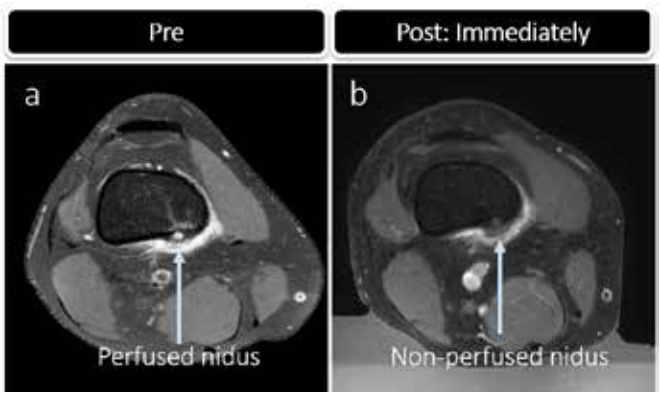

Figure 1. Representative images of an osteoid osteoma patient before (a) and immediately after (b) MR-HIFU ablation. The nidus was complete non-perfused, confirming treatment success.

Conclusions: Our early clinical experiences demonstrated that MR-HIFU ablation is a safe and effective alternative treatment for bone pain and tumor reduction.

CA-23

Tuesday

23 October 2018

Topic: Bone
Presentation Type: Oral

Cost-effectiveness analysis of magnetic resonance-guided focused ultrasound for palliation of painful bone metastases

Matthew Bucknor[1], Frandics Chan[2], Jessica Matuoka[3], James Kahn[1]

[1]University of California – San Francisco, San Francisco, California, United States
[2]Stanford University, Stanford, California, United States
[3]Universidade de São Paulo, São Paulo, Brazil

Background: To determine if in patients with refractory pain from bone metastases, if palliation with magnetic resonance guided focused ultrasound (MRgFUS), a novel non-invasive ablation technique, compared to medication alone, is cost-effective (incremental cost-effectiveness ratio or ICER), for a 24-month time horizon, from a health system perspective.

Methods: We constructed a Markov state transition model using TreeAgePro®. Probabilities, costs, and effectiveness data were derived from a combination of the available literature, expert opinion, and reimbursement data at two U.S. medical centers performing MRgFUS. In the model, costs and quality adjusted life years (QALYs), discounted at a rate of 3%/year, were accumulated each month over a 24-month time horizon. Willingness-to-pay level was estimated at $100,000/QALY. Multiple sensitivity analyses were performed.

Results: In the base case analysis, the MRgFUS treatment strategy cost an additional $8756.23 over the two year time horizon to accumulate an additional 0.22 QALYs, equal to a $40150.20/QALY ICER, thus making MRgFUS the preferred strategy. One way sensitivity analyses demonstrate that for the base case analysis, the crossover point at which Medication Only would instead become the preferred strategy is $25,711.58 per treatment. Micro-costing estimates demonstrated MRgFUS costs at each institution were well below both this estimated crossover point and the base case analysis MRgFUS cost at approximately $6000 at institution 1 and $11000 at institution 2.

If, in the base case, the costs of background medication for patients with relief of MRgFUS is increased from 25% to 50% of baseline pain medication usage, the ICER increases from $40150.20/QALY to $45,011.00/QALY with a new crossover point established at an MRgFUS cost of $24,841.62 per treatment. We also evaluated the results of our model with regard to the percentage of patients electing to repeat MRgFUS for persistent or relapsed pain. In the base case analysis, we had assumed approximately 50% of patients failing MRgFUS would elect to repeat the treatment each time. If that is increased to 100%, the ICER increases slightly to $40239.81/QALY. Finally, an additional sensitivity analysis was performed in which the efficacy of MRgFUS for a second treatment was decreased to 60% and then to 40% for a third treatment, compared to the 80% chance of pain relief following a first treatment. (In the base case analysis, HIFU efficacy remained at 80% for each of up to three treatments). With progressively decreasing MRgFUS efficacy, the ICER increased 13.5% from the base case to $45572.54/QALY.

Conclusions: Our base case and sensitivity analyses demonstrated that MRgFUS was a preferred treatment strategy across a wide range of transition state probabilities, costs, and QALYs. Our model was most sensitive to changes in the cost of MRgFUS and QALYs associated with persistent pain or pain relief.

CA-24

Tuesday

23 October 2018

Topic: Bone
Presentation Type: Oral

Focused ultrasound osteoid osteoma treatment registry: Moving towards centralized focused ultrasound data collection

Michael Temple[1], Joao Amaral[1], Pejman Ghanouni[2], Matthew Bucknor[3], Alessandro Napoli[4], Francesco Arrigoni[5], Alberto Bazzocchi[6], Manish Patel[7], Mahesh Prakash[8], Tim Meakem[9], Maria Lamberti-Pasculli[1], Simal Goman[1], James Drake[1]

[1]Hospital for Sick Children, Toronto, Ontario, Canada
[2]Stanford University, Stanford, California, United States
[3]University of California – San Francisco, San Francisco, California, United States
[4]Sapienza University of Rome, Rome, Italy
[5]San Salvatore Hospital, San Salvatore Hospital, L'aquila, IT-AQ [67100], Italy
[6]Rizzoli Orthopaedic Institute, Bologna, Italy
[7]Cincinnati Children's Hospital, Cincinnati, Ohio, United States
[8]PGI Chandigarh, PGI Chandigarh, Chandigarh, IN-CH [160012], India
[9]Focused Ultrasound Foundation, Charlottesville, Virginia, United States

Background: Osteoid osteomas are painful, benign bone tumours that are predominantly treated with thermal ablation. While the initial treatment effects of MRgFUS on Osteoid Osteoma (OO) have been very positive, it remains a small volume procedure, with variable patient selection, targeting, treatment parameters, outcome metrics, and follow up. An OO registry is an extremely important vehicle to collate a sufficient cohort of patients from multiple centers to demonstrate efficacy, but also to optimize and standardize the treatment. This will also help to more widely diffuse the procedure, and assist with regulatory approval. By including more invasive treatments such as laser ablation, radiofrequency ablation (RFA) and cryotherapy, in the same registry, with identical outcomes metrics, the true role of MRgFUS for OO can be evaluated. The Focused Ultrasound Osteoid Osteoma Treatment Registry was launched earlier this year.

Methods: Registry data collection design was developed with input from sites involved in the 2015 Cincinnati IGNITE pediatric consortium meeting and members of the Society for Pediatric Interventional Radiology (SPIR). A web-accessible prospective database was created using Research Electronic Data Capture (REDCap) software. All sites that perform osteoid osteoma (OO) treatment (in both children and adults), obtain ethics board approval and that agree to the registry governance charter, data sharing and publication policies are eligible for enrollment. Registry decisions will be made by the governance committee that includes site leads and 2 non-voting positions for representatives of the FUS Foundation and SPIR. Any researcher can request access to portions of the data in accordance with the data sharing policy. Initial estimates suggest that accrual of 300 patients over 5 years, will allow determination of relative efficacy of the primary outcome measure, pain free status within 2 weeks of performing the first intervention.

Results: At the present time, 1 site has completed enrollment and 8 sites are in the process of obtaining ethics approval for assessment of FUS OO treatment. Altogether 28 sites have expressed their intention to take part in assessment of percutaneous OO treatments.

Conclusions: The Focused Ultrasound Osteoid Osteoma Treatment Registry is open for enrollment. The registry was designed to be the initial step in creation of a Computational Data Center and Registry to capture information on multiple types of FUS research.

Acknowledgements: This work was supported by a Focused Ultrasound Foundation Research Award.

CA-25

Tuesday

23 October 2018

Topic: Bone
Presentation Type: Oral

Safety and feasibility of osteoid osteoma ablation with high-intensity focused ultrasound: Comparison to the radiofrequency ablation standard of care

Pavel Yarmolenko[1], Karun Sharma[2], Haydar Celik[2], Avinash Eranki[2], Ari Partanen[3], Anilawan Smitthimedhin[1], Aerang Kim[1], Matthew Oetgen[1], Domiciano Santos[1], Janish Patel[1], Peter Kim[4]

[1]Children's National Medical Center, Washington, DC, United States
[2]Sheikh Zayed Institute for Pediatric Surgical Innovation, Children's National Medical Center, Washington, DC, United States
[3]Profound Medical, Mississauga, Ontario, Canada
[4]George Washington University, Washington, DC, United States

Background: Osteoid osteoma (OO) is a painful bone tumor that commonly occurs in cortex of long bones of lower extremities in children and adolescents. It accounts for 10-14% of all benign bone tumors. In addition to pain, other symptoms of osteoid osteoma can include bony deformity, growth disturbance, and painful scoliosis. CT-guided radiofrequency ablation (CT-RFA) is the current standard of care for definitive treatment. Although CT-RFA is effective and less invasive than surgery, potential complications include bleeding, infection, skin and muscle burns, and nerve injury from drilling through tissue and heating along the RFA probe. The use of CT imaging required for treatment planning and guidance also exposes patients and operators to ionizing radiation, which can have potential long-term negative effects, especially for growing children. Magnetic resonance imaging-guided high-intensity focused ultrasound (MR-HIFU) is a non-invasive treatment modality capable of ablating tissues deep within the body without either incisions or exposure to ionizing radiation, and therefore it offers significant advantages over existing OO treatment approaches in children. The objectives of this work were to evaluate feasibility and safety of treatment of symptomatic osteoid osteoma and to compare clinical response with standard of care CT-RFA treatment.

Methods: Nine subjects with radiologically confirmed, symptomatic OO were treated with MR-HIFU (Sonalleve V2, Philips, Vantaa, Finland) on an IRB-approved clinical trial (NCT02349971). Treatment feasibility and safety were assessed. Analgesic requirement, Visual Analog Scale pain score, and sleep quality were used to evaluate clinical response. Anesthesia, procedure, and recovery times as well as clinical response indicators were compared between the group of patients treated with MR-HIFU and a historical control group of nine consecutive patients treated with radiofrequency ablation (RFA).

Results: Nine subjects with symptomatic extremity osteoid osteoma (7 males, 2 females; 16±6 years old) were treated with MR-HIFU without technical difficulties or any serious adverse events. There was significant decrease in their median pain scores four weeks after treatment (6 *vs.* 0, $p<0.01$). Total pain resolution and cessation of analgesics was achieved in 8/9 patients after four weeks. In the RFA group, nine patients (8 males, 1 female; 10±6 years old) were treated in routine clinical practice. All nine demonstrated complete pain resolution and cessation of medications by four weeks with significant decrease in median pain scores (9 *vs.* 0, $p<0.001$). One developed a second-degree skin burn, but there were no other adverse events. In both groups, treatment response remained constant over the 1-year follow-up period after treatment. Procedure times and treatment charges were comparable between the two groups.

Conclusions: This work demonstrates that MR-HIFU ablation of OO refractory to medical therapy is feasible and can be safely performed in pediatric patients. Clinical response following MR-HIFU ablation is comparable with standard of care treatment of osteoid osteoma over the course of a 1-year follow-up, but without any incisions or ionizing radiation exposure.

CA-26

Wednesday

24 October 2018

Topic: Prostate
Presentation Type: Oral

Advanced software support for MRgFUS of prostate cancer

Jürgen Jenne[1], Christian Rieder[2], Sven Rothlübbers[3], Lennard Tautz[2], Jan Hendrik Moltz[2], Alba Marina Malavé[1], Gilard Halevy[4], Shlomi Rudich[4], Caroline von Dresky[2], Stefan Hoffmann[1], Johannes Heitz[1], Johannes Gregori[1], Sabrina Haase[2], Yeruham Shapira[4], Matthias Günther[1], Tobias Preusser[2]

[1]Mediri GmbH, Heidelberg, Germany
[2]Fraunhofer MEVIS, Bremen, Germany
[3]Mediri GmbH, Bremen, Germany
[4]INSIGHTEC Ltd., Tirat Carmel, Israel

Background: Due to better preventive examinations, more and more small and localized prostate tumors can be discovered nowadays. Therefore, demand for therapies is increasing. There are many different, competitive treatment options for prostate cancer (PCa), e.g. surgery, radiation therapy and RF- or Cryo ablation. Therapeutic ultrasound for tissue ablation under US- or MR-guidance has shown very promising results, but is yet to be integrated into an efficient and safe workflow. In order to prevail in the clinic, MRgFUS therapy procedure has to be simple, fast and affordable. For this, the FUS therapy needs to be supported by tailored software tools for automatizing workflow, planning, guidance and follow up. Aim of the presented work is to analyze the MRgFUS therapy workflow and to develop software tools for improving MRgFUS therapy of prostate cancer.

Methods: Software tools based on MeVisLab (Medical image processing and visualization toolkit, MeVis Medical Solutions, Bremen) with several dedicated C++ modules for the image processing were developed. Advanced, 2D and 3D image viewers for detailed planning were created. An automated and interactive segmentation tool based on machine-learning algorithms was added to support the therapy planning stage. A quasi real-time prostate tracking software module working on MR thermometry images was implemented to detect prostate deformation and motion during the course of therapy. Moreover, an automated quality assurance (AQUA) module was developed. These tools were integrated into a software demonstrator, called "Prostate Therapy Planning Station" (PTPS) which could be used with INSIGHTEC's ExAblate Prostate system offering better automated processing blocks to the process of treatment management.

Figure 1. 3D and 2D visualization of MR images with segmented structures

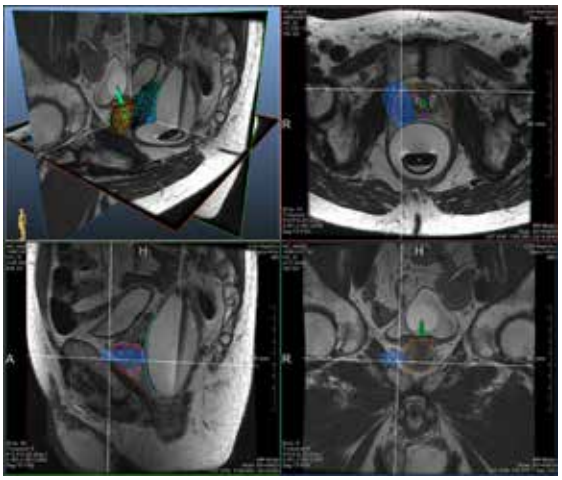

Figure 2. Example of prostate motion detection. L: reference image. R: arrows indicate the prostate motion

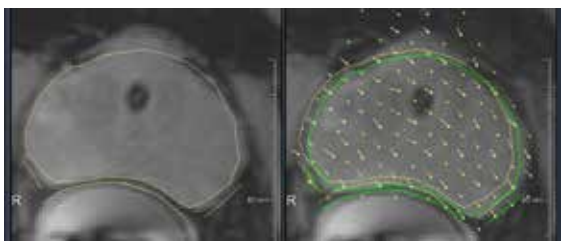

Results: PTPS allows a detailed visualization of the MR images along with segmented structures and organs displayed as opaque overlay or mesh (Fig. 1). Fully automated segmentation of the bladder, the catheterized urethra, the rectal wall and the adjacent cooling balloon is possible. Segmentation of the prostate capsule can be performed interactively with the augmented support of machine learning algorithms. The neurovascular bundle, a major organ at risk for PCa-therapy can be segmented manually. Automated real-time deformation and motion tracking of the segmented prostate capsule on consecutive image sets is possible (Fig. 2). In case of unwanted change of imaging parameters, protocols, non-matching reference images and prostate motion the AQUA module warns the physician instantaneously.

Conclusions: A consistent application of state of the art image processing tools, demonstrated in PTPS, may simplify, speed up and improve the precision of prostate MRgFUS. Real-time prostate motion and deformation tracking and the automated detection of unwanted deviation from the treatment protocol by the AQUA software will lead to a safer therapy procedure. A combination with advanced therapy workflow software, demonstrated in [1], supporting the management of the local disease from diagnostic imaging with multimodal MRI, to therapy, and to follow up will further increase the confidence in this kind of therapy. In the next steps, tools for fully automated segmentation, workflow management and follow up should be integrated.

Reference

1. Corr, et al. Software-supported analysis of MRgFUS therapy outcome. *Journal of Therapeutic Ultrasound.* 2015;3(133).

CA-27

Wednesday

24 October 2018

Topic: Prostate
Presentation Type: Oral

Initial assessment of boiling histotripsy for mechanical ablation of *ex vivo* human prostate tissue

Vera Khokhlova[1], Pavel Rosnitskiy[1], Sergey Tsysar[1], Oleg Sapozhnikov[1], Maria Karzova[2], Sergey Buravkov[1], Tanya Khokhlova[3], Adam Maxwell[4], Nurshat Gayfullin[1], Dmitriy Okhobotov[1], Armais Kamalov[1], George Schade[3]

[1]M.V. Lomonosov Moscow State University, Moscow, Russian Federation
[2]Moscow State University, Physics Faculty, Moscow, Russian Federation
[3]University of Washington, Seattle, Washington, United States
[4]University of Washington School of Medicine, Seattle, Washington, United States

Background: Boiling histotripsy (BH) is a HIFU method that uses milliseconds-long (<20 ms) pulses applied at low duty cycle to mechanically ablate targeted tissue. Compared to thermal ablation, BH has potential clinical advantages as it minimizes heat-sink effects and thermal spread, allows for real-time ultrasound feedback via the appearance of echogenic bubbles at the focus, and monitoring treatment outcome through production of a hypoechoic lesion. The method has been successfully used in pre-clinical studies to fractionate kidney and liver tissue *ex vivo* and *in vivo*. The goal of this study was to test the feasibility of BH ablation of fresh *ex vivo* human prostate tissue as a proof of principal for treating benign prostatic hyperplasia and prostate cancer.

Methods: Fresh human prostate tissue samples were obtained via rapid autopsy (<24 hours after death, n=4) using an IRB approved procurement program. Tissue was degassed in a polyacrylamide solution for 2 hours, then the final component was added to catalyze the polymerization of the gel containing the tissue (Figure 1A). Embedded tissue was placed in a custom holder submerged in degassed water (Figure 1B). BH pulses (10 ms duration, 1% duty cycle, peak focal pressures of p+=88 MPa, p-=17 MPa, 100 pulses/focus) were delivered to a rectangular grid with 2 mm spacing within the tissue using a 1.5-MHz custom-made transducer (80 mm diameter and 60 mm focal length). Real time-imaging of the sonications and evaluation of the BH treatment outcomes were performed using Verasonics Ultrasound Engines. A L7-4 probe operating in B-mode was oriented perpendicular to the HIFU beam axis and a P7-4 probe operating in B-mode/color Doppler was placed within the central opening of the BH transducer (Figure 1B). Doppler sequences were triggered by the BH driving electronics to generate images right after the end of each BH pulse. Following treatment, tissue was evaluated grossly or formalin-fixed for histologic assessment with H&E staining.

Results: During BH sonications, hyperechoic regions were visualized at the focus on B-mode and BH-induced bubbles were also detected using Color Doppler mode (Figure 2). As treatment progressed, hypoechoic regions of tissue appeared suggesting successful tissue fractionation. On gross assessment following treatment, fluid filled volumetric lesions were observed consistent with mechanical ablation without thermal denaturation (Figure 3). On histological analysis, lesions containing completely homogenized cell debris were observed consistent with histotripsy induced mechanical ablation of glandular elements. Close to the edge of the lesion, the regions of completely homogenized tissue were intermixed with regions of intact smooth muscle and collagen fibrils consistent with sparing of fibromuscular elements (Figure 4).

Conclusions: These data represent the first successful application of the BH method in *ex vivo* human prostate tissue and suggest that BH mechanical prostate ablation is feasible. Further work is ongoing to evaluate a prototype preclinical transrectal device while optimizing parameters of the BH pulsing scheme. This study was funded by RFBR 17-54-33034, NIH R21CA219793, and R01EB007643 grants.

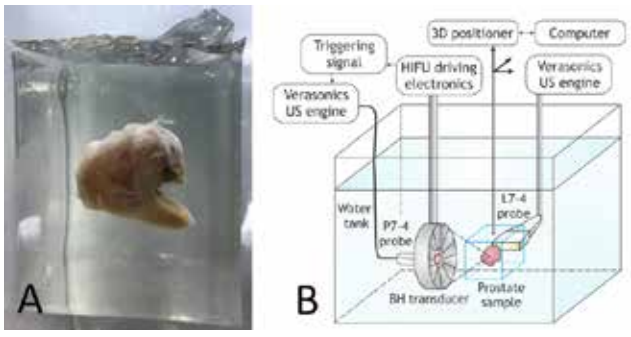

Figure 1. (A) Degassed *ex vivo* sample of human prostate tissue embedded in polyacrylamide gel. (B) Experimental arrangement of BH-irradiation of tissue under real time US-imaging.

Acknowledgements: This study was funded by RFBR 17-54-33034, NIH R21CA219793, and R01EB007643 grants.

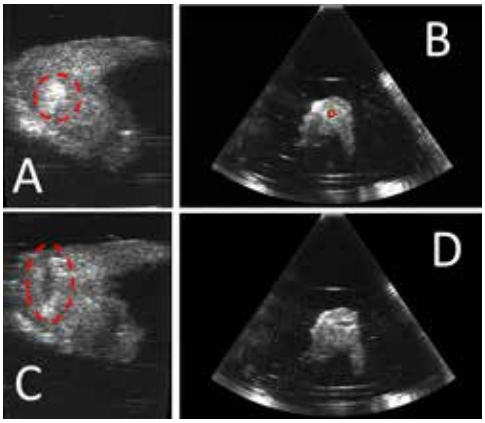

Figure 2. (A) Hyper-echogenic regions on B-mode and (B) Doppler images during BH exposure. (C, D) Hypo-echoic appearance of the line of lesions on B-mode images after BH exposure.

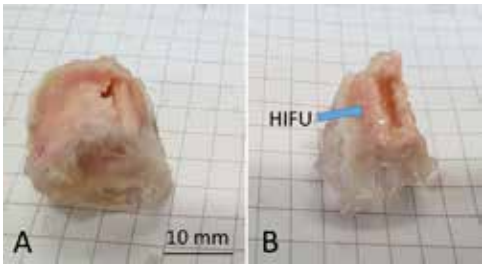

Figure 3. Cross-section of the line of BH-induced lesions in tissue. Direction of the HIFU beam is indicated by arrow.

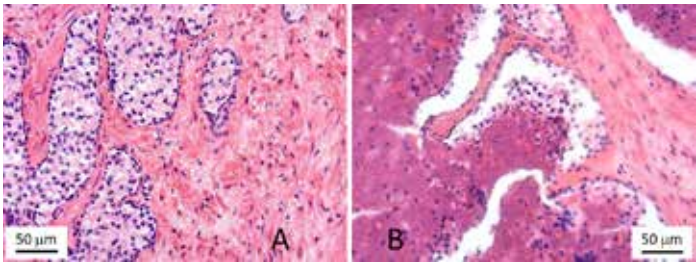

Figure 4. H&E histology images of the (A) intact prostate tissue and (B) region within the BH lesion.

CA-28

Wednesday

24 October 2018

Topic: Prostate
Presentation Type: Oral

Magnetic resonance-guided focused ultrasound (MRgFUS) focal treatment of localized prostate cancer: Initial experience and follow up from a multi-center trial

Clare Tempany[1], Pejman Ghanouni[2], Nathan McDannold[1], Behfar Ehdaie[3], Geoffery Sonn[2]

[1]Brigham and Women's Hospital, Boston, Massachusetts, United States
[2]Stanford University, Stanford, California, United States
[3]Memorial Sloan Kettering, New York, New York, United States

Background: To evaluate the initial experience, safety and feasibility of MR targeted focused ultrasound treatment of localized prostate cancer

Methods: Patients with biopsy proven prostate cancer enrolled in a prospective multi-center pivotal trial of the ExAblate 2100 prostate system. Eligibility criteria include men of 50 years or older, PSA < 20 ng/mL with either low or intermediate risk prostate cancer (Gleason Score 3+3, 3+4 or 4+3). A multi-parametric MR must confirm localized prostate cancer (Stage T1-T2) and tumor distance < 4cm from rectal wall. All men are treated in 1.5 or 3T GEHC MR devices

Results: 38 eligible men have been enrolled and treated from 7 sites. Mean age 62.8 years, mean PSA 6.0ng/mL. Prostate MR demonstrated dominant lesions in 32 men, no lesion in 4 men and MR data was not available in 2. Pre-treatment prostate biopsy results showed Gleason 3+3 in 14, 3+4 in 19 and 4+3 in 9. All men successfully underwent MRguided FUS ablation of their focal lesion. All except one were discharged home later on the treatment day. Currently 6 men have completed follow up, 34 men are at 9 months, 27 at 12 and 12 at 18 months. There were 131 combined device or protocol related adverse events, which were Grade 1 (mild) in 117, Grade 2 (moderate) in 13 and Grade 3 (severe) in 1 (severe suprapubic pain 1 week post treatment, resolved the following day without permanent injury). Overall 77 events were procedure related, 48 were transient, 5 biopsy related and 1 device related.

Conclusions: Initial experience indicates that MRgFUS focal prostate cancer ablation appears to be both feasible and safe. Enrolling men in a trial using image-guided focal therapy in prostate cancer is feasible. Accrual is ongoing in this pivotal trial.

CA-29

Wednesday

24 October 2018

Topic: Prostate
Presentation Type: Oral

Pivotal study of MRI-guided transurethral ultrasound ablation (TULSA) in patients with localized prostate cancer: Preliminary results

Aytekin Oto[1], Sandeep S. Arora[2], Masoom A. Haider[3], Michael Koch[4], Steven S. Raman[5], Christian Pavlovich[6], Gencay Hatiboglu[7], Jurgen Fütterer[8], Marc Serrallach[9], Carlos Nicolau[9], James Relle[10], Daniel N. Costa[11], Thorsten Persigehl[12], Robert Staruch[13], Mathieu Burtnyk[13], Axel Heidenreich[12], Yair Lotan[11], Gregory Zagaja[1], J.P. Michiel Sedelaar[8], David Bonekamp[14], Temel Tirkes[4], Joseph Chin[15], Laurence Klotz[16], Katarzyna Macura[6], David Penson[2], Scott Eggener[1]

[1]University of Chicago, Chicago, Illinois, United States
[2]Vanderbilt University Medical Center, Nashville, Tennessee, United States
[3]University of Toronto, Toronto, Ontario, Canada
[4]Indiana University, Indianapolis, Indiana, United States
[5]UCLA Health Sciences, Santa Monica, California, United States
[6]Johns Hopkins University, Baltimore, Maryland, United States
[7]University Hospital Heidelberg, Heidelberg, Germany
[8]Radboud University Medical Center, Nijmegen, Netherlands
[9]ResoFus Alomar (Hospital Universitari De Bellvitge), Barcelona, Spain
[10]Beaumont Health System, Royal Oak, Michigan, United States
[11]UT Southwestern Medical Center, Dallas, Texas, United States
[12]University Hospital Cologne, Cologne, Germany
[13]Profound Medical, Mississauga, Ontario, Canada
[14]German Cancer Research Center (DKFZ), Heidelberg, Germany
[15]Western University, London Health Sciences Centre, London, Ontario, Canada
[16]Sunnybrook Health Sciences Centre, Toronto, Ontario, Canada

Background: For men with low and intermediate-risk prostate cancer (PCa), MRI-guided transurethral ultrasound ablation (TULSA) of the prostate could bridge the gap between the uncertainty of active surveillance and the risk of side effects associated with radical treatment (surgery and radiation).

TULSA is an in-bore procedure that uses a minimally-invasive ultrasound applicator to emit directional high-intensity ultrasound from within the prostatic urethra, to achieve conformal ablation of targeted prostate tissue under real-time MR-thermometry feedback control. MR images are used to define patient-specific target boundaries for each of 10 independent 5-mm planar ultrasound transducer elements. MR-thermometry acquired continuously during treatment is used to control the ultrasound power, frequency, and device rotation rate, to achieve a desired three-dimensional ablation pattern. Water flowing through the ultrasound applicator and a passive endorectal cooling device protects the urethra and rectum. Ablation extent is confirmed qualitatively on post-treatment contrast-enhanced MRI.

A previously-reported Phase I study of TULSA delivered using a conservative safety margin 3 mm inside the prostate capsule demonstrated safety and ablation precision in 30 patients with predominately low-risk PCa.

We report preliminary safety and efficacy results from the larger TULSA-PRO Ablation Clinical Trial (TACT) pivotal study of whole-gland ablation for patients with mostly intermediate-risk localized PCa.

Methods: Between Sep 2016 and Feb 2018, the TACT study enrolled 115 patients with biopsy-proven organ-confined, low and intermediate-risk PCa across 13 centers in USA, Canada, and Europe. TULSA was delivered under general anesthesia, with intent of whole-gland ablation to the target boundary traced at the prostate capsule. Primary safety endpoint was the frequency and severity of adverse events (AEs) in the first 12 months. Primary efficacy endpoint was the proportion of patients achieving a PSA reduction ≥ 75%. Secondary endpoints include 12-month biopsy and MRI-measured prostate volume reduction, and quality of life (QoL) measures related to urinary, sexual, and bowel function.

Results: Median (IQR) age was 64 (59-69) years, PSA 6.5 (5.0-8.3) ng/ml. Gleason score was 3+3 in 39% and 3+4 in 61%; 34% had low-risk and 66% intermediate-risk disease (D'Amico). Treatment delivery time was 55 (41-70) min for prostate volumes of 40 (32-50) cc, with spatial ablation precision of ±1.4 mm on MRI thermometry.

There have been no rectal injuries or fistulae, no severe urinary incontinence, and no Grade ≥ 4 AEs. The most common serious attributable AEs were Grade 2 urinary retention (n=3) and Grade 3 infection (n=3), all resolved. The primary efficacy endpoint of PSA nadir ≤ 25% of pre-TULSA baseline was achieved in 95% of patients, with median (IQR) PSA reduction to-date of 95% (91-97%) and nadir of 0.36 (0.16-0.60) ng/ml. The number of patients with 12-mo MRI, biopsy, and QoL data is not yet large enough to assess.

Conclusions: Preliminary data of the TACT pivotal study of MRI-guided TULSA for whole-gland ablation in patients with localized prostate cancer showed that 95% of patients achieved the primary efficacy criteria of ≥ 75% PSA reduction, with a low rate of serious adverse events.

CA-30

Wednesday

24 October 2018

Topic: Prostate
Presentation Type: Oral

Salvage high-intensity focused ultrasound for locally recurrent prostate cancer after definitive brachytherapy: Oncologic and functional outcomes

Thomas Hostiou[1,2], Albert Gelet[3,4], Jean-Yves Chapelon[3], Olivier Rouvière[2], Florence Mège-Lechevalier[2], Lionel Badet[4], Sébastien Crouzet[4]

[1]LabTAU, Inserm, Lyon, France
[2]Edouard Herriot Hospital, Lyon, France
[3]LabTAU, Inserm, Lyon, France
[4]Université de Lyon, Lyon, France

Background: There is a lack of studies evaluating salvage therapies for locally recurrent prostate cancer (PCa) after low-dose-rate (LDR) brachytherapy. The objective of our study was to evaluate the oncologic and the functional outcomes of salvage high-intensity focused ultrasound (S-HIFU) for locally recurrent PCa after LDR brachytherapy.

Methods: Two institutional review board-approved phase II clinical studies (HIFU/F02.2 [EudraCT: 2002/09/016] or HIFU/F/10.08 [EudraCT: 2011-A00313-38]) has included 50 consecutive patients between 2003 and 2015 with post-brachytherapy PSA recurrence, histologically proven local recurrence and negative metastatic evaluation, treated by S-HIFU.

Initially, patients were treated using dedicated post-EBRT parameters. Since May 2008, specific post-brachytherapy parameters were applied, taking into account devascularisation and fibrosis created by brachytherapy. Whole gland treatment was realized; since 2009 in case of unilateral PCa identified with multiparametric magnetic resonance imaging and targeted biopsies, hemiablation was performed.

Figure 1

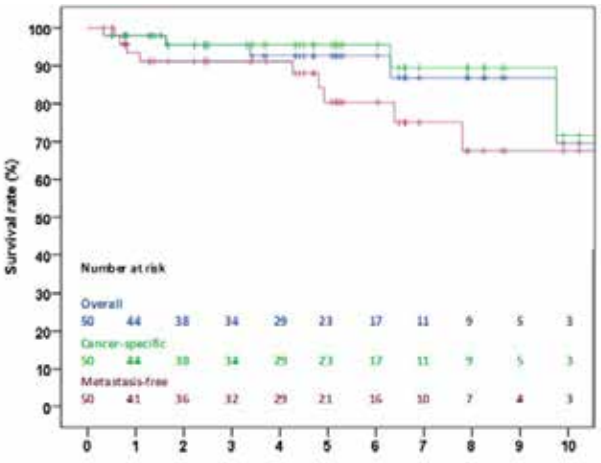

Figure 2

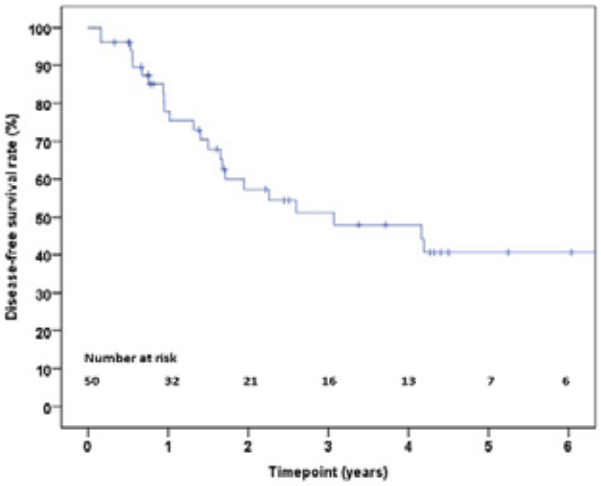

The primary outcome was the progression free survival (PFS) defined as PSA<nadir+2 ng/ml and absence of adjuvant therapy. The secondary outcomes were overall (OS), cancer-specific (CSS) and metastasis-free (MFS) survival rates, adverse events, Clavien-Dindo classification, continence (Ingelman-Sundberg score), erectile function (International Index of Erectile Function-5). Oncological outcomes were estimated using the Kaplan-Meier method.

Results: Thirteen patients treated with post-EBRT parameters, 37 with post-brachytherapy parameters, 35 with whole gland treatment, 15 with hemiablation. The pre-treatment median PSA was 5.3 ng/ml. The median follow-up was 4.6 years. After S-HIFU, median PSA was 0.3 ng/ml. At 5 years PFS, OS, CSS, MFS rates were 41%, 93%, 96% and 80% respectively. Complications grade III occurred in 48% of patients. Post-brachytherapy compared to post-EBRT parameters reduced grade 2-3 incontinence: 34% *vs.* 62% (p=0.015). Incontinence (regardless of rank), bladder outlet obstruction and grade≥III complications were significantly reduced with hemiablation compared to whole gland treatment (14% *vs.* 54%, p<0.001; 13% *vs.* 46%, p=0.03; 13% *vs.* 63% p=0.001 respectively). Before S-HIFU, 25 patients had IIEF-5 score≥17, maintained for 48% at 12 months. The main limitation was the adaption of S-HIFU during the study explained by technological developments.

Conclusions: This study describes the largest series of salvage therapy for local recurrence after LDR brachytherapy. Our data suggest that S-HIFU is efficient for local recurrence after LDR-brachytherapy. Using dedicated acoustics parameters and hemiablation could achieve a favourable efficacy/toxicity ratio. S-HIFU post-PB seems to have more treatment-related toxicity than S-HIFU after external beam radiation therapy.

Acknowledgements: L'Agence nationale de la recherche, Recherche Hospitalo-Universitaire PERFUSE

CA-31

Wednesday

24 October 2018

Topic: Miscellaneous Tumors

Presentation Type: Oral

In vivo image-guided catheter-based ultrasound thermal ablation of tumors in genetically engineered oncogenic pigs

Goutam Ghoshal[1], Lauretta Rund[2], Emery Williams[1], Paul Neubauer[1], Lance Frith[1], Patrick Roady[1], lawrence schook[2], Everette Burdette[1]

[1]Acoustic MedSystems, Inc., Savoy, Illinois, United States
[2]Univiersity of Illinois at Urbana-Champaign, Urbana, Illinois, United States

Background: One of the serious challenges faced in development of technologies for accurate and effective delivery of ablative therapies to solid organ malignancies is the lack of larger animal models which can simulate the size and scale aspects of the physical environment and the clinical workflow characteristics encountered while treating a human patient. Tumor mimics have been the only model available to examine technical aspects of minimally invasive treatment delivery. Thus far, no animal model has been reported that can truly simulate size or scale of tumors comparable to a human patient, which are suitable for device technical evaluation. We propose to assess the treatment efficacy of 3D spatially-registered real-time image-guided needle/catheter based ultrasound (CBUS) thermal therapy in an induced tumor grown in genetically engineered oncogenic pigs, specifically soft tissue sarcomas of the extremity and retroperitoneal regions, both clinically relevant sites closely simulating human disease.

Methods: A transgenic 'oncopig' line encoding a Cre recombinase inducible transgene encoding KRASG12D and TP53R17H, a commonly mutated oncogene and tumor suppressor, respectively, in human cancers was created. Treatment of cells derived from these oncopigs with adenoviral vector encoding Cre (AdCre) led to KRASG12D and TP53R17H expression, which rendered the cells transformed in culture and tumorigenic when engrafted into immunocompromised mice. Finally, injection of AdCre directly into these oncopigs led to the rapid and reproducible development of soft tissue sarcomas in the muscle. Ultrasound imaging was used to monitor the growth of these tumors. Once the tumor reached approximately 2cm by 3cm, it was treated with catheter based therapeutic ultrasound energy for thermal therapy (Fig. 1). Sectored tubular transducers were used to precisely deliver thermal energy to the treatment region. Ultrasound image guidance combined with 3D EM tracking were used to place the applicator in the target region.

Results: The tumors were successfully grown in the muscle within two weeks of injecting the AdCre virus into the oncopigs (Fig. 2). Skin incision less than 1cm length was sufficient to provide for insertion of catheter under image-guided ultrasound for ablating the muscle tumors. The tumors were treated for 6-9 minutes at 7 Watts acoustic power. Thermocouples inserted into the tumors showed temperature range of 55-65 C during the treatment (Fig. 2). Histopathology analysis showed complete ablation of the tumor using single applicator configuration (Fig. 3). Post ablation the survival animal showed diminishing of tumor size based in ultrasound imaging and gross pathology indicated fibrous connective tissue at the tumor site (Fig. 4).

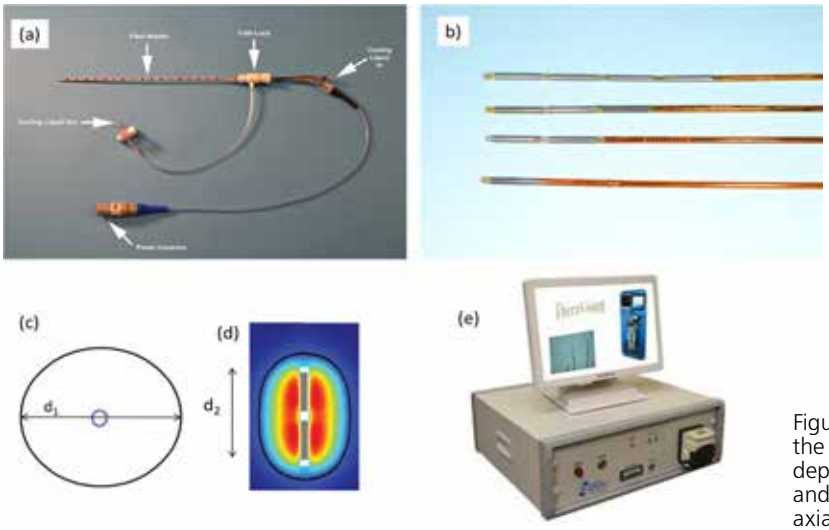

Figure 1. (a) Applicator used for the experiments, (b) tip of the applicator showing the 1-4 element configurations, (c) depiction of treatment patterns using a 360° applicators, and (d) an example thermal treatment pattern along the axial direction

Conclusions: The results suggest catheter-based therapeutic ultrasound can be used to perform fast volumetric ablation of the tumors. The tracked ultrasound image guidance is important to guide and precisely place the catheter at the target region.

Funding Sources: This work was supported by the National Cancer Institute (National Institutes of Health, Bethesda, MD) under NIH Grant R21 CA195433.

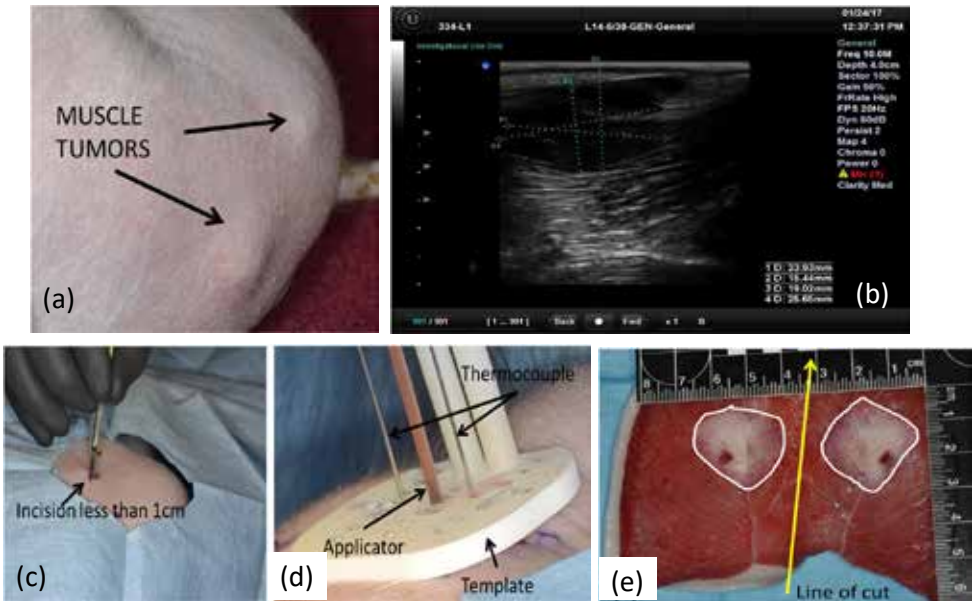

Figure 2. (a) Tumor grown into the oncopig, (b) B-mode ultrasound image before ablation to measure tumor size and the distance between the tumor surface and the skin so that applicator with appropriate active length can be used for treatment. (c) Small incision to insert the applicator, (d) template is used to hold applicator and thermocouples at specified depth and distances during treatment. (e) Post treatment TTC staining and imaging to determine gross ablation zone.

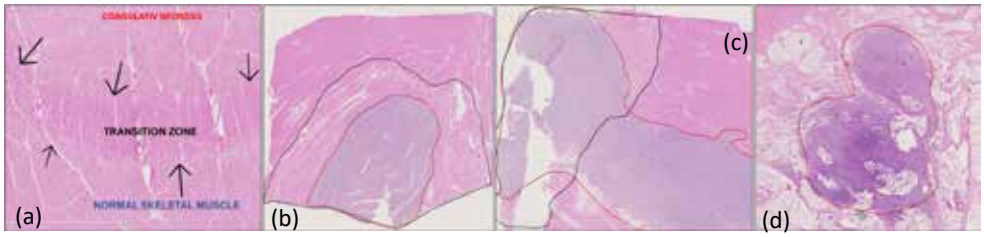

Figure 3. (a) Transitional zone (arrows) of intense injury between the skeletal muscle affected by peracute coagulative necrosis (above) and normal skeletal muscle (below)., (b) Sarcoma (red outline) that is within an area of skeletal muscle affected by acute coagulative necrosis (black outline) due to tissue ablation, (c) The sarcoma (red outline) extends beyond the edge of ablation zone (black outline), (d) Untreated RP sarcoma within red outline.

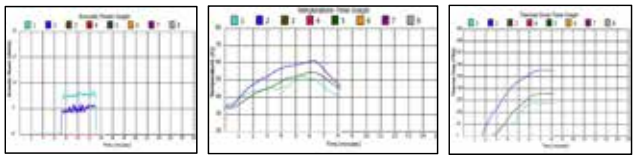

Figure 4a. Tumor treated with 360o transducers placed in the center of tumor, and thermocouples were placed 1 cm from applicator with 3 sensors 10mm apart.

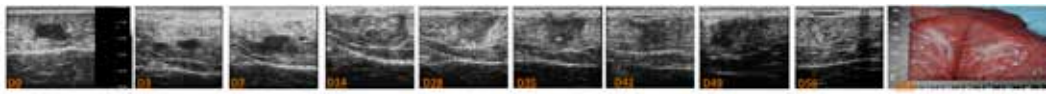

Figure 4b. Ultrasound images taken over the post treatment recovery period demonstrate the tumor tissue diminishing and scar tissue developing. Upon gross exam at necropsy revealed fibrous connective tissue at the original tumor site. Histopathologic exam of these areas is underway.

CA-32

Wednesday

24 October 2018

Topic: Miscellaneous Tumors

Presentation Type: Oral

Non-invasive treatment with MR-guided high intensity focused ultrasound for canine soft tissue sarcoma: A retrospective feasibility analysis

Marion Seward[1], Gregory Daniel[1], Jeffrey Ruth[1], Nikolaos Dervisis[1], Ari Partanen[2], Pavel Yarmolenko[3]

[1]Virginia-Maryland College of Veterinary Medicine, Blacksburg, Virginia, United States
[2]Profound Medical, Mississauga, Ontario, Canada
[3]Children's National Medical Center, Washington, DC, United States

Background: Soft tissues sarcomas (STS) are mesenchymal cell tumors in both people and dogs. In canines, STS account for 15% of all skin tumors and 7% of all subcutaneous tumors. They are locally aggressive and can proliferate through and along fascial planes making excision with clean margins difficult. Local recurrence is common and radical surgery, such as limb amputation, is often required to achieve adequate surgical margins. Magnetic resonance imaging-guided high intensity focused ultrasound (MR-HIFU) is a non-invasive treatment modality that may provide less traumatic treatment options. This modality precisely focuses ultrasound energy within a tumor and can be customized to result in a wide range of local bioeffects. The purpose of this study was to determine the feasibility of using MR-HIFU to treat soft tissue sarcoma (STS) in dogs.

Methods: A retrospective search of medical records of dogs admitted to the Virginia-Maryland College of Veterinary Medicine was performed. In the five-year period from January 1, 2012 to December 31, 2016, fifty-three (53) dogs were found with a diagnosis of sarcoma and available cross-sectional imaging of the tumor (MRI or CT). Targetability of these with a clinical MR-HIFU platform (Philips Sonalleve V2) was analyzed and distances to critical structures (vessels, nerve, bone, bowel) were measured. Tumor tissue (in bone as well as in soft tissue) was considered targetable unless: 1) the ultrasound path was completely obstructed by bone or gas, or 2) the MR-HIFU target was within the spinal cord or less than 1 cm from the margin of the spinal cord. Tumors were categorized as <50% targetable, ≥50% targetable, or non-targetable.

Results: Eighty-one percent of examined STS (81.1%, 43/53) were targetable. The majority of truncal and axillary tumors were ≥50% targetable (88.9%, 16/18) and all extremity tumors were considered ≥50% targetable (100%, 5/5). The highest proportion of non-targetable tumors (36%, 9/25) were found in the head and spine.

Conclusions: This is the first study to evaluate MR-HIFU targetability of canine STS. The majority of canine STS were targetable, and therefore MR-HIFU has potential as a therapeutic modality for treating STS in dogs. Furthermore, this veterinary application is a possible model for treatment of naturally-occurring STS in humans.

CA-33

Wednesday

24 October 2018

Topic: Miscellaneous Tumors

Presentation Type: Oral

Safety and feasibility of magnetic resonance-guided high intensity focused ultrasound (MR-HIFU) for the ablation of relapsed or refractory pediatric solid tumors

Aerang Kim[1], Karun Sharma[2], Pavel Yarmolenko[1], James Geller[3], John Racadio[3], Haydar Celik[2], Avinash Eranki[2], J. Matthew Lanier[3], Rosandra Kaplan[4], Ari Partanen[5], Peter Kim[1]

[1]Children's National Medical Center, Washington, DC, United States
[2]Sheikh Zayed Institute for Pediatric Surgical Innovation, Children's National Medical Center, Washington, DC, United States
[3]Cincinnati Children's Hospital Medical Center, Cincinnati, Ohio, United States
[4]National Institutes of Health, Bethesda, Maryland, United States
[5]Profound Medical, Mississauga, Ontario, Canada

Background: Acute toxicities and late effects of current multi-modal therapy in pediatric cancer are substantial and the prognosis for recurrent/refractory sarcomas and solid tumors remain dismal. MR-HIFU is an ultrasound based technology that can raise tissue temperature with millimeter spatial precision under the guidance of MR thermometry. Advantages over conventional local tumor control such as surgery or radiation therapy are that MR-HIFU is non-invasive, non-ionizing, and enables ablation of large tumor volumes under real-time image guidance. HIFU has been studied in a variety of solid tumors in adults and for relief of pain from bone metastases. There is evidence that HIFU may improve systemic disease by stimulating an anti-tumor immune response. MR-HIFU may provide an alternative to local treatment strategies in pediatric solid tumors. The primary objective of this clinical trial is to determine the safety and feasibility of MR-HIFU ablation in children, adolescents, and young adults with relapsed/refractory solid tumors. Secondary objectives include the evaluation of changes in functional imaging, quality of life, and immune markers in children treated with MR-HIFU.

Methods: In this multi-institutional trial (NCT02076906), patients ≤ 30 years of age with relapsed/refractory solid tumors including desmoid tumors are eligible. Tumor target lesions are limited to those located in or close to bone at sites accessible to MR-HIFU. Patients with target lesions in the skull or spine or any contraindication for MRI are excluded. Patient imaging and eligibility are reviewed by multi-disciplinary HIFU team. Patients undergo HIFU treatment of selected lesion(s) under general anesthesia. Tolerability is defined during the 14 days following MR-HIFU ablation. Disease status is evaluated using standard imaging techniques post treatment. Quality of life using patient reported outcomes and immune pharmacodynamic markers are collected at baseline and subsequent treatment intervals.

Results: As of 9/2017, the first cohort of six patients (3M, 3F; median age 14 years (range 4-21)) were enrolled at two study sites and received at least one treatment. Histologies were osteosarcoma, Ewing sarcoma, rhabdomyosarcoma (n=1 of each) and desmoid tumor (n=3). No patients had treatment limiting toxicity. All related toxicities were mild with transient pain and skin burn being most common. Two patients underwent 2nd MR-HIFU treatment of another target lesion and one patient underwent 2nd MR-HIFU of the same incompletely treated target lesion.

Conclusions: MR-HIFU ablation of solid tumors in children, adolescents, and young adults appears to be safe and feasible. Response and changes in quality of life patient reported outcomes and immune markers' analyses are underway. The study has been expanded to enroll six more patients for additional safety and feasibility experience and outcomes. The trial is open to enrollment and accrual is ongoing.

CA-34

Wednesday

24 October 2018

Topic: Miscellaneous Tumors

Presentation Type: Oral

The role of technical parameters on ablation volume during MR-guided focused ultrasound of desmoid tumors

Matthew Bucknor, Gabriela Beroukhim, Viola Rieke, Eugene Ozhinsky, Iryna Lobach

University of California – San Francisco, San Francisco, California, United States

Background: Desmoid tumors are benign, but locally aggressive monoclonal proliferations of fibroblasts arising in muscle and connective tissues. Conventional treatments for these tumors include surgery, radiation, and systemic medical therapy. However, recurrence is high even with multi-modality therapy. Magnetic resonance-guided focused ultrasound (MRgFUS) has emerged as a safe and effective treatment for control of desmoid tumors with a favorable side effect profile (Figure 1).[1,2] However, the use of MRgFUS devices and software for ablation of desmoid tumors relies on technical parameters that were developed for treatment of uterine fibroids, which can demonstrate very different responses to heating than desmoid tumors. For example, a T2 hyperintense fibroid classically heats very poorly during MRgFUS, whereas T2 hyperintense desmoid tumors frequently heat very well. The purpose of this study was to retrospectively review MRgFUS treatments of desmoid tumors at our institution to determine which technical treatment parameters contributed most significantly to accumulation of ablative thermal dose.

Methods: The study protocol was approved by the local Institutional Review Board. We retrospectively reviewed sonication data from all MRgFUS treatments performed in histologically confirmed desmoid tumors, over a period of 18 months from December 2014 through July 2016. Recorded sonication parameters included transducer roll (degrees), transducer pitch (degrees), power (W), sonication duration (s), sonication energy (J), focal height (mm), average temperature (Celsius), sonication type (short, nominal, or elongated) (Figure 2), and accumulated dose (cc). A linear mixed effects model was then used to determine the relative effect of each parameter on accumulated dose.

Results: 13 desmoid tumor treatments were performed at our institution over 18 months, in seven patients. In total, data from 946 individual sonications was reviewed. The average number of sonications performed in each treatment was 73 ± 40 with a range of 6 to 140. The generalized mixed effects model demonstrated that multiple technical parameters had significant standardized/ß coefficients: Roll (ß = 0.012, p=0.012), Power (ß =0.006, p=0.000), Duration (ß =0.057, p<0.001), Energy (ß =0.00035, p<0.001), Average Temp (ß = 0.03, p< 0.001), Dose Area (ß = 0.0068, p<0.001), suggesting that increases in these technical parameters were individually significantly associated with increases in accumulated dose volume. Interestingly, the most significant individual effect size was seen with spot type (ß=0.12, p<0.001).

Additional pending results include a determination of exactly which types of sonications (e.g as defined by energy, configuration), most frequently result in highly effective ablations (75% or more of the intended sonication volume).

Conclusions: These findings suggest that each of these technical parameters individually has a significant effect on the ablation volume dose for each sonication during MRgFUS of desmoid tumors. In our univariate linear mixed effects model, spot type appeared to demonstrate the largest effect size, suggesting that the choice of spot configuration plays a significant role in successful MRgFUS ablation of desmoid tumors. This work can serve as the basis for future more complex multivariate analyses to help build better treatment protocols for MRgFUS of desmoid tumors.

Figure 1. Post-treatment delayed delayed contrast enhanced segmented inversion recovery fast gradient echo (TR/TE/flip angle=1.5ms/15.2ms/15), LAVA 3D spoiled gradient echo sequences obtained following successful MRgFUS of a desmoid tumor. There is marked nonperfusion within the tumor centrally with a thin rim of peripheral enhancement consistent with tumor necrosis.

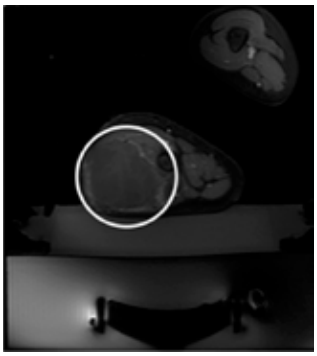

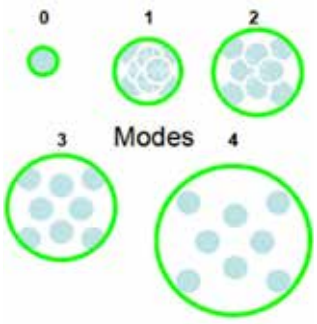

Figure 2. Schematics of the configurations of sub-sonications energy foci in the five different modes of nominal sonications. Short sonications also use eight sub-sonication foci. Elongated spots require between 8 and 25 sub-sonication foci.

References

1. Ghanouni P, Dobrotwir A, Bazzocchi A, et al. Magnetic resonance-guided focused ultrasound treatment of extra-abdominal desmoid tumors: a retrospective multicenter study. *Eur Radiol* 2016.
2. Avedian RS, Bitton R, Gold G, Butts Pauly K, Ghanouni P. Is MR-guided High-intensity Focused Ultrasound a Feasible Treatment Modality for Desmoid Tumors? *Clin Orthop Relat Res* 2016;474:697–704.

CA-35

Wednesday

24 October 2018

Topic: Miscellaneous Tumors

Presentation Type: Oral

Volumetric hyperthermia of soft tissue sarcoma using MR guided high intensity focused ultrasound: Case report

Edwin Heijman[1], Sin Yuin Yeo[2], Lukas Sebeke[3], Robert Staruch[4], Grischa Bratke[3], Michael Püsken[3], Armin Tuchscherer[3], David Maintz[3], Holger Gruell[2]

[1]Philips Research Germany, Cologne, Germany
[2]Klinikum der Universitaet zu Koeln, Cologne, Germany
[3]Uniklinik Köln, Cologne, Germany
[4]Profound Medical, Mississauga, Ontario, Canada

Background: Multiple studies have shown that mild hyperthermia improves treatment efficacy of radiotherapy, chemotherapy and chemoradiotherapy without adding extra toxicity. For example, Issels et al. recently showed that hyperthermia improves local tumor control[1] as well as local progression-free survival and overall survival of sarcoma patients[2]. While RF based hyperthermia devices are current standard for regional hyperthermia, MR-HIFU could potentially offer improved conformal hyperthermia (HT) thanks to temperature-based feedback in conjunction with targeted heating. Here, we describe the first three MR-HIFU hyperthermia treatments of a liposarcoma patient. Treatment was offered and approved as compassionate use.

Methods: The treatment was performed using a Sonalleve® V2 tabletop HIFU system including a DISC cooling (Profound Medical) integrated in a 3T Ingenia MRI scanner (Philips Healthcare). The hyperthermia control was based on the work of Tillander et al3. Seven treatment cells with 10 mm diameter each were spatially arranged within the tumor to yield a round treatment cell cluster with an overall diameter of 3.2 cm. Sonications were performed at an acoustic frequency of 1,0 MHz with a target temperature set to 42.5 °C. A newly developed Hyperthermia Manual Control (HMC) application tool (Figure 1) was implemented in the hyperthermia build of the Sonalleve therapy console software allowing the physician to manually pause sonications or an adjustment of sonication power during the treatment.

The patient (59 year old male) suffered from a dedifferentiated liposarcoma of the right spermatic cord infiltrating the femoral vein next to the pelvic bone and bladder inducing pain (VAS score of 6/10). Metastasis were found in the psoas major muscle and lungs. The patient received a chemotherapy combination of olaratumab, prior, and doxorubicin during MR-HIFU every 3 weeks. The MR-HIFU hyperthermia therapy was offered as a treatment option to alleviate pain and support the chemotherapy. To reduce risk, the tumor was only partially treated with the bladder in the far field. Each session was separated in a planning and therapy phase to relieve the patient pain and empty the bladder.

Results: The patient was treated in three sessions with total 56 min of hyperthermia duration. Figure 2 shows a temperature map, temperature curves and acoustic power output of the first therapy. Table 1 gives a summary of the three sessions. In the second session the treatment was restarted after emptying the bladder. No non-perfused-volume was found in the tumor although median Tmax was > 43 degrees during the first session. After the first session, liposarcoma became partially necrotic and local tumor control was reached. Over the sessions it became more difficult to maintain the temperatures in the tumor even after increasing the acoustic power. The patient did not received additional analgesia and tolerated the periods of sonication very well. No adverse events or discomfort was reported.

Conclusions: Technically, the MR-HIFU induced hyperthermia therapy was successful and safe. Overall, Tmean temperature were too low due to motion affected temperature mapping stability leading to variations in heating as well as the change in acoustic absorption probably caused by tumor necrosis.

References:

1. Issels, R. D. et al. Neo-adjuvant chemotherapy alone or with regional hyperthermia for localised high-risk soft-tissue sarcoma: A randomised phase 3 multicentre study. *The Lancet Oncology*. 2010;11:561–570.
2. Issels, R. D. High-risk soft tissue sarcoma: Clinical trial and hyperthermia combined chemotherapy. *International Journal of Hyperthermia*. 2006;22:235–239.
3. Tillander, M. et al. High intensity focused ultrasound induced *in vivo* large volume hyperthermia under 3D MRI temperature control. *Medical Physics*. 2016;43:1539.

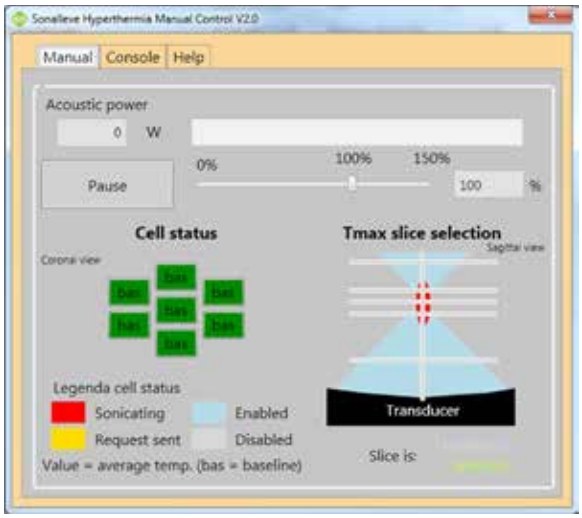

Figure 1. Graphical user interface of the Sonalleve Hyperthermia Manual Control (HMC) app.

Figure 2. Left: Temperature map in the tumor (white circle is the treatment cluster). Right: Temperature curves combined with the total acoustic power curve of the first treatment session.

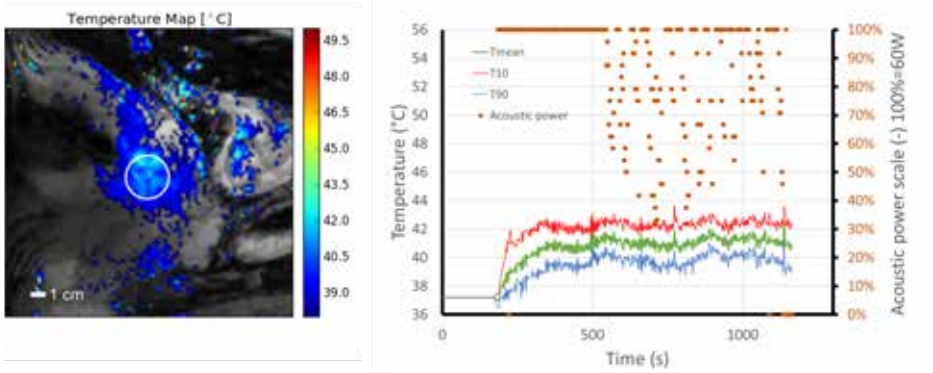

Table 1. Summary of the different treatment sessions. Therapy duration is the time of having a stable temperature in the treatment cell cluster.

Treatment session	1	2		3
Set temperature (°C)	42.5	42.5	42.5	42.5
Acoustic power (W)	60	60	80	80
Therapy duration (min)	13,6	22,8	5,3	13,8
Average mean temperature (°C)	41,1	40,0	39,1	39,6
Median max temperature (°C)	43,9	42,9	41,1	42,5
Reason of stopping sonication	Error: large motion detected	Stopped by patient	Error: large motion detected	Error: excessive heating
Temperature baseline measurement time (min)	3,1	3,1	3,1	3,0
Heating up time (sec)	2,7	1,5	1,0	2,8

CA-36

Wednesday

24 October 2018

Topic: Miscellaneous Tumors

Presentation Type: Oral

Focused ultrasound-mediated delivery of therapeutic agents for the treatment of head and neck cancer

Ali Mohammadabadi, Pavlos Anastasiadis, Jimena Dancy, Aniket Wadajkar, Jesse Smith, Jeffrey Winkles, Anthony Kim, Victor Frenkel

University of Maryland School of Medicine, Baltimore, Maryland, United States

In accordance with author request, this abstract is not available for publication.

CA-38

Wednesday

24 October 2018

Topic: Miscellaneous Tumors

Presentation Type: Oral

Towards FUS for lung cancer, which patient group with primary or secondary lung cancer is preferably accessible

Frank Wolfram, Uwe Funke, Joachim Böttcher, Thomas G Lesser

SRH Waldklinikum Gera, Gera, Germany

Background: Oncological manifestations in lung, such as primary Lung Cancer (LC) or Metastases are life threatening diseases with high incidence [1]. Surgical resection is the best treatment choice that can provide curativity. Most of LC patients are functionally inoperable at diagnosis and would benefit from minimal invasive - parenchyma sparing interventions [2]. In order to make FUS available for those, we previously investigated the condition of One Lung Flooding (OLF) [3] for sonographic guided HIFU ablation of central lung tumours [4].

In order to justify OLF, the appropriate clinical indication needs to be identified. Therefore, this study was aimed to investigate patient groups with primary and secondary lung tumours under aspects of accessibility to OLF, tumour volumes and locations.

Methods: Patient files from consecutive diagnosed patients with primary Lung Cancer (LC) and Lung Metastasis (MTS) have been included. The tumour board classifies inoperable cases regrading guideline. After anonymization, the cases were analysed by Excel (MS Office 2013) and SPSS (IBM, v20) and tested for significance (two sided $p<0,05$).

Data collection included clinical UICC staging, lung function status (FEV1, FVC, TLCO) and radiological datasets at the point of diagnosis (CT, PET). Accessibility to OLF was determined by the inclusion criteria for One Lung Ventilation. The tumour diameter, total tumour volume, number of nodules and depth of location were extracted from radiological images using LungVCAR (NEXUS, GE Healthcare) toolbox (Fig. 1).

Results: In total, 110 cases with inoperable primary Lung Cancer (83 male; 27 female; mean age 68.1y) and 80 with Lung Metastases (59 male; 21 female; mean age 69.2y) were included.

Out of the LC group, 55.5% (46/83) were accessible to OLF, as were 67.5%(54/80) of the MTS group. Advanced chronical obstructive lung disease (COPD) caused the exclusion in 83.7% of patients with primary LC and in 73% of the MTS group. All patients (LC and MTS) under the age of 50y showed no limitations to OLF. Increasing age shows a significant correlation with inaccessibility to OLF (Fig. 2). 64% of the Small Cell Lung Cancer (SCLC) subgroup showed accessibility to OLF, whereas 100% of those are inoperable due to advanced stages (17% IIIb; 73% IVa,b).

The mean tumour volume in the MTS group ($4.7cm^3$;min$0.15cm^3$max$45cm^3$) is significantly lower than in the Lung Cancer group ($45cm^3$;min$2.3cm^3$max$295cm^3$). Out of the MTS group, 44.3% had single metastases and only 7.7% had more than nine. The mean transcostal distance of the deepest tumour location was 80,5cm ± 28cm in the MTS group, and 93.2cm ± 33cm in the LC group.

Conclusions: Regarding Lung Flooding, approx. 50% of lung cancer and 2/3 of patients with lung metastases are accessible to OLF, and therefore FUS in Lung. Chronic obstructive lung disease (COLD) was the main cause of exclusion. The mean tumour volume and depth of tumour location was lower in the MTS group, which is therefore more favourable to FUS. Future work should be dedicated to combination strategies for the advanced LC stages.

References

1. R. Meza, C. Meernik, J. Jeon und M. Cote. Lung Cancer incidences trends by gender, race and histology. *PLOS ONE*. 2015;10(3):e0121323.
2. M. Guckenberger und M. Flentje. Lokal ablative nichtchirurgische Verfahren beim NSCLC. *Onkologe*. 2011;17:715-20.
3. T. Lesser, S. Klinzing, H. Schubert, U. Klein und M. Bartel. Lung flooding—a new method for complete lung sonography. *Res Exp Med*. 1998;198(2):83-91.
4. F. Wolfram, C. Boltze, H. Schubert, S. Bischoff und T. Lesser. Effect of lung flooding and high-intensity focused ultrasound on lung tumours: An experimental study in an *ex vivo* human cancer model and simulated *in vivo* tumours in pigs. *Eur J Med Res*. 2014;19(1).

Figure 1. Determination of tumour size, volume and localization using LungVCAR (Nexus, GE Healthcare)

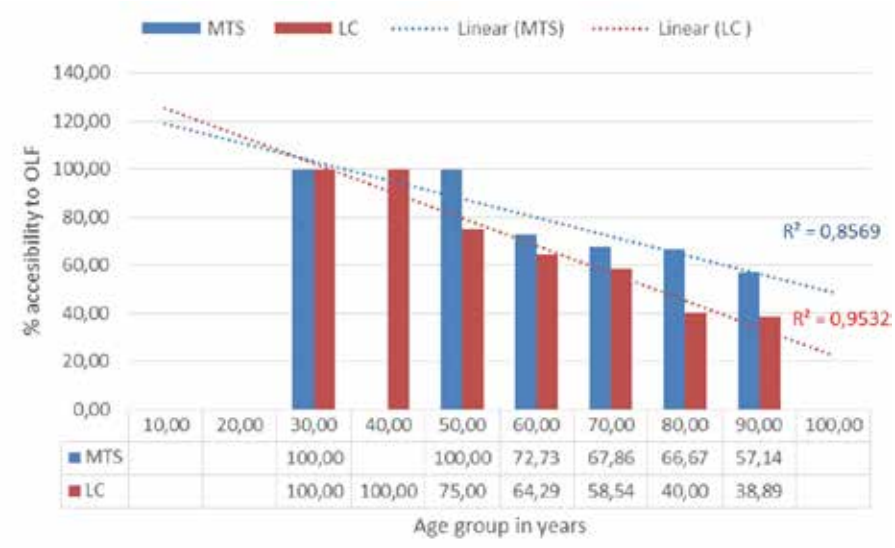

Figure 2. Relative accessibility to One Lung Flooding (OLF) with age from Lung Cancer and Lung Metastases group

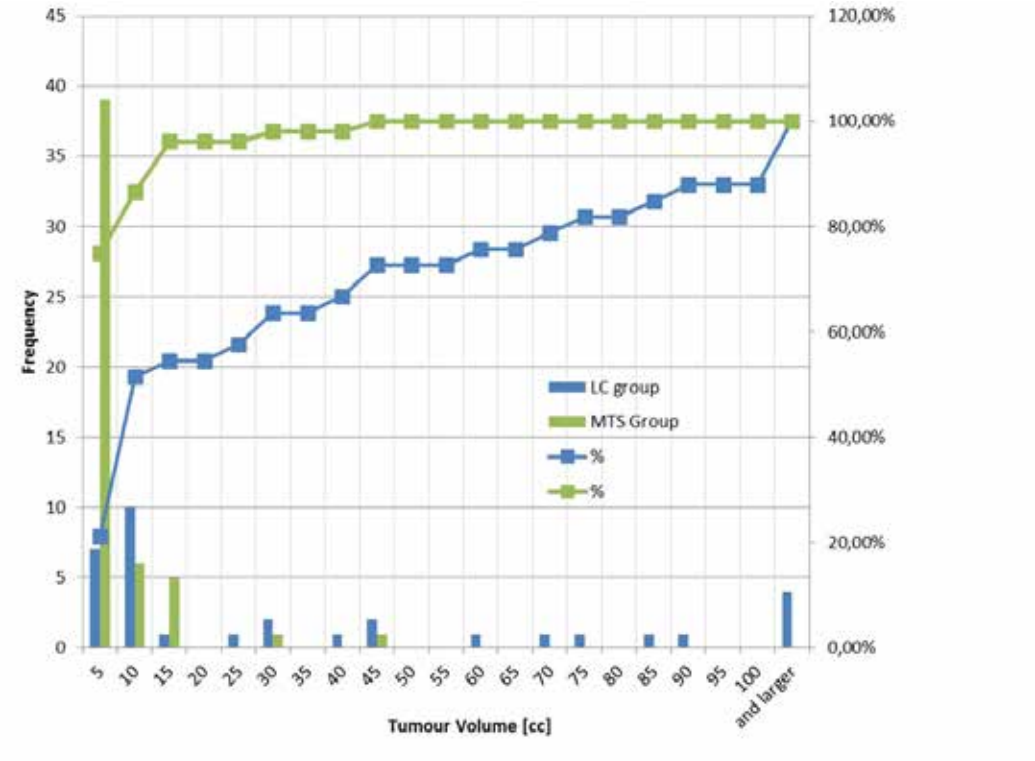

CA-39

Wednesday

24 October 2018

Topic: Miscellaneous Tumors

Presentation Type: Oral

Treatment of Ewing's sarcoma using localized delivery of thermosensitive liposomal doxorubicin and MR-HIFU mild hyperthermia

Chenchen Bing[1], Bingbing Cheng[1], Ming Xu[1], Imalka Munaweera[1], Debra Szczepanski[1], Theodore Laetsch[2], Rajiv Chopra[1]

[1]UT Southwestern Medical Center, Dallas, Texas, United States
[2]Children's Medical Center, Dallas, Texas, United States

Background: Ewing's sarcoma comprises approximately 15% of all pediatric cancers and its survival has been gradually improved via chemotherapy. Doxorubicin (DOX) delivery using thermosensitive liposomes (TSLs) and MR-HIFU hyperthermia (HT) might enable enhanced local control in solid tumors without increasing cardiotoxicity. This study evaluates the tumor control achieved using the combination of TSL-DOX and MR-HIFU mild hyperthermia in rodent pediatric tumor model (ES-1). ES-1 tumor cell cytotoxicity with DOX/TSL-DOX at different temperatures was investigated *in vitro*. The tumor growth in rats treated with TSL-DOX and MR-HIFU mild hyperthermia was measured and compared with controls.

Methods: In *in vitro* experiments, ES-1 growth viability with different concentration (0 to 100 μM) of DOX or TSL-DOX was measured at 72 hours after a brief exposure to 42°C *vs.* 37°C controls. For *in vivo* experiments, nude rats with unilateral ES-1 tumors were randomly assigned into 4 groups: control (n = 10), TSL-DOX only (n = 9), HT only (n = 5) and TSL-DOX + HT (n = 7). 9 days after tumor inoculation, the rats were treated with mild HT (42°C) for 30 minutes using a small animal MR-HIFU system (RK100, FUS Instruments) on a 3T MRI (Ingenia, Philips Healthcare) (Figure 1A). The frequency of focused ultrasound was 3.02 MHz. Data communication between the MRI scanner and the HIFU system was achieved via matMRI toolbox. PRF-shift based MR thermometry was acquired and temperature feedback control was performed using a PID controller. A sector vortex lens was used to create an enlarged heating region to cover the entire tumor (Figure 1B, C). TSL-DOX (2.5 mg/kg, Thermodox®, Celsion) was infused over 5 minutes through the tail vein starting when the tumor temperature reached 41°C. Tumor volume was measured every 2 days after treatment using a 1T MRI. The tumor volume of TSL-DOX + HT group was compared with other groups to evaluate the treatment effect.

Results: The *in vitro* results showed that TSL-DOX had similar cytotoxicity as DOX at temperature of 42°C due to release (Figure 2). For HT only and TSL-DOX + HT groups in the *in vivo* experiments, the mean temperature around the tumor was 41.4 ± 0.7°C, with 10th and 90th percentile to be 39.9 ± 0.7°C and 43.0 ± 1.0°C, confirming the capability of accurate temperature control (Figure 3). The duration when the mean temperature within the treatment region was in the range of 40-45°C was 30.5 ± 1.8 minutes, indicating adequate HT. TSL-DOX + HT group had a significant effect in controlling the tumor growth compared with control group (p-value = 0.0461) (Figure 4).

Conclusions: Cytotoxic doses of DOX can be locally delivered to ES-1 tumors in rats using MR-HIFU mild hyperthermia and TSL-DOX. The combined strategy showed an excellent and reliable controlling effect on the tumor growth.

Acknowledgements: Financial support for this study was provided by the National Institutes of Health (1R01CA199937).

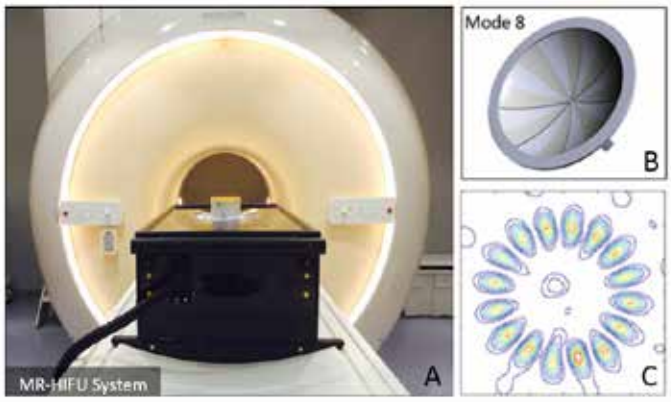

Figure 1 shows the experiment setup including the MR-HIFU system and 3T MRI scanner (A) and the sector vortex (B). Panel C is the heating pattern created when equipped the transducer with the lens.

Figure 2 is the ES-1 cell viability under different concentration of free doxorubicin (A) or thermosensitive doxorubicin (B) at different temperature. Similar behavior was observed with thermosensitive doxorubicin compared to free doxorubicin at 42°C.

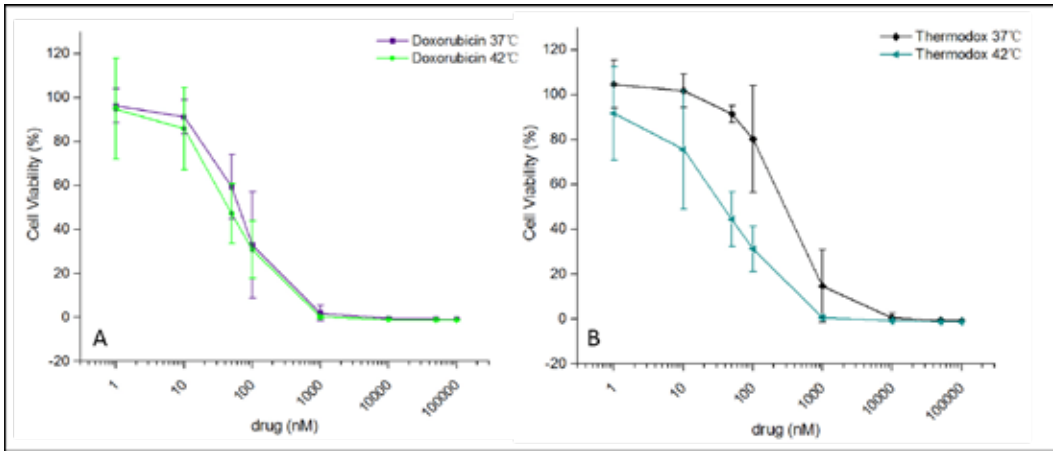

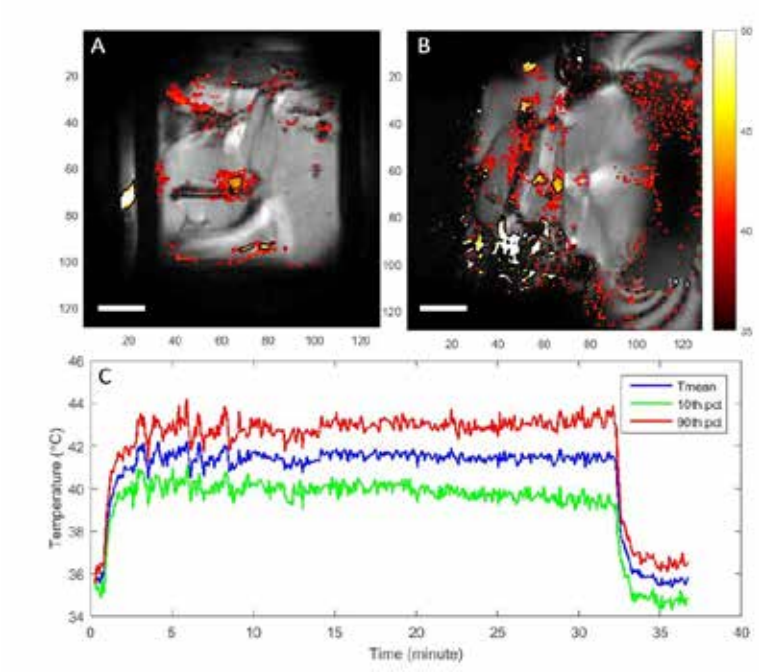

Figure 3 shows the temperature maps acquired during hyperthermia treatment (A, B). Good temperature control at target temperature of 42°C was achieved (C).

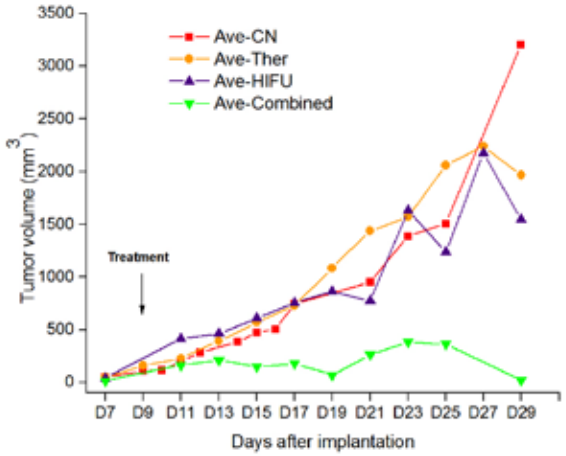

Figure 4 shows the tumor growth curves for different groups. The combined treatment with mild hyperthermia and thermo-sensitive doxorubicin had significant tumor control effect compared to the control group (paired t-test, $p = 0.0461$).

CA-40

Wednesday

24 October 2018

Topic: Miscellaneous Tumors

Presentation Type: Oral

The effect of high-intensity focused ultrasound treatment on thyroid and immune functions in patients with benign thyroid nodules

Brian Lang, E Lin

University of Hong Kong, Hong Kong SAR, China

Purpose: Studies have shown that thermal ablation by high intensity focused ultrasound (HIFU) can cause a rise in immune-related cytokines like tumor necrosis factor (TNF) and interleukin-6 (IL-6) in the early post-ablation period by generating large volume of tumor debris. The aim of this study was to investigate the effect of high-intensity focused ultrasound (HIFU) on local (thyroid) function and immune-related cytokines in patients with benign thyroid nodules.

Methods: From 2017 to 2018, consecutive patients who underwent a HIFU ablation for a benign thyroid nodule within a single session under IV sedation were analyzed. Venous blood samples were collected 1 hour before treatment (Baseline), during treatment when the target had been ablated by 50% in volume (t1), immediately after treatment (t2) and 96 hours after treatment (t3). Serum TSH, Free T4 (FT4), thyroglobulin, anti-thyroglobulin and anti-thyroid perioxidase auto-antibodies, erythrocyte sedimentation rate (ESR) and C-reactive protein (CRP) as well as levels of tumor necrosis factor (TNF) and interleukin-6 (IL-6) were checked at each time point. Levels were determined in the same laboratory using the same technique and assay.

Results: A total of 25 patients were eligible for analysis. Baseline serum TSH and FT4 remained similar at t1 ($p>0.05$) and t2 ($p>0.05$). However, serum TSH dropped significantly at t3 (1.03 mIU/L to 0.92 mIU/L, $p<0.001$) while baseline FT4 had a corresponding increase (from 16.27 ± 2.0 pmol/L to 18.5 ± 6.5 pmol/L, $p<0.001$). Baseline serum Tg began to rise from t2 ($p<0.05$) and peaked at t3 (106.5 ± 114.3 ng/mL to 1757.0 ± 1929.0 ng/mL, $p<0.001$). However, baseline TNF and IL-6 levels did not change significantly at t1 ($p>0.05$), t2 ($p>0.05$) or t3 ($p>0.05$). Similarly, baseline ESR and CRP also did not change significantly at t3 ($p>0.05$).

Conclusions: In the early post-ablation period (in the first 96 hours of ablation), HIFU ablation seemed to have a greater local effect (i.e. the thyroid gland itself) than a systemic effect or body immune system. Perhaps, future studies could focus on other potential immune-related cytokines and inflammatory markers in HIFU ablation of thyroid gland.

CA-41

Wednesday

24 October 2018

Topic: Miscellaneous Tumors

Presentation Type: Oral

Treating solid tumors and non-healing wounds in veterinary patients with focused ultrasound

Harshini Ashar[1], Kalyani Ektate[1], Danielle Dugata[1], Rajiv Chopra[2], Jack Hoopes[3], Steven Fiering[3], Jerry Malayer[1], Grant Rezabek[1], Ashish Ranjan[1]

[1]Oklahoma State University, Stillwater, Oklahoma, United States
[2]UT Southwestern Medical Center, Dallas, Texas, United States
[3]Dartmouth College, Lebanon, New Hampshire, United States

Background: The annual cancer incidence, tumor type and sites in canine patients are comparable to humans. Specifically, canine oral squamous and non-squamous masses are often well-established when detected in the oral cavity and metastasize aggressively. Similarly, the non-healing wounds caused by hard-to-treat biofilm-forming bacteria in canine patients replicate the infection profile in humans and often require long duration antimicrobial treatment, extensive surgical debridement, and in many cases amputations. The objective of our ongoing veterinary clinical trial is to determine the potential of focused ultrasound in treating privately owned dogs with spontaneous oral cancers, and infectious wound.

Material & **Methods:** Since late 2017, we have recruited three canine oral cancer and one non-healing wound patients for FUS clinical treatment in the hospital. Case#1 was a 9-year-old Shetland Sheepdog, castrated male with a plasmacytoma mass (Length = 25mm. Width = 20mm) on the lower right lip margin at the level of the canine/premolars that extended into the gum margin. Case # 2 was a 10 yr old, neutered male, castrated Border Collie that was presented with a 22mm x 16mm firm acanthomatous ameloblastoma mass on the mandible. Case # 3 was an 8-year-old spayed female Yorkshire Terrier with a large, raised, red, hairless cutaneous mast cell mass on the left upper lip extending into the lateral margin of the nostril. Case#4 was a dog patient with a non-healing infected wound in the elbow region. For treatments, we used the Alpinion FUS transducer of 1.5 MHz central frequency, 45 mm radius and 64 mm aperture diameter with central opening 40 mm in diameter. For FUS exposure, the tumor was aligned at a fixed focal depth for efficient coverage voxel size (5 x 5 x 10mm) using sector vortexed lens. 1-3 ablative focused ultrasound treatment for 3-5 min was performed for each patient. Endpoints were to measure tumor regression, and histopathological assessment of biopsies prior to treatment and then at the end of treatment to evaluate treatment success.

Results: Recheck evaluation in 3-weeks suggested clearance of plasmacytoma and ameloblastoma cancer in dogs with no ulcers present. Histopathological analysis indicated peritumoral inflammation with no evidence of tumor cells. For the cutaneous mast cell patient, a >50% reduction in the tumor volume was noted with erythema and mild ulcerations in the treatment regions that resolved over time. Lastly, bacterial culture performed in the non-healing wound patient to determine the presence of biofilm pathogens indicated the absence of infection at the end of first treatment.

Conclusions: Early clinical data suggests promising tumor remission and infection clearance following FUS treatment in veterinary patients. Additional studies to characterize the characteristics of tumor-infiltrating immune cells in the oral biopsy masses and efficacy of FUS to augment antimicrobial efficacy in patients are currently in works.

CA-42

Wednesday

24 October 2018

Topic: Bone
Presentation Type: Oral

The Horizon 2020 FURTHER project: Focused ultrasound and radiotherapy for non-invasive palliative pain treatment in patients with bone metastasis

Lenny Verkooijen[1], Wilbert Bartels[1], Clemens Bos[1], Chrit Moonen[1], Stephanie Stock[2], Holger Gruell[2], Sin Yuin Yeo[2], Dirk Mueller[2], Roberto Blanco[3], Alessandro Napoli[4], Martijn Boomsma[5], Erik Phernambucq[5], Alberto Bazzocchi[6], Matthew Brown[7], Nandita Desouz[7], Jessica Foley[8]

[1]University Medical Center Utrecht, Utrecht, Netherlands
[2]Klinikum der Universitaet zu Koeln, Cologne, Germany
[3]Varsinais-suomen sairaanhoitopiirin kuntayhtyma, Turku, Finland
[4]Universita degli studi di Roma la sapienza, Rome, Italy
[5]Stichting isala klinieken, Zwolle, Netherlands
[6]IRCCS Istituto Ortopedico Rizzoli, Bologna, Italy
[7]Institute of Cancer Research — Royal Cancer Hospital, London, United Kingdom
[8]Focused Ultrasound Foundation, Charlottesville, Virginia, United States

Background: The current standard of care for patients with painful bone metastasis includes palliative locoregional treatment using external beam radiotherapy (EBRT). While EBRT is a well-established treatment option, it takes up to four weeks for EBRT to induce adequate pain relief.[1] Unfortunately, thirty to forty percent of patients do not respond to EBRT, and 50% of responders experience recurrent pain (Figure 1). Re-irradiation is only effective in a small majority (58%) of patients.[2] Hurwitz[3] demonstrated in a multicenter randomized trial that MR-HIFU is a safe and effective, non-invasive treatment for alleviating pain caused by bone metastases. Response to MR-HIFU was typically rapid, with about two-thirds of responses seen within days after treatment. This study was however performed in patients who were ineligible, or who failed or declined radiation. As such, there is a lack of evidence that supports MR-HIFU as a standard first-line treatment alternative to EBRT. Evidence is lacking for wide-spread implementation of MR-HIFU as routine palliative care of painful bone metastases. Therefore, the FURTHER consortium sets out to demonstrate the effectiveness and cost-effectiveness of MR-HIFU compared to EBRT as a palliative treatment option to relieve bone pain caused by metastases. The FURTHER project starts in early 2019.

FURTHER Project objectives

- Generate Level I evidence to demonstrate that short-term pain relief is superior in treatment regimens with MR-HIFU (alone or in combination with EBRT) as compared to standard-of-care treatment with EBRT. Primary outcome of the trial will be pain at 14 days after randomization.
- Develop a prediction model to identify patients who are likely to benefit from MR-HIFU or radiotherapy in order to allow (cost-) effective use of the treatment.
- Investigate the added value of integrating MR-HIFU into a comprehensive pain management pathway that does not only focus on the pathophysiological component of pain but also takes into account psychophysical aspects of pain.
- Determine the cost-effectiveness of pain palliation using approaches based on MR-HIFU and EBRT.
- Identify strategies for the adoption of MR-HIFU into standard care, mapping and analysing socio-economic factors that influence uptake and access to MR-HIFU treatment.
- Raise awareness and acceptance of MR-HIFU as a treatment option for pain palliation amongst patients, care professionals and informal carers.

Methods: Effectiveness and cost-effectiveness will be studied in a three armed RCT, where patients will be randomized to standard EBRT, MR-HIFU only, or EBRT with MR-HIFU. In a pilot pathway trial, MR-HIFU will be integrated in a pain management strategy that tackles cancer induced bone pain in a comprehensive manner. In addition, the FURTHER consortium will map and analyse socio-economic factors that can influence the integration of MR-HIFU in routine care on a local level.

References

1. Westhoff et al. *IJROB* 2015;93(3)
2. *IJH*, 2015;31(3)
3. Hurwitz et al. *JNCI*, 2014;106(5).

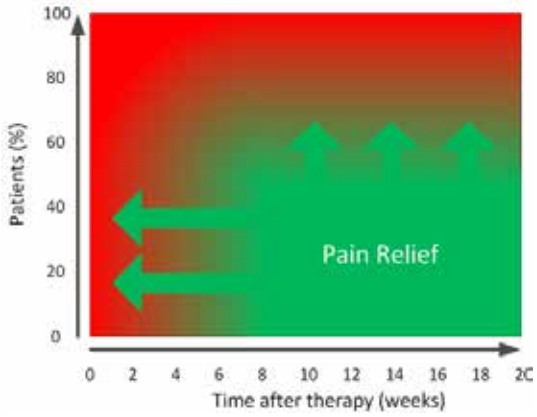

Figure 1. Radiotherapy achieves pain relief in 60-70% of patients after 4-6 weeks. There is a clinical need for more rapid pain relief, as well as for treatment options for the people that do not respond to EBRT, that MR-HIFU has the potential to address.

CA-43

Wednesday

24 October 2018

Topic: Cancer Immunotherapy

Presentation Type: Oral

Exploiting FUS as a strategy for myeloid cell modulation and repolarization in metastatic breast cancer

Natasha Sheybani[1], Cyril Lafon[2], Alexandra Witter[1], David Schlesinger[1], Frederic Padilla[1,2], Richard Price[1], Timothy Bullock[1]

[1]University of Virginia, Charlottesville, Virginia, United States
[2]LabTAU, Inserm, Lyon, France

Background: Myeloid cells serve as key players in the effective mounting of immune response against tumors. We hypothesize that understanding the differential impact of mechanical and thermal focused ultrasound (FUS) regimens on myeloid cells in the tumor microenvironment is essential for comprehending the antitumor effects of FUS, particularly when these FUS regimens are used in combination with immunotherapy. In the preliminary study presented herein, we evaluate whether FUS can impact the representation and polarization of myeloid cells in a murine model of metastatic breast cancer - 4T1 mammary carcinoma - characterized by a highly immunosuppressive microenvironment. This syngeneic mouse breast cancer model is known to have a strong hematopoietic cell infiltrate consisting predominantly of Gr-1+/CD11b+ myeloid cells that have been profiled as myeloid-derived suppressor cells (MDSCs) capable of inhibiting specific T-cell-mediated tumor immunity.

Methods: Mice bearing subcutaneous 4T1 tumors were exposed to one of three different ultrasound exposure conditions targeting ~50% tumor volume: boiling histotripsy, thermal ablation, or microbubble destruction. In a separate round of experiments, we compared these FUS regimens to single fraction radiation therapy. Seven days following treatment, animals were sacrificed and tumors, secondary lymphoid organs, and blood were harvested for analysis by flow cytometry. Two panels were used to quantify myeloid and T cell subsets. In the myeloid panel, immune cells were first gated as CD45.2+, and subsequently gated according to markers for CD11b+ with MDSC subsets, macrophages with DP, M1 and M2 subsets, dendritic cells and CD86+ subset, monocytes, and NK cells. Data were analyzed either as an absolute frequency of cells, as percentages of CD45.2+ cells, and as absolute cell counts normalized by tumor weight (for tumor samples). Data were compared either by Student's t-test or ANOVA followed by Tukey post-hoc test.

Results: Marked trends could be observed among all the conditions and tissues tested but statistical evaluation did not reveal significance. Most notably, we observed that thermal ablation and radiation induced an increase in the proportion of MDSCs among the immune cells in tumors. The activation status and function of these MDSCs, however, remains to be investigated.

Conclusions: Our preliminary results report a relatively weak impact of the FUS monotherapy on the myeloid compartment in 4T1 tumors, irrespective of regimen – with the exception of thermal ablation impacting MDSCs. This suggests that the mechanisms of action underlying FUS may be more T-cell driven, potentially through the release and repertoire of tumor-associated antigens, danger signals, and cytokines. These effects could be exploited to provide synergistic clinical benefits when combined with immunotherapy. However, if FUS alone cannot mitigate or reverse myeloid cell polarization, any combination of FUS with immunotherapy may see its efficacy limited by the predominating immune-suppressive compartment of the tumor if there is an imbalance in favor of immunosuppression over immune response. In these instances, additional targeted adjuvant therapies such as a chemotherapy, may be required to mitigate this immunosuppressive environment and lift the barrier to FUS-induced immunogenic modulation. The pre-treatment immunologic status of the host, particularly with respect to MDSC burden, may therefore prove to be an essential element of consideration when devising effective personalized combinatory FUS-immunotherapy treatments.

CV-1

Wednesday

24 October 2018

Topic: Cardiovascular
Presentation Type: Oral

Controlled luminal shrinkage with thermal HIFU for venous insufficiency treatment

Nesrine Barnat[1], Anthony Grisey[2], Björn Gerold[2], Jérémie Anquez[2], Sylvain Yon[2], Jean-François Aubry[3]

[1]Institut Langevin, CNRS UMR 7587, Inserm U979, ESPCI Paris, PSL, Paris, Theraclion, Malakoff, France
[2]Theraclion, Malakoff, France
[3]Institut Langevin, Paris, France

Background: Venous insufficiency is a common medical disease associated to refluxing veins of lower limbs. To treat this disease, incompetent veins are eliminated from the venous circulation. Veins can be surgically removed or occluded by chemical or thermal techniques. Thermal methods such as radiofrequency or laser act by inducing vein wall constriction through thermal denaturation of the vein wall collagen. We propose here to use extracorporeal high-intensity focused ultrasound (HIFU) to induce vein shrinkage. We used a sheep model to study lumen narrowing immediately after ultrasound exposure and after a follow-up period.

Methods: Saphenous veins of three ewes (12 months old, 54.5–59.5 kg body weight) were treated with the Echopulse® HIFU device (Theraclion, Malakoff, France). This system includes a therapy transducer operating at 3 MHz and a confocal image probe for real-time treatment monitoring. Six veins with a mean diameter of 5 mm were exposed to HIFU over a mean length of 22 mm. 8 seconds long continuous pulses were delivered in one to two rows along the vein with a spacing of 3.6 mm between subsequent spots. Blood flow was stopped during exposure by compression in order to reduce the heat sink effect. A minimal inter-pulse time of 50 s between two sonications was set. Ultrasound images were recorded immediately after HIFU procedures and after the follow-up time to assess vein wall constriction.

Lumen narrowing was quantified by a diameter contraction index measured with ultrasound imaging. This index is expressed by:

$$Diameter\ contraction\ index = 1 - dc/d0$$

where dc is the diameter of the vein in the treated section and $d0$ is the diameter outside the treated section. Both diameters were taken on the same longitudinal image plane of the vein. After euthanasia of the animals, veins were surgically exposed and visually inspected to evaluate macroscopic changes induced by HIFU.

Results: Stenosis was observed in all cases after HIFU procedures. The median vein diameter shrinkage measured directly after HIFU was 79% ± 14 % (Figure 1.A). After 30 days, lumen narrowing was still present with a median reduction of 51% ± 20 % (Figure 1.B). At excision, vein wall shrinking was also visible macroscopically (Figure 1.C). Whitening of the treated zone was observed for all veins. This is an indication of collagen fibers aggregation due to intense thermal exposure. Furthermore lumps observed on the vessels are signs of collagen fibers contraction. No carbonization nor perforations were identified in any of the targeted vessels.

Conclusions: All veins exposed to thermal HIFU showed significant wall shrinkage with a reduction of diameter of at least 50%. Moreover, the vein wall constriction persisted over time. These results demonstrate that like endovenous thermal treatments, HIFU can heat and shrink vein walls and produce a persistent reduction of lumen diameter.

Acknowledgements: This study was supported by Theraclion® France.

Figure 1.

A) US image of a vein wall constriction observed post HIFU

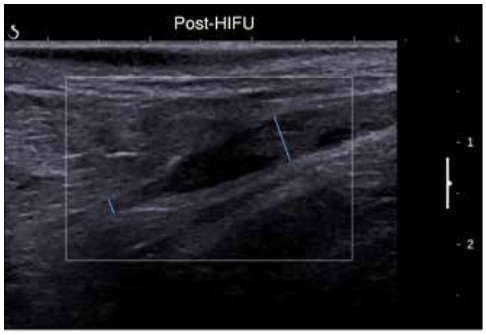

B) US image illustrating the persisting lumen shrinkage after 4 weeks

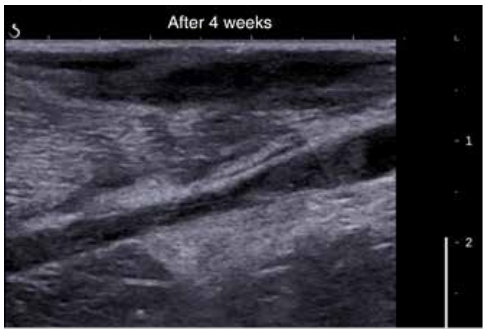

C) Macroscopic visualization of the venous narrowing

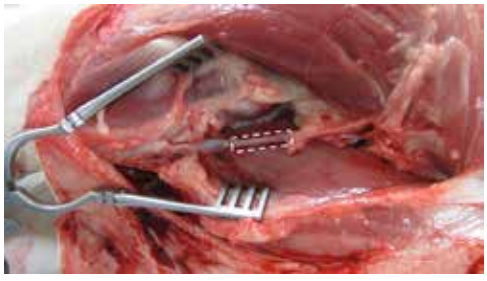

CV-2

Wednesday

24 October 2018

Topic: Cardiovascular
Presentation Type: Oral

Sub-chronic venous occlusion with thermal HIFU for venous insufficiency treatment: A preliminary study on rabbit saphenous veins

Nesrine Barnat[1], Anthony Grisey[2], Björn Gerold[2], Jérémie Anquez[2], Sylvain Yon[2], Jean-François Aubry[3]

[1]Institut Langevin, CNRS UMR 7587, Inserm U979, ESPCI Paris, PSL, Paris, Theraclion, Malakoff, France
[2]Theraclion, Malakoff, France
[3]Institut Langevin, Paris, France

Background: Venous insufficiency is a medical condition resulting from excessive hemodynamic pressure in the veins of the lower limbs. Thermal treatment options include the introduction of radiofrequency catheters or optical fibers into the vein to perform radiofrequency or laser ablation. These methods are challenging for the physician and can be traumatic for the patient. We propose here to use high-intensity focused ultrasound (HIFU) to occlude incompetent veins non-invasively. Several sonication strategies were investigated here, first numerically and second experimentally in an *in vivo* rabbit model.

Methods: Numerical simulations using the k-Wave toolbox were performed to identify sonication parameters ensuring the exposure of the entire diameter of a 2-cm vein segment. Thermal damages to the vein wall were computed based on a dedicated Arrhenius law associated to collagen denaturation, known to induce thermal venous occlusion. 4 seconds pulses in continuous wave mode were used with two different types of exposures: fix pulses and moving pulses at constant speed (0.75 mm/s) across the vein diameter. The same ultrasound exposures were evaluated *in vivo* on rabbit veins.

Twenty-nine veins were sonicated in fifteen rabbits (weighing 2.7 to 4.5 kg) with the Echopulse® HIFU device (Theraclion, Malakoff, France) including a therapy transducer operating at 3 MHz. The transducer was fitted with a balloon filled with degassed liquid to ensure good acoustic coupling. Treatments were US-guided. The mean vein diameter was 2 ± 0.6 mm. The legs were elevated to diminish blood flow and thus limit the heat sink effect of the blood. Rabbits were followed for up to 19 days and occlusion was evaluated by Duplex and histologic analysis.

Results: Simulations showed different sonication layouts depending on the vein diameter. Exposure parameters for the treatment of a 2 cm length portion of a vein included either 13 fix pulses 1.5 mm apart for diameter less or equal than 2 mm or 37 moving pulses 0.5 mm apart for larger vein diameters. In both cases, the acoustic power was adjusted to 85 W.

Simulated damaged area for both types of sonication are displayed in figure 1. For fix and moving pulse respectively, the damaged area was 19.2 x 2.4 mm^2 (Figure 1) and 19.2 x 3.9 mm^2 (Figure 2). Simulation results show that regardless the trajectory followed by the focal point, 85W ultrasound pulses are likely to induce significant damages to a vein segment of 2 mm in diameter and 2 cm in length. *In vivo*, both exposure parameters have been able to achieve rabbit veins occlusion, with a 82% success rate, as assessed by sub-chronic histology analysis.

Conclusions: These results demonstrate the feasibility of HIFU to induce durable occlusion of veins with a diameter higher or equal than 2 mm. To the best of our knowledge, it is the first time that durable occlusion (3 weeks) is demonstrated on 2 mm diameter veins without injection of additional products such as pro-inflammatory agents. Occlusion was 100% successful for veins treated with moving pulses. Further work is needed to translate these results to clinics.

Acknowledgements: This study was funded by Theraclion® France.

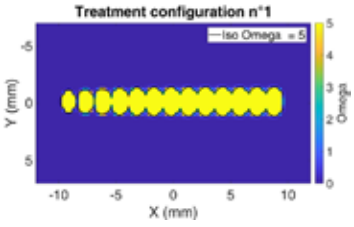

Figure 1. Thermal damage distribution at the end of 13 4-s pulses

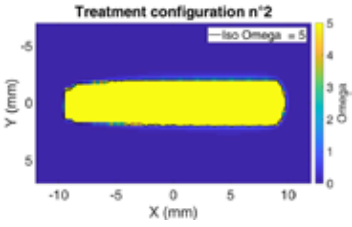

Figure 2. Damage map at the end of a treatment of 37 4-s pulses

CV-3

Wednesday

24 October 2018

Topic: Cardiovascular
Presentation Type: Oral

Development of an *ex vivo* porcine model of coarctation of the aorta: Possible treatment applications with MR-guided HIFU using boiling histotripsy

Sergio Vega[1], Aodhnait Fahy[1], Karolina Piorkowska[1], Adam Waspe[2], James Drake[2], Christoph Haller[1], Ted Gerstle[1]

[1]Sickkids, Toronto, Ontario, Canada
[2]Hospital for Sick Children, Toronto, Ontario, Canada

Background: Coarctation of the aorta is one of the most common types of congenital heart defects in neonates and is characterized by a narrowing of the aorta caused by a shelf-like obstructive lesion that leads to hypertension and heart failure. Current treatment strategies include open chest surgery with resection and end-to-end anastomosis or balloon-based catheter dilatation of the coarcted segment. These treatments are associated with risks that could be potentially avoided via a non-invasive technique, such as MR-guided high-intensity focused ultrasound (MRgHIFU). The purpose of this study was to create an *ex vivo* porcine model of a coarctation of the aorta and then determine if it was amenable to HIFU treatment of boiling histotripsy as a proof of concept.

Methods: To create a model of aortic coarctation, abdominal aortas were harvested from pigs and divided into 3 cm segments. Skin porcine gelatin at a concentration of 7% was injected under the intima using ultrasound image guidance (1 ml of solution) in order to create a gelatin mass within the lumen that would narrow the aorta, simulating a coarctation. One gelatin mass per aortic segment. Two segments were embedded into a 15% gelatin phantom. A 3 Tesla MRI (Philips Achieva, Best, Netherlands) was used for guidance, and one segment was sonicated on a Sonalleve V1 HIFU table (Profound Medical, Toronto, Canada) and the other segment left as an untreated control . Four adjacent sonications (900 Watt, 51 seconds duration, 20 pulses, duty cycle 0.21%) were performed within each treated gelatin mass. Post-treatment imaging was performed, and the pre- and post-treatment imaging was analyzed. The wall of the aorta was processed for histologic analysis.

Results: There were n= 8 aortic segments with a gelatin mass sonicated and n= 8 adjacent untreated gelatin mass controls. Longest diameter mean of the gelatin mass was 9.55 mm (13.8 mm to 6.6 mm). Post-treatment imaging revealed a smaller mass and wider lumen compared to pre-treatment imaging, with a mean reduction in the longest diameter of 11.4% (range from 5.2 to 28.4% with a standard deviation of 7.6), visualized on 2D in the T1w Vista. Boiling histotripsy did not grossly damage the endothelium nor adventitia.

Conclusions: We have developed a basic *ex vivo* porcine model for coarctation of the aorta that can be treated with MRgHIFU. It was possible to dissolve a portion of the narrowing that was simulating the coarctation without injuring the nearby adventitia nor the endothelium. This *ex vivo* porcine model as a proof of concept suggests that boiling histotripsy can be used to treat tissue narrowing the aorta without damaging the adjacent vessel. Future directions include evaluating the efficacy of histotripsy to dissolve the tissue normally found in the coarctation shelf, as well as to create an *ex vivo* pulsatile model of aortic coarctation.

Figure 1. MR scanning of the samples. A) pre-treatment images and B) shows the post-treatment images, both in T1W Vista, with a reduction of 11%.

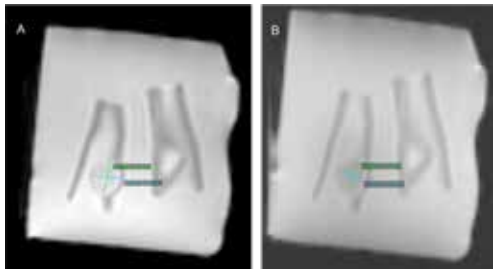

Figure 2. Gross anatomy cross section of a gelatin mass injected between the intima and adventitia of the aortic wall.

CV-4

Wednesday

24 October 2018

Topic: Cardiovascular
Presentation Type: Oral

Preliminary results of ultrasound-guided (US) high-intensity focused ultrasound (HIFU) treatment in superficial lower limb veins

Michel Nuta

Theraclion, Malakoff, France

Background: Chronic veins disease is highly prevalent, as up to 40% of the population in age between 30 and 70 is affected. Current modalities to treat varicose veins are including open surgery and endovenous thermal methods (radiofrequency and LASER) using a catheter inserted in the targeted vein. The endovenous thermal methods are widely accepted and surpassed since several years open surgery in the United States. However, these methods are invasive when compared to HIFU ablative modalities.

Methods: HIFU generated by the Echopulse Theraclion device penetrates through soft tissues and causes localized hyperthermia (around 80°C) responsible of irreversible protein denaturation and veinwall coagulation whereas overlying and surrounding tissues are spared, by focusing a beam into a given target. A focused piezoelectric transducer (3 MHz resonant frequency) generates the ultrasound field. At the center of the transducer, an imaging array of 7.5 MHz is integrated to allow perfect alignment between the imaging and the focal point.

A first in man prospective open study sponsored by Theraclion — approved by the Austrian competent authorities — is ongoing and a number of patients were followed up to 3M.

Results: Several examples of positive results after 3M follow-up are currently available. Most of the cases were performed without anesthesia, were well tolerated and no severe adverse events were observed.

A. A female patient presented recurrence after GSV (Great Saphenous Vein) stripping. A total of 12 pulses have been delivered with a mean power of 45W. No anesthesia was performed. The treated area was occluded acutely and this result is persistent at 3M.

B. An aged female patient (72 years old) presenting a refluxing stump and a neovascularization after GSV stripping as well as an active ulcer was treated at the groin level – over the stump and neo-vessels area. A total of 10 pulses have been delivered with a mean power of 42.9W. No anesthesia was performed. The recurrent flow was abolished and the ulcer was healed at 3M.

C. A male patient presenting a refluxing calf perforator was treated after unsuccessful surgery and sclerotherapy. A total of 9 pulses have been delivered, at mean power of 45W. No anesthesia was performed. The perforator was occluded acutely and this result persisted at 3M.

D. An aged male patient (76 years old) presenting a refluxing GSV and active ulcer was treated after unsuccessful surgery. A total of 39 pulses have been delivered with a mean power of 38W. Tumescent anesthesia was performed. The vein was occluded acutely and this result persisted at 3M. The ulcer was healed at 3M.

Conclusions: In this first study of the cure of refluxing lower limb veins by using HIFU, the preliminary results are encouraging and show that HIFU could be a credible alternative treatment in this field. More cases and longer follow-up are needed in the future studies.

Acknowledgements: This study was supported by Theraclion® France.

GI-1

Monday

22 October 2018

Topic: Neurodegenerative Disorders

Presentation Type: Oral

Effects of focused ultrasound on delivery of intranasal GDNF DNA nanoparticles to the rat brain

Qingxi Ma[1], Amirah Aly[1], Nathan McDannold[2], Barbara Waszczak[1]

[1]Northeastern University, Boston, Massachusetts, United States
[2]Brigham and Women's Hospital, Boston, Massachusetts, United States

Background: Glial cell line-derived neurotrophic factor (GDNF) provides a possible treatment for Parkinson's disease (PD) due to its ability to promote the survival of dopaminergic neurons in the brain. Our lab has previously shown intranasal administration of PEGylated lysine 30-mer (CK30PEG10K) plasmid DNA nanoparticles (NPs) encoding hGDNF to be a non-invasive, non-immunogenic approach that overcomes the blood-brain barrier (BBB) and generates a self-sustaining source of GDNF expression in the rat brain. We also showed with double-label immunohistochemistry (DL-IHC) that transgene expression occurred throughout the rat brain, primarily in cells adjacent to capillaries resembling pericytes. We then applied focused ultrasound (FUS) with circulating microbubbles to specific brain regions, in combination with intranasal administration of NPs, in an attempt to increase transgene expression in target areas for PD. After the application of FUS, we detected higher levels of GDNF expression in the sonicated brain regions in comparison to non-sonicated sites; however, DL-IHC showed that FUS changed the transfection pattern, causing the recruitment of a cell type that was neither astrocytes nor neurons, and not consistently perivascular in location. We speculated that the transfected cells at the sonication cite might be microglia. To test this hypothesis, we used DL-IHC to assess whether cells positive for GFP, a marker for transfected cells, also co-expressed Iba-1, a marker for microglia.

Methods: We used a reporter plasmid (pUGG), which produces an eGFP-GDNF fusion protein. We intranasally administrated to all rats 90 μg of pUGG NPs, a dose that was previously shown to yield significant transgene expression throughout the rat brain 1 week after delivery. FUS (32 msec bursts at 4 Hz for 100 sec at 274 kHz) was applied to the right forebrain and midbrain immediately before and after intranasal administration of the GDNF NPs, during the infusion of Optison microbubbles.

Results: Our data showed that pUGG transfected cells on the non-sonicated side of the brain are usually not positive for Iba1 (<50%). In addition, pUGG transfected cells on the sonicated side of the brain, but not at sonication sites, were also usually not positive for Iba1 (<50%). However, pUGG transfected cells on the sonicated side of the brain, and at apparent sonication sites, were often positive for Iba1 (>50%), and were ameboid in shape, resembling activated microglia.

Conclusions: The result of our study showed that FUS enhances the transfection of brain cells after intranasal administration of pUGG NPs. In areas distant from apparent sonication sites, transfected cells were widespread, commonly perivascular, and occasionally Iba1-positive. However, at sonication sites, the percentage of transfected cells that co-express the microglial marker greatly increased, leading to the conclusion that the transfected cells at sonication sites were predominantly microglia.

Acknowledgements: Qingxi Ma is the recipient of a Summer 2018 Global Internship from the Focused Ultrasound Foundation

MI-1

Tuesday

23 October 2018

Topic: Pancreas
Presentation Type: Oral

A planning strategy for combined self-scanned/gated MR-HIFU treatment in the pancreas

Cyril Ferrer, Clemens Bos, Baudoin de Senneville, Pim Borman, Rob Tijssen, Bjorn Stemkens, Chrit Moonen, Lambertus Bartels

UMC Utrecht, Utrecht, Netherlands

Background: Thermal ablation of tumors located in abdominal organs using MR-HIFU has been demonstrated to be feasible, but remains challenging, in particular due to respiratory motion 1. To overcome such problems, multiple solutions have been proposed: induced apneas, gating and beam steering2.

In a recent simulation study, Möri et al, investigated whether so-called self-scanned sonication, (i.e., a fixed HIFU sonication combined with respiratory motion to passively scan the target) could increase the time efficiency of HIFU treatment3.

Here, we present a combined self-scanned/gated approach that makes use of acquired 4D-MRI data to identify locations where self-scanned sonications could be used from those that should be targeted with gating. Based on volunteer data, this approach was tested using simulations. The number of sonications needed for ablation of the pancreas head using the self-scanned/gated approach was compared to the number needed with the gated approach and in the case without motion.

Methods: To generate a self-scanned/gated plan our pipeline is divided in four steps (figure 1):

1. From 4D-MRI4 data, the target displacement is evaluated in 3D throughout the respiratory cycle using image registration5.
2. All registered target positions are projected along the time axis. Self-scanned sonications are attributed to location where the target is always present (probability = 1), gated sonications otherwise.
3. For all locations thermal dose are simulated based on the Bio-Heat Transfer Equation6. Energy delivery was limited to the expiration plateau for gating7. Extracted motion patterns were applied as trajectory to simulate self-scanned sonications.
4. A voxel-wise optimization selects a set of locations to achieve complete ablation of the target.

Six healthy volunteers were scanned in prone position on a 3.0-T clinical scanner (Philips, Best, The Netherlands) using the body-coil array. For all volunteers and approaches (combined, gating and static), we compared the number of sonications needed to ablate the pancreas head.

Results: In a typical example, 94% of the target was assigned to self-scanning, figure 2a. After optimization, by comparing all evaluated strategies (combined, gating and static), lethal thermal dose was always delivered to the complete target. Spatial distribution of the sonication were similar for the combined and static strategy, however, with gating, sonications were more densely distributed, figure 2b.

The number of sonications was the lowest for a static target, 62 on average, figure 3. The gated approach required the largest number of sonications: 126. The combined self-scanned/gated approach, with an average of 78, was almost as efficient as sonication of a static target.

Conclusions: A combined self-scanned/gated sonication strategy that exploits the respiratory motion may reduce the number of sonications required to ablate a target volume in the pancreas.

References:

1. Maloney E, Int J Hyperth, 2014
2. de Senneville BD, Adv Exp Med Biol, 2016
3. Möri N, Phys Med Biol, 2016
4. Stemkens B, Int J Radiat Oncol Biol Phys, 2015
5. Zachiu C, Phys Med Biol, 2015
6. Ramaekers P, Med Phys, 2017
7. Wijlemans JW, Invest Radiol, 2015

Figure 1: Proposed planning pipeline for a combined self-scanned/gated MR-HIFU treatment.

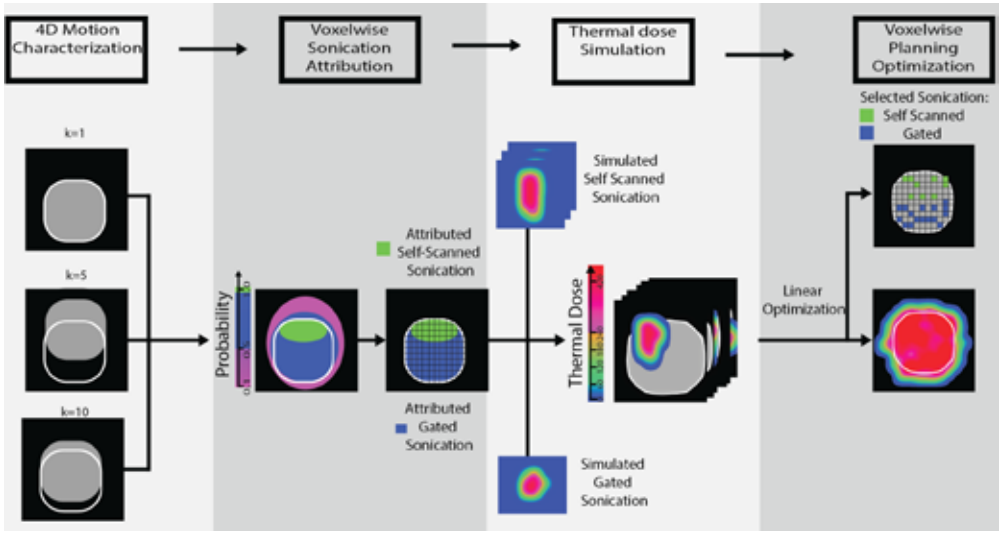

Figure 2: a) Time projection of all target positions through the respiratory cycle overlaid onto a reference image. b) Comparison of delivered thermal dose and planning sonications in the three evaluated scenarios. The target is outlined in white.

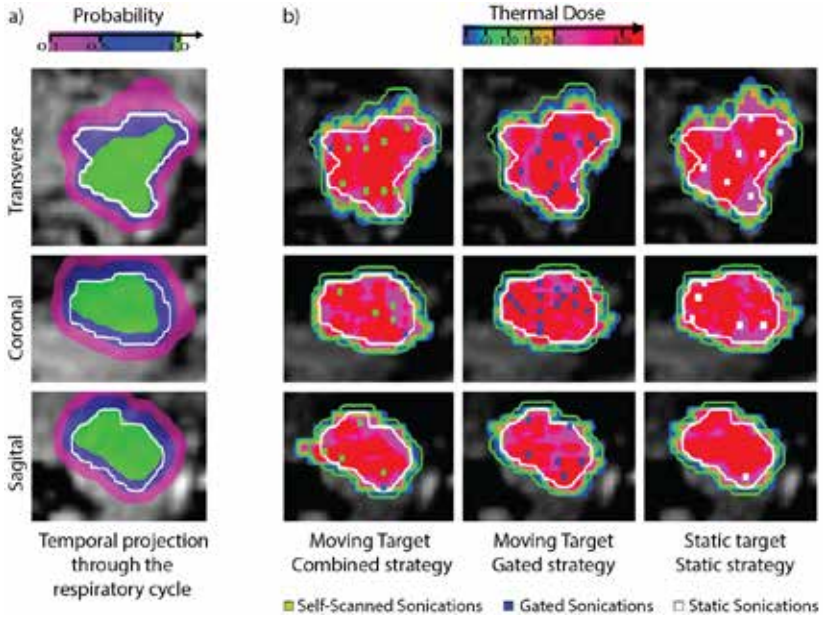

Figure 3: Number of sonications needed to ablate the complete target, in all volunteers, as a function of different energy delivery strategies: gating, combined self-scanned/ gated and static.

MI-2

Tuesday

23 October 2018

Topic: Liver/Kidney
Presentation Type: Oral

Comparison of Sonalleve V1 and V2 MR-HIFU systems for generating high-amplitude shock-wave fields

Maria Karzova[1], Petr Yuldashev[1], Wayne Kreider[2], Pavel Rosnitskiy[1], Tanya Khokhlova[2], Christopher Bawiec[2], Ari Partanen[3], Oleg Sapozhnikov[1,2], Vera Khokhlova[1,2]

[1]Lomonosov Moscow State University, Moscow, Russian Federation
[2]University of Washington, Seattle, Washington, United States
[3]Profound Medical, Mississauga, Ontario, Canada

Background: A Sonalleve V1 MR-HIFU clinical system (Philips, Vantaa, Finland) has been shown to generate nonlinear ultrasound fields with shocks up to 100 MPa at the focus as required for HIFU applications such as boiling histotripsy of hepatic and renal tumors. In the newer version of the Sonalleve system, the V1 transducer array has been replaced with the V2 version. The goal of this study was to compare the performance of the V1 and V2 transducers for generating high-amplitude shock-wave fields.

Methods: Transducer arrays of Sonalleve V1 and V2 systems comprise 256 circular elements arranged in different geometries with identical 6.6 mm diameters and 1.2 MHz operating frequencies (Fig.1). The V1 and V2 geometries are described by apertures 127.8 and 138.3 mm and radii of curvature 120 and 140 mm, respectively. Characterization of the corresponding nonlinear acoustic fields was performed using capsule PVDF hydrophone measurements in water (Fig. 1, top row) and nonlinear modeling. Low-power holography measurements were used to set boundary conditions for the model. Simulations based on the Westervelt equation were performed for increasing output levels and the results were compared to direct pressure measurements at the focus made with a fiber optic hydrophone.

Results: Figure 2 shows normalized linear pressure distributions along axial and transverse directions in the focal region for the V1 and V2 arrays. The plots compare direct field measurements with field projections based on holography measurements. While the width of the focal lobe in transverse directions is almost the same for both systems, its length in the axial direction is notably longer for the V2 system, which has a smaller focusing angle. At increasing power outputs, nonlinear waveform distortion occurs and shocks can form at the focus. Simulations of focal waveforms demonstrate that the V2 system produces fully developed shocks at a lower amplitude (82 MPa) than the V1 system (92 MPa) (Fig. 3). A shock is considered to be "fully developed", when the shock front (steep part) begins at a value of zero pressure, such that the shock amplitude is equal to the peak positive pressure. Figure 4 shows peak positive and peak negative pressures over a range of output levels from both simulations and direct measurements. Modeling results for shock amplitudes achieved at the focus are also presented demonstrating that fully developed shock forms at lower acoustic power for the V2 system. At high power levels, the V1 system provides about 10 MPa higher peak positive pressures and shock amplitudes than the V2 system.

Conclusions: In comparison with previous Sonalleve MR-HIFU V1 system, the new array of the V2 system has a smaller focusing angle and therefore at the same power output produces shocks with amplitudes that are about 10 MPa lower. Consequently, substantially higher power levels are required for the V2 system to reach the same shock-wave exposure conditions in histotripsy-type treatments.

Acknowledgements: The study was supported by FUSF Research Awards Program, NIH R01EB7643, R01EB025187, and RSF 14-12-00974.

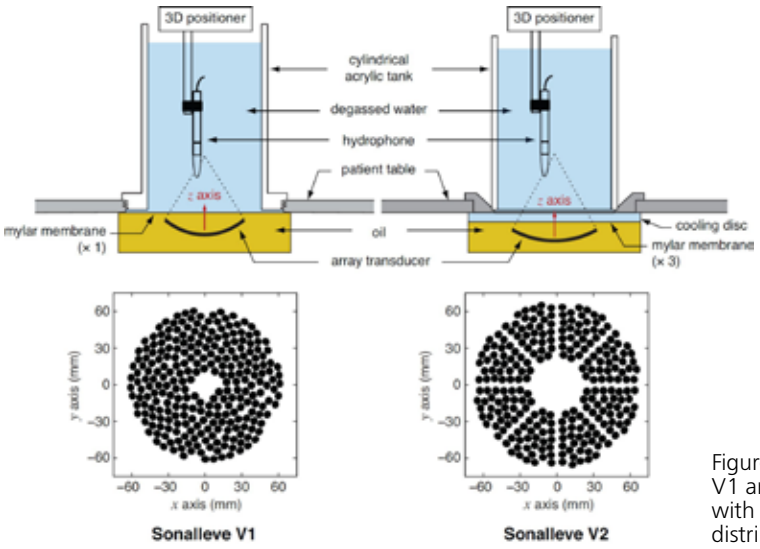

Figure 1. Schematics of the experimental arrangement of Sonalleve V1 and V2 MR-HIFU systems. Top row: measurement configuration with a custom tank mounted to the patient table. Bottom row: distribution of array elements over the transducer surface.

Figure 2. Normalized distributions of linear pressure amplitude in the focal region along axial (z) and transverse (x,y) directions, with the focus defined at the origin. Continuous lines represent modeling, while circles represent measurements.

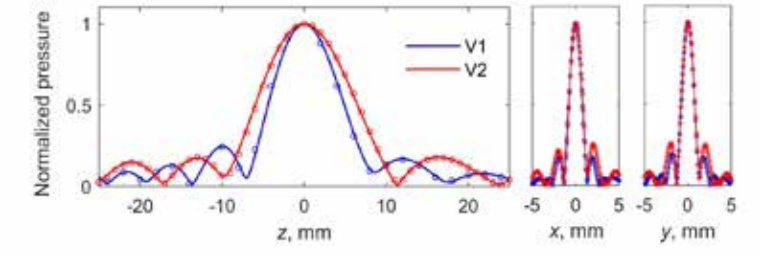

Figure 3. One cycle of the pressure waveforms with developed shocks simulated in water at the focus of the Sonalleve V1 (blue curve) and V2 (red curve) transducers.

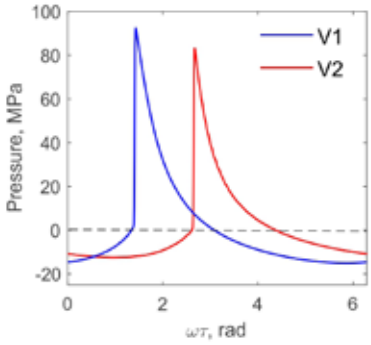

Figure 4. Comparison of the peak positive p+ and peak negative p- pressures at the focus as simulated (solid curves) and measured by hydrophone (circles). Simulated shock amplitudes are plotted as dashed curves.

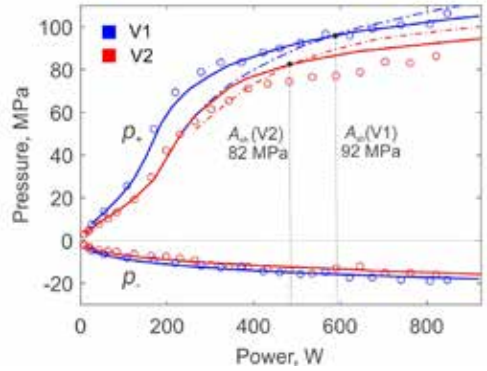

MI-3

Tuesday

23 October 2018

Topic: Liver
Presentation Type: Oral

Focused ultrasound with ultrasound guidance in liver cancer as suitable option for lesions in difficult locations

Joan Vidal-Jove[1], Angels Jaen[1], Marta Paraira[1], Manuela Velat[2], Eloi Perich[2]

[1]Hospital University Mutua Terrassa, Terrassa, Spain
[2]Institut Khuab, Barcelona, Spain

Background: FUS-HIFU is an Interventional Oncology procedure that is useful at obtaining local disease control with minimal invasive techniques. We describe the experience of the HIFU Ablation Oncology Unit of Hospital University Mutua Terrassa (Barcelona), and the Interventional Oncology group of Institute Khuab, Comprehensive Tumor Center, Barcelona, treating malignant primary and metastatic liver tumors. We underline some considerations about the role of hepatic tumor ablation in the present oncology stage.

Methods: From February 2008 to May 2016 we have treated 180 malignant cases. Of those, 40 cases of primary and metastatic liver tumors are included in this study. We include patients that were not candidates for surgery or other ablation available, Radiofrequency ablation, Microwave ablation or Embolization. All of the patients were allowed to continue on their systemic chemotherapy treatments after the ablation procedure was performed.

Results: We specially analyze the 40 liver tumors. Total treatment timings are between 60 and 180 minutes. Difficulties related to patient positioning, access to segments VII and VIII, and real-time response evaluation prolonged the procedures. Access to deep lesions its feasible (segment I, Inferior Vena Cava). Clinical responses (ablation obtained) were 92% in all cases. Major complications included skin burning grade III that required plastic surgery (1), and costal osteonecrosis (1). Overall Percent Survival is 28.5 % at 5 years follow up.

Conclusions: FUS-HIFU is an effective and safe Interventional Oncology ablation of malignant primary and metastatic hepatic tumors. Difficulties related to available devices makes it too cumbersome for accessible lesions at present compared with other ablations available. Access to deep lesions shows an opportunity for this system to increases its possibilities of use.

MI-4

Tuesday

23 October 2018

Topic: Liver
Presentation Type: Oral

TRANS-FUSIMO — Preliminary *in vivo* animal results of MR-guided focused ultrasound of liver under respiratory motion

Cesare Gagliardo[1], Angelo Gambino[1], Patrizia Toia[1], Jan Strehlow[2], Michael Schwenke[2], Luca Cicero[3], Giovani Cassata[3], Sabrina Haase[2], Tobias Preusser[2], Andreas Melzer[4], Massimo Midiri[1]

[1]University of Palermo, Palermo, Italy
[2]Fraunhofer Institute for Medical Image Computing MEVIS, Bremen, Germany
[3]Sicily Zooprophilactic Institute, Palermo, Italy
[4]The University of Dundee, Dundee, United Kingdom

Background: Treating liver tumors using FUS poses a great challenge due to the respiratory motion of the target and by the rib cage obscuring the anatomical location of the malignancy. In the EU FP7 project TRANS-FUSIMO (www.trans-fusimo.eu) a novel treatment software has been developed to support MR guided focused ultrasound treatment of liver lesions through electronic real-time beam steering of the ultrasound transducer. Prior to clinical use we conduct an *in vivo* animal trial using the TRANS-FUSIMO treatment system (TTS) to evaluate the safety and the technical efficacy and efficiency of generation predefined necrotic lesions in the healthy liver.

Methods: The pre-clinical animal trial includes a crossbred porcine model of thirty large white swine (all females; 55-85Kg) that will be treated using the TTS. Animals were sedated and underwent general anaesthesia with intubation. The following sampling time points have been scheduled: 1) acute, where the animal will be sacrificed immediately after therapy with completion of the post-operative MR imaging, dissected and sent for histopathological examination to assess the extent of the acute stage of the tissue destruction, 2) subacute, where after 5-7 days animals will be sacrificed after an MRI follow-up, the liver surgically dissected and sent for histopathological examination to assess the extent of the early stage of tissue necrosis and 3) late, where by day 28 animals will be scarified after an MRI follow-up, the liver surgically dissected and sent for histopathological examination to assess the extent of the late stage of tissue necrosis. All treatments haven been performed under ventilator-controlled breathing and using an improved non-clinical prototype version of INSIGHTEC's conformal bone system (iCBS) integrated with a 1,5T MRI unit (GE Signa HDxt); a set of interventional flexible coils (MRI Instruments DuoFLEX) were used. Before starting the treatment, a 3D LAVA sequence was scanned; 3D FIESTA sequences were then used for planning During each sonication, real-time multi reference thermal monitoring was achieved using a 3mm istotropic EPI-GRE slice (8Hz). At the end of the treatment session we injected 2ml/Kg of gadobenate dimeglumine (Multihance, Bracco) at 2ml/s followed by a saline flush of 20ml. A 3D LAVA sequence was than scanned to identified any necrotic lesion.

Results: The results from the first successfully treated animals will be presented (Figure 1). Liver lesioning was possible during both breath-hold and ventilator-controlled breathing due to the TTS motion compensation algorithm which allows the electronic steering to be controlled according to the MRI images. During all pre-clinical sessions, the TTS was used, including real-time multi reference thermal monitoring.

Conclusions: Although the TRANS-FUSIMO animal trial is still ongoing and subject to further optimizations, the preliminary results achieved using the TTS are promising. It was possible to confirm FUS induces lesions by both contrast enhanced MR imaging and post-operative pathological examination. The TRANS-FUSIMO treatment system is capable of compensating liver motion under ventilator controlled-respiration through real-time MR motion detection and real-time FUS beam steering.

Acknowledgements: The research leading to these results has received funding from the European Union's Seventh Framework Program (FP7/2007-2013) under grant agreement no. 611889 (TRANS-FUSIMO).

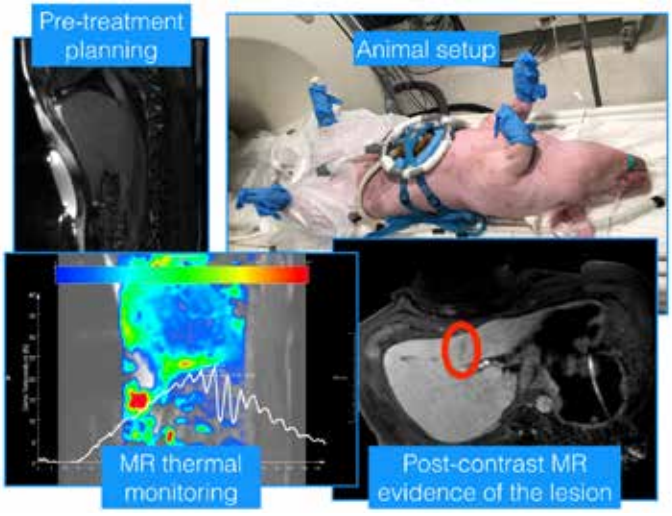

Figure 1 - Pre-treatment sag 3D FIESTA used for planning (top L); animal setup during one of the treating session (top R); screenshot from the thermal imaging monitoring sequence (bot L); ax post-Gd 3D LAVA to identify the FUS induced lesion (bot R).

MI-5

Tuesday

23 October 2018

Topic: Liver
Presentation Type: Oral

Ultrasound-induced insulin release as a potential treatment for type 2 diabetes

Tania Singh[1], Tyler Salvador[2], Ivan Suarez Castellanos[3], Diti Chatterjee Bhowmick[1], Joshua Cohen[4], Kevin Cleary[2], Aleksandar Jeremic[1], Vesna Zderic[1]

[1]The George Washington University, Washington, DC, United States
[2]Children's National Medical Center, Washington, DC, United States
[3]Inserm, Lyon, France
[4]GW Medical Faculty Associates, Washington, DC, United States

Background: Type 2 diabetes mellitus is a complicated and chronic metabolic disorder resulting from the interplay of systemic insulin resistance of peripheral tissues, insufficient secretion from pancreatic beta cells, and insufficient beta cells due to genetic and environmental factors. We have previously shown that therapeutic ultrasound is capable of stimulating insulin release from pancreatic beta cells, non-invasively, safely and effectively. The aim of this work is to study the translational potential of therapeutic ultrasound as a novel treatment for type 2 diabetes via preliminary animal studies and finite-element analysis.

Methods: Wild type hIAPP+/+ white FVB mice between twenty-eight and twenty-nine weeks of age were randomly assigned to either the ultrasound treatment group or the sham group. Mice in the ultrasound treatment group received one five-minute treatment of continuous 1 MHz ultrasound at 1 W/cm^2. Blood samples were collected via tail nick immediately prior to ultrasound application and immediately after ultrasound application. Blood samples were analyzed using a commercial glucometer and insulin ELISA kit to determine blood insulin levels. After sacrifice, the internal abdominal organs, particularly the stomach, liver, and large intestines, were examined for any signs of external damage. The pancreas was excised for histological analysis using H&E staining.

PZFlex, a finite-element analysis software, was used to develop a model of an axial slice of the human abdomen based on computer tomography imaging from patients with healthy and obese BMIs. The maximum temperature in the pancreas was recorded for the duration of treatment and for one minute after ultrasound application.

Results: Preliminary studies in a diabetic mouse model indicated no gross damage – including any burns on the skin – in the treatment area (shown in Fig. 1). There was no evidence of skin burning or internal damage of the abdominal organs, especially the pancreas, found during necropsy. Fig. 2 shows preliminary results from ongoing studies of insulin ELISA analysis indicating that treatment with ultrasound resulted in an increase in blood insulin concentration and a decrease in blood glucose concentration as compared to the sham treatment group.

Initial modeling results indicated that the stomach must be filled with fluid to avoid significant burning of the skin and to allow ultrasound energy to penetrate through the stomach to the pancreas. The maximum temperature observed in these models, 41.2 °C, was still below the threshold for tissue damage or death. Current work is focused on finding the optimal acoustic window for focused ultrasound application in patients with varying BMIs.

Conclusions: Our preliminary results from finite element analysis and animal studies show promise in the translational potential of therapeutic ultrasound in the treatment of type 2 diabetes. The significance of our work lies in its novel, cost-effective, target-specific, and non-invasive approach that utilizes the application of ultrasound energy to augment insulin release from pancreatic beta cells. We expect that our approach, with careful selection of ultrasound parameters, may provide a safe, controlled and targeted stimulation of insulin release from the pancreatic beta cells.

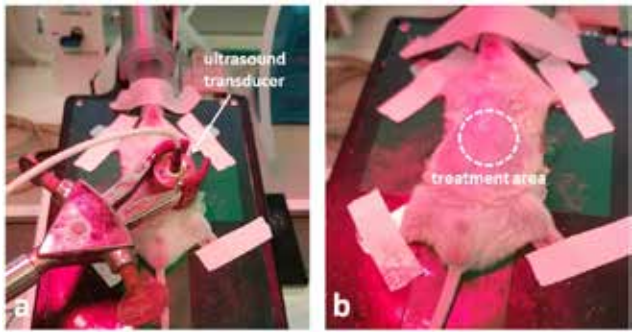

Fig. 1a: Image of the application of 1 MHz 1 W/cm^2 continuous ultrasound for five minutes to a diabetic mouse while under anesthesia. Fig. 1b: Image showing no visible evidence of burns or other injuries in the treatment area (white circle) after ultrasound application.

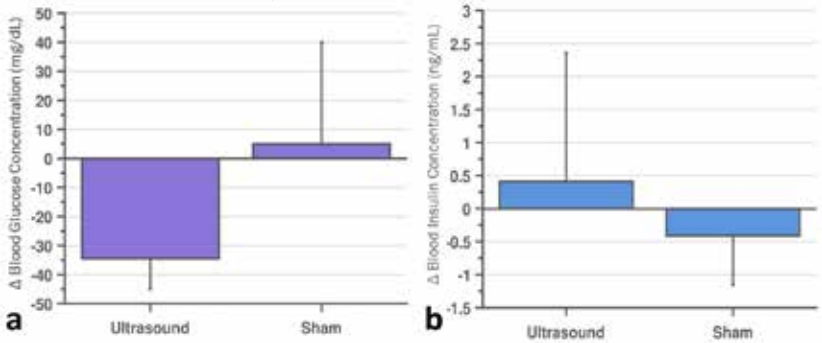

Fig. 2: Change in blood glucose concentrations (Fig. 2a) and blood insulin concentrations (Fig. 2b) after a five-minute continuous application of 1 MHz 1.0 W/cm^2 for an ultrasound (n = 2) and sham (n = 3) groups.

MI-6

Tuesday

23 October 2018

Topic: Liver/Pancreas/ Kidney

Presentation Type: Oral

US guided robotic strategy for continuous FUS treatment of moving organs

Andrea Cafarelli, Alessandro Diodato, Selene Tognarelli, Arianna Menciassi

The Biorobotics Institute, Scuola Superiore Sant'Anna, Pontedera, Italy

Background: Motion tracking for FUS therapies is not an available technology in clinical routine yet. Some motion tracking strategies were developed in research settings using both US and MR for motion monitoring; however, they all present some limitations (e.g. continuous modification of the acoustic window, complex electronic architecture) which limit their applicability in clinics. We propose herein the use of a US guided robotic approach intended for a continuous FUS treatment of moving organs (i.e. liver, kidney, pancreas), which is able to precisely compensate natural physiological movements of the target through an innovative method.

Methods: An innovative tracking strategy for compensating respiratory motion of moving organs under US monitoring was developed (Diodato, PMB 2018), by using the robotic platform FUTURA (http://www.futuraproject.eu/ - Figure 1). The method, schematically represented in Figure 2, consists in sonicating a moving target by exploiting an angular movement (i.e. pivot motion compensation) of the robotic manipulator that holds the HIFU transducer, while the focal depth is continuously adjusted thanks to the axial electronic steering capabilities of an annular transducer. By maintaining the same contact point between the transducer and the patient's skin, the modification of the acoustic window during all the breathing phases is minimized. Ultrasound image guidance and robotic manipulators control are used to automatically track, detect, and correct the target motion throughout the entire treatment. The HIFU transducer is equipped with a balloon filled with water, which guarantees the acoustic coupling between HIFU and US monitoring transducers and patient's skin. The entire procedure is performed also under robotic force control. US imaging is used to estimate and learn the periodic trajectory of the target and to monitor in real-time the treatment success.

The approach was tested *ex vivo* in a simulated breathing scenario. Lesions were induced on breast chicken in static and dynamic conditions (i.e. sinusoidal motion of 20 mm of amplitude and 0.2 Hz of frequency) by using the following sonication parameters: 1.2 MHz of frequency, 115 Watt of power, 20 seconds of duration. The test was repeated 10 times.

Results: The tracking error between a target point chosen at will from US images and transducer focus positions is always lower than 1 mm (Figure 3-a). Lesions performed in static conditions and dynamic conditions (Figure 3-b) appear similar in size and shape, thus qualitatively demonstrating the accuracy of the proposed strategy.

Conclusions: The feasibility of an innovative angular motion compensation strategy was demonstrated in a simulated respiratory-induced organ motion environment. Based on the experimental results, the proposed method appears to be significantly accurate, thus paving the way for the potential use of this technique for *in vivo* treatment of moving organs, and therefore enabling a wider use of HIFU in clinics.

Acknowledgements: Research supported by the European Commission in the framework of the FUTURA and FUTURA2020 project, grant agreements n. 611963 and n. 801451. The authors would like to thank Dr. Massimiliano Marciano and Dr. Franco Orsi for their valuble suggestions and comments and River Global Biomedical for its support.

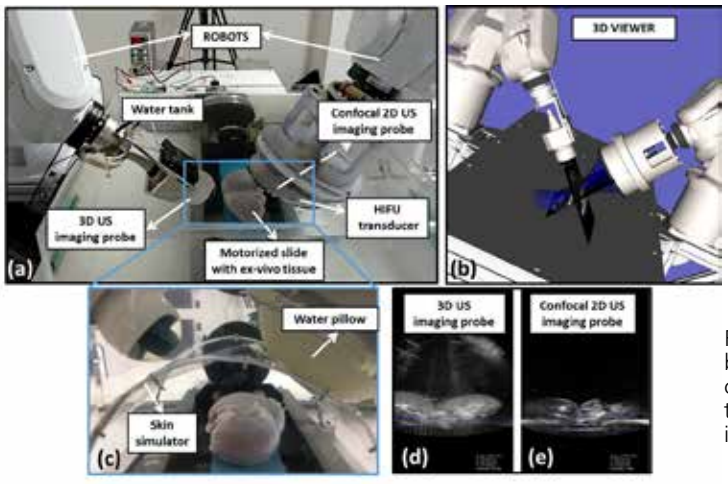

Figure 1. General representation of the FUTURA platform (a, b). Zoom on patient's abdomen simulator and HIFU acoustic coupling pillow (c) and images acquired simultaneously from the 3D US imaging probe (d) and from the confocal 2D US imaging probe (e)

Figure 2. Schematic representation of the angular motion compensation strategy used for FUS therapy of moving targets. The transducer rotates around a pivot point (P) chosen at will, and focal depth is continuously adjusted utilizing the electronic steering.

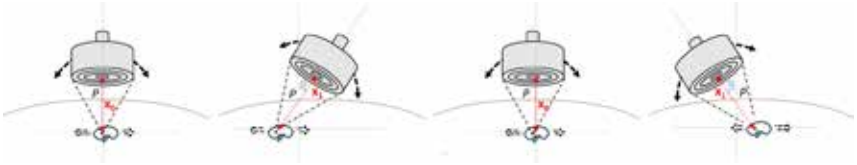

Figure 3. (a) Tracking error. (b) Lesions induced in chicken breast: static condition (left) and in dynamic conditions (middle); these lesions appear very similar. No visible lesions (right) were found when the compensation strategy was deactivated.

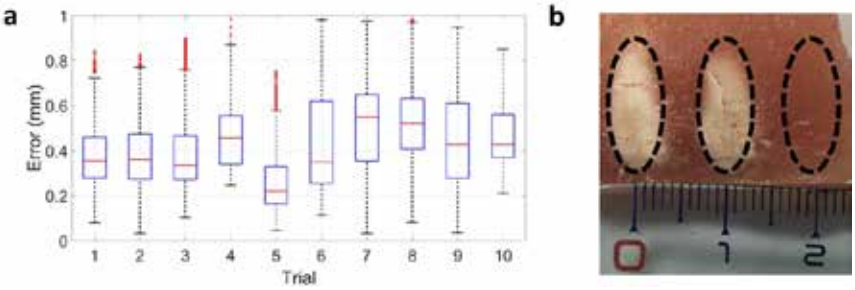

MI-7

Wednesday

24 October 2018

Topic: Miscellaneous Indications

Presentation Type: Oral

Boiling histotripsy liquefaction of large extravascular hematomas: *In vitro* optimization and device design considerations

Tanya Khokhlova[1], John Kucewicz[1], Christopher Hunter[1], Adam Maxwell[2], Vera Khokhlova[1], Thomas Matula[1], Wayne Monsky[1]

[1]University of Washington, Seattle, Washington, United States
[2]University of Washington School of Medicine, Seattle, Washington, United States

Background: Large extravascular hematomas are common sequelae of trauma and surgical bleeds. The consequences range from pain and infections to compartment syndrome and organ failure. Due to its gelatinous nature, the only efficient way to evacuate a hematoma is surgically, with associated co-morbidities. In previous *in vitro* studies we demonstrated the feasibility of using boiling histotripsy (BH) for liquefaction of hematomas, facilitating their fine needle aspiration. Here we aimed to correlate the size and shape of liquefied BH cavities with HIFU transducer field dimensions and the number of delivered BH pulses. BH cavity size also depends on material stiffness, which is unknown for clinical hematomas that autolyze over time, unlike vascular clots. Thus, the second goal was to identify the changes in stiffness of *in vitro* hematomas with retraction and alterations in composition and hence the susceptibility to BH liquefaction.

Methods: Hematoma phantoms of 40-200 mL volume were prepared with whole bovine blood either freshly clotted and allowed to retract over 0-9 days or anticoagulated with sodium citrate, degassed and mixed with varying concentrations of bovine thrombin (0-10 NIHU/mL) and calcium chloride (1.5-25 mM). Shear modulus of all samples was measured using custom built indentometer. Large volume samples were treated with BH using three spherically focused transducers (Figure 1A) with different F-numbers (0.77, 1 and 1.5), capable of operating at 1 MHz or 1.5 MHz. The following BH pulsing protocol was used: 10 ms (or 20 ms for F-number=1.5) pulses delivered at pulse repetition frequency of 1 Hz, with focal pressure amplitudes sufficient to produce boiling within each pulse. Separate BH cavities were created within each sample using varying number of BH pulses (2-120); the samples were then bisected and photographed.

Results: Shear modulus of freshly clotted and retracted samples varied within 0.2-1.2 kPa and did not depend on incubation time and degree of retraction. Shear modulus of samples prepared from anticoagulated blood could be varied within similar range (Figure 2), by altering concentrations of calcium chloride and thrombin. The BH cavity size saturated after delivery of 30 pulses for all HIFU transducers. Given the same sample stiffness, less focused transducers produced elongated, cylindrically shaped cavities, whereas more focused transducers produced shorter, tadpole-shaped cavities (Figure 1B). The increase in sample stiffness within 0.4-1.6 kPa led to significant decrease in transverse, but not axial size of the cavity. The latter corresponded to the distance from the focus to the first prefocal null in the HIFU axial pressure distribution (Figure 1C). Cavities produced by the same transducer at 1 MHz and 1.5 MHz had the same shape, with dimensions inversely scaled by a factor of 1.5.

Conclusions: Shear modulus measurements obtained here indicate that large hematomas are much softer than vascular clots and do not stiffen with retraction. The dimensions and shape of BH cavities correlate with the HIFU field structure which enables prediction of the liquefaction rate based on numerical modelling of the HIFU field of a certain transducer optimized for specific clinical scenarios.

Acknowledgements: Research supported by NIH R01GM122859.

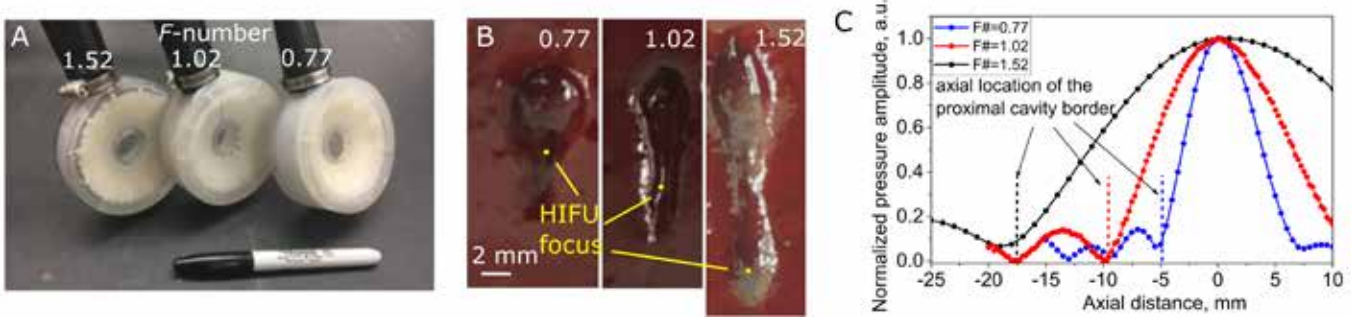

Figure 1. A Three HIFU transducers used in the experiments. B Representative photographs of the BH cavities produced using the three transducers. C Pressure distribution along the propagation axis of the HIFU transducers in linear regime (zero=focus)

Figure 2. A. Shear modulus of *in vitro* hematoma samples as a function of thrombin concentration, under two different concentrations of calcium chloride. B Hematoma stiffness as a function of calcium chloride concentration, with no added thrombin.

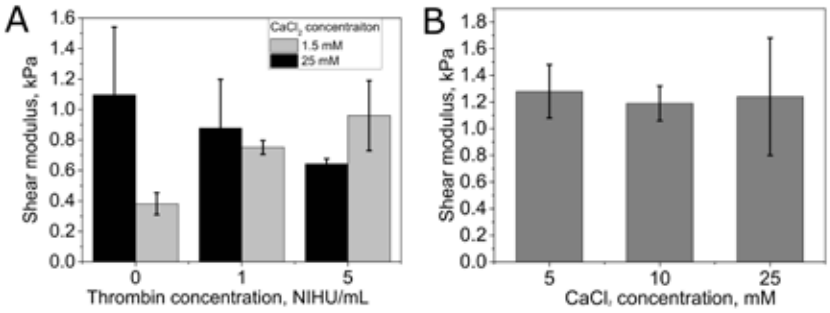

MI-8

Wednesday

24 October 2018

Topic: Miscellaneous Indications

Presentation Type: Oral

Introduction to a MOOC on focused ultrasound for therapy

Mailys Nier[1], Solenne Chassagne[2], Olivier Nier[2], Emily J White[3], Cyril Lafon[4]

[1]LabTAU, Inserm, Lyon, France
[2]University of Lyon, Villeurbanne, France
[3]Focused Ultrasound Foundation, Charlottesville, Virginia, United States
[4]Inserm, Lyon, France

As a center of excellence of the FUS Foundation and for educational purpose, LabTAU proposed to develop a MOOC (Massive Open Online Course) dedicated to focused ultrasound for therapy. The goal of this MOOC is to promote focused ultrasound to the medical community and more broadly to the general public.

For the first year, twelve presentations from world recognized experts were recorded. These presentations cover both clinical cases and more technical topics on focused ultrasound for therapy. Each presentation is followed by a questionnaire in order to assess the clarity of the message but also to be interactive with the community. For a similar purpose, a forum will be available to stimulate discussions between the participants. More resources will be available on-line like the State of the Field produced by the FUS Foundation, important dates for scientific meetings or information from the manufacturers…

The MOOC will be available for free from September 2018 on the educational platform of the University of Lyon (clarolineconnect.univ-lyon1.fr).

The goal of this presentation will be to introduce this MOOC to the community of therapeutic ultrasound.

Acknowledgements: MOOC realized with the support of the FUS Foundation – Warm thanks to the speakers for Year 1: Florent Aptel, Alexandre Carpentier, Sébastien Crouzet, Lawrence Crum, Jeff Elias, Pejman Ghanouni, Gail ter Haar, Chrit Moonen, Franco Orsi, Bruno Quesson, Oleg Sapozhnikov and Shin-ichiro Umemura – Acknowledgment to Sandrine Iochem for the administrative support.

MI-9

Wednesday

24 October 2018

Topic: Miscellaneous Indications

Presentation Type: Oral

Targeted optotriggering in PEG based hydrogels using high-intensity focused ultrasound

Gun Kim, Abigail Halmes, Michael Oelze, Jeffrey Moore, King Li

University of Illinois at Urbana-Champaign, Urbana, Illinois, United States

Background: Generating light *in vivo* for applications such as optogenetic research is generally achieved by the implantation of optical fibers. Here we introduce the concept of sono-optogenetics, a novel technology which couples high-intensity focused ultrasound (HIFU) with a mechanoluminescent hydrogel to generate a localized photon flux. We then review the applicability of mechanoluminescence in polyethylene glycol (PEG) based hydrogels generated by HIFU to existing optogenetic tools.

Methods: A known luminescent mechanophore was installed as a crosslinker in a PEG hydrogel using thiolene click chemistry (Fig. 1a). Upon excitation, the dioxetane based mechanophore generated a ketone in the excited state whose luminescence was enhanced by physically incorporating perylene as an energy acceptor into the gel. A HIFU transducer (FUS Instruments, Canada) with a center frequency of 500 kHz was employed to generate continuous wave ultrasound for a short period (10 seconds) that activated the prepared PEG hydrogel mounted onto a 3D micro-positioning system (positional accuracy of 2 micrometers and 0.02 degree) in a degassed water bath (temperature of 20.7 °C). The ultrasonic system (Fig. 1b) was calibrated to deliver known output pressures at the focus (Fig. 1c) so that we could differentiate effects of mechanical irradiation from thermal ablation. When exposed to HIFU irradiation, luminescence was observed.

Results: We first estimated that the threshold activation pressure was approximately 3.3 MPa at which there was no visible damage in the prepared hydrogel and an increase in temperature of less than 5 °C, indicating that the thermal effect was not significant during the activation process. A distinguishable light (blue) was detected in the luminescent hydrogel (Fig. 1d) during HIFU exposure. No reactivity due to mechanical irradiation was observed in the control sample not crosslinked with the mechanophore.

Conclusions: This study demonstrates the promise of HIFU remotely triggering mechanoluminescence in PEG based hydrogels. In combination with existing optogenetic tools, we envision a novel technology for generating targeted photon flux *in vivo* to benefit optogenetics research.

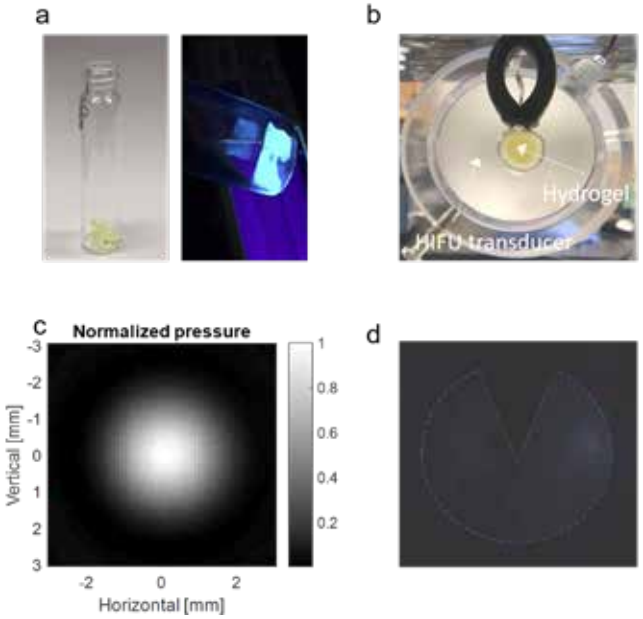

Figure 1. (a) PEG-based gel swelled with DMSO and solvated perylene; (b) example of the obtained pressure profile (500 kHz center frequency, electric power = 1.78 W); (c) HIFU-sample holder in degassed water; and (d) detected blue light.

MI-10

Wednesday

24 October 2018

Topic: Miscellaneous Indications

Presentation Type: Oral

Microbubbles: From imaging to therapy

Victor Jeannot[1], Thierry Bettinger[2]

[1]Bracco Suisse SA, Plan les Ouates, Switzerland
[2]Bracco, Plan les Ouates, Switzerland

Background: Since some decades, Bracco is involved in the field of contrast-enhanced ultrasound. This resulted in the approval and commercialization of the blood pool agent SonoVue® in 2001, and more recently, with the clinical development of BR55, an agent designed for molecular imaging of angiogenesis. Beyond imaging, a new application is emerging, combining ultrasound and microbubbles for therapy. This combination proves to be useful particularly for enhancing drug or gene delivery to organs, or for non-thermal ablation. In that context, microbubbles having optimized physico-chemical and acoustic properties could improve performance in terms of therapeutic efficiency and safety control. To this end, a new clinical grade microbubble formulation, namely BR38, has been proposed and evaluated for therapeutic applications in various preclinical studies. Here, the outcome of the preclinical evaluation of BR38 is reviewed and summarized.

Methods: BR38 is a lipid based GMP grade microbubble filled with a mixture of N2 and C4F10. Safety and toxicology studies were evaluated in nonclinical GLP studies conducted in rats, dogs and pigs. Then, safety and tolerability was evaluated in a single-center, single-blind, placebo-controlled Phase 1 Study1. Now this agent is under preclinical evaluation for therapeutic applications and has been tested in various animal models for applications such as sonothrombolysis and drug or gene delivery.

Results: BR38 evaluation in non-clinical studies conducted in rats and dogs demonstrated a good safety profile. In pigs, the effects on systemic and pulmonary arterial pressure at 0.02 and 0.04 µL gas/kg were non-significant. The clinical Phase 1 study confirmed this good safety profile in human volunteers with a good tolerability and without adverse events of clinical significance reported1. In terms of pharmacokinetic profile, BR38 has demonstrated persistence in the blood circulation for several minutes.

Efficacy of BR38 as a therapeutic agent has been evaluated in preclinical models for several indications. In the context of ischemic stroke treatment, BR38 has demonstrated in *in vitro* evaluations the feasibility to improve clot lysis in combination with rtPA2. Moreover, *in vivo* tests showed improved microvascular perfusion in a stroke rat model of cerebral "no reflow" following BR38-enhanced sonothrombolysis3.

The use of BR38 for gene delivery has also been investigated. Preclinical evaluations have revealed that BR38 is able to significantly induce gene transfection in skeletal muscle4 of mouse and in subcutaneously implanted tumor cells5. BR38 was also successfully used to disrupt the blood brain barier and to deliver LacZ gene into the brain6.

Finally, BR38 has been used for gene silencing and has demonstrated its efficiency to significantly reduce tumor growth of human HCC xenografts in mice7.

Conclusions: BR38 has completed its non-clinical development and demonstrated its safety in clinic. The collected preclinical data indicate its therapeutic efficiency for various preclinical applications. These evidences, prompt us to further evaluate the potential of BR38 as a possible 'first generation' of therapeutic microbubble agent.

References

1. *Invest Radiol.* 2011;46(8):486-94
2. *Ultrasound* Med Biol. 2012;38(7):1222-33
3. *PLoS One*. 2016;11(4):e0152898
4. *Theranostics*. 2012;2(11):1078-91
5. *Radiology*. 2012;264(3):721-32

MI-11

Wednesday

24 October 2018

Topic: Miscellaneous Indications

Presentation Type: Oral

Model-based control for conformal hyperthermia using MR-HIFU

Lukas Sebeke[1], Edwin Heijman[2], Daniel Deenen[3], Bert Maljaars[3], Bram de Jager[3], W.P.M.H. Heemels[3], Holger Gruell[4]

[1]Univeristy Clinic of Cologne, Cologne, Germany
[2]Philips Research Germany, Cologne, Germany
[3]Technical University of Eindhoven, Eindhoven, Netherlands
[4]Klinikum der Universitaet zu Koeln, Cologne, Germany

Background: Precise control of the spatial heat distribution is paramount for effective hyperthermia treatments using MR-HIFU. To address this need and to fully leverage the precision of HIFU, a model predictive control (MPC) algorithm was developed as well as a custom python-based software for flexible MR-HIFU treatment planning and real-time monitoring of the treatment. Here, we demonstrate the controller's capability to outperform the currently implemented on-off controller in pre-clinical experiments.

Methods: All experiments are performed on a 3T MRI (Achieva®, Philips Healthcare) with an integrated HIFU transducer (Sonalleve®, Profound Medical). Proton Resonance Frequency Shift (PRFS)-derived temperature measurements serve as feedback data. At each time instance, the controller uses the current temperature information and a discretized form of the Pennes bioheat equation to find the distribution of heating power among the target ROI's voxels which minimizes the discrepancy between the predicted and target temperature distribution. The solution is then approximated using rapid switching of the HIFU focus between voxels. The used model is adapted to each target tissue using temperature data from a test sonication and linear regression.

The controller's performance was assessed using homogenous tissue phantom material as well as material with an artificial blood vessel two millimeters away from the target region (Fig. 1). The sensitivity of the controller to errors in the model calibration step was assessed by varying the controller's model parameters between treatments. In all cases, the target region's diameter was 18mm. Currently, performance tests are ongoing *in vivo* using a porcine model with results expected by the time of presentation.

Results: In a homogeneous target ROI, the MPC controller achieves an average steady-state offset of 0.14K from the set-point temperature and a temperature range of 1.07K inside the ROI, while the on-off algorithm reaches 0.55K and 2.11K respectively (Fig. 2). In an equivalent experiment with a blood vessel present, the average temperature offset increases for both algorithms, but the MPC controller still outperforms the binary controller, showing a more narrow temperature distribution (MPC: 1.80K, on-off: 3.27K) and smaller temperature offset (MPC: 0.39, binary: 0.59).

The sensitivity of the MPC controller to varying model parameters A1 (diffusion parameter) and B (heating rate) was assessed for nine different combinations in a homogenous phantoms. The measurements show that the average offset from the target temperature and the temperature distribution in steady state are comparable for all scenarios (Fig. 4).

Conclusions: The experiments have shown that an MPC algorithm yields more narrow temperature distributions and smaller steady-state temperature offsets than an on-off control algorithm even if the exact model parameters are unknown. These improved control capabilities translate into safer and shorter treatments, as the required thermal dose in the coldest areas of the ROI is reached more quickly while overheating in other areas is avoided. It was also found that effects like localized heat sinks can impair the ability of our MPC algorithm to enforce the imposed safety constraints reliably. Nonetheless, this controller consistently outperforms the available alternative and thus will be developed further to address issues and extend its functionality.

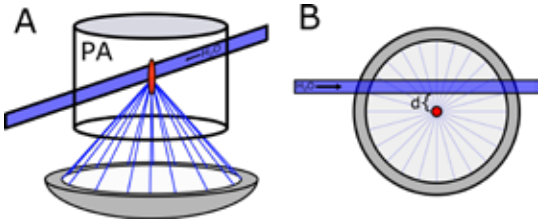

Figure 1. (A) The phantom is positioned above the transducer with the blood vessel running perpendicular to the beam axis. (B) The Transducer is positioned in such a way that the treatment area's edge is two millimeters away from the blood vessel.

Figure 2. Temperature distributions over time, achieved using an existing on-off controller and the newly developed MPC algorithm on a homogenous tissue-mimicking Polyacrylamide phantom.

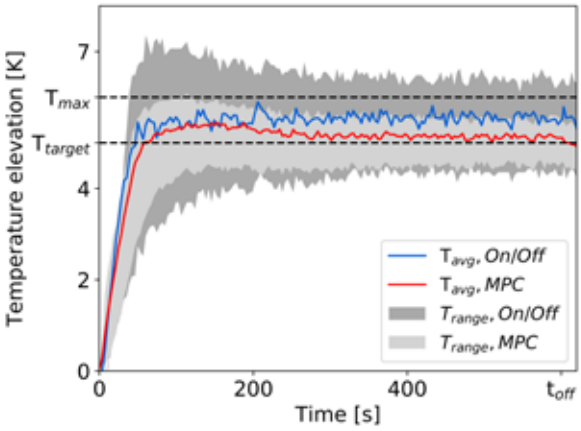

Figure 3. Temperature distributions over time, achieved using an existing on-off controller and the newly developed MPC algorithm on a tissue-mimicking phantom containing an artificial blood vessel.

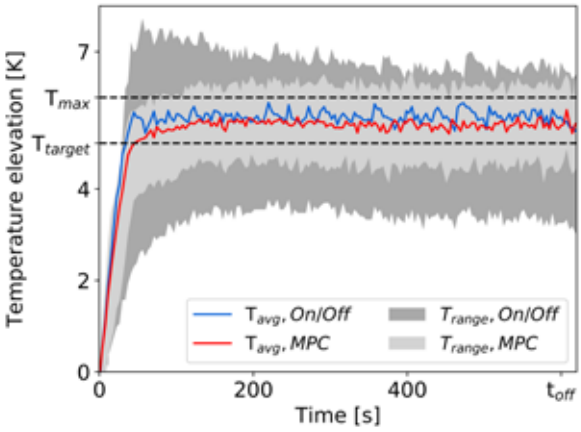

Figure 4. Temperature curves from experiments with varying controller models which were identified using linear regression and data from different test sonications.

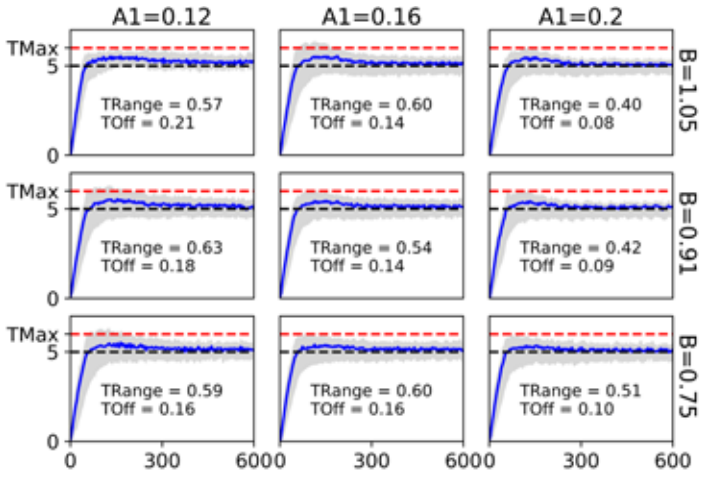

MI-12

Wednesday

24 October 2018

Topic: Miscellaneous Indications

Presentation Type: Oral

Pulsed focused ultrasound induces intracellular calcium signaling in multiple mammalian cell types

Rebecca Lorsung, Joseph A Frank, Scott R Burks

National Institutes of Health, Bethesda, Maryland, United States

In accordance with author request, this abstract is not available for publication.

MI-13

Wednesday

24 October 2018

Topic: Miscellaneous Indications

Presentation Type: Oral

Non-invasive, spatiotemporal control of transgene expression using hyperthermia generated by high intensity focused ultrasound

Alexander Moncion[1], Jonah Harmon[1], Yan Li[1], Sam Natla[1], Oliver D. Kripfgans[2], Jan Stegemann[1], Francisco Martín-Saavedra[3], Nuria Vilaboa[3], Renny Franceschi[1], Mario L. Fabiilli[2]

[1]University of Michigan, Ann Arbor, Michigan, United States
[2]University of Michigan Health System, Ann Arbor, Michigan, United States
[3]Hospital Universitario La Paz-IdiPAZ, Madrid, Spain

Background: The goal of tissue engineering is to develop biological substitutes facilitating the regeneration of impaired or injured tissues. These substitutes have the potential to overcome current problems associated with surgical reconstruction and organ transplantation. Conventional tissue engineering approaches rely on the scaffold-based delivery of exogenous proteins, genes, and/or cells to stimulate regeneration via growth factor signaling. However, scaffold-based approaches do not allow active control of the dose, timing, or spatial localization of a delivered growth factor – crucial parameters in promoting tissue regeneration. To address this limitation, we developed stable cell lines containing a heat-activated and rapamycin-dependent gene expression system that controls expression of firefly luciferase (fLuc), vascular endothelial growth factor 165 (VEGF165), or bone morphogenetic protein 2 (BMP2). Here, we demonstrate how high intensity focused ultrasound (HIFU) can induce spatiotemporally-controlled expression of fLuc both *in vitro* and *in vivo* via the controlled generation of hyperthemia within composite scaffolds.

Methods: Composite scaffolds were fabricated using 5 mg/mL fibrin, 20% (v/v) serum, 50 mg/mL hydroxyapatite powder (HA, ∅: <200 nm), 10 nM rapamycin, and 2 U/mL thrombin. Cell-loaded scaffolds (0.4 mL volume) were made by incorporating C3H/10T1/2 cells carrying the gene switch for controlling fLuc expression (i.e., C3H-fLuc) in the scaffolds at 106 cells/mL. Transgene activation was evaluated as a function of acoustic intensity following exposure to HIFU (2.5 MHz, f-number: 0.83, Sonic Concepts). Cell-loaded scaffolds without HA served as a control. Separately, spatial patterning of transgene activation was demonstrated by mechanically rastering the HIFU transducer across cell-loaded scaffolds (1 mL volume) in a 10 mm line. For *in vivo* studies, scaffolds (0.4 mL volume) containing C3H-fLuc cells were injected subcutaneously in the lower back of C3H/HeNCrl mice (2 scaffolds/mouse). One and seven days after implantation, 46 μg rapamycin was injected subcutaneously into each scaffold and HIFU was applied. fLuc activity was measured longitudinally using an IVIS Spectrum Imaging System (Perkin Elmer).

Results: Significant fLuc activity was observed in composite scaffolds after exposure to 2 min of continuous wave HIFU at ≥ 201 W/cm^2. Residual fLuc activity was observed in fibrin only scaffolds across all tested intensities (Figure 1). The spatial pattern of transgene activation matched the raster pattern of the HIFU transducer. The width of the activated region - characterized by the full width half maximum (FWHM) of the luminescence data - correlated inversely with transducer velocity (Figure 2). *In vivo*, significant fLuc activity was observed following HIFU on day 1 and 7 (Figure 3).

Conclusions: Composite scaffolds containing HA have a higher attenuation than fibrin only scaffolds, which enabled transgene activation at lower HIFU exposures. HA, the mineral component of bone, is osteoconductive and used in bone graft substitutes. *In vitro* and *in vivo* results indicate HIFU can spatiotemporally control transgene activation. C3H-fLuc cells could be reactivated one week after implantation. Future studies will investigate how HIFU can generate gradients of VEGF165 and BMP2, with the goal of inducing spatially-controlled blood vessel and bone growth.

Acknowledgements: This work is supported by the Focused Ultrasound Foundation.

Figure 1. Transgene activation occurred at lower HIFU intensities in composite (+HA) *versus* fibrin only (-HA) scaffolds.

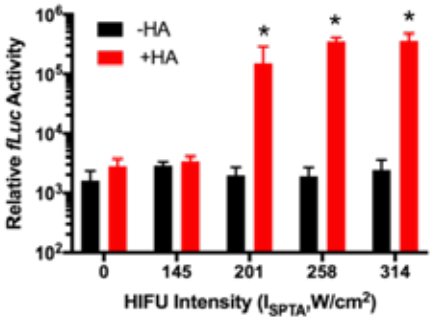

Figure 2. The width of the scaffold region containing transgene activation correlated inversely with transducer velocity. Inset: Luminescence image showing a 10 mm line of fLuc activity.

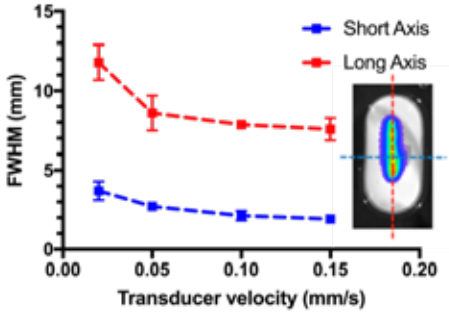

Figure 3. The timecourse of transgene activation, with significantly greater expression in scaffolds exposed to HIFU.

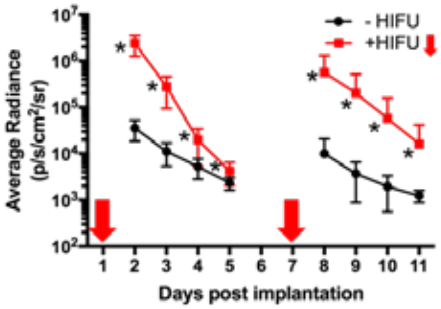

MI-15

Wednesday

24 October 2018

Topic: Miscellaneous Indications

Presentation Type: Oral

Thermal-energy memory based photoacoustic thermometry (TEMPT) in deep tissue

Yuan Zhou[1], Jianwen Luo[2], Pei Zhong[1], Junjie Yao[1]

[1]Duke University, Durham, North Carolina, United States
[2]Tsinghua University, Beijing, China

Background: Monitoring the temperature in deep tissues during HIFU therapy can help precisely control the heating process, efficiently kill the tumor cells, and minimize collateral damage to healthy tissues. Photoacoustic (PA) tomography (PAT) is a promising technology for noninvasive temperature sensing. However, traditional PA thermometry can measure only the changes in temperature relative to a baseline. Here we report a new thermal-energy-memory-based PA thermometry (TEMPT) to quantify the Grüneisen parameter and recover the absolute temperature distribution in deep tissues. Unlike the previous PA thermometry methods, TEMPT is calibration-free, and can directly provide absolute temperature map at clinically relevant depths.

Methods: In TEMPT, instead of using a single laser pulse, a train of high-speed laser pulses are sequentially delivered into the target within the thermal relaxation time, and the corresponding PA signals probe the target's local temperatures right before each laser strike (Fig. 1). While the first PA signal carries the information of the tissue's baseline temperature, the following PA signals reflect the slightly elevated temperature induced by the consecutive laser pulses due to the lingering thermal energy within the target. Using the acquired PA signals, we have developed a nonlinear mathematical model that correlates the signal time course with the tissue's Grüneisen parameter (Fig. 2). A ratiometric measurement can then be performed to estimate the absolute temperature, by canceling out the remaining temperature-irrelevant quantities that are challenging to calibrate for. A tomographic map of absolute temperature distribution can then be reconstructed.

Results: To validate the feasibility of TEMPT, two transparent plastic tubes filled with black ink solution were sandwiched between the chick tissues (Fig. 3a). TEMPT measurements were performed as the black ink temperature in the two tubes was adjust within the range of 20–55 °C (Fig. 3b). A highly linear correlation (R2=0.98) is observed between the calculated TEMPT temperatures and the referenced temperatures (Fig. 3c), with an average measurement error of ~0.5 °C.

In vivo experiments were conducted to further validate TEMPT in mice . A 5-second HIFU heating was applied to elevate the temperature inside the mouse limb, during which the TEMPT measurements were repeatedly performed. Figure 4 shows the region around the HIFU focus had substantial temperature rise, mainly due to the thermal diffusion from the heating focus.

Conclusions: Here, we report a novel technology TEMPT that is capable of noninvasive, calibration-free and absolute temperature mapping in deep tissues, based on the thermal energy memory effect. The major innovation of TEMPT over previous PA thermometry technologies is that the absolute temperature can be computed from the ratiometric measurement derived from the nonlinear mathematical model, without calibrating the PA signals by invasively measuring and changing the temperature of the target.

Acknowledgements: Duke MEDx Basic Science Pilot Grant, Duke Center for Genomic and Computational Biology Faculty Pilot Research Grant, and American Heart Association Collaborative Sciences Award 18CSA34080277.

Figure 1. Schematic of the thermal-energy memory effect in TEMPT. A train of laser pulses (a) excite the target and induce local temperature rise at each laser strike (b), which can be probed by the resultant PA signals (c).

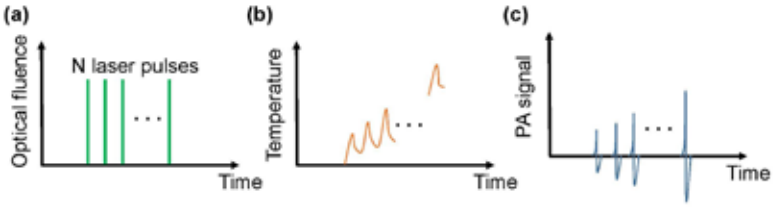

Figure 2. Workflow of the temperature mapping in TEMPT, including the mathmatical model that correlates the measured PA signals to the Grüneisen paramter at the baseline temperature.

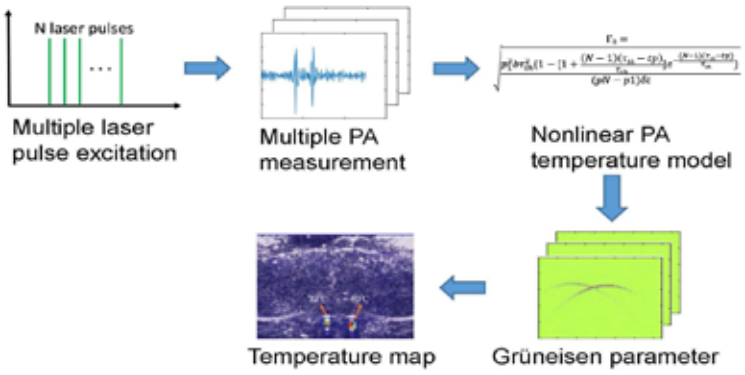

Figure 3. TEMPT meaurement on tissue phantoms (a) Reconstructed PAT image of the phantom. The white arrows indicate the two tubes. (b) TEMPT temperature map (shown in color) overlaid on the ultrasound image (shown in gray). (c) The temperatures in the tubes measured by TEMPT as a function of the reference temperatures measured by the thermometer.

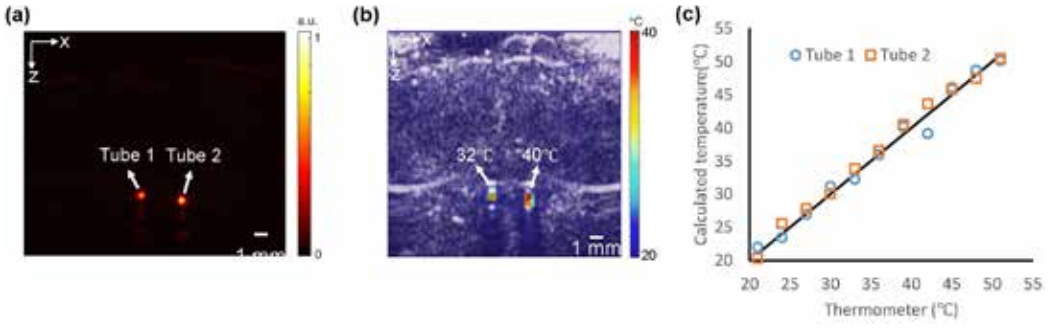

Figure 4. *In vivo* TEMPT measurement on a mouse with HIFU treatment. (a) TEMPT temperature maps of the mouse leg at different HIFU heating time points, showing the elevated temperatue in the HIFU focus. (b) Absolute temperature maps overlaid on the corresponding ultrasound images.

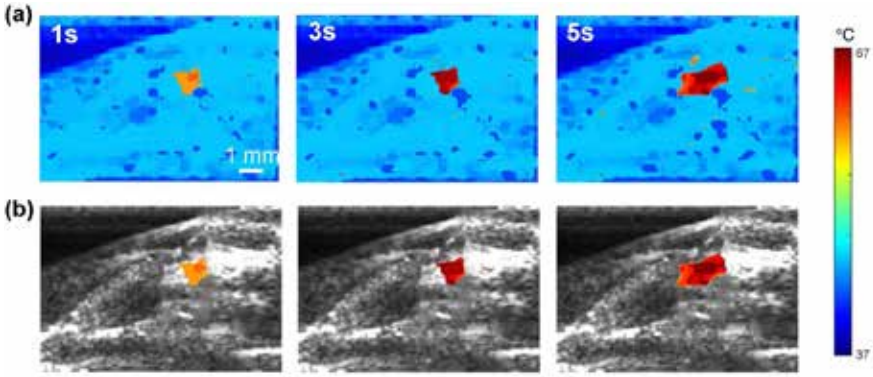

MI-16

Wednesday

24 October 2018

Topic: Miscellaneous Indications

Presentation Type: Oral

Mechanical damage induced by rectified bubble growth during boiling histotripsy

Ki Joo Pahk[1], Matheus Oliveira De Andrade[2], Pierre Gélat[2], Hyungmin Kim[1], Nader Saffari[2]

[1]Center for Bionics, Biomedical Research Institute, Korea Institute of Science and Technology (KIST), Seoul, Republic of Korea

[2]University College London, London, United Kingdom

Background: In boiling histotripsy, the presence of a boiling vapour bubble and understanding of its dynamic behaviour are crucially important for the initiation of the tissue fractionation process and for the control of the size of the lesion produced. Whilst many *in vivo* studies have shown the feasibility of using boiling histotripsy in mechanical fractionation of solid tumours, not much is known about the evolution of a boiling vapour bubble in soft tissue induced by boiling histotripsy. In general, the shape of a lesion induced by boiling histotripsy, consists of a head and a tail with the head closest to the High Intensity Focused Ultrasound (HIFU) transducer. The formation of boiling bubbles in a localised-heated region at the HIFU focus and the subsequent production of an inertial cavitation cloud are respectively responsible for the tail and the head of the tadpole-shaped lesion [1]. The main objective of this present study is therefore to investigate the formation and the dynamic behaviour of a boiling vapour bubble created under boiling histotripsy insonation.

Methods: Experimental studies on the bubble dynamics induced in optically transparent tissue-mimicking gel phantoms exposed to the field of a 2.0 MHz HIFU transducer were performed with a high speed camera. Numerical studies using the Gilmore bubble model coupled with the Zener viscoelastic, the Khokhlov-Zabolotskaya-Kuznetsov and the Bio-heat Transfer equations were conducted to simulate bubble dynamics driven by nonlinear-shocked wave excitation in a viscoelastic medium as functions of temperature and tissue elasticity variations. *In vivo* animal experiments were also conducted to examine cellular structures around a freshly created lesion in the liver resulting from boiling histotripsy.

Results: To the best of our knowledge, this is the first study reporting the numerical and experimental evidence of the appearance of rectified bubble growth in a viscoelastic medium (Figure 1 and 2). Accounting for tissue phantom elasticity adds a mechanical constraint on vapour bubble growth, which improves the agreement between the simulation and the experimental results. In addition the numerical calculations showed that the asymmetry in a shockwave and water vapour transport can result in rectified bubble growth which could be responsible for boiling histotripsy-induced tissue decellularisation (Figure 3). Strain on liver tissue induced by this radial motion can potentially damage liver tissue while preserving blood vessels (Figure 3 and 4).

Conclusions: In this study, a numerical and experimental study of bubble dynamics in a viscoelastic medium induced by boiling histotripsy was performed with a high speed camera. Results presented suggest that the asymmetry in a shockwave together with water vapour transport can result in rectified bubble growth in a viscoelastic medium that can potentially tear off liver tissue while preserving blood vessels.

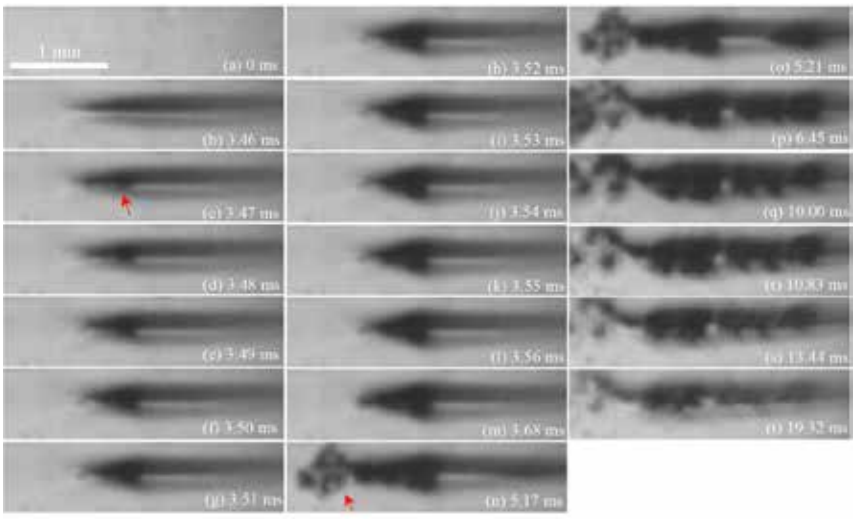

Figure 1. A sequence of high-speed camera images obtained in an optically transparent liver tissue mimicking gel phantom during the single 10-ms HIFU exposure with P+ of 85.4 MPa and P- of −15.6 MPa. The 2.0 MHz HIFU beam propagates from left to right.

Acknowledgments: This work was funded by Department of Mechanical Engineering, University College London (UCL, London, UK) and Korea Institute of Science and Technology (KIST, Seoul, Korea, 2E27980).

Reference

1. Ki Joo Pahk, Pierre Gélat, David Sinden, Dipok Kumar Dhar, Nader Saffari. Numerical and experimental study of mechanisms involved in boiling histotripsy. *Ultrasound in Medicine and Biology*. 2017;43(12):2848-2861.

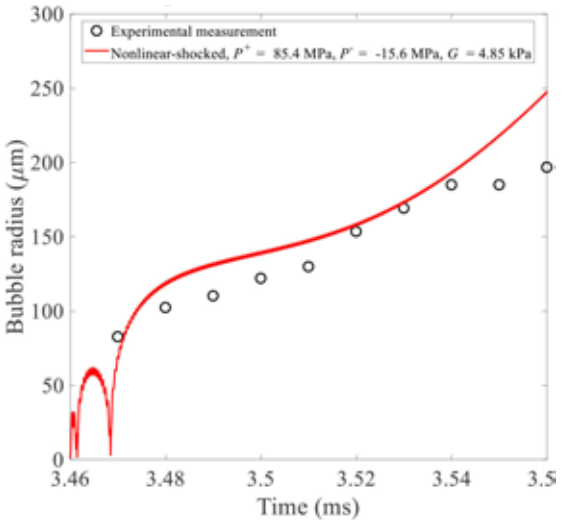

Figure 2. A comparison between the experimentally measured bubble radius and the simulated radius *vs.* time curves. The simulation was performed at the temperature of T0 = 95.62degC which was obtained from the BHT simulation at t = 3.47 ms. R0 = 1 μm.

Figure 3. Calculated a time-varying strain produced in the liver caused by rectified bubble growth at 100degC with varying shear modulus G. (a) Strain *vs.* time curve over 100 acoustic cycles. (b) A percentage difference in strain relative to at G = 2 kPa.

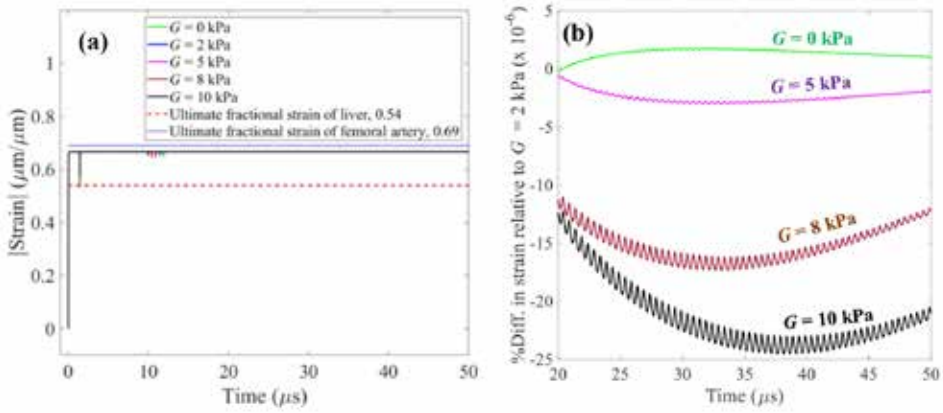

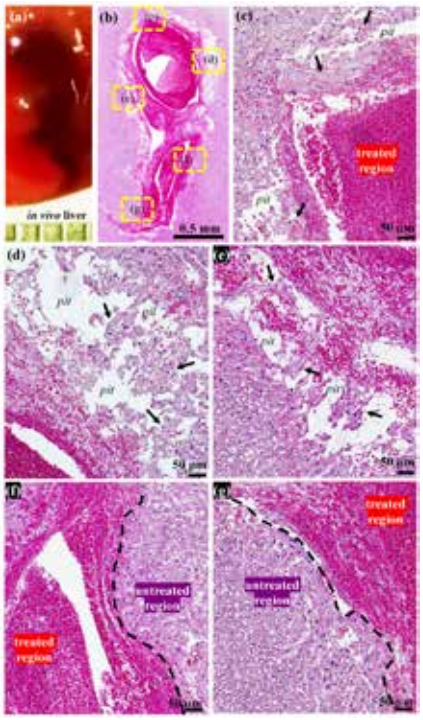

Figure 4. Histological examination around a freshly created cavity produced by boiling histotripsy (P+ = 80 MPa, P- = - 15.6 MPa, 1% DC, 1 Hz PRF, 10 HIFU pulses). The 2.0 MHz HIFU beam propagates from top to bottom. Arrows indicate broken hepatocyte plates.

MS-1

Wednesday

24 October 2018

Topic: Musculoskeletal
Presentation Type: Oral

Development of a custom LIPUS system with uniform far-field exposure and demonstration of LIPUS-induced increase in collagen synthesis in annulus fibrosus cells

Devante Horne, Peter Jones, Matthew Adams, Jeffrey Lotz, Chris Diederich

University of California –San Francisco, San Francisco, California, United States

Background: Low back pain (LBP) is the most common musculoskeletal condition, affecting 80% of the population at some point in their lifetime. Common causes of LBP include damage to the annulus fibrosus (AF) of the intervertebral disc (IVD), which is characterized by its limited intrinsic healing capacity. Recently emerging therapies, including intra-discal growth factor injections, are invasive and limited due to sustainability and safety concerns. Mechanical stimulation of IVD cells by Low-intensity Pulsed Ultrasound (LIPUS) may be a safer alternative that is both noninvasive and regenerative. In this study, a LIPUS exposimetry system was designed to mitigate confounding factors often ignored in previous studies including nonuniform near-field (NF) exposure, beam reflections, and temperature elevation within the sample. This custom system was used to test the hypothesis that collagen synthesis in AF cells can be increased by far-field LIPUS exposure.

Methods: LIPUS systems were devised and fabricated following our general schematic (Figure 1), specific to delivering calibrated and uniform energy to cells cultured in standard 6-well plates. Our configuration consisted of two 2.5cm diameter PZT-4 planar transducers (1.5MHz). Well plates were positioned at an acoustic standoff distance within temperature-regulated degassed water, placing them within the transducer's uniform far-field (FF) zone. Acoustically transparent alginate rings were inserted into wells to constrain cells within the Full Width at Half Maximum Intensity (Figure 1B). Custom silicone absorbers were placed distally to eliminate standing wave formation. Temperature elevation within the well plate was measured using thermocouples positioned in parallel with ultrasound propagation (sonication parameters: 1.5MHz, ISPTA=120mW/cm^2, 20-minute exposure).

Bovine AF cells were encapsulated in alginate beads and cultured in 6-well plates. One group received media supplemented with BMP-7, a well-known anabolic growth factor. The LIPUS group was exposed to a LIPUS waveform (1.5MHz, ISPTA=120mW/cm^2) for 20 minutes each treatment day. To simulate environmental conditions without LIPUS, control and BMP-7 samples were placed in the LIPUS exposimetry system for 20 minutes with the ultrasound turned off. All samples were cultured for 14 days, with treatments taking place on 8 of the 14 days. On day 14, collagen content was evaluated by hydroxyproline assay.

Results: Our design demonstrates delivery of uniform FF intensity with a 92% reduction in gradient magnitude compared to typical NF configurations (Figure 2). Additionally, our system demonstrates minimal temperature elevation of 0.81 ± 0.15°C within alginate beads. Bovine AF cells demonstrated greater collagen concentration than controls when treated with BMP-7 (3.3-fold) or LIPUS (2.6-fold), with no significant difference between the BMP-7 and LIPUS groups (Figure 3).

Conclusions: A custom LIPUS *in vitro* system was designed and characterized to deliver uniform energy and mitigate confounding factors often ignored in previous studies. We

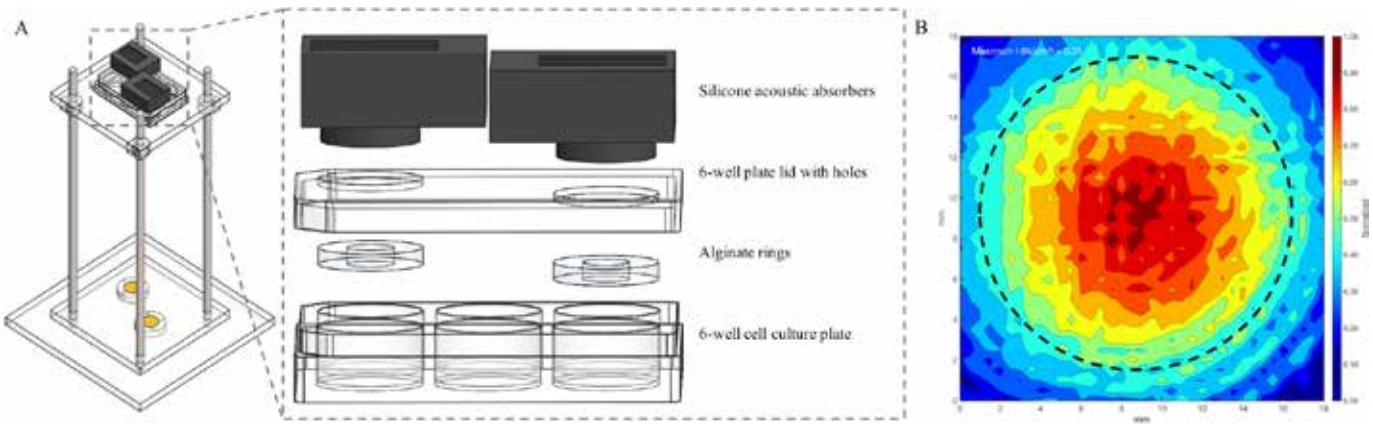

Figure 1. A) Schematic of custom LIPUS exposimetry system. B) Beam plot of normalized intensity demonstrates uniform FF intensity at cell culture level. Cell culture area is restricted within dashed circle, which is the inner diameter of alginate rings.

demonstrate a LIPUS-induced upregulation in collagen synthesis in bovine AF cells that is of similar magnitude to growth factor treatment, suggesting that LIPUS may be a safer alternative for stimulating AF repair.

Acknowledgements: Supported by NIH R21EB024347; Focused Ultrasound Foundation

Figure 2. Beam uniformity was quantified by assessing the magnitude of the intensity gradient across the cell culture area. Typical configurations place 24-well plates within the transducer's near-field (NF-24-well).

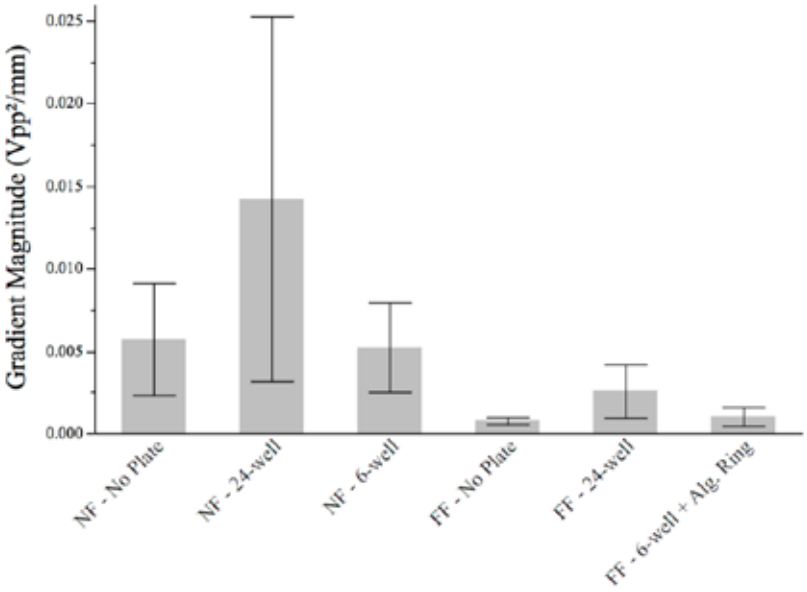

Figure 3. LIPUS exposure as well as treatment with BMP-7, a well-known anabolic and anti-catabolic growth factor, demonstrated a significant increase in collagen concentration compared to control. n=12

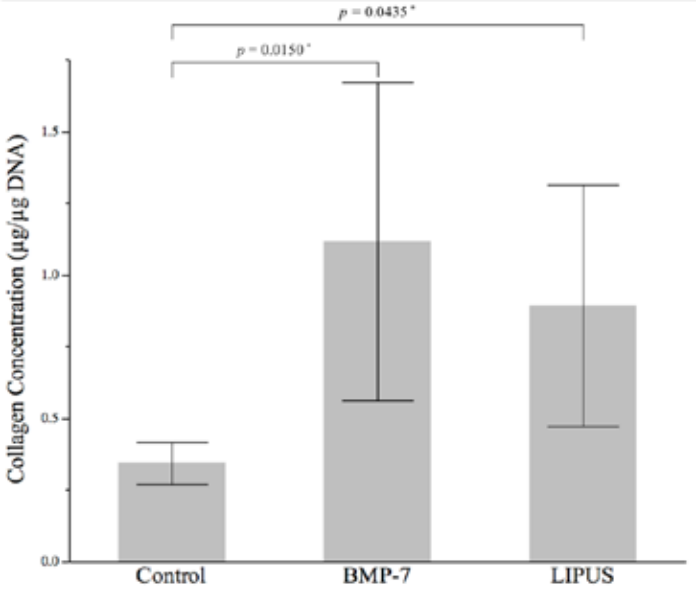

MS-2

Wednesday

24 October 2018

Topic: Musculoskeletal
Presentation Type: Oral

Histotripsy as a novel therapeutic approach to rotator cuff tendon injury

Julianna Simon, Meghan Vidt

The Pennsylvania State University, University Park, Pennsylvania, United States

Background: Mechanical high intensity focused ultrasound, or histotripsy, has been used to fractionate soft tissues through the oscillation and collapse of cavitation bubble clouds or through shock wave heating and millisecond boiling. While these histotripsy approaches have successfully liquefied soft organs such as the liver, heart, and prostate, highly collagenous tissues, like tendons and ligaments, have proven resistant to mechanical fractionation with histotripsy. Rotator cuff tears are a highly prevalent cause of shoulder pain, estimated to affect 5-40% of people. However, surgery fails in up to 90% of patients. Non-surgical treatments, such as dry needling and extracorporeal shock wave therapy, have been introduced to facilitate healing by intentionally inducing microdamage to promote inflammation and the release of healing factors. Yet, success rates are mixed, in part due to user variability. Here, we propose developing ultrasound-guided histotripsy protocols to create microdamage in highly collagenous tissues, such as tendons, to induce a healing response. Histological and mechanical results will be compared between histotripsy and the conventional dry needling therapy to evaluate tissue integrity.

Methods: Thirty supraspinatus tendons were harvested from fifteen rats and mounted in a custom-designed holder that allows for mechanical testing of the treated samples. The 10 samples in the histotripsy treatment group were aligned at the focus of a 1.5 MHz or 3.6 MHz focused ultrasound transducer using a Verasonics® ultrasound system with the L22-14 transducer for image-guidance (Fig. 1). The transducer was operated with 1-20 ms pulses repeated at 1-10 Hz pulse repetition frequencies. The 10 samples in the dry needling treatment group had a fine-gauge needle inserted 5-10 times to "pepper" the tendon as per standard dry needling practice (scaled for rat tendon). The final 10 samples were used as controls. After treatment, 5 samples from each group were processed for histological analysis and the other 5 samples were exposed to stress-relaxation and load-to-failure mechanical testing.

Results: Preliminary results show that histotripsy can disrupt tendon tissues, and we expect that parameters can be tuned to create controllable microdamage. Results comparing histotripsy to dry needling histologically and mechanically are forthcoming.

Conclusions: Histotripsy has potential as a non-invasive, non-surgical treatment for rotator cuff tendon tears by inducing microdamage to initiate a healing response. By using ultrasound imaging for guidance of the histotripsy therapy, we hope to reduce the user variability associated with other non-surgical therapeutic techniques while preserving the mechanical integrity of the healing tendon. If successful, this therapy could lead to reduced sequelae associated with rotator cuff and other tendon tears.

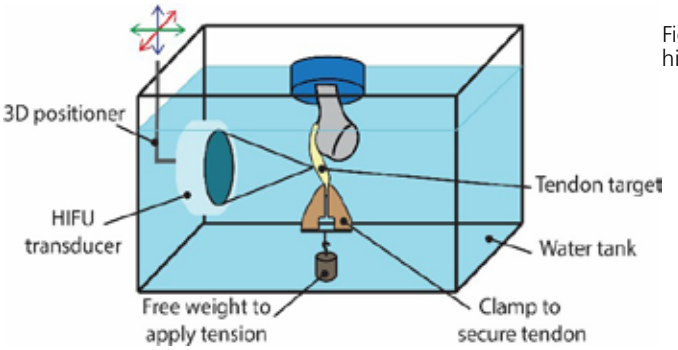

Figure 1. Experimental arrangement for histotripsy of *ex vivo* rat tendons.

MS-3

Wednesday

24 October 2018

Topic: Musculoskeletal
Presentation Type: Oral

In vivo measurements of medial branch nerve depth for FUS ablation of facet-related back pain: Predictors of patient candidacy

Hannah Zwiebel[1], Daniel Baldor[2], Suzanne LeBlang[3], Arik Hanannel[4], Ron Aginsky[5], Fred Steinberg[3]

[1]Tufts University, Boca Raton, Florida, United States
[2]University of Miami Miller School of Medicine, Miami, Florida, United States
[3]University MRI & Diagnostic Imaging Centers, Boca Raton, Florida, United States
[4]FUSMobile Inc., Alpharetta, Georgia, United States
[5]FUS Mobile, Boca Raton, Florida, United States

Background: To evaluate candidacy for direct focused ultrasound ablation of the medial nerve branch in patients with facet-related back pain.

Methods: 100 patient lumbar noncontrast CAT scans were retrospectively evaluated, and the depth from the skin to the medial branch nerve (MBN) from L2-L5 was recorded bilaterally. Other measurements included the smallest width of the pedicle and the three dimensions of the transverse process. A step-wise linear regression model was built to identify the strongest predictors of MBN depth with independent variables including age, gender, vertebral level, BMI, and pedicle side.

Results: The average distance of skin-to-MBN increased as the lumbar level increased measuring 64.6mm at L2, 72.0mm at L3, 79.2mm at L4, and 79.1mm at L5. The linear regression model returned BMI, vertebral level, and gender as significant predictors of MBN depth ($p<0.001$ and $r2= .61$). Analysis also demonstrated that MBN depth increases more rapidly in men than in women as BMI increases. A regression equation was generated that can predict patient candidacy based on MBN depth: MBN depth (mm) = 2.2*BMI + 4.9*(lumbar vertebral level) + 3.6(if female) - 5.4.

Conclusions: Overall, it was found that a FUS beam capable of 85mm and 97mm penetration would be adequate to treat 75% and 90% of the patient population respectively. We believe that FUS ablation of this more proximal MBN could provide more complete and durable pain relief from facet-related back pain compared to ablation of the more distal branches along the facet joint. As a noninvasive treatment, FUS ablation decreases the risks associated with more invasive procedures such as bleeding and infection, thus reducing morbidity and recovery times.

MS-4

Wednesday

24 October 2018

Topic: Musculoskeletal
Presentation Type: Oral

RNA-seq reveals differential transcriptome-wide responses to pulsed-focused or therapeutic ultrasound in skeletal muscle

Scott R Burks, Rebecca Lorsung, Joseph Frank

National Institutes of Health, Bethesda, Maryland, United States

In accordance with author request, this abstract is not available for publication.

MS-5

Wednesday

24 October 2018

Topic: Musculoskeletal
Presentation Type: Oral

Sacroiliac joint ablation using MRgFUS in a chronic swine model

Viola Rieke, Eugene Ozhinsky, Matthew Bucknor, Ellen Liebenberg, Carol Stillson, Colin Yee, Teri Moore, Roland Krug

University of California – San Francisco, San Francisco, California, United States

Background: There is evidence that MRgFUS might be a very safe and effective minimally invasive technique to treat facet and sacroiliac joint pain caused by arthritis and other degenerative changes. In contrast to radiofrequency neurotomy, MRgFUS is non-invasive, eliminates the risk of bleeding or infection, is radiation free, and can be repeated if necessary. However, due to safety concerns it has not yet been approved by the FDA. In this study, we longitudinally evaluated the safety and effectiveness of MRgFUS ablation of the SI joint in a chronic swine model.

Methods: All animal procedures received approval from the Institutional Animal Care and Use Committee. Five animals have undergone MRgFUS treatment with the INSIGHTEC ExAblate 2000 system in a 3T scanner using two different energies (n = 3 with 700J, n=2 with 1000J) at 1.35 MHz frequency. Sonications were planned in oblique coronal slices lateral and in a semicircle around the foramina (S1: 7 sonications, S2: 6 sonications, S3: 0-4 sonications) targeting the lateral branches of the nerve roots, as seen in Figure 1. The beam was angled to achieve close to normal incidence onto the surface of the sacrum. The left side was treated, the right side served as control. After post-treatment imaging (baseline), the animals were recovered from anesthesia, assessed for pain, behavior, ambulation, and gait, and followed for 5 weeks. The animals were euthanized after an additional MR imaging session (follow-up) and the sacrum removed for histopathological analysis and confirmation of the imaging results.

Results: Treatment dose and temperature rise (~60oC) were clearly seen on MR temperature imaging in all experiments. Treatment effects were not seen on MRI images immediately after treatment in all animals. One animal (1000J) had some clearly visible bulge directly under the skin in the field of treatment (Figure 2), with sonication effects visible on the T2-weighted and T1-weighted post-contrast images. However, the animal did not seem to have pain in that region and had completely subsided after five weeks at follow-up imaging. Figure 3 shows an additional example of MRgFUS treatment assessment.

There was no sign of lameness or impairment in any animal and no changes in animal behavior or appetite was observed.

In order to assess the treatment effectiveness, the specimens are currently undergoing histopathological (Figure 4).

Conclusions: This study in a chronic swine model attempts to show safety and effectiveness of MRgFUS sacroiliac joint ablation. At the current stage of this study, we demonstrated SI joint ablation using MRgFUS is a safe treatment. Our ongoing histological assessment will show the effectiveness of this treatment once it is concluded. The results of this study will be paramount for obtaining regulatory approval for a clinical trial for this promising alternative to radio frequency ablation.

Acknowledgements: This work was funded by the Focused Ultrasound Foundation and a Departmental Seed Grant.

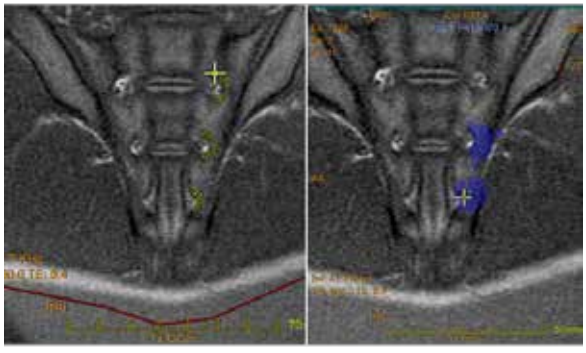

Figure 1. Oblique coronal planning images with the sonication spots indicated as yellow circles (left) targeting the lateral branches of the S1 to S3 nerve roots. The thermal does accumulated in the treatment area dose is shown for S2 and S3 (right).

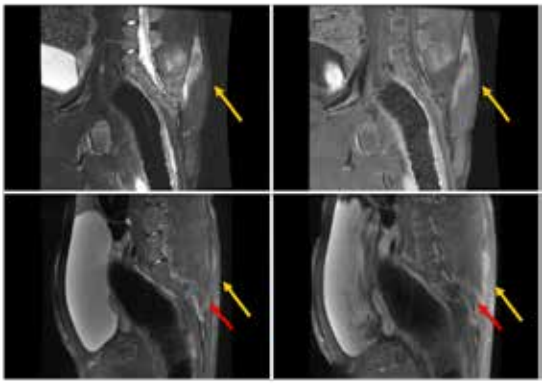

Figure 2. On this animal, a swelling (orange arrows) was visible on the baseline images (top), which was also visible and palpable on/ underneath the surface of the skin. The T2 (left column) and post-contrast T1 (right column) weighted images clearly show changes in the treatment regions and in the beam path to the target. However, there was no indication of pain in the area and swelling disappeared within a few days. Follow-up images (bottom row) show that treatment effects are still visible after five weeks (red arrows).

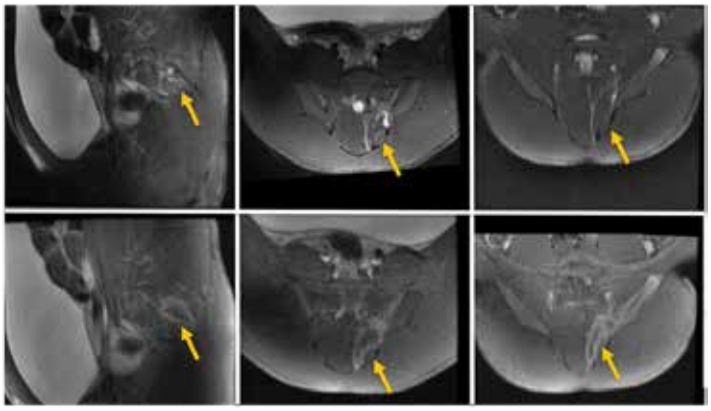

Figure 3. Follow-up images of an animal treated with the lower energy of 700J in sagittal, axial and coronal orientations. The arrows indicate the region of treatment. T2 weighted images before contrast (top row) provide better tissue contrast and show clearly the regions of edema. T1 weighted post-contrast images (bottom row) clearly show the effects in the treatment area, where the ablated/coagulated area appears dark surrounded by a hyper-enhancing ring.

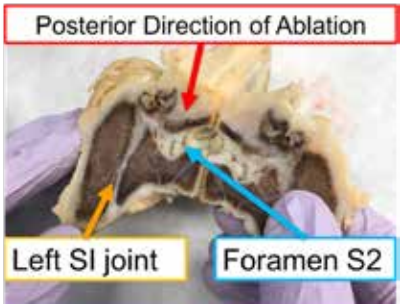

Figure 4. This figure shows a section of the specimen after decalcifying. The SI joint and foramen can be seen. Histology will be performed on these sections.

MS-6

Wednesday

24 October 2018

Topic: Musculoskeletal
Presentation Type: Oral

MR-HIFU ablation of lumbar facet joints: Effects of varying acoustic powers

Sin Yuin Yeo[1], Juan Castillo[2], Edwin Heijman[3], Alexandra Maul[4], Lukas Sebeke[4], Pia Rademann[4], Hannsjörg Schröder[4], Holger Gruell[1]

[1]Klinikum der Universitaet zu Koeln, Cologne, Germany
[2]University Hospital of Cologne, Cologne, Germany
[3]Philips Research Germany, Cologne, Germany
[4]Uniklinik Köln, Cologne, Germany

Background: Lumbar facet joint osteoarthritis is one of the main causes of low back pain (LBP). Though there is a selection of treatment options available, for instance, non-steroidal anti-inflammatory drugs, intra-articular injection of anesthetic or corticosteroid, or radiofrequency ablation, pain recurrence is common. Magnetic resonance-guided high intensity focused ultrasound (MR-HIFU) is an attractive alternative non-invasive treatment, which has been demonstrated to alleviate pain in a preliminary study in patients with LBP. However, there is limited insight into the effects of different ablation parameters on facet joints. Here, we systematically investigated the effects of varying acoustic powers on facet joint ablation using imaging and histological analyses.

Methods: Five female landrace pigs with an average weight of 51±3kg were used in this study. For each pig, 4 lumbar facet joints were ablated with the contralateral side serving as controls. A 4 mm treatment cell was planned on each facet joint. The acoustic powers used were 80, 100, 120, 140, 160 and 190W, with 190W being the maximum power allowed by a Sonalleve® MR-HIFU system (Profound Medical). Each power was repeated 3 times, and all facet joints were sonicated once for 16s using a frequency of 1.2MHz. The highest temperature in the soft tissue adjacent to the facet joint was analyzed from the temperature maps. All animals were followed-up for 7 days for treatment effects and complications. Edema formation and non-perfused volume (NPV) were assessed using T2-weighted and subtracted contrast-enhanced T1-weighted MR images, respectively, and correlated to acoustic powers. Thereafter, animals were euthanized and facet joints were excised for histological analysis.

Results: Figure 1 shows representative images of a facet joint ablation in 3 orthogonal planes. In line with our expectation, with increasing power, the soft tissue temperatures increased from 74.8°C (80W) to 85.6°C (190W). Immediately and at 7 days after the treatments, edema formation around the treated facet joints was evident, and the volume increased from 0.6cm^3 (80W) to 2.5cm^3 (190W). In conjunction to edema formation, NPV was observed in the soft tissue and within the facet joints, and the NPV increased from 0.5cm^3 (80W) to 2.3cm^3(190W). Histological analyses revealed ablation of bone, bone marrow, and cartilage of a facet joint. In addition, hemorrhages were observed within the ablated bone marrow. There were no complications related to the treatments.

Conclusions: MR-HIFU ablation is safe and effective for treatment of facet joints at high acoustic powers. There is a positive correlation between increasing powers and the resulting edema and NPV. This knowledge can be used to tailor a facet joint ablation protocol.

Acknowledgements: We would like to thank Carolin Debuschewitz, Susan Vlachakis, Katrin Wiesmann and Bernadette Disler for supporting the *in vivo* experiments, and Manuela Lerwe, Irmgard Henke, and Kirsten Pilz for their assistance in histology.

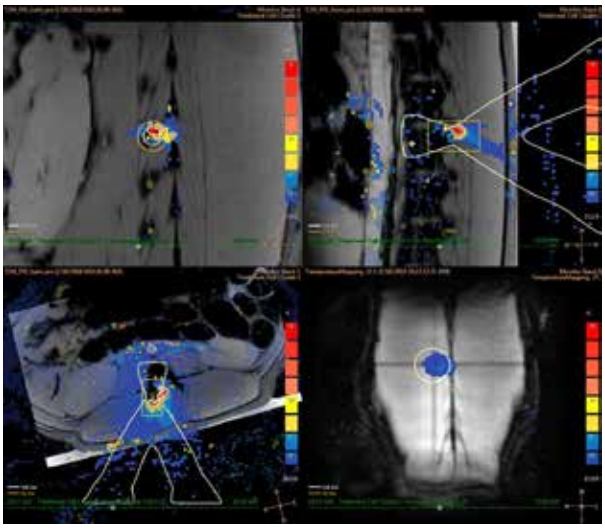

Figure 1. Representative images of a MR-HIFU ablation of facet joint using a 4mm treatment cell, 120W, 1.2MHz and 16s.

MS-7

Wednesday

24 October 2018

Topic: Musculoskeletal
Presentation Type: Oral

In vivo measurements of sacral nerve lateral branch depth for focused ultrasound ablation of patients with sacral iliac joint pain: Predictors for patient candidacy

Jude Jaraki[1], Daniel Kushner[1], Ron Aginsky[2], Arik Hananel[2], Fred Steinberg[3], Suzanne LeBlang[3]

[1]Florida Atlantic University College of Medicine, Boca Raton, Florida, United States
[2]FUS Mobile, Boca Raton, Florida, United States
[3]University MRI & Diagnostic Imaging Centers, Boca Raton, Florida, United States

Background: To evaluate candidacy for focused ultrasound ablation of lateral branches of the sacral nerves in patients with sacral iliac joint (SIJ) pain.

Methods: 20 CT scans of the sacrum and were retrospectively evaluated in 9 male and 11 female patients and charts were reviewed for age and BMI. Bilateral measurements were obtained from 2D and 3D images and included: distance between the lateral aspect of the posterior sacral foramina to the medial margin of the sacroiliac joint (LSIJ), depth from the skin to the midpoint of the LSIJ at 0o , 15o , and a maximal angle without interacting the spinous processes (θmax), curved length of the posterior sacrum through the midpoints of the LSIJ, the angle between LSIJ and the iliac crest (α), sacral foraminal width, and the AP thickness of the sacrum measured at the midpoint of the LSIJ. For patients with sacroiliac anatomy where the perpendicular depth from the skin to the LSIJ midpoint intersected the iliac crest, a maximal cone was constructed simulating a range for the focused ultrasound beam. A regression model evaluated the most statistically and clinically significant predictors for the distance from the skin to the LSIJ midpoint at 0o, 15o, and θmax.

Results: The average depth from the skin to the sacral LSIJ midpoint perpendicularly decreased as the vertebral levels increased. The average distances were 57.2 mm at S1 (range: 31.2-87.9 mm) and 40.97 mm at S2 (range: 23.6-66 mm). The average depth from the skin to the midpoint at θmax decreased slightly as vertebral level increased, from 98.43 mm at S1 (range: 53.9-146.8 mm) to 92.71 mm at S2 (range: 40.4-146.1 mm). The average AP diameter at S1 was 40.72 mm (range: 22.2-60.6 mm) and increased at S2 to 44.79 mm (range: 29.2-67 mm), then decreased at S3 to 22.5 mm (range: 9.6-51.8 mm) and decreased again at S4 to 9.69 mm (range: 6.6-13.5mm) due to angulation of the sacrum. The average curved length of the posterior sacrum was 122.7 mm. Average BMI of all patients was 26.51 (range: 18.3-43.65) and average age was 65.25 years old (range: 27-86).

Conclusions: The average distance from the skin to the posterior border of the sacrum at the LSIJ was 49.1 mm and decreased as the vertebral level increased and the average curved length of the posterior border of the sacrum was 12.3 mm. To date, no clinical studies have published *in vivo* measurements of the posterior sacrum. Currently, SIJ pain is treated with percutaneous injections and ablation. These results will help determine the feasibility of noninvasive FUS ablation of the lateral sacral branches for patients with sacroiliac joint pain.

MS-8

Wednesday

24 October 2018

Topic: Musculoskeletal
Presentation Type: Oral

Evaluation of magnetic resonance guided focused ultrasound in the management of osteomyelitis: Targeting feasibility

Amanda Beserra[1], Samuel Pichardo[1], David Kisselgoff[2], Shalyn Littlefield[2], Valentina Peeva[2], Laura Curiel[1]

[1]University of Calgary, Calgary, Alberta, Canada
[2]Thunder Bay Regional Health Sciences Centre, Thunder Bay, Ontario, Canada

Background: Osteomyelitis is a serious complication linked to diabetes that increases the possibility of limb amputation. It is a complex inflammatory process involving infection of the bone and adjacent structures, often not responding to antimicrobial therapy. There exists a clinical need to improve management of osteomyelitis, especially for diabetic patients. Magnetic resonance guided focused ultrasound (MRgFUS) can offer an option for patients with osteomyelitis by providing a non-surgical treatment option. This minimally invasive approach could be proposed as an adjuvant treatment that can be combined with standard care, including administration of antibiotics.

Methods: In this study we evaluated the feasibility of targeting osteomyelitis sites using a clinically-approved MRgFUS device. We performed MRgFUS virtual treatment planning on images from 16 clinical cases using an in-house adaptation of the treatment planning software for the Sonalleve platform. Images were obtained from cases with an osteomyelitis diagnosis for which magnetic resonance imaging (MRI) or computed tomography (CT) was available. Targets were evaluated based on their location and surrounding structures within the ultrasound beam path. The criteria to disqualify a case was: 1) target less than 1 cm from the skin, 2) target close to a neuro-vascular bundle, 3) defect in overlying skin or 4) metallic device adjacent to the treatment region close to a vital organ. The in-house software allowed for virtual repositioning of the patient to reach the target with the Sonalleve platform. Images were initially processed to place a target volume at the infection site and treatment planning was then conducted. The calculated treated volume was taken from the Sonalleve planning calculation and the total target volume was obtained using Osirix 3D reconstruction from 2D user-defined ROIs on the osteomyelitis site. The percentage of cases that could be treated as well as the percentage of the bone infection that could be targeted on cases that qualified after accounting for safety margins was calculated.

Results: The cases covered in this work included limb, pelvis and thorax locations. Five out of the 16 cases were disqualified (31.25%) with 3/5 because of proximity to skin. For the cases that qualified, 88.2±5.7% of the osteomyelitis target was considered reachable using treatment cells available at the Sonalleve system. The main limitation to full coverage was the localization of a treatment cell close to the skin, and this reduced the treatment volume to 79% for two cases.

Figure 1 shows the treatment planning for a knee case where the software was first used to virtually position the patient in a feet first decubitus left orientation. The final coverage of the osteomyelitis site was 90.7%.

Three of the cases presented a large lesion site where the calculated a total exposure volume averaged 48.57±41.41mL and the total treatment time was estimated more than 3 hours. For all other cases the average treated volume was significantly lower at 1.59±1.75mL.

Conclusions: This retrospective study was performed as a first step to evaluate feasibility of MRgFUS treatment of osteomyelitis. Osteomyelitis sites located in the extremities seem to be very promising for this non-invasive treatment. This approach can be well indicated for patients with strong associated comorbidities and it could be proposed as an adjuvant to antibiotic therapy. Future work will include some *ex vivo* experiments to evaluate the feasibility of thermometry follow as well as *in vivo* experiments in animal models of osteomyelitis.

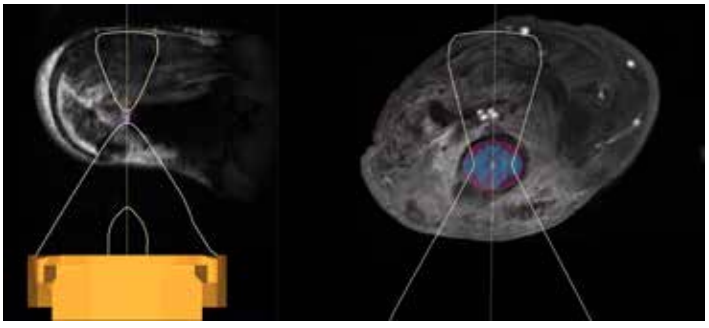

Figure 1. MR image of a knee case with patient repositioned and cells planned. The osteomyelitis site volume was 1.29mL with a treated volume estimated at 1.17mL by the planning software (90.7% coverage)

MS-9

Wednesday

24 October 2018

Topic: Musculoskeletal
Presentation Type: Oral

Acoustic radiation and cavitation forces in non-ablative pulsed focused ultrasound independently activate a pro-stem-cell-homing molecular response in murine skeletal muscle

Rebecca Lorsung, Ritika Jain, Joseph A Frank, Scott R Burks

National Institutes of Health, Bethesda, Maryland, United States

In accordance with author request, this abstract is not available for publication.

WH-1

Wednesday

24 October 2018

Topic: Breast
Presentation Type: Oral

Focused ultrasound therapy combined with pembrolizumab in metastatic breast cancer

Patrick Dillon, Bethany Horton, Timothy Bullock, Christiana Brenin, David Brenin

University of Virginia, Charlottesville, Virginia, United States

Background: Focused ultrasound (FUS) perturbs the microenvironment of a tumor by mechanical, thermal and vascular permeability effects. Carefully controlled FUS can induce apoptotic cell death and/or sub-lethal cellular damage as means of immune stimulation. FUS induces heat shock proteins, cytokine release and cellular mediated mechanisms resulting in T cell activation and recognition of tumor antigens. FUS has been demonstrated to be an effective method for inducing tumor antigen exposure and presentation to dendritic cells, thus acting as an auto-vaccine. Pembrolizumab (PBZ) is a PD-1 targeted antibody used in the treatment of multiple solid tumors to augment T cell activation. It is hypothesized that the combination of these two modalities will result in T cell infiltration into breast tumors as well as systemic immune responses.

Methods: In this pilot study, PBZ therapy is combined with FUS to assess for immune stimulation and antitumor effects at local ablation sites, distant non-treated sites and in the blood. Biopsy before, after and 10 weeks post-FUS will examine the tissue in the peripheral zone of ablation, central ablation zone, and distant metastatic sites for CD8 and CD4 T cells, MDSC's, T-regulatory cells and cytokine responses. Twelve patients will be randomized to receive either PBZ 14 days before or 7 days after a single time FUS partial tumor ablation on day 15. FUS will be delivered by Theraclion Echopulse device at 45W power, with a skin cooling device. Biopsies will be on days 1, 22 and 64 and tumor imaging will be every 12 weeks after baseline. Patients must have metastatic or unresectable breast cancer, adequate organ function, and prior therapy in the metastatic setting. They must also have a tumor in the breast or axilla amenable to FUS and biopsy.

Results: Five patients have been treated to date. The median age is 62. All patients had metastatic breast cancer and accessible primary tumors in breast or axilla. Ultrasound ablations of 30-42% of each lesion was accomplished at 45W power using checkerboard patterns. Increases in CD8+, FOXP3- tumor cells were observed in the periablation zones. Increased numbers of PD-L1+ cells were also observed in peri-ablation zones. Clinical responses will be measured by RECIST criteria. The treatments were reasonably well tolerated and no auto-immune toxicity is observed to date. The trial is ongoing.

Conclusions: To date, focused ultrasound ablation in combination with pembrolizumab is safe and results in observable changes to the immune microenvironment in patients with metastatic breast cancer.

WH-2

Wednesday

24 October 2018

Topic: Breast
Presentation Type: Oral

Ultrasound guided high intensity focused ultrasound ablation of breast fibroadenoma: Final results of the first United States study

David Brenin[1], Jonathan Nguyen[1], George Stukenborg[2], Carrie Rochman[1]

[1]University of Virginia Medical Center, Charlottesville, Virginia, United States
[2]University of Virginia School of Medicine, Charlottesville, Virginia, United States

Background: Fibroadenoma is a common benign breast mass that can cause pain, a palpable lump, and anxiety. Current management includes observation or surgical excision. This study evaluated the safety and feasibility of Ultrasound guided High Intensity Focused Ultrasound (USgHIFU) delivered by the Echopulse device (Theraclion, Paris) for treatment of breast fibroadenomas. Patient safety, cosmetic outcome, tumor response, and patient experience were assessed.

Methods: Twenty women with a palpable, core biopsy confirmed, breast fibroadenoma were enrolled in a single arm IRB and FDA approved clinical trial. Patients underwent treatment utilizing the Echopulse device (Theraclion, France). All patients had tumors with a minimum diameter >1 cm with volume between 0.3cc and 10cc. Volume calculation formula = length (mm) x width (mm) x height (mm) x π / (6 x 1000) in cc. Optimal energy delivered per sonication was established by determining the minimal setting found to produce a hyperechoic mark observed on real-time B-mode image. Patient treatment experience, toxicity, cosmesis, and change in tumor size on both physical examination (palpability) and ultrasound measurement were obtained before and immediately after treatment, and at 3, 6, and 12 months.

Results: Twenty of 20 patients successfully completed therapy. Pre-treatment mean tumor volume was 1.8cc (SD = 1.23, Range 0.57–5.7). Mean patient age was 35.3 years. Forty percent of patients were Caucasian, 40% Latino, and 20% were Black. Fifty percent reported a painful mass prior to treatment. Mean power/sonication = 38.0 (28.2 – 47.0) watts. Mean number of sites treated/patient = 34.3 (8-103). Median duration of treatment was 39.5 minutes (95% CI, 34.5 – 53.0). Hyperechoic marks were observed in 15/20 (75%) of patients. All adverse events were grade 1 or 2; no burns, damage to adjacent structures, or other toxicities were observed. The most common toxicity was mild pain, reported by 15/20 (75%) of patients during treatment, and 14/20 (60%) at day 7. Mean pain score during treatment was 16 on a scale from 0 to 100 (100 = worst pain). Mean pain score at day 7 was 12.2. Patient satisfaction was 4.4 on a scale of 1-5 (5 = most satisfied), likelihood of recommending it to a friend or family member was 4.7 (5 = strongly agree). Two patients were lost to follow-up at 12 months.

At 12 months follow-up, mean % reduction in volume of the fibroadenoma was 65%, (98% to 25%, $p < 0.0001$). A mass was no longer palpable in 80% of patients, no patients reported pain, and cosmesis was rated by both patients and physicians as excellent in 100% of subjects.

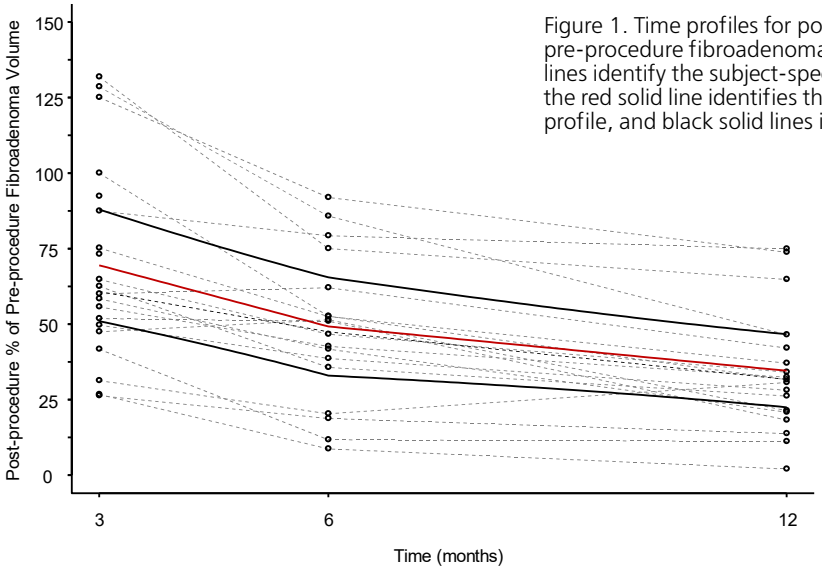

Figure 1. Time profiles for post-procedure % of pre-procedure fibroadenoma volume. Hatched lines identify the subject-specific time profiles, and the red solid line identifies the predicted mean time profile, and black solid lines identify 95% CI

Conclusions: USgHIFU is an effective, safe, and well tolerated treatment for breast fibroadenomas resulting in minimal toxicity. Based on the above results, a larger multi-center clinical trial is currently open to accrual in both the United States and Europe.

Acknowledgements: Research funding provided by Theraclion

Figure 2. Relationship between assessment time and the predicted frequency of reported palpable mass. The solid red line identifies the predicted frequency as a function of time. Vertical black lines identify 95% CI, and blue dots are the observed frequency.

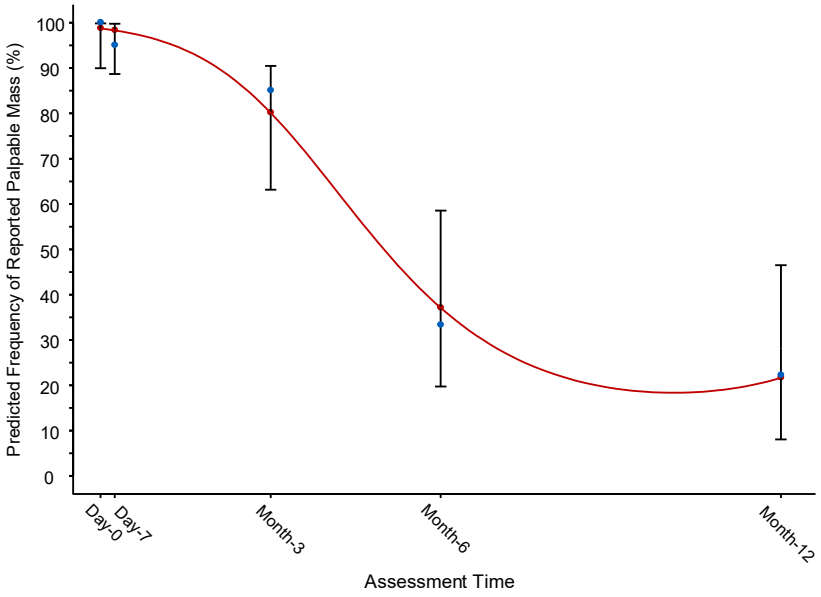

Figure 3. Relationship between pain assessment and the predicted frequency of pain (%). Solid red line is the predicted frequency of pain as a function of time. Vertical black lines are 95% CI, and blue dots were the observed frequency of pain.

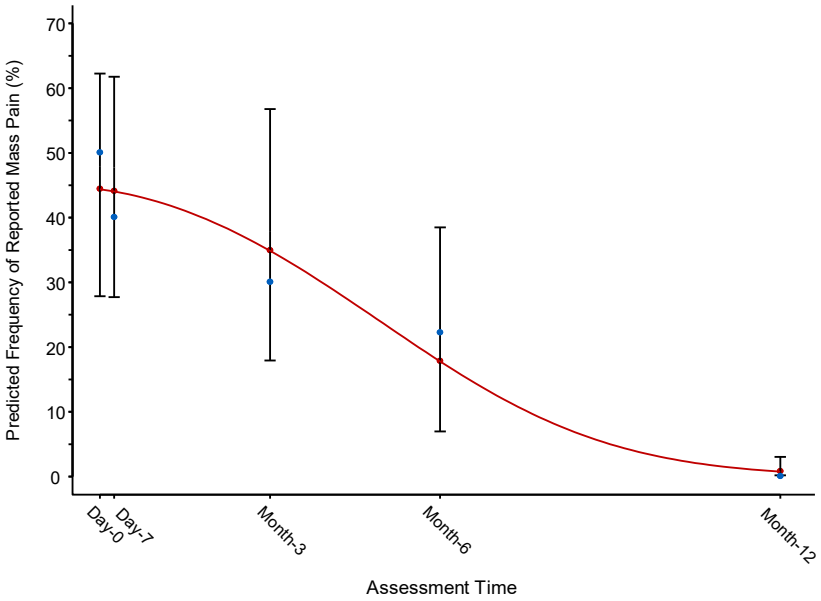

WH-3

Wednesday

24 October 2018

Topic: Breast
Presentation Type: Oral

A feasibility study of *in vivo* human breast tumor detection and differentiation using Harmonic Motion Imaging (HMI)

Niloufar Saharkhiz[1], Yang Han[1], Alireza Nabavizadehrafsanjani[1], Richard Ha[2], Elisa Konofagou[2]

[1]Columbia University, New York, New York, United States
[2]Columbia University Medical Center, New York, New York, United States

Background: Breast cancer, the second most common cancer in American women, is associated with alterations in the mechanical properties of breast tissues. Several methods have been proposed for breast cancer imaging with high sensitivity. However, false-positive cases resulting from low specificity have led to unnecessary biopsies, in particular in women with dense breasts. Harmonic Motion Imaging (HMI) is a non-invasive ultrasound-based elasticity imaging technique that assesses viscoelastic properties of the underlying tissue based on displacements induced by a periodic acoustic radiation force. The capability of HMI in mapping, characterization and High Intensity Focused Ultrasound (HIFU) ablation monitoring of breast masses in post-surgical human specimens has been previously shown. In this study, we demonstrate clinical application of HMI for the first time. The objective is to assess the potential of HMI as a complementary tool for *in vivo* human breast tumor detection and differentiation.

Methods: The HMI system consisted of two confocally aligned transducers: a 4-MHz focused ultrasound (FUS) transducer to generate the 25 Hz oscillating acoustic force, and a 7.8-MHz phased array imaging probe to track the induced tissue displacements. A 1-D point-by-point raster scan of the HMI setup with a step size of 2 mm was performed automatically with a robotic arm controlled by a PC workstation. The scan area location was selected based on the B-mode image (Figure 1) to include both the tumor area and normal peripheral tissue. The sonication time was 0.08 seconds at each point during which 80 RF frames were acquired. The data was transferred to the host workstation at a frame rate of 1 kHz. The axial displacements were estimated offline from acquired RF lines using 1-D cross correlation with a 0.98 mm window and 95% overlap.

Results: HMI displacement maps of 15×50 mm^2 were reconstructed from peak-to-peak displacements amplitude. An example of the overlaid displacement map on B-mode image taken from a 53-year-old female patient diagnosed with fat necrosis is shown in Figure 2. A 5-mm diameter circular region of interest was used to average the displacements, resulting in 1) A mean of 2.38±0.46 μm within the tumor area with a maximum of 3.16 μm, and 2) A mean of 3.70±1.09 μm within the normal tissue with a maximum of 6.63 μm. The size of the mass estimated from HMI displacements was correlated with the B-mode image and the mass was found to be twice stiffer than the surrounding tissue, based on the maximum HMI displacement.

Conclusions: Clinical application of HMI was demonstrated for breast tumor detection and characterization. As a non-ionizing elasticity imaging technique, HMI estimates the relative stiffness of the underlying tissue precisely due to the induced localized displacements. Since the technique benefits from FUS to generate the radiation force, it could probe both stiff and deep seeded breast masses in humans. Ongoing clinical studies focus on the optimization of the current setup for real-time acquisition , potentially distinguishing masses from normal tissues and characterizing different tumor types based on HMI displacements, as well as HIFU ablation application.

Figure 1. B-mode image of a breast mass in patient

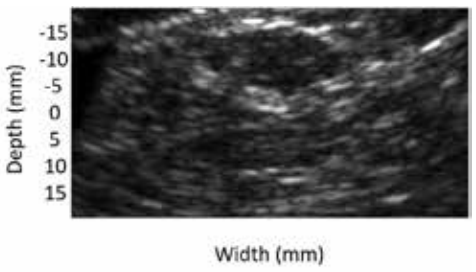

Figure 2. Overlaid image (B-mode + HMI displacement map) of the mass where blue shows low displacements and red shows high displacements

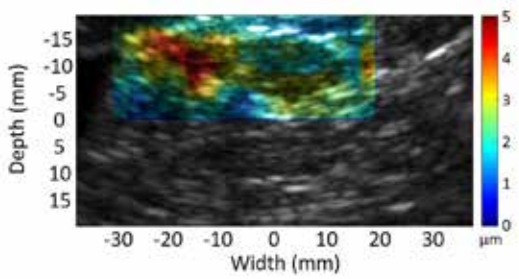

WH-4

Wednesday

24 October 2018

Topic: Gynecological
Presentation Type: Oral

Decrement of screening and treatment failure rates by application of manipulation techniques in our patients

Inez Verpalen[1], Jolien de Boer[1], Joke Schutte[1], Erwin de Boer[1], Rolf van den Hoed[1], Miranda Van 't Veer-ten Kate[1], Martijn Boomsma[2]

[1]Isala, Zwolle, Netherlands
[2]Stichting isala klinieken, Zwolle, Netherlands

Background: Magnetic Resonance-High Intensity Focused Ultrasound (MR-HIFU) therapy is a complete noninvasive treatment of symptomatic uterine fibroids. However, the clinical applicability is often limited due to the limit in focal depth of the MR-HIFU system or interposition of small bowel loops in the sonication path. To decrease the screening and treatment failure rates, manipulation techniques are widely used.[1,2,3,4] The aim of this retrospective study was to describe our manipulation protocol for MR-HIFU treatment of uterine fibroids.

Methods: From June 2016 to June 2018, 145 women underwent a screening MRI examination of which 54 women were consecutively treated with MR-HIFU at our institution. We obtained informed consent from all patients. Procedures were performed on an outpatient basis under conscious sedation. Bowel preparation was done using a fast-acting micro-enema. Patients received oral premedication. A Foley catheter and intravenous line were inserted. Treatments were conducted using a clinical HIFU system (Sonalleve V1, Profound Medical Inc., Toronto, Canada) integrated with a 1.5-T MRI system (Achieva; Philips Healthcare, Best, the Netherlands). We reassessed the location of the fibroid on T2W images. If necessary, we followed our manipulation protocol which included three different techniques:

Step 1 — The BRB maneuver; sequential applications of urinary bladder filling, rectal filling and urinary bladder emptying.2,4 Compared to this classical BRB maneuver, we filled the rectum with multiple syringes (60 mL) using a solution of ultrasound gel (30 mL), saline solution (30 mL) and 1 sachet psyllium fiber (3,4 gram). The amount of rectal filling ranged from 240-480 mL, based on patient tolerance. This BRB manipulation moved the fibroid anteriorly (figure 1) or displaced bowel loops (figure 2). If step 1 failed to succeed, we moved on to step 2 or 3 depending on the position of the uterus.

Step 2 — Uterus axial or retroverted; we manipulated the uterus manually into anteflexion. Afterwards, we fixated the position of the uterus with an speculum (figure 3).

Step 3 — Anteverted uterus; patients were positioned into Trendelenburg to move the small bowel out of the pelvis. Additionally, abdominal massage was performed on both sides of the lower abdomen with movements towards the upper abdomen (figure 4).

Results: The first 20 treatments we only used the classical BRB manipulation technique. Our overall screening failure rate was 53% (47/88), of which 18% (16/88) was due to a retroverted uterus or the distance between fibroid and abdominal wall. Although no bowel interposition was observed on the screening MRI, still 20% (4/20) of the treatments failed due to the interposition of bowel loops, suggesting a reversible situation. Therefore, we implemented new manipulation techniques and our screening failure rate decreased from 53% to 28% (16/57). Our treatment failure rate due to the interposition of bowel loops decreased from 20% to 0% (0/34). Although this could be partially explained by a learning curve.[5] There were no complications or thermal injuries to the bowel or uterus from the manipulation.

Conclusions: We implemented a manipulation protocol using three different techniques which has led to a decrease in our screening and treatment failure rates.

References

1. Zhang L, et al. Feasibility of Magnetic Resonance Imaging-Guided High Intensity Focused Ultrasound Therapy for Ablating Uterine Fibroids in Patients with Bowel Lies Anterior to Uterus. *European Journal of Radiology*. 2010;73(2):96–403. doi:10.1016/j.ejrad.2008.11.002.
2. Park MJ, et al. Technique to Displace Bowel Loops in MRI-Guided High-Intensity Focused Ultrasound Ablation of Fibroids in the Anteverted or Anteflexed Uterus. *American Journal of Roentgenology*. 2013;201(5):61–4. doi:10.2214/AJR.12.10081.

3. Pulanic TK, et al. Vaginal Pessary for Uterine Repositioning during High-Intensity Focused Ultrasound Ablation of Uterine Leiomyomas. *Gynecologic and Obstetric Investigation*. 2016;81(3):285–8. doi:10.1159/000441782.
4. Kim YS, et al. Magnetic Resonance Imaging-Guided High-Intensity Focused Ultrasound Ablation of Uterine Fibroids: Effect of Bowel Interposition on Procedure Feasibility and a Unique Bowel Displacement Technique. *Plos One*. 2016;11(5):0155670. doi:10.1371/journal.pone.0155670.
5. Okada A, et al. Non-Invasive Magnetic Resonance-Guided Focused Ultrasound Treatment of Uterine Fibroids in a Large Japanese Population: Impact of the Learning Curve on Patient Outcome. *Ultrasound in Obstetrics and Gynecology*. 2009;34(5):579–583. doi:10.1002/uog.7454.

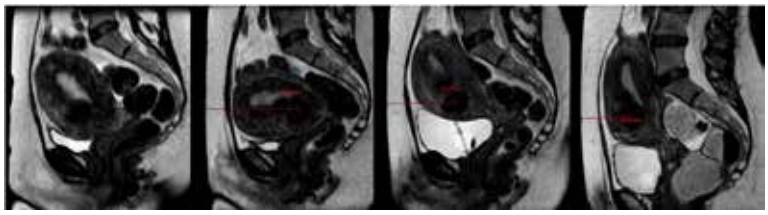

Figure 1. The first image on the left is the screening MRI. The three images on the right are from treatment day and the show the BRB manipulation technique, in this case used to shorten the distance between the fibroid and anterior abdominal wall.

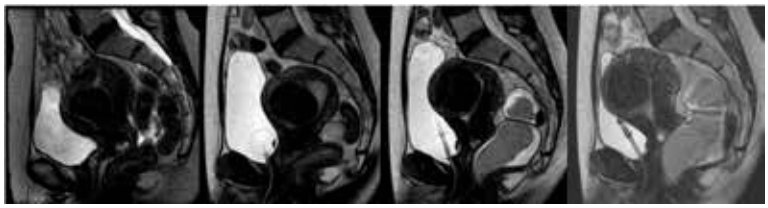

Figure 2. Another example of the BRB manipulation technique, in this case used to displace small bowel loops and to move the fibroid more anteriorly. The first image on the left is the screening MRI.

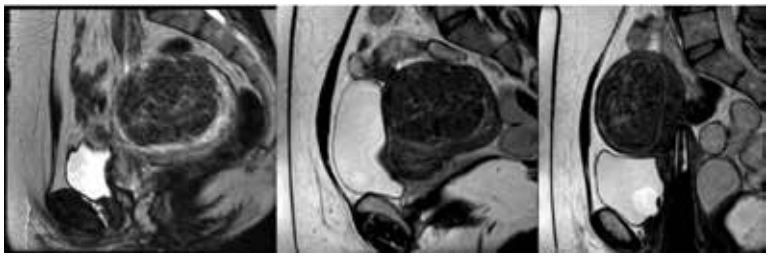

Figure 3. The left image shows the screening MRI of an retroverted uterus. BRB manipulation is not sufficient (middle image). Thus, we manually manipulated the uterus into anteversion. Afterwards, we fixate the uterus with a speculum (right image).

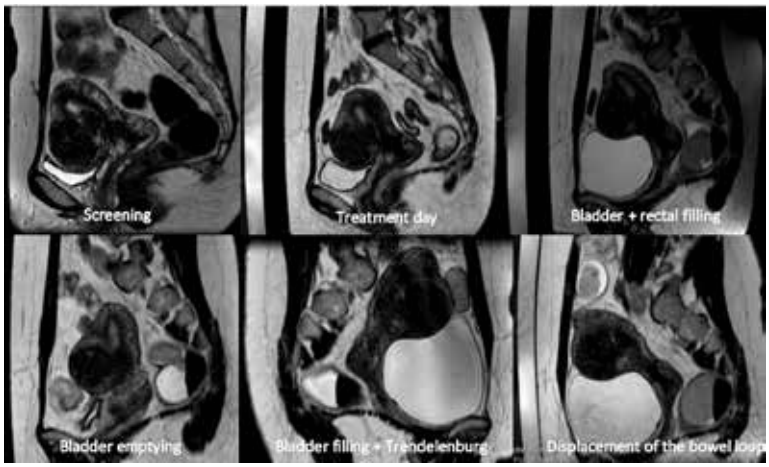

Figure 4. Trendelenburg maneuver with bowel massage. The BRB maneuver failed, so after bladder filling we placed the patient in supine position with a pillow below the hips. Bowel massage was performed and the patient was moved back into prone position.

WH-5

Wednesday

24 October 2018

Topic: Gynecological
Presentation Type: Oral

The Focused Ultrasound Myoma Outcome Study (FUMOS): Long-term results of MR-HIFU treatment

Inez Verpalen[1], Jolien de Boer[1], Marlot Linstra[2], Charles Mougenot[3], Chrit Moonen[3], Manon Braat[3], Martijn Boomsma[4]

[1]Isala, Zwolle, Netherlands
[2]University of Utrecht, Utrecht, Netherlands
[3]University Medical Center Utrecht, Utrecht, Netherlands
[4]Stichting isala klinieken, Zwolle, Netherlands

Background: Since 2010 fibroids have been treated with Magnetic Resonance-High Intensity Focused Ultrasound (MR-HIFU) at the UMC Utrecht within a research setting1. To date, there is no reimbursement, because insurance companies are doubting long-term efficacy. Early clinical studies reported high retreatment rates, although those treatment protocols were limited to partially ablating fibroids.[1,2] Long-term outcome data after MR-HIFU treatments aiming for complete ablation is scarce.[3] Therefore, the Focused Ultrasound Myoma Outcome Study (FUMOS) evaluates long-term outcomes of MR-HIFU treatments without restrictive guidelines. This abstract presents preliminary results and the purpose of this sub-analysis was to assess our primary outcome, the reintervention rate.

Methods: This is a retrospective, single-center study of 140 patients with symptomatic uterine fibroids who underwent MR-HIFU therapy. Patients will be requested to complete a questionnaire that includes symptom severity, quality of life, pregnancy outcomes, patient satisfaction, and requirement for additional treatments.

The presented preliminary results are based on a sample of 28 patients who have been continuously monitored by a gynecologist in the UMC Utrecht. The other 80% patients of the study population were referrals from other hospitals. We used medical records for data-collection. Our main study endpoint was the reintervention rate, stratified by follow-up duration. Another study parameter was the Non-Perfused Volume (NPV) ratio directly after treatment. The NPV was calculated by volumetric measurements in IntelliSpace Portal Software (Philips). Furthermore, reintervention rate was stratified by NPV ratio and duration of follow-up.

Results: The average NPV ratio of the sample of 28 patients was 56% and the average NPV of the entire study population is 57%, indicating a representative study sample. The 28 patients had an average follow-up of 46 ±30 months. A total of four reinterventions were reported, three abdominal uterine extirpations and one embolization. The total incidence of additional treatments was 14.3% (figure 1). Comparison of two subgroups NPV<50% *versus* NPV>50% resulted in reintervention rates of 30% and 5.6%. This finding supports the hypothesis that NPV percentage is a predictor of treatment success.[4,5] Additionally, it is suggested that the reintervention rate increases with time. Interestingly, in our sample all four reinterventions were all performed within the first year. However, stratification by follow-up duration showed a substantial effect of time on the reintervention rate. No reinterventions were reported in the group with a follow-up shorter than 3 years. In the group with a follow-up longer than 3 years (average follow-up of 70 ±14 months) the reintervention rate increases to 25% (figure 2). Stratification by NPV% (figure 3), showed a decreased reintervention rate of 11.1% (1/9) in the subgroup NPV>50%. Importantly, in retrospect this patient was not an ideal candidate for MR-HIFU due to multiple fibroids.

Conclusions: These preliminary results support our hypothesis that long-term reintervention rates after MR-HIFU therapy are comparable with other reimbursed uterine-sparing treatment options. Patients with NPV ratio <50% were more likely to require additional treatment. Therefore, patient screening remains important and physicians should always aim for complete ablation.

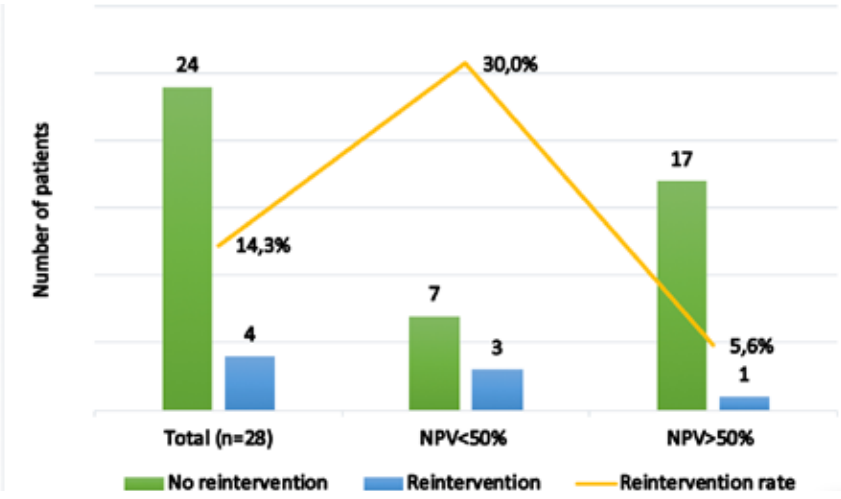

Figure 1: the total numbers of reinterventions in the study sample, including comparison of two subgroups NPV<50% *versus* NPV>50%.

References

1. Ikink ME, Voogt MJ, Verkooijen HM, Lohle PNM, Schweitzer KJ, Franx A, et al. Mid-term clinical efficacy of a volumetric magnetic resonance-guided high-intensity focused ultrasound technique for treatment of symptomatic uterine fibroids. *Eur Radiol.* 2013;23(11):3054-3061.
2. Froeling V, Meckelburg K, Schreiter NF, Scheurig-Muenkler C, Kamp J, Maurer MH, et al. Outcome of uterine artery embolization *versus* MR-guided high-intensity focused ultrasound treatment for uterine fibroids: Long-term results. *Eur J Radiol.* 2013;82(12):2265-2269.
3. Kim HSM, Baik JM, Pham LDM, Jacobs MAP. MR-guided High-intensity Focused Ultrasound Treatment for Symptomatic Uterine Leiomyomata: Long-term Outcomes. *Acad Radiol.* 2011;18(8):970-976.
4. Gorny KRP, Borah BJP, Brown DLM, Woodrum DAM, PhD, Stewart EAM, Hesley GKM. Incidence of Additional Treatments in Women Treated with MR-Guided Focused US for Symptomatic Uterine Fibroids: Review of 138 Patients with an Average Follow-up of 2.8 Years. *Journal of Vascular and Interventional Radiology.* 2014;25(10):1506-1512.
5. LeBlang SD, Hoctor K, Steinberg FL. Leiomyoma shrinkage after MRI-guided focused ultrasound treatment: report of 80 patients. *American Journal of Roentgenology.* 2010;194(1):274-80.
6. Dobrotwir Andrew A. Clinical 24 month experience of the first MRgFUS unit for treatment of uterine fibroids in Australia. *Journal of Medical Imaging and Radiation Oncology.* 2012 -8;56(4):409-16.

Figure 2: the effect of time on the reinterventions, the reintervention rate increases from 0% to 25%. No reintervention in the 12 patients with a follow-up <3 years. Four reinterventions were reported in the 16 patients with a follow-up >3 years.

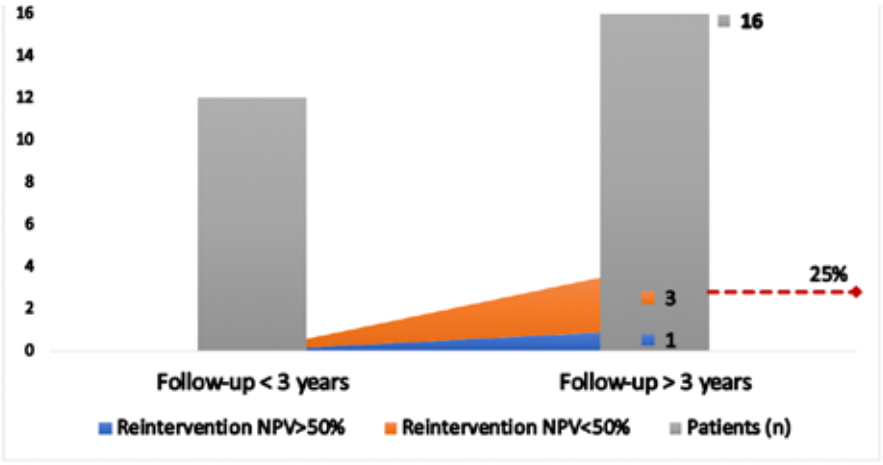

Figure 2: the effect of time on the reinterventions, the reintervention rate increases from 0% to 25%. No reintervention in the 12 patients with a follow-up <3 years. Four reinterventions were reported in the 16 patients with a follow-up >3 years.

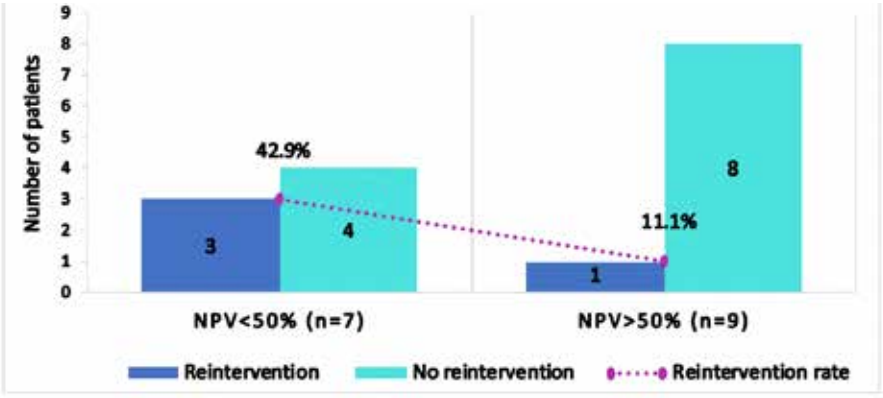

WH-6

Wednesday

24 October 2018

Topic: Gynecological
Presentation Type: Oral

Efficacy of MR guided focused ultrasound surgery in treatment of uterine fibroids — a study of 1221 fibroids, Indian experience

Shrinivas Desai, Ritu Kashikar

Jaslok Hospital and Research Center, Mumbai, India

Background: The aim of this study was:

- To evaluate the role of Magnetic Resonance guided Focussed Ultrasound Surgery (MRgFUS) in management of Uterine Fibroids in terms of clinical improvement in symptoms as suggested by decrease in Symptom Severity Score (SSS) and reduction in Non perfused volume
- To access early and late adverse effects of treatment
- To evaluate the role of MRgFUS in management of Uterine Fibroids in terms of clinical improvement in symptoms as suggested by decrease in Symptom Severity Score (SSS) and reduction in Non perfused volume ,and to access early and late adverse effects of treatment.

Methods: 1221 symptomatic fibroids in 722 Indian women were selected.Patients with uterine fibroids showing enhancement on screening MRI were recruited for the study.Patients with non enhancing /calcified fibroids were excluded.Pretreatment raw and transformed symptom severity score was was calculated.Treatment was performed on a 1.5-T whole-body system (Signa; GE Healthcare) in the ExAblate 2000 (INSIGHTEC) device. During treatment the patient lies prone and a gel pad couples the patients abdomen to a phased array coil in a sealed water bath. The system generates a high intensity acoustic beam that is focused on target,leading to tissue necrosis.Post treatment results were evaluated by assessing non perfused volume on contrast enhanced scans. All patients were followed up at 6 months with post contrast MR pelvis Symptom severity score and Non perfused volume was calculated ,delayed adverse events were enquired.

Results: The reduction in both mean raw and transformed SSS before and 6 months post treatment was statistically significant (p=0.0001). The mean volume of fibroids before treatment was 145.76 cc with SD 81.22 cc .At 6 months follow up there was statistically significant reduction in the volume of fibroids with mean being 105.75 cc and SD 59.95 cc (p value 0.0001).The Non Perfused Volume (NPV) achieved after the procedure was 88.21% with a SD of 7.60%. And this has transformed into greater reduction of fibroid volume at 6 months.65%patients had no adverse effects following treatment .Leg pain was seen in 15% patients immediately after treatment and 2% continued having mild leg pain after 6 months .2 patients (0.2%)had intestinal perforation.

Conclusions: MRgFUS provides statistically significant reduction in symptom severity index and fibroid volumes at 6 month follow up The adverse effect profile is acceptable with major events occurring in a very small percentage of patients.

MRgFUS is a good ,safe, non invasive replacement to conventional invasive therapies like hysterectomy and myomectomy for uterine fibroids with comparable success rates and lower side effect profile.

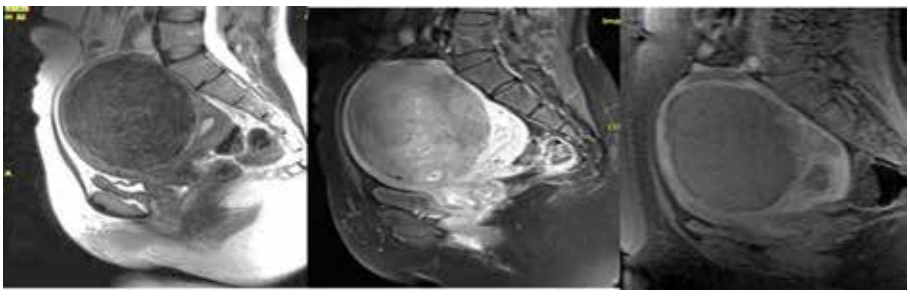

Figure 1. Pretreatment T2W1 and postcontrast T1W1 images showing enhancing viable fibroid and post treatment post contrast image showing non enhancing non viable tumoura

WH-7

Wednesday

24 October 2018

Topic: Gynecological
Presentation Type: Oral

Efficacy of MR guided focused ultrasound surgery (MRgFUS) in adenomyosis — a study of 115 symptomatic adenomyosis in 94 Indian patients

Shrinivas Desai, Ritu Kashikar

Jaslok Hospital and Research Center, Mumbai, India

Background: To assess the efficacy of MR guided focused ultrasound surgery (MRGFUS) in treating adenomyosis by evaluation of non-perfused volumes (NPV) and symptom severity score (SSS).

Methods: 94 Indian women with 115 significant symptomatic adenomyosis (SSS > 21) were selected after approval from ethics committee.Adenomyosis with definable treatable areas(>2cm) were included.Patients with SSS <21 and non definable treatable areas were excluded.Pre treatment raw and transformed SSS were calculated.Treatment was performed on a 1.5-T whole-body system (Signa; GE Healthcare) in the ExAblate 2000 (INSIGHTEC) device.During treatment the patient lies prone and a gel pad couples the patients abdomen to a phased array coil in a sealed water bath in the treatment table. The system generates a high intensity acoustic beam that is focused on target ,leading to tissue necrosis .Post treatment results were evaluated by assessing non perfused areas on contrast enhanced scans. Patients were called for follow up at 6 months .SSS was enquired and MRI pelvis with contrast was performed to calculate the non-perfused volume.

Results: 74% of our patients had significant reduction in symptom severity score following treatment.The reduction in mean raw and transformed SSS pre and 6 months post treatment was statistically significant .The mean volume of adenomyosis prior to treatment was 139.47± 102.497 SD, while non perfused volumes 6 months after treatment were 71.26 ± 51.15 SD.This difference was found to be statically significant (0.000134). We used Non-perfused Volume (NPV) and its percentage of the total adenomyotic volume before the treatment (NPV%) and correlated these with the Reduction in the Symptom Severity Score at 6 months and found the correlation strong and positively linear (Pearsons correlation of .644 and .928 with NPV and NPV %).

Conclusions: MRgFUS is able to achieve NPV values that will result in clinically significant reduction in symptoms. The reduction in the SSS and percentage of adenomyosis reduction follows the NPV very closely and linearly, which means that achieving greater NPV will essentially result in significant symptom reduction.

MRgFUS is a non invasive ,safe and effective modality for the treatment of Adenomyosis providing good symptomatic relief and long term results

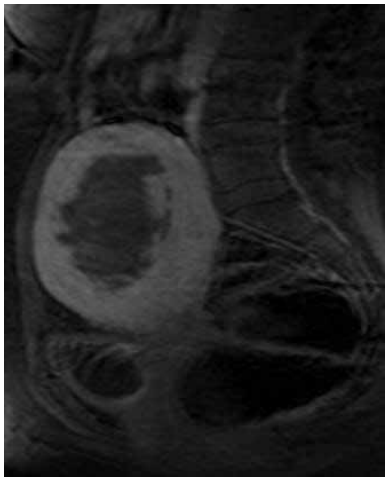

Figure 1. Pretraetment T2W1 image showing anterior wall adenomyosis

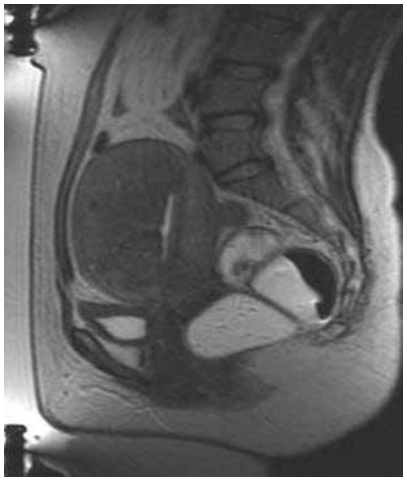

Figure 2. Post treatment T1W1 image showing absence of enhancement indicating non viable lesion

WH-9

Wednesday

24 October 2018

Topic: Gynecological
Presentation Type: Oral

Outcome of MRgFUS treatments for uterine fibroids in a private practice setting

Daniel Kushner[1], Jude Alrahm Jaraki[1], Fred Steinberg[2], Suzanne LeBlang[2]

[1]Florida Atlantic University Charles E. Schmidt College of Medicine, Boca Raton, Florida, United States
[2]University MRI & Diagnostic Imaging Centers, Boca Raton, Florida, United States

Background: The FDA relaxed the guidelines to perform MRgFUS in women who wish to preserve and enhance fertility in 2015. Since then, our practice has treated younger women. The objective of this study is to evaluate the efficacy of MRgFUS treatment in this new patient population.

Methods: Of the 90 patients that received MRgFUS ablation of uterine fibroids from May 2016 to December 2017, 68 were interviewed by phone while 22 patients were unavailable for follow up. Patients were asked if their symptoms improved, stayed the same, or worsened, as well as if they underwent alternative procedures. Patient records were then reviewed and non-perfused volume (NPV), number of fibroids, average fibroid size, and age at time of treatment were recorded. A multinomial logistic regression was created to determine the relationship among changes in symptoms and independent variables including NPV, average fibroid size, number of fibroids, and age at treatment.

Results: There were 10 patients under 35 years of age, 37 patients between 35-45 years, and 21 who were over 45 years. Overall, 36 (52.9%) of the 68 patients reported an improvement of symptoms, 17 (25%) reported no change in severity, and 15 (22.1%) reported worsening of symptoms. Of the patients under 35, 4 improved, 4 had no change, and 2 worsened. Of the patients 35-45 years, 21 improved, 10 had no change, and 6 worsened. Of the patients over 45, 11 improved, 3 had no change, and 7 worsened. The average age of patients with improved symptoms was 41.3 years, no change in symptoms 40.9 years, and worse symptoms 42.1 years. The average treated fibroid volume was 172.4 cc. There was a total of 4 patients with a NPV <50%, 17 patients with a NPV of 50-70%, and 47 patients with a NPV of >70%. 59.6% of patients with a NPV >70% reported improvement of symptoms, while 75% of patients with a NPV <50% reported worsening of symptoms. The patients who experienced worsening symptoms with a NPV <50% had an average of 3.7 fibroids compared to the average of 2.3 fibroids in the total study population. 10 of the patients who reported worsening of their symptoms and 1 patient with no change in symptoms underwent alternative treatment (5 hysterectomies, 5 myomectomies, and 1 UAE). There was a weakly positive correlation between NPV and improved outcome ($r = 0.365$), as well as between number of fibroids and improved outcome ($r = 0.017$).

Conclusions: In this small patient population of varying ages, 52.9% of patients MRgFUS reported an overall improvement of their symptoms. A majority (75%) of patients with a post-procedure NPV <50% experienced worsening of symptoms but did not have a significantly higher number of fibroids compared to the other groups. Of the patients with worsening symptoms, 60% went on to have an alternative procedure. Approximately 20% of patients under 35, 17% between 35 and 45, and 33% over 45 had worsening symptoms.

WH-10

Wednesday

24 October 2018

Topic: Gynecological
Presentation Type: Oral

Prospective clinical trial for uterine adenomyosis using portable ultrasound-guided high intensity focused ultrasound

Jae Young Lee[1], Hyun Hoon Chung[1], Maria Lee[1], Soo Yeon Kang[1], Keonho Son[2]

[1]Seoul National University Hospital, Seoul, Republic of Korea
[2]Alpinion Medical Systems Co., Ltd, Seoul, Republic of Korea

In accordance with author request, this abstract is not available for publication.

WH-11

Wednesday

24 October 2018

Topic: Gynecological
Presentation Type: Oral

Transrectal high-intensity focused ultrasound as focal therapy for rectal endometriosis

Gil Dubernard[1], Charles- André Philip[2], Albert Gelet[3], Nicolas Guillen[4], Françoise Chavrier[3], Hélène Tonoli[4], Jean-Yves Chapelon[3], Cyril Lafon[5]

[1]Hospices Civils de Lyon - LabTAU, Lyon, France
[2]Croix-Rousse University hospital, Lyon, France
[3]LabTAU, Inserm, Lyon, France
[4]EDAP-TMS, Vaulx-en-Velin, France
[5]Inserm, Lyon, France

Background: Deep invasive endometriosis (DIE) includes lesions of the rectosigmoid. Theses lesions are associated with painful symptoms that can alter quality of life. High Intensity Focused Ultrasound (HIFU) is a non-invasive ablative procedure using a high-intensity ultrasound probe to induce tissue devitalization using acoustic cavitation and thermal ablation. FocalOne is a transrectal HIFU device, which is validated to treat prostatic cancer. The aim of the study was to assess the feasibility, safety and clinical efficacy of FocalOne in patients presenting posterior DIE with rectal involvement.

Methods: We are conducting a Phase I, non-controlled, prospective monocentric clinical study. In the first part 11 patients have been included. The inclusion criteria were patients older than 25 years old, without project of pregnancy in the next 3 months, who presented a single lesion with rectal invasion and after hormonal therapy failure. All lesions were assessed using a sonography, pelvic MRI and a transrectal sonography. The probe was inserted inside the rectum under spinal anesthesia. Real-time guided ultrasonography was used to determine the location of the endometriotic nodule. Succession of HIFU exposure was then used to treat maximum lesion volume, excluding a security margin of 3mm with the digestive mucosae to prevent risk of fistulae. Patients filled-out questionnaires on gynecological and intestinal symptoms and on quality of life before treatment and at 1 and 6 months after HIFU procedure. We are currently performing the second part of thestudy including 12 patients with endometriotic lesions located exclusively in the lower and mid-rectum while following the same protocol but the MRI will be performed at six months.

Results: The first study was carried-out between September 2015 and January 2018. All lesions were visualized with sonographic probe. Only 9 patients complied with security conditions allowing treatment. The "feasibility rate" was 81.8%. The treatment of the entire lesion was feasible for 3 patients, while for the remaining 6 patients, approximately 50% of the lesion was treated. The median duration of the procedure was 56 minutes (± 22, [25-91]). At 6 months We observed a significant improvement for dysmenorrhea (-4.0, p=0.008), spasms (-4.6, p=0.02), constipation (-3.2, p=0.02), false urges to defecate (-2.7, p=0.04), posterior irradiation pain (-4.4, , p=0.01) and asthenia (-4.0, p=0.01).There was also a significant improvement of the MOS-SF36 with an increase of both Physical Composite Score of 22.7% (53.1 *vs.* 43.2, +9.9, p=0.015) and Mental Composite Score of 45.8% (50.0 *vs.* 34.3, +15.7, p=0.015). No significant complications occurred during and after the procedure. All patients left hospital the day after the procedure. We will present the early follow-up results of the second part of the study, which started in May 2018, including the assessment of the treatment volume and the early postoperative complications.

Conclusions: HIFU therapy for posterior DIE can be considered as feasible and safe. It could be an interesting alternative to surgery for the treatment of posterior DIE. Further studies are required to confirm these preliminary results and also to optimize the selective criteria enabling the treatment of rectal lesions with Focal One device. This is the objective of the second part of the study.

Acknowledgements: Work supported by EDAP TMS.

WH-12

Wednesday

24 October 2018

Topic: Gynecological
Presentation Type: Oral

Artifact from myomectomy/C-section scars on MRI images — What does this mean for MRgFUS candidacy for uterine fibroids?

Vikash Sinha[1], Shahil Mehta[2], Georgios Kalantzis[3], Fred Steinberg[4], Suzanne LeBlang[4]

[1]FAU College of Medicine, Boca Raton, Florida, United States
[2]University of Miami Miller School of Medicine, Boca Raton, Florida, United States
[3]Florida Atlantic University, Boca Raton, Florida, United States
[4]University MRI & Diagnostic Imaging Centers, Boca Raton, Florida, United States

Background: MRgFUS is currently being used for the non-surgical treatment of uterine fibroids providing a non-invasive, effective treatment to decrease symptoms and preserve fertility without undergoing a traditional myomectomy. One of the contraindications for MRgFUS of uterine fibroids includes MRI artifacts along the beam path. A previous published report describes post op MRI scans in patients s/p myomectomy show healing of the uterus and endometrial cavity at around 12 weeks but often artifacts of unknown origin persist for many years afterwards. While potential problems arising from superficial scar artifacts can be largely circumvented through scar patching, positional changes, or bladder and bowel distention, deeper artifacts can be difficult to bypass. Consequently, many patients with these deep artifacts are excluded from treatment. Interestingly, the surgical reports from such patients describe the use of resorbable sutures and no use of metallic clips, thus the etiology of the MRI artifacts is unclear. To date, there are no published studies on whether artifacts from prior uterine surgeries have a significant effect on MRgFUS treatment efficacy or safety.

Methods: 56 patients were identified with a search for "myomectomy", "c-section", or "abdominal scar." The search yielded 25 patients with prior uterine surgery (12 myomectomy and 13 c section). Of those 19 had artifacts along the FUS beam path visible on MRI. 31 patients were excluded from study due to no evidence of prior surgery or missing information in the chart. Charts, screening MRI scans, and MRgFUS treatment scans were reviewed and artifacts were graded as mild, moderate, or severe. In addition, operative reports were reviewed.

Results: Average patient age was 44 years (range 32-51) and average time from surgery to MRgFUS treatment was 8.3 years. In total 36 fibroids were treated with an average volume of 103cc (range 7-478cc). One-way ANOVA showed no significant correlation with artifact severity and % NPV ($p=0.41$) or with fibroid size and % NPV ($p=0.49$). There were no adverse events in this patient population except for one case of endometritis that occurred months after the operation, and thus unlikely related to the MRgFUS treatments. Artifacts from prior surgeries appear more visible on post contrast T1 fat saturation images *versus* pre-contrast T1 and T2 weighted images.

Conclusions: Postoperative artifacts do not impede MRgFUS ablation. A possible etiology of the artifact could be from a small electrical field formed by the residual carbon compounds from the dye (D and C Violet No. 2) in the sutures that leaked into the tissues. Patients with a history of prior uterine surgery deserve a treatment attempt with MRgFUS, even with MRI artifacts, as long as they are aware of the potential risks.

YI-1/P-YI-1

Monday

22 October 2018

Topic: Movement Disorders

Presentation Type: Oral; Poster

MRgFUS in chronic therapy-resistant Parkinson's disease: Anatomical reappraisal and technical strategy

Marc Gallay[1], David Moser[2], Christian Federau[3], Daniel Jeanmonod[2]

[1]Center for Functional Ultrasound Neurosurgery, Sonimodul, Solothurn, Switzerland
[2]Sonimodul, Solothurn, Switzerland
[3]ETH Zürich and University Zürich, Institute for Biomedical Engineering, Zürich, Switzerland

Background: After 60 years of history in the field of functional neurosurgery, the issue of target coverage remains primordial and sub-optimally addressed and solved. The possibility of intraoperative visualization and monitoring of a selected target heated with MR-guided high intensity focused ultrasound (MRgFUS) offers new perspectives for safe and efficient lesioning inside the brain. The aim of this technical development is to provide an optimized planning and operative strategy to perform a pallidothalamic tractotomy (PTT), i.e. an intervention on the pallidothalamic tract, with the technology of MRgFUS, using postmortem histological evidence of interindividual variability and correlations between MR imaging and a thermal dose model of cumulative equivalent minutes at 43°C (CEM).

Methods: Histological sections and maps from 6 human brain hemispheres cut in their axial stereotactic plane were aligned on their mid-commissural line (MCL) at intercommissural level and outlines of the identified pallidothalamic tract on Myelin stained sections were drawn and superimposed. A standardized PTT with 5 to 7 target sub-units was then performed using MRgFUS. Each sonication had the shortest possible time and the corresponding power in order to reach 240 CEM at each target sub-unit. MR and thermal dose parameters were analyzed in 31 consecutive treatments between January and December 2017 in patients suffering from chronic therapy-resistant Parkinson's disease (PD).

Results: Good correlations were found between 1) the mean axial T2 lesion diameter immediately post-treatment and the mean 240 CEM thermal dose diameter (r=0.52), 2) the mean axial T2 diameter 48 hours post-treatment and the mean 18 CEM thermal dose diameter (r=0.62), and 3) the mean axial T2 diameter immediately post-treatment and 48 hours post-treatment (r=0.62).

Conclusions: Neither repetition of high temperature (54-60°C) sonications nor prolonging sonication time without moving the focal point, both strategies aiming to increase the 240 CEM thermal dose surface area, brought sufficient consistency in patient's symptom control in our previous experience. We hereby present our current approach to the MRgFUS pallidothalamic lesioning taking into account interindividual variability.

YI-2/P-YI-2

Monday

22 October 2018

Topic: Movement Disorders

Presentation Type: Oral; Poster

Longitudinal analysis of lesion microstructural changes after focused ultrasound thalamotomy

Francesco Sammartino

The Ohio State University, Dublin, Ohio, United States

Background: Focused ultrasound thalamotomy (FUS-T) is an emerging, incision-less treatment of patients with essential tremor (ET). Currently, the presence of edema in the acute phase and decreased definition of the lesion boundaries in longer term limit *in vivo* investigations into the patterns of tissue reorganization after FUS-T. This research is critical to refining the ablation technique and gain insights into mechanisms underlying loss of efficacy after FUS-T.

Restricted diffusion imaging (RDI) is a non-parametric tensor algorithm which can selectively quantify restricted diffusion and may be more sensitive to tissue reorganization following surgical lesioning. We utilized RDI to non-invasively study the *in vivo* tissue reorganization after FUS-T both immediately after (n=18) and one year after lesioning (n=9).

Methods: Structural and 60-directions diffusion-weighted MRI scans were obtained at several time points: preoperative, one day and one year after FUS-T. We studied microstructural changes at the lesion site using RDI. RDI analysis was performed in two regions: local (around the lesion epicenter) and whole brain. To understand the local microstructural changes, RDI was compared between pre & immediately post, immediately post & 1year and pre and 1 year imaging. The resulting maps were statistically thresholded at the group level using a general linear model with non-parametric permutation (up to 5000 permutations) to correct for false discovery. This voxel-wise analysis was also adjusted for tremor improvement in the contralateral hand.

Results: The restriction in diffusivity extended beyond the conventional lesion boundaries on T2 imaging. Using RDI, microstructural changes could be detected at lesion site immediately after and 1 year after FUS-T. We discovered two distinct zones of microstructural changes locally - the lesion core: significant increase in RDI immediately after FUS-T without normalization at the 1 year; zone of reorganization: increase in RDI immediately after FUS-T and a subsequent significant decrease at 1 year. The zone of reorganization was localized anterior and medial to the lesioned area.

The group-level whole-brain comparison, adjusting for tremor improvement, revealed two clusters, one anterior the the group lesion and another at the level of the Gpi .

Conclusions: RDI analysis is a novel technique for studying microstructural changes after FUS-T. We observed significant reorganization around the lesion especially antero-medially which could represent zone of partial ablation. These findings have clinical implications for FUST ablation technique and planning of retreatment in patients with loss of efficacy.

Figure 1. RDI changes at the lesion site revealed two clusters; the lesion is green in color and the zone of reorganization is yellow.

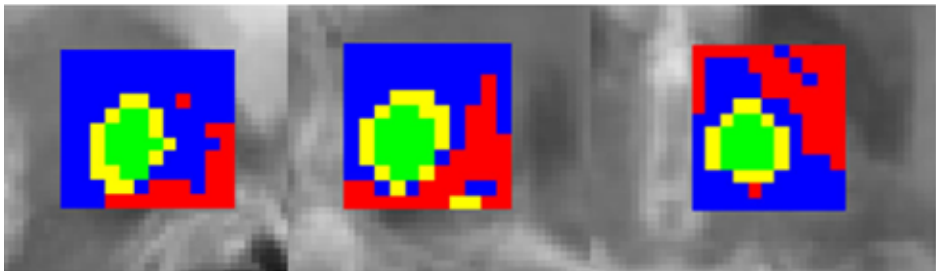

YI-3/P-YI-3

Monday

22 October 2018

Topic: Stroke
Presentation Type: Oral; Poster

Focused ultrasound-mediated transfection of cerebral vasculature independent of blood-brain barrier opening

Catherine Gorick, Ji Song, Caitleen Copeland, Alexander Klibanov, Richard Price

University of Virginia, Charlottesville, Virginia, United States

Background: Approximately 15 million people suffer from strokes annually. Gene therapy approaches to revascularization after stroke could benefit from endothelial cell-selective transfection, which could permit modulation of the vasculature without affecting the blood-brain barrier (BBB). We have previously demonstrated targeted transfection of brain structures using focused ultrasound (FUS) and microbubbles (MBs). Here, we develop a novel gene therapy approach for FUS-targeted endothelial-selective transfection in the brain.

Methods: A 1 MHz FUS transducer was aligned to target the right striatum of mice. Cationic lipid-shelled MBs (1-3 microns) were electrostatically coupled with reporter gene-bearing plasmid DNA (luciferase or mCherry) and injected intravenously. Mice were treated with a FUS pulsing sequence at a range of peak-negative acoustic pressures. Transfection was assessed by bioluminescence or immunofluorescence. Acoustic emissions were recorded during each treatment. In separate studies, mice received plasmid-coupled microbubbles intravenously along with Evans Blue dye in order to assess blood-brain barrier disruption. Dye leakage from the vasculature was quantified.

Results: Bioluminescent imaging demonstrated spatially-specific expression of the luciferase transgene (Fig.1A). At each of the pressures, mCherry expression was robust in the FUS-treated region, but virtually undetectable in the contralateral side (Fig. 1B-I). At increasing pressures, there was significantly more transfection of extravascular cells (Fig. 1J). At 0.1 MPa, over 95% of the mCherry+ sites overlapped completely with GSI lectin staining, indicating highly endothelial-selective transfection. Despite the increased selectivity, there was no significant decrease in the area of vessels transfected (Fig.1K), suggesting that we can modulate transfection selectivity without sacrificing transfection efficiency. Importantly, endothelial-selective transfection at 0.1 MPa was achieved without detectable BBB opening, as evidenced by the absence of Evans Blue in the striatum after treatment. In contrast, brains treated with higher pressures exhibited significant BBB opening (Fig. 2A-D). While sample sizes were too small (n=2-5) to determine statistical significance, the 0.3 and 0.4 MPa groups trended toward more extensive Evans Blue leakage due to BBB disruption, while no leakage was observed at 0.1 or 0.2 MPa (Fig. 2E-F). BBB integrity as assessed by contrast-enhanced T1w MRI recapitulated the trends of the Evans Blue assay (Fig. 3). Acoustic emissions analysis revealed a correlation between peak-negative pressure and stable and inertial cavitation doses (Fig. 4A-B), as well as between T1w MRI contrast enhancement and cavitation doses (Fig. 4C-D). Animals in which BBB disruption was visible on T1w MRI demonstrated greater cavitation doses than those without visible disruption (Fig. 4E-F).

Conclusions: Our results indicate that endothelial-selective transfection of targeted regions of cerebral vasculature (independent of BBB disruption) is possible with FUS and that the degree of selectivity can be modulated according to the peak-negative pressure of the ultrasound waves. The results suggest an acoustic signature of BBB disruption that could be used to inform future treatments to prevent BBB opening, and we expect cavitation dose to correlate with transfection selectivity in future studies. This platform provides possibilities for targeted gene therapy for stroke applications, wherein potential risks may be associated with BBB disruption.

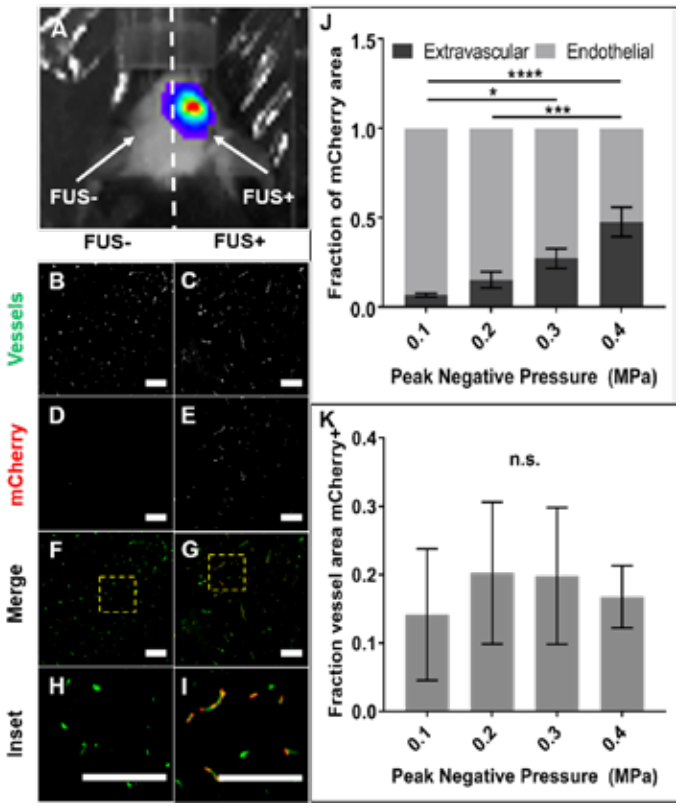

Figure 1. Endothelial-selective transfection. A) Luciferase expression in striatum. B,C) Lectin staining for blood vessels. D,E) mCherry expression. F,G) Merged images. H,I) F and G insets. J) mCherry localization. K) Fraction vessels mCherry+.

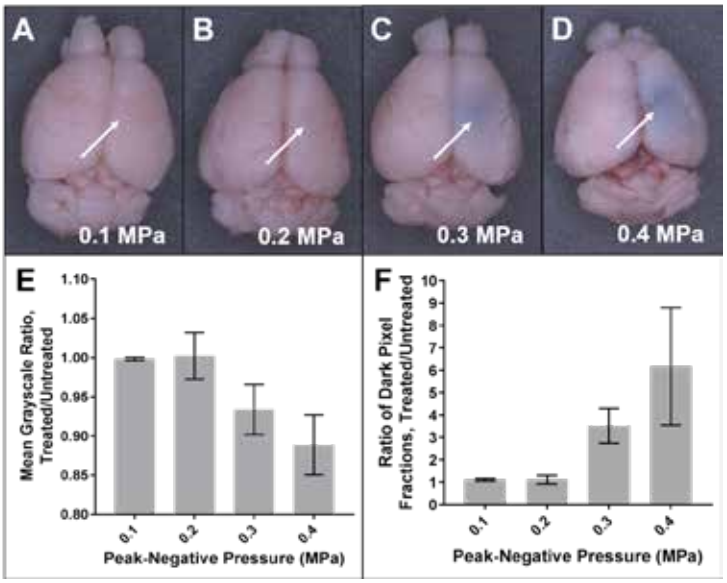

Figure 2. Pressure-dependent BBB disruption. A,B,C,D) Evans Blue extravasation across pressures. E) Mean grayscale value in FUS-treated *vs.* contralateral regions. F) Ratio of fraction pixels with lower grayscale values than whole brain median.

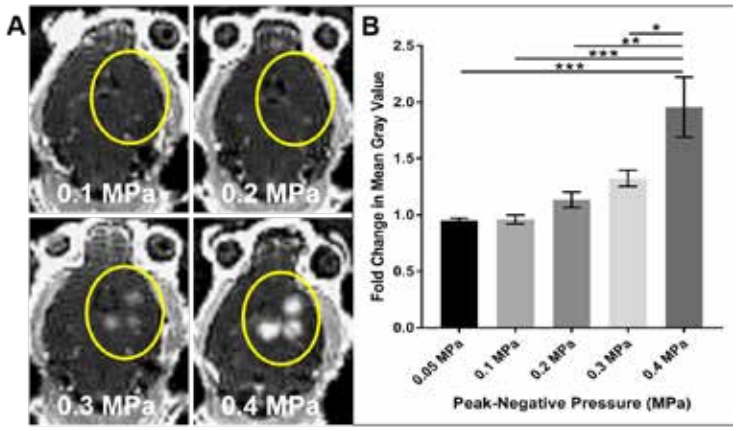

Figure 3. Pressure-dependent gadolinium extravasation. A) Contrast-enhanced T1-weighted MR images following FUS+MB treatment across pressures B) Fold change in mean gray value in the FUS-targeted region relative to contralateral across pressures.

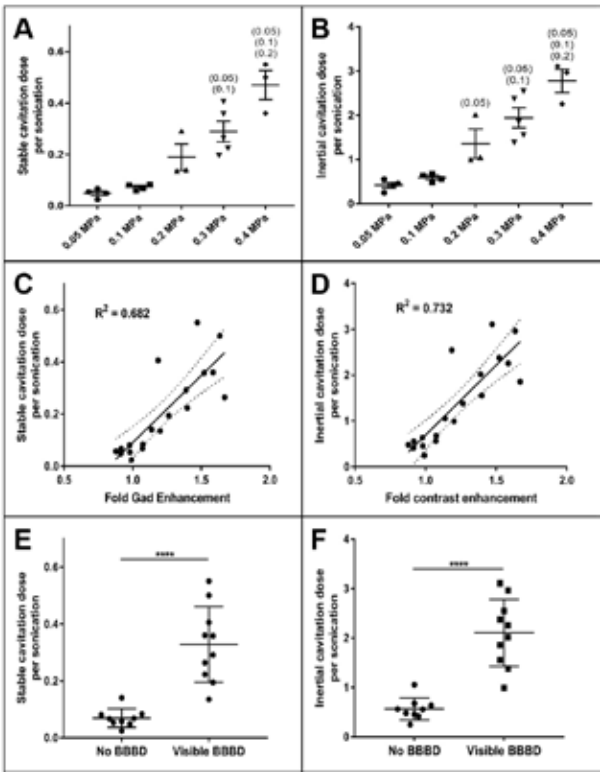

Figure 4. Acoustic emissions correlate with FUS pressure and BBB opening. A,B) Cavitation doses across pressures. C,D) Cavitation doses *vs.* MRI contrast enhancement. E,F) Cavitation doses for animals with visible BBB opening on T1w-MRI *vs.* without.

YI-4/P-YI-4

Monday

22 October 2018

Topic: Neuromodulation
Presentation Type: Oral; Poster

Histological study of focused ultrasound neuromodulation and MR-ARFI in sheep

Pooja Gaur, Kerriann Casey, Ningrui Li, Jan Kubanek, Morteza Mohammadjavadi, Yamil Saenz, Gary Glover, Kim Butts Pauly

Stanford University, Stanford, California, United States

Background: Neuromodulation is an emerging application of non-ablative focused ultrasound (FUS) that enables non-invasive exploration of neural processing. However, further assessment of tissue safety following FUS neuromodulation is needed. Dallapiazza et al. found no tissue damage following FUS neuromodulation in pigs, whereas Lee et al. reported microhemorrhages in sheep after FUS neuromodulation. To address the unmet need for a controlled study of tissue safety in large animals, we evaluate histological findings in sheep with and without exposure to FUS.

Methods: Seven anesthetized male Dorset cross sheep were included. Five underwent transcranial FUS (1024 element, 550 kHz transducer). Two animals did not receive ultrasound but otherwise underwent the same experimental procedures.

In the five that had transcranial FUS, MR-ARFI verified focal spot location in one or more areas away from the neuromodulation site(s). Neuromodulation pulses were then applied at 1-4 subcortical locations in the left hemisphere.

Figure 1(a) illustrates MR-ARFI parameters: FUS was on for 16 ms each TR of 500 ms, repeated 128 times at acoustic powers between 127.5-195.5 W. Figures 1(b)-(d) illustrate neuromodulatory parameters in which FUS was on 200-300 ms every 1 s with pulsed (50% duty cycle) or CW ultrasound at acoustic powers between 8.5-17 W. Table 1 summarizes experimental parameters for each sheep.

Animals were euthanized zero to seven days after study. The skull cap and brain were extracted and fixed in 10% neutral buffered formalin for 10 days prior to tissue sectioning and H&E staining. Brain regions were selected based on gross tissue comparison to MRI locations of FUS targets. For each location, 5 μm-thick sections were obtained from the left and right hemisphere and stained with H&E. A fiberoptic hydrophone was used to measure peak negative pressure transmitted through each skull cap to obtain an *in situ* intensity estimate, provided in Table 1.

Results: Sheep euthanized <24 hours following MRI (+/- FUS) exhibited extravascular red blood cells within the meninges as well as rare extravascular red blood cells within neural parenchyma, regardless of hemispheric location (left *vs.* right) or FUS application. In this cohort, no additional histologic findings (i.e. macrophage infiltration, erythrophagocytosis, hemosiderin-laden macrophages, tissue necrosis) were noted in areas of extravascular red blood cells. Sheep euthanized >72 hours following MRI (+/- FUS) exhibited similar findings, regardless of hemispheric location (left *vs.* right) or FUS application. Furthermore, even >72 hours following MRI (+/-FUS), there was no evidence of concurrent histologic lesions (i.e. listed above) in regions of red cell extravasation.

Conclusions: The results of this study suggest that the transcranial FUS did not result in histologic tissue damage (i.e. pre-mortem meningeal or perivascular hemorrhage). The absence of concurrent histologic lesions suggests that areas of extravascular red blood cells seen across both hemispheres and experimental groups were artifact due to post-mortem tissue extraction.

Figure 1. Focused ultrasound protocols for focal spot localization with MR-ARFI (500 ms TR) (a) and neuromodulation (b)-(d).

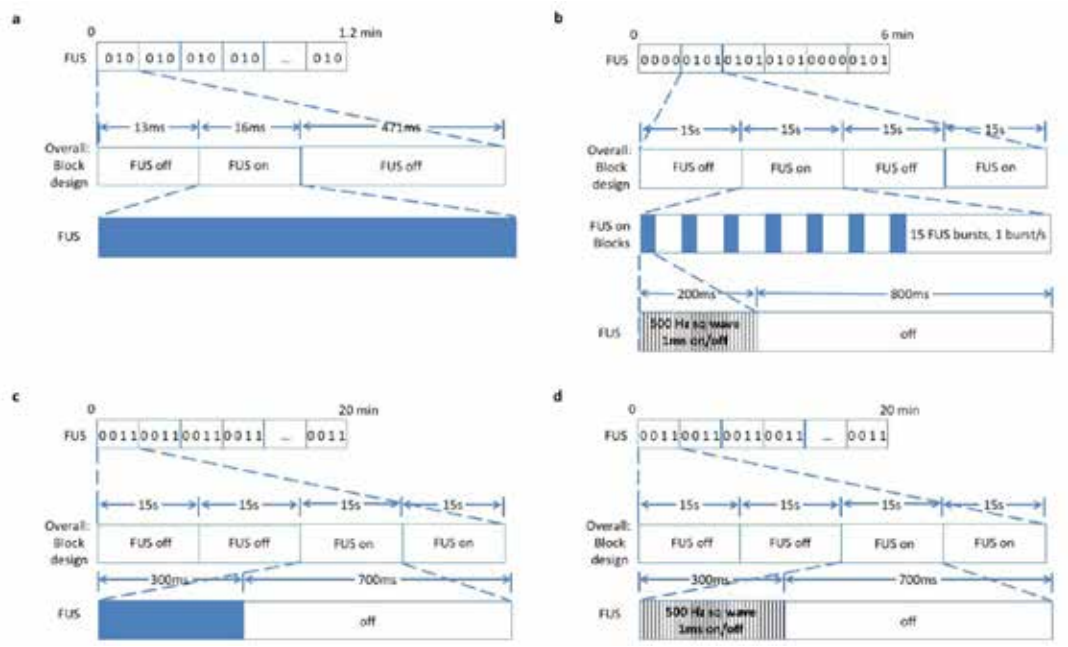

Table 1. Summary of study parameters.

Study group	Animal number	Weight (kg)	Number of neuromodulation sonications	Maximum neuromodulation I_{SPTA} *in situ* estimate (W/cm^2)	Number of MR-ARFI localization sonications	Maximum localization I_{SPTA} *in situ* estimate (W/cm^2)	Days post FUS survival
FUS	1	20	1200	11.24	1408	63.35	0
	2	28	3600	20.41	1792	232.54	0
	3	22	2100	31.9	1664	268.26	0
	4	25	4200	38.6	512	250.08	7
	5	26	3600	25.84	384	368.74	4
Control	1	22	N/A	N/A	N/A	N/A	N/A
	2	34	N/A	N/A	N/A	N/A	N/A

YI-5/P-YI-5

Tuesday

23 October 2018

Topic: Brain – Technical
Presentation Type: Oral; Poster

Efficient transcranial ultrasound delivery *via* excitation of Lamb waves

Kamyar Firouzi, Pejman Ghanouni, Pierre (Butrus) T. Khuri-Yakub

Stanford University, Stanford, California, United States

Background: Transcranial focused ultrasound is being researched as a noninvasive means of ablating brain tumors and of increasing delivery of cancer therapeutics through the blood-brain barrier. However, the currently realized version of the device for tumor ablation operating at approximately 650 is implemented by means of a large-aperture spherical transducer, which has a treatment envelope limited to the center of the brain, whereas most metastases occur along the periphery of the brain. In addition, these transducers create waves that impinge perpendicularly on the skull, which is inefficient. A normal incident transmission also sets up standing waves in the skull, which along with high attenuation leads to excess heating and a requirement for active cooling.

Methods: We have developed an array of ultrasound wedge transducers capable of efficiently delivering focused ultrasound energy into the brain with minimal heating of the skull and the ability to address regions in the brain that are close to or far from the skull. A wedge transducer utilizes guided Lamb waves in the skull as an efficient way of transmitting the ultrasound beam into the brain. Transmission efficiency is by virtue of a double-mode-conversion mechanism, one from the wedge into selective Lamb waves in the skull and the other from Lamb waves into the brain. Additionally, Lamb waves exhibit less attenuation than normal-incident bulk waves. The main constituents of the transducer array are wedge transducer elements arranged over a wedge ring to provide a focusing mechanism. The benefits of our approach is in improved efficiency, reduction in heating of the skull, and the ability to address regions in the brain that are close to the skull.

Results: We have conducted experiments to demonstrate the transmission efficiency of the mode-conversion mechanism in samples such as an Aluminum plate, which exhibit low attenuation. As a cranial phantom, we have used human skull fragments, with natural variations in thickness and heterogeneous porous structure. In order to benchmark our technique against the normal-incident technique, we have utilized a single element 1 MHz commercial immersion transducer to emulate both wedge and normal-incident transmissions. The field measurements are shown in Figure 1. The wedge technique exhibits around 14 dB total loss as opposed to the normal-incident technique, which shows around 21 dB total transmission loss. Furthermore, we have fabricated wedge transducer prototypes and tested them on the skull fragments to prove the feasibility of transcranial delivery close to the expected value.

Conclusions: The results demonstrate the validity of our approach both for mode-conversion and overcoming attenuation.

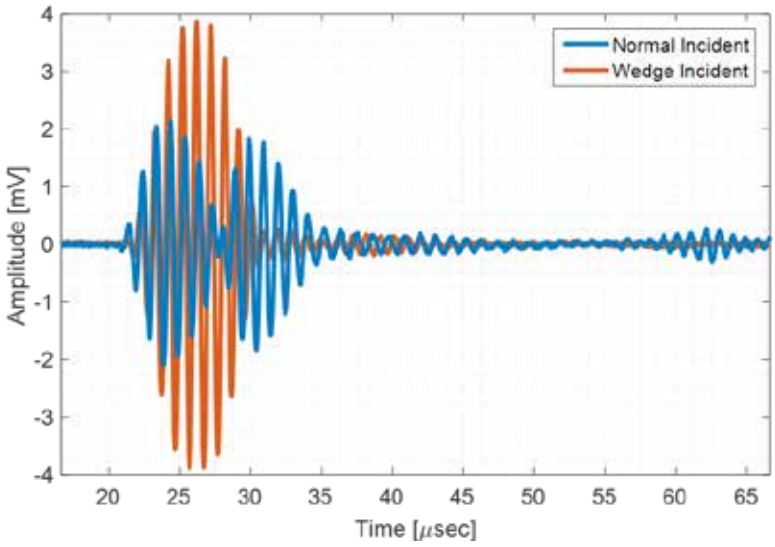

Figure 1. RF data recorded at the location of peak transmitted pressure in both normal-incident and wedge transmission cases.

YI-6/P-YI-6

Tuesday

23 October 2018

Topic: Brain Tumors
Presentation Type: Oral; Poster

Blood-brain barrier opening in primary brain tumors: A demonstration of safety and feasibility with non-invasive MR-guided focused ultrasound

Todd Mainprize[1], Nir Lipsman[1], Yuexi Huang[2], Ying Meng[1], Allison Bethune[1], Sarah Ironside[1], Chinthaka Heyn[1], Ryan Alkins[1], Maureen Trudeau[1], Arjun Sahgal[1], James Perry[1], Kullervo Hynynen[3]

[1]Sunnybrook Health Sciences Centre, Toronto, Ontario, Canada
[2]Sunnybrook Research Institute, Toronto, Ontario, Canada
[3]University of Toronto, Toronto, Ontario, Canada

Background: The blood-brain barrier (BBB) has long limited therapeutic access to brain tumor and peritumoral tissue. Pre-clinical evidence of low-intensity MR-guided focused ultrasound (MRgFUS) has shown precision in disrupting the BBB without surgery. The objective of this Phase I, single-arm open-label study is to investigate the safety and feasibility of BBB opening with chemotherapy delivery using MRgFUS for the first time in patients with glioma.

Methods: Five patients with previously confirmed or suspected high-grade glioma underwent a single MRgFUS BBB opening with concurrent chemotherapy (n=1 liposomal doxorubicin, n=4 temozolomide) administration. Surgical resection of the tumor was performed the following day, and tissue samples of 'sonicated' and 'unsonicated' tissue were obtained for analysis where accessible. Participants continued with standard neuro-oncology care and followed for three months.

Results: The BBB within the target volume showed radiographic evidence of increased permeability to gadolinium immediately following focused ultrasound procedure, resolving on the MRI approximately 20 hours. No adverse clinical or radiologic events occurred with BBB opening. Biochemical analysis of tissue from the tumor margin suggests evidence of chemotherapy delivery.

Conclusions: MRgFUS BBB opening of tumor and peri-tumor tissue with concurrent administration of chemotherapy was well tolerated by patients with glioma. The characterization of therapeutic delivery and clinical response to this treatment paradigm requires further investigation.

Acknowledgements: This study was supported by the Focused Ultrasound Foundation.

YI-7/P-YI-7

Tuesday

23 October 2018

Topic: Brain Tumors
Presentation Type: Oral; Poster

Towards a model of FUS-mediated blood-brain barrier disruption in non-enhancing, glioma-invaded brain regions for testing improvements in therapeutic delivery

Pavlos Anastasiadis[1], Nina Connolly[1], Ali Mohammadabadi[1], Joseph Frank[2], Graeme Woodworth[1], Victor Frenkel[1]

[1]University of Maryland School of Medicine, Baltimore, Maryland, United States
[2]National Institutes of Health Clinical Center, Bethesda, Maryland, United States

In accordance with author request, this abstract is not available for publication.

YI-8/P-YI-8

Tuesday

23 October 2018

Topic: Brain Tumors
Presentation Type: Oral; Poster

Histotripsy mediated immunomodulation in a mouse gl261 intracranial glioma model

Tyler Gerhardson, Anupama Pal, Lindsay Scheetz, Jonathan Sukovich, Jonathan Lundt, Timothy Hall, Beata Chertok, Charles Cain, Alnawaz Rehemtulla, Zhen Xu

University of Michigan, Ann Arbor, Michigan, United States

Background: Glioblastoma (GBM) is the most common and most malignant primary brain tumor in adults. Despite aggressive standard therapy including surgery, radiotherapy, and concomitant and adjuvant temozolomide the prognosis is poor with a median overall survival (OS) of less than 15 months. GBM is a highly invasive and diffuse tumor with no clear margin between tumor and healthy brain tissue, making full surgical resection impossible. Recent success of immunotherapies in treating cancers such as melanoma has sparked interest in applying such therapies to GBM. Although beneficial effects of immunotherapies in treating mouse models of GBM have been demonstrated, their limited efficacy has hampered immediate clinical translation. In an effort to enhance anti-tumor immunity in GBM, we hypothesized that histotripsy, due to its ability to induce tumor ablation in a safe and targeted manner, could be used to increase tumor permeability and activity of the anti-tumor immune response. In this initial study, we investigated the immune response of a mouse GL261 intracranial glioma model after histotripsy ablation of a fraction of an intracranial GBM.

Methods: A total of 27 male mice were inoculated with GBM according to a GL261-luc2 C57 BL/6 albino mouse model protocol. Tumor monitoring was performed using T2-weighted MRI and bioluminescence imaging. Histotripsy treatment was applied to a portion of the tumor in 15 of the 27 mice. The remaining 12 were left untreated as controls. A 1 MHz, 8 element transducer with aperture diameter of 58.6 mm and focal length of 32.5 mm was used for treatment. A phased array imaging probe was inserted coaxially within the transducer to allow tumor targeting and treatment monitoring. Tumors were targeted using features visible on both pretreatment MRI and B-mode ultrasound. 50 histotripsy pulses were applied through the skull to a single point within the tumor at a pulse repetition frequency (PRF) of 1 Hz and an estimated peak-negative pressure of 40 MPa. Preliminary experiments in healthy mice showed well-defined lesions using these treatment parameters (Fig. 1). Treatment was applied 2 weeks after inoculation and mice were survived for 1 week after histotripsy treatment after which point they were euthanized. Directly following euthanasia in both treatment and control mice, brain tumors, spleens and lymph nodes were harvested for flow cytometry. In addition, for both groups, immunohistochemistry staining was performed on the primary tumor. The overview of the study and specific time points is shown in Figure 2.

Figure 1. The brain of a healthy mouse after applying 50, 1 MHz histotripsy pulses to a single point through the skull at a PRF of 1 Hz. The lesions as observed in both T2-weighted MRI (top) and H&E stained histology (bottom).

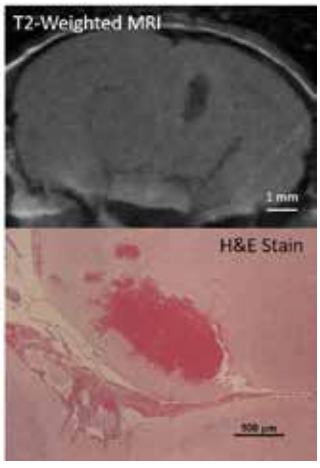

Results: Of the 15 mice treated with histotripsy, 14 survived treatments, all with lesions visible in post-treatment MRI. 12 of these mice were confirmed to have lesions in a portion of the bulk tumor volume as observed via MRI. Of the 12 control mice, 11 survived until the euthanasia date with 1 mouse dying 3 days prior to euthanasia. Figure 3 shows the pre- and post-treatment T2-weighted MR images from tumor monitoring of a treated mouse . Flow cytometry results yielded a two-fold decrease ($\alpha = 0.05$) in the number of myeloid derived suppressor cells (MDSCs) in the brain tissue of mice treated with histotripsy relative to that of the control mice (Fig. 4a). Additionally, a large increase in interferon gamma (IFN-γ) was observed in mice treated with histotripsy (Fig. 4b). As interpreted by a pathologist, Giemsa staining of sections of brain tumors from treated mice sampled from regions away from the histotripsy lesion showed shrunken cells with shrunken and pyknotic nuclei separated by edema with insufficient cells to assess the mitotic index (Fig. 4c). This contrasted with the sections of brain tumors from control mice where intact tumor cells and a high mitotic index were observed (Fig 4d).

Conclusions: In this initial study, we investigated the immune response of a mouse GL261 intracranial glioma model after treating a portion of the brain tumor with histotripsy. Flow cytometric analysis showed a decrease in highly immunosuppressive MDSCs in histotripsy treated tumors compared to untreated brain tumors. In addition, the IFN-γ production was found to be extremely low in the untreated control tumors (consistent with literature), whereas histotripsy treated tumors showed relatively large amounts of IFN-γ, suggesting that the decrease in MDSC resulted in a decreased immunosuppressive inratumoral environment. Analysis of tumor immunohistochemistry revealed that histotripsy treated tumors showed

shrunken tumor cells with shrunken and pyknotic nuclei separated by edema which contrasted with the untreated brain tumors, which appeared relatively healthy. These initial results provide a compelling rationale for the safety of GBM therapy using histotripsy, while changes in immunomodulatory cell populations provide evidence of potential mechanisms that may be at work in increasing the immunogenicity of the tumors following histotripsy treatment.

Figure 2. The overview of the study and specific time points.

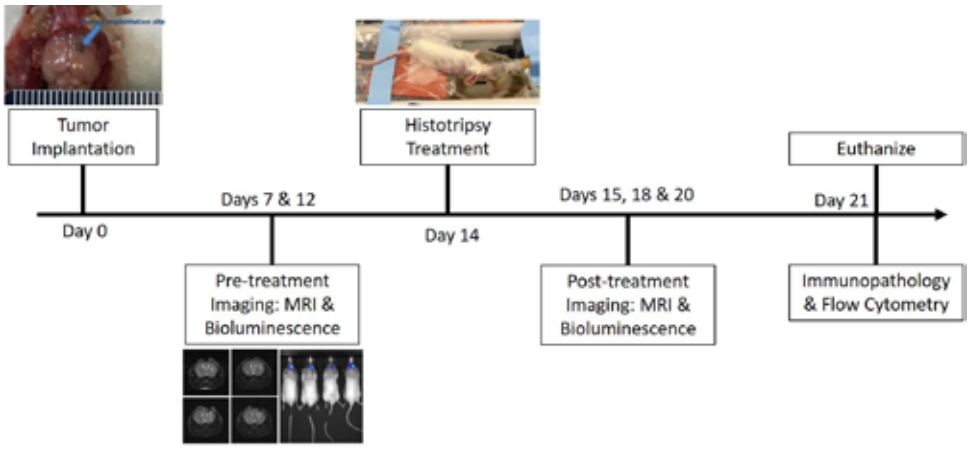

Figure 3. The pre- and post-treatment T2-weighted MR images from tumor monitoring of a treated mouse. A well defined lesion is evident within the tumor in the first post-treatment image (day 15).

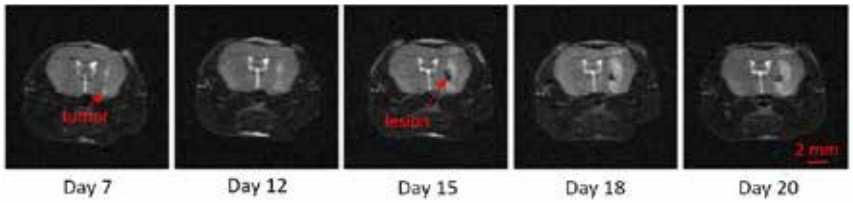

Figure 4. (a) Flow cytometry results for brain tissue (BT), spleen, sentinel lymph node (SLN) and draining lymph node (DLN). (b) IFN-gamma concentration in control *vs*. treated mice. Giemsa staining of tumor from (c) treated and (d) control mice.

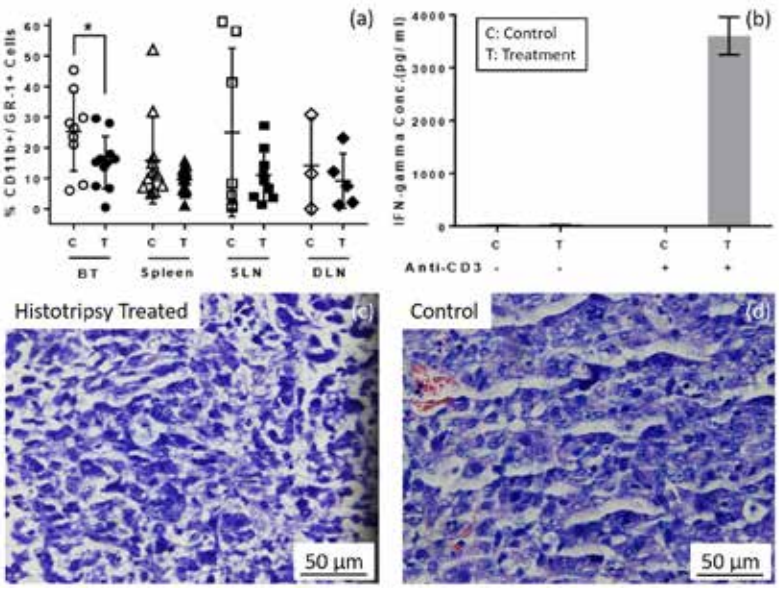

YI-9/P-YI-9

Tuesday

23 October 2018

Topic: Brain Tumors
Presentation Type: Oral; Poster

Leveraging MR image-guided focused ultrasound to potentiate immunotherapy for glioblastoma

Natasha Sheybani, Alexandra Witter, William Garrison, G. Wilson Miller, Timothy Bullock, Richard Price

University of Virginia, Charlottesville, Virginia, United States

Background: Glioblastoma (GB) is the most common and malignant brain tumor, its diffuse nature and proclivity for recurrence rendering it largely intractable. Immunotherapy (ITx) approaches (e.g. anti-PD1) may hold promise for treating GB; however, the blood-brain (BBB) and blood-tumor (BTB) barriers hinder delivery of systemically administered ITx drugs. A potential approach to enhancing ITx delivery is MRI-guided focused ultrasound (FUS), a non-invasive technique that, when combined with concomitant systemic injection of microbubbles (MB), can transiently disrupt the BBB/BTB and mechanically perturb the tumor microenvironment. Here, we investigate whether localized BBB/BTB disruption with FUS+MB enhances anti-tumor immune responses and inhibits tumor growth in an orthotopic murine glioma model.

Methods: At 14 days following intracranial implantation of GL261 cells stably transfected with luciferase (GL261-luc2), mice were ultrasonically coupled to a 1.1 MHz small animal MR image-guided FUS system. In animals bearing MRI-visible tumors, albumin-shelled MB were injected intravenously and a 4-spot grid of sonications was applied to the tumor-bearing region immediately following (0.4-0.6 MPa peak negative pressure (PNP), 0.5% duty cycle, 120s period). BBB/BTB disruption was confirmed by post-treatment MR imaging. Tumor outgrowth was monitored serially by IVIS imaging. One week following treatment, whole brains and peripheral lymphoid organs were harvested for flow cytometry.

Results: MR imaging of GL261-luc2 tumors treated at the stated parameters evidenced successful BBB/BTB disruption (Fig.1a). Analysis of acoustic emissions detected by passive cavitation monitoring discretized stable and inertial cavitation activity as a function of PNP (Fig.1b,c). Seven days following BBB/BTB disruption at 0.6 MPa, CD86 (a marker of maturity) mean fluorescence intensity (MFI) on dendritic cells (DC) increased ~3-fold in deep cervical lymph nodes (DCLN) (Fig.1d). Accordingly, intratumoral CD86+ DC trended towards increased absolute frequency while CD86 MFI on intratumoral DC was significantly different across the two PNPs evaluated (Fig.1e). One week following BBB/BTB disruption, intratumoral CD4+ T cells doubled and intratumoral CD8+ T cells increased by ~17%. Within the intratumoral CD8+ T cell population, a significant differential increase in antigen-experienced (CD44+) PD1+ T cells was observed as a function of FUS+MB treatment at both 0.4 and 0.6 MPa (Fig.1f), thereby inciting a rationale for future implementation of anti-PD1 therapy. Bioluminescence imaging revealed a significant reduction in total photon flux as early as 6 days following FUS+MB at 0.6 MPa (Fig.1g), indicating early growth inhibition of GL261-luc2 tumors.

Conclusions: These findings demonstrate that BBB/BTB disruption with FUS+MB can potentiate anti-tumor immunity against glioma, independent of drug delivery. Ongoing studies entail combining FUS+MB with checkpoint inhibitor (i.e. anti-PD1, anti-TIGIT) delivery to evaluate whether an allied treatment approach can promote an even more robust anti-glioma response.

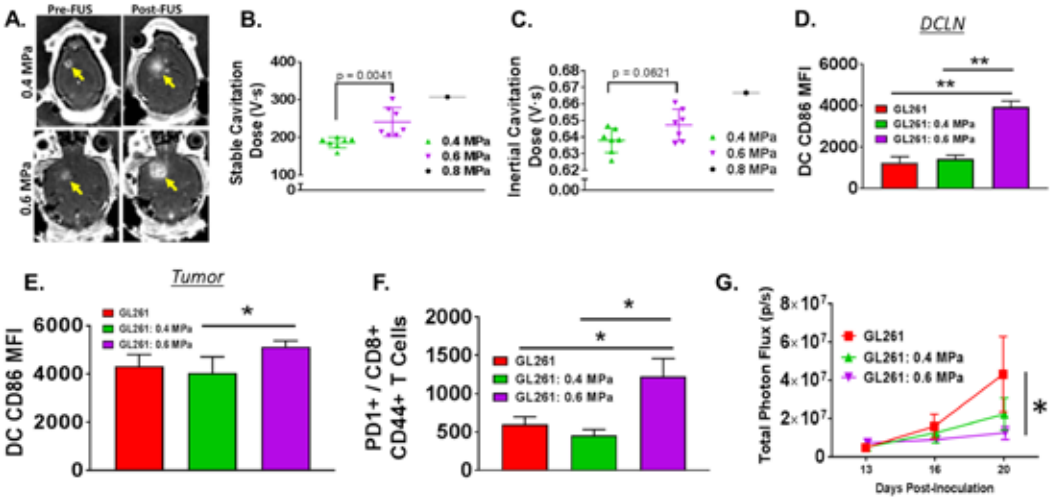

Figure 1. (A) Representative axial contrast-enhanced T1-weighted MRI images demonstrating BBB/BTB disruption in GL261-luc2 tumors. (B-C) Stable and inertial cavitation doses calculated from harmonic and broadband acoustic emissions, respectively. (D-E) MFI of CD86 on CD11c+ DC in DCLN and tumor one week following FUS+MB (groups: untreated GL261-luc2 tumors, GL261-luc2 tumors exposed to 0.4 MPa or 0.6 MPa FUS). (F) Absolute frequency of CD8+CD44+PD1+ T cells in GL261-luc2 tumors one week following FUS+MB. (G) Serial bioluminescence imaging quantification demonstrating early tumor growth inhibition. *p<0.05. **p< 0.01.

YI-10/P-YI-10

Tuesday

23 October 2018

Topic: Cancer Immunotherapy

Presentation Type: Oral; Poster

Developing synergy between immunotherapy and focused ultrasound ablation for metastatic breast cancer

Natasha Sheybani, Alexandra Witter, Aaron Stevens, Timothy Bullock, Richard Price

University of Virginia, Charlottesville, Virginia, United States

Background: Metastatic breast cancer (BrCa) remains incurable, with a 5 year survival of only 22%. Immune rejection of BrCa is very rare due to such limitations as poor functional CD8+ T cell infiltration and immunosuppression in the tumor microenvironment. Thus, adjunct strategies that render BrCa tumors responsive to immunotherapy (ITx) are in critical demand. Focused ultrasound (FUS) ablation has been demonstrated to cause tumor cell damage and death while preserving the integrity of sensitive surrounding tissues, mediating increased tumor antigen presentation, heat shock protein release, cytokine release, and upregulation of other mechanisms capable of bolstering systemic CD8+ T cell responses. The goal of this study is to evaluate the hypothesis that ultrasound-guided FUS thermal ablation can serve as an auto-vaccine for treatment of BrCa with ITx.

Methods: In an ectopic model of metastatic mammary carcinoma, mice were inoculated subcutaneously with 4T1 cells expressing hemagglutinin (4T1-HA). At 14 days following tumor implantation, tumors were partially thermally ablated using a 3 MHz single-element transducer operating at 30W derated acoustic power for 4 seconds in order to reach temperatures exceeding 60oC. Concomitant with FUS, treatment with gemcitabine (GEM) was initiated to abrogate the substantial contribution of myeloid-derived suppressor cells (MDSCs) to the immunosuppressive tumor microenvironment in the 4T1-HA tumor model. GEM was administered intraperitoneally once every 7 days. Tumor outgrowth was monitored by digital caliper measurements. 4T1-HA tumors, lungs and secondary lymphoid organs including tumor-draining lymph nodes (TDLN) were harvested for flow cytometry upon conclusion of the outgrowth study. Pulmonary metastasis of tumors was additionally assessed by India ink staining and histology.

Results: FUS thermal ablation of 4T1-HA tumors under ultrasound guidance was demonstrated feasible, with post-ablative hyperechoic signatures appearing on occasion at targeted sites (Fig.1a). At one week following FUS treatment, we observed a ~3-fold increase in mature dendritic cells (CD11c-hi/CD86+), as well as an increasing trend in M1 macrophage representation by flow cytometry (Fig.1b). Nonetheless, FUS did not confer concomitant changes in intratumoral CD8+ and CD4+ T cells, presumably due to an overwhelming MDSC population. However, combining FUS with MDSC abrogation via GEM application (i.e. FUS+GEM) elicited a significant decrease in 4T1-HA tumor outgrowth when compared to Untreated, FUS, and GEM alone groups (Fig 1c). Importantly, this tumor growth-control response was sustained for nearly two weeks after the termination of treatment(s) (Fig.1d). Gross assessment of whole lungs by India ink staining revealed reduced pulmonary metastatic burden in mice treated with FUS+GEM as compared to untreated controls (Fig.1e).

Conclusions: Taken together, these results suggest that combination of partial ablation with FUS and immunoadjuvants abrogating immunosuppression (e.g. GEM) may enable FUS to stimulate anti-tumor immunity in BrCa. Ongoing studies capitalize on this platform for evaluation of interaction between FUS and anti-PD1 therapy in 4T1-HA tumors. Histological and flow cytometric analyses of tissue samples harvested from these studies are currently underway.

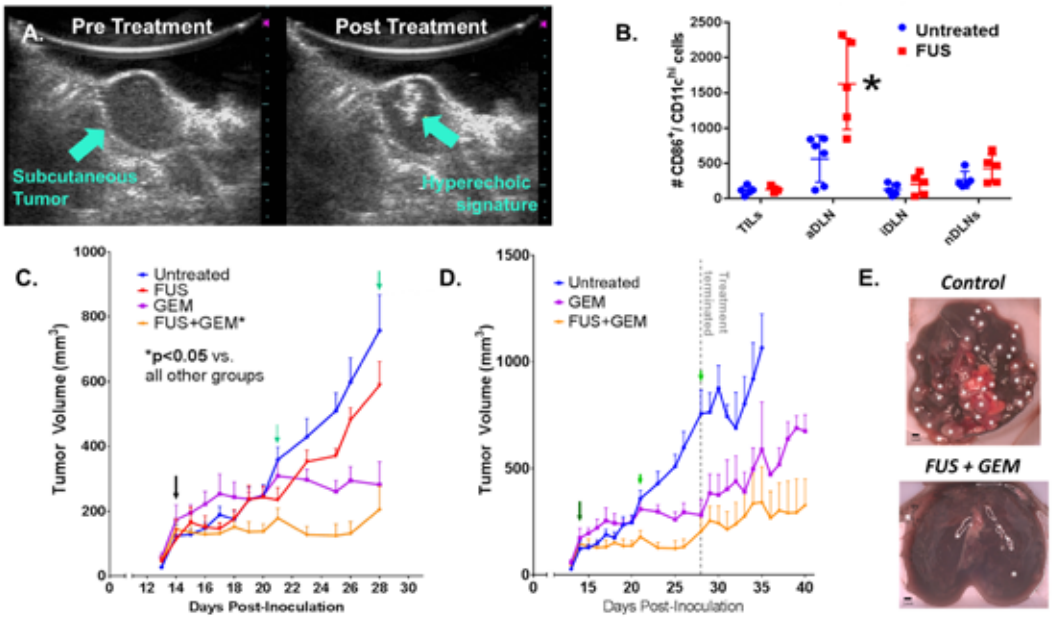

Figure 1. (A) Representative B-mode ultrasound image of subcutaneous 4T1-HA tumor before and after FUS thermal ablation. Hyperechoic marks occasionally appear at the site of sonication. (B) Absolute frequency of CD86+ CD11c-hi dendritic cells across harvested organs one week following FUS ablation (4T1-HA tumor infiltrating leukocytes, TILs; axillary DLN, aDLN; inguinal DLN, iDLN; non-DLN, nDLNs). (C) 4T1-HA tumor outgrowth (dark green arrow: initiation of FUS and GEM treatments; light green arrows: GEM re-administration) up to termination of treatment(s) at 28 days. (D) 4T1-HA tumor outgrowth up to termination of experiment at 40 days. (E) Representative India ink staining depicting macroscopic surface pulmonary metastatic burden (metastases denoted by white asterisks) in 4T1-HA tumor-bearing mice. *p<0.05 vs. untreated unless otherwise specified.

YI-11/P-YI-11

Tuesday

23 October 2018

Topic: Cancer Immunotherapy

Presentation Type: Oral; Poster

RNA sequencing of focused ultrasound-treated melanoma reveals that thermal ablation and hyperthermia elicit differential immunogenicity

Alexander Mathew, Andrew Thim, Timothy Bullock, Richard Price

University of Virginia, Charlottesville, Virginia, United States

Background: Focused Ultrasound (FUS) is a non-invasive thermal energy deposition technology under widespread evaluation for treatment of solid tumors. In addition to causing localized necrosis through thermal damage, preclinical and clinical studies suggest that FUS attenuates immunosuppression in the tumor microenvironment (TME), thereby promoting resistance to recurrence and metastasis. The dominant mechanisms behind this immunomodulation remain unclear, though several have been proposed. The challenge in identifying a unifying mechanistic principle arises from the fact that FUS simultaneously affects tumor, microvasculature, stroma, and lymphatics, inducing a complex cascade of heterogeneous bioeffects that must be simultaneously considered. We propose that integrating RNA sequencing with computational modeling is necessary to solve this inherently systems-level problem. In this study, we use this approach to evaluate and compare mechanisms of immunogenicity in two common FUS regimens: ablation and hyperthermia.

Methods: Male C57BL/6 mice were inoculated subcutaneously with B16F10 melanoma cells and treated 13 days later with FUS in either ablative or hyperthermia heating regimens (Figure 1). Eight hours after treatment, tumors were harvested and stored in RNAlater solution. cDNA libraries generated from purified mRNA were sequenced at a depth of 25 million 2 x 75 bp paired end reads per sample. Reads were aligned to the mouse genome and quantified using the Salmon method to yield differential gene expression. Gene set enrichment analysis (GSEA) was performed on significantly (p adjusted < 0.05) differentially expressed genes using the MsigDB hallmark gene set.

Results: RNA sequencing revealed significant (p adjusted < 0.05) differential expression of 2666 and 560 transcripts for tumors treated with ablation and hyperthermia respectively (Figure 2). Ablation generated a variety of immunomodulatory effects including massive upregulation of HSP70, IL-6, CXCL3, and CCR4. Downregulation of immune markers, including CD209b, CD209g, C6, and IRF6, was also observed. These findings are consistent with a phenotype of local inflammation, increased antigen presentation, and possible mobilization of dendritic cells to the lymphatics. Surprisingly, hyperthermia produced potent immunosuppressive effects on the TME. We observed substantial (> 4 fold) downregulation of TNFα, IL-33, CD-28, and IL-2R, all of which are critical mediators of innate and adaptive immunity. GSEA performed on differentially expressed transcripts revealed distinct phenotypes induced by ablation *vs.* hyperthermia (Table 1). While both treatments induced an unfolded protein response, ablation additionally induced TNFα signaling and apoptosis. Interestingly, ablation also downregulated multiple metabolic pathways, possibly reflecting disruption of normal circulation in the TME. Hyperthermia, however, caused downregulation of multiple immune pathways, reinforcing the concept that hyperthermia may be acutely immunosuppressive.

Conclusions: High throughput unbiased approaches are essential in identifying the mechanisms of FUS-induced immunogenicity toward the goal of designing immunotherapeutic regimens that optimally cooperate with FUS. Using RNA-sequencing, we demonstrated substantially different expression profiles and phenotypes in the TME induced by partial thermal ablation and hyperthermia. We are currently extending these approaches to multiple time points post-treatment to more completely understand expression changes induced by FUS.

Acknowledgements: Supported by NIH R01CA197111 and R01EB020147.

Figure 1. A. Ultrasound guided FUS treatment of a flank melanoma tumor. B. Differential bioeffects in the TME induced by partial thermal ablation *vs.* hyperthermia. C. Parameters used to apply thermal ablation or hyperthermia.

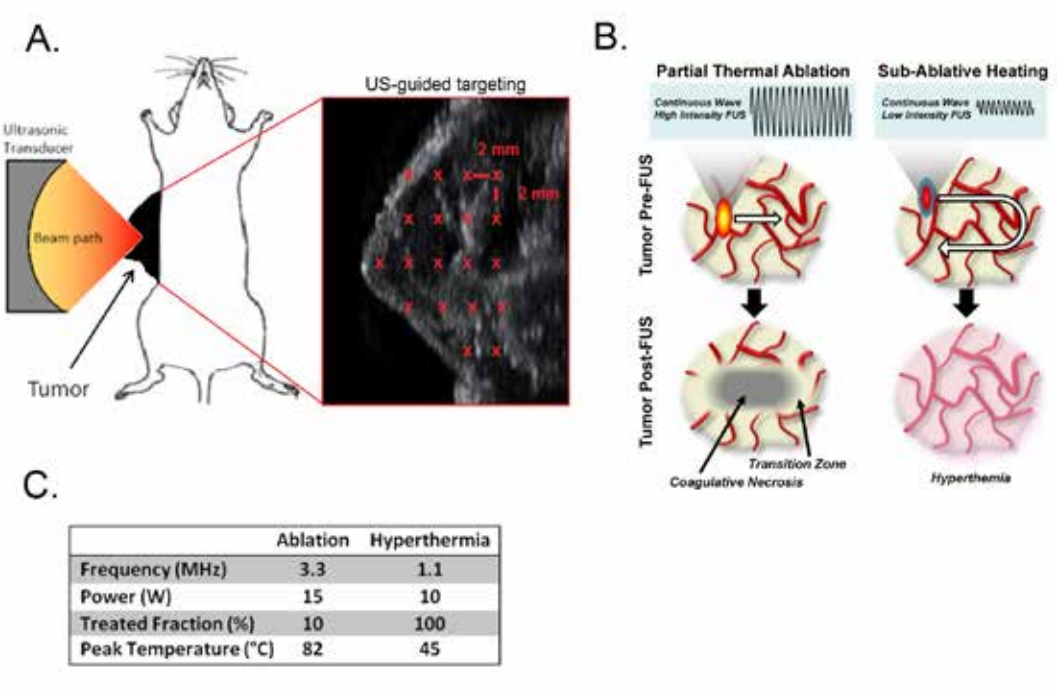

C.

	Ablation	Hyperthermia
Frequency (MHz)	3.3	1.1
Power (W)	15	10
Treated Fraction (%)	10	100
Peak Temperature (°C)	82	45

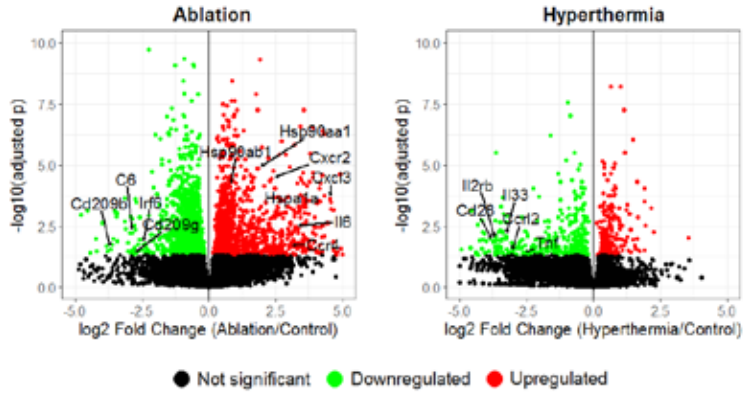

Figure 2. Volcano plots showing transcriptome changes induced by ablation and hyperthermia. Selected damage associated molecular patterns and immune markers are labeled.

Table 1. Selected Hallmark gene signatures either induced or downregulated by ablation and hyperthermia determined by GSEA with p value < 0.00001.

	Ablation		Hyperthermia	
	Hallmark Signature	-log10(p val)	Hallmark Signature	-log10(p val)
Induced	APOPTOSIS	9.20	UNFOLDED_PROTEIN_RESPONSE	9.84
	UV_RESPONSE_UP	7.80		
	TNFA_SIGNALING_VIA_NFKB	7.49		
	DNA_REPAIR	7.41		
	UNFOLDED_PROTEIN_RESPONSE	5.32		
Downregulated	GLYCOLYSIS	30.31	COMPLEMENT	14.17
	CHOLESTEROL_HOMEOSTASIS	26.78	INTERFERON_GAMMA_RESPONSE	13.01
	G2M_CHECKPOINT	25.13	TNFA_SIGNALING_VIA_NFKB	11.87
	MITOTIC_SPINDLE	22.18	INTERFERON_ALPHA_RESPONSE	9.98
	FATTY_ACID_METABOLISM	16.15	ALLOGRAFT_REJECTION	9.69
	ADIPOGENESIS	15.79	INFLAMMATORY_RESPONSE	9.69
	UV_RESPONSE_DN	9.27	IL2_STAT5_SIGNALING	8.64
	BILE_ACID_METABOLISM	8.74		
	UNFOLDED_PROTEIN_RESPONSE	7.84		
	HEME_METABOLISM	7.37		
	OXIDATIVE_PHOSPHORYLATION	6.72		

YI-12/P-YI-12

Tuesday

23 October 2018

Topic: Bone
Presentation Type: Oral; Poster

Treatment of painful bone tumors using MR-guided focused ultrasound with conformal bone system

Daniele Mercatelli[1], Chiara Gasperini[2], Maria Pilar Aparisi Gómez[3], Alessandro Napoli[4], Alberto Bazzocchi[5]

[1]Istituto Ortopedico Rizzoli, Bologna, Italy
[2]University of Bologna, Bologna, Italy
[3]Auckland City Hospital, Auckland, New Zealand
[4]Sapienza University of Rome, Rome, Italy
[5]IRCCS Istituto Ortopedico Rizzoli, Bologna, Italy

Background: Some bone lesions are difficult to treat with MR-guided Focused Ultrasound (MRgFUS) due to positioning problems and lesion accessibility to the ultrasound beam. The conformal bone system (CBS) developed by INSIGHTEC integrates new features for bone applications that could help interventional radiologists to treat bone lesions in locations that are difficult to reach using conventional MRgFUS systems or other devices. The aim of the present work is to report our experience in treating painful bone lesions using the CBS at the Rizzoli Orthopaedic Institute (IOR).

Methods: Ten patients with painful bone lesions were treated at IOR with MRgFUS using the CBS between 2013 and 2016. All patients suffered from painful bone metastases, except one, who was submitted to MRgFUS for osteoid osteoma. VAS scores were acquired at baseline and at 3 months after treatment. Adverse events (any untoward medical occurrence, unintended disease or injury or any untoward clinical signs in subjects, users or other persons whether or not related to the investigational medical device) were collected.

Results: Ten procedures were performed in 9 patients affected by painful bone metastases (8 males, 1 female; mean age 61 ± 19 years). Mean VAS at baseline was 5.4±2.4; at 6 months patients experienced a mean reduction in VAS score of 4.6 ± 3.1, except two patients: one patient, affected by a bone metastasis at the ischiopubic branch from colon cancer experienced progression of pain, and a patient with a lesion at the iliac wing had no pain improvement. A patient with a secondary lesion from prostate cancer at the proximal humerus was treated two times with MRgFUS, achieving a complete response in terms of VAS. A male patient (22 years old) presenting a painful osteoid osteoma at the first metatarsal bone (VAS at baseline: 2) was treated with the CBS. A complete relief from pain was achieved with a single MRgFUS treatment. No adverse events were reported.

Conclusions: MRgFUS with CBS is a safe and effective procedure for pain palliation in patients with bone lesions at locations not or not easily accessible with conventional MRgFUS systems. No adverse events were experienced.

Acknowledgements: This work has been supported by the "Programma di ricerca Regione-Università," Regione Emilia-Romagna, bando Giovani Ricercatori "Alessandro Liberati" 2013 to AB "Magnetic Resonance guided High Intensity Focused Ultrasound treatment of bone metastases: pain palliation, and local tumor control?"

Poster Abstracts

P-BR	Brain	208
P-CA	Cancer	250
P-MI	Miscellaneous Indications	273
P-MS	Musculoskeletal	295
P-WH	Women's Health	298
P-YI	Young Investigator	317

In accordance with author requests, the following abstracts are not included in this publication:

P-BR-34 P-BR-36 P-CA-2 P-MI-5

The following abstracts were withdrawn by the authors:

P-BR-9 P-BR-14 P-BR-39 P-CA-6 P-MI-18
P-BR-12 P-BR-24 P-CA-18 P-WH-7

P-BR-1

Topic: Brain
Presentation Type: Poster

In vitro/*in vivo* characterization of ultrasonic drug uncaging from phase change nanoparticles for neuromodulation

Muna Aryal, Jeffery Wang, Qian Zhong, Raag Airan

Stanford University, Stanford, California, United States

Current neuromodulation techniques suffer from invasiveness, limited tissue penetration, or limited spatiotemporal resolution. We have proposed that polymeric perfluorocarbon nanoemulsions can be used to uncage neuromodulatory drugs with focused ultrasound (FUS), enabling noninvasive pharmacological neuromodulation. Here, we present an improved synthesis of phase-change polymeric nanoparticles that encapsulated the small molecule anesthetic propofol. We report the *in vitro* drug release threshold at different ultrasonic parameters and show that these particles can be used for spatially and temporally resolved noninvasive neuromodulation with ultrasonic propofol uncaging in rats.

We synthesized phase-change nanoparticles (1 mg/kg propofol encapsulated in poly (ethylene glycol) - poly(lactide-co-glycolic) acid PEG: PLGA, mol. wt. 2 kDa: 5 kDa), with a perfluoropentane core by sonication and membrane extrusion methods. We used dynamic light scattering (DLS) to measure polydispersity, particle size, and stability and also measured the total drug loading. We also determined the *in vitro* drug release thresholds. We used visual evoked potentials (VEPs) to determine the temporal kinetics and dose-response relationship of the neuromodulatory effect *in vivo*. Visual evoked potentials were recorded from subdural electrodes implanted in male Long-Evans rats (~200gm). FUS (650 kHz, 1 Hz burst frequency) was used while varying in-situ pressure, burst length, and the brain target.

With DLS, Z-averaged diameter was 397.3 ± 10.0 nm, with polydispersity index of 0.068 ± 0.023, zeta potential of -26.7 ± 0.6 mV, and drug loading of 1.19% of nanoparticle weight. The nanoparticles uncaged propofol with an estimated *in vitro* pressure threshold of 0.8 MPa with 650 kHz sonication, with uncaging efficacy increasing with both sonication pressure and burst length. Percentage change of the N1P1 VEP amplitude was measured before, during, and after ultrasonic drug uncaging after administration of nanoparticle-encapsulated propofol (1 mg/kg) *versus* blank nanoparticles. With visual cortex (V1) sonication, VEPs were attenuated by 15±5% and 34±10% with 1.2 and 1.8 MPa peak FUS pressure, respectively (Fig.1). VEPs were attenuated by 13±8%, 15±5%, and 27±8%, with 10, 50, and 100ms ultrasound bursts, respectively at 1.2 MPa (Fig.B). While sonicating lateral geniculate nucleus (LGN), VEPs were attenuation by 9±3%, but were not attenuated at motor cortex (M1, Fig.B). The temporal kinetics of these effects had half-lives of 8.8-14.8 sec.

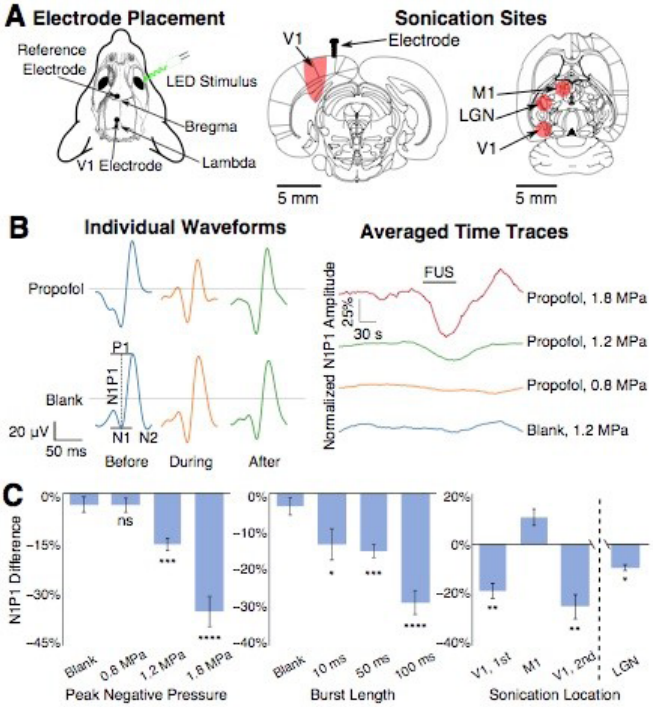

This work establishes that noninvasive pharmacological neuromodulation with ultrasonic drug uncaging is temporally precise with respect to sonication, with dose-response relationships with sonication pressure and burst length, and with spatial specificity to the sonicating site. Data presented as mean +/- S.E.M., N=5-10. ns: not significant; *: $p<0.05$, **: $p<0.01$, ***: $p<0.001$; ****: $p<0.0001$ by two-tailed t-tests.

Figure 1. (A) Schematic of recording electrode placement (left) and sonication sites (right), represented by the expected full-width half-maximum of the ultrasound field in each location. (B-C) Dose-response relationship and spatial specificity of the ultrasonication site

P-BR-2

Topic: Brain
Presentation Type: Poster

Kranion: A tool for transcranial focused ultrasound surgical analysis

Dylan Beam[1], Francesco Sammartino[1], John Snell[2], Vibhor Krishna[1]

[1]Ohio State University, Columbus, Ohio, United States
[2]Focused Ultrasound Foundation, Charlottesville, Virginia, United States

Background: Transcranial focused ultrasound (FUS) ablation is an emerging incision-less treatment option for patients with movement disorders such as Essential Tremor (ET) and Parkinsons' Disease (PD). Several technical challenges currently limit the efficiency and broader applications of this technology, including the inherent complexities of the physics that govern the interactions between ultrasound waves and biological tissues. Here we introduce a new software, Kranion, developed by Dr. John Snell at the FUS Foundation. This is an open-source software that allows the user to simulate the planning stages of FUS treatment, and to 'replay' FUS treatment for offline analysis. Using Kranion, we investigated the predictors of ultrasound penetration through the skull and created a new metric to estimate the energy penetration through the skull during FUS treatment (Beam Value). This metric was then used to predict the average temperature rise for individual sonications.

Methods: Anonymized head CT DICOM images from 28 subjects evaluated for FUS ablation for ET or PD were analyzed. Kranion was used to simulate treatment at 4 different common FUS targets (Ventral Intermediate Nucleus, Globus Pallidus pars Interna, Anterior Thalamic Nucleus, and Nucleus Accumbens) bilaterally. For each target within each subject, individual transducer element incident angles, SDR, skull thickness measurements, and distance traveled by the ultrasound beam were recorded. The Beam Value was calculated for each treatment dataset by combining the energy loss from incident angles of ultrasound beams and skull thickness values. Two-sample t-tests were used to compare datasets, and a linear-mixed-effects model was used to predict the temperature rise during treatment using the Beam Value and energy output from the system as covariates.

Results: There were no significant differences between the standard of care and Kranion calculated SDR values ($p=0.7895$), and number of effective elements (incident angle $< 20°$) ($p=0.075$). SDR estimation changed with the variation of CT bone filter. The mean and median SDR values did not change significantly between targets as expected.

Beam Value significantly varied between targets reflecting the energy penetration percentage at different locations in the treatment envelope. For example, Beam Value was significantly lower in the anterior (e.g. nucleus accumbens) and lateral targets (e.g. globus pallidus). We were able to predict the average temperature rise at the focal point during ablation within 21% error or less ($55\pm3.8°C$) in 75% of sonications, and within 44% error or less ($55\pm7.9°C$) in 97% of sonications.

Conclusions: Kranion can provide accurate and realistic measures of skull and treatment parameters that are useful for planning transcranial FUS procedures. The novel penetration metric suggests that utilization of other skull parameters, in addition to SDR, may be effective in estimating the efficiency of FUS treatments.

P-BR-3

Topic: Brain
Presentation Type: Poster

A pre-clinical HIFU system with integrated passive cavitation mapping for investigating the pharmacokinetics and pharmacodynamics of drug delivery by FUS-mediated blood-brain barrier disruption (BBBD)

Adam Canfield, P. Jason White

Brigham and Women's Hospital, Harvard Medical School, Boston, Massachusetts, United States

Background: High-intensity focused ultrasound (HIFU) has been shown to elicit temporary blood-brain barrier disruption (BBBD), an effect that could allow for effective drug delivery into the brain parenchyma. As HIFU-mediated BBBD has entered into clinical studies, the detailed relationship between cavitation levels and subsequent pharmacodynamics/pharmacokinetics requires detailed investigation. Currently, tools for this level of investigation are not available.

Methods: We designed, constructed, and tested a HIFU transducer that incorporates an ultrasound imaging array for monitoring and tracking the level and location of HIFU-induced intracranial cavitation. We considered each of three commercial imaging probes and the implications of their integration into the device: a 2-D phased array (ATL P4-2, Philips Healthcare, Bothell, WA) and two linear arrays (ATL L12-5 and ATL L7-4, Philips Healthcare, Bothell, WA). Specifically, we optimized between imaging efficacy and therapy transducer surface area. To allow for co-registered operation, we placed a port at the central axis of the HIFU transducer to allow for the insertion of the 2-D phases array to effectively detect and map cavitation activity at the focal target. The HIFU transducer was air-backed in an acrylic housing, impedance matched, characterized, and calibrated. To ready the system for experiments, the combined HIFU transducer and imaging probe were characterized, calibrated, and tested with *in vivo* animal models.

Results: The surface area loss of the HIFU transducer was calculated for multiple scenarios to determine the optimal size of the port for the imaging probe. We assessed three different probe geometries and determined that the 2-D phased array resulted in the least amount of surface area loss (18.35%), as opposed to the linear arrays (29.14% and 30.48%, respectively). The demonstration of effective cavitation detection while performing ultrasound- and microbubble-mediated BBBD established a device that is ready for continued *in vivo* experiments.

Conclusions: We have designed, constructed, and tested a pre-clinical HIFU system that enables us to better investigate effects of ultrasound-mediated BBBD as it is related to localized cavitation activity.

P-BR-4

Topic: Brain
Presentation Type: Poster

Feasibility of brain temperature estimation during HIFU procedures using temporal derivatives of the ultrasonic attenuation coefficient

Daniel Dahis, Haim Azhari

Technion Institute of Technology, Haifa, Israel

Background: Noninvasive intracranial treatments using high intensity focused ultrasound (HIFU) are on the course of translation into clinical applications. They include, among others, tumor ablation, hyperthermia, blood-brain-barrier (BBB) penetration and neuromodulation. For safety and efficacy, thermal monitoring is essential. MRI is the currently leading modality for temperature mapping. Nevertheless, MRI is an expensive non-portable modality with limited accessibility. Ultrasonic thermal monitoring, on the other hand, could provide a modular cost-effective alternative with higher temporal resolution and accessibility. Previous studies have suggested various methods for ultrasonic thermometry at different body locations. However, ultrasonic brain monitoring techniques are relatively scarce. Although brain ultrasonic attenuation as a function of temperature has been investigated, to the best of our knowledge, no proposed method utilizes the time related attenuation changes for brain temperature estimation. In order to assess the feasibility of ultrasonic brain thermal monitoring, this study investigated the usage of brain tissue attenuation coefficient (AC) temporal changes.

Methods: Newton's Law of Cooling describes a temporal exponential decay behavior for the temperature of a heated object immersed in a relatively colder surrounding. Accordingly, in the case of cerebral HIFU treatments, the temperature in the region of interest, i.e. focal zone, during the cooling phase following acoustic energy deposition, is expected to also present a characteristic time related pattern. In addition, the AC of the irradiated tissue is hypothesized to follow a similar temporal exponential behavior during the cooling stage. Thus, in this work, it is suggested that the encephalic thermal changes may be assessed by analyzing the time-related AC changes. Three *ex vivo* bovine brain tissue specimens were inserted into plastic containers along with four thermocouple probes in each sample. The containers were placed inside a specially built ultrasonic tomographic scanner and scanned at room temperature. The corresponding pixel-averaged AC was acquired for each specimen and used as a reference. Subsequently, the containers were placed in a beaker containing hot water and gradually heated to about 45oC. They were then repeatedly rescanned during cool down using ultrasonic through-transmission raster until reaching about 30oC. From the obtained images, the normalized AC temporal trajectories and their derivatives as a function of temperature and time were registered.

Results: The results have demonstrated high correlation ($R2 > 0.95$) between the AC temporal derivative and temperature (Figure 1). This indicates the validity of the hypothesis and the possibility of obtaining noninvasive brain tissue temperature estimation from the temporal AC thermal changes. It is important to note that each brain yielded different AC values and slopes. This implies a required calibration step for each specimen.

Figure 1

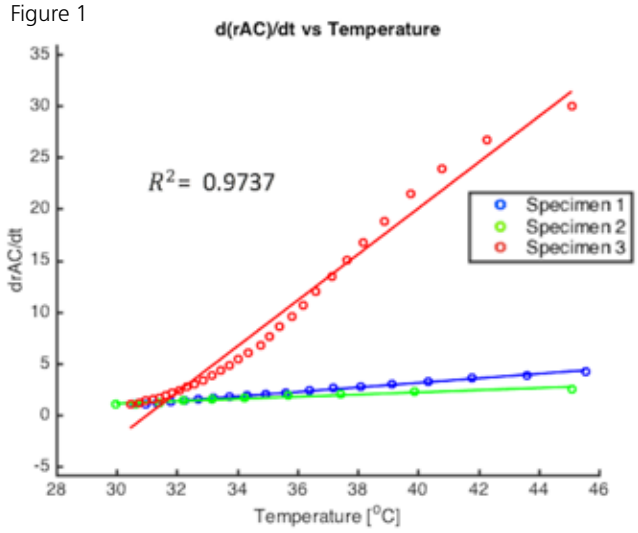

Conclusions: A three step strategy for thermal monitoring of the brain, is suggested. The first step consists of simply estimating the AC at the focal zone at normal body temperature. The second step is to induce a small temperature elevation. The third step entails measuring the normalized AC trajectory as a function of time and estimating the temperature.

P-BR-5

Topic: Brain
Presentation Type: Poster

Novel MRI guided focused ultrasound positioning devices for small animals

Christakis Damianou[1], Marinos Giannakou[2], Georgios Menikou[1]

[1]Cyprus University of Technology, Limassol, Cyprus
[2]University of Cyprus, Limassol, Cyprus

Background: MRI-guided focused ultrasound (MRgFUS) positioning devices were developed that can be used for small animal experiments. One positioning device is dedicated for prostate ablation. The second device is for application in the abdominal area and brain (animal is in supine position). The third positioning device is for small animals (mice and rats) and can be integrated in a 9.4 T MRI system.

Methods: A single element spherically focused transducer of 5 cm diameter, focusing at 10 cm and operating at 0.5 MHz was used. The positioning devices incorporate only MRI compatible materials. The propagation of ultrasound is bottom to top, top to bottom or lateral.

Results: The system was tested successfully in agar/silica/evaporated milk phantoms, in mice and rabbits for various tasks using MR thermometry.

Conclusions: These positioning devices have the potential to be marketed as cost effective solutions for performing experiments in small animals. With minimum changes the positioning devices can be converted into devices for performing interventions with focused ultrasound in humans in the brain, thyroid, abdominal area and breast.

P-BR-6

Topic: Brain
Presentation Type: Poster

Trans-cranial magnetic resonance-guided focused ultrasound (tcMRgFUS) system integrated with a 1.5T: An SNR study on DQA phantoms

Cesare Gagliardo[1], Giorgio Collura[1], Maurizio Marrale[1], Alessandro Napoli[2], Tommaso Vincenzo Bartolotta[1], Carlo Catalano[2], Massimo Midiri[3]

[1]University of Palermo, Palermo, Italy
[2]Sapienza University of Rome, Rome, Italy
[3]Universita Degli Studi Di Palermo, Palermo, Italy

Background: In recent years transcranial Magnetic Resonance-guided Focused Ultrasound Surgery (tcMRgFUS) treatments have been performed only using 3T units. Since following some internal analysis, planning images obtained using a 1.5T MRI's body RF coil (as usually done with 3T systems) showed generally reasonable quality in terms of anatomy visualization and SNR but thermal images noise was above acceptable standard for treatments, a dedicated 2-channels head coil was developed (INSIGHTEC Ltd.) to ensure an adequate signal-to-noise ratio (SNR). Hence, we present the imaging protocol and the technological methods successfully used with the world-first installation of a certified tcMRgFUS system (ExAblate 4000, INSIGHTEC Ltd.) integrated with a 1.5T scanner (Signa HDxt, GE Medical Systems).

Methods: We used the NEMA (2008) test methods for measuring the SNR of both MRI's body RF coil and the dedicated coil. T2w-FRFSE images were obtained from a dedicated tcMRgFUS daily quality assurance (DQA) phantom using the same MRI protocol subsequently used for real treatments planning.

Results: Compared to that achieved using MRI's body RF coil, the dedicated coil resulted in significantly larger values of the SNR on all planes. In particular, for the axial plane, using the body RF coil we measured a SNR equal to 2.5, 5.1 and 6.0 at 1, 4 and 6 NEXs respectively whereas it was equal to 27.5, 51.5 and 67.3 when using the dedicated 2-ch head coil: therefore, an increase of more than 10 times was achieved. For the coronal and the sagittal planes, we measured a gain of about 6 and 3 times respectively.

Conclusions: Even though the SNR linearly increases with magnetic field strength, it should be underlined that on a 1.5T scanner the use of a dedicated coil enabled us to obtain images with a SNR roughly 5 times larger than those acquired on 3T scanners using MRI's body RF coil.

Acknowledgements: The installation of the tcMRgFUS equipment used in this work was funded by the Italian Ministry of Education, University and Research (MIUR) within the project "Programma Operativo Nazionale 2007-3013" (PONa3_00011; Project Leader: Prof. Carlo Catalano).

P-BR-7

Topic: Brain
Presentation Type: Poster

Thalamic parcellation for target identification in trans-cranial MR-guided focused ultrasound (tcMRgFUS) thalamotomies: A preliminary probabilistc tractography study

Cesare Gagliardo[1], Giorgio Collura[1], Maurizio Marrale[1], Alessandro Napoli[2], Marco D'Amelio[1], Domenico Gerardo[1], Carlo Catalano[2], Massimo Midiri[3], Roberto Lagalla[1]

[1]University of Palermo, Palermo, Italy
[2]Sapienza University of Rome, Rome, Italy
[3]Universita Degli Studi Di Palermo, Palermo, Italy

Background: Trans-cranial MR-guided Focused UltraSound (tcMRgFUS) allows a neurofunctional exploration of thalamic nuclei to confirm and optimize the target before inducing a permanent brain lesion. However, the choice of the target is based on stereotactic coordinates that do not take into account the anatomical variability of each single patient. Thus, the optimization of the treatment target is based on the patient's feedback during lower power sonications. The aim of this work is to retrospectively evaluate the possible role of thalamic parcellation for the identification of the intermediate ventral nucleus (VIM) in patients undergoing tcMRgFUS.

Methods: A 1.5T MR scanner (GE Signa HDxt) was used to acquire morphological (3D-FSPGR T1w) and ultrastructural morphological sequences (Diffusion Tensor Imaging) in patients that subsequently underwent tcMRgFUS thalamotmy. A segmentation of the eloquent cerebral areas was then used as seed for a probabilistic tractography algorithm aimed at representing the cortical projections to and from the thalamus with particular reference to the primary and supplementary motor areas and the premotor cortex. The thalamic parcellation maps obtained were then compared with tcMRgFUS induced lesions.

Results: In all cases it was possible to represent the major groups of thalamic nuclei that receive from or project towards brain cortex. It was possible to identify a good overlap between the thalamic parcellation maps thus obtained (with particular reference to the VIM nucleus) and the lesions induced by tcMRgFUS.

Conclusions: These preliminary results are very encouraging. Even if the requested pre- and post-processing pipeline behind such an innovative approach are still extremely complex and time consuming, the use of such a technique could result very helpful during tcMRgFUS treatment target optimization, especially in that cases where the optimal treatment target does not perfectly match conventional stereotactic coordinates.

Acknowledgements: The installation of the tcMRgFUS equipment used in this work was funded by the Italian Ministry of Education, University and Research (MIUR) within the project "Programma Operativo Nazionale 2007-3013" (PONa3_00011; Project Leader: Prof. Carlo Catalano). The research leading to these results has received funding from the Italian Ministry of Health's "Ricerca Finalizzata 2016" (GR-2016-02364526; Principal Investigator: Dr. Cesare Gagliardo).

P-BR-8

Topic: Brain
Presentation Type: Poster

Evaluation of DCE-MRI as a correlate for antibody delivery outcomes in a murine glioma model

Maeghan Garrison, William Garrison, Natasha Sheybani, Richard Price, G. Wilson Miller

University of Virginia, Charlottesville, Virginia, United States

Background: The ability to perform image-based assessments of treatment efficacy is an important component of a clinically-relevant focused ultrasound (FUS) treatment regimen. In this work, we intend to assess dynamic contrast-enhanced MRI (DCE-MRI) as a benchmark for antibody delivery efficacy in the context of FUS-modulated antibody delivery to intracranial murine glioma. We will perform this work with an eye toward identifying a mathematical relationship between Ktrans, a quantitative DCE-MRI output characterizing the rate of contrast agent transfer across the capillary endothelium, and antibody delivery outcomes. Demonstration of such a relationship could indicate a potential role for DCE-MRI as a clinical indicator of treatment efficacy in the context of FUS-modulated antibody delivery to glioma.

Methods: GL261-luc2 glioma cells will be implanted into the right striatum of syngeneic C57BL/6 mice. Two weeks following inoculation, tumor-bearing mice will be coupled to an MR-compatible 1.1 MHz FUS transducer for treatment. FUS treatments will consist of intravenous injection of albumin-shelled microbubbles and fluorescently labeled αGLAST (glutamate aspartate transporter; an extracellular surface marker of astrocytes within the CNS), followed by targeted blood-brain/blood-tumor barrier (BBB/BTB) opening. Treatments will be performed using peak-negative pressures (PNPs) ranging from 0.4-0.8 MPa. DCE-MRI will be performed immediately after FUS-modulated BBB/BTB opening. The DCE imaging will be performed continuously over a span of 10 minutes, with a gadolinium-based contrast agent injected 30 seconds after the start of imaging. Brains will be excised between 4 and 24 hours after antibody delivery for both flow cytometry and immunofluorescence staining to ascertain changes in intensity and spatial localization of GLAST staining on astrocytes. DCE-MRI image series will be analyzed using standard methods, and the volume transfer coefficient Ktrans will be extracted for each animal. Ktrans values will then be benchmarked to quantitation of GLAST staining.

Results: We hope to show that there is a quantifiable relationship between degree of BBB/BTB permeabilization conferred by discrete FUS PNPs as measured by Ktrans and antibody penetration in glioma. We will describe the functional form of the relationship, and its goodness-of-fit to the acquired data.

Conclusions: We hope to successfully demonstrate a relationship between quantitative DCE-MRI results and antibody delivery efficacy as a prelude to immunotherapeutic antibody delivery to glioma. This study will enable a framework for understanding the relationship between FUS BBB/BTB disruption PNP and antibody delivery/penetration in glioma. Findings indicating that Ktrans values can be used to benchmark this relationship could potentiate DCE-MRI as an accessible clinical strategy for assessing glioma treatment efficacy in the context of FUS-modulated immunotherapeutic antibody delivery.

Acknowledgements: This work was supported by the FUS Foundation Global Internship Program.

P-BR-10

Topic: Brain
Presentation Type: Poster

Ray-based phase correction using Kranion software for transcranial focused ultrasound on a clinical system

Changzhu Jin[1], Dave Moore[2], John Snell[2], Juyoung Park[1], Dong-Guk Paeng[3]

[1]Daegu-Gyeongbuk Medical Innovation Foundation, Daegu, South Korea
[2]Focused Ultrasound Foundation, Charlottesville, Virginia, United States
[3]Jeju National University of Korea, Jeju City, South Korea

Background: The numerical compensation of skull bone induced phase aberration significantly recover the focal quality in the transcranial focused ultrasound. In spite of the high accuracy of a full wave simulation approach, it is not feasible for this technology to be adopted in a clinical environment because of long computation time. A clinical system compatible rapid phase correction software was developed in this study based on ray tracing.

Methods: A visualization platform utilizing the Open Graphics Library was constructed to visualize and registrat the array transducer (650 kHz transducer, INSIGHTEC, Israel) with the patient anatomy which rendered from prior medical imaging. A two-layered medium approach was applied to account the refraction of transmitting longitudinal wave on water-to-skull and skull-to-brain boundaries. The length of the beam trapped in between outer skull and inner skull layer was collected to calculate the phase delay. An average speed of sound (2900 m/s) on skull bone was utilized. The corrected phase from 1024 elements was saved in a local phase correction file and feed in the controller PC of The clinical system (ExAblate 4000, INSIGHTEC, Israel). Needle hydrophone based transcranial pressure field scanning was applied to measure the transcranial focal point shift on three collected human skull caps.

Results: The comparison of corrected focal quality based on clinical system software and proposed ray method were presented. An averaged focal shift of 0.44±0.5 mm, 0.34±0.37 mm and 0.17±0.15 mm corresponding to without correction, ExAblate based correction and Kranion based correction were comparable. Both ExAblate and Kranion correction were improved the level of peak pressure by 152.8±29.7 % and 140.5±17.0 %.

Conclusions: This suggest that the ray-based phase correction by using Kranion software could compensate the skull aberration on the clinical environment with a faster visualization and comparable refocusing performance.

P-BR-11

Topic: Brain
Presentation Type: Poster

Factors related to successful energy transmission of focused ultrasound through a skull: A study in human cadavers and its comparison with clinical experiences

Na Young Jung, Jin Woo Chang

Yonsei University College of Medicine, Seoul, Korea

Background: Although magnetic resonance guided focused ultrasound (MRgFUS) has been used as minimally invasive and effective neurosurgical treatment for several neurological disorders, it exhibits some limitations, mainly related to acoustic properties of the skull barrier. This study was undertaken to identify skull characteristics that contribute to optimal ultrasonic energy transmission, using *ex vivo* skulls and patient skull analyses.

Methods: For *ex vivo* skull experiments, various acoustic fields were measured under different conditions, using five non-embalmed cadaver skulls in our institute, corroborating with Department of Anatomy. For patient skull analyses, brain computed tomography data of 46 patients who underwent MRgFUS ablation at Severance Hospital were retrospectively reviewed. Clinical sonication data comprised the following procedures: 18 unilateral thalamotomy, nine unilateral pallidotomy, and 19 bilateral capsulotomy. Patients` skull factors and sonication parameters were comparatively analyzed with respect to the cadaveric skulls.

Results: We identified three important factors related skull penetration of ultrasound in skull experiments, including skull density ratio (SDR), skull volume, and incidence angle of ultrasonic energy. In clinical analysis, SDR positively correlated with acoustic transmission and maximal temperature, whereas it negatively correlated with energy requirement to achieve peak temperature. Skull volume negatively correlated with maximal temperature ($p=0.043$) and energy requirement to achieve peak temperature ($p=0.045$). Incidence angle of ultrasonic energy, determined by brain target location, was crucial for successful and effective sonication. Less energy was required to reach peak temperature in the central, rather than lateral targets, particularly when compared between thalamotomy and capsulotomy ($p=0.015$).

Conclusions: This study reconfirmed previously identified skull factors, including SDR and skull volume, for successful MRgFUS; it identified an additional factor, incidence angle of acoustic rays against the skull surface, for effective MRgFUS. To guarantee successful MRgFUS treatment for all neurological disorders without suffering these various skull issues, further technical improvements are required.

Acknowledgements: This study was made possible with funding from the Michael J. Fox Foundation (New York, USA) and the Focused Ultrasound Surgery Foundation (Virginia, USA).

P-BR-13

Topic: Brain
Presentation Type: Poster

Transcranial ultrasound focusing using customizable printed lenses

Graham Keeley, Matt Eames, Dave Moore, John Snell, Neal Kassell

Focused Ultrasound Foundation, Charlottesville, Virginia, United States

Background: Phased array ultrasound transducers currently approved for select non-invasive neurosurgical applications are made with costly electronic systems that enable per-element phase delay to account for variations in skull thickness. We propose a low-cost, per-treatment disposable as a potential alternative. We demonstrate here a direct-3D-printed acoustic lens that could be designed for a given patient's skull. Such lenses would conform to the inside of the transducer array and vary in thickness over the transducer surface. Based on the speed of sound of the printed material, the thickness of 3D printed plastic would be designed to induce the phase delays currently generated by the system electronics for skull aberration correction. If this method proves comparable to the current phase-delay approach, it could enable the use of less expensive single-element transducers for transcranial application of focused ultrasound.

Methods: An *ex vivo* skull CT was used to calculate phase delay data for a 650 kHz INSIGHTEC Neuravive transducer. The speed of sound of Vero White resin material printed with a Connex3 Objet 500 PolyJet 3D printer (Stratasys, Eden Prairie, MN) at the University of Virginia Rapid Prototyping Lab was measured using an unfocused, single-element transducer (SonicConcepts, Bothell, WA) and a custom hydrophone. The lens was 3D printed (figure 1) using the data from the transducer elements in the bottom 12mm of the array. The lens was then placed in the transducer array with a mounted skull and the resulting focus was measured with needle hydrophone (ONDA Corp., Sunnyvale, CA) scans.

Results: Hydrophone scans in the XY and XZ plane were taken in three configurations: without transducer phase correction, with phase correction, and without phase correction with the lens in place. All of the scans were taken with the skull mounted between the transducer and the hydrophone. The XY scan with no phase correction resulted in a focus 2mm to the left of the natural focus with a full width at half max (FWHM) of 16.5mm. The XY scan with phase correction resulted in a focus 6mm to the right of the natural focus with a FWHM of 16mm. The XY scan with no phase correction and the lens in place resulted in a focus 2mm to the left of the natural focus with a FWHM of 11mm (figure 2). In the XZ scans, the focus was in the center with a FWHM of 15mm in the scan without phase corrections, shifted to the right with a FWHM of 17mm in the scan with phase corrections, and centered with a FWHM of 10mm in the scan with the lens (figure 3).

Conclusions: These preliminary results show that the printed lens created a sharper focus through the skull as compared to the uncorrected and electronically corrected sonications. The lens, however, only covered a small portion of the transducer elements. Further tests with lenses that cover every element of the transducer array should be performed to validate the results obtained with the current, smaller lens.

Figure 1. A top view of the printed lens

Figure 2. XY Scans in each of the three transducer configurations. Each scan is sliced at the horizontal axis where it reaches its highest pressure and graphed.

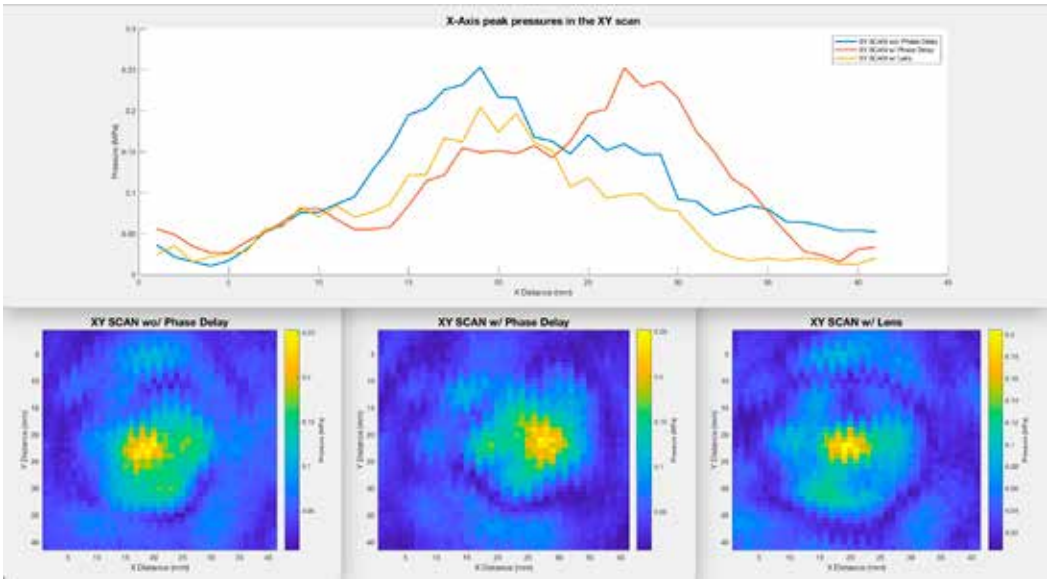

Figure 3. XZ Scans in each of the three transducer configurations. Each scan is sliced at both the horizontal and vertical axis where it reaches its highest pressure and graphed.

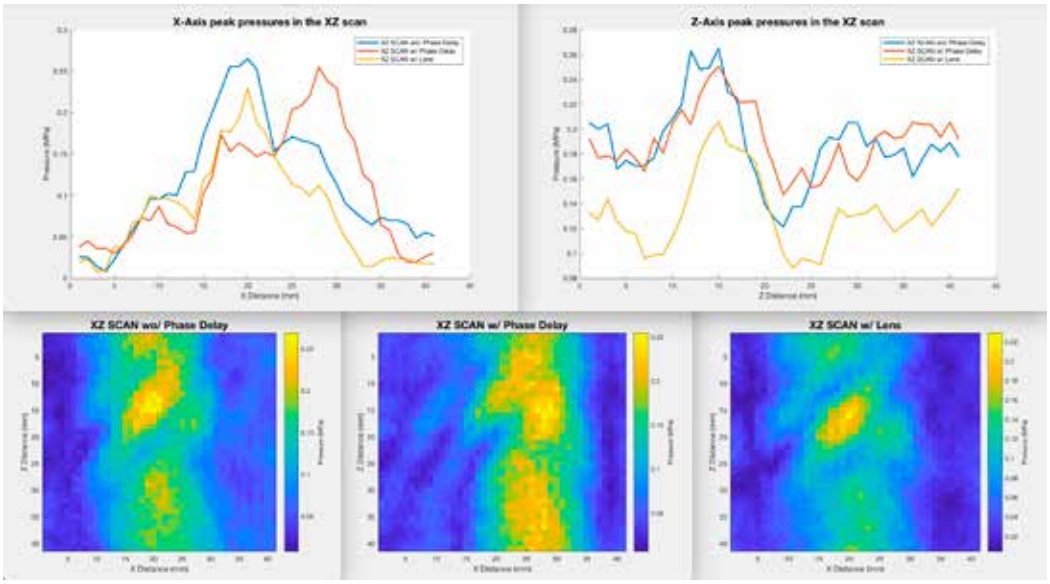

P-BR-15

Topic: Brain
Presentation Type: Poster

Simulation of ultrasound propagation through human skull: Parametric study to investigate the acoustical properties of the skull

Frédéric Padilla[1,2,3,4], Raphaël Loyet[1,2], David Moore[3], Achour Ouaked[1,2], John Snell[3,4], Matt Eames[3,4], Sylvain Chatillon[5], Cyril Lafon[1,2,3,4]

[1]LabTAU, Inserm, Lyon, France
[2]University of Lyon, Lyon, France
[3]Focused Ultrasound Foundation, Charlottesville, Virginia, United States
[4]University of Virginia School of Medicine, Charlottesville, Virginia, United States
[5]CEA, LIST, Gif-sur-Yvette, France

Transcranial focused ultrasound (FUS) is a non-invasive therapeutic modality that can be used to treat essential tremor via local thermal ablation of a small volume in the thalamus. Acoustic energy is focused through the skull using a multi-element transducer. Per-element phase delay is derived using individual patient's skull CT to compensate for skull heterogeneity, but MRI thermometry is still required for precise targeting and localization of the focal spot.

An accurate simulation system would help to improve the refocusing of the beam in the targeted zones. Here, we report a parametric study that aims to evaluate the acoustical parameters to be used in such a simulation (attenuation, speed of sound and density). The simulations are based on a pencil tracing algorithms developed in the CIVA Healthcare platform. Those algorithms, have the ability to simulate the linear propagation in heterogeneous anisotropic mediums, as well as transverse / shear wave conversions. The thermal propagation is simulated using a finite volume solver of Penne's BioHeat Transfer Equation. The parametric study will be compared to measurements performed on an ExAblate Neuro 650 kHz (INSIGHTEC) clinical system with acoustic signals acquired with a hydrophone and MRI thermometry.

Acknowledgements: CIVA Healthcare platform supported by French Nation Research Agency (ANR SATURN -15-CE19-0016)]. Project supported by FUS Foundation.

P-BR-16

Topic: Brain
Presentation Type: Poster

Pseudo-random gated sonications for reducing cavitation during thermal ablations in the brain

Frederic Padilla[1,2,3,4], David Moore[3], Matthew Eames[3,4], John Snell[3,4], Cyril Lafon[1,2,3,4]

[1]LabTAU, Inserm, Lyon, France
[2]University of Lyon, Lyon, France
[3]Focused Ultrasound Foundation, Charlottesville, Virginia, United States
[4]University of Virginia School of Medicine, Charlottesville, Virginia, United States

Background: Transcranial HIFU is a clinically approved modality for treatment of essential tremor, and under clinical trials several other brain disorders. In some instances however, HIFU-induced thermal ablation in the brain requires high energy can resulting in undesired cavitation and potential side effects. We present a study aiming at: 1- to evaluate the potential of pseudo-random gated sonications, as compared to conventional CW exposure, to increase the cavitation threshold, and 2- to assess the heating and steering capabilities with such sonications.

Methods: The experiments were performed with the transcranial MR-compatible ExAblate Neuro system (INSIGHTEC). It is a 1024-element, 30 cm diameter, 15 cm focal length, transducer operating at a frequency of 660 kHz. Transducer efficiency and delivered acoustic power were measured with a radiation force balance. Four methods of sonication were compared: continuous wave (CW), gated emissions with pseudo-random 2 ms (p-Rand2ms) or 33 us (p-Rand33us) -period codes and 30 kHz square (Squ30kHz). The duty cycle (DC) was set to 50% for the gated sonications.

First, cavitation threshold was evaluated by increasing electrical driving power was increased step by step from 20 to 500W, and recording the acoustical noise with integrated passive cavitation detectors. The spectral energy was averaged over a subharmonic and the sonication duration. Secondly, heating experiments were performed in a hydrogel tissue mimicking material (TMM, ATS Laboratories). The electrical power was set to 15, 30 or 60 W, the exposure duration to 9 or 18 s. For comparison with CW, 50% DC gated sonications had either the electrical power or the exposure duration doubled. The temperature was measured by MR-thermometry when focusing at the geometrical focus and when steering the beam off-focus by 5mm-steps.

Results: Among the tested gates, 2ms period pseudo-random codes seem to be the modulation that increases the cavitation threshold the most while preserving heating capabilities. Indeed, very fast switches may be associated to electronic difficulties for non-demonstrated benefit in terms of cavitation reduction. The settings used did not allow to heat the TMM when electronically steering the focus more than 15mm-off the geometrical focus. Doubling the exposure duration did not allow to compensate the 50% DC because of thermal diffusion. At a power of 30W, a maximal temperature rise of 9°C was measured with gated sonications applied for 18s while CW 30W sonication for 9 s gave a 13°C increase in temperature. However, the heating patterns obtained at 60W with p-Rand2ms and 30 W in CW were very similar for a constant 9s duration. For the same conditions, lower temperature rises were measured for p-Rand33us and Squ30kHz. Several assumptions can be made to explain this difference: the gating is too rapid for reaching steady state, the amplifier struggles to switch so quickly, or cavitation enhanced heating is reduced.

Acknowledgements: Work sponsored by the FUS Foundation through the Robert Merkin Fellowship and performed with the technical support of INSIGHTEC.

P-BR-17

Topic: Brain
Presentation Type: Poster

Automatic focused ultrasound system for targeted drug delivery in central nervous system

Hohyun Lee[1], Scott Schoen[1], Costas Arvanitis[1,2]

[1]Georgia Institute of Technology, Atlanta, Georgia, United States
[2]Emory University, Atlanta, Georgia, United States

Background: Blood-brain barrier (BBB) opening with focused ultrasound (FUS) and microbubbles is a promising drug delivery strategy for treatment of neurological diseases such as Parkinson's, Alzheimer's, and brain cancer. Magnetic resonance imaging–guided FUS (MRIgFUS) has been the gold standard for this procedure due to its high image quality, which provides the ability to target regions of the brain with high precision. However, widespread use of this technology in both preclinical and clinical settings is hindered due to its high-cost and lack of portability. Ultrasound-guided FUS (USgFUS) systems have potential to address these limitations. Here, with the implementation of FUS and MATLAB algorithm, we attempt to replicate the functionality of MIRgFUS systems with the design of an automatic USgFUS system with capability of more cost-effective imaging and therapy.

Methods: The designed system comprises i) 3D positioning system, ii) imaging probe, iii) FUS transducer, iv) digital oscilloscope, v) pulser/receiver, vi) and a power amplifier. The system first operates in imaging mode: it creates an arbitrary grid around the object to be scanned (a rodent skull was used), and, with the aid of 3D positioning system performs a pulse and receive sequence at each of the grid points. The recorded echoes are then analyzed with cross-correlation method to calculate the ultrasound time of flight, from which the height of each grid points is computed. Next, all grid points are plotted with MATLAB after median filtering. Finally, the system uses the location of bregma and mouse brain atlas to position the FUS transducer for therapy mode. For the registration process of locating bregma, the system follows the same imaging procedure, but with a small reflector (1 mm) on the bregma. With Canny edge detection and centroid calculation, the two centroids (those of the skull and the reflector) are calculated. After undergoing 10 imaging processes, the distance between bregma and centroid of skull is calculated; in this way the bregma is able to be located without the reflector. Using the mouse atlas and estimated location of bregma, the system then moves FUS transducer to a desired location, for microbubble disruption.

Results: A rodent skull was scanned in 3 cm x 3 cm grid with step size of 1 mm. For the specific type and size of the scanned skull, the distance from centroid of outer edge of skull to centroid of reflector (the bregma) was approximately 1 mm (Figure 1). Using distance between two centroids, an estimation of bregma location was obtained for images that were scanned without reflector (Figures 2, 3).

Conclusions: The result of imaging process with implementation of mouse brain atlas showed the potential of USgFUS system, possibly allowing us to target desired location with sub-millimeter precision. More data will be collected to determine feasibility of this algorithm to localize relevant anatomical features with the necessary accuracy. Following verification, FUS microbubble disruption combined with the imaging mode will be performed *in vivo*.

Acknowledgements: Focused Ultrasound Foundation

Figure 1. (top) Image with reflector (1mm)

Figure 2. (bottom, left) Bregma estimation in image without reflector

Figure 3. (bottom, right) Bregma estimation in image without reflector

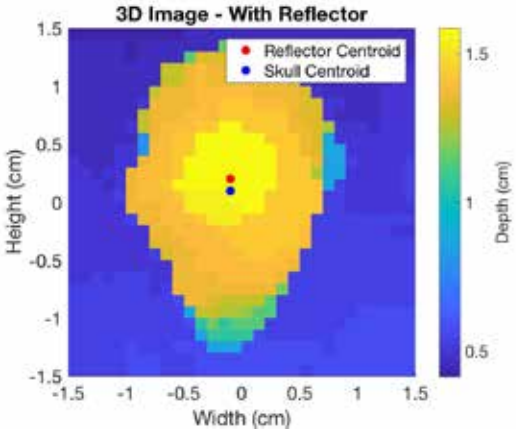

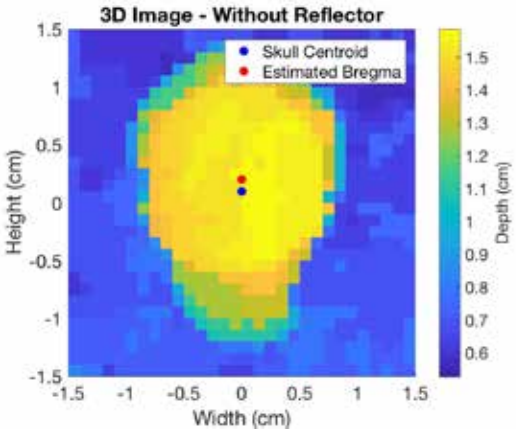

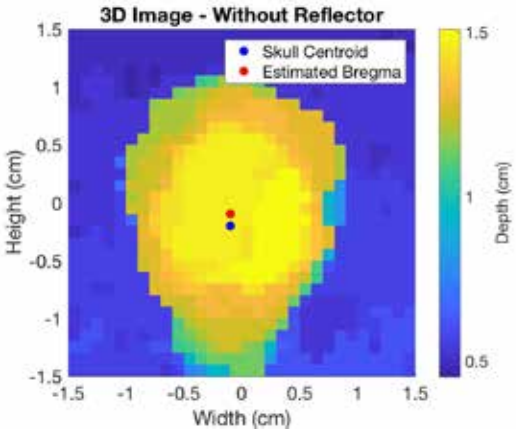

P-BR-18

Topic: Brain
Presentation Type: Poster

Measurement of attenuation coefficients of the human skull cadaver using shock wave generated from a CNT-PDMS transducer

Jooho Lee[1], Cheongah Lee[1], Soohong Min[1], Dong-Guk Paeng[1], Kanglyeol Ha[2], Kwansuk Kang[1], Minjoo Choi[1]

[1]Jeju National University, Jeju City, South Korea
[2]Pukyong National Univiversity, Busan City, South Korea

Background: Sound wave generated by focused ultrasound transducer is distorted at the focus through the human skull. Attenuation by the skull is important for transcranial ultrasound and various studies have been conducted to measure attenuation by the human skull and brain tissue. However, most measurements were performed by narrow band due to limitation in the bandwidth of the piezoelectric transducers. The shock wave generated from a focused CNT-PDMS transducer has a wide band of up to several MHz in a single pulse, and the attenuation coefficient up to several MHz can be measured by the single CNT transducer. The object of this study is to measure the attenuation through the human skull cadavers using the broadband frequency of the shock wave generated by the CNT transducer. The measurement results will be analyzed by a finite element method (FEM) commercial software.

Methods: In this experiment, the measurement was first done without a skull for a reference and then with a skull. The focal length and diameter of the focused CNT transducer used in the experiment were 5 cm. Three human skull cadavers were used for measurement. The average densities and sound speeds of the three skulls were computed to 1.908±0.047, 1.85±0.032 and 1.995±0.052 g/cm^3 and 2836±51, 2750±48, 2963±63 m/s, respectively. The shock wave from the CNT transducer generated by a laser(wave length is 532nm, 175mJ of Energy) is transmitted through the skull and measured by a needle hydrophone(TNU001A, Onda, Sunnyvale, CA, USA). Another narrow band HIFU transducer (H-101, Sonic concepts Inc, Bothell, WA, USA) with a center frequency of 1.1MHz was used to confirm the broadband measurement. To compare experimental and computational results, we used the commercial software, Sim4life.

Results: Sound pressure at the focal point was measured to 84kPa from the HIFU transducer without a skull and 8.8kPa with the skull. The center frequency was measured to 800kHz with the skull which was decreased from 1.1 MHz without the skull. The sound pressure ratio at the focus with and without the skull was 0.10 from the measurement and 0.09 from the simulation. Using the CNT-PDMS transducer, attenuation by the skull was measured with the frequency band up to 1.6MHz. The average attenuation coefficients of the three skulls were 4.38, 4.72, 2.98 np/cm/MHz. The simulation results were similar to the experimental results.

Conclusions: We measured the attenuation using broadband shock wave by a laser-generated CNT transducer, and the measurements were confirmed by the HIFU transducer and FEM simulation. The broadband measurement of the attenuation by a single CNT transducer was efficient and economic, which would be helpful for transcranial focused ultrasound applications.

P-BR-19

Topic: Brain
Presentation Type: Poster

Online data processing with GE human clinical MRI scanners

Craig Macsemchuk[1], Marc Lebel[2], Samuel Pichardo[1]

[1]University of Calgary Foothills Medical Centre, Calgary, Alberta, Canada
[2]General Electric Healthcare, Calgary, Alberta, Canada

Background: Online processing of magnetic resonance imaging (MRI) data is an essential component in developing MR guided high intensity focused ultrasound (MRgHIFU) therapies. Online data processing allows for MRI interventional applications such as acquiring thermometry data for MRgHIFU procedures. Traditionally, online data processing platforms for research development have been limited and manufacturer specific. Proteus is a software library that aims to be a comprehensive software infrastructure that facilitates the development of new therapeutic applications of MRgHIFU (18th Int. Sym. Ther. Ultrasound, 2018, Nashville, USA). Currently, Proteus includes support for clinical and preclinical MRI scanners from Brucker, Philips, and Siemens along various clinical HIFU platforms including Sonalleve (Profound Medical, Mississauga, ON, Canada), Image-Guided Therapy (IGT, Bordeaux, France), and RK-100 (FUS Instruments, Toronto, ON, Canada). The addition of support for General Electric (GE) MRI scanners to Proteus will help it achieve its goal of being vendor agnostic. Challenges presented by online data processing for MRI scanners include the need for low-latency transfer, proprietary scanner interfaces, variable data formats, and documentation on protocols that may not be available to research users.

Methods: In GE human clinical MRI scanners online data collection takes place over two interfaces. After consultation with GE, we were able to identify the operation of these interfaces. Investigation with standard Unix/Linux networking tools verified the operational outline as provided by GE. Preliminary design planning led to the adoption of both synchronous and asynchronous networking paradigms. The Twisted event-driven networking engine was selected to accommodate this communication topology. A Python class was then prototyped to test control and image reception. After verification of image reception, data stream processing was implemented to convert the continuous data stream into individual images. Once divided, these images were placed in a queue and sent to the MRgHIFU user interface. Finalization of the Python class included adding provisions for scanner operation and parameter control and documentation of both the image receiver implementation and scanner side data flow.

Results: The successful integration of GE human clinical MRI scanners into Proteus enable online data processing for use in MRgHIFU applications. Implementation of client authentication, image reception, and data stream processing has been shown.

Conclusions: The first steps towards a fully functional software library to integrate GE human clinical MRI scanners into MRgHIFU treatment planning and therapy software have been made. The addition of GE scanner support further progresses Proteus as the first and only vendor-neutral software platform to aid in the development of MRgHIFU therapies. Further work into full scanner parameter and operation control will be investigated next.

P-BR-20

Topic: Brain
Presentation Type: Poster

Electrophysiological findings after unilateral MRIgFUS subthalamotomy

Raul Martínez-Fernández, Danielle Urso, Fernando Alonso-French, Guglielmo Foffani, Michele Dileone, Jorge Máñez-Miró, Marta del Álamo, Frida Hernández-Fernandez, Lydia Vela, José Obeso

CINAC, Hospital Universitario HM Puerta del Sur, Móstoles, Universidad CEU-San Pablo, Madrid, Spain

Background: Our group has recently demonstrated that MRI-guided Focused Ultrasound (MRIgFUS) unilateral subthalamotomy can safely improve Parkinson disease's (PD) motor features according to the validated Movement Disorders Society- Unified Parkinson's disease rating scale (MDS-UPDRS) III.[1] However, this scale suffers from non-negligible both intra and inter-rater variability.[2] Electrophysiological techniques can help to provide more objective measures for demonstrating motor clinical changes. The objective of this study was to support with objective neurophysiological evaluation the positive clinical findings observed with unilateral MRIgFUS subthalamotomy.

Methods: PD patients who were selected for MRIgFUS unilateral subthalamotomy were analyzed in the OFF-medication state at baseline and six months after treatment. For the electromyography (EMG) movement analysis, patients performed two tasks while surface EMG was recorded: upper limb ballistic movement and 10-second finger tapping. Proximal simple reaction time after an acoustic signal and number, amplitude and rhythmicity of taps were recorded. Cortical silent period elicited through transcraneal magnetic stiu,ation (TMS) was measured. For both EMG and TMS all measurements were assessed on both sides of the body (ipsilateral/contralateral to the subthalamotomy). Off-line analysis was blinded to treated/untreated side. Comparison was done by means of t-test for paired samples.

Results: Seven patients (4 male) were included in the study. Mean age was 62.5 years (range 42-70) with a mean disease evolution f 6.4 years (range 3-10). EMG findings showed that distal simple reaction time in the treated body side improved from 176 ± 23 ms at baseline to 140 ± 23 ms at 6 months (a mean reduction of 20%, p=0.02). No change was found in reaction time in the untreated hemibody. While the number of taps between both hands differed at baseline (29 ± 8 for the most impaired hemibody *vs.* 34 ± 11 for the less affected, p=0.01), it was equivalent between the treated and untreated body side at 6 months (39.2 ± 9 *vs.* 40.2 ± 11 respectively, p=0.08). Moreover, the number of taps in the treated hand significantly increased after subthalamotomy 34.4% improvement). Rhythmicity in the treated body side had improved by 6 months (0.119 *vs.* 0.092 of tapping variability) without reaching statistical significance (p=0.2). No significant differences were found between each hemisphere before the procedure (139.6 + 21.4 *vs.* 160.6 + 44.1 ms for the most affected and less affected hemisphere respectively: p=0.26), although the duration of the cortical silent period was significantly longer at 3 and 6 months after subthalamotomy in the treated (p <0.01) but not the untreated hemisphere.

Conclusions: This study shows that the clinical improvement reported with MRIgFUS subthalamotomy is corroborated by EMG movement analysis and changes in motor cortex excitability.

References

1. Martinez-Fernández et al. Focused ultrasound subthalamotomy in patients with asymmetric Parkinson's disease: a pilot study. *Lancet Neurology*. 2018
2. Siderowf et al. Test-retest reliability of the unified Parkinson's disease rating scale in patients with early Parkinson's disease: Results from a multicenter clinical trial. *Mov Disord*. 2002.

Figure 1. Individual finger-tapping EMG recording.

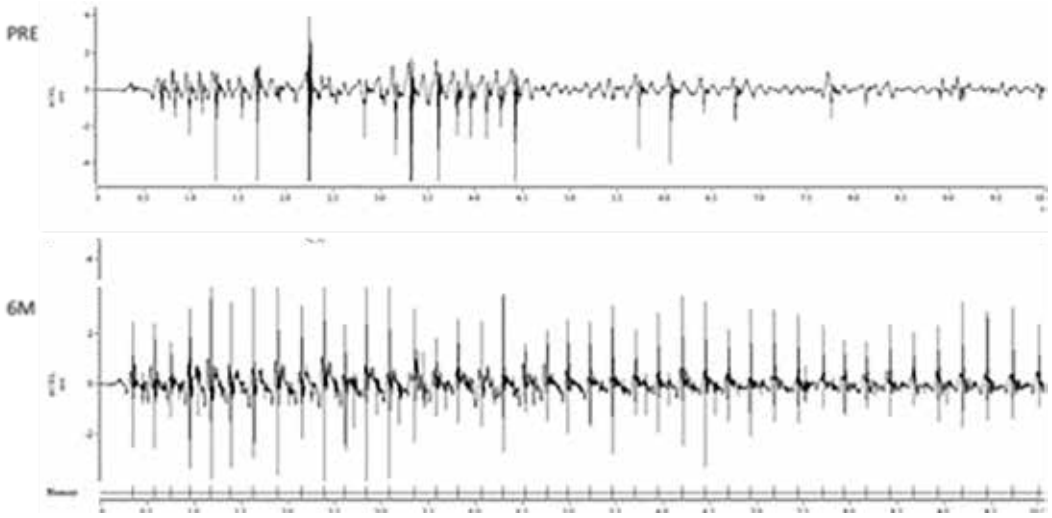

Figure 2. Transcranial magnetic stimulation (TMS) findings for the cortical silent period.

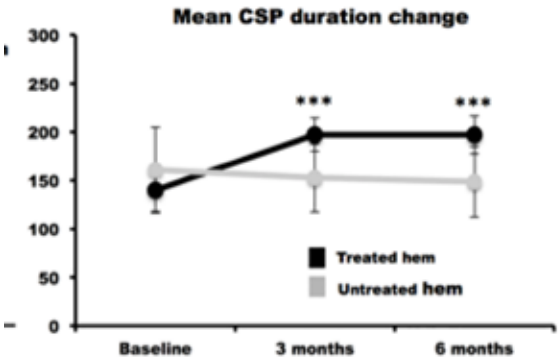

P-BR-21

Topic: Brain
Presentation Type: Poster

MR-guided focused ultrasound for essential tremor: Initial MRI observations

Erin Mazerolle[1], Robyn Warwaruk-Rogers[1], Rob Sevick[1], Tejas Sankar[2], Samuel Pichardo[3], Menashe Zaaroor[4], Davide Martino[1], Zelma Kiss[1], Bruce Pike[1]

[1]University of Calgary, Calgary, Alberta, Canada
[2]University of Alberta, Edmonton, Alberta, Canada
[3]University of Calgary Foothills Medical Centre, Calgary, Alberta, Canada
[4]Technion, Tiberias, Israel

Background: Little is known about how the brain networks involved in tremor change after MR-guided focused ultrasound (MRGFUS) treatment. We describe the initial MRGFUS study at our site, in which thalamotomies targeting the ventral intermediate nucleus are performed in patients with essential tremor (ET). We focus on tracking lesion volumes and evaluating structural connectivity changes with diffusion MRI.

Methods: Patients who have been diagnosed with ET by a movement disorder neurologist, have failed medical management, and have passed neuropsychology and CT screening are enrolled. Clinical assessments (e.g., accelerometry, Clinical Rating Scale for Tremor) are performed before treatment, as well as 1 day, 3 months, and 1 year post-treatment. A comprehensive research MRI protocol, including resting state functional MRI (fMRI) and diffusion MRI, is also acquired at each time-point. Lesion volume was determined manually on the basis of T1-weighted (T1w) images for 1 day and 3 month time-points.

To explore the effects of MRGFUS treatment on structural connectivity, initial analyses of post-treatment diffusion changes used day 1 lesions as seeds for probabilistic tractography. Streamlines were excluded if they passed through the midsagittal plane of the corpus callosum, or had a length of less than 10 mm to ensure streamlines exited the lesion. Voxels were further excluded from the analysis if they intersected less than 1% of streamlines. Mean fractional anisotropy (FA) was considered in the resulting tract as a surrogate for MRGFUS-related changes in white matter microstructure.

Results: As of April 2018, 11 patients have been treated at our site. One had been previously treated with deep brain stimulation (DBS) and is excluded from these analyses because it was difficult to distinguish between the boundary of the MRGFUS lesion and electrode-related scarring on T1w images. For all patients, good to excellent tremor suppression has been achieved. Lesion volumes on T1w images acquired 1 day post treatment averaged 279 ± 112 mm^3 (mean ± standard deviation; N=10). For the seven patients with 3 month data available, T1w lesion volume decreased from 250 ± 110 mm^3 to 35 ± 34 mm^3 (N=7).

With respect to the structural connectivity analysis, one patient was excluded for excessive head motion unrelated to ET on diffusion MRI scans. Outside of the lesion, changes in FA were generally restricted to the thalamus portion of the lesion-seeded tract, and recovered by 3 months (N=6; see Figures 1 and 2).

Conclusions: MRGFUS thalamotomy for ET presents novel opportunities to study how brain networks change after lesioning, particularly because these networks can be studied in the absence of other surgical-related trauma and/or DBS electrodes, which may cause MRI artifacts. Ongoing work is aimed at linking the MRI results to clinical findings, considering functional connectivity, and implementing advanced atlas-, fMRI- and diffusion-based treatment targeting.

Figure 1. Tractography-derived regions of interest (ROIs) used for the fractional anisotropy (FA) analysis.

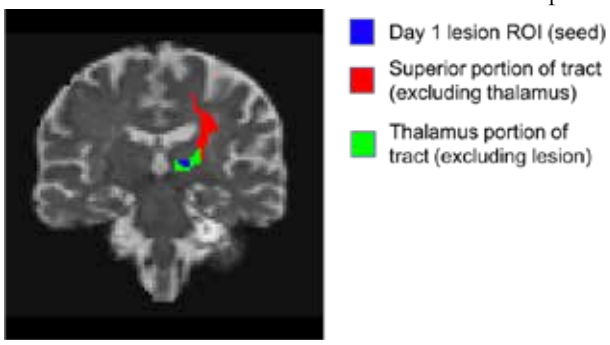

Figure 2. Fractional anisotropy (FA), a surrogate measure of white matter microstructure, at the three time-points: pre-treatment, 1 day after, and 3 months after MRGFUS treatment.

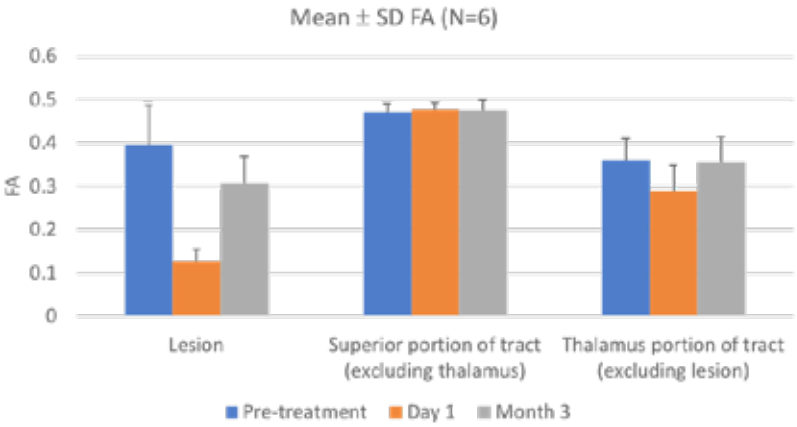

P-BR-22

Topic: Brain
Presentation Type: Poster

Microbubble-enhanced nonthermal ablation in rats using a clinical transcranial MRI-guided focused ultrasound system

Nathan McDannold, Yongzhi Zhang, Chanikarn Power, Natalia Vykhodtseva

Brigham and Women's Hospital, Boston, Massachusetts, United States

Background: Sonication combined with intravenously-administered microbubbles can be used to mechanically ablate tissue at exposure levels significantly lower than what is required for thermal ablation and is a promising approach to expand the "treatment envelope" within the brain where transcranial MRI-guided focused ultrasound (TcMRgFUS) is feasible. With this non-thermal mode of ablation, the ultrasound effects are concentrated on the vasculature, leading to tissue necrosis via ischemia. Here, we investigated the feasibility of nonthermal ablation with a low-frequency clinical TcMRgFUS system.

Methods: The experiments were performed with the ExAblate Neuro TcMRgFUS system (INSIGHTEC), a 1024-element hemisphere transducer (diameter: 30 cm) operating at 230 kHz. The sonications were planned, monitored, and evaluated using a 3T MRI (GE Healthcare) and a surface coil. MR temperature imaging (MRTI) was acquired during the sonications, and the acoustic emissions were recorded to monitor microbubble activity. Sonications were delivered at acoustic power levels of 0.7-0.9 W (approximately 186-211 kPa peak pressures in water) simultaneous with intravenous injection of 50-200 µl/kg Optison (GE Healthcare; 1-4× a clinical dose). The sonications consisted of 500 ms bursts applied at 1 Hz for 90 s. Overall, 16 locations were sonicated in experiments in 11 male rats, first without microbubbles and then with microbubbles. The lesions were evaluated after sonication and 2-9 days later with MRI, and the animals were sacrificed for histological examination. Numerical simulations of the transcranial focusing were also performed using k-Wave and a micro-CT scan of a rat head.

Results: During sonication, low-level focal heating was observed in the brain in 13/16 locations; the other two had flow artifacts and could not be interpreted. The peak temperature ranged from 2.1-5.4°C (mean: 3.8±1.1). While substantial variation was observed, the heating level generally increased with increasing acoustic power and microbubble dose. Enhanced subharmonic emissions were detected throughout sonication. Tissue changes were evident immediately after sonication as slightly darkened areas in T2*-weighted imaging. Blood-brain barrier disruption was evident in and around the sonicated region. In histology, the tissue damage was similar to previous investigations of this approach, with inflammation and macrophage infiltration at 2 days, and with formation of a scar or small cyst evident at 4-9 days. The severity of tissue damage depended on the microbubble dose; scars were evident with a dose of 50 µl/kg, and the cysts were evident with 200µl/kg. Simulations suggest that a tight focus can be achieved in the rat brain without significant standing wave formation, in agreement with the experiments. Figure 1 shows an example contrast-enhanced image acquired after sonication and MRTI obtained during sonication.

Conclusions: Despite the low frequency used by this TcMRgFUS system, discrete lesions could be created via nonthermal ablation with the hemispherical transducer. While the low-level heating evident during sonication was below the threshold for thermal damage, it did enable us to visualize the location of the ablation during sonication. These results are promising since microbubble-enhanced effects are frequency-dependent. Being able to use a low frequency clinical TcMRgFUS system in a small animal model will enable us to investigate this ablation approach in tumor models.

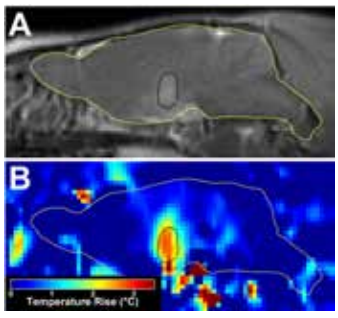

Figure 1. A. Contrast-enhanced MRI showing localized BBB disruption in the focal region shortly after sonication. B. MRTI obtained during sonication shows localized focal heating with a peak temperature rise of only a few degrees.

P-BR-23

Topic: Brain
Presentation Type: Poster

Different brain states are differentially responsive to ultrasonic stimulation

Pierre Mourad

University of Washington, Seattle, Washington, United States

It is well known that direct, non-invasive, spatially specific ultrasonic stimulation of the brain can activate neural responses, however it is less studied how the brain's state itself affects the responses. This thesis explores the differential responses to different brain states in mice, particularly the anesthetized brain state as induced by isoflurane and the sedated, awake-like brain state as induced by medetomidine. The electrocorticographic (ECoG) technique was utilized to record responses in the visual cortex (V1), the somatosensory cortex, and the auditory cortex when a flash of light was cast on the retina of the eye and when a burst of pulsed ultrasound was focused on V1. It was found that the responses due to these two stimulation techniques of the same brain state were largely similar. For example, under isoflurane, each stimulation generated slow waves (brain responses not only significantly longer than the stimulus duration but also distributed throughout the brain) ; under medetomidine, they did not. This preliminary result serves to confirm the effects of different brain states regardless of stimulation technique. Taken together, these preliminary results pave the way to further investigation of the similarities and differences of direct ultrasonic stimulation of the cortex and indirect neural stimulation of the cortex via light cast on the retina of the eye, as well as other sensory input such as sound and pinching, when applied to mice experiencing various brain states.

P-BR-25

Topic: Brain
Presentation Type: Poster

Acute activation of microglia and astrocytes after BBB opening with low intensity pulsed focused ultrasound and microbubbles in a mouse model

Aurea Pascal-Tenorio, Ningrui Li, Donna M. Bouley, Kim Butts Pauly

Stanford University, Stanford, California, United States

Background: Kovacs et al. recently demonstrated an upregulation of pro- and anti-inflammatory cytokines, neurotrophic, and neurogenesis factors after BBB opening with pulsed focused ultrasound (pFUS) and microbubbles (MB) in a rat model [1]. This was also associated with microglial and astrocyte activation. The goal of our study was to assess pFUS parameters, in terms of broadband acoustic emissions (AEs) and signal enhancement on contrast-enhanced MRI (CE-MRI), that produce microglial and astrocyte activation in a mouse model.

Methods: Twenty-eight healthy female CD1 mice (7 to 9 weeks of age, 20-40 g) were anesthetized with isoflurane carried on medical air during application of pFUS and either MB or saline. 650 kHz ultrasound (10 ms bursts, 1 Hz PRF) was delivered to the left hemisphere at peak negative pressures (PNPs) ranging from 0.10 to 0.35 MPa. Diluted Definity MB (1:20 v/v) were delivered intravenously (5 μL of dilution per gram body weight) prior to pFUS. Control mice were sonicated at 0.35 MPa after saline injection. BBB opening was assessed via AEs from a passive cavitation detector (1.95 MHz, 51% fractional bandwidth), CE-MRI, gross pathology, and H&E histology. In the treated hemisphere, a grade of "none", "mild", "moderate", or "severe" was assigned based on red blood cell density (hemorrhage), tissue pallor (edema), and cell morphology (neuronal/glial damage). Immunohistochemistry (IHC) for activated microglia (Iba1+) and astrocytes (GFAP+) was performed. A grade of "none", "mild", and "moderate" was assigned based on intensity of fluorescence (dim to bright) and cell morphology (resting state to hypertrophy) when compared to the non-treated side of the brain.

Results: There was BBB opening without hemorrhage at PNPs below 0.20 MPa (Fig. 1). Hemorrhage was present at PNPs above 0.25 MPa, with mild rarefaction of the parenchyma activation of microglia and astrocytes (Fig. 2). The degree of microglial and astrocyte activation is associated with broadband AEs (> 3 dB above baseline) around the subharmonic frequency (325 ± 2 kHz, Fig. 3). Any signal enhancement on CE-MRI is associated with microglial activation. However, mild astrocyte activation was observed without signal enhancement, and signal enhancement was also observed without any astrocyte activation (Fig. 4).

Conclusions: Microglial and astrocyte activation were observed on IHC one hour after BBB opening at PNP ranging from 0.10 to 0.35 MPa. AEs have potential for predicting the degree of activation.

Acknowledgements: This work was supported by NIH T32 EB009653 and NIH R01 CA227687. The authors would like to thank Roberta Moorhead, Elias Godoy, and Sergio Koba (Stanford Veterinary Service Department) for their assistance processing brain samples. We would also like to thank Patrick Ye and Kendra Lechtenberg for helpful discussions on IHC grading.

Reference

1. Kovacs, Zsofia I., et al. Disrupting the blood–brain barrier by focused ultrasound induces sterile inflammation. *Proceedings of the National Academy of Sciences*. 2017;114(1):E75-E84.

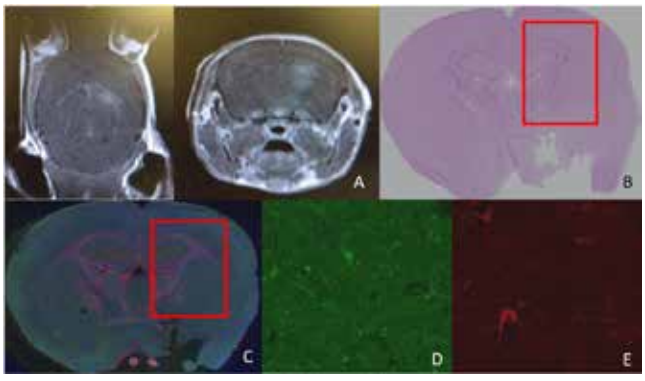

Figure 1. CE-MRI (A) after BBB opening (0.15 MPa). Histological analysis (B). Anti-Iba1 and anti-GFAP antibodies (C) show mild activation of microglia (D) and astrocytes (E).

Figure 2. CE-MRI (A) after BBB opening (0.35 MPa). Gross anatomy (B). Histological analysis (C). Anti-Iba1 and anti-GFAP antibodies (D) show activation of microglia (E) and astrocytes (F).

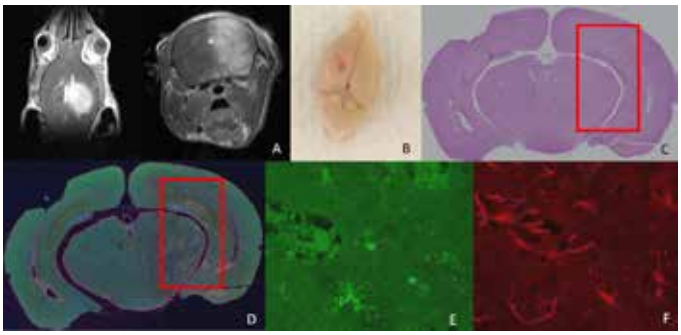

Figure 3. Broadband AEs in mice with varying grades of astrocyte and microglial activation.

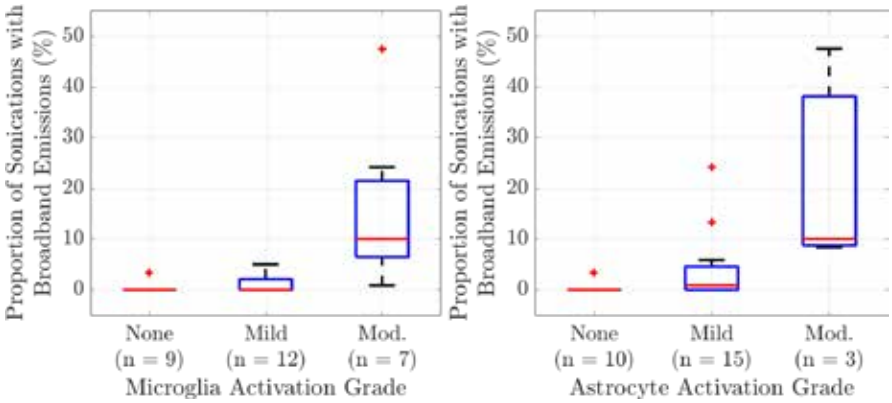

Figure 4. CE-MRI signal enhancement in mice with varying grades of astrocyte and microglial activation.

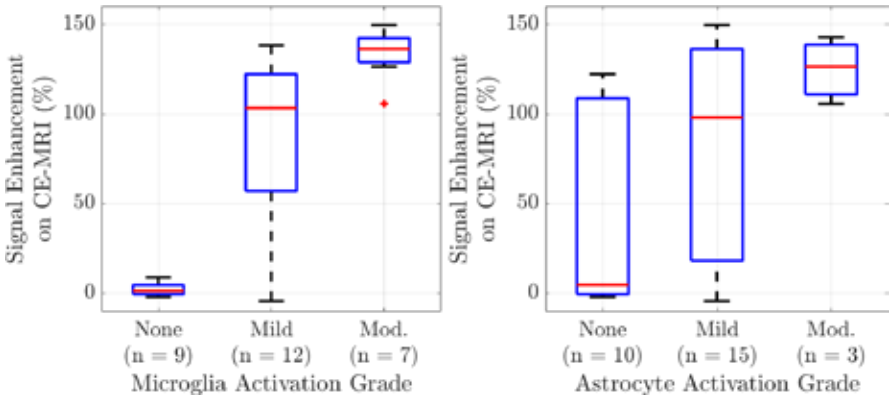

P-BR-26

Topic: Brain
Presentation Type: Poster

Navigational analysis and sensory responses of MR-guided focused ultrasound thalamotomy: Early results

Catherine Weiner, Erin Mazerolle, Craig Macsemchuk, Bruce Pike, Zelma Kiss, Davide Martino, Samuel Pichardo

University of Calgary, Calgary, Alberta, Canada

Background: MR-guided focused ultrasound (MRgFUS) is a new way to perform thalamotomy for essential tremor (ET). It is not known whether sub-lesional US-based thalamic mapping can help with targeting. In this study, we present our preliminary results, showing the energy level and location in the anterior–posterior commissural plane (AC-PC) relative to the sensory responses associated with correct targeting (flipping backwards, spinning).

Methods: Patients, diagnosed with ET by a movement disorder neurologist, who have failed medical management, pass neuropsychology and CT screening are enrolled. Assessments consisting of accelerometry, Clinical Rating Scale for Tremor (CRST), Scale for the Assessment and Rating of Ataxia, Purdue Pegboard, Beck Depression Inventory, and quality of life scales are performed pre-, post- at month 3 and yearly thereafter. MR imaging is performed at these time points as well as on day 1 post-op. During each treatment, we initially used the targeting suggested by the manufacturer, which was the ventral intermediate thalamus target, anterior to PC by 0.25 the length of the AC-PC line (anterior to the PC; i.e., 5.75-6.5 mm anterior to the PC), and 14 mm lateral to midline on the AC-PC plane.

Results: Twelve patients (11 M, 1 F) have had MRgFUS thalamotomy (2 R, 10 L). The number of sonications ranged from 13-29. All patients experienced "flipping backwards" or "spinning" during sonications that improved tremor. Fifty percent of patients required energy levels above lesioning levels before reporting the flipping backwards sensation; e.g. average temperature at focus greater or equal to 53°C. Figure 1 shows treatment locations showing average temperature at focus greater or equal than 45°C. Each sonication and the path taken to it in each patient is a separate colour. The size of the circles represents the temperature achieved, e.g. larger circles represent sites where the temperature exceeded 53°C. Black circles indicate the first location of sensory movement response (flipping backwards, spinning) with an average temperature <53°C. Red circles indicate the first location of sensory response (flipping backwards, spinning) with an average temperature >53°C. Using an AC-PC plane coordinate system, with the posterior commissure (PC) as origin, the average location (±s.d) in medial-lateral (-M+L), posterior-anterior (-P+A) and inferior-superior (-I+S) of the first location showing sensory response was -M+L =+14.2(±0.9) mm, -P+A=+6(±1.2) mm and -I+S=1.1(±1.3) mm. The location with therapy level (average temperature greater or equal than 53°C) was -M+L =+13.9(±0.8) mm, -P+A=+7(±1.3) mm and -I+S=1.1(±1.2) mm.

Figure 1. The location of all sonications applied reaching temperatures higher than 45°C, shown in axial (or Medial-Lateral Posterior-Anterior, ML-PA) plane (left) and coronal (or Medial-Lateral Inferior-Superior, ML-IS) plane (right), relative to origin at PC

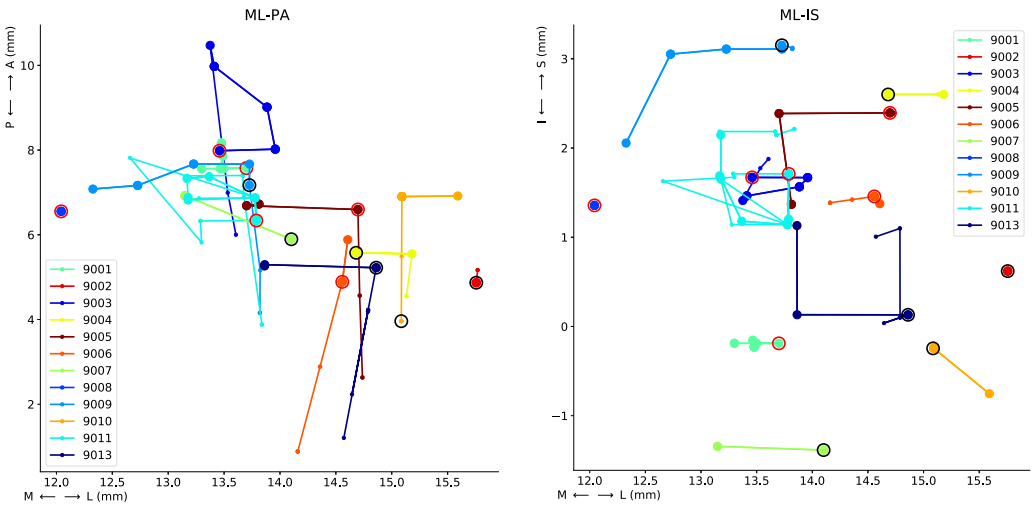

Conclusions: Our early results indicated that an adjustment of 1.1 mm in the superior direction and 0.5-1.25 mm in the anterior direction of the target recommended by the manufacturer is required to produce both a sensory response and tremor reduction. These results can provide supplemental guidance during MRgFUS-based thalamotomy for essential tremor.

P-BR-27

Topic: Brain
Presentation Type: Poster

Metabolic changes following transcranial magnetic resonance-guided focused ultrasound subthalamotomy

Rafael Rodriguez-Rojas[1], Jose A. Pineda-Pardo[1], Raul Martínez-Fernández[2], Marta Del-Alamo[2], José Obeso[2]

[1]Centro Integral de Neurociencias AC, University Hospital HM Puerta del Sur, Madrid, Spain
[2]CINAC, Hospital Universitario HM Puerta del Sur, Móstoles, Universidad CEU-San Pablo, Madrid, Spain

Background: Subthalamotomy is effective in alleviating motor symptoms in Parkinson's disease (PD). As part of a pioneer trial to investigate the use of transcranial magnetic resonance-guided focused ultrasound (MRgFUS) subthalamotomy in PD, this study addresses the effects of sonication on resting-state cerebral glucose metabolism and examines the associations between lesions size and modulation of brain metabolism.

Methods: Eight PD patients receiving MRgFUS-STN underwent simultaneous FDG-PET/MRI at rest in off-medication, both previous and three months after procedure. MRI were segmented and normalized using the DARTEL method and volume of lesions were computed. PET were corrected for partial volume effect, normalized and smoothed using a 6-mm gaussian kernel. Standardized uptake ratios (SUVRs) were computed using pons as reference. We performed voxel-based statistical non-parametric mapping (SnPM) based upon 10.000 random permutations to identify significant changes in regional metabolism that occurred with MRgFUS-STN. To identify MRgFUS subthalamotomy-associated metabolic brain network changes, we computed the expression of a PD-related spatial covariance pattern (PDRP) on a subject-by-subject basis using a scaled subprofile scaling model/principal component analysis.

Results: All treatments were recognized by MRI. Average volume of lesions was 0.32 cc, involving the sensorimotor STN and dorsal white matter. SnPM analysis revealed a significant metabolic reduction in the STN area, ipsilateral GPi, primary motor cortex (precentral and paracentral region, Brodmann area 4), superior frontal and cingulate gyruses (Brodmann areas 6 and 23, respectively), and in the contralateral cerebellar lobules IV-VI, compared to baseline ($P < 0.001$, uncorrected). Patient PDRP expression was significantly reduced following MRgFUS subthalamotomy ($P < 0.05$). On an individual subject basis, network activity was reduced in 7/8 patients. Treatment-mediated modifications in metabolic network showed a significant correlation with changes in MDS-UPDRS motor scores ($R2 = 0.88$; $P = 0.001$)

Conclusions: MRgFUS-STN modulates the activity of PD-related metabolic brain networks. Contrary to classical approach using DBS, our data are consistent with deactivation of the inhibitory basal ganglia output and subsequent long-range effects on motor cortices. ROI-based analysis documents a neurobiologically expected relation between the size of the lesion and the amplitude of changes in metabolism. Our results suggest that suppression of abnormal network activity is a feature of subthalamotomy. These findings suggest that MRgFUS subthalamotomy regulates the entire neural network rather than merely exciting or inhibiting certain nuclei.

P-BR-28

Topic: Brain
Presentation Type: Poster

Quantitative diffusion tensor tractography predict clinical improvement induced by MRgFUS subthalamotomy

Rafael Rodriguez-Rojas[1], Jose A. Pineda-Pardo[1], Raul Martínez-Fernández[2], José Obeso[2]

[1]Centro Integral de Neurociencias AC, University Hospital HM Puerta del Sur, Madrid, Spain
[2]CINAC, Hospital Universitario HM Puerta del Sur, Móstoles, Universidad CEU-San Pablo, Madrid, Spain

Background: The feasible and safety of transcranial thermal ablation of the dorso-lateral subthalamus (STN) in patients with Parkinson's disease (PD) has recently been explored by our group. While that pilot study showed the feasibility of revert the main motor symptoms, clinical outcomes are not homogenous. We hypothesized that the impact of sonication over specific fibber bundles could explain the disparity in clinical response. In this study we evaluate the capacity of quantitative diffusion tensor tractography (DTI) to segment the subthalamic regions according to their cortical connections. We analyze 3 white matter connections important in the pathophysiology of PD: motor cortex – STN, supplementary motor cortex (SMA) – STN and cerebello – thalamo – cortical pathways, in order to investigate the relationship between changes in diffusivity measures and clinical measures.

Methods: Motor and imaging assessment was performed at baseline and 3 months after subthalamotomy while off-medication. Motor status were assessed using the MDS-UPDRS part III scale at baseline Lesion tissue was segmented by two independent raters. Imaging data was acquired in a hybrid 3T Biograph tomograph (Siemens, Erlangen) at baseline and 3 months post-treatment. DWI was acquired using EPI sequence (2 mm^3 and b=1000s/mm^2 along 60 encoding directions). DWI data of each subject are reconstructed in a standard space using q-space diffeomorphic reconstruction (QSDR). Local connectome is estimated from local fiber directions. Relevant tracts are reconstructed on a high-definition fiber tracking template (HCP-842 atlas). Track-based analysis compare diffusivity measures (QA, nQA, gFA, iso) along the tracks.

Results: Lesion topography is consistent with the dorsal-lateral (motor) region of the STN in the Morel atlas. Average lesion size was 270 mm^3. DTI analysis showed marked reduction in gFA 3-months post-treatment. Structural connectograms show that significant differences are restricted to the treated hemisphere. Our preliminary DTI analyses and the spatial correlation with lesion topography proposed that fibres connecting to the primary motor cortex are more markedly reduced in patients with major improvement in rigidity and tremor. More anterior lesions might be more affected in patients with major improvement in bradykinesia, suggesting an involvement of the STN-SMA cortical fibres.

Conclusions: Interruption of basal ganglia pathways is a feature of MRgFUS-subthalamotomy. A combination of complex DTI processing and lesion morphometry may be able to predict motor performance in patients undergoing unilateral MRgFUS-subthalamotomy. This is a proof of concept study, exploring the possibility of investigating by quantitative tractography the impact of MRgFUS subthalamothomy on specific cortico-subcortical tracts. This study is therefore expected to prompt future research with the aim of creating imaging reference to assess the lesion effect on a single subject basis. This might eventually have an impact on MRgFUS-subthalamotomy planning.

P-BR-29

Topic: Brain
Presentation Type: Poster

Skull induced aberration corrections by an indirect wavefront sensing approach

Elisabetta Sassaroli

Brigham and Women's Hospital, Boston, Massachusetts, United States

Background: A method for focusing ultrasound through the skull, based on an intuitive idea of focus formation, is proposed. An ideal focus is formed when the beamlets emitted by the elements of a transducer form a spherically converging wavefront with the rays intersecting at a common point in phase to produce maximum constructive interference. The skull may be approximated as a thin layer inducing ray refraction, attenuation and a phase shift. In such a situation, a wavefront can still be defined but the rays will no longer all converge to a common point in phase. The goal is to reconstruct this wavefront in order to correct for refraction, phase shift and possibly attenuation (Figure1).

Methods: The transducer elements are divided into N groups and one group at the time is focused through the skull at the intended location. Using only one group at the time permits dividing the wavefront into zones and isolating a beamlet of refracted rays. The resulting focal spot is enlarged, has reduced intensity and is displaced. The centroid of the aberrated focus is determined and the displacement of the centroid relative to the intended focus is determined using MRI thermometry and/or MRI-ARFI. From this displacement, the steering angle required to bring the beamlet to focus at the intended focused is obtained. Once the procedure is repeated for all the groups, the beamlets intersect at the intended focus, i.e. ray refraction is corrected, but they are not necessarily in phase. To bring all the beamlets into phase for constructive interference, two approaches may be applied. In one approach, the phase of one beamlet is changed while keeping the phases of the remaining beamlets constant. For each beamlet, the phase that produces maximum constructive interference is chosen. In the second approach the phase is reconstructed algorithmically using the displacements determined above and taking into account that they are proportional to the gradient of the wavefront. The calculation of the aberrated wavefront from its gradient permits determining the phase shift to be applied to each group.

Results: In Figure 2, an example of simulated displacements is illustrated. The corresponding aberrated wavefront is reconstructed algorithmically using a modal method in Figure 3 and an iterative method in Figure 4. The modal method provides an approximate estimate of the aberrated wavefront as it uses only a limited number (25) of Zernike polynomials. In. Figure 4, the results from the modal method are used as initial guess for the iterative method.

Conclusions: The proposed technique needs to be validated experimentally. It could be very accurate if the array is divided into a sufficient number of groups of elements and the division of the groups is optimized. It could be used for constructing look up tables for a given transducer. It could be used the day of treatment with a smaller group of elements if only a small adjustment to the focus location is required. The Zernike coefficients could be used to classify the aberration type.

Figure 1. Aberrated wavefront.

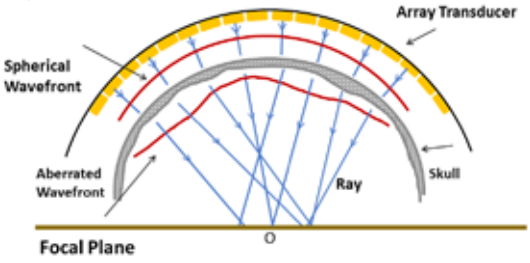

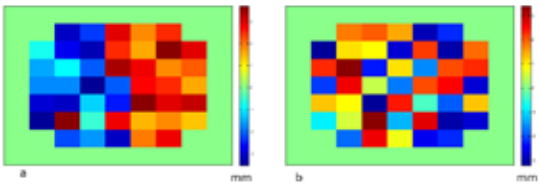

Figure 2. Displacements in mm in the focal plane (a) along the x direction (b) along the y direction for a transducer divided in 45 groups.

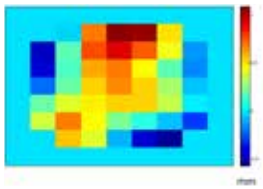

Figure 3. Aberrated wavefront in mm for a transducer divided in 45 groups. Modal method used.

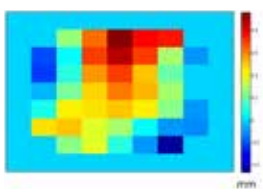

Figure 4. Aberrated wavefront in mm for a transducer divided in 45 groups. Zonal method used.

P-BR-30

Topic: Brain
Presentation Type: Poster

Online data processing of MRI raw-data for an MRgHIFU software library

Eric Song[1], Samuel Pichardo[2], Warren Foltz[3], Marcus Couch[4], Adam Waspe[4], James Drake[4]

[1]CIGITI, The Hospital for Sick Children, Toronto, Ontario, Canada
[2]University of Calgary, Calgary, Alberta, Canada
[3]STTARR Innovation Centre, University Health Network, Toronto, Ontario, Canada
[4]The Hospital for Sick Children, Toronto, Ontario, Canada

Background: Magnetic Resonance guided High Intensity Focused Ultrasound (MRgHIFU) therapeutics rely on real-time MR imaging for focal targeting and thermal feedback. Previously, online MR data processing applications for conjoined use with HIFU controllers have been limited by accessibility or by manufacturer. The vendor agnostic software library "Proteus" aims to provide a comprehensive foundation for the development of new MRgHIFU applications for therapy and research (18th Int. Sym. Ther. Ultrasound, 2018, Nashville, USA). New support for Siemens MRIs would increase the number of supported MRI vendors, which include Philips, General Electric, and Bruker.

Methods: From a Siemens 1.5T Aera MR scanner, raw data was converted into the ISMRM Raw Data (ISMRMRD) format and streamed over TCP/IP to Gadgetron, an image reconstruction framework. The open-source framework was necessary to reconstruct spatial domain images, which was not a necessary step for other MRI vendors that provided specifications for directly exporting image data. A Gadgetron instance running natively on the processing computer received ISMRMRD files from the network and reconstructed the images based on a customizable chain of processing functions. Next, a custom implemented data exporter for Gadgetron packaged the processed image into either DICOM or ISMRMRD image formats and exported to Proteus via TCP/IP. Lastly, Proteus's Twisted-based network interface received the images, parsed relevant data, and performed post-processing (phase difference calculations) to develop thermal mapping.

Results: An online data pipeline for Siemens MRIs with Proteus was successfully implemented and tested. A reliable stream of real-time thermometry was performed by an application using Proteus. Integrity of data after network transmission and transformation by Gadgetron and Proteus were confirmed to be preserved.

Conclusions: Online image reconstruction and thermometry with Siemens MR scanners is now possible for the Proteus software library. Compatibility with Siemens MRIs greatly increases the usability of Proteus for MRgHIFU research.

P-BR-31

Topic: Brain
Presentation Type: Poster

Development of an MRI-guided robotic platform for focused ultrasound induced sonothrombolysis of brain intraventricular blood clots

Nathan Soucier

University of Toronto - The Hospital for Sick Children, Toronto, Ontario, Canada

Background: One in every ten babies are born premature and many with a low-birthweight. Nearly 50% of low-birthweight premature babies develop an intraventricular hemorrhage. This can lead to an intraventricular blood clot, which obstructs the flow of cerebrospinal fluid leading to hydrocephalus. This is characterized by increased pressure and enlarged ventricles resulting in secondary brain injury if untreated. Currently, minimally invasive neurosurgery is the only available therapy for these infants, which aims to care for the symptoms of hydrocephalus long-term, instead of treating the actual underlying condition. Our aim is to provide a non-invasive method of treatment by dissolving the blood clot directly in the ventricles, thereby eliminating the need for shunt surgery and reducing the effects caused by hydrocephalus. This proposed treatment platform is composed of a focused ultrasound (FUS) transducer to perform thrombolysis and the development of a robotic platform to target the blood clot using real-time MRI.

Methods: A 256-element FUS transducer is mounted on an MRI-safe robot that operates in the bore of a clinical 3T MRI scanner to achieve precise image-guided targeting. This is a five degree-of-freedom robot that was designed using MR-safe materials and integrated into existing Sonalleve electronics (Profound Medical) and software interfaces. Fiducial markers are placed on the transducer which are imaged by the MRI (Figure 1) and transferred as DICOM's to the robot software (Figure 2) so that its location can be determined. The robot software has an interface that allows for its maneuverability, initiation of sonication and monitoring the treatment. Once the FUS parameters are set, the sonication is initiated and thermal map images are displayed (Figure 3). These images are initially planned and captured on the MR software, then continually pushed to the robot software to provide real-time feedback of the sonication. When sonicating a clot, the volume reduction and targeting accuracy will be assessed with a goal of more than 50% decrease in volume with targeting capabilities within ±2mm. This will initially be tested using *in vitro* phantom models and porcine cadaver heads, followed by *in vivo* animal tests using an established piglet model of an intraventricular hemorrhage.

Results: The robot software has been developed to import the DICOM files that are pushed from the MRI and provide a graphical user interface that allows for control of the robot and FUS. The transducer can be operated in both a thermal mode (continuous sonication) and histotripsy mode (pulsed sonication). This platform also monitors the treatment in real-time as MR thermal images are continually streamed to the robot user interface. We will be testing the recently developed robot platform using an established porcine model of an intraventricular hemorrhage.

Conclusions: The results from this work will provide a method of treating premature babies with intraventricular clots that is non-invasive, thus eliminating the need for shunt surgery.

Acknowledgements: SickKids HIFU and CIGITI Lab (T. Looi, K. Piorkowska, W. Chu-Kwan), Brain Canada (MIRI) and FUS Foundation

Figure 1. MRI Fiducial Markers

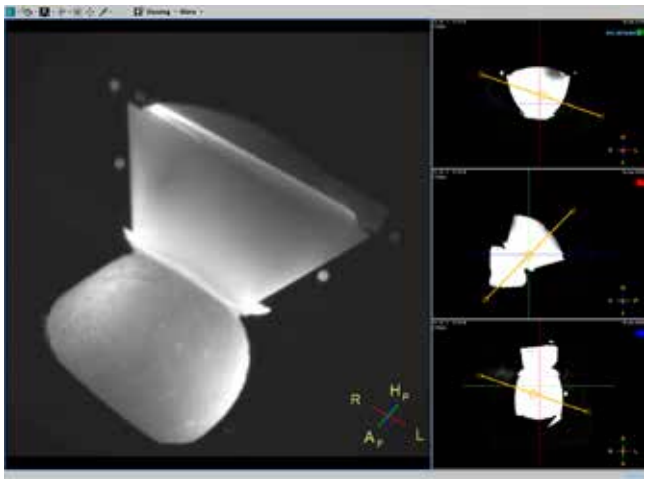

Figure 2. Robot Software Fiducial Markers

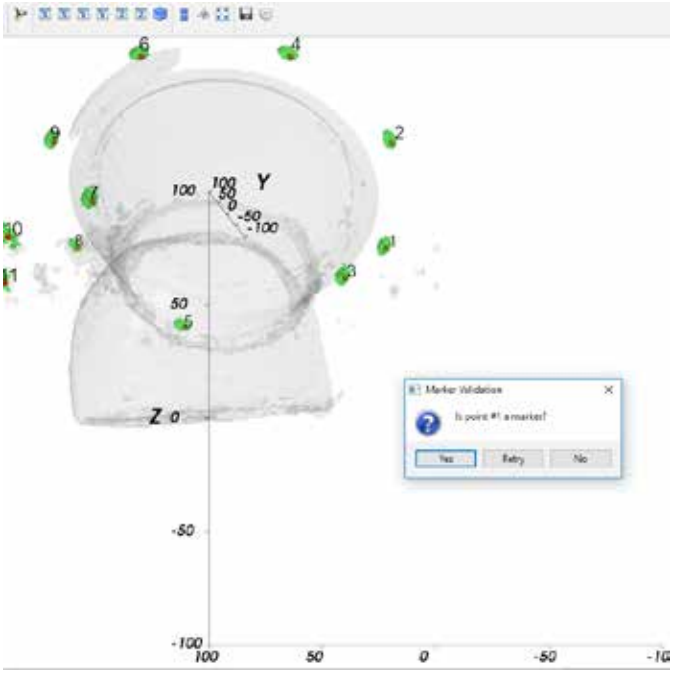

Figure 3. Robot Software Thermal Maps

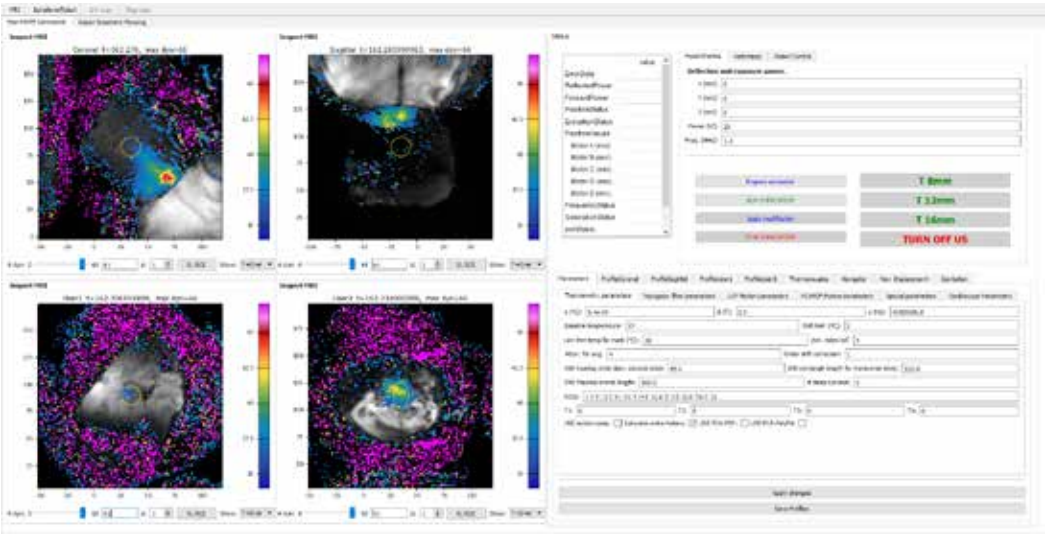

P-BR-32

Topic: Brain
Presentation Type: Poster

Non-linear temperature modeling for MR-guided focused ultrasound thalamotomy

Kevin Tsai, Wei-Chieh Chang, Hui-Chin Lai, Cheng-Yu Wei

Chang Bing Show Chwan Memorial Hospital, Taiwan

Background: MR-guided focused ultrasound (MRgFUS) thalamotomy recently became an available alternative for the refractory essential tremor patients. By increasing the temperature in the selected target, e.g. ventro-intermediate nucleus in thalamus, the tremor of patients would be mitigated immediately. In order to produce a lesion for permanent control the tremor, the temperature is expected to achieve higher than 54 degree. However, the parameter manipulation in the MRgFUS thalamotomy heavily relays on the empirical experience of the operator to achieve the expected temperature. Therefore, we proposed a non-linear model to describe the temperature changes across different sonications as well as different individuals.

Methods: The treatment data was collected from twenty-three patients with written informed consents. Specifically, the actual energy (AE), maximum power (MP), focal power (FP), and the maximum of the averaged temperature (T) of each sonication as well as the skull scores (SS) from all the patients were collected. For each patient, the correlation between the MP and the FP was described by FP = pa x MPpb [1], where pa and pb were the coefficients. The correlation between T, AE, FP, and the accumulated thermal dose calculated by CEM43 (aCEM43) was described by T = IC + a x AE + b x FP + C x aCEM43 [2], where IC, a, b, and C were the coefficients. The correlation between SS and the coefficients a and b were described by a = a1 x SSa2 [3] and b = b1 x SSb2 [4], respectively. Put equation [1] to [4] together T = aIC + (a1 x SSa2) x AE + (b1 x SSb2) x (apa x MPapb) + aC x aCEM43, where aIC, apa, apb, and aC were the averaged coefficients of IC, pa, pb, and C, respectively.

Results: The mean and the standard deviation of the SS of all the patients were 0.45±0.10. The mean and the standard deviation of the adjusted coefficients of determination of fitting [1] across all the patients were 0.9996±0.0005, and that of fitting [2] were 0.9562±0.033. Figure 1 showed all the modeled and the empirical temperature of all the patients. Figure 2 showed the fitting of [3] and [4]. Figure 3 was an exemplar on MATLAB that given the SS, temperatures and the durations of previous sonicaitons as well as the energy and the MP we want to deliver for this sonication, the script showed the expected temperature. Given the temperature we want to achieve for this sonication, the script also showed the required energy according given maximum power.

Conclusions: Our results showed that there was a high correlation between the maximum and the focal power. The linear combination of the actual energy, focal power, and the thermal dose could be used to synthesize the temperature. The coefficients of AE and FP were correlated with SS. This model could be used to predict the temperature given the parameters we used in the thalamotomy.

Figure 1

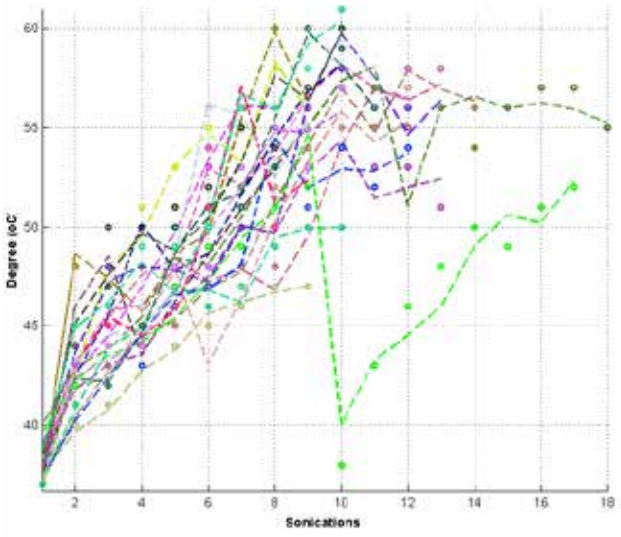

Figure 2

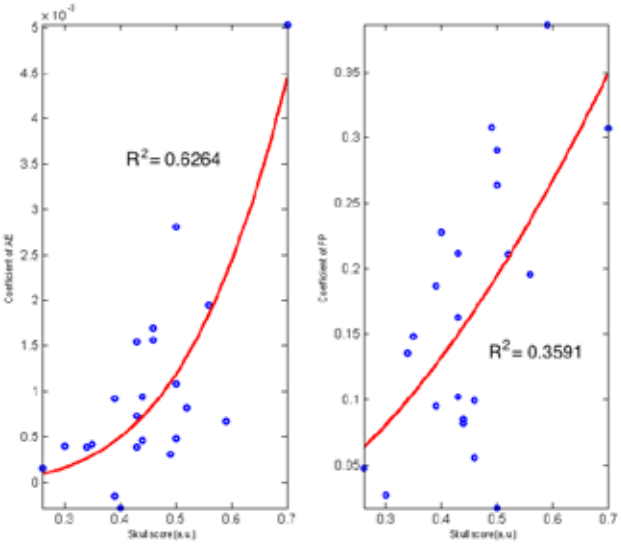

Figure 3

```
SDR = 0.43;
T_target = 56;

actual_energy = [
    8000;
    ];
max_power = [
    800;
    ];
T_done = [
    37,0;
    41,11.5;
    43,10;
    ];
```

Command Window

```
>> FUS_temperature_predict
Estimated T = 54.132131
Required E = 10863.641312
```

P-BR-33

Topic: Brain
Presentation Type: Poster

Trabecular bone associates more than cortical bone with skull score for MR-guided focused ultrasound

Kevin Tsai, Hui-Chin Lai

Chang Bing Show Chwan Memorial Hospital, Taiwan

Background: The trans-cranial magnetic resonance-guided focused ultrasound (MRgFUS) has been widely used to treat various neurological disorders by using the thermal ablation to the specific target in human brain. A volumetric computed tomography (CT) scan is used to not only delineate the entire skull for the phase aberration correction during the MRgFUS treatment, but also estimate a skull score (SS) to determined patient's feasibility before the MRgFUS treatment. Patient with low SS indicates a low energy-temperature efficiency in MRgFUS treatment. Different from the conventional skull density ratio (SDR) calculation, the SS is calculated by averaging all the ratios between the minimum and the maximum of the CT number of the skull along thousands of the spatial pathway from the ultrasound transducer to the simulated target. In this study, the linear correlation between the SDR and SS was calculated, and the influence of the cortical and trabecular bone to SDR was investigated.

Methods: 120 patients received a CT scan by using a 16-slise CT scanner (LightSpeed, GE, USA) for the screening of the MRgFUS treatment. The imaging parameters followed the routine scan, and reconstructed slice thickness = 0.625 mm. A high-pass filtering Bone+ was applied to the reconstructed CT images. These CT images of each patient were uploaded into the MRgFUS (Exablate Neuro, INSIGHTEC Ltd. Isreal) platform, and the SS of each patient was calculated. The same data sets were used to calculate the skull density ratio by first defining the whole skull using the region growing procedure through all the CT slices. The Otsu' method was then used to obtain the image intensity threshold of the cortical bone and trabecular bone of the skull. The SDR was calculated by dividing the averaged cortical bone intensity (aCBI) by the averaged trabecular bone intensity (aTBI). The bootstrap sampling was applied to produce twelve thousand pairs of SDR-SS pairs. The correlation between the SS and the SDR after the bootstrap sampling were estimated by calculating the Pearson's correlation coefficient across all the patients. The linear fitting to aCBI-SDR and aTBI-SDR pairs across all the patients was respectively performed to evaluate influence of the aCBI and the aTBI to the SDR.

Results: The Pearson's correlation coefficient (R) between SS and SDR was 0.7995 (Figure 1). Figure 2 showed that The aCBI was less correlated (R = 0.2293) and less influent (slope = 597) to SDR than that of aTBI to SDR (R = 0.8565, slope = 3018) (Figure 3).

Conclusions: Our results suggested that SS has a highly linear correlation with SDR, and aTBI had stronger influence to SDR than aCBI. Accordingly, aTBI had stronger influence to SS, indicating that the SS could be efficiently increased by increasing aTBI to improve the energy-temperature efficiency in MRgFUS treatment.

Figure 1

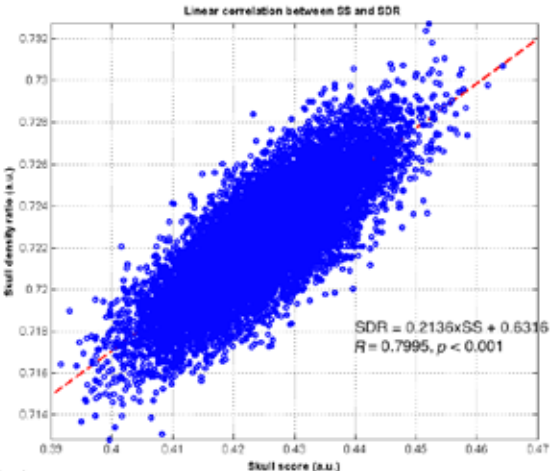

Figure 2

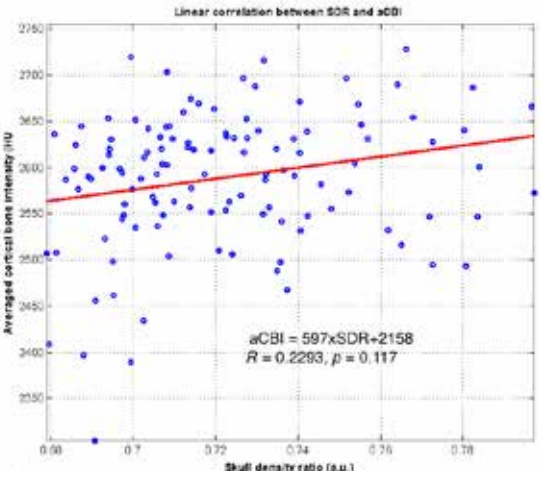

Figure 3

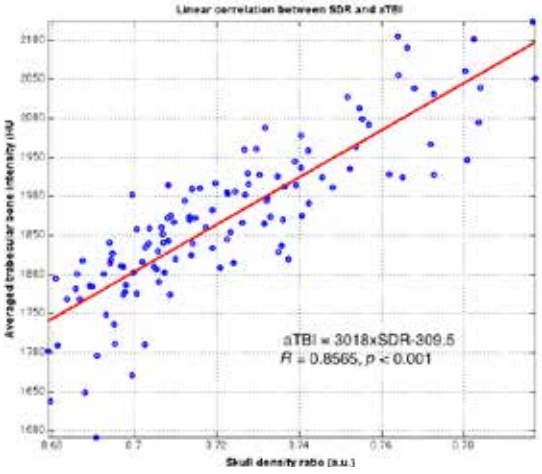

P-BR-34

Topic: Brain
Presentation Type: Poster

Invertebrate *in vivo* nervous model for the mechanistic study of ultrasound neurostimulation

Jérémy Vion-Bailly[1], W. Apoutou N'Djin[1], Alexandre Carpentier[2], Jean-Yves Chapelon[1]

[1]LabTAU, Inserm, Lyon, France
[2]APHP, Paris, France

In accordance with author request, this abstract is not available for publication.

P-BR-35

Topic: Brain
Presentation Type: Poster

Correlating acoustic velocity with UTE and ZTE MRI

Taylor Webb, Steven Leung, Pejman Ghanouni, Jeremy Dahl, Norbert Pelc, Kim Butts Pauly

Stanford University, Stanford, California, United States

Background: Transcranial MR guided focused ultrasound treatments (tcMRgFUS) could be greatly simplified by replacing pre-treatment CT scans with MR. Miller et al[1] showed that ultra short echo time (UTE) imaging could be used to segment the skull with an accuracy comparable to CT but a more complete MR solution requires a quantitative mapping of MR parameters to acoustic velocity as has been achieved with CT.[2-4] In this work we measure the acoustic velocity in 84 skull fragments and compare the results to the average MR magnitude measured with UTE and zero echo time (ZTE) imaging and to a T2* estimate.

Methods: Samples were acquired from two dried human skulls (Skulls Unlimited, Oklahoma City, OK). The sample preparation and measurement of acoustic velocity and average HU is described in.[4] The velocity and HU values were compared to MR Imaging and the correlation was measured using the r-squared value.

MR Imaging: UTE (TE=32 μs, TR=0.78 ms, FOV=18 cm, slice thickness=0.7 mm, in-plane resolution=0.63 mm, flip angle=5°) and ZTE (TE=0.02 μs, TR=150 ms, FOV=18 cm, slice thickness=0.8 mm, in-plane resolution=0.7 mm, flip angle=5°) images were acquired at 3T. Coil shading was removed by normalizing the images to an image of an agar phantom acquired with the same parameters. A UTE sequence was used to obtain estimates of T2* (TE=32, 200, 500, 700, 900 μs, TR=10 ms, FOV=16 cm, slice thickness=0.7 mm, in plane resolution=0.63 mm, flip angle=10°).

Results: Figure 1 shows example ZTE, UTE, and T2* images. Dual energy CT images reconstructed at 80 and 140 keV are shown for comparison. Qualitatively, the MR image brightness is opposite that of the CT images, with brighter images in the medullary and darker images in cortical bone. This inverse correlation is shown quantitatively in Figures 2a-2c. The r-squared values for these correlations range from 0.69-0.79 and the slope of the relationship depends on the photon energy of the CT scan. For comparison, Figures 2a and 2b also show the correlation measured by Wiesinger et al,[5] who measured the relationship between ZTE magnitude and HUs *in vivo*.

The same MR-derived parameters are compared to the velocity in each fragment in Figure 3. The r-squared values range from 0.31-0.41.

Conclusions: The MR-derived parameters are strongly correlated with HUs. The slope of this correlation depends on the energy used to obtain the CT image. Acoustic velocity is also correlated with all three MR parameters and the r-squared values are comparable to those measured between HU and velocity in.[4]

Acknowledgements: NIH Grant #s R01 MH111825, PO1 CA159992, the FUS Foundation, GE Healthcare, and INSIGHTEC.

Figure 1. Sample CT and MR images of fragments from inner table, diploe, and outer table. CT images were acquired with a dual energy scan and reconstructed at 80 and 140 keV.

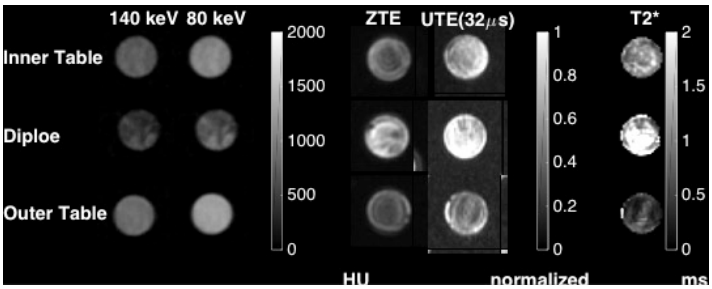

Figure 2. The average HU of each fragment as a function of a) ZTE magnitude, b) UTE magnitude, and c) T2*. The black dotted line in a) and b) shows the relationship measured by Wiesinger et al between ZTE and CT HU.

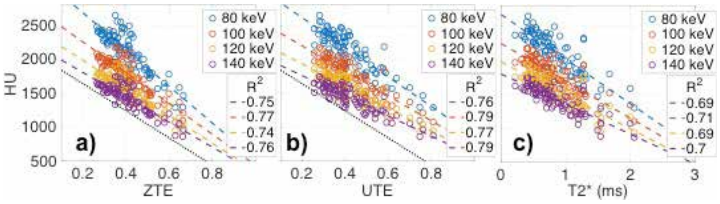

Figure 3. The measured acoustic velocity of each fragment as a function of a) ZTE magnitude, b) UTE magnitude, and c) T2*.

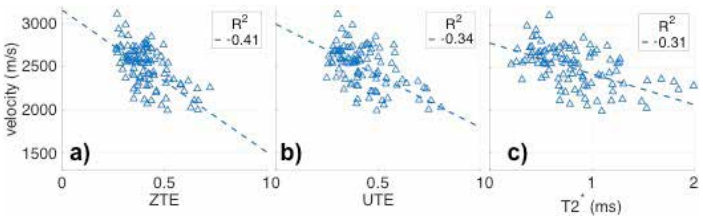

References

1. Miller et al. UTE MRI *versus* CT… *Med. Phys.* 2015.
2. Aubry et al. Experimental demonstration… *J. Acoust. Soc. Am.* 2003.
3. Connor et al. A unified model … *Phys. Med. Biol.* 2002.
4. Webb et al. Measurements of The Relationship … *IEEE TUFFC.* In press.
5. Wiesinger et al. ZTE MR bone imaging… *Magn. Reson. Med.* 2016.

P-BR-36

Topic: Brain
Presentation Type: Poster

Ultrasonic neuromodulation of pharmacologically isolated cultured neurons using a single extremely short pulse

Eyal Weinreb, Rony Paz, Elisha Moses

Weizmann Institute of Science, Rehovot, Israel

In accordance with author request, this abstract is not available for publication.

P-BR-37

Topic: Brain
Presentation Type: Poster

Fractional anisotropy value ratio after MR-guided focused ultrasound thalamotomy for essential tremor: correlation with one-year clinical outcome

Toshio Yamaguchi[1], Hiroki Hori[1], Takaomi Taira[2]

[1]Shin-yurigaoka General Hospital, Kawasaki, Japan
[2]Tokyo Women's Medical University, Tokyo, Japan

Background: Although the clinical rating scale for tremor (CRST) has been used for quantitative clinical assessment for transcranial magnetic resonance imaging-guided focused ultrasound (TcMRgFUS) thalamotomy in patients with essential tremor (ET), no definite quantitative imaging biomarker for degeneration of treated area has been introduced for TcMRgFUS thalamotomy. The aim of this study was to investigate the clinical significance of the Fractional Anisotropy (FA) value as an imaging biomarker, through investigation of the correlation between the FA value ratio and the CRST ratio recorded followings TcMRgFUS treatment.

Methods: We conducted a retrospective study in 12 patients, which consisted of two groups. The groups were the tremor improvement group and the tremor recurrence group. The FA value ratio was defined as a FA value at the treated side divided by a FA value at an untreated side. The receiver operating characteristic (ROC) analysis were performed to find out the optimal cut-off values of the FA value ratio.

Results: A significant decrease of the FA value ratio was observed after the treatment when compared to the pre-treatment FA ratio value seen in the group of improvement ($P = 0.0009$). The FA value ratio of the tremor recurrence group at one year after treatment recovered to the FA value ratio equivalent to the pre-treatment FA value ratio ($P = 0.4705$). The cut-off value of the FA value ratio was 0.537.

Conclusions: It was suggested that the FA value ratio is one of the imaging biomarker indicated for clinical outcome for TcMRgFUS thalamotomy with ET.

P-BR-38

Topic: Brain
Presentation Type: Poster

Hemodynamic imaging of mouse cortical response to multi-parametric transcranial ultrasound stimulation

Zhijie Wang[1], Yi Yuan[2], Shy Shoham[2]

[1]Yanshan University, Qinhuangdao, China
[2]New York University, New York, New York, United States

Background: Transcranial ultrasound stimulation (TUS) is a powerful new modality for targeted, reversible neuromodulation. However, the dependence of cortical responses on TUS dose parameters was only characterized indirectly using motor response-related measures.

Methods: We measured direct hemodynamic cortical responses to multi-parametric TUS delivered to mouse motor cortex, using effective short stimulation protocols. To capture both cerebral blood flow and blood oxygenation metabolism we used laser speckle contrast imaging and intrinsic signal optical imaging, respectively.

Results: Our stimulation protocol consistently evoked significant visible muscle contraction and movement. The imaging results demonstrate that both the relative cerebral blood flow and blood oxygenation reach the peak values at roughly 2.5 - 2.6 sec. and display a quantitative relationship between blood flow and oxygenation metabolism and ultrasonic intensity and stimulation duration.

Conclusions: These results could significantly contribute to our understanding of the dose-response characteristics of ultrasonic neuromodulation.

P-BR-40

Topic: Brain
Presentation Type: Poster

Reformatting MR temperature imaging data to identify anatomic landmarks during focused ultrasoundthalamotomy

Nathan McDannold, Reese Cosgrove

Brigham and Women's Hospital, Boston, Massachusetts, United States

Background: The ventral intermediate (VIM) target for transcranial MRI-guided focused ultrasound (TcMRgFUS) thalamotomyfor essential tremor is commonly selected using measurements relative to the intercommissural line. DifferentMRI sequences can delineate thalamic nuclei, but such imaging is currently not practical to obtain duringtreatment. Here, we demonstrate that phase imaging obtained for MR temperature imaging (MRTI) can directlyvisualize the red nucleus (RN), the substantia nigra (SN) and the subthalamic nucleus (STN), and these landmarkswere consistently oriented with respect to the VIM target.

Methods: Data from 11 TcMRgFUS thalamotomies were reviewed. The treatments were performed using the ExAblateNeuro device (INSIGHTEC) installed on a 3T MRI (GE). The VIM was targeted 14 mm lateral and ~1 mm superior tothe intercommissural line, and posterior to the anterior commissure by 25% of the intercommissural distance.Adjustments were made by the neurosurgeon based on individual patient anatomy and from functional testsbetween sonications. MRTI was obtained with the body coil (TR: 28 ms; TE: 3.1:4.7:21.9 ms; voxel:1.1×2.2×3mm, bandwidth: ±36 kHz) in a single plane. The complex data for every image obtained during in thesonication (typically 10) were averaged to improve SNR. A high-pass filter was applied to the phase data afterunwrapping. Anatomic structures were manually segmented.

Results: The filtered phase maps created by reformatting the MRTI data clearly depicted the RN, STN, and SN (Figure 1-3)in 10/11 patients. The VIM targets were reliably aligned in the AP direction with the RN observed in axialimaging, in the LR direction with the SN in coronal imaging, and were placed slightly above or partiallyoverlapping the SN visible in coronal and sagittal imaging. The mean AP distance between the RN centroid andthe target was 0.54±0.55 mm; it was was less than the dimension in 9/10 patients. The LR distance between theSN and the target in the coronal images was −0.16 ± 0.84 mm and less than the voxel dimension in 10/11patients.

Conclusions: Filtered phase maps with high SNR enabled delineation of the RN and the SN/STN with the patient within theTcMRgFUS device. These structures were consistently oriented with respect to the VIM target. The images werecreated by reformatting the data obtained for MRTI. Being able to visualize relevant anatomic structures withthe same images used for thermometry can enable greater confidence in targeting, as issues related to imagedistortion, patient/table motion, and registration to previously-acquired MRI are removed. It may prove usefulin ensuring consistent targeting during ET treatments. The images could potentially provide information fordifferent targets for TcMRgFUS such as the globus pallidus and the STN. Higher resolution imaging within theTcMRgFUS device should also be possible with this approach.

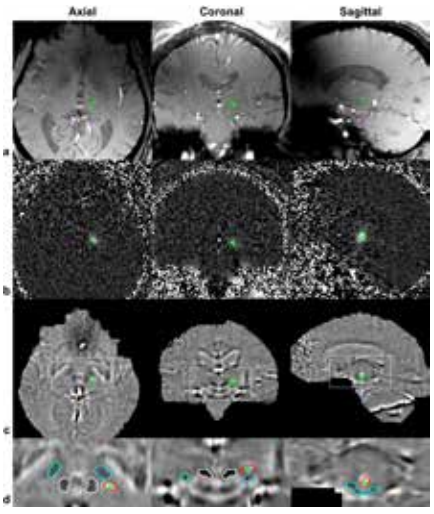

Figure 1.

Figure 2.

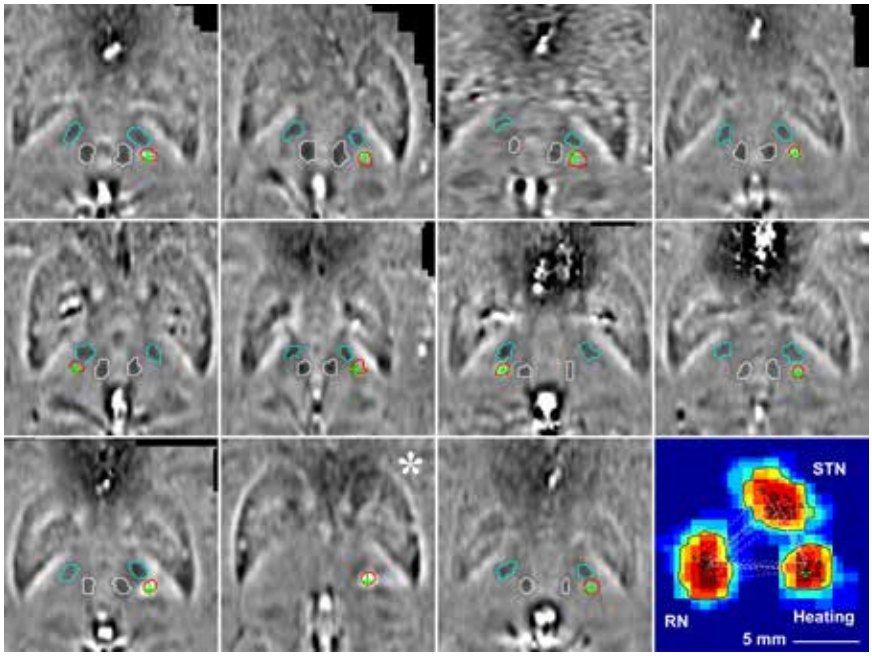

Figure 3.

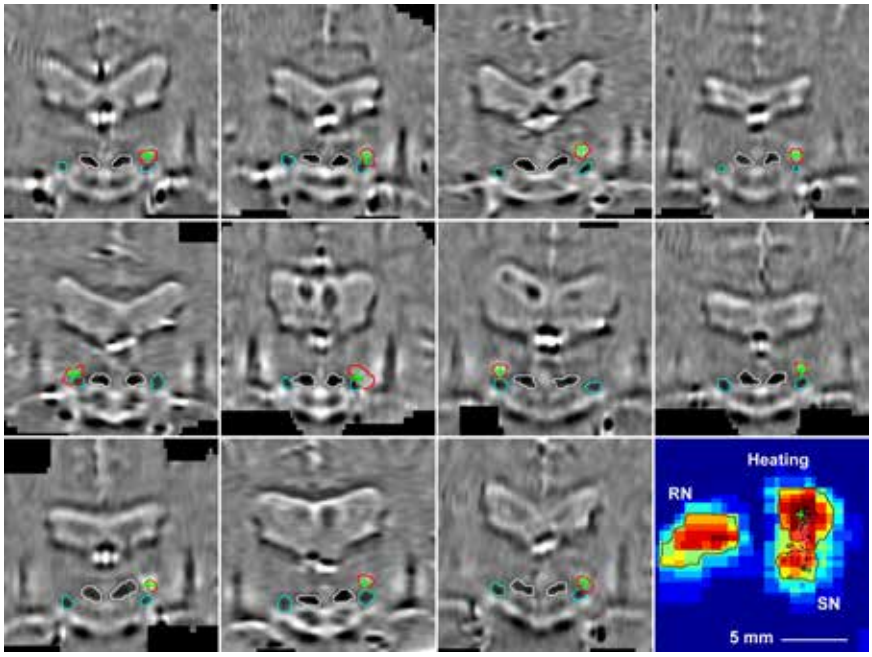

P-BR-41

Topic: Brain
Presentation Type: Poster

Focused ultrasound-mediated disruption of the blood-brain barrier alters the brain's neurovascular response to external stimulation

Nick Todd[1], Yongzhi Zhang[1], Margaret Livingstone[2], David Borsook[3], Nathan McDannold[1]

[1]Brigham and Women's Hospital, Boston, Massachusetts, United States
[2]Harvard Medical School, Boston, Massachusetts, United States
[3]Boston Children's Hospital, Boston, Massachusetts, United States

Background: Focused ultrasound (FUS) with microbubbles can transiently open the blood-brain barrier (BBB) for targeted delivery of pharmaceuticals into the brain without causing tissue damage. However, open questions remain about the severity of secondary effects that FUS BBB opening can have on the immune response, neuronal function and vascular hemodynamics.

In this study, we use two types of functional MRI to characterize the effects that FUS-BBB opening has on the neurovascular response to external stimuli in the rat brain.

Methods: N=9 Sprague Dawley rats underwent separate MR imaging sessions with and without FUS-BBB opening. Functional MRI data was acquired using two different imaging sequences: blood-oxygen level dependent (BOLD) imaging captured the hemodynamic response associated with standard fMRI and arterial spin labeling (ASL) imaging was used to isolate cerebral blood flow (CBF) in particular.

BBB disruption (0.34 MPa, 0.41 MI) was targeted to the right somatosensory cortex in one hemisphere only. Bilateral hind paw electrical stimulation was used to activate the somatosensory cortex in both hemispheres at short (6 s) and long (18 s) stimulus durations.

MR imaging was done one hour after BBB opening on a Bruker 7T scanner, using a single shot 2D EPI sequence for the BOLD data (TR = 1.5 s, TE = 18 ms, 18 slices, 0.5 x 0.5 x 1.0 mm resolution, 300 images) and a continuous ASL sequence for the CBF data (TR = 3000 ms, TE = 15.5 ms, 2000 ms labeling duration, 350 ms post-label delay, interleaved label/control).

Results: The location and extent of BBB opening is shown in Figure 1, along with histology from the first 5 rats showing no signs of tissue damage. The BOLD results in Figure 2 show that FUS-BBB opening leads to a marked decrease in the changes in the BOLD signal due to stimulation. The baseline CBF results are shown in Figure 3. The BBB Open cohort had slightly lower overall baseline flow, but there were no differences in baseline flow between the targeted right hemisphere and the non-targeted left hemisphere. Figure 4 shows changes in flow due to stimulation. BBB opening appears to fully suppress any changes in flow due to stimulation.

Conclusions: The brain's neurovascular response to external stimulation is a complex cascade of mechanisms from neuronal activity to neurovascular signaling to a hemodynamic response. Functional MRI can probe the final step in this chain, the changes in blood flow that arise to support local brain activity. The FUS power in this study used was below the threshold that others have shown could cause suppression of neuronal firing. It appears that FUS-BBB opening, at this low power level and one hour after sonication, still affects either the signaling mechanism from the neurons to the vessels that is supposed to initiate increased blood flow to the active region or the ability of the vessels to respond to this signal.

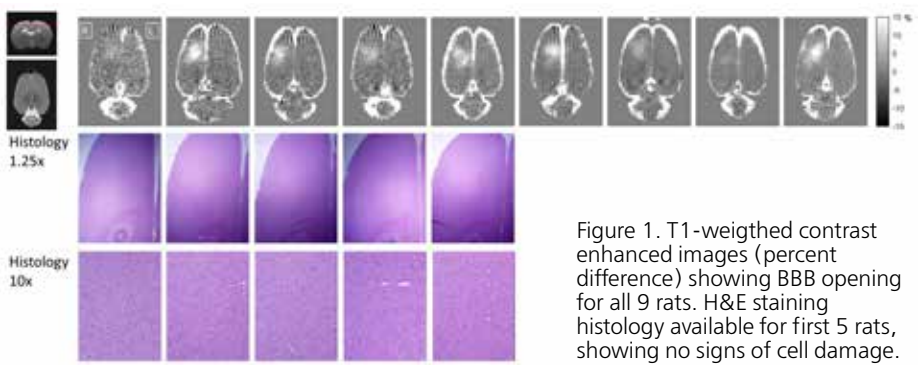

Figure 1. T1-weigthed contrast enhanced images (percent difference) showing BBB opening for all 9 rats. H&E staining histology available for first 5 rats, showing no signs of cell damage.

Figure 2. BOLD time course and whole brain maps (percent signal change) for BBB Closed and BBB Open cohorts at two different stimulus durations.

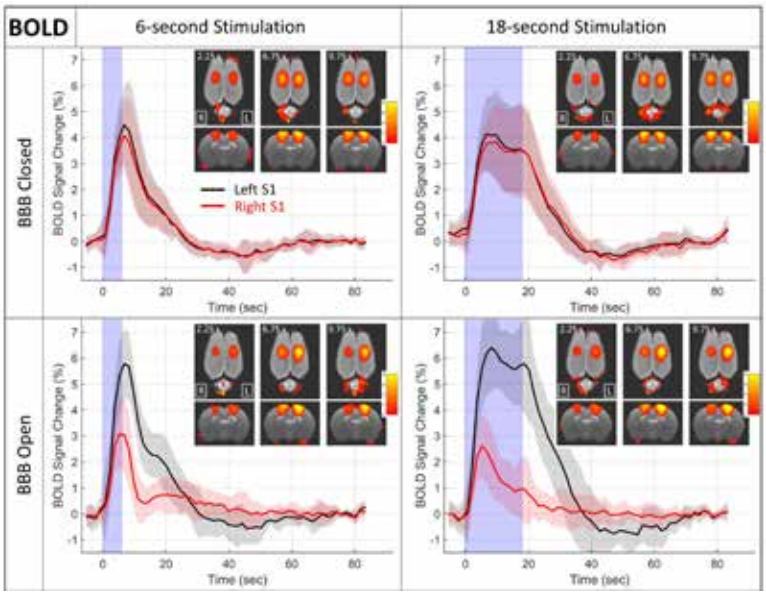

Figure 3. Baseline CBF maps for BBB Closed and BBB Open cohorts.

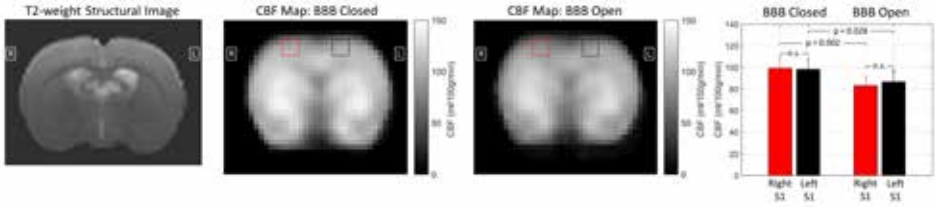

Figure 4. Time course plots and single-slice maps of CBF changes in response to stimulus for BBB Closed and BBB Open cohorts.

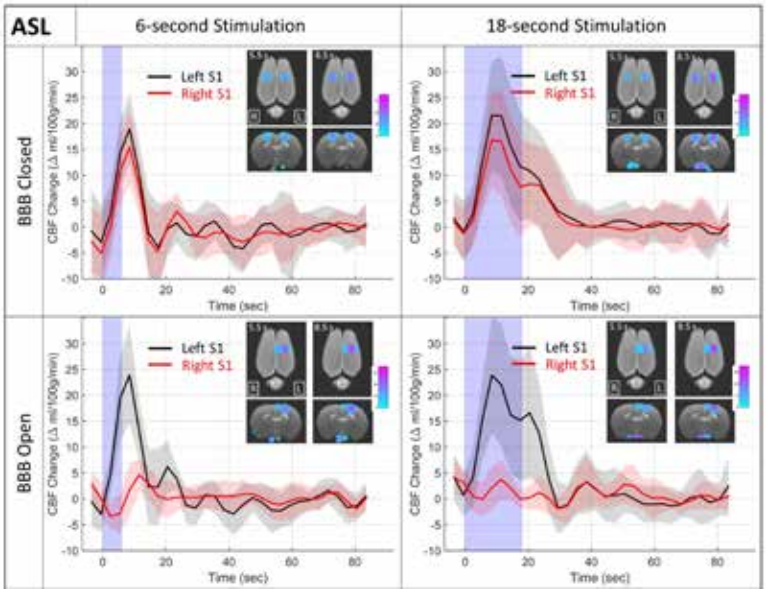

P-CA-1

Topic: Cancer
Presentation Type: Poster

Targeted drug delivery systems using shape memory polymers

Neema Ahmadian, Shima Shahab

MInDS Laboratory, Blacksburg, Virginia, United States

Background: The goal of the project is to design and perform *in vitro* testing of a novel mechanism for using focused ultrasound in targeted drug delivery applications. Targeted drug delivery systems would serve to act as a powerful medical tool and could save many lives. Targeted drug delivery is a way of more accurately administering a drug to its desired location in the body with less of the drug going to waste or potentially causing adverse effects. The proposed research has many medical applications such as treating a range of conditions across neurology and cardiovascular disease. This more efficient way of drug delivery results in less of the drug going to other parts of the body, thus reducing drug waste and side effects.

Methods: One way of achieving targeted drug delivery is through the use of shape memory polymers actuated by focused ultrasound. Shape memory polymers (SPM) are smart plastics that can be heated, deformed, and then reheated to return to their original state. A shape memory polymer capsule allows for a more dynamic system than traditional drug delivery methods. Once ingested by the patient the specially designed SPM capsule can be safely actuated from outside of the body through the use of HIFU as to not cause harm to natural body tissue. By creating a system in which pharmaceutical compounds can be selectively released into the body, this technology could also potentially be used in creating longer-term drug delivery systems in which the drug would be released part by part over an extended period of time.

Results: An oversized prototype has already been created by casting and curing the SMP into a custom acrylic mold. This prototype, however, is nonfunctional and has significant inaccuracies. The process of using a physical mold limits the usability and scalability of any prototype created. By developing a stereolithography method of 3D printing shape memory polymers, it becomes possible to fabricate much smaller, more intricate, and more accurate prototypes of this technology. The use of 3D printing as a manufacturing method also allows for many new capsule designs that wouldn't be possible with conventional methods. This ongoing research is being pursued through designing and testing custom 3D printing machines with modified tanks that can hold the special resigns needed for SMPs. Once accurate manufacturing of SMPs has been achieved, testing of focused ultrasonic actuation of polymer-based drug containers in laboratory conditions will commence.

Conclusions: The outcome of this internship can be used as the preliminary results for using focused ultrasound in controlled drug delivery applications to achieve high efficiency in releasing pharmaceutical compounds at targeted locations with controlled time rates, for a stable and effective drug concentration. Although there remain challenges in adapting 3D printing techniques to adequately manufacture SMPs, we remain optimistic that the research will lead to new methods for improved drug delivery systems through the use of high intensity focused ultrasound.

P-CA-2

Topic: Cancer
Presentation Type: Poster

Mechanisms of enhanced drug delivery in brain tumors with focused ultrasound-induced transient blood-tumor barrier disruption

Xiaoxiao Dong[1], Xiaofang Lu[1], Kailee Kingston[1], Emily Brewer[1], Oliver D. Kripfgans[1], J. Brian Fowlkes[1], Renny Franceschi[2], Zheng Liu[3], Andrew Putnam[2], Mario L. Fabiilli[1]

[1]University of Michigan Health System, Ann Arbor, Michigan, United States
[2]University of Michigan, Ann Arbor, Michigan, United States
[3]Xinqiao Hospital, Army Medical University, Chongqing, China

In accordance with author request, this abstract is not available for publication.

P-CA-3

Topic: Cancer
Presentation Type: Poster

DNA double-strand breaks induced by combined doxorubicin and unseeded controlled stable cavitation treatment in murine mammary tumor cells

FANT Cécile[1], Adeline Granzotto[2], Thais Moraes Vieira[1], Jean-Louis Mestas[1], Jacqueline Ngo[1], Cyril Lafon[1], Nicolas Foray[2], Frederic Padilla[1]

[1]LabTAU, Inserm U1032, Lyon, France
[2]Radiobiology, Inserm U1052, Lyon, France

Background: Doxorubicin (DOX) induces cell cytotoxicity through DNA damage. Recent studies have reported the occurrence of DNA damage in different cell lines exposed to cavitational ultrasound (US). We hypothesized that a combined treatment with doxorubicin and stable cavitation would lead to increased DNA damage in cells and would impact cell viability. . The objectives of this study were to evaluate the impact of such combined treatment on DNA in 4T1 murine mammary tumor cells *in vitro*, to investigate the possible causative mechanisms and to assess the impact on cell proliferation and viability.

Methods: 4T1 cells, a mouse mammary cancer cell line, were treated *in vitro* using a confocal device generating and monitoring pulsed cavitational ultrasound, with or without addition of DOX (frequency 1.1 MHz, PRF 25 HZ, DC = 15 %). The regulation of cavitation is based on two distinct modes: a high-power mode (peak negative pressure 6.7MPa), aimed at creating a population of bubbles, and a low-power mode (PNP 2.9MPa) aimed at maintaining their oscillations. After treatment, the occurrence of DNA damage was assessed by scoring γ-H2AX foci number in cell nuclei by immunofluorescence. The role of a bystander effect through calcium release was assessed by exposing untreated cells to the supernatant of sonicated cells with or without the addition of calcium chelator PBS solution. Cell viability and cell proliferation were assessed at 48h and 72h post treatment.

Results: The study of DNA damage through γ-H2AX foci showed that cells treated with stable cavitation, with or without DOX, elicited double strand breaks (DSB). However, without DOX, these DSB did not impact cell proliferation nor viability. The combination of stable cavitation and DOX led to premature DSB from 1h post treatment compared to DOX alone (DSBs observable only from 4h post treatment). Significant decrease of cell viability and proliferation was observed for the US+DOX group compared to the DOX group. The exposure of untreated cells to sonicated cells supernatant showed 40% of untreated cells with γ-H2AX foci from 10 min after treatment. The addition of PBS in the supernatant prevented the occurrence of g-H2AX foci in the cells.

Conclusions: A combined treatment of 4T1 tumor cells with DOX and controlled stable cavitation led to premature DSB induced by a bystander effect and significant decreases in cell proliferation and viability compared to a treatment with DOX or US alone. The role of calcium in this effect was further confirmed, as the addition of PBS counteracted this effect. These data suggest that cavitational ultrasound may potentiate the action of DOX through induction of DSB, therefore increasing the cytotoxicity of DOX.

P-CA-4

Topic: Cancer
Presentation Type: Poster

Focused ultrasound-induced blood-brain barrier opening increases antibody penetration and abscopal effect in mice with bilateral intracranial melanoma metastases treated with anti PDL1 and stereotactic radiosurgery

Fred C.C. Wu, Kunal Chaudhary, Shutao Wang, Elisa Konofagou, Simon Cheng

Columbia University Medical Center, New York, New York, United States

Background: The objective of this study was to determine if blood-brain barrier (BBB) opening with focused ultrasound (FUS) can increase antibody penetration and local control of non-irradiated tumor in the setting of bilateral brain metastases treated with unilateral targeted stereotactic radiosurgery (SRS) and antiPDL1 therapy.

Methods: C57B6 mice underwent bilateral intracranial injection of B16-F10 melanoma cells. In this 4 arm study, Arm 1: bilateral injection with no treatment. Arm 2: unilateral SRS only. Arm 3: unilateral SRS + antiPDL1 (Bioxcell). Arm 4: unilateral SRS + antiPDL1 + FUS. T1-post contrast MRI was performed on day 11 post intracranial injection using a 9.4 Tesla MRI. DICOM images were fused with CBCT simulation with SARRP (Xstrahl). Gross tumor volume (GTV) and non-irradiated contralateral tumor (AVOID) were contoured. A single sagittal arc using the 3 mm collimator was used to plan a 60 degree arc encompassing the GTV to avoid lateral scatter. 18 Gy was delivered to a point dose on the same day. Mouse phantom with radiochromic film was irradiated to assess lateral dose fall off. Animals treated with antiPDL1 received 4 cycles of 200 microgram every 3 days starting 1 hour prior to SRS. FUS-induced BBB disruption with microbubbles was performed targeting the irradiated tumor with 1.5 MHz FUS, 0.5 MPa peak negative pressure, 1000 cycle pulses, 5 Hz pulse repetition frequency, 30 second treatment duration at each spot. A 3 x 3 mm exposure grid was performed to cover the targeted tumor 1 hour prior to each cycle of antiPDL1 injection. MRI was obtained on day 18. To assess permeability of antibody status post FUS-induced BBB opening, western blot was performed of brain tumors with and without FUS.

Results: FUS-mediated BBB-opening was associated with approximately 5 times increase in antiPDL1 delivery. In addition, BBB-opening was feasible in an irradiated field. On day 18, volume of the tumor in the SRS treated side (GTV) *versus* the non-irradiated side (AVOID) were 19.0±9.6 *vs.* 91.9±24.4 mm^3 (Avg±SEM) (Arm 2), 4.6±1.6 *vs.* 61.7±13.6 mm^3 (Arm 3), 0.8±0.7 *vs.* 21.4±7.6 mm^3(Arm 4). In the untreated arm (Arm 1), tumor volumes were 54.9±5.2 mm^3 *vs.* 66.9±35.5 mm^3. DVH analysis for GTV and Avoid tumors are listed in table below. Radiochromic film using axial mouse phantom treated with 18 Gy SRS showed rapid dose fall off with the projected contralateral Avoid tumor located within the 1%-5% isodose lines. Increased permeability of IgG status post FUS was demonstrated with IgG tagged gadolinium and serial T1-post contrast MRI. Median OS for Arms 1-4 were 19.3, 19.6, 21.2, and 26 days respectively.

Conclusions: FUS-induced BBB opening increases local IgG permeability. FUS plus radiation and antiPDL1 seems to suggest increased local control in non-treated brain tumor. Further data needed to validate these findings.

P-CA-5

Topic: Cancer
Presentation Type: Poster

Magnetic Resonance guided high intensity focused ultrasound (MRgHIFU) virtual treatment planning for abdominal neuroblastoma utilizing retrospective diagnostic 3D CT images

Aodhnait Fahy[1], Stephanie Tung[1], Maria Lamberti-Pasculli[1], Adam Waspe[1], Samuel Pichardo[2], Ted Gerstle[1]

[1]The Hospital for Sick Children, Toronto, Ontario, Canada
[2]University of Calgary, Calgary, Alberta, Canada

Background: Despite significant advances in multimodal therapies, prognosis for high risk neuroblastoma remains poor. Magnetic Resonance-guided High Intensity Focused Ultrasound (MRgHIFU) is a potentially new therapy for neuroblastoma, which uses ultrasound-induced thermal ablation with real-time MR thermometry to treat solid tumours. The potential therapeutic impact of this approach is partly dependent on whether the tumour is anatomically targetable with MRgHIFU. Targetability must take into account patient safety, minimizing the risk of injury to surrounding structures; treatments are unpredictable outside of formal MRgHIFU planning platforms. MRgHIFU planning to evaluate targetability currently relies predominantly on MR scans which, for the pediatric patient, can involve general anesthesia, longer imaging times, longer wait times and increased cost relative to abdominal CT scans; moreover, MR scans are a distinctly uncommon part of the standard neuroblastoma workup. We have previously presented pilot data as a proof of principle showing a technique to enable virtual planning for MRgHIFU therapy based entirely on the patient's existing 3D CT scans. In this follow up analysis, we use this technology to ask what proportion of patients' abdominal neuroblastomas were potentially targetable with MRgHIFU based on their initial CT scans at diagnosis.

Methods: Abdominal CT images of 88 patients with neuroblastoma were processed with a custom Python-based software script to incorporate data fields required by the Philips Sonalleve MR-HIFU treatment-planning platform, as well as to numerically re-center and rotate the tumor into the Sonalleve's intrinsic workspace. Targetability was calculated as the percentage of treatment volume to tumor volume by two independent research analysts with training in MRgHIFU targeting.

Results: All patients' CT scans were imported into the Philips Sonalleve MRgHIFU system in order to complete treatment planning for MRgHIFU. Average tumor size (± s.d.) was 191 (± 195) cubic centimeters and tumor depth was 29 (± 17) millimeters. 73 and 78 of the 88 patients had targetable tumors when a two- and one-centimeter safety margin (around vital structures including bowel and nerves) was adopted, respectively. Of those with targetable tumors, the percent volume of targetable tumor ranged from 5% to 67% with two-centimeter margins, and from 7% to 79% with one-centimeter margins. Tumor targetability was highest in right upper quadrant lesions, tumors greater than 200 milliliters in size, and tumors less than 3 centimeters from the skin surface. Over 90% of lesions were limited to some degree in their targetability due to proximity to bowel and almost 80% limited due to ribs.

Conclusions: This study demonstrates the feasibility of using patients' CT imaging for MRgHIFU treatment planning in a larger patient cohort. Our results show that MRgHIFU can partially treat the majority of patients with intra-abdominal neuroblastomas and that certain tumor characteristics as size and anatomical location within the abdomen (right upper quadrant and superficial position) make a lesion more amenable to MRgHIFU targetability. Patient safety with the application of this treatment, including potential thermal injury to the bowel, bone, and nerve, limits whole tumor targetability and ablation in most cases.

P-CA-7

Topic: Cancer
Presentation Type: Poster

A compressible multiscale model for mathematical modeling of microbubble enhanced high intensity focused ultrasound (HIFU)

Aswin Gnanaskandan, Chao-Tsung Hsiao, Georges Chahine

Dynaflow Inc, Jessup, Maryland, United States

Background: HIFU uses the focused energy of ultrasound to elevate temperature locally, causing thermal ablation of tissues. A major impediment with the current use of HIFU to efficiently treat deep seated cancer is the need for deep penetration using higher intensity ultrasound and longer treatment times. Such high intensity sound waves may cause unwanted tissue damage along its passage before reaching the targeted region. It is therefore desirable to develop mechanisms to achieve higher temperature elevations at the focal region while still using moderate intensity levels (100 – 1000 W/cm^2). Introducing microbubbles in the form of contrast agents has been shown to increase temperature levels in both *in vitro* and *in vivo* experiments. However, understanding the exact mechanism of how the microbubbles contribute to the heat increase requires well validated numerical models to shed light on the underlying phenomena.

Methods: A fully compressible multiscale model for simulation of High Intensity Focused Ultrasound (HIFU) both in the absence and presence of microbubbles is presented. The non-linear ultrasound field is modeled using compressible Navier-Stokes equations, while the microbubbles dynamics is handled using discrete singularities in a Lagrangian framework. These two models are coupled such that both the acoustic field and the bubbles influence each other. The energy absorbed by the medium locally due to the focused ultrasound and bubble dynamics is then used to compute the temperature rise by solving a bio-heat transfer equation over the entire insonation time period.

Results: We first demonstrate HIFU simulation without microbubbles and characterize the pressure and temperature fields by validating against available experiments. Experimental validation in the presence of microbubbles is then carried out to demonstrate the accuracy of the model. The effects of the initial void fraction on the attenuation of the primary ultrasound and on the enhanced heat deposition near the focal region is examined. The partial contribution of ultrasound, bubble acoustics and bubble viscous damping to the heat enhancement are analyzed in detail. We then study the effect of localizing the microbubbles in the focal region and the effects of the localization on altering the temperature rise obtained in the focal region.

Conclusions: For *in vitro* studies in tissue phantom without microbubbles, a good agreement with experiments for temperature rise in the focal region is obtained. The method, when applied in the presence of bubbles, gives a good qualitative agreement. Quantitative validation of the method is hampered at this point by the lack of details from the experiment. It is shown that for the considered configuration, viscous damping of the bubble oscillations is the primary contributor to the enhanced heat deposition. Enhanced attenuation of the focused ultrasound and prefocal heating is demonstrated at higher void fractions. Concentrating the bubbles close to the focal region results in higher temperature increase due to reduced attenuation of the amplitude of the ultrasound wave.

Acknowledgements: This work is support by NIH under SBIR Grant No. 1R43CA213866-01A1.

P-CA-8

Topic: Cancer
Presentation Type: Poster

Characterization of metabolic stress response on murine melanoma cells after therapeutic ultrasound

Tejas Karwa[1], Sanjay Pandey[1], Saurabh Singh[2], Claudia Gutierrez[2], Indranil Basu[2], Chandan Guha[2]

[1]Albert Einstein College of Medicine - Montefiore Medical Center, Bronx, New York, United States
[2]Institute of Oncophysics, Albert Einstein College of Medicine, Bronx, New York, United States

Background: Treatment of localized primary tumor by focused ultrasound (FUS) utilizes a range of input energy predominantly for in-situ tumor ablation. While clinically used high-intensity FUS (HIFU) thermally ablate the tumor at the focal spots, low-intensity FUS (LOFU) on the other hand, releases immunogenic molecules into the tumor microenvironment by generating a mild thermal and cavitation effects. HIFU is not very effective in terms of long-term protection from local recurrence or metastasis. We have recently shown that treating mouse melanoma tumors with LOFU inhibits the induction of T cell tolerance. In the proposed study, we will measure the induction of significant metabolic burden of LOFU in combination with another mode of ablation in a murine B16 F10 melanoma cell line. The simultaneous assessments of physiological responses during the treatments will help to investigate the stress generated by the failure to fulfill the metabolic demand of the melanoma cells.

Methods: B16 F10 melanoma cell line will be cultured in DMEM media with 10% fetal bovine serum and divided into 4 groups: Control, LOFU treatment, Ablative treatment, and LOFU + Ablative treatment. LOFU treatment will be performed on the Philips Therapy and Imaging Probe System (TIPS, Philips Research Briarcliff, USA). Treated cells will be processed and analyzed at 4 hours or 24 hours after treatment for flow-based assays and at 2, 24, 48, and 72 hours for MTT assay to assess the metabolically viable cells. Annexin V and PI staining will be conducted to determine the percentage of cell death because of either treatment initiated apoptosis or necrosis respectively. The expression of HSP70, CRT, and GRP78 on the cells membrane surface will be determined using flow cytometry.

Results: *In vitro* treatment of B16F10 cells with LOFU is expected to increase the cell surface localization of stress markers CRT, HSP70, and GRP78 as early as 4 hours after LOFU treatment. Simultaneous staining of Annexin V-FITC and the non-vital dye PI (propidium iodide) should discriminate the early apoptotic (FITC+PI-) from the late apoptotic or necrotic cells (FITC+PI+). The combination of LOFU treatment and ablation therapy is expected to increase the expression of immunogenic markers that might play a key role in the process of cell death. These key markers of the immune system recognize and eradicate the tumor cells that have the ability to bypass the immune system's survey of malignant tumors. The expected low cell viability will be detected by MTT cell proliferation assay in combination treatment group.

Conclusions: The increase in tumor susceptibility to the immune system can allow for better anticancer immunotherapy treatment of primary tumors and prevention of metastasis. LOFU in combination with ablation therapy has the potential to successfully cut off the metabolic pathway of highly metastatic B16 melanoma cells. The characterization of metabolic stress response will lead the way for a more effective combination therapy options with either immune or other forms of energies or anti-tumor drugs.

Acknowledgements: Einstein Institute of Oncophysics and Summer 2018 FUSF Global Internship Program

P-CA-9

Topic: Cancer
Presentation Type: Poster

Concepts for robot-assisted focused ultrasound to support radiation therapy

Johann Berger[1], Michael Unger[1], Thies Jochimsen[2], Bernhard Sattler[2], Upasana Roy[1], Lisa Landgraf[1], Thomas Neumuth[1], Osama Sabri[2], Andreas Melzer[1]

[1]Innovation Center Computer Assisted Surgery, Leipzig, Germany
[2]University Leipzig, Leipzig, Germany

Background: Radiation therapy (RT) belongs to the routinely applied treatment modalities of cancer disease whereas still causing side effects. Hyperthermia (40-45°C) of tumor cells causes radio-sensitizing effects. Hence, a combined therapy of both modalities should improve treatment outcome. Focused ultrasound (FUS) is able to generate hyperthermia precisely and non-invasively. FUS may prove to be the optimal method to combine hyperthermia and radiation in one treatment in the clinic. However, positioning ultrasound transducer can be challenging. Robotic arms provide the means to place tools in regions that are difficult to reach. The aim of this work is to present novel ideas for the combined FUS-RT treatment and to propose concepts for an effective realization.

Methods: For simultaneous hyperthermia and RT the robotic workflow needs to be (i) integrated into radiation room or (ii) MR-compatible systems should be installed in an MR-guided radiation device (e.g. MR-linac, Elekta).

Collaborative robotics provides the means to reduce complexity and increase user experience. Towards integrating the dual-robot setup (i), first steps were made by implementing a framework for the vendor-independent communication of a KUKA LBR iiwa 7 robotic arm using the open surgical communication protocol (OSCP). A service-oriented mobile platform was developed to evaluate touch gesture interaction concepts for the use case of ultrasound guided biopsies. A validation was conducted on an abdominal phantom (Triple Modality 3D Abdominal Phantom, CIRS Inc., USA) with nine participants of varying technical and clinical expertise.

To realize FUS in an MR-guided radiation device (ii) an MR-compatible robotic arm system (InnoMotion by InnoMedic GmbH) was integrated into a Biograph mMR PET/MRI system (Siemens Healthineers) in Leipzig. For integration into the clinical infrastructure, the hardware, which contains the planning software of the robotic arm, was virtualized using Oracle VirtualBox. This virtual machine was placed on the Linux server which is attached to the PET/MRI system for post-processing, storage and distribution of data. Thereover, image data can be transferred easily to the planning software which acts as a DICOM receiver.

Results: The mobile robotic platform (i) was tested for needle targeting of two lesions inside the phantom. Manually, participants had to advance the needle up to five times until hitting the targets, whereas with robot assistance the targets were hit on the first try. In a questionnaire the interaction concept was rated to be intuitive and improve the workflow (Fig. 1).

For the realization of (ii) MR-guided FUS and radiation therapy, a robotic arm system was successfully integrated into the Biograph mMR PET/MRI system. The attenuation caused by the robotic arm was measured to correct this influence in future studies (Fig. 2).

Conclusions: Our approach for the interaction and integration of a dual robotic arm system for a combined therapy using FUS-induced hyperthermia and radiation is technically feasible. The usability and user acceptance of interacting with the robotic system using touch control was rated positively. The presented technical setup with an MR-compatible arm represents a starting point to gain clinical experience.

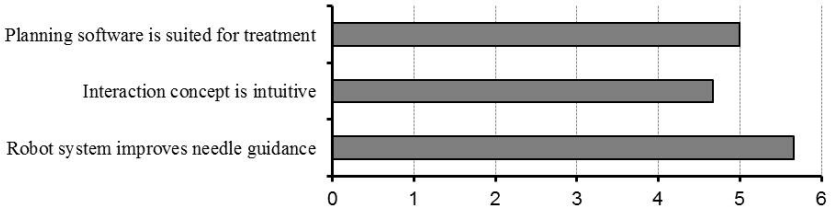

Figure 1. Evaluation of the questionnaire on the systems performance and usability (6 – very good, 1 – very bad). Values are given as mean over all participants.

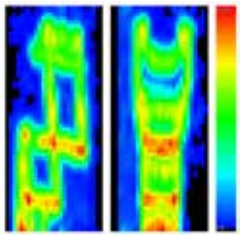

Figure 2. Attenuation map of the robotic arm visualized by two perpendicular maximum-intensity projections of the linear attenuation coefficient of 511-keV PET annihilation photons (in 1/cm) obtained by a stand-alone PET scanner equipped with Ge-/Ga-68

P-CA-10

Topic: Cancer
Presentation Type: Poster

3T MRI-guided High Intensity Focused Ultrasound setup for treatment and evaluation of mouse models of pancreatic ductal adenocarcinoma

Donghoon Lee[1], Yasser Nazari[1], Joshua Park[1], Stella Whang[1], Helena Son[1], Ezekiel Maloney[1], Yak-Nam Wang[1], Wayne Kreider[1], Ari Partanen[2], Feng Zhang[1], Tanya Khokhlova[1], Joo Ha Hwang[3],

[1]University of Washington, Seattle, Washington, United States
[2]Profound Medical, Mississauga, Ontario, Canada
[3]Stanford University, Stanford, California, United States

Background: Pancreatic ductal adenocarcinoma (PDA) is the fourth leading course of cancer-related death in the United States. MRI-guided high intensity focused ultrasound (MRgHIFU) has recently demonstrated potential treatment efficacy of PDA. One major challenge in MRgHIFU preclinical research is developing a setup appropriate for mouse models of PDA and establishing MRI methods to assess responses to MRgHIFU therapy. In this study an MRgHIFU preclinical setup and MRI methods were developed to treat PDA mouse models, monitor tumor progression and assess response to therapy on a clinical 3 Tesla (T) MRgHIFU system.

Methods: An orthotopic model and transgenic (KPC) mouse model of PDA was used in this study. The experiments were performed on a 3T clinical MRI scanner (Ingenia, Philips Healthcare, Best, the Netherlands) equipped with a clinical HIFU system (Sonalleve V2, Profound Medical Inc., Mississauga, Canada). A surface radiofrequency (RF) coil was developed to image mouse pancreas tumors *in vivo* at 128 MHz. The RF coil was placed within a custom mouse holder mounted on top of a degassed water tank that was positioned above the HIFU patient table acoustic window. A high pass filter was fabricated to minimize potential interaction from HIFU signals at 1.2 MHz. We established multi-parametric MRI (mpMRI) methods including high-resolution T2 weighted imaging, and quantitative T2 maps, diffusion weighted, magnetization transfer ratio, and chemical exchange saturation transfer (CEST) parameters for comprehensive characterization of PDA tumors pre- and post-treatment. Two HIFU regimes were evaluated for PDA treatment: continuous wave mild hyperthermia (HT) treatment at around 41 C (three sets of 10 min duration) and cavitation-based pulsed HIFU treatment (450 W acoustic power, 1 ms pulse duration and 1 Hz pulse repetition frequency).

Results: Both mild HT and pulsed HIFU treatments were successfully performed in pancreatic tumor models *in vivo*, with sets of mpMRI performed before and after the treatment. T1 weighted images were first acquired for both a mouse body and a gel phantom next to the animal. The T1 weighted image was selected from multi-slice 2D slices showing detailed features of the animal body. The tumor target was identified by high-resolution T2 weighted images. MRI parameter values including T2, MTR, ADC and gagCEST were quantified and compared before and after HIFU sonication. Initial results show slight decrease of T2, ADC, and gagCEST, and increase of MTR after both HIFU treatment modes in comparison to those before HIFU.

Conclusions: A preclinical setup for treatment of PDA with a clinical MRgHIFU system was developed along with mpMRI methods for monitoring tumor progression and response to different modes of HIFU treatment. The developed setup and mpMRI methods will be used for future HIFU treatments with the PDA mouse models for targeted drug delivery.

Acknowledgements: This work was supported by NIH R01CA154451 and R01CA188654.

P-CA-11

Topic: Cancer
Presentation Type: Poster

Focused Ultrasound-Induced Immunomodulation in Breast Cancer

Christopher Margraf, Timothy Bullock, Alexandra Witter, Richard Price, Natasha Sheybani

University of Virginia, Charlottesville, Virginia, United States

In many instances, cancer immunotherapy is revolutionizing patient outcome, however, breast cancer patients have yet to receive much benefit from this treatment option, in part due to the immunosuppressive tumor microenvironment. This project aims to use focused ultrasound technology to stimulate an anti-tumor immune response. Focused ultrasound is a non-invasive technology that uses high-powered acoustic waves to damage cancer cells. This stimulation is known to have a multitude of effects, including heat and mechanical tissue damage, depending on the wave type, which can do direct damage to tumor and lead to decreased tumor growth, both directly and via induction of anti-tumor immunity. Activated T cells are required for tumor killing based on their ability to target the tumor and release cytokines in the tumor environment. A major hypothesis to explain the weak immunogenicity of breast cancers is the lack of the availability of both antigen and immune-stimulatory materials (DAMPs) from dying tumor cells. Low antigen availability in the tumor limits the ability of dendritic cells (DCs) to activate T cells, while limited DAMPs lessens the activation of DCs. Methods of increasing antigen and DAMP availability are therefore important for improving cancer therapies. Herein, we use single cell multi-parameter flow cytometry and TCR transgenic T cell lines to explore the impact of different FUS regimens on the acquisition of antigen from tumors by DCs, the subsequent activation of DCs, and their ability to stimulate T cells.

P-CA-12

Topic: Cancer
Presentation Type: Poster

The effect of mechanical stress *versus* thermal stress of therapeutic ultrasound on murine prostate and breast cancer cells

Dia Shah, Karin Skalina, Saurabh Singh, Claudia Gutierrez, Indranil Basu, Chandan Guha

Institute of Oncophysics, Albert Einstein College of Medicine, Bronx, New York, United States

Background: Current focused ultrasound (FUS) therapies used in the clinical setting fall under the category of High intensity focused ultrasound (HIFU) which sends sound energy to a targeted region in the tissue, causing a fast increase in the temperature of the tissue over around 80°C, inducing immediate necrosis at the tissue focal point, serving as an ablator. HIFU, though, is insufficient in the prevention of long-term metastases, or cancer recurrence, due to its border zone treatment nature. Low intensity focused ultrasound (LOFU) has the ability to induce a less severe thermal and mechanical effect, which allows for the release of immunogenic molecules, thereby inducing an immune response. In the proposed study, we will compare the effects of mechanical and thermal stress by varying peak negative pressure and duty cycle while delivering LOFU to the TPSA23 (murine prostate tumor) and 4T1 (murine breast tumor) cells. The simultaneous assessments of cell viability, altered mitochondrial inner cell membrane potential, and analysis of HSP family of proteins and other immunogenic cell death markers will help to investigate the stress generated by the LOFU treatment inside the prostate and breast tumor cells.

Methods: The first phase of this study includes treating 4T1 and TPSA23 cell lines *in vitro* by performing mitochondrial stress and immune cell proliferation assays measuring changes in metabolic viability and T cell tolerance of 4T1 and TPSA23 cells under the LOFU treatment. LOFU will be performed using the Phillips Therapy and Imaging Probe System (TIPS, Philips Research Briarcliff, USA). The second phase of this study includes treating 4T1 and TPSA23 cell lines *in vitro* with LOFU alone, radiation therapy alone and a combination of LOFU + radiation therapy. Various LOFU parameters (3W – 9W of power and 75%–100% duty cycle) will be utilized for each cell type based on our previous studies and published literature. The viability and proliferation of cells in each of the treatment groups will be monitored by MTT and clonogenic assays. The expression of HSP family of proteins and ICD markers will be determined by using flow cytometry.

Results: In phase one of the study, parameters which were previously established as non-lethal are expected to produce a significant amount of mitochondrial stress and reduced cell proliferation in 4T1 and TPSA23 tumor cell lines. In phase two of the study, *in vitro* treatment of both the cell lines with LOFU is expected to increase the cell surface localization of HSP70. The combination of LOFU and radiation therapy is expected to increase the expression of immunogenic markers. The expected low cell viability will be detected by MTT cell proliferation assay in combination treatment group.

Conclusions: The establishment of the parameters at which LOFU serves as a mitochondrial stressor and immune response activator allows for a baseline at which further therapeutic combination studies can be built. The proposed study will help to characterize the mechanical and thermal effect of LOFU treatment on murine tumor models and predict the most translationally effective therapy to control the primary and systemic tumor growth.

Acknowledgements: Einstein Institute of Oncophysics and Summer 2018 FUSF Global Internship Program

P-CA-13

Topic: Cancer
Presentation Type: Poster

Characterization of acoustic emissions and tumor outgrowth in the setting of FUS-mediated blood/tumor barrier disruption in murine glioma

Sophie Meyer, Natasha Sheybani, William Garrison, G. Wilson, Richard Price

University of Virginia, Charlottesville, Virginia, United States

Background: Glioblastoma (GB) is the most common and malignant brain tumor, its diffuse nature and proclivity for recurrence rendering it largely intractable. Immunotherapy (ITx) approaches (e.g. anti-PD1) may hold promise for treating GB; however, the blood-brain (BBB) and blood-tumor (BTB) barriers hinder delivery of systemically administered ITx drugs. A potential approach to enhancing ITx delivery is MRI-guided focused ultrasound (FUS), a non-invasive technique that, when combined with concomitant systemic injection of microbubbles (MB), can transiently disrupt the BBB/BTB and mechanically perturb the tumor microenvironment. Here, we investigate whether localized BBB/BTB disruption with FUS+MB enhances anti-tumor immune responses and inhibits tumor growth in an orthotopic murine glioma model.

Methods: At 14 days following intracranial implantation of GL261 cells stably transfected with luciferase (GL261-luc2), mice were ultrasonically coupled to a 1.1 MHz small animal MR image-guided FUS system. In animals bearing MRI-visible tumors, albumin-shelled MB were injected intravenously and a 4-spot grid of sonications was applied to the tumor-bearing region immediately following (0.4-0.6 MPa peak negative pressure (PNP), 0.5% duty cycle, 120s period). BBB/BTB disruption was confirmed by post-treatment MR imaging. Tumor outgrowth was monitored serially by IVIS imaging. One week following treatment, whole brains and peripheral lymphoid organs were harvested for flow cytometry.

Results: MR imaging of GL261-luc2 tumors treated at the stated parameters evidenced successful BBB/BTB disruption (Fig.1a). Analysis of acoustic emissions detected by passive cavitation monitoring discretized stable and inertial cavitation activity as a function of PNP (Fig.1b,c). Seven days following BBB/BTB disruption at 0.6 MPa, CD86 (a marker of maturity) mean fluorescence intensity (MFI) on dendritic cells (DC) increased ~3-fold in deep cervical lymph nodes (DCLN) (Fig.1d). Accordingly, intratumoral CD86+ DC trended towards increased absolute frequency while CD86 MFI on intratumoral DC was significantly different across the two PNPs evaluated (Fig.1e). One week following BBB/BTB disruption, intratumoral CD4+ T cells doubled and intratumoral CD8+ T cells increased by ~17%. Within the intratumoral CD8+ T cell population, a significant differential increase in antigen-experienced (CD44+) PD1+ T cells was observed as a function of FUS+MB treatment at both 0.4 and 0.6 MPa (Fig.1f), thereby inciting a rationale for future implementation of anti-PD1 therapy. Bioluminescence imaging revealed a significant reduction in total photon flux as early as 6 days following FUS+MB at 0.6 MPa (Fig.1g), indicating early growth inhibition of GL261-luc2 tumors.

Conclusions: These findings demonstrate that BBB/BTB disruption with FUS+MB can potentiate anti-tumor immunity against glioma, independent of drug delivery. Ongoing studies entail combining FUS+MB with checkpoint inhibitor (i.e. anti-PD1, anti-TIGIT) delivery to evaluate whether an allied treatment approach can promote an even more robust anti-glioma response.

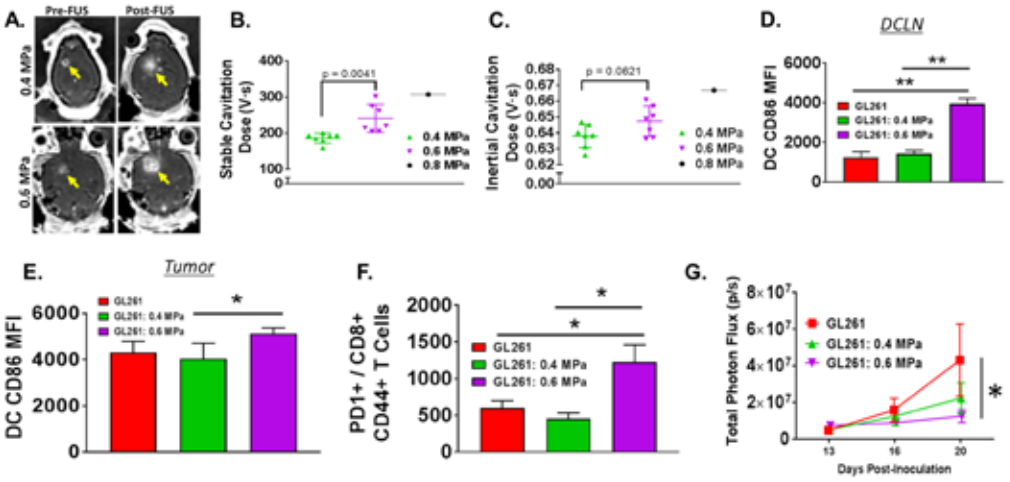

Figure 1. (A) Representative axial contrast-enhanced T1-weighted MRI images demonstrating BBB/BTB disruption in GL261-luc2 tumors. (B-C) Stable and inertial cavitation doses calculated from harmonic and broadband acoustic emissions, respectively. (D-E) MFI of CD86 on CD11c+ DC in DCLN and tumor one week following FUS+MB (groups: untreated GL261-luc2 tumors, GL261-luc2 tumors exposed to 0.4 MPa or 0.6 MPa FUS). (F) Absolute frequency of CD8+CD44+PD1+ T cells in GL261-luc2 tumors one week following FUS+MB. (G) Serial bioluminescence imaging quantification demonstrating early tumor growth inhibition. *p<0.05. **p< 0.01.

P-CA-14

Topic: Cancer
Presentation Type: Poster

Nonlinear acoustic and acoustic-electromagnetic interactions for prospective bio medical applications

Alexander Sutin

Stevens Institute of Technology, Hoboken, New Jersey

Background: We present a review of research and new ideas based on effects investigated in various physics areas that are being investigated for medical applications. These effects include:

1. Nonlinear acoustic effects. The most known application of this effect is nonlinear ultrasonic imaging of Ultrasonic Contract Agents (UCA) and nonlinear acoustic methods of bone assessment.
2. Time Reversal Acoustic (TRA) focusing that provides precise concentration of acoustic energy to chosen areas of the body. Measurements of nonlinear effects in the TRA focus are the basis for a new diagnostic method of precise focusing.
3. Interaction of acoustic and Electro-Magnetic (EM) waves is a new topic for medical applications and research. The investigations of modulation of EM waves by ultrasound for breast tumor detection started a few years ago.

Methods: We suggest the improvement of currently investigated and new methods of cancer diagnostics and treatment.

Results: The following prospective medical applications of nonlinear acoustic, TRA and acoustic electromagnetic interaction effects are discussed.

1. Nonlinear acoustic effect for diagnostics and their enhancement using Time Reversal Acoustic focusing; early osteoporosis detection — The previously conducted experiments demonstrated that an osteoporotic bone exhibits stronger acoustic nonlinearity compared to healthy bones. Among many tested nonlinear acoustic methods, the nonlinear TRA is one of the simplest. In the conducted tests, the concentration of acoustic energy of two signals with different frequencies in a small volume of bone was provided by TRA focusing. The measurements of the scattered signal in human calcanei bone samples demonstrated a much higher level of nonlinearity for bones of older women (91 and 93 years old) than for younger healthy women.
2. Cancer diagnostics using modulation of EM waves by ultrasound — Proposed methods for detecting breast cancer are based on different physical properties, such as tissue elasticity, temperature, acoustic, optical or electrical parameters. The interaction of EM and acoustic waves depends on the combination of these parameters. Stevens has substantial experience in measuring similar interactions for nondestructive testing and all necessary acoustic and EM systems for these investigations.
3. Application of nonlinear ultrasound contrast agents scattering for TRA focusing — Focused ultrasound with Ultrasonic Contract Agents (UCA) has numerous clinical applications. We suggest applying nonlinear TRA focusing to UCA that is based on the reception of signals of nonlinear scattering from UCA and their frequency transformation and application of transferred signals for TRA focusing.
4. TRA focusing using thermoacoustic and optoacoustic effects — TRA systems can provide precise focusing to a tissue area where the transformation of the EM or optical wave to sound takes place. Numerous research of thermoacoustic and photoacoustic tomography for breast cancer diagnostic demonstrated increasing of ultrasonic radiation from the cancer cells that can be used as a beacon for precise TRA focusing to this area.

Conclusions: The presented suggestions for several new methods of ultrasound and EM diagnostics and treatment require significant research for their possible transfer to medicine. Stevens team will be happy to collaborate with medical organizations in this research.

P-CA-15

Topic: Cancer
Presentation Type: Poster

Effective tumor growth suppression by the combination of microbubble mediated ultrasound and immunotherapy

Ryo Suzuki, Daiki Omata, Lisa Munakata, Saori Kageyama, Tadamitsu Shima, Johan Unga, Kazuo Maruyama

Teikyo University, Tokyo, Japan

Background: Microbubbles oscillate and collapse in an ultrasound field. Especially, higher acoustic power leads to collapse of microbubbles and result in generating jet stream and heat. This phenomenon induces the damage the cells nearby collapse of microbubbles. It is expected that microbubbles enhance the mechanical and thermal effects of ultrasound. We have also studied about the anti-tumor effects by the microbubble mediated ultrasound. In our study, we found out that CD8+ T lymphocytes contributed to tumor growth suppression in the treatment of microbubbles and ultrasound. In this therapy, it is thought that the tumor associated antigens and molecules of damage associated molecular patterns (DAMPS) might be released from the damaged tumor cells. Therefore, we hypothesized that anti-tumor immune response could be modulated after microbubble mediated ultrasound therapy. If so, we have a chance to enhance the anti-tumor effects by the combination of immune therapy. In this study, we examined about the enhancement of anti-tumor effect by the combination of microbubble mediated ultrasound therapy and dendritic cell (DC)-based immunotherapy.

Methods: Colon-26 cells (mouse colon carcinoma) were inoculated into the backs of mice. After 8 days, house made lipid bubbles (LBs) were intratumorally injected and ultrasound was transdermally exposed toward tumor tissue. DCs were intratumorally immunized on days 9, 10, 11, and 13 after tumor inoculation. The anti-tumor effect was evaluated by measuring tumor volume. To analyze the effector cells for anti-tumor effects, we also examined the anti-tumor effects with this combination therapy in the CD8+ cells depleted mice by injecting anti-CD8 antibody.

Results: In either ultrasound therapy with LBs or DC-based immunotherapy, we obtained only slight anti-tumor effect. On the other hand, the combination of LBs mediated ultrasound and DC-based immunotherapy efficiently suppressed tumor growth. In addition, the tumor growth suppression was disappeared in the CD8+ cells depleted mice.

Conclusions: It seems that LBs mediated ultrasound supports the induction of effective anti-tumor immunity. Therefore, the combination of LBs mediated ultrasound and DC-based immunotherapy would be a useful strategy for cancer therapy.

Acknowledgements: This study was supported by JSPS KAKENHI (26560264), the MEXT-Supported Program for the Strategic Research Foundation at Private Universities 2013-2017.

P-CA-16

Topic: Cancer
Presentation Type: Poster

Oligometastatic disease: Not a new concept and its implications in focused ultrasound ablation and immunotherapy approaches

Joan Vidal-Jove[1], Manuela Velat[2]

[1]Hospital University Mutua Terrassa, Barcelona, Spain
[2]Institut Khuab, Barcelona, Spain

Background: The concept of oligometastases was developed in the late 90's by R. Weichselbaum. The hypothesis suggests that some metastases are limited in its extent and can be cured with focal therapies.

Favorable outcomes have been observed in selected patients with oligometastases that are treated with local ablative therapies, which include surgical extirpation, stereotactic body radiation therapy, and ablation.

We are searching explanations for recent favorable results with the use of focused ultrasound in advanced and metastatic liver and pancreatic tumors.

We review the recent literature in the light of new immunotherapy approaches. Tumor microenvironment, abscopal effects, and immune-modulation are keywords that may explain the successful results.

Our hypothesis suggests that there is a subgroup of selected patients that may benefit from combined approaches that include focal ablation and immune activation. Strategies to identify those patients and availability of synergistic treatments should come in the picture in the coming years.

We will propose different options to confront the challenge that advanced and metastatic patients present to clinicians today.

P-CA-17

Topic: Cancer
Presentation Type: Poster

Development of perfluorohexane "nanocones" as histotripsy agents for nanoparticle-mediated histotripsy

Jennifer Khirallah[1], Faith Robinson[1], Justin Howell[1], Tanzeel Ur Rehman[2], Yasemin Yuksel Durmaz[2], Eli Vlaisavljevich[1]

[1]Virginia Polytechnic Institute and State University, Blacksburg, Virginia, United States
[2]Istanbul Medipol University, Istanbul, Turkey

Background: Histotripsy is a non-thermal ultrasonic ablation method that destroys tissue through the precise control of acoustic cavitation. Nanoparticle-mediated histotripsy (NMH) is a treatment strategy being developed for multi-focal tumor ablation by utilizing nanoparticles to reduce the histotripsy cavitation threshold. Since the nanoparticles are small (<400 nm), they can be selectively delivered to tumors to generate cavitation at lower pressures than histotripsy, which often requires negative pressures >28MPa, giving NMH the potential to be used for tumor selective ablation. In previous studies we used nanodroplets (ND), which are about 200 nm in size as a first generation histotripsy agent. In this study, we develop acoustically active nanocones (NCs) as a new histotripsy agent with an optimal size of <50nm and high stability at room temperature. We hypothesize that NCs will reduce the cavitation threshold similar to the NDs used in our previous studies. We further hypothesize that the cavitation threshold will decrease with increasing NC concentration.

Methods: Perflourohexane (PFH) NCs were synthesized through host-guest interactions of PFH and methylated β-cyclodextrin (MCD) by mixing at room temperature in aqueous solution and collecting precipitated NCs through simple filtration (Fig.1). The cavitation threshold was tested using a custom-built 500 kHz focused transducer and a high-speed camera to capture images of the cavitation bubbles. The cavitation threshold was tested at NC concentrations ranging from 1x10^-4 mL-PFH/cm^3 to 10^-10 mL-PFH/cm^3. For each concentration, 100 pulses were applied at 1 Hz pulse repetition frequency (PRF) at driving voltages (i.e pressures) ranging 5-100V in 5V increments. The ability of NMH to effectively ablate tissue using NCs was also investigated in red blood cell (RBC) tissue phantoms with and without NCs (1x10^-5 mL-PFH/cm^3) using acoustic parameters chosen based on the results from the cavitation threshold experiments.

Results: Results demonstrated a significant decrease in the cavitation threshold when using PFH NCs compared to histotripsy alone. For example, Figure 2 shows a comparison of samples containing no NCs, empty NCs (no PFH) and PFH-NCs at a concentration of 1x10^-5 mL-PFH/cm^3, with cavitation only observed in the sample containing PFH-NCs (Fig.2). In addition, results showed a significant decrease in the cavitation threshold with increasing concentration. Finally, results demonstrated NCs were capable of achieving effective NMH ablation in RBC tissue phantoms at pressures significantly below the histotripsy intrinsic threshold.

Conclusions: This work demonstrates that ~50nm PFH-NCs can effectively lower the histotripsy cavitation threshold similar to the larger NDs used in our previous studies. Clearly defined bubble clouds were generated at lower pressures than with histotripsy alone, suggesting that these NCs can be used for targeted tumor ablation. Furthermore, our results affirmed our hypothesis in increasing concentration of NCs will decrease the cavitation threshold. Overall, the results of this study support our hypothesis and demonstrate the potential of NCs as a future histotripsy agent for NMH therapy.

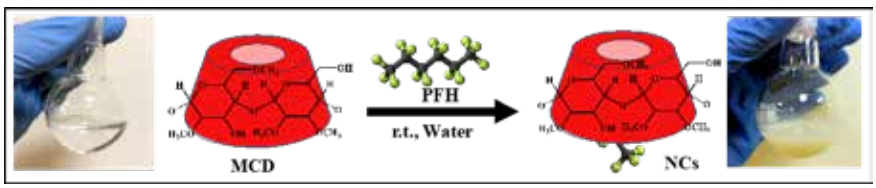

Figure 1. NC synthesis *via* host-quest interaction between PFH and MCD.

Figure 2. 15MPa pulses applied to tissue phantoms containing (A) no particles, (B) empty NCs, and (C) PFH-NCs.

P-CA-19

Topic: Cancer
Presentation Type: Poster

Aspects of MR guidance on flooded lung: Which sequence protocol for pre-treatment imaging should be considered?

Frank Wolfram[1], Daniel Güllmar[2], Joachim Böttcher[1], Thomas G Lesser[1]

[1]SRH Waldklinikum Gera, Gera, Germany
[2]Friedrich Schiller University Jena, Jena, Germany

Background: One-lung flooding (OLF) enables acoustic access to central lung tumours[1] and therefore HIFU application under sonographic guidance.[2] Regarding MRgFUS on lung cancer, we investigated the MR morphology in the lung during OLF. Herein, the question arose as to which sequence protocol should be considered for pretreatment planning during OLF. Because of limited flooding time, the acquisition using standard MR sequences, should be performed in an efficient time regime, giving optimal tumor demarcation and visualization of intraparenchymal sensitive structures at a high level of detail.

Methods: OLF was performed *in vivo* on six pigs (female 35-60 kg) in 3T MRT (Prisma, Siemens, Germany). After narcosis, mechanical ventilation was performed with an ICU respirator (Servo 900, Siemens, Germany) through a double-lumen tube (Mallinckrodt, Ireland). After ventilation with FIO2 = 1.0 for 30 min, flooding (saline, 35°C) of the left lung was performed. MR imaging was performed with spine and body array coils in lateral position using T1, PD and T2, weighted GRE and SE sequences. *Ex vivo* MR imaging was performed on ten human lung lobes containing lung cancer (NSCLC) and lung metastases (MTS). Two independent observers categorized the nodule detection, visualization of bronchial and vascular structure, as well as intrapulmonary anatomic orientation. Tumour sizes out of preoperative CT images were compared with those derived by MRI *ex vivo* using Bland Altman plot.

Results: Lung tumours and metastases appear strongly hyperintense in T1 w GRE (Fig. 1) and hypointense in T2w images with clear demarcation from lung parenchyma. Bronchial wall and vascular structures in flooded lung were imaged at high level of detail in T2w MRI (Fig. 2) but appeared in T1w 2D and PDw GRE images with low contrast. Cross correlation of nodule diameters revealed the best agreement for CT to be with T1w 3D GRE (Fig. 3). The duration of the thoracic MR image acquisition during OLF *in vivo* was 115 sec ± 26 for T1w 3D GRE, and 85 sec ± 18 for T2w HASTE.

Figure 1. T1w 3D GRE (5 ms/244 ms) image of flooded human lung lobe with hyperintense metastasis of a colorectal carcinoma

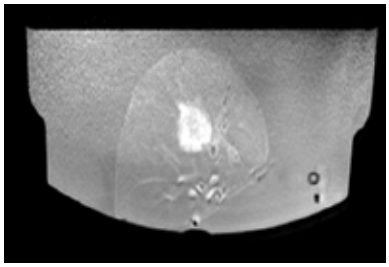

Figure 2. *In vivo* T2w (84ms/900ms) image of porcine lung, right ventilated, left flooded lung with visualization of bronchial and vascular structure as well as intralobular fissure

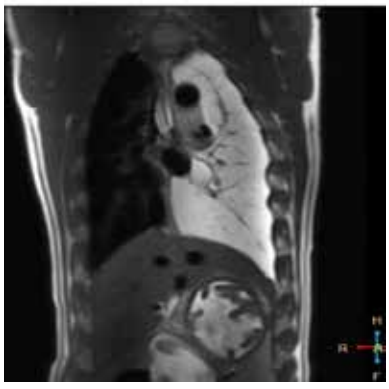

Discussion: For pre-treatment planning a fast T1w 3D GRE sequence should be considered because of both superior tumor-lung parenchyma contrast, and also giving best agreement with CT tumour size. A T2w HASTE is superior for anatomic orientation and definition of sensitive structures. The proposed sequences can be acquired within less of 10% of the treatment time limiting flooding (OLF) procedure.

References

1. T. Lesser, H. Schubert, S. Bischoff und F. Wolfram. Lung flooding enables efficient lung sonography and tumour imaging in human *ex vivo* and porcine *in vivo* lung cancer models. *European Journal of Medical Research*. 2013;18(23).
2. F. Wolfram, H. Schubert, S. Bischoff und T. Lesser Effect of lung flooding and high-intensity focused ultrasound on lung tumours: an experimental study in an *ex vivo* human cancer model and simulated *in vivo* tumours in pigs. *Eur J Med Res*. 2014;19(1).

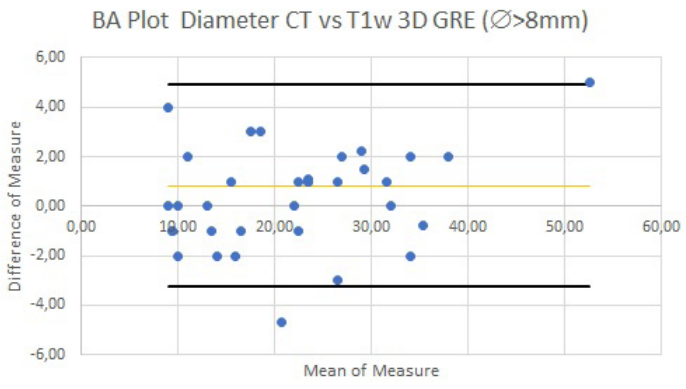

Figure 3. Bland Altman Plot of two measures showing lung nodule diameter of CT pre-operative and T1w 3D GRE on *ex vivo* flooded lung model

P-CA-20

Topic: Cancer
Presentation Type: Poster

Control of endothelial network formation *via* the ultrasound-triggered delivery of basic fibroblast growth factor (bFGF) from acoustically-responsive scaffolds

Xiaoxiao Dong[1], Xiaofang Lu[1], Kailee Kingston[1], Emily Brewer[1], Oliver D. Kripfgans[1], J. Brian Fowlkes[1], Renny Franceschi[2], Zheng Liu[3], Andrew Putnam[2], Mario L. Fabiilli[1]

[1]University of Michigan Health System, Ann Arbor, Michigan, United States
[2]University of Michigan, Ann Arbor, Michigan, United States
[3]Xinqiao Hospital, Army Medical University, Chongqing, China

Background: Blood vessel formation is a crucial process in the development, homeostasis, and regeneration of most types of tissue. Vessel formation is regulated by the concentration, spatiotemporal presentation, and sequence of pro-angiogenic growth factors (GFs). Methods to stimulate vessel formation could impact the treatment of ischemic diseases as well as improve the viability of transplanted organs and tissue substitutes. However, the understanding of how the aforementioned delivery parameters impact vessel formation is not very well understood, which ultimately hinders the clinical translation of administered GFs. We have previously shown that focused ultrasound (FUS) can be used to control the delivery of bioactive payloads from composite scaffolds, termed acoustically-responsive scaffolds (ARSs).

Here, we demonstrate how FUS can temporally control the release of bFGF from an ARS, thereby stimulating endothelial network formation in an *in vitro* model of vasculogenesis.

Methods: A schematic of the *in vitro* model, which was polymerized in a 6-well BioFlex plate, is shown in Figure 1. The inner gel consisted of an ARS (0.4 mL volume) containing 2.5 mg/mL fibrin, 2 U/mL thrombin, and either 0.25% or 1% (v/v) double emulsion with bFGF. The water-in-perfluorocarbon-in water (W1/PFC/W2) double emulsion was prepared in a microfluidic device. The W1 phase consisted of 10 mg/mL bovine serum albumin, 0.75 U/mL heparin, and 1 mg/mL bFGF in PBS, whereas the PFC phase was perfluorohexane (C7F16)

The outer gel (1.5mL volume) consisted of 2.5 mg/mL fibrin, 2 U/mL thrombin, 75 microcarrier beads coated with human umbilical vein endothelial cells (HUVECs), and 2.5x104/mL normal human dermal fibroblasts. The gels were covered with complete media following polymerization. The next day, the overlying media was replaced with starvation media and the ARSs were exposed to pulsed FUS (2.5 MHz, f-number: 0.83, 3.3 MPa or 8.8 MPa peak rarefactional pressure (PRP)) via a computer-controlled raster pattern at three z-planes from top to bottom. Seven days after FUS exposure, the scaffolds were fixed and stained with rhodamine labeled Ulex Europaeus Agglutin I (UEA-I) for HUVECs and DAPI separately. The beads were imaged via fluorescence microscopy (Figure 2) and the length of the HUVEC sprouts (i.e., total tube length per bead) was quantified using image analysis software. Cells cultured in fully-supplemented or starvation media, but without ARSs, served as positive and negative controls, respectively.

Results: The emulsions had a mean diameter of 6.2±0.9 μm and a coefficient of variance of 19.5%±7.5%. As seen in images taken on day 7, bubble formation in the ARS correlated with FUS pressure and emulsion volume (Figure 3). Similarly, tubule length correlated with FUS pressure and emulsion volume (Figure 4).

Conclusions: The study indicates that FUS can temporally control endothelial tubule formation in an *in vitro* model of vasculogenesis via the controlled release of bFGF from ARSs. Future studies are aimed at understanding how different spatiotemporal profiles of bFGF release impact sprouting and the *in vivo* performance of these materials.

Acknowledgements: This work is supported by NIH grant R01HL139656 and National Key R&D Program of China 2017YFC0107300.

Figure 1. Schematic of the *in vitro* model showing side (A) and top (B) views. The red numbers in panel A denote the order of z-plane exposures.

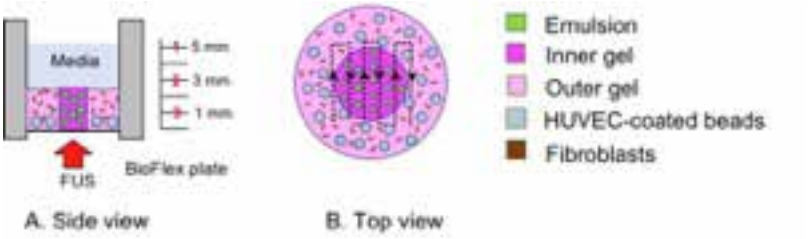

Figure 2. Examples of HUVEC sprouts stained with rhodamine-labeled UEA-I. A and B correspond to ARS with 1% emulsion +FUS at 8.8 MPa PRP and ARS with starvation media, respectively, at day 7. Scale bar: 200 μm.

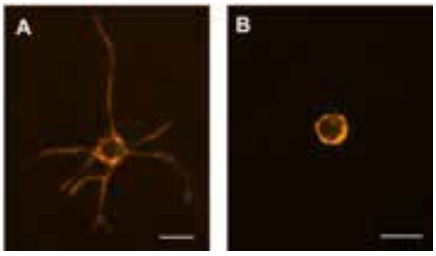

Figure 3. Images, taken on day 7, of the *in vitro* model. The experimental groups are as follows: A) fully supplemented media; B) starvation media; C) ARS with 1% emulsion and -FUS; D) ARS with 1% emulsion and +FUS at 3.3 MPa PRP; E) ARS with 1% emuls

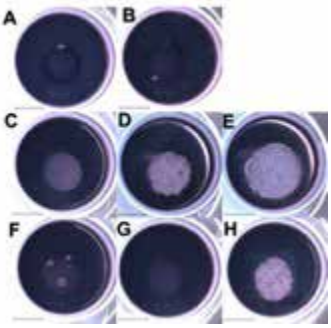

Figure 4. Total tubule length after 7 days. Statistically significant differences ($p<0.05$) are denoted by *. For gels containing 1% emulsion, the beads in gels exposed to FUS at 8.8 MPa PRP (Group E) had the longest tube length, significantly higher

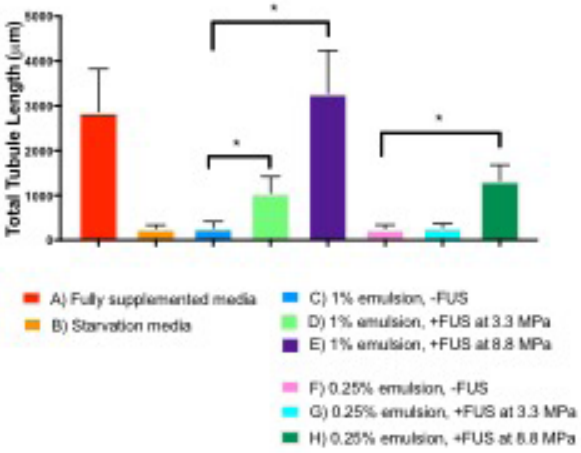

P-CA-21

Topic: Cancer
Presentation Type: Poster

Relief of lower urinary tract symptoms after MRI-guided transurethral ultrasound ablation (TULSA): Retrospective subgroup analysis of a Phase I clinical trial in men with localized prostate cancer

Robert Staruch[1], Dean S. Elterman[2], Gencay Hatiboglu[3], Khalil Hetou[4], James Relle[5], Mathieu Burtnyk[1], Joseph Chin[4]

[1]Profound Medical, Mississauga, Ontario, Canada
[2]University Health Network, University of Toronto, Toronto, Ontario, Canada
[3]University Hospital Heidelberg, Heidelberg, Germany
[4]London Health Sciences Centre, London, Ontario, Canada
[5]Beaumont Health System, Royal Oak, Michigan, United States

Background: MRI-guided transurethral ultrasound ablation (TULSA) is a minimally-invasive technique for the ablation of benign and malignant prostate tissue. Clinical evaluations of TULSA have focused on men with localized prostate cancer; here we explore the feasibility of using transurethral ultrasound ablation to alleviate lower urinary tract symptoms associated with benign prostatic hyperplasia (BPH).

TULSA uses a transurethral ultrasound applicator to achieve conformal ablation of targeted prostate tissue using directional high-intensity ultrasound under real-time MR-thermometry feedback control. Patient-specific target boundaries are defined on MR images corresponding to each of 10 independent 5-mm planar ultrasound transducer elements. MR-thermometry acquired during treatment is used to control the ultrasound power, frequency, and device rotation rate, to achieve a desired three-dimensional ablation pattern. The urethra and rectum are thermally protected by water flowing through the ultrasound applicator and a passive endorectal cooling device. Ablation extent is confirmed qualitatively on post-treatment contrast-enhanced MRI.

A previously-reported Phase I study demonstrated the safety and ablation precision in 30 patients with predominately low-risk prostate cancer, where TULSA was delivered using a treatment plan designed for men with cancer rather than BPH. We report a retrospective analysis of lower urinary tract symptoms in a subgroup of Phase I study patients who had symptomatic benign prostatic hyperplasia in addition to their cancer at baseline.

Methods: The Phase I trial treated 30 pts with organ-confined low or intermediate-risk PCa (T1c-T2a, PSA ≤ 10 ng/ml, Gleason Score 3+3 or ≤ 3+4 in Canada only). MRI-guided TULSA was delivered with 3 mm margins at the gland periphery, without attempting to spare the ejaculatory ducts.

A subgroup of patients who had lower urinary tract symptoms at baseline was defined based on an international prostate symptom score (IPSS) ≥12. Measures of urinary symptom relief assessed 12 months post-TULSA included IPSS, IPSS quality of life (QoL), and uroflowmetry peak flow rate (Qmax). Ablation efficacy was also assessed by reduction in prostate volume on 12-month MRI. Safety measures included adverse events (AE, CTCAEv4), self-reported urinary continence, erectile function (IIEF-15), and erections sufficient for penetration (IIEF question 2 ≥2).

Results: Of 30 men with localized prostate cancer treated in the Phase I study, 9 had baseline IPSS scores consistent with at least moderately symptomatic benign prostatic hyperplasia. In this subgroup, the mean ± SD age was 70 ± 3 years, PSA 5.9 ± 2.2 ng/ml, prostate volume 54 ± 23 cc. Baseline IPSS was 16.1 ± 3.8, IPSS QoL 2.8 ± 1.1, and QMax 14.5 ± 4.1 ml/s. Treatment delivery time was 39 ± 10 min, for prostate ablation volumes of 52 ± 21 cc measured by MR-thermometry and confirmed by contrast-enhanced T1.

At 12 months after TULSA, IPSS improved by 9.8 ± 7.1 (58 ± 34%) to 6.3 ± 5.0 (paired t-test p=0.0033), with at least a moderate (> 5 point) reduction experienced by 8/9 patients (89%). IPSS QoL improved by 2.0 ± 1.7 to 0.8 ± 1.0 (p=0.0068), with 8/9 patients (89%) reporting as "pleased" or "delighted". QMax increased to 21.9 ± 12.7 ml/s, but did not reach significance (p=0.13). Prostate volume measured on T2-weighted MRI (less the non-perfused cavity) decreased by 70 ± 19% to 14 ± 5 cc (p=0.001).

There were no rectal injuries or fistulae. In this subgroup there were no attributable Grade ≥3 or serious AEs. The most common attributable Grade ≤2 AEs were urinary tract infection (3/9), acute urinary retention (3/9), urinary urgency (3/9), and hematuria (3/9),

which all resolved by the 1-month visit. All patients (9/9) had full urinary continence (leak-free, pad-free) at 6 and 12 months. Erectile function was stable from 15 ± 9 at baseline to 16 ± 9 at 12 months (p=0.81), as was the proportion of patients with erections sufficient for penetration, 7/9 at baseline to 8/9 at 12 months.

Conclusions: This retrospective analysis demonstrates the feasibility of using TULSA to relieve lower urinary tract symptoms attributed to BPH, with a mean IPSS reduction of 9.8 ± 7.1 down to 6.3 ± 5.0 at 12 months, similar to levels reached with modern surgical therapies [Cornu et al, European Urology 2015]. This analysis is limited by the fact that the original study was designed to assess safety and precision of whole-gland ablation in an oncological patient population. Promising relief of lower urinary tract symptoms, with acceptable morbidity and minimal impact on urinary continence and sexual function, warrant further development of TULSA for men with symptomatic benign prostatic hyperplasia.

P-CA-22

Topic: Cancer
Presentation Type: Poster

Investigation of the mechanisms involved in boiling histotripsy-induced immune response *in vitro*

Ki Joo Pahk, Cheol-Hee Shin, Seung Ja Oh, Hyungmin Kim

Center for Bionics, Biomedical Research Institute, Korea Institute of Science and Technology (KIST), Seoul, South Korea

Background: Boiling histotripsy (BH) is a High Intensity Focused Ultrasound (HIFU) technique that can mechanically fractionate soft tissue without causing significant thermal damage. Studies have demonstrated the feasibility of applying BH in mechanically destroying solid tumours. There has been growing recent interest in the study of BH-mediated cancer immunotherapy. An *in vivo* preliminary study showing the release of an increased amount of T-cells in the treated region by BH has been reported at the previous FUS symposium in 2016.[1] Though the high potential of BH for triggering immune response has been demonstrated, the question of what causes this remains unclear. In the present study we aim to investigate (a) the mechanisms behind immune response to BH and (b) the relationship between the degree of mechanical damage induced and the corresponding level of immune response.

Methods: Two different sets of *in vitro* HIFU experiments were performed. A cluster of MDA-MB-231 cells (human breast adenocarcinoma) in the form of spheroids embedded in 0.6% collagen gel was exposed to the field of a 2.0 MHz HIFU transducer with simulated *in situ* peak positive and negative pressures of +78 and –14 MPa at the HIFU focus (1 Hz PRF, 1% DC). The HIFU exposed collagen gel sample was then collected for analysis under confocal microscope. Additional experiments were conducted with MDA-MB-231 cells cultured in the liquid media in a customised container with the variation of the number of BH pulses. Cell death pathway and proteome cytokine arrays were respectively carried out to classify the types of cell death (apoptosis, autophagy or necrosis) and of antigenic factors secreted by mechanically damaged tumour cells resulting from BH exposure. Lastly MDA-MB-231 cells treated with BH were co-cultured with human monocytes (THP-1 cells) to analyse macrophage polarisation (M1 or M2 differentiation) using quantitative polymerase chain reaction (qPCR) array.

Results: Boiling histotripsy-induced mechanical damage on MDA-MD-231 tumour cells was clearly observed under confocal microscope (Figure 1). The treated tumour cells eventually underwent immunogenic cell death through necrosis and apoptosis. Increased levels of damage-associated molecular patterns (DAMPs) and of pro-inflammatory cytokines (IL-18, IL-1α, IL-1β, ICAM-1, IL-8) in the damaged cancer cell microenvironment were observed compared to those in the control group (i.e., no BH treatment, see Figure 2), which also increased with the HIFU pulses. Interestingly and most importantly, these secreted immunogenic molecules resulted in M1 macrophage polarisation (Figure 3).

Conclusions: Here we investigated the mechanisms of immune response to boiling histotripsy *in vitro*. Our experimental results clearly suggest that BH might be an invaluable tool for immunotherapy not only mechanically destroying solid tumours but also inducing immunogenic cell death to trigger antitumor immunity.

Acknowledgements: This work was funded by Korea Institute of Science and Technology (KIST, Seoul, Korea, 2E27975 & 2E27980).

Reference

1. G Schade et al. Characterizing the immune response to boiling histotripsy ablation of renal carcinoma in the Eker rat. Presented at the 5th International Symposium on Focused Ultrasound, Bethesda, MD, USA, 28 Aug – 1 Sept 2016.

P-MI-1

Topic: Miscellaneous Indications
Presentation Type: Poster

Evaluation of changes in bone density, microstructure, and composition following MRgFUS in a swine model

Matthew Bucknor[1], Harsh Goel[2], Galateia Kazakia[1]

[1]University of California - San Francisco, San Francisco, California, United States
[2]University of Iowa, Iowa City, Iowa, United States

Background: Magnetic resonance-guided focused ultrasound treatments of bone lesions can produce dramatic changes in bone morphology and microarchitecture, for example, new bone formation at the site of a treated bone metastasis. The purpose of this study was to better characterize changes in bone following MRgFUS ablation.

Methods: Experimental procedures received approval from the local institutional animal care and use committee. MRgFUS was used to create distal and proximal ablations in the right femurs of eight pigs. The energy used at the distal target was higher (mean, 419 J; range, 390–440 J) than that used at the proximal target (mean, 324 J; range, 300–360 J). Animal specimens were subsequently obtained at 3 and 6 weeks and evaluated with high-resolution peripheral quantitative computed tomography (HR-pQCT) to evaluate changes in bone mineral density, bone volume, and cortical thickness. Additionally, Fourier Transform Infrared Spectroscopy (FTIR) was used to evaluate compositional changes in bone maturity following MRgFUS treatment. For both analyses, untreated regions of the femur with similar morphology were used as a control. Means and standard deviations were calculated for all indices and compared with t-tests and 95% confidence intervals were calculated.

Results: On HR-pQCT, the high energy ablations overall demonstrated a prominent focus of new bone formation along the cortical margin of the bones, not seen in the control regions, with associated decreased bone mineral density within the area of new bone formation (Image 1), compared to the untreated opposite bone surface (mean density 421 ± 83 mg/cm^3 *vs.* 900 ± 46 mg/cm^3; $p<0.001$). High energy regions also demonstrated a consistent pattern of evolution over time with progressively increased bone mineral density at 6 weeks (490 ± 80 mg/cm^3) compared to 3 weeks (352 ± 42 mg/cm^3), $p<0.001$. Low energy ablations also demonstrated an increase in cortical thickness (3.12 ± 0.47 mm) compared to control regions (2.50 ± 0.63 mm). FTIR analysis of specimens from the high energy sonications demonstrated a lower bone immaturity index and increased crystallinity compared to control samples.

Conclusions: MRgFUS of bone can produce specific changes in bone mineral density, bone volume, and cortical thickness. Progressively increased bone mineral density and cortical thickness were associated with higher energy sonications. Additionally, in this study, MRgFUS ablations demonstrated increased maturity compared to untreated control regions. Additional research is needed in order to better understand the patterns of bone remodeling following MRgFUS ablation.

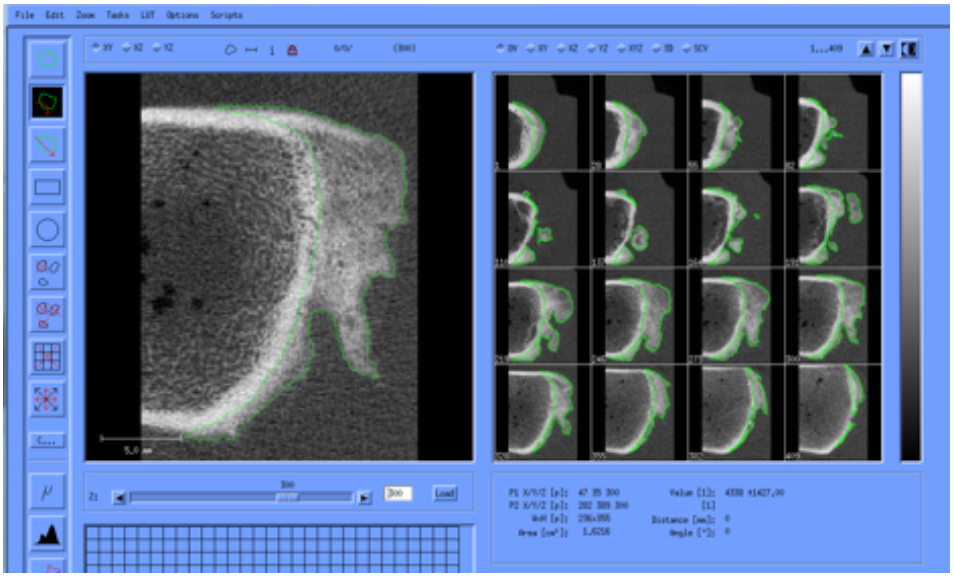

Figure 1. Segmented axial HR-pQCT images demonstrate a large area of subperiosteal new bone formation 6 weeks following MRgFUS.

P-MI-2

Topic: Miscellaneous Indications

Presentation Type: Poster

Reusable, cross validation, focused ultrasound phantom for image guided therapy

Andrew Dennison, Joyce Joy, Andreas Melzer

The University of Dundee, Dundee, United Kingdom

Background: Tissue mimicking material (TMM) phantoms can be used for preclinical validation of focused ultrasound (FUS) systems. Many TMM's for testing FUS systems have been published to date, examples including polyacrylamide (PAA) doped with egg-white or albumin proteins or thermally responsive colour changing ink. These constitute a class of single-use TMM phantoms requiring destructive dissection after FUS application for optical lesion cross validation. Commercial quality assurance (QA) phantoms can also be purchased which are reusable, but only for their intended imaging modality. This has resulted in requirement of both single-use and reusable phantoms for a typical image guided therapy (IGT) FUS validation workflow.

Methods: In this work a N-Isopropylacrylamide (NIPAM) TMM phantom was developed as a FUS preclinical validation target for image guided therapies (IGT). The objectives were to test the material for reusability and repeatability under FUS treatment conditions, relevant to hyperthermia >42°C and thermal ablation >52°C and to cross validate the thermal lesion with optical imaging assessment. NIPAM has comparable material properties (density, elasticity, water content) to soft tissues and other TMM phantoms. NIPAM is optically transparent at temperatures below its thermal transition or cloud point and above this it becomes opaque. This transition allows for optical lesion assessment. Upon cooling NIPAM becomes transparent again, making it repeatably reusable for thermal and optical cross validation studies. The cloud point of NIPAM can also be adjusted by variation of the acrylic acid content during phantom fabrication.

Results: 50ml NIPAM sealed samples with a range of acrylic acid concentrations (1.3 to 3.7ml per litre phantom) were bulk heated in a water bath starting at (body temperature) 37°C and increasing the water bath temperature by 1°C every 30 minutes. The cloud point transition was optically observed for each sample concentration, figure 1.

NIPAM with a bulk heating cloud point above 52°C was chosen for FUS testing using an Exablate 2100 MRgFUS system (INSIGHTEC, Israel) and a 1.2MHz confocal HIFU system (IGT, France) figure 2. Lesion assessment was cross validated by MRI PRF shift baseline thermometry methods and by optical image assessment. The NIPAM phantom produced thermal and optically visible opaque lesions using both FUS systems successfully. At low power values (<50W) a smooth temperature curve was observed with a steady increase in maximum temperature relative to increasing applied powers, figure 3, 4. At higher temperatures beyond the NIPAM cloud point threshold, there was significantly decreased signal to noise observed, this obscured MRI based thermal measurement.

Conclusions: Here we present results for an N-Isopropylacrylamide (NIPAM) tissue mimicking material (TMM) phantom, with a chemically tuneable temperature threshold (cloud point), that offers reusability and optical cross validation without the need for destructive dissection post FUS application. This material allows lesion visualisation and thermal monitoring during focused ultrasound treatment, using MRI baseline thermometry and optical imaging characterisation techniques. This provides a single phantom material for benchmarking and pre-clinical validation in image guided therapy focused ultrasound (IGT-FUS) system calibration workflows.

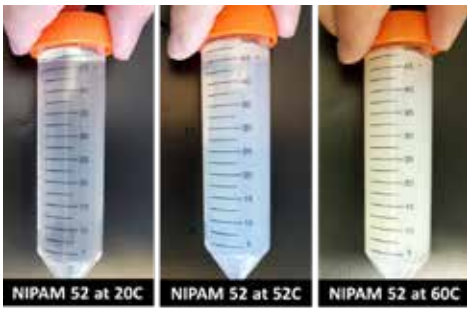

Figure 1. Bulk heating N-Isopropylacrylamide samples to verify thermal cloud point material transition, left to right NIPAM 52 at 20, 52 and 60°C

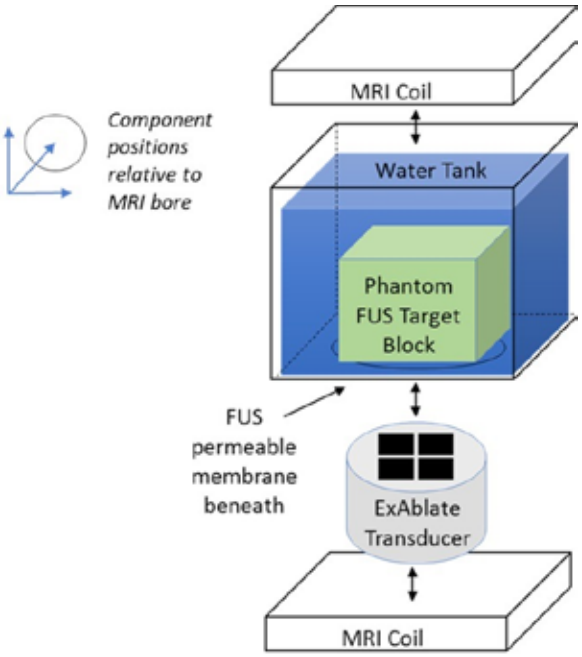

Figure 2. Magnetic Resonance Guided Focused Ultrasound (MRgFUS) phantom target experimental assembly schematic

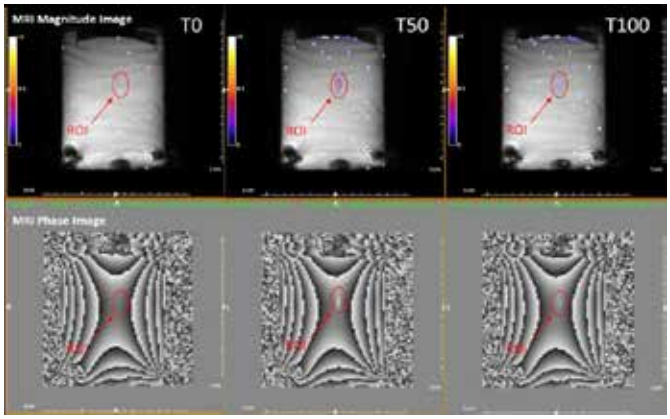

Figure 3. Thermoguide software (Image Guided Therapy, France) screencast at region of interest, targeting NIPAM phantom with focused ultrasound before T0, During T50, After T100 treatment

Figure 4 – Magnetic Resonance guided Focused Ultrasound (MRgFUS) preliminary results, left - using 1.2MHz Confocal FUS transducer (Image Guided Therapy, France) and right using a 550kHz Exablate 2100 FUS transducer (INSIGHTEC, Israel) on NIPAM 52

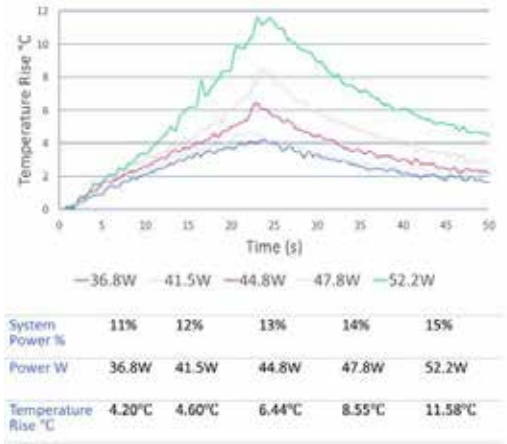

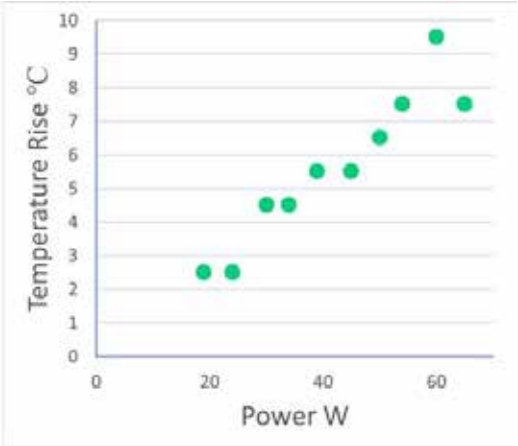

P-MI-3

Topic: Miscellaneous Indications

Presentation Type: Poster

TRANS-FUSIMO – A novel system for treatment support for FUS applications in moving abdominal organs

Sabrina Haase[1], Mario Bezzi[2], Thomas Lango[3], Sebastien Muller[3], Yoav Levy[4], Yeruham Shapira[4], Massimo Midiri[2], Michael Müller[5], Christine Tanner[6], Nagy Naguib[7], Jürgen Jenne[8], Giora Sat[9], Andreas Melzer[10], Tobias Preusser[1]

[1]Fraunhofer Institute for Medical Image Computing MEVIS, Bremen, Germany
[2]Universita Degli Studi Di Roma La Sapienza, Rome, Italy
[3]SINTEF AS, Trondheim, Norway
[4]INSIGHTEC, Tirat Carmel, Israel
[5]IBSmm, Brno, Czech Republic
[6]ETH, Zurich, Switzerland
[7]Johann Wolfgang Goethe University, Frankfurt, Germany
[8]Mediri GmbH, Heidelberg, Germany
[9]GE Medical Systems, Tirat Carmel, Israel
[10]The University of Dundee, Dundee, United Kingdom

Background: FUS treatment of abdominal organs like the liver is challenged by the target's breathing motion and its occlusion by the rib-cage. In the EU project TRANS-FUSIMO (www.trans-fusimo.eu) we developed a software system that connects to a FUS transducer and an MRI and allows for real-time beam steering in order to conduct safe, effective and efficient ablation of tumors in the moving liver.

Methods: The TRANS-FUSIMO treatment system (TTS) includes a real-time motion compensation pipeline which runs during a sonication. In update cycles of up to 8 Hz, patient specific image data is retrieved from the connected MRI which is on the one hand used to capture and track the motion of the liver and especially the target region and on the other hand to monitor the induced tissue effects . The real-time information from the motion tracking is fed into a motion model that calculates a short-time prediction of the movement of the target focal point. The predicted real-time information is sent to the transducer to steer the FUS beam accordingly. The real-time monitoring information enables the physician to stop the procedure when unwanted effects show up, e.g. heating of the near or far field. Furthermore, the TRANS-FUSIMO treatment system recognizes ribs that occlude the beam path and switches off transducer elements that would sonicate these ribs. The transducer power is then re-distributed to all remaining elements.

Results: To validate the TTS and its complete motion compensation pipeline and the models, phantom studies have been performed in static as well as moving scenarios first. We could prove that the software meets the defined requirements regarding system's safety as well as functionality. During each sonication, the complete pipeline of motion compensation and rib detection is running in the background in real-time and based on real-time patient specific information. Furthermore, we showed in our currently ongoing *in vivo* animal study that the software can sonicate safely in a living pig using an improved non-clinical prototype version of INSIGHTEC's conformal bone system (iCBS). We were able to introduce deep liver lesions that have been confirmed by contrast enhanced MR imaging and pathological examination.

Conclusions: In *ex vivo* as well as in *in vivo* experiments we could show that the TRANS-FUSIMO treatment system is capable of compensating organ motion through real-time motion detection, motion modelling and real-time beam steering. With the ongoing animal study we intend to prove that MRgFUS in moving organs can be performed safely, efficaciously and effectively. In the next step, we will show the feasibility of a treatment using the TTS in the clinical setting on human patients. To this end an adjuvant treatment with the TTS is planned for patients that will undergo surgical resection.

Acknowledgements: The research leading to these results has received funding from the European Union's Seventh Framework Program (FP7/2007-2013) under grant agreement no. 611889 (TRANS-FUSIMO).

P-MI-4

Topic: Miscellaneous Indications

Presentation Type: Poster

Magnetic resonance shear wave elastography in ablated *ex vivo* bovine liver

Lorne Hofstetter, Henrik Odeen, Allison Payne, Dennis Parker

University of Utah, Salt Lake City, Utah, United States

Background: Mechanical properties of diseased and ablated tissues differ from those of healthy tissues.[1-3] Tissue stiffness imaging may be a useful tool for assessing MRI-guided focused ultrasound (MRgFUS) procedures, and can be used independently or in conjunction with evaluating thermal dose. In this work we use a recently developed magnetic resonance shear wave elastography (MRSWE) technique[4] to volumetrically image post ablation tissue stiffness changes in *ex vivo* bovine liver.

Methods: Acoustic radiation force (ARF) impulses from a FUS transducer were applied to a set of spatial positions. A 3D gradient echo segmented echo planar imaging (EPI) sequence with motion encoding gradients was used to acquire volumetric images of the shear wavefront at multiple propagation times from each point. Shear wave speed was calculated as distance between each encoded wavefront position divided by the propagation time (see Figure 1).

MRSWE was performed in a fresh *ex vivo* bovine liver sample. The experimental setup is shown in Figure 2. A phased array transducer (256 element, 950 kHz, Imasonic, Besançon, France) was used to generate short FUS excitations (4 ms, 106 acoustic watts) at 16 positions. MRSWE imaging was performed on a 3T scanner (Siemens PrismaFIT, Erlangen, Germany) with scan parameters: TR/TE = 46/28 ms, Flip angle = 34°, Matrix = 128×112×12, Resolution = 1×1×5 mm, Bandwidth = 752 Hz/Pixel, Echo Train Length = 7, MEG amplitude = 75 mT/m, MEG duration = 4 ms. After a baseline MRSWE measurement, FUS ablation was performed followed by another post-ablation MRSWE measurement. For the ablation a 3x3 square grid (2 mm spacing) was sonicated at 43.3 acoustic Watts for 21.5 seconds per point, and this was repeated twice. During the ablations a segmented EPI thermometry protocol was used to measure temperature change, and thermal dose[5] was calculated.

Results: Figure 3a and 3b depict the MRSWE shear wave speed before and after ablation. Figure 3c shows the maximum intensity projection of MR thermometry readings acquired during the ablations, and Figure 3d shows the total calculated thermal dose distribution. In Figure 3b the 240 CEM43 dose line is displayed as a black line circumscribing the ablated region. Within the thermal dose boundary, the mean shear wave speed increased from 1.65 to 2.52 m/s after ablation.

Conclusions: Magnetic resonance shear wave elastography can be used to evaluate ablation-induced changes in *ex vivo* tissue shear wave speed. Regions of increased stiffness and shear wave speed agreed well with 240 CEM isodose contours, demonstrating the potential feasibility of using MRSWE for endpoint assessment of MRgFUS procedures. One benefit with MRSWE is that the same transducer is used for ablation and as an excitation source for elastography–this cannot be done with conventional harmonic MR elastography techniques, which need a separate external driver.

References

1. Pepin et al. *NMRS*. 2015.
2. Larrat et al. *PMB*. 2010.
3. Vappou et al. *PMB*. 2018.
4. Hofstetter et al. *ISMRM*. 2018.
5. Sapareto & Dewey. *IJROBP*. 1984.

Figure 1. MRSWE shear wave speed calculation. MR phase difference images are depicted in row (a). Detected wavefront locations are shown in (b). Shear wave maps for each ARF point are shown in (c) and median combined map in (d).

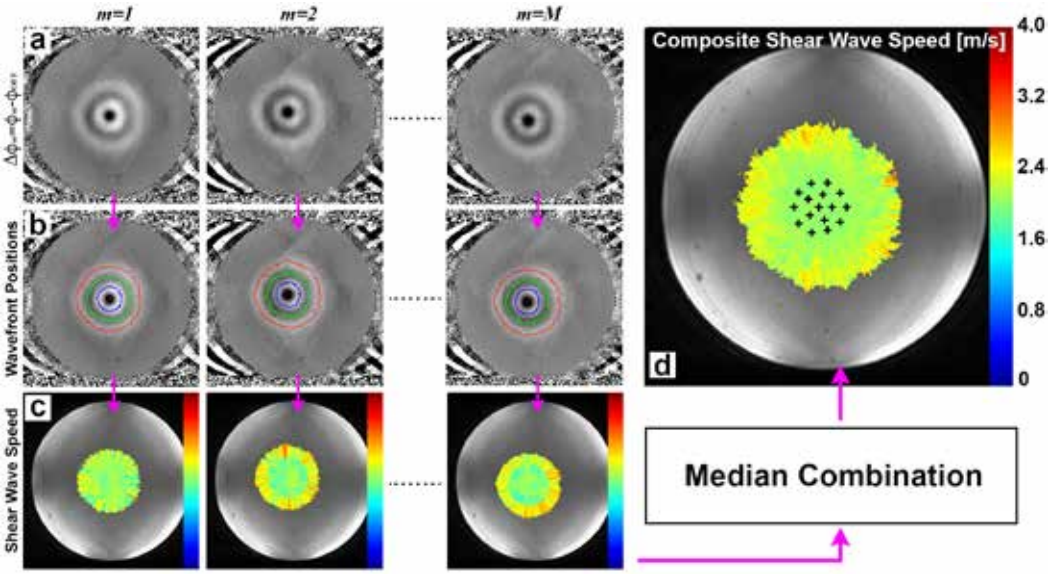

Figure 2. Experimental setup depicting orientation of liver tissue sample and FUS transducer.

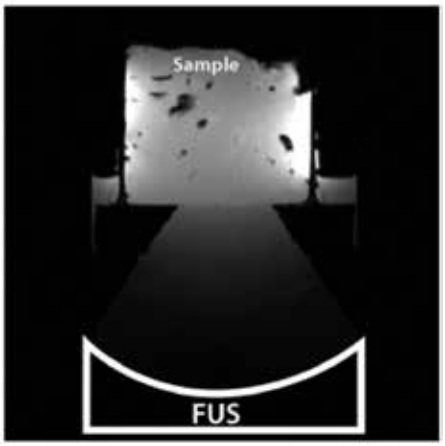

Figure 3. *Ex vivo* results. The thermal dose threshold of 240 CEM is overlayed as a black line in (b).

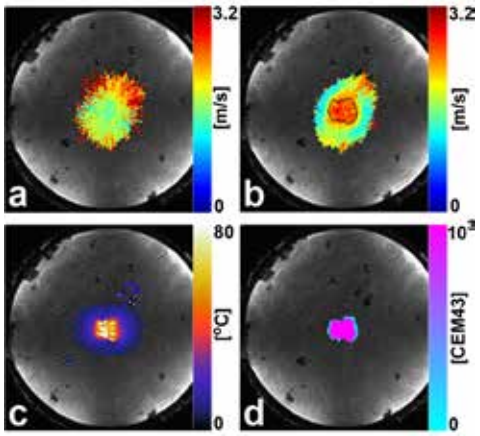

P-MI-5

Topic: Miscellaneous Indications
Presentation Type: Poster

Drug delivery system with mechanical effects of pulsed HIFU and droplet sensitizers

Ken-ichi Kawabata[1], Reiko Ashida[2], Takashi Maruoka[1], Kazuhiro Yamanaka[1]

[1]Research & Development Group, Hitachi, Ltd., Kokubunji, Japan
[2]Osaka International Cancer Institute, Osaka, Japan

In accordance with author request, this abstract is not available for publication.

P-MI-6

Topic: Miscellaneous Indications

Presentation Type: Poster

Single-beam acoustic trapping of a single microparticle or levitated cells at high frequency: A new approach for drug delivery

Hae Gyun Lim, Hyung Ham Kim

Pohang University of Science and Technology (POSTECH), Pohang, South Korea

Background: Acoustic tweezers can levitate and manipulate a single object or objects through air and water. Compared to other tweezer technologies: optical tweezers and magnetic tweezers, acoustic tweezers have a huge advantage on trapping larger objects and generating aggregates with strong trapping forces. Recently, acoustic levitation technique appeared to be promising in targeted drug delivery in the human body. The single beam acoustic trapping (SBAT) has a definitive advantage over other acoustic tweezer methods since it only employs a single transducer. In the present study, we demonstrated that the SBAT could levitate and manipulate red blood cells (RBCs) aggregation in 3 dimensions. This study is a significant step forward in the manipulation of cell aggregates using high-frequency acoustic tweezers.

Methods: Lithium niobate single crystal, Esolder-3022, and 2-3 μm Silver epoxy were selected as a piezoelectric material, a backing layer and a matching layer, respectively. By press-focusing technique, a focused transducer with the f-number of 1.5 (the focal distance of 5 mm and the aperture size of 3.3 mm) was obtained. The center frequency of 45 MHz and -6 dB fractional bandwidth of 70% were measured by the pulse echo test. Schematic diagram of experimental systems for manipulation of levitated cell aggregates with SBAT was shown in Fig. 1.

Results: A single microbead at the size of cellular level plays a vital role in cellular experiments because micron-sized particles are favorable for drug delivery through blood vessels. Fig. 2 described the manipulation of a single levitated 10-μm polystyrene bead. Fig 2 (a), the focal plane of the microscope was set at the bottom of the cell dish to prove that the trapped particle was levitated. In contrast, in Fig. 2 (b~d), the focal plane was at the same level as the levitated microparticle, and the particle was manipulated along the movement of the transducer. Fig. 3 showed the optical image of manipulation of levitated RBCs aggregates. In the same manner of Fig 2 (a), an image of Fig. 3 (a) was unfocused on RBCs aggregation resulting blurry image of RBCs. The RBCs was in-focused in Fig 3 (b~d) which proved that the transducer could effectively levitate cells, form and manipulate 2-D cell aggregates in the space.

Conclusions: The main interest of this new technique, cell trapping and transporting is drug delivery. In this study, we ascertained that SBAT was a potential tool for manipulation of levitated RBCs aggregates with non-contact and label-free. Using focused ultrasound field generated by a high-frequency single-element transducer, we first report the levitation and transportation of cell aggregates. Further development of this method will be the manipulation of cells or particles injected into the microtube, demonstrating the efficacy of micro-objects delivery.

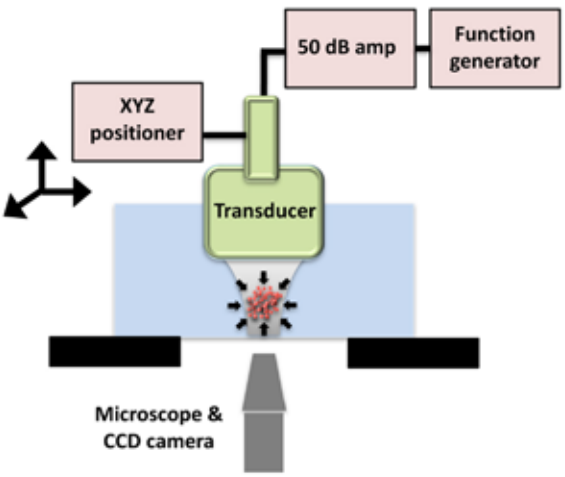

Figure 1. Schemical diagram of experimental setup for SBAT.

Figure 2. Manipulation of a levitated 10 μm particle. (a) The focal plane of the microscope was located at the bottom of the cell dish. (b~d) The optical images of a levitated and trapped single particle were shown.

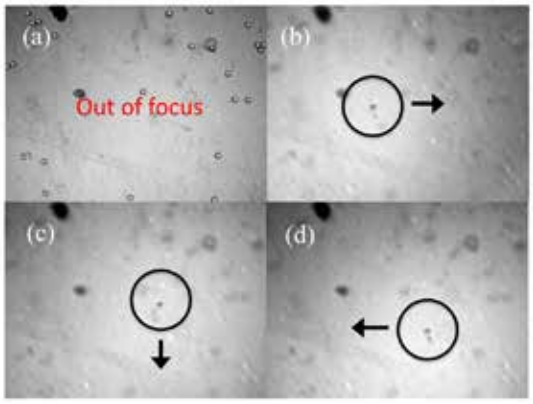

Figure 3. Manipulation of levitated RBCs aggregates. (a) The focal plane of the microscope was located at the bottom of the cell dish. (b~d) The optical images of manipulation of cell aggregates were displayed with the focal plane of the microscope.

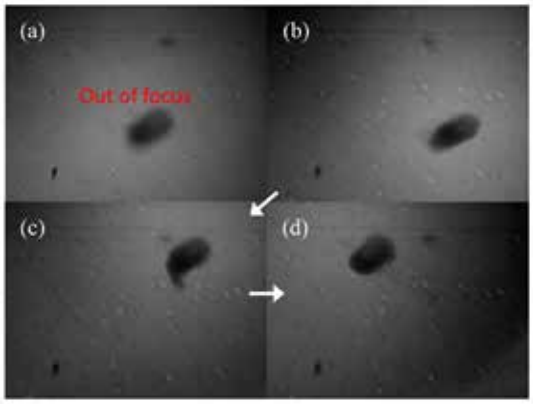

P-MI-7

Topic: Miscellaneous Indications

Presentation Type: Poster

In vivo assessment of stone fragmentation and kidney injury with burst wave lithotripsy

Adam Maxwell[1], Yak-Nam Wang[2], Christopher Hunter[2], Bryan Cunitz[2], Jeff Thiel[1], Frank Starr[2], Jessica Dai[1], Yasser Nazari[2], Donghoon Lee[2], James Williams[3], Michael Bailey[2], Wayne Kreider[2]

[1]University of Washington School of Medicine, Seattle, Washington, United States
[2]University of Washington, Seattle, Washington, United States
[3]Indiana University - Purdue University at Indianapolis, Indianapolis, Indiana, United States

Background: Shock wave lithotripsy was clinically introduced over 30 years ago to noninvasively fragment urinary stones with focused shock waves. Although preferred by patients, its use has been declining due to its limited success rate. We are developing an alternative approach called burst wave lithotripsy (BWL) that uses focused sinusoidal pulses of ultrasound delivered at lower amplitude to fragment stones more safely and effectively. This research investigated the efficacy and acute safety of BWL in an *in vivo* porcine model of nephrolithiasis.

Methods: Three female pigs weighing 55-60 kg each were used to assess stone fragmentation and renal injury from BWL. The animal was placed under general anesthesia and stones were implanted by surgical incision in the ureter. Natural human calcium oxalate monohydrate stones with a maximum dimension between 6 and 7 mm were used. Acoustic coupling was achieved by a water bath with an acoustically-transparent membrane coupled to the skin. BWL exposures were delivered by a 350-kHz therapy transducer powered by a pulse generator and guided with a coaxially aligned ultrasound imaging probe. The transducer had an aperture of 85 mm and focal distance of 100 mm. The transducer delivered 20-cycle pulses at a pulse repetition frequency of 10 Hz. BWL was delivered to the stone for 30 minutes total in 10-minute intervals at peak negative pressure levels between 6.5 and 7 MPa. Following treatment, the animal was euthanized and the kidneys were excised. Each kidney was photographed, then placed in an MRI system with several scans performed to evaluate injury. Kidneys were then bivalved to recover stone fragments and fixed in glutaraldehyde for later MRI and histology. Recovered fragments were sieved through mesh filters. All stone fragments <2 mm were considered disintegrated. Larger fragments were weighed and compared to the original stone weight to determine the mass fraction successfully treated.

Results: On average, 82% by mass of the 5 treated stones was fragmented to <2 mm. In all cases, ≥58% of the stone mass was disintegrated <2 mm, with 3 of 5 stones being completely disintegrated. One stone implanted in the remaining kidney did not receive BWL treatment due to lack of a suitable acoustic window. Gross examination of kidneys revealed minor petechial injury to the collecting space where the stone was targeted. No effects to the skin or overlying tissues were observed. MRI indicated minimal injury to the parenchyma of all treated kidneys.

Conclusions: We developed a porcine model of nephrolithiasis to perform clinical simulation of BWL to noninvasively fragment kidney stones. The results demonstrate that BWL can consistently fragment urinary stones with clinically relevant size in the kidney while avoiding significant injury to functional renal tissue.

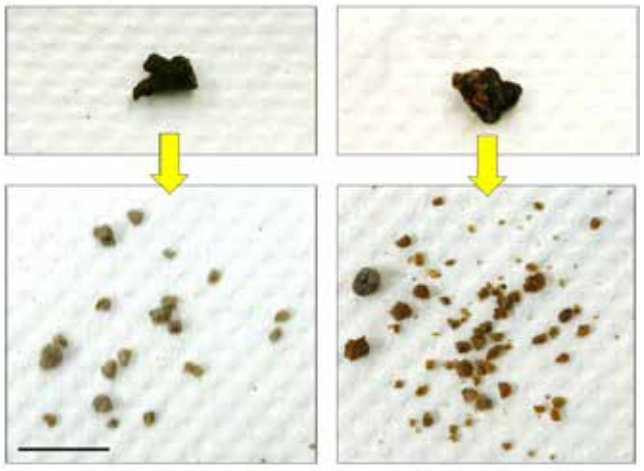

Figure 1. Two stones before BWL treatment (top) and fragments recovered after treatment (bottom). The scale bar corresponds to 1 cm.

Acknowledgements: Work supported by NIH through NIDDK P01 DK043881 and K01 DK104854. Adam Maxwell, Bryan Cunitz, and Michael Bailey have equity in and consulting agreements with SonoMotion, Inc, which has licensed technology related to this work from the University of Washington.

P-MI-8

Topic: Miscellaneous Indications
Presentation Type: Poster

An Analysis of the Mechanical Response of Biological Tissue

Alexander Mueller[1], Lorne Hofstetter[2], Dennis Parker[2]

[1]Utah Center for Advanced Imaging Research, Salt Lake City, Utah, United States
[2]University of Utah, Salt Lake City, Utah, United States

Background: Magnetic resonance elastography (MRE) may be a useful tool for improved endpoint assessment of magnetic resonances guided focused ultrasound (MRgFUS) procedures. In some cases, use of traditional MRE may not be feasible in conjunction with MRgFUS since an additional mechanical excitation source is needed. Focused ultrasound shows promise as a means for mechanical excitation of tissue for MRE because the same transducer can be used for both ablation and for generating shear waves whose propagation can then be tracked using MRI. However, since FUS can deposit large quantities of energy into a small region of tissue, it is possible to damage healthy tissue when using FUS as an excitation source for MRE. It is then important to maximize the total displacement for a given energy to provide a clear image of mechanical tissue properties and to avoid harm to healthy tissue.

Methods: A Green's function solution to the viscoelastic Navier-Stokes equation was used to model the displacement induced by an FUS pulse. This model was then used to simulate MR phase contrast images in 1-D using a single-lobe motion encoding gradient (MEG) of length 3 ms and amplitude 60 mT/m to visualize the displacement caused by FUS pulses of durations between 5 μs and 10 ms while maintaining a constant deposition of energy. General trends about the mechanical behavior of a viscoelastic medium were inferred from these simulation.

Results: Figure 1 shows simulated displacement curves for 4 different values of T (FUS pulse duration). The kinks in the graphs of the displacements occur where the FUS pulse ends. Figure 2 shows a graph of the average displacement in a 1 mm radius circle in the plane of the ultrasound focus as a function of FUS pulse length for tissue of shear modulus 4 kPa and kinetic shear viscosity of 2e-3 m^2/s.

Conclusions: We have modeled the displacement induced by FUS pulses of different durations. We have shown that when energy deposition is kept constant, shorter FUS pulses can attain higher phase accruals. This has implications for FUS powered MRE because it shows that the maximum displacement can be generated using shorter pulses and higher operating power.

Acknowledgements: Funding source from the FUS foundation global internship program, the Mark H. Huntsman endowed chair, and NIH Grants R01CA172787, R03EB023712 and F30CA228363.

Figure 1. Examples of displacement curves for FUS pulse durations of T = .5 ms, 1 ms, 2 ms and 4 ms

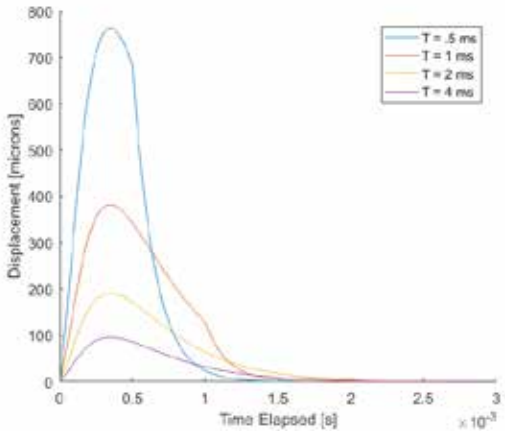

Figure 2. Graph showing the relation between the phase in a simulated phase contrast image and the duration of the FUS pulse for a single-lobed motion encoding gradient of 3 ms

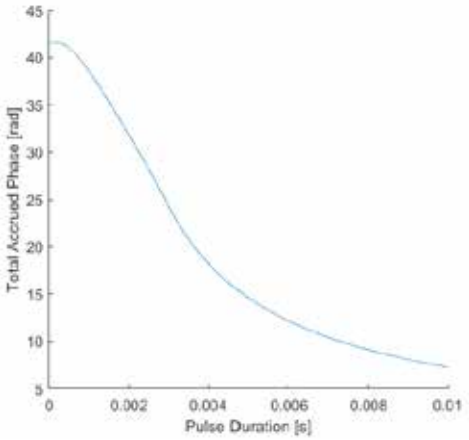

P-MI-9

Topic: Miscellaneous Indications

Presentation Type: Poster

The discontinuous galerkin method for parallel simulations of acoustic wave propagation

Drew Murray, James Kelly, Robert McGough

Michigan State University, East Lansing, Michigan, United States

Background: Realistic three dimensional (3D) simulations of acoustic waves are resource-intensive tasks that require high performance computing solutions. Performing these calculations on compute clusters with distributed memory systems enables a dramatic reduction in the compute time for these simulations.

Methods: The discontinuous Galerkin (DG) method demonstrates excellent scalability, which is advantageous for parallel ultrasound simulations. For these calculations, the spatial grid is split into equal sections (called blocks), where each is run on one core. Inter-block communication is implemented using halo elements along the faces of each block. Each halo element in a block corresponds to a interior element on the corresponding neighboring block. Communication is performed with MPI, which sends the state variables of the interior element to the corresponding halo element on the neighboring core.

Results: For preliminary evaluations, a standing wave solution to the 3D wave equation was computed on a three dimensional (3D) grid. The (3,2,1) mode of a rectangular cavity was simulated on a grid of 51200 elements for 4000 timesteps using 20 cores on a distributed memory computer cluster, and a factor of 19.56 speedup was achieved relative to a serial implementation with the same simulation parameters.

Further evaluations on additional cores are presently underway.

Conclusions: Simulations of standing waves in a rectangular cavity with the DG method demonstrate excellent scalability. We ultimately intend to extend these promising results to ultrasound simulations with the discontinuous Galerkin method for simulations of shock waves generated for histotripsy.

P-MI-10

Topic: Miscellaneous Indications

Presentation Type: Poster

Brain targeting drug delivery with lipid bubble and ultrasound

Daiki Omata[1], Ryo Suzuki[1], Fumiko Hagiwara[1], Johan Unga[1], Takashi Azuma[2], Shu Takagi[2], Kazuhiko Seki[3], Kazuo Maruyama[1]

[1]Teikyo University, Tokyo, Japan
[2]University of Tokyo, Tokyo, Japan
[3]National Institute of Neuroscience, National Center of Neurology and Psychiatry, Tokyo Japan

Background: Recently, the combination of ultrasound and microbubbles has appeared as a promising technology for therapeutic use. There are few microbubbles approved for ultrasound imaging, and those microbubbles may not ideal for therapy. There could be improvements to the stability in the blood circulation, equipping targeting function, and the loading of drug. The stability of microbubbles is an important property not only for diagnostics, but also therapy. Long-circulating microbubbles could image blood vessels in detail and remain in the blood stream long enough to be exposed to ultrasound, leading to therapeutic effect. We have developed new lipid-based bubbles (LB), which have shown long-circulation, for diagnostics and therapeutics. In this study, to assess the potential of the LB for therapy, we examined whether the LB and ultrasound could enhance the drug delivery into brain.

Methods: A mixture of LB and evans blue (EB), which was used as model drug, was injected into tail vein of ddY mice. Immediately, the right part of brain was exposed to transcranial non-focused ultrasound (Frequency: 1 or 3 MHz, Intensity: 0.1-2.0 W/cm^2, Duty: 50%, PRF: 10 Hz, Exposure time: 3 min). After 1 h, coronal brain sections were observed by stereoscopic microscopy, and EB concentration from brain section was determined. In addition, to evaluate the toxicity of the combination of LB and ultrasound, coronal brain sections were observed after Hematoxylin-Eosin (HE) staining.

Results: To evaluate the drug delivery to the brain, we examined the delivery of EB to brain by LB and ultrasound of different frequencies and intensities. EB delivery to the right side of brain, which was exposed to ultrasound, was observed when ultrasound intensities were higher than 0.5 W/cm^2. The EB concentrations in the right side of brain was also higher than in the left side. These results suggest that the LB and ultrasound can deliver EB into a specific part of the brain. Further, to assess damage to the brain, we observed coronal brain sections after HE staining. Extravasation of red blood cell was observed in coronal brain sections treated with LB and 1 MHz ultrasound. Still, there were no notable damage to the brain treated with LB and 3 MHz ultrasound. These results suggest that optimizing ultrasound conditions could reduce damage to the brain. Thus, it indicates that the long-circulating LB we have developed can be used for drug delivery to the brain. In the next study, we will attempt to combine HIFU and LB to achieve site specific drug delivery.

Acknowledgements: This work was supported by JSPS KAKENHI Grant Numbers JP17H07119, JP15J10508 and AMED under Grant Number JP16dm0107115.

P-MI-11

Topic: Miscellaneous Indications

Presentation Type: Poster

Focused ultrasound-hyperthermia and radiation therapy for combined treatment of brain and prostate tumors — preliminary studies *in vitro*

Xinrui Zhang[1], Lisa Landgraf[1], Michael Unger[1], Upasana Roy[1], Ina Patties[2], Damian McLeod[3,4], Thomas Neumuth[1], Andreas Melzer[1]

[1]Innovation Center Computer Assisted Surgery, Leipzig, Germany
[2]University of Leipzig, Leipzig, Germany
[3]OncoRay - National Center for Radiation Research in Oncology, Dresden, Germany
[4]University Hospital Carl Gustav Carus, Technische Universität Dresden, Dresden, Germany

Background: Focused ultrasound (FUS) is able to generate hyperthermia (HT) (40-46°C) localized to target tumors in a non-invasive way. HT treatment has previously been reported to support radiation therapy (RT) and chemotherapy. However, there is no HT technique currently used in routine clinical practice. Furthermore, there are limited studies that have investigated the biological effects of acoustic waves on cancer cells when ultrasound-induced hyperthermia (US-HT) is combined with RT. The aim of this study is to analyse the molecular effects of combined FUS-HT and RT *in vitro* on human glioblastoma (T98G) and prostate (PC-3) cancer cell lines.

Methods: An existing FUS *in vitro* system (IMSaT, Dundee) with a customized 1.14 MHz single transducer made by piezoelectric ceramic material (Meggitt-Ferroperm Piezoceramics, Kvistgaard) at an acoustic intensity of 142 W/cm2 was reconstructed to generate HT (40- 44°C) in special US-penetrable 96 well cell culture plates (Greiner bio one, GmbH). Target temperature was set at 43°C for treatment of 3 wells in parallel. LabVIEW program (National Instruments, Newbury) and a motion system were utilized to control the movement of the plate. The temperature of each well was monitored in real-time by an infrared thermal camera (PI450 by Optris GmbH) with the imaging software (PI connect version 2.10) with a feedback loop to the motor. Thermal block HT at 43°C was performed to determine optimal treatment duration and interval time. Cells were irradiated with a 150 kV X-ray device (DARPAC 150-MC) at a single dose of 10 Gy in combination regime. Cellular metabolism (WST-1 assay, Roche Diagnostic GmbH) and cell apoptosis (Annexin V assay, Cayman chemical) were evaluated at different time points after therapy.

Results: Cells treated with combined thermal block HT (43°C, 30 min) and RT (10 Gy) showed a decreased cellular metabolism (T98G: 47 %, PC-3: 60 %) compared to RT group (T98G: 84%, PC-3: 70 %). Regarding the treatment regime, a greater reduction in cellular metabolism was observed in T98G cells when RT was performed 15 min (47 % viable cells) compared to 60 min post thermal block HT (58 % viable cells). Brain and prostate cancer cell lines were treated by combined FUS-induced HT with the single focused 1.14 MHz transducer (40-43°C, 15 min) and RT (10 Gy). First results showed slightly lower cellular metabolism in FUS-HT combination group in comparison to single treatment groups. Fluorescence microscopy images demonstrated that FUS-HT induced early apoptosis (annexin V-positive/PI-negative) and necrosis in T98G and PC-3 cells 24 h post treatment.

Conclusions: Our preliminary data suggest that combined HT and RT had additional effects on glioblastoma and prostate cancer cell lines compared to RT alone. A shorter time interval between the two treatment modalities was more effective. In the future, duration of FUS-HT treatment needs to be prolonged and compared to thermal block HT at the same thermal dose. More accurate temperature measurement inside the wells will be performed with fiber optics.

P-MI-12

Topic: Miscellaneous Indications

Presentation Type: Poster

Effect of temperature elevation on short duration focused ultrasound for hyperthermia mediated drug delivery using thermosensitive liposomes

Marc Santos, David Goertz, Kullervo Hynynen

University of Toronto, Toronto, Ontario, Canada

Background: Preclinical studies have shown that MRI-guided focused ultrasound (MRgFUS) can achieve spatially localized thermal exposures in the range of 41-43°C. It has been found that MRgFUS is capable of inducing the targeted uptake and release of doxorubicin (DOX) from thermosensitive liposomes (ThermoDox®, Celsion Corporation) in tumor models, and that this gives rise to potent antitumor effects. To enable the treatment of a broad spectrum of tumor types, improved heating methods must be developed to overcome issues relating to respiratory motion, bone shielding, and large blood vessel cooling during clinical MRgFUS. We have shown previously that 10 short 30s exposures of hyperthermia to 42°C can release substantial amounts of DOX from ThermoDox®. Here we investigate the effect of temperature elevation on the spatiotemporal drug release and distribution of DOX from ThermoDox® during 30s of hyperthermia using a mouse tumor model and *in vivo* two-photon microscopy (2PM).

Methods: FaDu tumors expressing GFP were implanted in the window chambers of nude mice (Figure 1(A)) and allowed to grow for 9-12 days whereupon experiments commenced. Temperature-based PID feedback from implanted thermocouples was used to control of the output power was used to maintain the tissue temperature at the desired level (41°C, 42°C, 43°C or 45°C) for 10 short 30s heating bursts. The short duration was chosen from a clinical perspective to be long enough to release DOX from ThermoDox®, but also short enough to be applied during a breath hold and also to overcome perfusion-related limitations on sustained temperature elevations *in vivo*. The temperature elevations were chosen to be close to the phase transition temperature of ThermoDox® (~41.3°C) but not so high as to cause thermal damage to the microvasculature of the tumor. Serial 3D vascular and DOX images were acquired in tumor regions before, during and after each hyperthermia exposure all in the presence of ThermoDox® (example shown in Figure 1(B)).

Results: ThermoDox® drug release was successfully visualized at each temperature elevation with 2PM during FUS hyperthermia. The PID controller was able to achieve the desired temperature response with a variable temperature elevation within the hyperthermia regime (Figure 2). Quantification of the drug penetration and real-time release from ThermoDox® during each thermal exposure is currently underway. Preliminary results suggest that the amount of drug released depends on the amount of time the tumor temperature is above 41°C.

Conclusions: We have developed the use of 2PM to image the release of DOX from ThermoDox® in real-time during FUS hyperthermia in mouse tumors. This capability will enable the evaluation of standalone or cavitation-enhanced FUS schemes for hyperthermia-mediated drug delivery to overcome limitations on clinical MRgFUS hyperthermia. Future work will involve comparing the short duration temperature elevations in the presence of ThermoDox on their tumor control capability in a larger animal model.

P-MI-13

Topic: Miscellaneous Indications

Presentation Type: Poster

TRANS-FUSIMO — In silico First-stage evaluation and parameter optimization of a FUS system for moving targets

Michael Schwenke[1], Jan Strehlow[1], Daniel Demedts[1], Sabrina Haase[1], Diego Barrios Romero[1], Sven Rothlübbers[1,2], Caroline von Dresky[1], Stephan Zidowitz[1], Joachim Georgii[1], Senay Mihcin[3], Mario Bezzi[4], Christine Tanner[5], Giora Sat[6], Yoav Levy[7], Jürgen Jenne[1,2], Matthias Günther[1,2], Andreas Melzer[3,8] and Tobias Preusser[1,9]

[1]Fraunhofer Institute for Medical Image Computing MEVIS, Bremen, Germany.
[2]Mediri, Heidelberg, Germany
[3]Institute for Medical Science and Technology, Dundee, Scotland
[4]Universita Degli Studi Di Roma La Sapienza, Rome, Italy
[5]Computer Vision Laboratory, Eidgenössische Technische Hochschule, Zurich, Switzerland
[6]GE Medical Systems Israel, Haifa, Israel
[7]INSIGHTEC, Tirat Carmel, Israel
[8]Innovation Center Computer Assisted Surgery, Leipzig, Germany
[9]Jacobs University, Bremen, Germany

Background: Currently, no clinically available Focused ultrasound (FUS) treatment system features automated respiratory motion compensation. In the EU FP7 project TRANS-FUSIMO we have developed a system for real-time motion compensation through beam steering. Quality assurance of such a complicated system is challenging and involves great efforts for manual experimentation. In the work presented here, we suggest to utilize numerical FUS simulations for automatic system testing with the aim of reducing the efforts of manual testing.

Methods: The TRANS-FUSIMO treatment system (see Figure 1) consists of a clinically available MR device and FUS transducer system. The controller is generic and could work with any suitable MR or FUS device. MR image sequences (echo planar imaging) are acquired for combined motion observation and thermometry. Image-based anatomical feature tracking is performed and motion predictions are estimated to compensate for processing delays. FUS control parameters are computed repeatedly and sent to the hardware to steer the focus to the (estimated) target position. The system is currently integrated with INSIGHTEC's CBS system and GE 3T MR scanner.

To allow for extensive in-silico testing of the motion compensation over wide ranges of parameters and algorithmic choices, we replace the actual MR and FUS devices by a virtual system equipped with a numerical FUS model to predict the outcome of the treatment during respiratory motion. The actual motion compensation controller is not aware of this change and the testing is as close as possible to the real-world use.

Within the motion compensation calculation pipeline, all system components produce individually known errors with, however, unknown impact on the overall therapy outcome. To analyze the overall impact and to optimize the system parameters, we define an intuitive quality measure that compares the achieved temperature to the static scenario, resulting in an overall efficiency with respect to temperature rise combining all individual errors. Figure 2 shows the maximum efficiency possible with discrete focusing when no errors are introduced in the computations.

Results: With a clinically available monitoring image rate of 6.67 Hz and 20 Hz FUS control update rate, normal respiratory motion is estimated to be compensable with an estimated efficiency of 80%. This reduces to about 70% for motion scaled by 1.5. Extensive testing over wide parameter ranges involving 6347 simulated sonications shows that the most influential component is the temporal motion prediction. Utilizing a history-based motion prediction method has advantages over a linear extrapolator for normal respiratory motion as turning points in the respiratory motion can be anticipated.

Conclusions: Using the in-silico testing we have been able to evaluate and optimize the efficiency of the treatment system towards suitability for clinical applications. The simulation-based in-silico testing as a first-stage validation reduces the efforts of real-world testing. Due to the extensible modular design of the system in combination with automatic testing, the described approach might lead to faster translations from research to clinical practice also for other hardware systems.

Acknowledgements: The research leading to these results has received funding from the European Union's Seventh Framework Programme (FP7/2007-2013) under grant agreements no. 270186 (www.fusimo.eu) and no. 611889 (www.trans-fusimo.eu).

P-MI-14

Topic: Miscellaneous Indications

Presentation Type: Poster

Establishing a correction factor for porcine kidney tissue shrinkage due to histological processing after HIFU treatment

Tess Seip[1], Liang Cheng[2], Narendra Sanghvi[3], Ralf Seip[1]

[1]SonaCare Medical, Charlotte, North Carolina, United States
[2]Indiana University School of Medicine, Indianapolis, Indiana, United States
[3]SonaCare Medical, Indianapolis, Indiana, United States

Background: To quantitatively analyze and compare the volume ablation performance of a newly-developed laparoscopic high-intensity focused ultrasound (HIFU) kidney probe to planned and targeted ablation volumes defined using ultrasound image guidance, renal tissue shrinkage effects due to formalin fixation during histological processing must be considered. Tissue shrinkage was compensated for by determining a correction factor, extracted from features visible on both the freshly excised kidney tissues and histologically processed kidney slides.

Methods: In order to calculate this factor, histology slides containing HIFU ablations and non-ablated tissues were registered with corresponding photographs of the kidneys obtained right after tissue harvesting. Ablated regions visible on both the histology slides and the surface of the organ were used as fiducial markers to guide the alignment of the samples. Data processing included digitization of the histology slides, identification and tracing of the ablated regions, scale normalization across all datasets, and generating an equivalent novel one-dimensional projection of each slide to enable alignment and registration with each kidney photograph. Applying the same registration metrics as a boundary condition across multiple slides covering the same ablated volume increased the registration accuracy between the two different datasets. Once aligned, the length of the kidney along the line of the corresponding slide position was measured and divided by the length of the kidney as captured on the slide in order to calculate the correction factor. This process was repeated on a total of 366 slides across 37 lesions on 22 kidneys.

Results: The mean correction factor was found to be 1.136 ± 0.142. The effects of operator dependence during the registration step, changes in the angle of alignment, changes in the thickness of slide spacing, and the impact of the number of days the samples were preserved in formalin prior to processing on the value of the correction factor were also examined, and were found to affect the correction factor by less than 6%.

Conclusions: It is well known that formalin fixation and histological processing shrinks tissues being processed. If the gold standard of histology is to be used in the context of HIFU volume ablation quantification and device validation, it is imperative that such shrinkage be taken into account. The robustness of the developed method (relying on multiple slides and ablation volumes for estimating such shrinkage) and small variability of the resulting correction factor allow for a high degree of confidence for applying the established correction factor for HIFU ablation quantification analyses.

P-MI-15

Topic: Miscellaneous Indications

Presentation Type: Poster

Thermal-Mechanical focused ultrasound ablation for stiff tissue ablation

Alexander Simon[1], Faith Robinson[2], Pete Weber[2], Eli Vlaisavljevich[1]

[1]Virginia Polytechnic Institute and State University, Blacksburg, Virginia, United States
[2] Virginia Tech Carilion School of Medicine and Research Institute, Blacksburg, Virginia, United States

Background: Histotripsy is a non-invasive and non-thermal ablation method that mechanically breaks down tissue via controlled acoustic cavitation. Histotripsy is highly dependent upon tissue mechanical properties, with previous studies showing that tissues with higher mechanical strength are more resistant to histotripsy-induced tissue damage. In this work, we develop a dual-modality focused ultrasound (FUS) ablation method combining thermal HIFU with histotripsy for the treatment of stiff tissues such as cholangiocarcinoma and uterine fibroids. We hypothesize that thermal HIFU will significantly reduce tissue stiffness when treated at specific temperatures due to collagen denaturing, allowing for the complete and efficient ablation of these tissues with histotripsy.

Methods: Two sets of experiments were conducted in order to test the feasibility of thermal-mechanical FUS ablation using *ex vivo* bovine tissue with a wide range of mechanical properties (liver, kidney, tongue, tendon). First, tissue samples were heated in a constant temperature water bath at ~60˚C or ~90˚C followed by histotripsy using a 700kHz therapy transducer (HistoSonics), 5-cycle pulses, a pulse repetition frequency (PRF) of 500 Hz, and peak pressures of ~19/60 MPa (P-/P+). In a second set of experiments, the same 700kHz transducer was used to apply thermal HIFU and histotripsy to bovine samples with thermal HIFU applied using 30-35 cycle pulses at pressures of ~8/25 MPa (P-/P+) and a PRF varying from 1300-1750 Hz. During HIFU, the temperature measured by three type T thermocouples was allowed to increase to the desired maximum temperature (60°C or 90°C) and then the PRF was modulated to maintain a nearly constant temperature for the duration of the HIFU exposure. For all experiments, tissue mechanical properties were measured before and after HIFU with a soft tissue elastometer, and ablation was assessed histologically using a Masson's trichrome stain.

Results: Results demonstrated that thermal pre-treatment at ~60˚C significantly softened tissues due to collagen denaturing, therefore enhancing tissue susceptibility to histotripsy (Fig.1). In contrast, heating at ~90˚C resulted in the stiffening of most tissues due to collagen contraction, resulting in tissues being less susceptible to histotripsy (Fig.1). An exception to this trend was observed for bovine tendon, which saw significant tissue softening when heated at ~90˚C due to collagen hydrolysis, resulting in complete histotripsy ablation after the thermal pretreatment (Fig.1). Current studies are underway to optimize this thermal-mechanical FUS ablation method in order to determine the optimal acoustic parameters for the treatment of various tissue types.

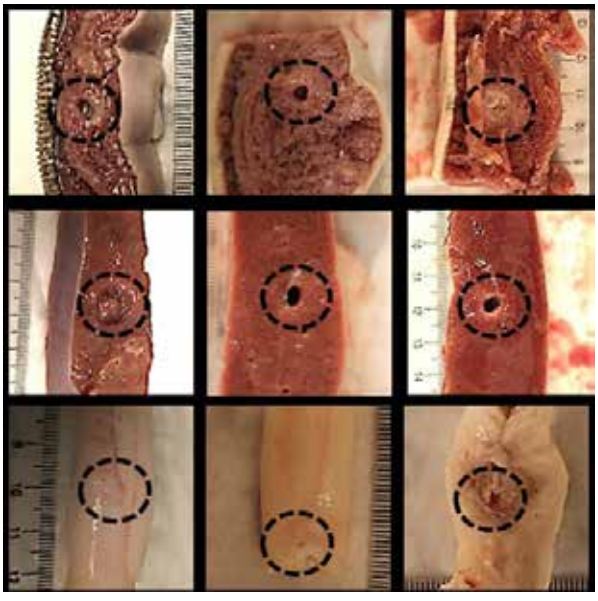

Figure 1. Morphological analysis of bovine tissues treated with thermal HIFU followed by histotripsy showed an increase in susceptibility to histotripsy for tongue, liver, and tendon heated for 10 minutes at ~60°C. Tongue and liver samples heated for 10 minutes at ~60°C. Tongue and liver samples heated for 10 minutes at ~90°C were less susceptible to histotripsy while tendon became more susceptible.

Conclusions: The results of this study demonstrate the potential of thermal-mechanical FUS for the efficient and complete ablation of a variety of tissue types, including tissues with higher mechanical properties that are resistant to traditional histotripsy. Additional studies are currently underway to optimize this method for treating specific tissues of interest and to develop imaging feedback methods for real-time modulation of therapy parameters.

Acknowledgements: The authors would like to thank the Virginia Tech Department of Biomedical Engineering and Mechanics for providing funding for these studies.

P-MI-16

Topic: Miscellaneous Indications

Presentation Type: Poster

TRANS-FUSIMO — Safety and efficacy evaluation of a novel motion compensated FUS treatment system for clinical use

Jan Strehlow[1], Andrew Dennison[2], Michael Schwenke[1], Joyce Joy[2], Sabrina Haase[1], Mario Bezzi[3], Andreas Melzer[2], Tobias Preusser[1]

[1]Fraunhofer Institute for Medical Image Computing MEVIS, Bremen, Germany
[2]University of Dundee, Dundee, United Kingdom
[3]Universita Degli Studi Di Roma La Sapienza, Rome, Italy

Background: Motion compensated Focused Ultrasound offers a promising new approach for treating hepatic tumor diseases. Despite plenty of research, no clinically approved system has been presented so far. In the EU FP7 project TRANS-FUSIMO a generic and extensible framework for motion compensated FUS has been developed, validated, and optimized via in-silico experiments. The resulting TRANS-FUSIMO treatment system (TTS) is capable of treating abdominal organs that move under breathing motion. Both organ motion and target temperature are monitored via a Signa 1.5T MR scanner (GE Healthcare Systems Chicago). An automated feature tracking component determines the motion captured across 2D images and feeds it into a motion model which can extrapolate feature positions both spatially and temporally. An independent FUS controller queries the position of a target at a given time and updates the focal position of a CBS 2100 FUS transducer from INSIGHTEC accordingly.

Methods: The proposed TTS system is evaluated with respect to clinically motivated safety, performance and efficacy parameters using dedicated setups and phantoms. In a first series of system safety experiments we evaluate if prescribed sonication parameters such as power, duration and focus position are accurately replicated by the system and if a sonication can be interrupted instantaneously. Further we compare the temperature monitoring of our system to that of the clinically approved EXABLATE 2100 (INSIGHTEC Ltd., Tirat Carmel, Israel) treatment system. In a second series of experiments we analyze the latencies and computation times of our system and its components. Last, motion compensation efficacy is evaluated in a respiratory motion phantom and compared to our estimates from the in-silico experiments.

Results: The TTS executes sonications according to the clinical requirements while being interruptible instantaneously and safely. The observed peak temperature during similarly prescribed sonications with the TTS system and EXABLATE 2100 differ by less than 10%. Latencies are analyzed and the median time from motion observation to focus update is 409 ms, with image acquisition and transfer being the main contributor. Despite this considerable system latency the system can compensate motion in a respiratory motion phantom with an efficiency of 89.6%, which is in-line with the predictions of our in-silico evaluation.

Conclusions: Our results suggest that safe, efficient and effective motion compensated FUS is possible with the proposed system. The system is currently being evaluated on porcine animal models in a pre-clinical site to show safety, efficiency, and efficacy in an *in vivo* model.

P-MI-17

Topic: Miscellaneous Indications

Presentation Type: Poster

Bowel safety margins with MRgHIFU thermal ablation in a preclinical porcine model

Sergio Vega, Aodhnait Fahy, Karolina Piorkowska, Adam Waspe, James Drake, Ted Gerstle

The Hospital for Sick Children, Toronto, Ontario, Canada

Background: MRgHIFU is currently approved for thermally ablative treatments of uterine fibroids and bone metastasis in adults. Abdominal soft tissue masses, such as neuroblastoma and pelvic rhabdomyosarcoma, are under investigation as potential targets for thermally ablative HIFU. However, one of the significant potential risks of abdominal HIFU is thermal injury to nearby bowel (necrosis and/or perforation). To minimize the risk of injury to the bowel, current protocols for treating other pathologies using HIFU recommend maintaining a safety margin of 4 cm. However, the extent of this safety margin has not been scientifically delineated. In the pediatric abdomen, maintaining 4 cm from any edge of the bowel would significantly limit the amount of tumor tissue that could be treated or debulked, and practically, this type of margin would prevent a significant proportion of patients' tumors from being treated. The objective of this study was to create an *in vivo* porcine model to refine bowel safety margins for thermal ablation using MRgHIFU.

Methods: Pigs (n=2, mean weight of 22 kg) underwent a laparotomy under general anesthesia. A 4cm gel marker (Aquaflex®, Parker Labs) was placed in a pocket within the retroperitoneal muscle, lateral to the lower pole of the kidney and caudal to the rib cage. A 10 cm segment of small bowel was fixed to the retroperitoneal wall with a Penrose drain through the mesentery. The same procedure was performed on the contralateral side. Pigs were imaged with a 3 Tesla MRI (Philips Achieva, Best, Netherlands) which enabled localization of the gel markers. HIFU treatment was performed on a Sonalleve V1 HIFU table (Profound Medical, Toronto, Canada) using a soft tissue ablation protocol consisting of an acoustic power of 100 W for a sonication duration of 20s at 1.2MHz. Sonications on the gel marker within the muscular layer was 1.0 cm and 1.5 cm from the nearest bowel. After post-treatment imaging, bowel segments were collected for histological analysis.

Results: The Penrose drain allowed stable but not restrictive fixation of small bowel near to the fiducial marker, directly against the retroperitoneal wall. The distance from the fiducial marker and sonication to the bowel wall was quantifiable via MRI. This method simulated the naturally fixed duodenum, which could not be used due to its nearby relation with ribcage. Immediate necrosis on the bowel occurred at both 1.0 cm and 1.5 cm distance from HIFU therapy. Future experiments will also assess injury due to therapy, at 2 cm to 4 cm from the bowel.

Conclusions: This preclinical porcine model enables reproducible positioning of fixed bowel in relation to the abdominal wall, which will help to determine a safety margin to bowel with thermal ablation using MRgHIFU. Further investigations will vary the distance between the HIFU focus and the bowel in order to refine the proximity to bowel at which MRgHIFU thermal ablation can be safely used with various MRgHIFU treatment parameters.

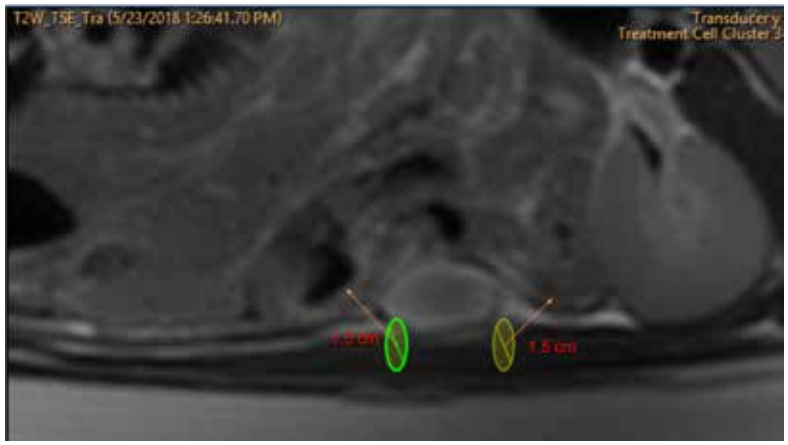

Figure 1. Fiducial marker placement and areas sonicated

P-MI-19

Topic: Miscellaneous Indications

Presentation Type: Poster

Numerical analysis to develop an image-guided tilt and displaceable HIFU transducer for patient-specific allergic rhinitis treatment

Prasad Bibin[1], Suzy Kim[1], Jung Kyung Kim[2]

[1]SMG Seoul National University, Boramae Medical Center, Seoul, South Korea
[2]Kookmin University, Seoul, South Korea

Background: Allergic rhinitis (AR) is a non-infectious inflammation of the nasal mucosa mediated by immunoglobulin E. Recognition of safe and efficient treatment is an imperative topic for clinical examinations. This study puts emphasis on to develop an effectual image-guided tilt and displaceable focused ultrasound transducer for patient-specific AR treatment.

Methods: Numerical simulations were performed using a nonlinear acoustic model on phantom and human models to develop a HIFU transducer which is capable to displace and tilt for AR treatment. Parametric studies were conducted on phantom models to determine the effect of frequency range and transducer design. Comparisons were made with spherical and cylindrical transducers to investigate the influence of size and exposure time for controllable energy deposition near the focal point. Simulations on human anatomy were conducted to predict effective deployment of temperature distribution by displacing and tilting ultrasound irradiation to foresee the tissue damage in short duration for patient-specific AR treatment.

Results: Transducer with an optimum radius of curvature of 6 mm and frequency around 3 MHz was derived from the parametric study for effective energy deposition. Cylindrical transducer provides more controllable temperature distribution in terms of transducer size and exposure time compared to spherical transducers. Human anatomy study elucidated effective deployment of temperature distribution at the inflammatory region (nasal submucosa) in short time with appropriate displacement (2-5 mm) and tilting (30-90°) of transducers. Thermal dose calculations show the ablation of lesion without damaging the superficial tissue of nasal mucosa.

Conclusions: This work depicts the preliminary studies for developing an image-guided tilt and displaceable HIFU transducer for AR treatment. Transducer shape and size are pivotal factors for optimizing the energy deposition at focal point. Human anatomy simulations elucidate that tilt and displaceable HIFU transducer can provide effectual coagulative necrosis with minimal superficial tissue damage. The study would contribute to effective image-guided AR treatment planning strategies in clinics.

Acknowledgements: This research was supported by the National Research Foundation (NRF-2016R1A2B4012095) sponsored by the Ministry of Science, ICT and Future Planning, Republic of Korea.

P-MS-1

Topic: Musculoskeletal
Presentation Type: Poster

Benefits of personalized gel pads for magnetic resonance-guided focused ultrasound

William Chu Kwan, Michael Temple, Adam Waspe, James Drake

The Hospital for Sick Children, Toronto, Ontario, Canada

Background: To minimize the attenuation and reflection of ultrasound energy emitted by a transducer, coupling mediums are employed. Existing coupling agents include mineral oils, degassed water, and hydrogels such as agar. During Magnetic Resonance-guided Focused Ultrasound (MRgFUS) treatments, standard discoid gel pads (Aquaflex, Parker Labs) coated with diluted ultrasound gel are typically used between transducers and patients. Of concern is the ultrasound energy reflection due air and coupling at the skin-gel interface. Energy is absorbed by the medium and converted into heat, leading to skin necrosis. Other drawbacks include decreased surface area contact on smaller patients, and positional changes throughout treatment. Ultimately, these factors diminish the overall effectiveness of treatment and increase treatment time and cost.

Our goal is to determine the benefits of using personalized agar gel pads. The aim is to analyze if there is an increased effectiveness of ultrasound energy coupling, and to explore if it is both practical and advantageous to construct these personalized agar gel pads.

Methods: We prepared 2 personalized agar gel pads and compared them to 3 control setups consisting of the standard Aquaflex pads. A total of 5 porcine leg specimens were harvested. The mould consisted of a permanent section designed to fit in the HIFU sonication window encompassing the complete conical sonication beam. For the personalized section, a modular piece was 3D-printed based on anatomic MRI scans (Figure1). After mould assembly, the gel pads were prepared with a mixture of 2% purified agar in water (Figure2).

For testing, the specimens were sonicated using a V1 Sonalleve HIFU table (Profound Medical). For each specimen, 10 treatment cells of 2mm were ablated at a power of 100W for 20 seconds. Near-field temperature mapping at the skin-gel interface was obtained with an Achieva 3T MRI (Philips Healthcare). The distance between the sonication plane and the temperature mapping plane were comparable.

Results: Visual inspection of the near field temperature map demonstrated a significant decrease in energy scattering in the personalized gel pad when compared to the standard gel pad (Figure3 and Figure4). The maximum temperature recorded on the personalized gel pad ranged from 45.7oC to 56.3oC with a maximal area of 90.1 mm^2 at a distance of 14 mm from the treatment plane. In contrast, the maximum temperate recorded on the standard gel pad ranged from 45.9oC to 67.7oC with an area of 205.98 mm^2 at an average distance of 14 mm from the treatment plane. Other notable differences were the ease of sample positioning on the personalized gel pad and the lack of motion or shifting of the sample throughout testing.

Figure 1. 3D printed mould

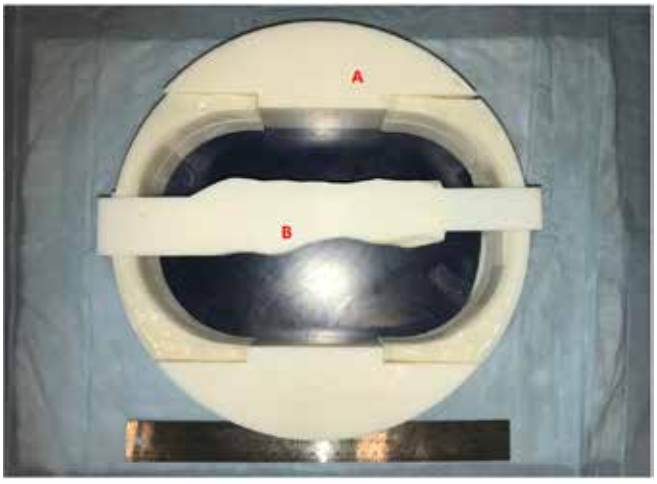

A: permanent section of mould modelled for HIFU table
B: modular personalized section of mould modelled for specimen

Conclusions: Our results demonstrate a reproducible and feasible method of preparing patient-specific personalized agar gel pads for MRgFUS treatment. The benefits of these personalized gel pads include greater acoustic coupling and effective energy delivery, which translates into improved patient safety. Additionally, the ease of positioning and the lack of motion provide a shorter treatment time and reduced therapy cost.

Figure 2. Personalized agar gel pad

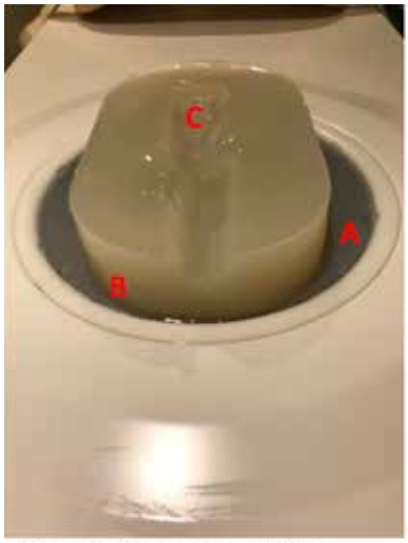

A: sonication window cylinder
B: gel pad elevation
C: personalized mould

Figure 3. Comparison of near-field temperature mapping

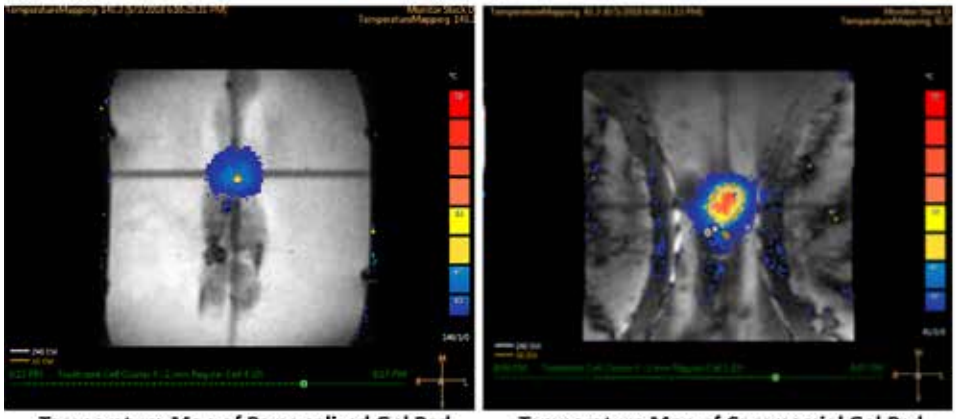

Temperature Map of Personalized Gel Pad
Tmax = 56 °C

Temperature Map of Commercial Gel Pad
Tmax = 67.7°C

Figure 4. Comparison of near-field temperature mapping

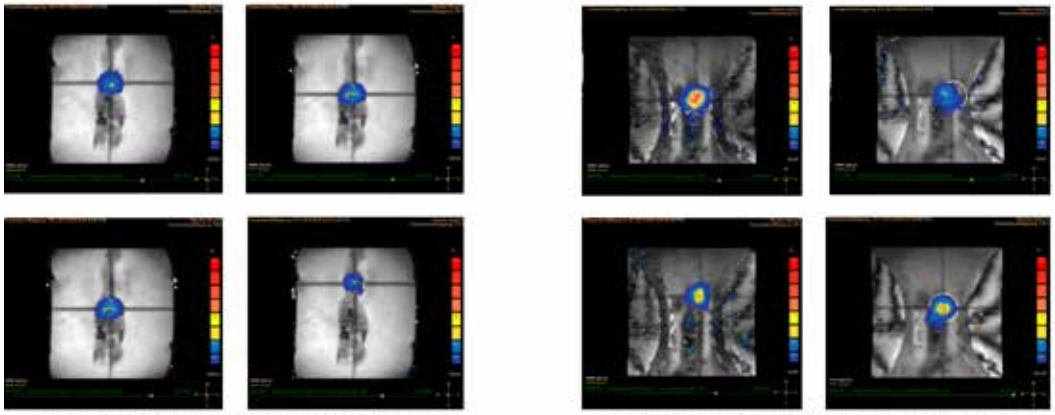

Temperature Map of Personalized Gel Pad

Temperature Map of Commercial Gel Pad

P-MS-2

Topic: Musculoskeletal
Presentation Type: Poster

Biomechanical changes of porcine tendons following high-intensity focused ultrasound ablation

William Chu Kwan, Adam Waspe, James Drake

The Hospital for Sick Children, Toronto, Ontario, Canada

Background: Diabetic foot ulcer, pediatric toe-walking, and cerebral palsy are musculoskeletal conditions that can be corrected with surgical resection of tendons. Given current trends towards non-invasive procedures, Magnetic Resonance-guided Focused Ultrasound Surgery (MRgFUS) is an ablation technique that has the potential to provide an incisionless non-invasive treatment for these conditions. This could translate into less exposure to anesthetics, less prophylactic antibiotics use, better pain management medication , reduced hospitalization time, and ability to perform conservative treatments with retreatments.

Our goal in this study is to perform a quantitative analysis of biomechanical changes in tendons after MRgFUS ablation. Understanding these effects sets the foundation for future studies in non-invasive MRgFUS tendon transection.

Methods: To standardized this experiment, 4 agar phantoms were prepared. Each phantom contained 4 pairs of matching porcine deep digital flexor tendons. One tendon in each pair would be treated with MRgFUS ablation while the other tendon would serve as a control. Physical properties such as temperature, length, and diameter were recorded during preparation, verified to be consistent between control and treatment tendons, and used for analysis.

Ablation treatment was performed using a V1 Sonalleve (Profound Medical). The treated tendon from each pair was randomly assigned to one of four groups based on ablation parameters. Group 1 did not receive any treatment serving as an additional control. Group 2 had 1 treatment with a power of 50W for 20 seconds. Group 3 had 1 treatment with a power of 100W for 20 seconds. Group 4 had 2 treatments of 100W for 20 seconds each. MR imaging and temperature maps were performed throughout the experiment (Figure1).

Figure 1. Post-sonication tendon in Instron tester

Following ablation, the tendon biomechanical properties were analyzed using an Instron MicroTester. This machine applied a tensile force on the tendon and generated a stress *versus* strain curve, yielding the Young's modulus (Figure2).

Results: Overall, there was a decrease in Young's modulus as more power was used to ablate the tendon. Treated tendons from Group 3 and 4 experienced a rupture while subjected to the Instron tester. The treated tendons in Group 2 had a decrease of 16.07% in Young's modulus and no tendon rupture observed. The tendons in Group 3 had a decrease of 41.97% in Young's modulus and a maximum tensile stress of 6.59 MPa. Finally, the tendons in Group 4 had a decrease of 73.01% in Young's modulus and a maximum tensile stress of 4.48 MPa.

Given the Instron's tensile force maximum of 500N, there was no data to report Young's modulus or fracture strain for all the untreated controls. These tendons did not rupture during testing and remained intact.

Conclusions: Our results demonstrate that MRgFUS ablation changes the biomechanical properties of tendon by decreasing the Young's modulus and its elasticity. As more power is delivered on a treatment cell, the maximum tensile stress required to rupture the tendon decreased. This demonstrates that MRgFUS ablation could be a feasible intervention for non-invasive tendon transection for many musculoskeletal conditions.

Figure 2. MRI images and sonication temperature map

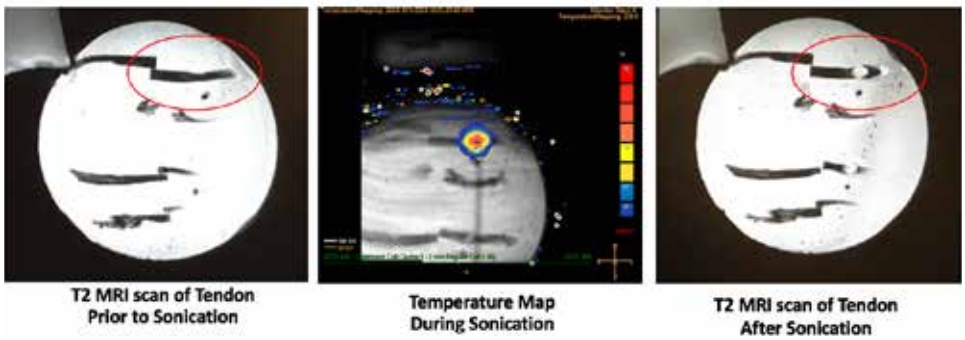

P-WH-1

Topic: Women's Health
Presentation Type: Poster

Validation in phantoms of a rapid beam modeling method for breast therapy

Megan Dearden, Douglas Christensen, Allison Payne

University of Utah, Salt Lake City, Utah, United States

Background: To optimize the treatment efficacy of MRgHIFU breast therapies, ultrasound beam propagation in the targeted tissue must be modeled quickly and accurately. For this purpose, the system developed for the treatment of breast cancer at the University of Utah utilizes the hybrid angular spectrum (HAS) method, which is a novel and rapid wave propagation technique for inhomogeneous media.[1] To quantitatively validate the HAS-predicted beam focusing patterns in both homogeneous and heterogeneous media, we are performing studies with both types of phantoms.

Methods: Multiple phantoms were created to compare the HAS-predicted and hydrophone-measured volumetric pressure patterns. All simulated and experimental pressure patterns are using a 940-kHz, 256-element phased-array transducer. Homogeneous 250-bloom gelatin phantoms (n=9) were constructed with varying amounts of evaporated milk (30%, 50% and 70% by volume) to modify their acoustic properties (speed of sound and attenuation).[2] Radiation force balance and through-transmission techniques were used to measure beam attenuation, and through-transmission measured speed of sound. The HAS algorithm utilized these experimental values (along with the calculated density) to simulate wave propagation through these samples into a distal water region to obtain a three-dimensional (3D) pressure pattern. Then, a two-dimensional transverse complex pressure pattern near the beam focus in water (after propagation through the sample) was recorded with a hydrophone and propagated longitudinally with HAS to create the 3D experimental beam pattern. In addition, heterogeneous phantoms (n=5) are being constructed with breast tissue-mimicking inclusions. These are undergoing equivalent testing using the methods described above.

Results: The density, speed of sound and attenuation values determined for the three phantoms with different milk percentages are given in Table I with a comparison to values for the same type of gelatin phantoms from Johnson et al.[1] and to breast tissue values from an international database. These values were used to simulate 3D beam profiles in the phantoms using the HAS technique and a model of the breast system transducer. Figure 1 shows a longitudinal slice of the pressure pattern at the location of the focus, while Figures 2 and 3 are plots of the pressure profile both transverse and parallel to beam propagation. Analysis of the propagated hydrophone pressure data and comparison to the simulated beams is ongoing along with construction of heterogeneous phantoms.

Table I – Measured Values of Phantoms with Different Milk Concentrations and Representative Tissue Values

Material	Material Density (kg/m^3)	Speed Of Sound (m/s)	Attenuation at 1 MHz (np/cm)
30% Phantom	1040 ± 10	1552.6 ± 0.6	0.029 ± 0.004 (Through-Transmission) 0.03 ± 0.01 (Radiation Force)
50% Phantom	1060 ± 20	1565.8 ± 0.8	0.044 ± 0.001 (Through-Transmission) 0.044 ± 0.007 (Radiation Force)
70% Phantom	1080 ± 20	1579.4 ± 0.8	0.057 ± 0.001 (Through-Transmission) 0.06 ± 0.01 (Radiation Force)
30% Phantom ref. 3	1050 ± 8	1552 ± 2	0.027 ± 0.004
50% Phantom ref. 3	1040 ± 8	1560 ± 2	0.042 ± 0.007
70% Phantom ref. 3	1050 ± 8	1572 ± 2	0.053 ± 0.008
Breast Fat*	911 ± 53	1440.2 ± 21.9	0.044
Breast Glandular*	1041 ± 45	1505.0 ± 47.3	0.086

* Foundation for Research on Information Technologies in Society.

Conclusions: The hybrid angular spectrum method has been shown to be rapid and flexible beam modeling technique that is currently undergoing validating with hydrophone scanning by comparing pressure pattern size and overall magnitude. The accuracy of this method is dependent on determining media properties correctly, including density, speed of sound and attenuation. Extending these results to heterogeneous tissue-mimicking phantoms will add to the *in vitro* validation of the HAS algorithm.

Acknowledgements: Summer 2018 FUSF Global Internship program and NIH R01224141.

References:

1. Vyas et al. *IEEE Trans Ultra Ferro Freq*. 2012;59(6).
2. Farrer et al. *J Ther Ultrasound*. 2015.
3. Johnson et al. *Int J Hyperthermia*. 2016;32(7).

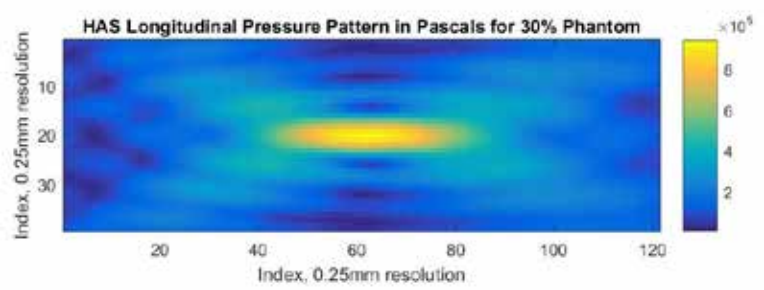

Figure 1. Simulated pressure pattern in Pa for a 30% milk phantom in a longitudinal plane at the beam focus using attenuation and speed of sound values obtained by through-transmission

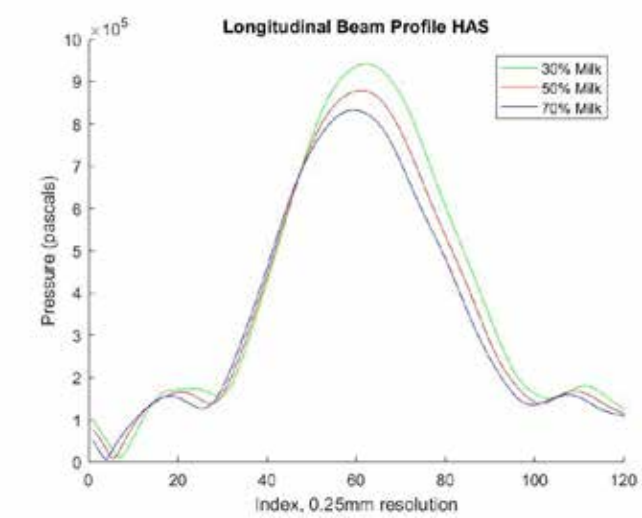

Figure 2. Simulated longitudinal beam profiles for 30%, 50% and 70% phantoms through the beam focus using through-transmission property values

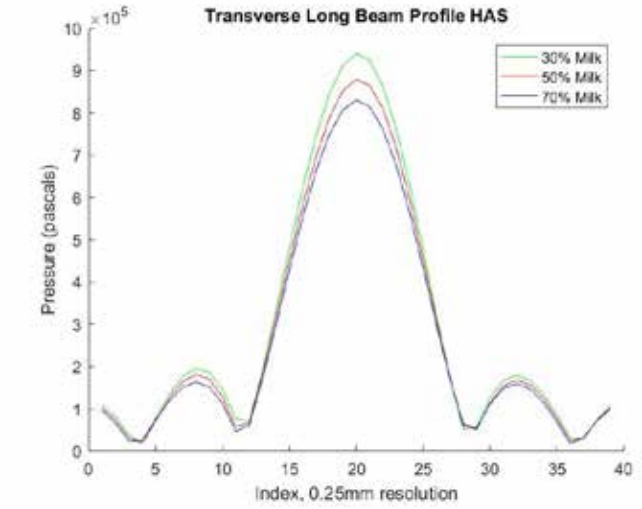

Figure 3. Simulated beam profiles for 30%, 50% and 70% phantoms using through-transmission property values along the longer transverse axis of the oblong beam focus

P-WH-2

Topic: Women's Health
Presentation Type: Poster

Ultrasound guided high intensity focused ultrasound ablation of breast fibroadenoma: Results of the first United States study

Bilgin Keserci[1], Nguyen Minh Duc[2], Mohd Shafie Abdullah[1]

[1]School of Medical Sciences, Hospital Universiti Sains Malaysia, Kota Bharu, Malaysia
[2]Pham Ngoc Thach University of Medicine, Ho Chi Minh, Vietnam

Background: Fibroadenoma is a common benign breast mass that can cause pain, a palpable lump, and anxiety. Current management includes observation or surgical excision. This study evaluated the safety and feasibility of Ultrasound guided High Intensity Focused Ultrasound (USgHIFU) delivered by the Echopulse device (Theraclion, Paris) for treatment of breast fibroadenomas. Patient safety, cosmetic outcome, tumor response, and patient experience were assessed.

Methods: Twenty women with a palpable, core biopsy confirmed, breast fibroadenoma were enrolled in a single arm IRB and FDA approved clinical trial. Patients underwent treatment utilizing the Echopulse device (Theraclion, France). All patients had tumors with a minimum diameter >1 cm with volume between 0.3cc and 10cc. Volume calculation formula = length (mm) x width (mm) x height (mm) x π / (6 x 1000) in cc. Optimal energy delivered per sonication was established by determining the minimal setting found to produce a hyperechoic mark observed on real-time B-mode image. Patient treatment experience, toxicity, cosmesis, and change in tumor size on both physical examination (palpability) and ultrasound measurement were obtained before and immediately after treatment, and at 3, 6, and 12 months.

Results: Twenty of 20 patients successfully completed therapy. Pre-treatment mean tumor volume was 1.8cc (SD = 1.23, Range 0.57–5.7). Mean patient age was 35.3 years. Forty percent of patients were Caucasian, 40% Latino, and 20% were Black. Fifty percent reported a painful mass prior to treatment. Mean power/sonication = 38.0 (28.2 – 47.0) watts. Mean number of sites treated/patient = 34.3 (8-103). Median duration of treatment was 39.5 minutes (95% CI, 34.5 – 53.0). Hyperechoic marks were observed in 15/20 (75%) of patients. All adverse events were grade 1 or 2; no burns, damage to adjacent structures, or other toxicities were observed. The most common toxicity was mild pain, reported by 15/20 (75%) of patients during treatment, and 14/20 (60%) at day 7. Mean pain score during treatment was 16 on a scale from 0 to 100 (100 = worst pain). Mean pain score at day 7 was 12.2. Patient satisfaction was 4.4 on a scale of 1-5 (5 = most satisfied), likelihood of recommending it to a friend or family member was 4.7 (5 = strongly agree). Two patients were lost to follow-up at 12 months.

Figure 1.

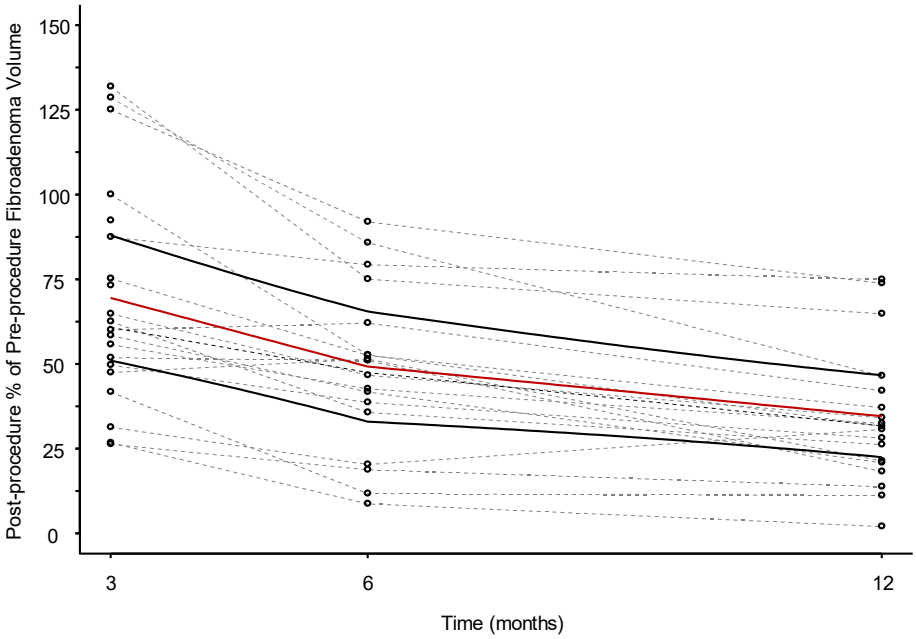

At 12 months follow-up, mean % reduction in volume of the fibroadenoma was 65%, (98% to 25%, $p < 0.0001$). A mass was no longer palpable in 80% of patients, no patients reported pain, and cosmesis was rated by both patients and physicians as excellent in 100% of subjects.

Conclusions: USgHIFU is an effective, safe, and well tolerated treatment for breast fibroadenomas resulting in minimal toxicity. Based on the above results, a larger multi-center clinical trial is currently open to accrual in both the United States and Europe.

Acknowledgements: Research funding provided by Theraclion

Figure 2.

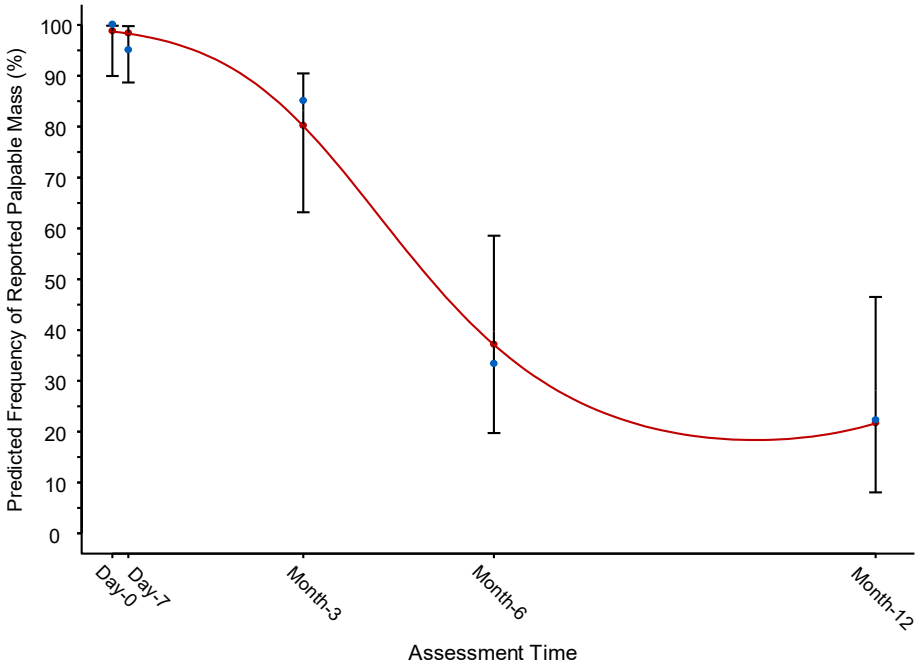

Figure 3.

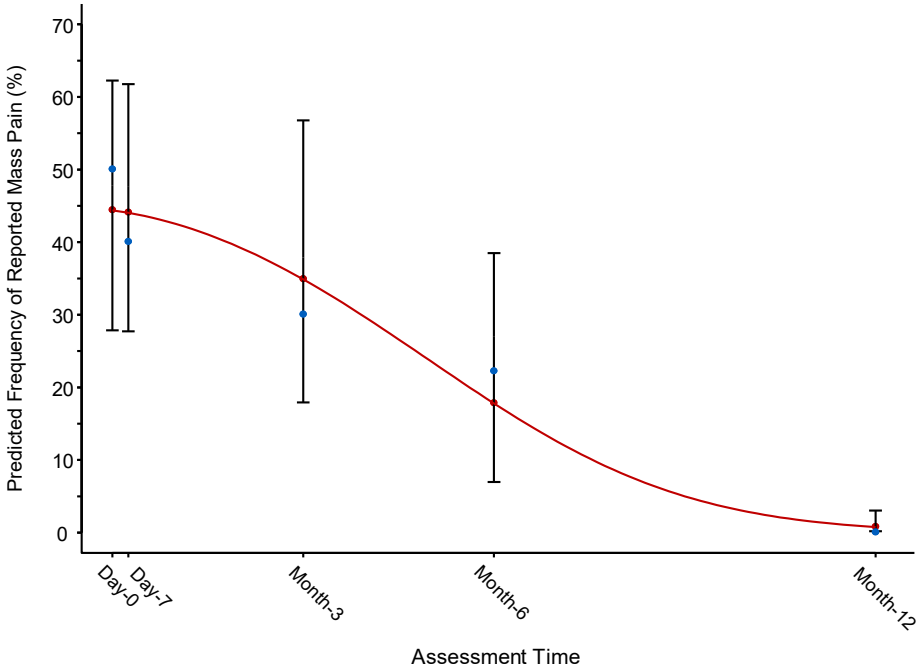

P-WH-3

Topic: Women's Health
Presentation Type: Poster

Comparison of therapeutic efficacy in volumetric magnetic resonance imaging-guided high-intensity focused ultrasound ablation of uterine fibroids: T1-perfusion and T2 signal intensity-based classification

Bilgin Keserci[1], Nguyen Minh Duc[2], Mohd Shafie Abdullah[1]

[1]School of Medical Sciences, Hospital Universiti Sains Malaysia, Kota Bharu, Malaysia
[2]Pham Ngoc Thach University of Medicine, Ho Chi Minh, Vietnam

Background: To comparatively evaluate therapeutic efficacy in magnetic resonance imaging (MRI)-guided high-intensity focused ultrasound (HIFU) ablation of uterine fibroid (UF) based on T1-perfusion and T2 signal intensity (SI)-based classifications.

Methods: This retrospective study was approved by the institutional review board, and informed consent was obtained from all participants. The fibroids of 67 women (age, 39.2 ± 5.9 years; range, 22–53 years) who underwent HIFU treatment were classified according to (i) T2 SI-based classification as type I (n = 10, if SI of UF lower than or equal to that of skeletal muscle), type II (n = 40, if SI of UF lower than that of the myometrium but higher than that of skeletal muscles) and type III (n = 17, if SI of UF higher than that of the myometrium), and (ii) T1 perfusion-based classification as group A (n = 44, if the time-SI curve of UF is lower than that of myometrium) and group B (n = 23, if the time-SI curve of UF is equal or higher than that of myometrium). The uterine fibroids volume, non-perfused volume (NPV) ratios immediately after treatment and volume reduction ratios and transformed symptom severity scores (tSSS) at the 6-month follow-up were retrospectively assessed.

Results: The mean UF volume of type I, II, III and group A and B was 155.4ml, 207.7ml, 156.5ml, 206.1ml and 150.0ml, respectively. The mean NPV ratio was significantly higher in group A than in group B (95.6%, 51.9%, respectively; $p<0.05$). However, we found no statistically significant difference in the immediate NPV ratio among patients with type I, II and III (80.6%, 79.5%, 83.2%, respectively; $p>0.05$). The 6-month fibroid volume reduction ratio in group A was significantly greater compared to that in group B (52.7% and 3.6%, respectively; $p<0.05$), whereas we found no statistically significant difference among type I, II and III (44.3%, 32.8%, 38.2%, respectively; $p>0.05$). The corresponding tSSS improvement ratio was 70.3%, 53.7%, 55.3% in type I, II and III and 80.9% and 10.1% in group A and group B, respectively.

Conclusions: The preliminary results of this study revealed that T1-perfusion based classification method could play an important role in not only classifying the UF but also predicting the treatment outcome of MRI-guided HIFU ablation.

Acknowledgement/Funding sources

This research received no specific grant from any funding agency in the public, commercial, or not-for-profit sectors.

P-WH-4

Topic: Women's Health
Presentation Type: Poster

Volumetric magnetic resonance imaging-guided high-intensity focused ultrasound ablation of uterine fibroids and adenomyosis: ASEAN experience

Bilgin Keserci[1], Nur Hartini MohdTaib[1], Nguyen Minh Duc[2], Wan Aireene Binti Wan Ahmed[1], Mohd Shafie Abdullah[1]

[1]School of Medical Sciences, Hospital Universiti Sains Malaysia, Kota Bharu, Malaysia
[2]Pham Ngoc Thach University of Medicine, Ho Chi Minh, Vietnam

Background: Magnetic Resonance-High Intensity Focused Ultrasound (MR-HIFU) therapy is a complete noninvasive treatment of symptomatic uterine fibroids. However, the clinical applicability is often limited due to the limit in focal depth of the MR-HIFU system or interposition of small bowel loops in the sonication path. To decrease the screening and treatment failure rates, manipulation techniques are widely used.[1,2,3,4] The aim of this retrospective study was to describe our manipulation protocol for MR-HIFU treatment of uterine fibroids.

Methods: From June 2016 to June 2018, 145 women underwent a screening MRI examination of which 54 women were consecutively treated with MR-HIFU at our institution. We obtained informed consent from all patients. Procedures were performed on an outpatient basis under conscious sedation. Bowel preparation was done using a fast-acting micro-enema. Patients received oral premedication. A Foley catheter and intravenous line were inserted. Treatments were conducted using a clinical HIFU system (Sonalleve V1, Profound Medical Inc., Toronto, Canada) integrated with a 1.5-T MRI system (Achieva; Philips Healthcare, Best, the Netherlands). We reassessed the location of the fibroid on T2W images. If necessary, we followed our manipulation protocol which included three different techniques:

1. The BRB maneuver; sequential applications of urinary bladder filling, rectal filling and urinary bladder emptying.2,4 Compared to this classical BRB maneuver, we filled the rectum with multiple syringes (60 mL) using a solution of ultrasound gel (30 mL), saline solution (30 mL) and 1 sachet psyllium fiber (3,4 gram). The amount of rectal filling ranged from 240-480 mL, based on patient tolerance. This BRB manipulation moved the fibroid anteriorly (figure 1) or displaced bowel loops (figure 2).

   If step 1 failed to succeed, we moved on to step 2 or 3 depending on the position of the uterus.

2. Uterus axial or retroverted; we manipulated the uterus manually into anteflexion. Afterwards, we fixated the position of the uterus with an speculum (figure 3).
3. Anteverted uterus; patients were positioned into Trendelenburg to move the small bowel out of the pelvis. Additionally, abdominal massage was performed on both sides of the lower abdomen with movements towards the upper abdomen (figure 4).

Results: The first 20 treatments we only used the classical BRB manipulation technique.

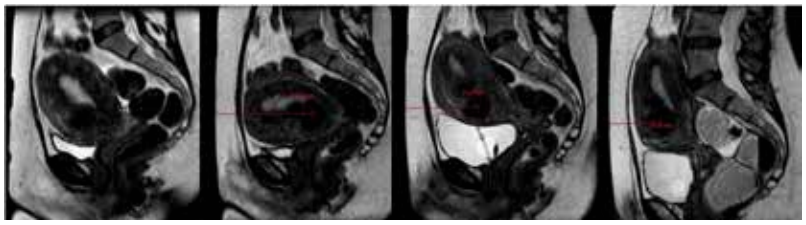

Figure 1.

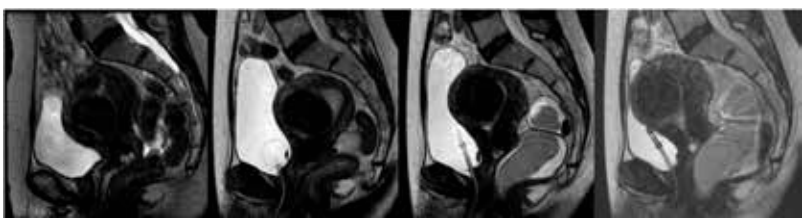

Figure 2.

Our overall screening failure rate was 53% (47/88), of which 18% (16/88) was due to a retroverted uterus or the distance between fibroid and abdominal wall. Although no bowel interposition was observed on the screening MRI, still 20% (4/20) of the treatments failed due to the interposition of bowel loops, suggesting a reversible situation. Therefore, we implemented new manipulation techniques and our screening failure rate decreased from 53% to 28% (16/57). Our treatment failure rate due to the interposition of bowel loops decreased from 20% to 0% (0/34). Although this could be partially explained by a learning curve.[5]

There were no complications or thermal injuries to the bowel or uterus from the manipulation.

Conclusions: We implemented a manipulation protocol using three different techniques which has led to a decrease in our screening and treatment failure rates.

References:

1. Zhang L, et al. Feasibility of Magnetic Resonance Imaging-Guided High Intensity Focused Ultrasound Therapy for Ablating Uterine Fibroids in Patients with Bowel Lies Anterior to Uterus. *European Journal of Radiology*. 2010;73(2):396-403. DOI:10.1016/j.ejrad.2008.11.002.
2. Park MJ, et al. Technique to Displace Bowel Loops in MRI-Guided High-Intensity Focused Ultrasound Ablation of Fibroids in the Anteverted or Anteflexed Uterus. *American Journal of Roentgenology*. 2013;201(5):761-4. DOI:10.2214/AJR.12.10081.
3. Pulanic TK, et al. Vaginal Pessary for Uterine Repositioning during High-Intensity Focused Ultrasound Ablation of Uterine Leiomyomas. *Gynecologic and Obstetric Investigation*. 2016;81(3):285-8., DOI:10.1159/000441782.
4. Kim YS, et al. Magnetic Resonance Imaging-Guided High-Intensity Focused Ultrasound Ablation of Uterine Fibroids: Effect of Bowel Interposition on Procedure Feasibility and a Unique Bowel Displacement Technique. *Plos One*. 2016;11(5):0155670. DOI:10.1371/journal.pone.0155670.
5. Okada A, et al. Non-Invasive Magnetic Resonance-Guided Focused Ultrasound Treatment of Uterine Fibroids in a Large Japanese Population: Impact of the Learning Curve on Patient Outcome. *Ultrasound in Obstetrics and Gynecology*. 2009;34(5):579-583. DOI:10.1002/uog.7454.

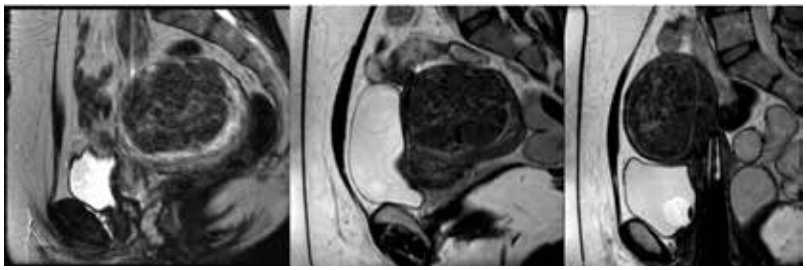

Figure 3.

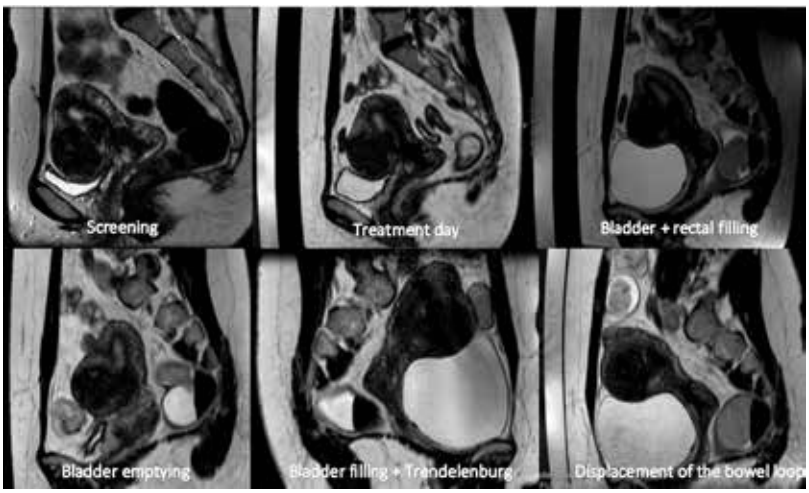

Figure 4.

P-WH-5

Topic: Women's Health
Presentation Type: Poster

Apparent diffusion coefficient as a biomarker to evaluate the uterine fibroid suitability for high-intensity focused ultrasound therapy

Teija Sainio[1], Jani Saunavaara[1], Kirsi Joronen[1], Visa Suomi[1], Roberto Blanco[2]

[1]Turku University Hospital, Turku, Finland
[2]Varsinais-suomen sairaanhoitopiirin, Turku, Finland

Background: High-intensity focused ultrasound (HIFU) therapy is a noninvasive treatment method that can be used to thermally ablate a variety of tumors, e.g., uterine fibroids. A drawback of HIFU therapy is that ablation feasibility of a particular fibroid cannot reliably be assessed before treatment, thus increasing the risk for suboptimal therapy outcome. While the Funaki classification (based on relative T2 signal intensity) is widely used, it only provides qualitative assessment of fibroid suitability for HIFU therapy. The purpose of this study is to assess apparent diffusion coefficient (ADC) as a biomarker to evaluate suitability of uterine fibroids for HIFU therapy.

Methods: 37 patients presenting 42 uterine fibroids who underwent the diffusion-weighted imaging (DWI) before HIFU treatment were enrolled in this study. All Funaki types were present in the analyzed fibroids. Treatment was performed using a clinical magnetic resonance imaging (MRI) -guided HIFU system (Sonalleve V2, Profound Medical Inc.) coupled with clinical 3T MRI scanner (Ingenia, Philips). The DW images were acquired with b-values of 0, 100, 400, 600, and 800 s/mm^2. ADC maps were reconstructed from the DW images for quantitative analysis with different combinations of b-values using commercial software (Philips). Regions of interest were drawn on ADC maps in three sequential slices covering the whole fibroid, and averaged quantitative ADC values were obtained. Treatment outcome was assessed from T1-weighted contrast-enhanced (CE) images as non-enhancing regions also known as non-perfused volume (NPV). The NPV and uterine fibroid volumes were calculated from CE and T2W images, respectively, using image analysis software (AW-server 3.2, GE Healthcare). Finally, the NPV ratio, recognized as a good predictor of HIFU clinical outcome, was calculated as NPV/fibroid volume.

Results: Higher ADC value prior to treatment correlated with a lower NPV ratio, i.e., poorer clinical outcome: regression analysis showed statistically significant negative correlation (Pearson's r = - 0.63, p-value <0.0001) between ADC values and therapy outcome (Figure 1). ADC mapping could provide a more reliable, quantitative method to evaluate uterine fibroid suitability for HIFU, as compared to the qualitative Funaki classification method.

Conclusions: ADC is a promising biomarker to evaluate the suitability of uterine fibroids for HIFU therapy, and to potentially establish new inclusion/exclusion criteria. DWI and ADC maps could be added to the MRI screening protocol to provide consistent, quantitative assessment of uterine fibroid suitability for HIFU therapy.

Funding sources: This work was supported by Finnish Cultural Foundation, Varsinais-Suomi Regional fund.

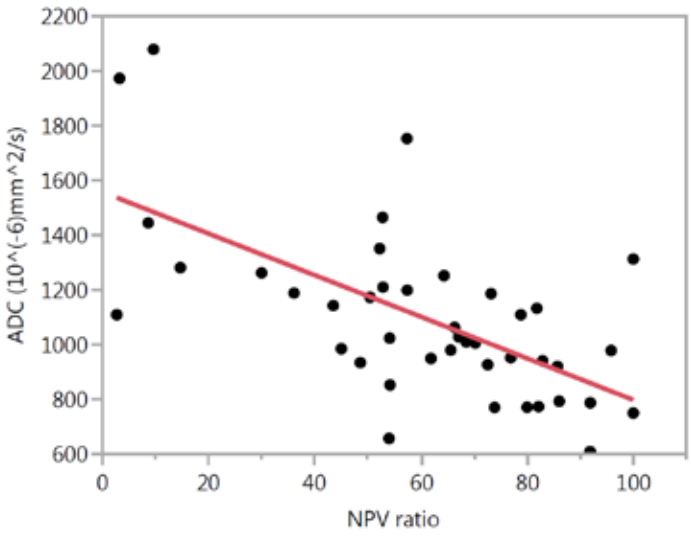

Figure 1. ADC values before HIFU therapy of 42 uterine fibroids as function of NPV ratio with linear fit (Pearson's r = -0.63, p-value < 0.0001).

P-WH-6

Topic: Women's Health
Presentation Type: Poster

Preclinical HIFU treatment of human breast tissues recovered from mastectomies using a toroidal transducer

Marine Sanchez[1], Victor Barrere[1], Nicolas Chopin[2], David Melodelima[1]

[1]LabTAU, Inserm U1032, Lyon, France
[2]Centre Léon Berard, Lyon, France

Background: Breast cancer affects one in eight women. Breast-conserving surgery is the standard early-stage therapeutic approach. Lesser invasive treatments (like radiofrequency and laser) have shown promising results with reduced morbidity, psychological trauma and hospital stay. HIFU is one of the most attractive technology due to its non-invasiveness. We recently developed a toroidal HIFU transducers to treat liver metastases that enable fast and large volume treatments. We report here the first use of a completely non-invasive treatment of breast human tissues using a toroidal HIFU device.

Methods: The toroidal HIFU transducer was divided into 32 concentric rings of equal surface (78mm^2). The diameter of the transducer and its radius of curvature were 70 mm. The operating frequency was 2.5 MHz. A 7.5 MHz ultrasound imaging probe was placed in the center of the HIFU device. Due to the geometrical characteristics of a torus, the ultrasound beams coming from each of the 32 emitters intersect between the principal focal ring and the transducer to form a secondary focal zone, which contributes to reinforce the size and homogeneity of the lesion.

Ablations in breast tissues were performed by placing the HIFU probe on the skin and using electronic beam steering to place the lesion at 15 mm under the skin. Trials were conducted in 23 human samples of normal breast tissue recovered from mastectomies. The free-field acoustic power varied from 100 to 140 watts and was applied for durations ranging from 45 to 180 seconds. Attenuation measurements were performed in the frequency range of 2 to 4 MHz, using the pulse-echo method, before and after HIFU treatment.

Results: 10 HIFU lesions were created. The dimensions of the lesion had an average diameter of 22.5 ± 4.4 mm while preserving skin integrity. The average distance between the skin and the HIFU lesion was 15.1 mm. Necrosis of the treated zone was histologically confirmed. The attenuation coefficient was higher in HIFU-treated breast tissues (0.27 ± 0.08 Np.cm-1.MHz-1) than in the untreated tissues (0.16 ± 0.09 Np.cm-1.MHz-1).

Conclusions: These results suggest that it should be possible to ablate a breast tumor of 10-15 mm in diameter with safety margins using a fully non-invasive HIFU exposure performed by this toroidal transducer. These results highlight the creation of large ablation zones in a short time without the need of mechanically juxtaposing several lesions or the need to displace the HIFU device.

These preliminary study supports the translation of the toroidal HIFU transducer to a Phase I – II clinical trials of breast cancer treatment.

Take home message: Our project consisted in developing a preclinical HIFU treatment of human breast tissues recovered from mastectomies using a toroidal transducer. Our results show the creation of large ablation zones in a short time without the need of mechanically juxtaposing several lesions or the need to displace the HIFU device.

Acknowledgements: Financial support was partly received from EDAP TMS France (N°09757A40) and the LyriCAN (INCa_INSERM_DGOS_12563).

P-WH-8

Topic: Women's Health
Presentation Type: Poster

The effect of transducer orientation on the efficacy of high-intensity focused ultrasound treatment of uterine fibroids

Visa Suomi[1], Bradley Treeby[2], Jiri Jaros[3], Antti Viitala[1], Teija Sainio[1], Gaber Komar[1], Roberto Blanco[4]

[1]Turku University Hospital, Turku, Finland
[2]University College, London, United Kingdom
[3]Brno University of Technology, Brno, Czech Republic
[4]Varsinais-suomen sairaanhoitopiirin kuntayhtyma, Turku, Finland

Background: High-intensity focused ultrasound (HIFU) therapy is a non-invasive treatment method which can be used to treat uterine fibroids (i.e., myomas). The clinical treatment of patients with uterine fibroids using HIFU therapy is nowadays a standard practice, but the outcome of the treatment is sometimes unsuccessful due to the diminished heating efficacy in the target region. The lower heating effect in some patients can be attributed to several factors such as the local perfusion rate, the location and depth of the myoma, and the attenuation of ultrasound energy. Furthermore, in some cases, the transducer has to be positioned at an angle in order to avoid intervening tissue structures or to reach deep-laying targets. All of these effects reduce the heating efficacy resulting in a poor response to the HIFU treatment. The aim of this study is therefore to investigate how the positioning of the transducer affect the ultrasound focal point and the treatment efficacy.

Methods: Three-dimensional ultrasound simulations were conducted on a clinical patient image data acquired during a clinical HIFU treatment at the Turku University Hospital, Finland. The image data were segmented into water/bladder, fat, muscle and uterine fibroid tissues. The simulations were conducted on a clinical HIFU system (Sonalleve V2, Philips, Vantaa, Finland) by rotating the transducer at different angles around the left-right axis between 0 and -20 degrees relative to the target location inside the myoma. Focal point deformation, maximum pressure values and focal shifts in axial, lateral and elevation directions were characterised and the results were then compared to the actual treatment outcome of the same patient.

Results: Changing the transducer rotation angle between 0 and -20 degrees did not have a large effect on the focal point shape where nearly ellipsoidal -6 dB focal region of the same size was observed in all the cases (see Fig. 1). Similarly, the maximum pressures inside the focal points did not change considerably with the average maximum pressure of 2.07 MPa and a standard deviation of ±0.06 MPa (see Fig. 2). The effect of rotation angle on the focal shift was more pronounced (see Fig. 3). In the axial, lateral and elevation directions average focal shifts of -2.2 ± 1.3 mm, 0.5 ± 0.2 mm and -1.0 ± 0.2 mm were observed, respectively. When compared to the clinical treatment outcome, the changes in the ultrasound focal point did not seem to be the major cause for the experienced poor heating efficacy, but other factors, such as local perfusion and attenuation, likely play a more significant role in this case.

Conclusions: Changing the orientation of the transducer during a uterine fibroid HIFU treatment did not result in a significant loss of acoustic efficacy in terms of the ultrasound focal parameters. Only a slight axial shift might be encountered when using extreme rotation angles during the treatment. However, these results might differ when using another patient data, which still requires further research.

Figure 1. The -6 dB ultrasound focal points with different transducer rotation angles (-20 blue, -15 green, -10 red, -5 yellow, 0 magenta)

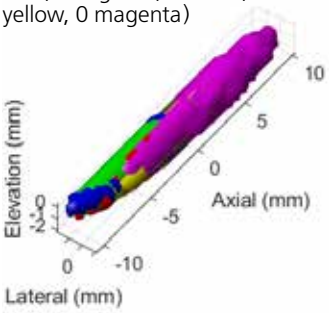

Figure 2. Maximum pressure values with respect to the transducer rotation angle

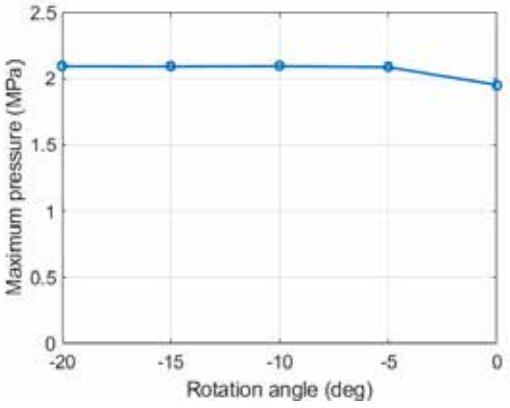

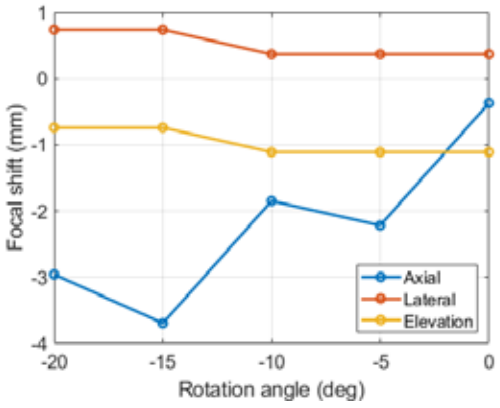

Figure 3. Focal shifts with respect to the transducer rotation angle

P-WH-9

Topic: Women's Health
Presentation Type: Poster

The preliminary value of combination with DCE-MRI quantitative parameters and diffusion-weighted imaging in MR-guided high intensity focused ultrasound (MRgHIFU) ablation's immediate effect for uterine fibroids

Juan Wang, Shou-guo Zhou, Yao-qu Huang

Guangzhou University of Chinese Medicine, Foshan, China

Background: To evaluate the immediate value of combination with dynamic contrast-enhanced MRI(DCE-MRI) quantitative parameters and diffusion-weighted imaging(DWI) after MRgHIFU treatment of uterine fibroids.

Methods: Thirty-six patients with 54 uterine fibroids were scanned with DCE-MRI and DWI before and after MRgHIFU ablation. The correlation between the quantitative parameters and the non-perfused volume ratio (NPVR) was evaluated. According to the Ktrans value of myometrium, these uterine fibroids were divided into complete and non-complete Ktrans group, respectively. Statistical analysis was carried out in Ktrans value and NPVR of uterine fibroids between complete and non-complete Ktrans groups. Compared the changes of the routine MRI and DWI before and after MRgHIFU ablation.

Results: In the quantitative parameters of uterine fibroids, only the Ktrans value was statistically correlated with the NPVR ($r = -0.384$, $P<0.01$). Significant difference of NPVR and Ktrans value was found between complete and non-complete Ktrans group (all $P<0.01$). The mean ADC value of uterine fibroids before MRgHIFU ablation was $1.97 \times 10\text{-}3\ mm^2/s$, and decreased to $1.64 \times 10\text{-}3 mm^2/s$ after MRgHIFU ablation, and the difference was significant.

Conclusions: DCE-MRI quantitative parameters and DWI have reference value in MRgHIFU treatment's immediate effect evaluations for uterine fibroids.

P-WH-10

Topic: Women's Health
Presentation Type: Poster

Uterine fibroids with homogeneous hyperintense on T2-weighted magnetic resonance imaging: The efficacy of gonadotrophin releasing hormone agonist therapy (cases report)

Huang Yaoqu

China

Background: Uterine fibroids with homogeneous hyperintense on T2-weighted MR imaging may have particularly pathologic structure that consisted of more cell components or blood flow and less collagens than other types of fibroids, many researchers agreed that it might not be an indication of magnetic resonance guided focused ultrasound(MRgFUS). Gonadotrophin releasing hormone (GnRH) agonist has been proven to reduce the size of uterine fibroids and reduce their blood supply. The purpose of this study was to determine that weather pretreatment of leiomyomata with GnRH agonists could change its signal, increasing the number of women who could benefit from this noninvasive technique.

Methods: Three patients with uterine fibroids were enrolled,including 3 lesions. The inclusion criteria of lesion was with a high signal range of leiomyomata of ¡Ý70% and a fibroid/muscle signal ratio of ¡Ý2 on T2-weighted MR imaging before treatment. These women received a 2-month course of GnRH agonist. On T2WI sagittal images, we analyzed the following indicators: uterine volume, fibroid volume, high signal range, fibroid/muscle signal ratio. The pre-treatment data were used as baseline to analyze the changes in the above indicators before and after treatment.

Results: In Case 1, the volume of uterine decreased by 78.5% after 2 months of treatment, the volume of fibroid decreased by 64.5%, the high signal range decreased by 6.5%, and the fibroid/muscle signal ratio decreased by 3.0%. Case 2, the uterine volume was reduced by 58%, the fibroid volume was reduced by 50.3%, the range of high signal increased by 3.2%, and the fibroid / muscle ratio increased by 13.2%. Case 3, the volume was reduced 30.0% for uterine and 31.3% for fibroid after 2-months treatment, and the high signal range was decreased 5.7%, the ratio of fibroid / muscle decreased 2.2%.

Conclusions: For uterine fibroids with homogeneous hyperintense on T2WI, the use of GnRH agonist therapy could significantly decrease both uterine volume and fibroid size. However, the hyperintensity characteristics of fibroids after GnRH agonist treatment were not significantly changed, suggesting that even with GnRH agonist pretreatment, fibroids with homogeneous hyperintense may still not be suitable for the preferred MRgFUS treatment. But this view needs more cases to be confirmed.

Acknowledgements: Guangdong Provincial Medical Research Fund

P-WH-11

Topic: Women's Health
Presentation Type: Poster

A camera-based in-vivo focused-ultrasound switchable fluorescence imaging

Shuai, Yu, Tingfeng Yao, Yang Liu, Baohong Yuan

The University of Texas at Arlington, Arlington, Texas, United States

Background: Ultrasound-switchable fluorescence (USF) imaging is a novel technique which provides high-resolution fluorescence imaging in centimeter-deep tissue. In this study, we showed *in vivo* USF imaging in live mice, using a camera-based USF imaging system. Also, micro-CT imaging was conducted to validate the USF imaging results.

Methods: BALB/cJ mice (female) were used in this study. Indocyanine green (ICG)-encapsulated poly(N-isopropylacrylamide) (PNIPAM) nanoparticles (ICG-NPs, Tth = ~37 °C) was adopted as USF contrast agents and ExiTron nano 12000 as the CT contrast agent. An aqueous mixture of ICG-NPs and ExiTron nano 12000 agents (total volume = 20 uL, volume ratio: ICG-NPs/ ExiTron nano 12000 = 3:1) was intramuscularly-injected on the left hind leg. The animal was placed on the USF imaging system. The excitation light was from a diode laser (785 nm, 2 Watts). The emitted fluorescence was filtered by a set of long-pass interference filters (edge wavelength: 846 nm) and captured by the camera on the top. A high intensity focused ultrasound (HIFU) transducer (central frequency: 2.5 MHz) was submerged in water and placed right below the animal. It was controlled by a function generator and a power amplifier to send ultrasound pulses to the subject. Also, it was mounted on a motorized 3-dimensional (3D) translation stage for mechanical scanning. Meanwhile, the camera was synchronized with the ultrasound signal, for purpose of capturing USF signals. The 3D USF imaging result was compared with that of 3D micro-CT imaging.

Results: By raster scanning of the HIFU transducer and acquiring USF signals at each scan point, a 3D USF image was acquired. The total scan area is 9.144 × 8.128 × 3.048 mm^3. The lateral step size is 1.016 mm and the axial step size is 1.524 mm. Figure 1 (a) shows the 2-dimensional (2D) background fluorescence image of around the injected area acquired via the camera. The yellow dash square indicates the USF scanning area on the horizontal plane. Figure 1(b) shows the 3D micro-CT image, and the red dash square corresponds to the same USF scan area. Figure 1 (c) shows one of the 2D USF image slices and Figure 1 (d) shows the 3D USF image in the entire scanning volume. In both Figure (c) and (d) the signal intensities are normalized and interpolated. In Figure (d), a threshold of 0.5 is applied for viewing the distribution of USF signals. Comparing Figure 1 (a) and (b), it indicates the ICG-NPs and ExiTron nano 12000 are likely to stay together. The 3D micro-CT image (Figure (b)) and 3D USF image (Figure (d)) show similar distribution and the *in vivo* USF imaging is validated. A quantitative comparison will be presented during the conference.

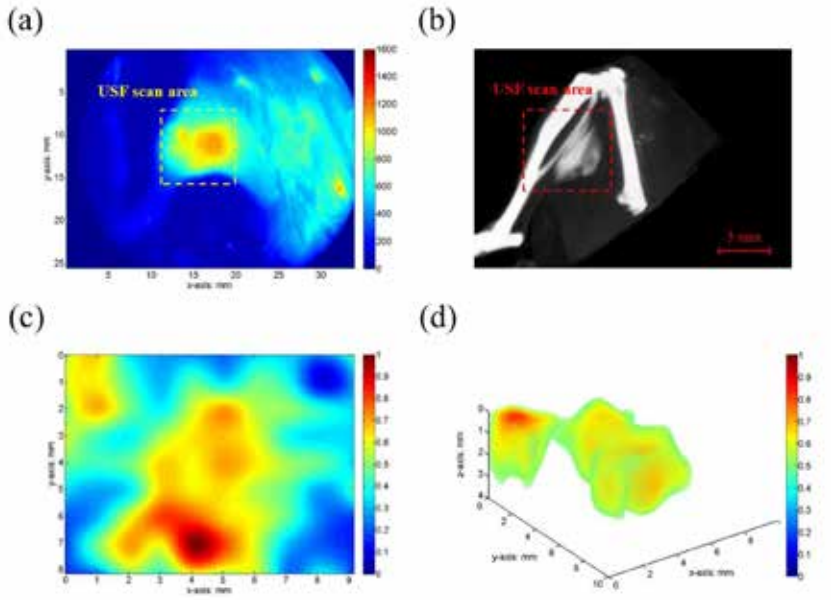

Figure 1 | (a) 2D background fluorescence image of left hind leg in a mouse. The yellow dash square represents the USF scanning area on the horizontal plane. (b) 3D micro-CT image of the same area. The red dash square represents the same scanning area. (c) One of 2D USF image slices of the same scan area. (d) 3D USF image of the entire scanning volume.

Conclusions: This work demonstrated that *in vivo* 3D USF imaging was achieved using a camera-based USF imaging system, and the result was validated by micro-CT imaging. This work shows *in vivo* feasibility of USF imaging.

Acknowledgements/Funding Sources: Supported in part by funding from the CPRIT RP170564 (Yuan) and the NSF CBET-1253199 (Yuan).

P-WH-12

Topic: Women's Health
Presentation Type: Poster

Magnetic resonance-high intensity focused ultrasound (MR-HIFU) treatment of symptomatic uterine fibroids: A systematic review and meta-analysis

Inez Verpalen[1], Kimberley Anneveldt[1], Ingrid Nijholt[1], Mireille Edens[1], Martijn Boomsma[2]

[1]Isala, Zwolle, Netherlands
[2]Stichting Isala Klinieken, Zwolle, Netherlands

Background: MR-HIFU is the only non-invasive treatment option for women with symptomatic uterine fibroids. MR-HIFU was shown to be effective in relieving symptoms at short-term follow-up. However, studies with prolonged follow-up reported a relatively high re-intervention rate.[1,2] These high re-intervention rates may be explained by the initial use of restrictive treatment protocols for safety measures which are no longer in clinical use. Nowadays, treatment protocols aim for complete ablation. Therefore, the effectiveness of MR-HIFU therapy needed re-evaluation.

In our systematic review we assessed the effectiveness of MR-HIFU focusing only on studies which used treatment protocols that aim for complete ablation.

Materials and **Methods:** The National Guideline Clearinghouse, The Cochrane Library, TRIP, PubMed/MEDLINE, EMBASE and the WHO International Clinical Trials Registry Platform databases were searched. Randomized controlled trials (RCT's), first phases of cross-over trials and prospective or retrospective non-randomized studies were evaluated for inclusion. We did not include case reports, study protocols or ongoing trials in this review. Guidelines, systematic reviews, meta-analyses and narrative reviews were consulted, but only the original articles were used. Studies with ultrasound guided devices or a follow-up of less than three months were excluded. We also eliminated studies with treatment protocols not aiming for complete ablation. Only studies that reported the Non Perfused Volume (NPV) ratio[3] and our primary outcome, the transformed symptom severity score (tSSS) assessed by the uterine fibroid symptom and health related quality of life questionnaire (UFS-QoL)[4] were included. We stratified outcomes by device, the use of mitigation and duration of follow-up.

Results: A total of 19 articles (1409 patients) met our inclusion criteria (figure 1). The mean NPV ratio directly post MR-HIFU was above 50% (figure 2), indicating successful treatment.[5] Stratification by mitigation suggested that mitigation strategies may lead to higher NPV ratios. All studies reported symptom reduction (figure 3) and fibroid shrinkage after treatment (figure 4). Stratification by system insinuated a difference in fibroid shrinkage between the INSIGHTEC, Sonalleve and Chongquing system (figure 4). Although the number of adverse events was very low, stratification of adverse events by system also resulted in a significant association with Sonalleve and INSIGHTEC. Unfortunately, we were unable to determine the long-term reinvention rate, because of the lack of sufficient data. Short-term and mid-term re-intervention rates showed that the effect of time was associated with a higher risk of further interventions, whereas re-intervention rates were not associated with NPV ratio or baseline symptom severity. The reported re-intervention rates are comparable to other uterine-sparing treatment options such as uterine artery embolization and myomectomy.[6]

Conclusions: MR-HIFU treatment of uterine fibroids is a safe treatment option and is shown to be effective until a follow-up of at least 12 months. Further studies should evaluate long-term efficacy and reproductive outcomes. Moreover, controlled trials are necessary to directly compare the effectiveness of MR-HIFU to other uterine sparing treatment options.

Figure 1. Selection process

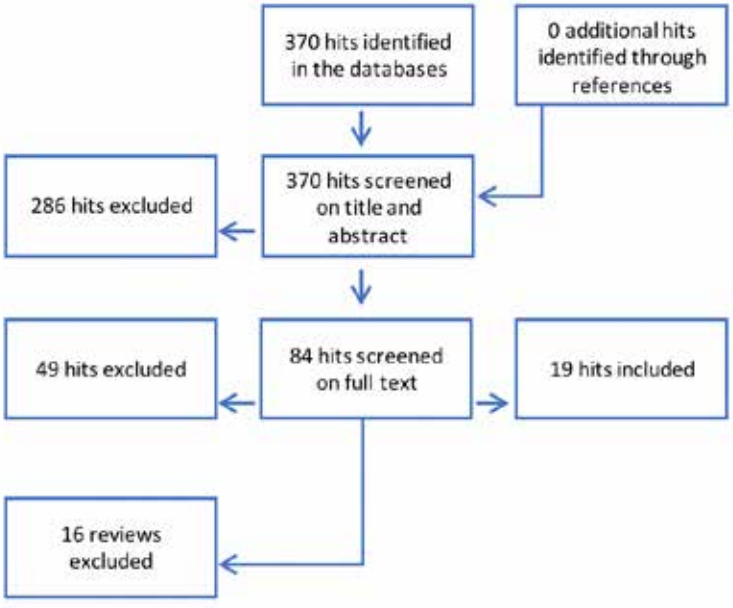

References:
1. Froeling V, Meckelburg K, Schreiter NF, Scheurig-Muenkler C, Kamp J, Maurer MH, et al. Outcome of uterine artery embolization *versus* MR-guided high-intensity focused ultrasound treatment for uterine fibroids: Long-term results. *Eur J Radiol.* 2013;82(12):2265-2269.
2. Kim HSM, Baik JM, Pham LDM, Jacobs MAP. MR-guided High-intensity Focused Ultrasound Treatment for Symptomatic Uterine Leiomyomata: Long-term Outcomes. *Acad Radiol* 2011;18(8):970-976.
3. LeBlang SD, Hoctor K, Steinberg FL. Leiomyoma shrinkage after MRI-guided focused ultrasound treatment: report of 80 patients. *American Journal of Roentgenology.* 2010;194(1):274-80.
4. Spies JB, Coyne K, Guaou Guaou N, Boyle D, Skyrnarz-Murphy K, Gonzalves SM. The UFS-QOL, a new disease-specific symptom and health-related quality of life questionnaire for leiomyomata. *Obstet Gynecol.* 2002;99(2):290-300.
5. Dobrotwir Andrew A. Clinical 24 month experience of the first MRgFUS unit for treatment of uterine fibroids in Australia. *Journal of Medical Imaging and Radiation Oncology.* 2012 -8;56(4):409-16.
6. Gupta JK, Sinha A, Lumsden MA, Hickey M. Uterine artery embolization for symptomatic uterine fibroids. *The Cochrane Database of Systematic Reviews.* 2014(12):CD005073.

Figure 2. Forest plot of NPV percentage directly post MR-HIFU

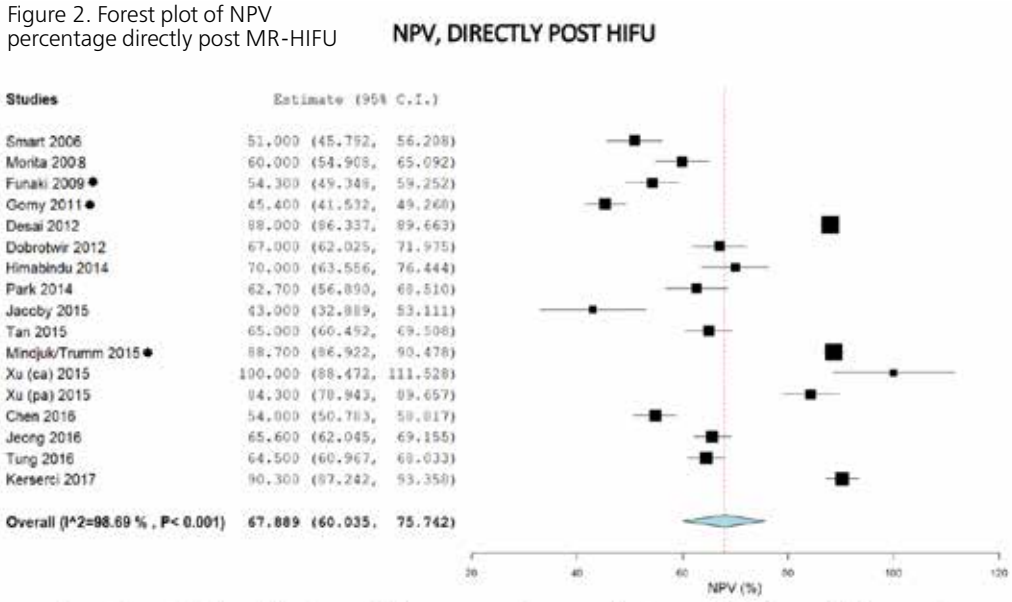

●studies with multiple publications of the same patient populations with different follow-up time.

Figure 3. Forest plots of tSSS decrease percentage, stratified by follow-up category

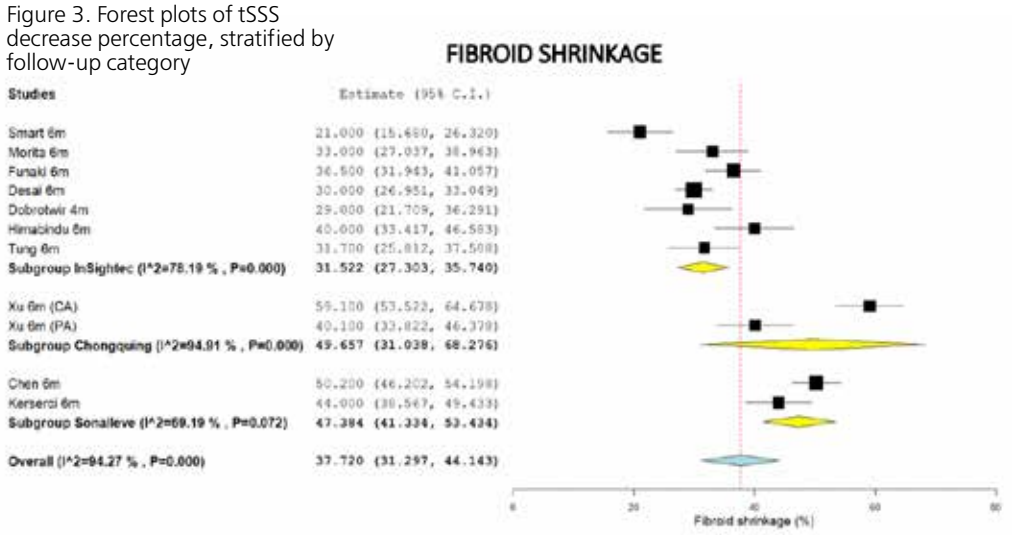

Figure 4. Forest plots of fibroid shrinkage at six months follow-up, stratified by system

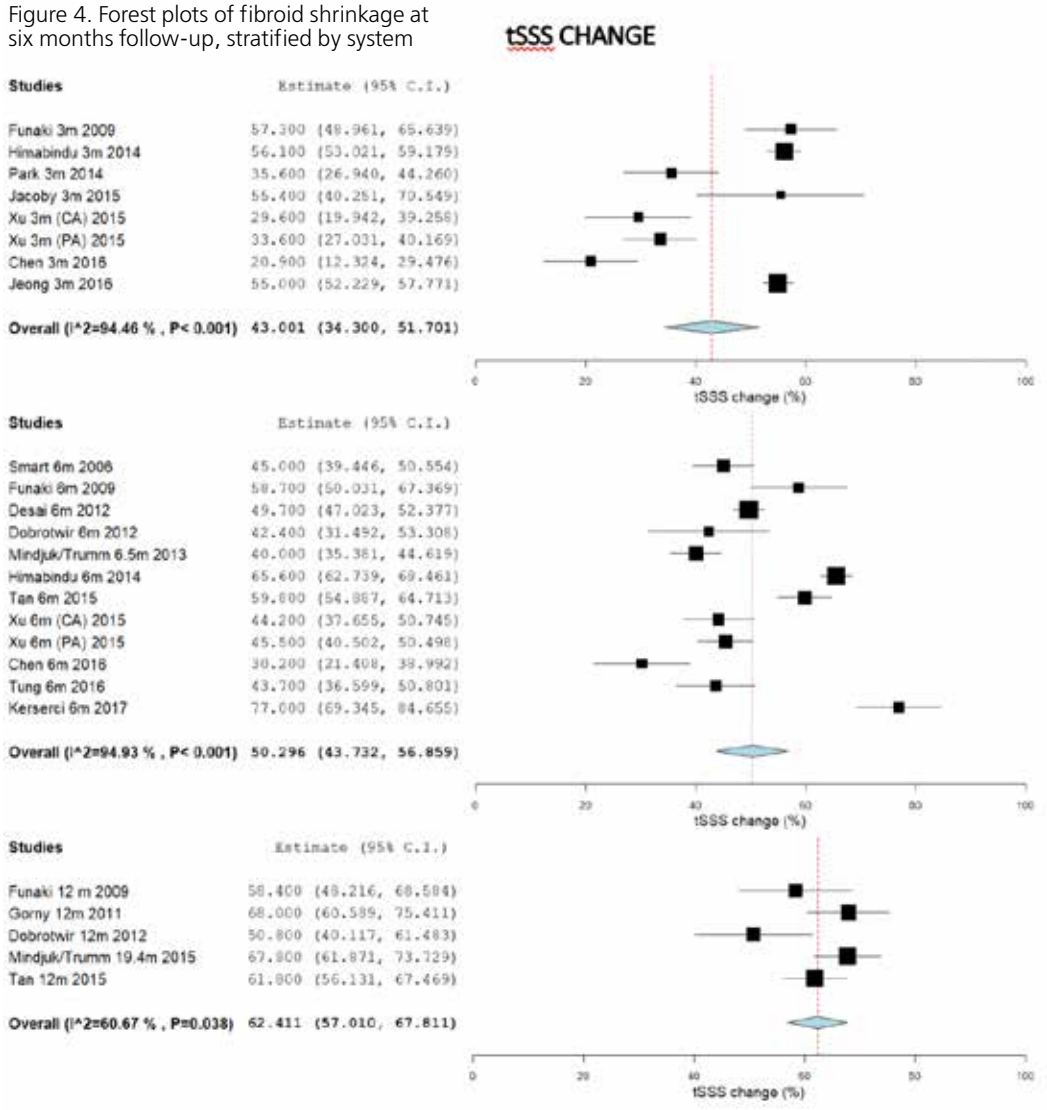

P-WH-13

Topic: Women's Health
Presentation Type: Poster

Multiparametric MRI sequences have the potential of a new screening tool for MR-HIFU treatment in treatment of uterine fibroids

Inez Verpalen[1], Kimberley Anneveldt[1], Mireille Edens[1], Pieter Vos[2], Edwin Heijman[3], Jeroen Dijkstra[1], Joke Schutte[1], Martijn Boomsma[4]

[1]Isala, Zwolle, Netherlands
[2]Philips, Eindhoven, Netherlands
[3]Philips Research Germany, Cologne, Germany
[4]Stichting Isala Klinieken, Zwolle, Netherlands

Background: Uterine fibroids are the most common gynaecological benign tumours affecting a high percentage of women. Currently, the Funaki classification[1] is the most used screening tool for Magnetic Resonance-High Intensity Focused ultrasound (MR-HIFU) therapy, but is limited in characterizing uterine fibroids because of its heterogeneity. To refine characterisation of uterine fibroids, more biological information is needed on tissue level. Advanced multi-parametric MRI sequences might be used as non-invasive biomarkers. Therefore, in this study we want to investigate a multi-parametric MRI-protocol for characterization of uterine fibroids and compare these results with the Funaki classification and symptom severity.

Methods: This prospective single-centre explorative research was conducted at the Isala Hospital Zwolle, The Netherlands. Clinical symptoms were examined by the uterine fibroid symptom and health related quality of life questionnaire (UFS-QoL).[2] MR-scans were performed on a clinical 1.5-T MRI system (Achieva; Philips Healthcare, Best, the Netherlands). The multi-parametric MRI-sequence set contained quantitative T2-mapping and diffusion weighted imaging (DWI) sequences. Data were analysed using IntelliSpace Portal software (Philips). In order to analyse MRI-parameters of the uterine fibroids, Regions-Of-Interest (ROIs) were manually drawn in T2 weighted images. A comparison was made between fibroid and myometrium for the different mean MRI-parameters, T2, ADC by different b-values and mean signal of DWI with long echo time. Statistical analyses were performed using the IBM SPSS version 24 and the statistical software package R, version 3.4.2, The R Foundation for Statistical Computing.[3] The Spearman's rank correlation or Wilcoxon Signed Rank Test were calculated for statistical testing the different relationships. Correlations were determined for the different Funaki classes for the mean T2 fibroid, mean ADC fibroid (all b-values) and Scaled Signal Intensity (SSI).[4] The different UFS-QoL scores were also correlated to the different parameters.

Results: 87 patients, their characteristics are described in table 1, were imaged and analysed. The Funaki distribution is shown in figure 1. Table 2 shows the differences in values between fibroid tissue and myometrium. Only the ADC with low b-values did not show a significant difference between fibroid and myometrium. A significant correlation was found between Funaki and the SSI score ($p<0{,}001$), although we found a large overlap between the SSI values for Funaki 1 and Funaki 2. Only correlation was found between SSI and mean T2 fibroid (see figure 2). No or weak correlations were found between the UFS-QoL and the fibroid characteristics.

Conclusions: The implemented MRI-screening protocol was able to show variation between fibroids and myometrium. No good separation was found in the different MR parameters between the Funaki class 1 and 2, although expected for the mean T2 fibroid. Further cluster analysis should reveal if a more objective way can be found to separate Funaki classes 1 and 2, to refine characterisation of uterine fibroids.

References:

1. Funaki K, Fukunishi H, Funaki T, Sawada K, Kaji Y, Maruo T. Magnetic resonance-guided focused ultrasound surgery for uterine fibroids: relationship between the therapeutic effects and signal intensity of preexisting t2-weighted magnetic resonance images. *American Journal of Obstetrics and Gynecology.* 2007;196(2):184.
2. Spies JB, Coyne K, Guaou Guaou N, Boyle D, Skyrnarz-Murphy K, Gonzalves SM. The UFS-QOL, a new disease-specific symptom and health-related quality of life questionnaire for leiomyomata. *Obstet Gynecol.* 2002;99(2):290-300.
3. R Core Team. R: A language and environment for statistical computing. R Foundation for Statistical Computing, Vienna, Austria. 2017. URL https://www.R-project.org/.

4. Kang SH, Lee SJ, Jeon GS, Yoon S-W. Scaled signal intensity of uterine fibroids on T2-Weighted MR imaging as a predictor of the potential response to uterine fibroid embolization. *Journal of Vascular and Interventional Radiology*. 2017;28(6):844–849.

Table 1

Patient characteristics:	Average/±SD (N %)
Age (years)	46 / ±5,4
tSSS	49 / ±20,9
Number of myomas:	
1	36 (41,4%)
2	14 (16,1%)
3	15 (17,2%)
4	4 (4,6%)
≥ 5	18 (20,7%)
Maximal diameter (mm)	63 / ± 0,9
Total volume (mL)	171 / ±182,0
Funaki classification:	
I	24 (27,6%)
II	46 (52,9%)
III	17 (19,5%)
Myoma classification:	
1	2 (2,3%)
2	6 (6,9%)
3	9 (10,3%)
4	33 (37,9%)
5	23 (26,4%)
6	13 (14,9%)
7	1 (1,1%)
Myoma location:	
Anterior	19 (21,8%)
Cervix	3 (3,4%)
Fundus	21 (24,1%)
Posterior	23 (26,4%)
Side wall	21 (24,1%)

Figure 1. Patient distribution over the 3 Funaki classes

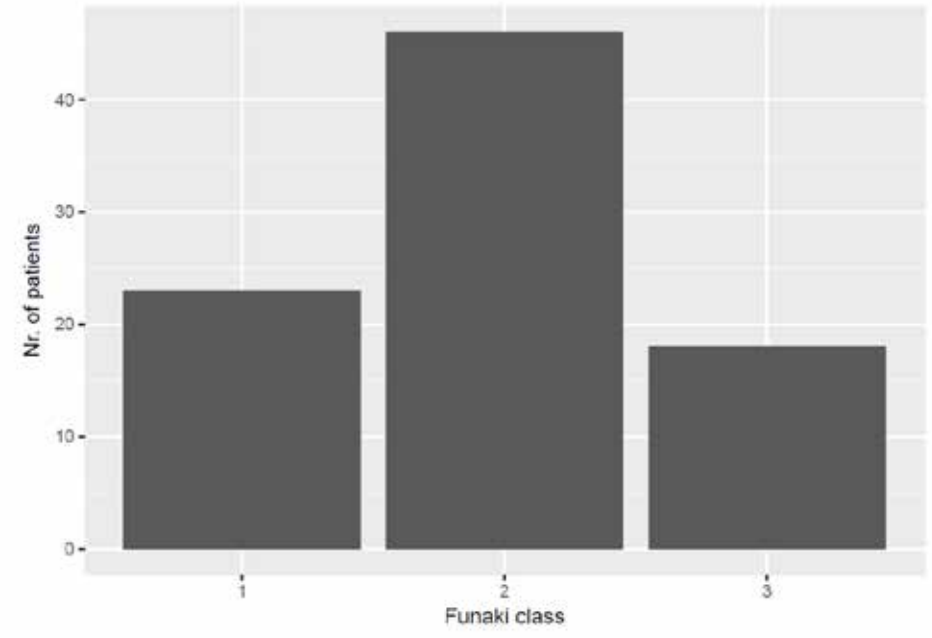

Table 2. Average signal intensity (SI) uterine fibroid tissue and myometrium tissue

	SI uterine fibroid tissue (SD)	Coefficient of Variation (CV)	Range (min-max)	SI myometrium (SD)	P-value
T2-relaxometry	73,187 (17,2252)	23,5%	38,8-117,5	79,497 (13,5529)	,004
ADC with all b-values(mm^2/s)	1,286 (1,9288)	15%	0,93-1,97	1,438(2,2462)	,000
ADC with low b-values(mm^2/s)	3,176 (0,8367)	26,3%	0,6-5,4	3,391 (1,0121)	,110
ADC with high b-values(mm^2/s)	1,007 (0,1784)	17,7%	0,7-1,8	1,121 (0,2052)	,000*
DWI with long TE(mm^2/s)	2,491 (0,6606)	26,5%	0,5-3,8	2,876 (0,9252)	,002

**Calculated using the Wilcoxon Signed Rank Test*

Figure 2. Pair plots of the different Funaki classes and T2,mean, mean ADC, both in fibroid, and SSI

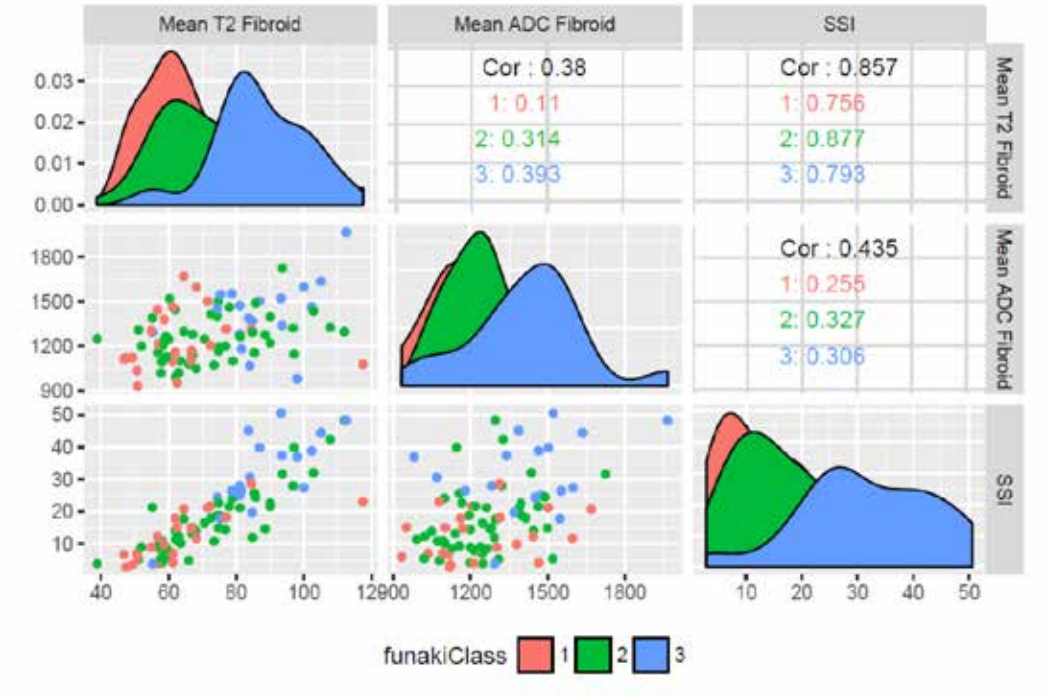

P-YI-1 through P-YI-12

Topic: Young Investigator
Presentation Type: Poster

The following posters also were presented orally:

Poster	Oral presentation	Abstract page
P-YI-1	YI-1	189
P-YI-2	YI-2	190
P-YI-3	YI-3	191
P-YI-4	YI-4	193
P-YI-5	YI-5	195
P-YI-6	YI-6	196
P-YI-7	YI-7	197
P-YI-8	YI-8	198
P-YI-9	YI-9	200
P-YI-10	YI-10	202
P-YI-11	YI-11	204
P-YI-12	YI-12	206

The abstract for P-YI-13 is published on page 318.

P-YI-13

Topic: Young Investigator
Presentation Type: Poster

Detecting T1-based signal reduction in focused ultrasound heating of bone using a 3D spiral ultra-short echo time sequence

Yekaterina Gilbo[1], Helen Sporkin[1], Samuel Fielden[1], John Mugler[1], G. Wilson Miller[1], Steven Allen[1], Joseph Pfeuffer[2], Berthold Kiefer[2], Craig Meyer[3]

[1]University of Virginia, Charlottesville, Virginia, United States
[2]Siemens Healthcare, Erlangen, Germany
[3]University of Utah, Salt Lake City, Utah

Background: MR-guided Focused Ultrasound (MRgFUS) is used transcranially to ablate brain tissue for the treatment of essential tremor. Despite evidence of skull damage,[7] there is no direct monitoring of heating in bone. We demonstrate a rapid volumetric thermometry method using a T1-weighted 3D Spiral Ultra-short Echo Time sequence in focused ultrasound heated bone.

Methods: A fiberoptic thermocouple was placed in bovine femur cortical bone (Fig. 1). The bone was placed on an ultrasound transparent film above a water bath of a small animal transducer (FUS Instruments Inc.) (Fig. 1c). Imaging was performed using a prototype spiral UTE pulse sequence (Fig. 2)[4] on a 1.5 T scanner and a 3T scanner (Siemens). The bone was ablated with a 45W continuous sonication six times for 135 seconds. Imaging parameters were: flip angle = 44°, matrix 96x96x16, slice thickness = 3 mm, TR = 11 ms, TE = 50 μs, and 203 linear variable density spiral interleaves.

Results: In 1.5T, a linear reduction of signal with increasing temperature was observed in both cortical bone and in marrow from 27.4-60.2 °C (Fig. 3). The mean signal difference of cortical bone (relative to 60.2 °C), analogous in composition to a patient's skull, decreased by 1.39% per °C with a strong correlation (R^2 = 0.93) and substantial mean SNR (>20). The mean signal difference of marrow (analogous to marrow or fat in or near the skull) decreased by 3.63% per °C (R^2 = 0.98). This linear model supports the hypothesis that signal decrease (T1-weighted) can be approximated as linearly dependent on temperature over the range we investigated. However, mixed results were observed on the 3T (Fig. 4). To ensure a more controllable experiment, we will use the GE-INSIGHTEC clinical system and RTHawk to acquire data in clinical conditions.

Conclusions: The clinical rise of MRgFUS necessitates improvements in the accuracy of MR thermometry to address concerns of unintended dangerous heating.[2] 3D spiral UTE allows fast volumetric imaging between clinical transcranial sonications.[4] Our preliminary results at 1.5T show the possibility of whole-brain T1-based thermometry, which can increase treatment safety by enabling dose monitoring of the skull. Ultimately, we aim to validate the sequence for thermometry in patients to increase safety for many treatments, including for neuroglioma.

References

1. Han M. et al. *ISMRM*. 2014;22:0262.
2. Cohen-Inbar O. et al. *World Neurosurg*. 2016;91:661-665
3. Miller GW. *3rd International Symposium on Focused Ultrasound*. 2012:65-BN.
4. Fielden S. et al. *ISMRM*. 2015;233867.
5. Rieke, V. & Butts Pauly, K. *JMRI*. 2008;27:376–390.
6. Ramsay E. et al. *MRM*. 2015;74(4):1095-102.

Figure 1. Left: Fresh cortical cow bone probed by a thermocouple and ablated by ultrasound during imaging. Center: Coronal spiral UTE image of cow bone at 60.2 °C from a 3D acquisition with TE = 50 μs. 1c). Right: Experimental setup.

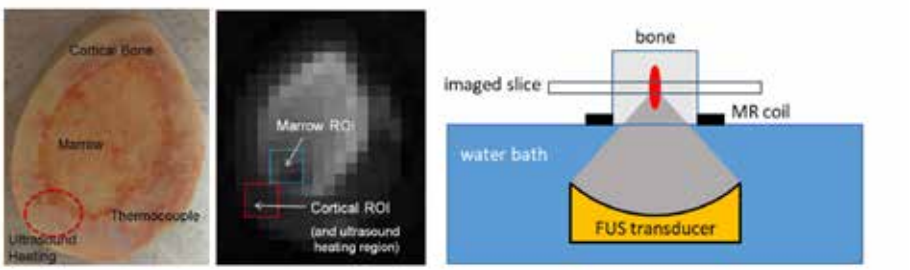

Figure 2. 3D spiral UTE pulse sequence. The shortest TE is acquired at the center of k space in the z direction, when the phase-encode lobe has zero area

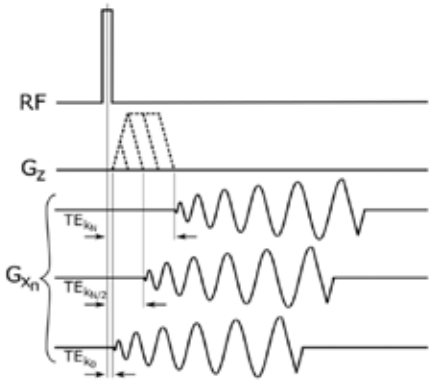

Figure 3. Mean signal difference of cortical and marrow bone from the hottest temperature (T = 60 °C). The signal decreases as temperature increases in both cortical bone (-1.39% per °C) and in marrow (-3.63% per °C).

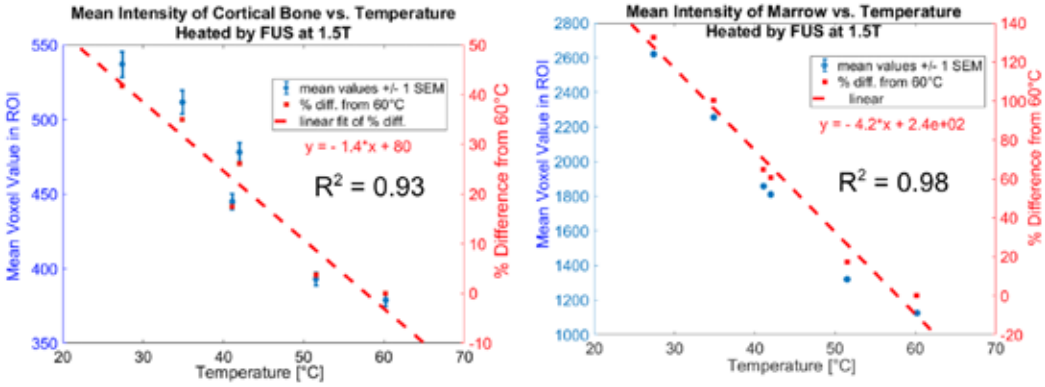

Figure 4. 3T Results with opposite (of expected) trend.

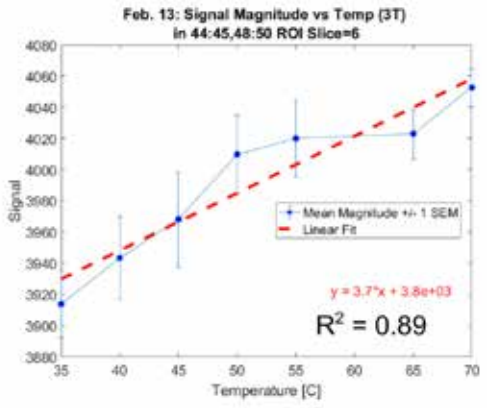

Notes

Awards

Ferenc Jolesz Memorial Award

Seung-Schik Yoo, PhD, MBA

Seung-Schik Yoo, PhD, MBA

The Ferenc Jolesz Memorial Award was established in 2016 to honor the life of a true pioneer in focused ultrasound. The award, supported by INSIGHTEC, has a two-fold purpose: to honor Ferenc's memory and to recognize and encourage this same innovative spirit in mid-career researchers and clinicians who continue to advance focused ultrasound.

We are honored to present the award to Seung-Schik Yoo, PhD, MBA.

Dr. Yoo is an associate professor of Radiology at Harvard Medical School and a director of the Neuromodulation and Tissue Engineering Laboratory (NTEL) at Brigham and Women's Hospital. He also serves as a faculty member of Mind Brain Behavior at Harvard University.

His early pioneering work involved developing real-time functional MR-imaging to interpret the human mind and applying the technology to interface the brain function with machines and computers. Dr. Yoo's current research is in exploring a new mode of noninvasive brain stimulation modality utilizing focused ultrasound to control regional neural functions, including the activity of the brain. He is primarily interested in advancing the technique for various neurotherapeutics, but also likes to seek out new ways to link thoughts/brain processes between individuals.

"On behalf of all the splendid researchers that I have worked with, I am deeply honored to receive the recognition," says Yoo. "I would like to thank the inspirations and encouragement that I have received from my mentors, Drs. Tempany, Panych, and Jolesz. I would like to express my gratitude to Drs. Seltzer and Boland who provided us with a vibrant research environment, and thank the Foundation and INSIGHTEC for the award."

Dr. Yoo will be acknowledged during the Sunday evening Welcome Reception. He will deliver a presentation on his research on Monday morning. He also receives up to $5,000 toward Symposium registration, travel and lodging expenses and a $5,000 award.

The Ferenc Jolesz Memorial Award is sponsored by INSIGHTEC

Ferenc Jolesz, MD

In Memoriam — Ferenc Jolesz, MD

Ferenc Jolesz, MD, was a world-class visionary whose passion for pushing surgery into the 21st century led from developing image-guided minimally invasive therapy to pioneering focused ultrasound as a completely noninvasive approach. He passed away suddenly in December 2014.

Dr. Jolesz helped create the world's first MR-guided focused ultrasound system, and an early device was installed at Brigham and Women's Hospital. Research was conducted for several years under his guidance, eventually leading to the FDA approval of a system to treat uterine fibroids and establishing the technology's potential to noninvasively treat a range of serious medical conditions. Dr. Jolesz spent the last few years of his life championing the use of focused ultrasound for the brain, and was especially interested in exploring treatents for Alzheimer's disease.

Awards (continued)

2018 Visionary Award

Narendra Sanghvi

Narendra Sanghvi

Established in 2014, the Visionary Award is given every two years at our Symposium to recognize an individual who has created a larger vision for what the future of focused ultrasound may hold and whose effort, passion, and persistence have been crucial to advancing the field.

We are honored to present the award to Narendra (Naren) Sanghvi.

A focused ultrasound technology pioneer and entrepreneur, Mr. Sanghvi began working with focused ultrasound in the Fry brothers' laboratory at Indiana University School of Medicine more than 45 years ago. Following several years of work on a system to treat brain disorders, he began the pursuit of treating the prostate with focused ultrasound and formed a company, Focus Surgery Inc., now a part of SonaCare Medical. Currently, Mr. Sanghvi is the Chief Scientific Officer at SonaCare; he is also the inventor and developer of the company's Sonablate® HIFU device, which has treated approximately 20,000 patients with prostate cancer at more than 120 clinical sites worldwide.

"Today, diagnostic ultrasound is a major medical imaging modality due to its noninvasiveness and high temporal and spatial resolutions," says Mr. Sanghvi. "Similarly, highly focused ultrasound has the same attributes to be a significant player for therapeutic applications. Receiving this award from the Focused Ultrasound Foundation is a surprise and very exciting. The Foundation has played an important role in integrating the interests of scientific, medical, and commercial entities in this field, and it continues to provide timely synergism to make these novel therapeutic applications a reality."

Mr. Sanghvi will be acknowledged during the Symposium's Welcome Reception on Sunday, 21 October 2018, where he will briefly share his journey in focused ultrasound and vision of the future.

Young Investigator Awards Program

The Focused Ultrasound Foundation established the Young Investigator Awards Program to encourage quality research by clinicians and scientists-in-training and to support their presentation of meritorious scientific papers at venues such as the 6th International Symposium on Focused Ultrasound.

Graduate students, research fellows, clinical fellows, and junior faculty members are eligible to apply for the awards, which include complimentary event registration and up to an additional $2,000 in reimbursement for travel and lodging expenses. One of the 2018 Young Investigator Awards is sponsored by Bracco Suisse SA.

Twelve Young Investigators are participating in the 6th International Symposium on Focused Ultrasound and being acknowledged in several ways:

Pre-Symposium Publicity: To emphasize the significance of the Young Investigator Awards, the Foundation announced this year's award recipients in our monthly e-newsletter.

Name Badges and Announcement: Award recipients have received unique name badges that indicate their status as Young Investigators.

Evening Poster Session and Young Investigator Spotlight: Young Investigators have a designated section of the poster room. On Tuesday, 23 October 2018, during the poster session and reception, they will have an opportunity to showcase and present their work to the larger focused ultrasound community.

2018 Young Investigator Awards

YI-7/P-YI-7

Abstract: page 197

Award sponsored by

BRACCO
LIFE FROM INSIDE

Pavlos Anastasiadis, PhD

Awarded for: Towards a model of FUS-mediated blood-brain barrier disruption in non-enhancing, glioma-invaded brain regions for testing improvements in therapeutic delivery

Pavlos Anastasiadis joined the Translational Focused Ultrasound Research Laboratory in the Department of Diagnostic Radiology and Nuclear Medicine at the University of Maryland School of Medicine in 2016. The lab, under the directorship of Victor Frenkel, PhD, is part of the Focused Ultrasound Foundation-Designated Center of Excellence at the University of Maryland School of Medicine. His research efforts make up a key component of the lab's mandate to develop focused ultrasound-based procedures. His projects include the use of MRgFUS for targeted delivery of therapeutics, cancer immunotherapy for the treatment of brain tumors, and the delivery of cellular-based therapies. He was previously a Fellow of the German Research Foundation, the Max Planck Foundation, and the Fraunhofer Foundation. Prior to moving to Maryland, he worked at the National Cancer Institute-Designated University of Hawaii Cancer Center. Currently, as an NIH T32 Cancer Biology Fellow, he is associated with the University of Maryland Marlene and Stewart Greenebaum Comprehensive Cancer Center. His NIH T32 advisory committee is composed of Victor Frenkel, PhD, Graeme F. Woodworth, M.D., Joseph A. Frank, M.D., Eduardo Davila, PhD, and Jeffrey A. Winkles, PhD. Pavlos is a member of the American Association for Cancer Research, the American Society for Biochemistry and Molecular Biology, the International Society for Electrical Bioimpedance, the Acoustical Society of America, the International Society for Therapeutic Ultrasound and the German Society for Cell Biology.

YI-5/P-YI-5

Abstract: page 195

Kamyar Firouzi, PhD

Awarded for: Efficient transcranial ultrasound delivery via excitation of lamb waves

Kamyar Firouzi received his MS degree in mechanical engineering from University College London (UCL) in 2010 and a PhD degree in mechanical engineering from Stanford University in 2016. For his doctoral dissertation, he focused on the localization of objects in chaotic and reverberant enclosures, based on which he developed a lamb-wave multitouch ultrasonic touchscreen system. He was a Research Assistant with UCL from 2010 to 2011, where he developed a predictive computational tool for evaluation of photoacoustic imaging techniques for detection of brain tumors. He has worked on numerous problems in ultrasound/MEMS technologies, including modeling and design of ultrasonic transducers, photoacoustics, microbubbles, wave propagation, and numerical methods. His current research interests include transcranial ultrasound, ultrasound neuromodulation, ultrasonic flow-measurement, and ultrasound signal processing and inverse problems.

YI-1/P-YI-1

Abstract: page 189

Marc N. Gallay, MD

Awarded for: MRgFUS in chronic therapy-resistant Parkinson's disease

Marc Gallay currently works as a neurosurgeon at the Center for Focused Ultrasound Neurosurgery Sonimodul, Switzerland, led by neurosurgeon Daniel Jeanmonod. He received his medical degree at the University of Zurich in 2008. His doctoral dissertation, "Human cerebello- and pallidothalamic tracts: Stereotactic localization, interindividual variability and MR correlations," was obtained in 2009 at the University Hospital Zürich under the supervision of Dr. Anne Morel and Prof. Daniel Jeanmonod. There, he further studied the monkey and human insular cortex as a postdoc fellow before training in neurosurgery at the Kantonsspital St.Gallen and at the University Hospital Geneva. He completed his neurosurgical training in 2015.

2018 Young Investigator Awards (continued)

YI-4/P-YI-4

Abstract: page 193

Pooja Gaur, PhD

Awarded for: Histological study of focused ultrasound neuromodulation and MR-ARFI in sheep

Pooja Gaur earned her BS in biomedical engineering at Johns Hopkins University and her PhD at Vanderbilt University under the mentorship of Dr. William Grissom. During her doctoral research, she developed MRI methods for measuring temperature changes in the body during focused ultrasound heating treatments. As a postdoctoral scholar working with Dr. Kim Butts Pauly at Stanford University, Dr. Gaur is investigating focused ultrasound through the skull and assessing tissue safety in the brain.

YI-8/P-YI-8

Abstract: page 198

Tyler I. Gerhardson

Awarded for: Histotripsy mediated immunomodulation in a mouse gl261 intracranial glioma model

Tyler Gerhardson is a PhD candidate in the Department of Biomedical Engineering at the University of Michigan. He received a BS degree in biomedical engineering from Western New England University in 2015 and an MS Degree in biomedical engineering from the University of Michigan in 2017. Selected honors include the Dean's Award for Academic Excellence and Biomedical Engineering Department Award for Outstanding Senior from Western New England University, a Scholarship and Fellowship from Tau Beta Pi, and a National Science Foundation Graduate Research Fellowship. Tyler's research interests include ultrasonic standing wave separators, ultrasound transducers, and focused ultrasound therapies.

P-YI-13

Abstract: page 318

Yekaterina Gilbo

Awarded for: Detecting T1-based signal reduction in focused ultrasound heating of bone using a 3D spiral ultra-short echo time sequence

Yekaterina Gilbo graduated from the University of Virginia (UVA) in 2017 with a BS in physics and is pursuing a PhD in biomedical engineering at UVA. She is currently working on a project in MRgFUS that uses the magnetization properties of bone to detect potentially harmful skull heating.

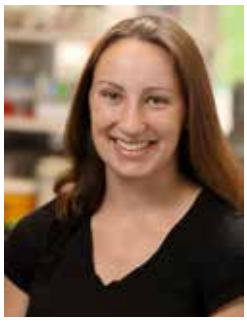

YI-3/P-YI-3

Abstract: page 191

Catherine Gorick

Awarded for: Focused ultrasound-mediated transfection of cerebral vasculature independent of blood-brain barrier opening [YI-3/P-YI-3]

Catherine Gorick received an undergraduate degree in biological engineering from MIT in 2015. There, she was a four-year member of the varsity lightweight crew team, a member of the Tau Beta Pi engineering honor society, and a mentor for an undergraduate leadership development program. Now in her fourth year of a PhD program in biomedical engineering at the University of Virginia, Ms. Gorick is working in the Price Lab and her research focuses on developing a platform for ultrasound-mediated gene delivery to the cerebral vasculature for stroke applications.

YI-11/P-YI-11

Abstract: page 204

Alexander S. Mathew

Awarded for: RNA sequencing of focused ultrasound-treated melanoma reveals that thermal ablation and hyperthermia elicit differential immunogenicity

Alex Mathew received his BS in chemistry and BA in mathematics from the University of Virginia (UVA) where he is pursuing an MD/PhD at UVA in the Price Lab. Currently, he is integrating high throughput sequencing with systems biology approaches to uncover the mechanisms behind FUS immunomodulation to inform FUS and immunotherapy combination strategies.

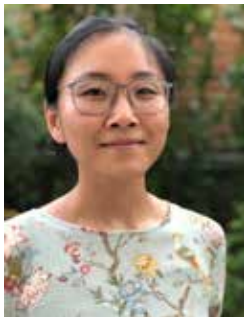

YI-6/P-YI-6

Abstract: page 196

Ying Meng, MD

Awarded for: Blood-brain barrier opening in primary brain tumors: A demonstration of safety and feasibility with noninvasive MR-guided focused ultrasound

Ying Meng is a neurosurgery resident at the University of Toronto, researching neurologic applications of FUS under Dr. Nir Lipsman's supervision. Her interests and activities span from preclinical to clinical investigations involving neurological conditions such as movement disorders, traumatic brain injury, and neurodegenerative disorders.

2018 Young Investigator Awards (continued)

YI-12/P-YI-12

Abstract: page 206

Daniele Mercatelli, PhD

Awarded for: Treatment of painful bone tumors using MR-guided focused ultrasound with conformal bone system

Daniele Mercatelli is a postdoc research fellow active in the field of imaging and oncology at the Istituto Ortopedico Rizzoli. He holds a master's degree in cellular and molecular biology and a PhD in oncology and experimental pathology from Alma Mater Studiorum - University of Bologna. He has been working on the team headed by Dr. Alberto Bazzocchi since 2016, where he has been involved in managing and coordinating clinical trials investigating MRgFUS and its current applications in bone malignancies. His main research interests involve the potential application of focused ultrasound in the experimental treatment of osteoarthritis and benign bone and soft tissue tumors, broadened to wider aspects of cellular and molecular research.

YI-2/P-YI-2

Abstract: page 190

Francesco Sammartino, MD

Awarded for: Longitudinal analysis of lesion microstructural changes after focused ultrasound thalamotomy

Francesco Sammartino received his MD from the University of Udine in 2008 and completed his neurosurgery residency at the University of Padova in 2015. In 2016, he completed a functional neurosurgery fellowship at the University of Toronto under the supervision of Prof. Andres Lozano. He is currently a research fellow at Ohio State University in the Center for Neuromodulation. Dr Sammartino's main interest is neuroimaging applied to functional neurosurgery. During his fellowship in Toronto he chose to dedicate his research to personalizing the targeting and improving the outcomes after MRgFUS thalamotomy for essential tremor. He developed a methodology to help define the VIM region with the use of tractography, and he is currently involved in developing new methods to understand the mechanisms of tremor efficacy in the thalamus and the longitudinal microstructural changes associated with tissue ablation.

YI-9/P-YI-9
Abstract: page 200

YI-10/P-YI-10
Abstract: page 202

Natasha Sheybani

Awarded for: Leveraging MR image-guided focused ultrasound to potentiate immunotherapy for glioblastoma

Developing synergy between immunotherapy and focused ultrasound ablation for metastatic breast cancer

Natasha Sheybani is a fourth-year PhD Candidate and member of the Price Lab in the Department of Biomedical Engineering at the University of Virginia (UVA). Her graduate research centers on leveraging FUS to potentiate immunotherapy for primary and disseminated solid cancers. Natasha received her BS in biomedical engineering (with honors) from Virginia Commonwealth University. She is a recipient of the NSF Graduate Research Fellowship and UVA Robert R. Wagner Fellowship.

Charles Steger Memorial Internship Program

Charles Steger, PhD

Claude Moore
CHARITABLE FOUNDATION

The Focused Ultrasound Foundation's Summer Internship Program was established in 2012 with the goal of giving accomplished high school, undergraduate, and graduate students the opportunity to collaborate with leaders in the field on a variety of projects that address preclinical, clinical, and business challenges.

In May 2018, the Foundation's internship program–which encompasses both local and global interns–was named in memory of Board of Directors member Charles Steger, PhD. The Foundation's summer technical internships are generously funded by the Claude Moore Charitable Foundation. The Claude Moore Summer Internship Program is part of the Charles Steger Focused Ultrasound Internship Program and is designed to foster interest in focused ultrasound technology among the next generation of researchers.

In the summer of 2017, the talented group of interns included four college students who worked on projects ranging from focused ultrasound patient registries to the use of 3D-printed lenses for transcranial focused ultrasound.

This summer, the Foundation welcomed seven students, including more nontechnical interns than in previous years. The group completed a wide variety of projects, working on everything from graphic design to the newly launched FUS Partners Program, to more technical projects like 3D-printed acoustic lenses and the use of software to automate and simplify research.

2017 Summer Interns
(Left to Right)

Sara Hunter Chang
Derek Fang
Lindsey Abramson
Kassandra Tulenko

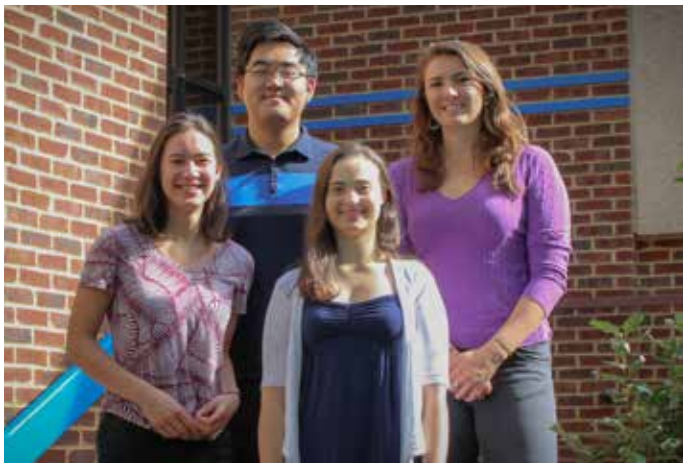

2018 Summer Interns
(Left to Right)

George Brown
Lola Manning
Kate Snell
Marysia Serafin
Graham Keeley
Runmeng Zhai

Not pictured: Mailys Nier

Global Internship Program

Qingxi (Brooke) Ma

Receiving the highest peer-reviewed rating among submissions from the 2017 and 2018 FUSF Global Interns, Brooke Ma's abstract, entitled "Effects of focused ultrasound on delivery of intranasal GDNF DNA nanoparticles to the rat brain" earned her travel support to attend and present her work at the Symposium.

The Focused Ultrasound Foundation offers an international internship opportunity for high school and university undergraduate students interested in the physical and life sciences. Interns supported through this program work in an established focused ultrasound laboratory under a researcher recognized in the field.

2017 Global Interns

Jessica Cahill
Georgia Institute of Technology
Atlanta, Georgia, United States
Mentor: Costas Arvanitis, PhD

Nikolas Evripidou
Cyprus University of Technology
Limassol, Cyprus
Mentor: Christakis Damianou, PhD

Afton Holzer
University of Utah
Salt Lake City, Utah, United States
Mentor: Allison Payne, PhD

Yixuan Huang
Vanderbilt University
Nashville, Tennessee, United States
Mentor: Charles Caskey, PhD

Diana Kim
Columbia University
New York, New York, United States
Mentor: Elisa Konofagou, PhD

Jennifer Kunes
Brigham and Women's Hospital
Boston, Massachusetts, United States
Mentor: Nick Todd, PhD

Roxanne Lahady
University of Paris
Paris, France
Mentor: Jean François Aubry, PhD

Jie Man Low
Institute of Cancer Research
London, United Kingdom
Mentor: Gail ter Haar, PhD

Ilia Mezdrokhin
Moscow State University
Moscow, Russia
Mentor: Vera Khokhlova, PhD

Alex Mueller
University of Utah
Salt Lake City, Utah, United States
Mentor: Dennis Parker, PhD

Andreas Mylonas
Cyprus University of Technology
Limassol, Cyprus
Mentor: Christakis Damianou, PhD

Shivani Patel
University of Maryland
College Park, Maryland, United States
Mentor: Rao Gullapalli, PhD, MBA

Andrey Polyanskiy
Moscow State University
Moscow, Russia
Mentor: Oleg Sapozhnikov, PhD

Lauren Puumala
Lakehead University
Thunder Bay, Ontario, Canada
Mentor: Laura Curiel, PhD

Tess Seip
SonaCare Medical
Charlotte, North Carolina, United States
Mentor: Narendra Sanghvi

Bruno Souchu
University of Paris
Paris, France
Mentor: Jean François Aubry, PhD

Jinchao Wu
Stanford University
Stanford, California, United States
Mentor: Kim Butts Pauly, PhD

Yoko Zecchini
University College London
London, United Kingdom
Mentor: Wladyslaw Gedroyc, MBBS

Global Internship Program (continued)

2018 Global Interns

Neema Ahmadian
Virginia Polytechnic Institute and State University
Blacksburg, Virginia, United States
Mentor: Shima Shahab, PhD

Dylan Beam
Ohio State University
Columbus, Ohio, United States
Mentor: Vibhor Krishna, MBBS

Anastasia Bobina
Moscow State University
Moscow, Russia
Mentor: Oleg Sapozhnikov, PhD

Adam Canfield
Brigham and Women's Hospital
Boston, Massachusetts, United States
Mentor: Phillip Jason White, PhD

Megan Dearden
University of Utah
Salt Lake City, Utah, United States
Mentor: Doug Christensen, PhD

Nikolas Evripidou
Cyprus University of Technology
Limassol, Cyprus
Mentor: Christakis Damianou, PhD

Maeghan Garrison
University of Virginia School of Medicine
Charlottesville, Virginia, United States
Mentor: Wilson Miller, PhD

Tejas Karwa
Albert Einstein College of Medicine
Bronx, New York, United States
Mentor: Indranil Basu, PhD, MBA

Hohyun Lee
Georgia Institute of Technology
Atlanta, Georgia, United States
Mentor: Costas Arvanitis, PhD

Qingxi (Brooke) Ma
Northeastern University
Boston, Massachusetts, United States
Mentor: Barbara Waszczak, PhD

Craig Macsemchuk
University of Calgary
Calgary, Alberta, Canada
Mentor: Samuel Pichardo, PhD

Chris Margraf
University of Virginia
Charlottesville, Virginia, United States
Mentor: Timothy Bullock, PhD

Sophie Meyer
University of Virginia
Charlottesville, Virginia, United States
Mentor: Richard Price, PhD

Swadhin Nalubola
University of Maryland
Baltimore, Maryland, United States
Mentor: Rao Gullapalli, PhD, MBA

Somang Paeng
Seoul National University Hospital
Seoul, Korea
Mentor: Eun-Joo Park, PhD

Ekaterina Ponomarchuk
Moscow State University
Moscow, Russia
Mentor: Vera Khokhlova, PhD

Dia Shah
Albert Einstein College of Medicine
Bronx, New York, United States
Mentor: Indranil Basu, PhD, MBA

Alexander Simon
Virginia Polytechnic Institute and State University
Blacksburg, Virginia, United States
Mentor: Eli Vlaisavljevich, PhD

James Woznak
University of Virginia
Charlottesville, Virginia, United States
Mentor: Kevin Lee, PhD

Lin Zhang
Columbia University
New York, New York, United States
Mentor: Elisa Konofagou, PhD

Sponsors and Exhibitors

	Exhibit Booth	Description Page	Advertisement Page
Diamond Sponsor			
INSIGHTEC	8	334	342
Platinum Sponsor			
Profound Medical Corp.	1	334	343
Gold Sponsor			
Koch Disruptive Technologies	not exhibiting	334	
Silver Sponsors			
Bracco Suisse SA	not exhibiting	335	
International Society for Therapeutic Ultrasound (ISTU)	9	335	344
KAI Research, Inc., an Altarum Company	11	335	
Meggitt A/S	3	335	
Exhibitors and Supporters			
Electronics & Innovation, Ltd.	4	336	
European Focused Ultrasound (EUFUS) Charitable Society	10	336	
HistoSonics, Inc.	not exhibiting	336	
Image Guided Therapy	12	337	
IMASONIC	2	337	
Korean Society for Therapeutic Ultrasound (KSTU)	9	337	
Sonic Concepts, Inc.	5–7	337	
Verasonics, Inc.	5–7	337	
Focused Ultrasound Foundation			
7th International Symposium on Focused Ultrasound			345
Focused Ultrasound Foundation		336	Back cover
FUS Foundation Board of Directors and Council			346
FUS Foundation Research Funding			345

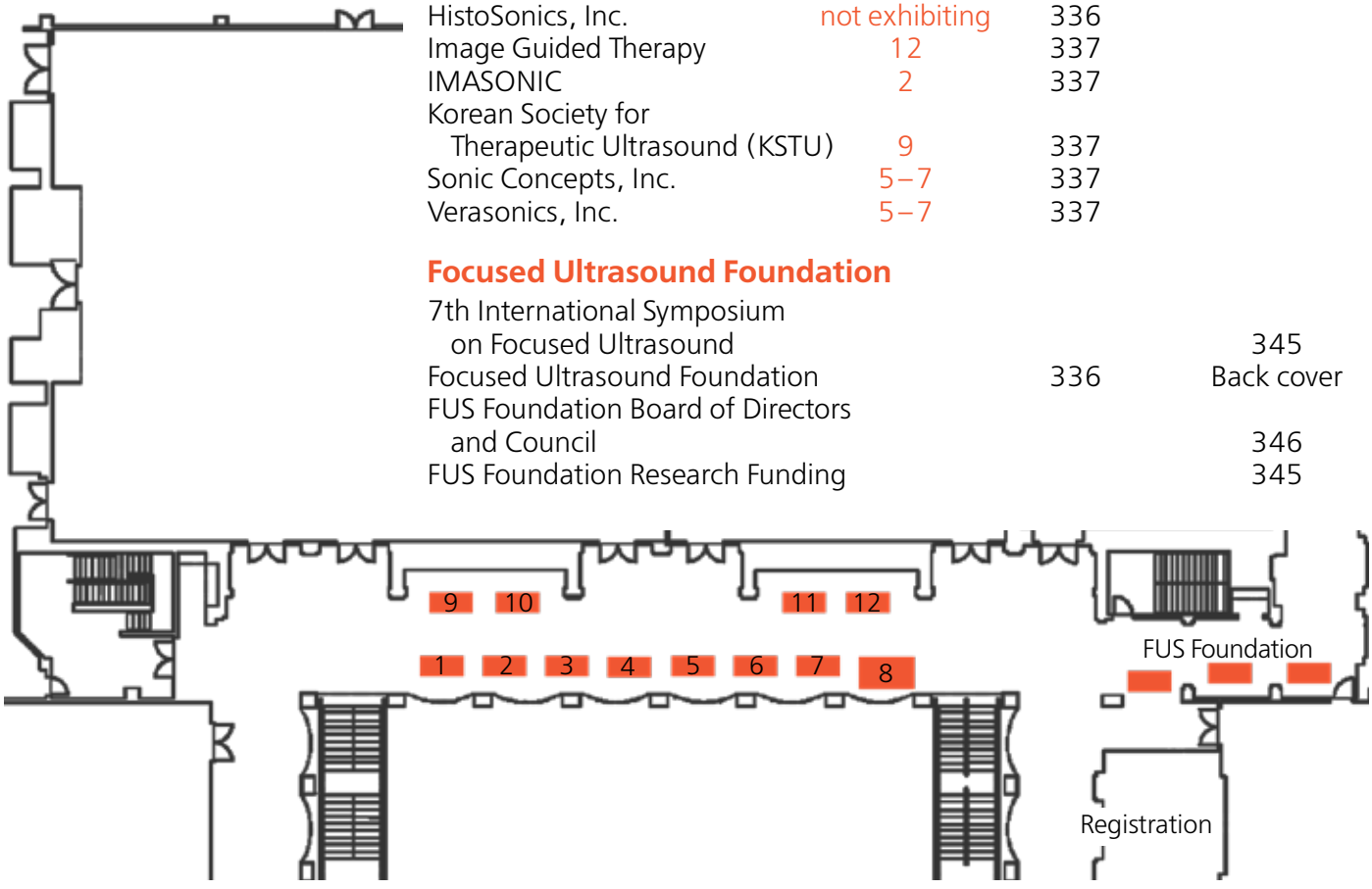

Diamond Sponsor

INSIGHTEC

www.insightec.com

Advertisement: page 342

INSIGHTEC® is a global medical technology innovator transforming patient lives through incisionless brain surgery with MR-guided focused ultrasound. With no incisions, there is no risk of infection, hospitalization is minimized or avoided altogether, and patients can quickly return to their lives.

The company's award-winning platform, Exablate Neuro™, is being used to treat medication-refractory essential tremor. The result for many patients is immediate and durable tremor relief with minimal complications. Research for future brain applications is underway in partnership with leading academic and medical institutions. INSIGHTEC is headquartered in Haifa, Israel, and Miami, with offices in Dallas, Tokyo, and Shanghai.

Platinum Sponsor

Profound Medical

www.profoundmedical.com

Advertisement: page 343

Profound Medical is creating a therapeutics platform that provides the precision of real-time MRI combined with the safety and ablation power of both directional and focused ultrasound. We are commercializing TULSA-PRO® and SONALLEVE® which have CE marking for the ablation therapy of prostate, uterine fibroids, and bone metastases pain.

Gold Sponsor

Koch Disruptive Technologies

www.kochind.com

Koch Disruptive Technologies (KDT) invests in highly transformative growth companies that disrupt current market alternatives. KDT has a mutual benefit mindset, offering bespoke capital solutions and access to Koch Industries' global, multi-industry network.

Silver Sponsors

Bracco Suisse SA

www.bracco.com

Bracco Imaging, part of the Bracco Group, is one of the world's leading companies in the diagnostic imaging business. Headquartered in Milan, Italy, it operates in more than 100 markets worldwide. Manufacturing activities are located in Italy, Switzerland, Japan, China, and Germany, while R&D activities are managed in three research centers located in Italy, Switzerland, and the U.S.

International Society for Therapeutic Ultrasound (ISTU)

www.istu.org

Advertisement: page 344

The International Society for Therapeutic Ultrasound (ISTU) is a nonprofit organization founded in 2001 to increase and diffuse knowledge of therapeutic ultrasound to the scientific and medical community, and to facilitate the translation of therapeutic ultrasound techniques into the clinical arena for the benefit of patients worldwide.

KAI Research

www.kai-research.com

KAI is a collaborative, "high-touch" clinical research company that conducts clinical trials, provides clinical research consultation, and implements data management and standardization services. For more than 30 years, we've helped commercial, academic, and federal clients bring innovative drug treatments and medical devices to market, including many years supporting focused ultrasound and related technologies.

Meggitt A/S

www.meggittferroperm.com

With 60 years of experience in manufacturing high quality piezoelectric ceramics, Meggitt A/S aims to provide materials and components with the highest possible reproducibility of properties and parameters, and to obtain the lowest aging rates in the industry. This strategy enables customers to optimize design and improve performance and production flow.

Exhibitors and Supporters

Electronics & Innovation, Ltd.

www.eandiltd.com

Electronics & Innovation Ltd (E&I) is a world leader in providing rugged and reliable RF power products. We want to work with you from research to production, benchtop to module. In addition to our standard product lines, we offer custom modules and pallets – designed specifically to fulfill your OEM requirements. Operating globally and continuing to expand our technology, E&I is committed to providing RF power solutions of the highest quality, durability, and ruggedness.

EUFUS - European Focused Ultrasound Charitable Society

www.eufus.org

The European Focused Ultrasound Charitable Society is a research and education organization serving as a philanthropic forum to establish research funding, sharing experiences, reviewing best practices, and promoting cooperation in the field of Focused Ultrasound for better patient treatment.

Focused Ultrasound Foundation (FUSF)

www.fusfoundation.org

Overview: Inside back cover
7th International Symposium: page 345
Board of Directors: page 346
Research funding: page 345

The Focused Ultrasound Foundation is a medical technology research, education, and advocacy organization dedicated to improving the lives of millions of people with serious medical disorders by accelerating the development and adoption of focused ultrasound. The Foundation works to clear the path to global adoption by organizing and funding research, fostering collaboration, building awareness at our various workshops and symposia, and cultivating the next generation through internships and fellowships.

HistoSonics, Inc.

www.histosonics.com

(not exhibiting)

HistoSonics is a venture-backed medical device company whose mission is to redefine cancer treatment with a noninvasive, highly precise, cost-effective method of tumor destruction called Robotically Assisted Sonic Therapy (RAST™). The team at HistoSonics is currently developing a completely non-invasive robot that has the potential to deliver personalized treatments over a broad range of cancers in an outpatient setting. RAST™ is based on the science of histotripsy, a noninvasive ablation modality developed at the University of Michigan that uses the pressure created by focused sound energy to completely destroy tissue at a subcellular level.

Exhibitors and Supporters (continued)

Image Guided Therapy

www.imageguidedtherapy.com

Image Guided Therapy develops MR guided HIFU systems for preclinical research, based on phased array generators and transducer with up to 256 independent channels. IGT systems are used by renowned academic centers in diverse applications ranging from drug delivery to hyperthermia, ultrasound mediated blood-brain barrier opening, neurostimulation, and plain thermal ablation.

IMASONIC

www.imasonic.com

IMASONIC is a French independent, privately-owned company that develops and produces ultrasonic transducers and complete probes for health and safety applications. Since its creation in 1989, IMASONIC has been contributing to improving ultrasonic medical applications by designing and manufacturing transducers for therapeutic use, diagnosis, and monitoring. The company has 100 employees.

Korean Society for Therapeutic Ultrasound (KSTU)

www.kstu.or.kr

Exhibiting with ISTU

The Korean Society for Therapeutic Ultrasound (KSTU) was founded in 2014. Since inception there has been rapid membership growth with approximately 100 attendees at our annual meetings. This year, KSTU began an official exchange program with Japanese Society for Therapeutic Ultrasound (JSTU). We are looking to expand this program to other Asian societies for therapeutic ultrasound. KSTU is honored to host the symposium of the International Society for Therapeutic Ultrasound (ISTU) at Gyeongju, Korea, May 17-20, 2020.

Sonic Concepts, Inc.

www.sonicconcepts.com

Sonic Concepts, Inc. manufactures high-power, wide-bandwidth ultrasound transducers and related equipment. SCI supplies single- or multi-element transducers, as well as annular, linear, and 2D arrays, transmit electronics, passive cavitation detectors, high-intensity hydrophones, radiation force balances, water degassing equipment, and more. SCI supports customer orders from initial prototyping into full-scale production.

Verasonics, Inc.

www.verasonics.com

Verasonics offers leading-edge capabilities for focused ultrasound research and development. The Vantage systems are real-time, software-based programmable ultrasound platforms that provide flexible and precise imaging and HIFU including targeting, guidance, treatment, and monitoring. Verasonics sells research systems and software, licenses its technology, and provides consulting services to academic and commercial investigators.

Notes

Partners

BIRD Foundation	34
Cancer Research Institute	34
Epilepsy Foundation	34
International Essential Tremor Foundation	35
Melanoma Research Alliance	35
The Michael J. Fox Foundation	35

Partners

BIRD Foundation

www.birdf.com

The Israel-US Binational Industrial Research and Development (BIRD) Foundation's mission is to accelerate growth through strategic partnerships. The BIRD Foundation promotes and facilitates collaboration between US and Israeli companies in various technological fields for the mutually beneficial purpose of developing and commercializing promising innovations for the global market. Providing conditional grants of up to 50 percent of a joint project budget, the BIRD Foundation assists companies by identifying potential strategic partners in either Israel or the US and facilitating introductions. In almost 40 years since its inception, BIRD has funded over 900 projects worth $10 billion in direct and indirect investment. Some of the recent collaborations that have matured into successfully commercialized products include ReWalk™, Poise™, Hockey IntelliGym™; OnVu™ and many more.

Cancer Research Institute

www.cancerresearch.org

The Cancer Research Institute is motivated by a very simple but important scientific fact: the human body has the ability to defend itself from cancer. The mission is straightforward — save more lives with cancer immunotherapy. Our founding scientists believed that the key to long-term survival lay in learning how to manipulate the immune system to strengthen its defenses against cancer. We set out more than 60 years ago not only to prove this could be done, but also to do something with this knowledge that would truly help cancer patients. This work is now beginning to pay off: immunotherapies are transforming cancer treatment and bringing us closer to cures for all cancers.

Epilepsy Foundation

www.epilepsy.com

The Epilepsy Foundation and affiliates provide information and referral assistance; maintain individual and family support services; serve as advocates for the rights of those with epilepsy; and offer community-based education to employers, emergency first-responders, school nurses, and other allied health professionals.

Partners (continued)

International Essential Tremor Foundation

www.essentialtremor.org

The mission of the International Essential Tremor Foundation (IETF) is to provide global educational information, services, and support to children and adults challenged by essential tremor (ET), to their families and health care providers, as well as to promote and fund ET research.

Melanoma Research Alliance

www.curemelanoma.org

The mission of the Melanoma Research Alliance (MRA) is to end suffering and death due to melanoma by collaborating with all stakeholders to accelerate powerful research, advance cures for all patients, and prevent more melanomas. We are the largest private funder of melanoma research. Since its founding in 2007, MRA has committed more than $79 million in funding to advance our understanding of this disease. MRA funds projects in the areas of prevention, diagnosis, and treatment, with the majority of funding allocated for melanoma treatment.

The Michael J. Fox Foundation

www.michaeljfox.org

The Michael J. Fox Foundation is dedicated to accelerating a cure for Parkinson's disease and improved therapies for those living with the condition today. As the world's largest nonprofit funder of Parkinson's research, the Foundation manages an aggressively funded research agenda. The Foundation works to ensure the patient voice is at the center of our efforts with one urgent goal in mind: Accelerating breakthroughs patients can feel in their everyday lives.

INTERNATIONAL SOCIETY FOR THERAPEUTIC ULTRASOUND

Registration is now open for the 19th Annual International Symposium for Therapeutic Ultrasound

Join scientists, engineers, clinicians and industry from around the world as we come together in Barcelona, Spain for the first joint meeting with the European Focused Ultrasound Charitable Society (EUFUS).

- Attend sessions covering topics ranging from Immunotherapy to Thermal Ablation, Modeling and Physics, and much more.
- Exchange ideas, collaborate, and envision novel applications of therapeutic ultrasound.
- Enjoy Barcelona's world-renowned art and architecture, and explore the beauty of the cosmopolitan capital of Spain's Catalonia region right on the Mediterranean Sea.

Save the dates now for the 20th Annual International Symposium for Therapeutic Ultrasound!

We look forward to your contribution to these exciting meetings.

Learn more and register today at ISTU.org

Funding Available for Focused Ultrasound Research

Grants of up to $100,000 for 12-month projects

The Foundation's **External Research Awards Program** supports technical, preclinical, and pilot clinical research to accelerate adoption of image-guided focused ultrasound.

For more information visit the **For Researchers** page at **fusfoundation.org** or contact **Matt Eames**, Director of Extramural Research, at meames@fusfoundation.org.

Research award recipient Dong-guk Paeng, PhD

FOCUSED ULTRASOUND FOUNDATION

Save the Date

7th International Symposium on Focused Ultrasound

2020

Washington, DC area • November 2020

FOCUSED ULTRASOUND FOUNDATION

Thank you!

The Focused Ultrasound Foundation wishes to thank its exceptional Board of Directors and Council for their steadfast dedication to helping make focused ultrasound a clinical reality and improve the lives of millions of patients.

BOARD OF DIRECTORS

Dorothy N. Batten
Founder, iThrive Initiative
Former Director, Landmark Communications

Lodewijk J.R. de Vink
Founding Partner, Blackstone Healthcare Partners
Former Chairman & CEO, Warner-Lambert

Eugene V. Fife
Founding Principal, Vawter Capital
Former Chairman, Goldman Sachs International

John R. Grisham
Author

William A. Hawkins, III
Former Chairman & CEO, Medtronic

Daniel P. Jordan, PhD
President Emeritus, Thomas Jefferson Foundation, Inc.

Neal F. Kassell, MD
Chairman, Focused Ultrasound Foundation
Professor of Neurosurgery, University of Virginia

Edward J. "Ned" Kelly, III
Former Chairman, Institutional Clients Group, Citigroup

Edward D. Miller, MD
Former CEO, Johns Hopkins Medicine

Frederic H. Moll, MD
Co-founder, Intuitive Surgical
Chairman & CEO, Auris Health, Inc.

Charles W. "Wick" Moorman, IV
Former CEO, Amtrak
Former Chairman & CEO, Norfolk Southern

Stephen H. Rusckowski
President and CEO, Quest Diagnostics Inc.
Former CEO, Philips Healthcare

Andrew C. von Eschenbach, MD
President, Samaritan Health Initiatives
Former Commissioner, U.S. Food and Drug Administration
Former Director, National Cancer Institute

Carl P. Zeithaml, PhD
Dean and F.S. Cornell Professor of Free Enterprise,
McIntire School of Commerce, University of Virginia

COUNCIL

Co-Chairs
Jane P. Batten
Charles H. Seilheimer, Jr.

John B. Adams, Jr.
Ellen H. Block
Charles F. Bryan, Jr., PhD
Thomas and Nancy Chewning
Norwood and Marguerite Davis
Diane Heller
William and Cecelia Howell
Dean Kamen
Robert C. Khayat, JD, LLM
Ann Kingston
Syaru Shirley Lin, PhD
Amanda Megargel
Tony and Jonna Mendez
Michael Milken
Paula F. Newcomb
Wyndham G. Robertson
Mary Lou Seilheimer
Alice H. Siegel
Aaron Stern, MD, PhD
Howard and Fredericka Stevenson
Jane Tolleson
Meredith Jung-En Woo, PhD
Linda K. Zecher

FOCUSED ULTRASOUND FOUNDATION

www.fusfoundation.org

Your partner *in advancing the field*

FOCUSED ULTRASOUND FOUNDATION

The Focused Ultrasound Foundation was created to improve the lives of millions of patients by accelerating the development and adoption of focused ultrasound.

We leverage our independent status to drive progress by:

Funding Research

A key priority for the Foundation is funding translational studies, applying the growing body of knowledge to complex problems.

We fund internal research exploring technical aspects of treating the **brain** and **cancer immunotherapy.** Our **External Awards Program** also funds investigator-initiated clinical, preclinical and technical projects through a competitive peer-reviewed process.

Fostering Collaboration

We act as a global connector, hosting a variety of **workshops and biennial symposia** to stimulate innovation and increase awareness.

Overcoming Barriers

We **partner with industry** to help usher this technology through the regulatory and reimbursement processes and move the technology closer to patients.

FOCUSED
ULTRASOUND
FOUNDATION

Focused Ultrasound Foundation
1230 Cedars Court, Suite 206, Charlottesville, VA, USA
(434) 220.4993
www.fusfoundation.org